Mechanistic insights into biased agonism at the Glucagon-like peptide 1 receptor

Lachlan Charles Clydesdale
Bachelor of Science (Honours)

A thesis submitted for the degree of (Doctor of Philosophy) at
Monash University in 2020
Monash Institute of Pharmaceutical Sciences

Copyright notice

Abstract

The GLP-1R is a key target in the treatment of type 2 diabetes with multiple therapeutics already approved that target this receptor. Despite the success of these drugs, there is a need to develop new and better therapeutics. One avenue for this is to take advantage GLP-1Rs natural ability to couple to multiple signalling effectors. Different ligands at the GLP-1R can promote distinct signalling profiles, which has the potential lead to different combined physiological profiles. This phenomenon, known as biased agonism, has been well documented at the GLP-1R, however, to exploit this for therapeutic development requires knowledge of the ideal profiles of signalling for therapeutic benefit and a greater understanding of mechanistic basis for which this phenomenon arises at the GLP-1R.

To identify the ideal profiles of GLP-1R signalling for development of improved therapies requires a wide range of tool compounds with differing signalling properties to enable a thorough investigation of the functional consequences of biased agonism in vivo. In this thesis, a series of 11mer peptide ligands based on the first 11 residues of the native peptide (GLP-1(7-36)NH_2 with novel chemistry have been synthesised and gifted to our group, and comprehensively assessed at the GLP-1R to quantify their profiles of signalling. We identified a wide range of peptides with differing pharmacology. These included peptides with differences in their biased agonism profile that could be correlated with the composition of the first residue of the peptide.

To exploit biased agonism for rationale development of novel ligands requires detailed mechanistic understanding of how biased agonism and differential efficacy arises. The fourth chapter of this thesis identified contributions of individual transducer subfamilies to the downstream signalling profiles of different GLP-1R ligands, which included both full length and 11mer peptide ligands. While Gαs and Gαq, as expected, were both essential for cAMP and calcium signalling respectively, we identified surprising roles of Gα12/13 and β-arrestins in modulating these signalling pathways, which occurred in a ligand-dependent manner.

To date, a number of large structural and mutagenesis programs have been undertaken for the GLP-1R. An understanding of how different ligands interact with the GLP-1R, and how this promotes coupling of intracellular signalling components is required to link structural

information to the function of ligands of different pharmacology. A combination of structural biology, performed by Lynn Liang and Xin Zhang in combination with molecular pharmacology, mutating residues in a pocket that encases the extreme N terminus of ligand in the final binding pose, enables linking of specific topographical areas of the receptor to distinct signalling pathways and provide critical information that can be exploited for rational development of novel agonists.

The third results chapter of this thesis reports mutagenesis of receptor residues to alanine and the influence of this on receptor function. The selection of these was guided by structural biology efforts (performed by others in the laboratory) where we identified residues that were located within the pocket within the 7 transmembrane core that accommodates the N-terminus of different peptide ligands. This study provides unprecedented information of how different biased ligands interact with the GLP-1R with molecular details into the role individual residues play in both ligand affinity and cAMP efficacy. While individual residues within the GLP-1R TM binding site had little impact on exendin P5 affinity compared to GLP-1, exendin 4 and oxyntomodulin, this region of the receptor was more important for cAMP efficacy for exendin P5. This can be explained by the a more open binding pocket in the exendin P5 structure allowing for greater mobility in the pocket whereby any one individual receptor interaction was less important for this ligand than other agonists and this is confirmed in MD simulations (from Chris Reynolds group). In addition, distinct regions within the GLP-1R were linked to divergent pharmacological profiles of the four agonists where three receptor regions were identified for differences in both the structure and functional variances observed upon GLP-1R receptor binding to distinct ligands. These included TM1, the TM2-ECL1-TM3 region and the TM6-ECL3-TM7 area that displayed differences not only in the structural conformation induced in the receptor (as revealed by novel structural information), but also in the role of individual residues within these regions in ligand-dependent affinity and efficacy of the biased ligands assessed.

In summary, this thesis furthers our understanding of GLP-1R biased agonism and provides novel insights into the structural and mechanistic basis of how this phenomenon arises. This enhanced understanding will allow future rational drug development to design ligands with select pharmacologies that will enable the identification and development of better therapeutics with the potential for greater therapeutic efficacy and fewer side effects for the treatment of diseases, such as diabetes.

Published works during studies

Hager, M. Clydesdale, L. Gellman. S. Sexton, P. Wootten. D: Characterization of signal bias at the GLP-1 receptor induced by backbone modification of GLP-1, *Biochemical Pharamcology* (2017) 136;99-108.

Liang, L. Khoshouei, M. Glukhova, A. Furness, S. Zhao, P. Clydesdale, L. Koole, C. Truong, T. Lei, S. Thal, D. et al; Phase-plate cryo-EM structure of a biased agonistbound human GLP-1 receptor-Gs complex, *Nature* (2018) 555; 121-125

Lei, S. Clydesdale, L. Dai, A. Cai, X. Feng, Y. Yang, D. Liang, L. Koole, C. Zhao, P. Coudrat, T. Two distinct domains of the glucagon-like peptide-1 receptor control peptide-mediated biased agonism, *Journal of Biological Chemistry,* (2018) 293(3); 9370-9387

Fletcher, M. Halls, L. Zhao, P. Clydesdale, L. Christopolous, A. Sexton, P. Wootten, D: Glucagon-like peptide-1 receptor internalisation controls spatiotemporal signalling mediated by biased agonists, *Biochemical Pharmacology* (2018) 156; 406-419

Zhao, P. Liang, L. Belousoff, M. Deganutti, G. Fletcher, M. Willard, F. Bell, M. Christe, M. Sloop, K. Inoue, A. Truong, T. Clydesdale, L et al.: Activation of the GLP-1 receptor by a non-peptidic agonist, *Nature* (2020) 577; 432-436

Acknowledgments

I am sure there have been many wise words written by much smarter people that chronicle the arduous task that is the completion of a PhD. It is an undertaking that is not for the impatient nor quick to anger though at times I have been both. It requires all you have and even that might not be enough. As the famous line by John Donne states, no man is an island, and I have most definitely been a continent.

Amy, you have been seen the evolution of me throughout the whole process, from unbridled enthusiasm to desperate pessimism. You lit up my darker days and got me to this point and I cannot wait for the next phase of our life. You pushed me when I did not want to push myself and helped me more than you will ever realise. I love you.

My family, Mum you have given me unlimited love and support which I hope to pay back in kind. Dad, you always understood the choices I've made, and your wisdom and love has been invaluable. My siblings; Angus, Hamish, Isobel, Beitris and Fergus your support and friendship has been invaluable.

Denise, keeping my head above water and in line was I'm sure no easy task. I have been your student for close to 6 years now and you have moulded me into the professional I am today, and I cannot thank you enough for your guidance and tutelage.

Patrick your gruff exterior hides a man who truly cares about his charges and you have always steered me back in the right direction when I have gone astray.

To all the student who have come before me and remain at MIPS I thank you for the inspiration and hope that there is a life after. Thomas, Tess, Maddy and Alice, thank you. Wess and Daisy, good luck.

And finally, to Lotti and Willow, thank you for always being available for a cuddle when I needed it. You can't read this, but I hope you can feel how much I appreciate those.

Table of Contents

TITLE PAGE ..... **I**

COPYRIGHT NOTICE ..... **II**

ABSTRACT ..... **III**

DECLARATION ..... **V**

PUBLISHED WORKS DURING STUDIES ..... **VI**

TABLE OF CONTENTS ..... **VIII**

LIST OF ACRONYMS **1**

CHAPTER 1 : GENERAL INTRODUCTION **3**

1.1 G-PROTEIN COUPLED RECEPTORS 4

1.1.1 General Introduction *4*

1.1.2 GPCR Classification *5*

1.1.3 G protein mediated signalling *5*

1.1.4 GPCR regulation of signalling *8*

1.1.5 Non-canonical signalling *9*

1.1.6 Biased agonism *9*

1.1.7 Analytical models to quantify GPCR activity and biased agonism *13*

1.1.9 Biophysical methods to study conformation and dynamics of GPCRs *17*

1.2 CLASS B GPCRS 18

1.2.2 Class B GPCR ligand binding *19*

1.2.3 Class B GPCR signalling and regulation *20*

1.2.4 Class B GPCR structural information *20*

1.2.4.1 Class B GPCR structure comparison 22

..... *24*

1.2.5 Structure function studies of class B GPCRs *25*

1.3 THE INCRETIN SYSTEM 26

1.3.1 Glucose homeostasis and the incretin system *26*

1.3.2 Glucagon-Like Peptide 1 ..... *27*

1.3.2 Targeting the GLP-1 system in disease *27*

1.4 THE GLUCAGON-LIKE PEPTIDE 1 RECEPTOR 30

1.4.1 GLP-1R Ligands *30*

1.4.2 GLP-1R signalling *32*

1.4.3 GLP-1R and biased agonism *33*

1.4.4 Structural studies on the GLP-1R *36*

1.4.5 Structure-function studies on the GLP-1R *40*

1.5 SCOPE OF THESIS 41

CHAPTER 2: METHODS **43**

2.1 REAGENTS 43

2.2 CELL CULTURE 44

2.3.1 Transient transfections *45*

2.3.2 Generation of stable cell lines *45*

2.3 CELL SIGNALLING ASSAYS 45

2.3.1 cAMP accumulation *45*

2.3.3 iCa2+ mobilisation assay. *47*

2.3.4 Bioluminescence Resonance Energy Transfer *48*
2.5 ELISA 50
2.6 GLP-1R MUTAGENESIS 50
2.6.1 Primer generation *50*
2.6.2 Quikchange site directed mutagenesis *50*
2.6.3 DNA expansion (transformation and minipreps) *51*
2.6.4 DNA sequencing *51*
2.7 DATA AND STATISTICAL ANALYSIS 51
2.8 STATISTICAL TESTS 53
2.9 GRAPHICAL SOFTWARE 54

CHAPTER 3: ASSESSING THE BIAS OF NOVEL 11MER LIGANDS AT THE GLUCAGON-LIKE PEPTIDE 1 RECEPTOR. **55**

3.1 INTRODUCTION 56
3.2 RESULTS AND DISCUSSION: 58
3.2.1 Comparison of GLP-1 full length peptide vs scaffold 11mer 1B *60*
3.2.2 1B scaffold modifications retaining linearity and H^1 at the N-terminus *61*
3.2.3 Cyclised peptides. *65*
3.2.4 1B scaffold with X^1/X^3 substitutions at position 1 ..... *72*

CHAPTER 4: ASSESSING THE ROLE OF DIFFERENT SIGNALLING EFFECTORS IN G PROTEIN AND β ARRESTIN DEFICIENT CELL LINES FOR GLP-1R LIGANDS. **82**

4.1 INTRODUCTION 83
4.2 RESULTS 85
4.2.1 GLP-1R expression profiles in different HEK293 cell lines *85*
4.2.2 GLP-1R cAMP accumulation profiles in the absence of distinct G protein families or β arrestins *86*
4.2.3 GLP-1R calcium mobilisation profiles in the absence of distinct G protein families or β arrestins *87*
4.3.4 GLP-1R β arrestin-1 recruitment profiles in the absence of distinct G protein families or β arrestins *91*
4.3 DISCUSSION 92

CHAPTER 5: THE ROLE OF INDIVIDUAL RESIDUES OF THE EXTRACELLULAR SURFACE PLAY IN AFFINITY AND CAMP EFFICACY FOR LIGANDS AT THE GLP-1R **104**

5.1 INTRODUCTION 105
5.2 RESULTS 108
5.2.1 Effects of alanine mutations on receptor expression *108*
5.2.2 Effects of alanine mutations on ligand binding affinity *112*
5.2.3 Effects of alanine mutations on ligand-induced cAMP signalling *117*
5.2.3.1 Effects of alanine mutations on pKA 119
5.2.3.2 Effects of alanine mutations on efficacy (τ) 126
5.3 DISCUSSION 129

CHAPTER 6: SUMMARY AND FUTURE DIRECTIONS **142**

CHAPTER 7: BIBLIOGRAPHY **149**

APPENDIX I: CHARACTERIZATION OF SIGNAL BIAS AT THE GLP-1 RECEPTOR INDUCED BY BACKBONE MODIFICATION OF GLP-1 ..... **162**

APPENDIX II: PHASE-PLATE CRYO-EM STRUCTURE OF A BIASED AGONISTBOUND HUMAN GLP-1 RECEPTOR-GS COMPLEX **163**

APPENDIX III: TWO DISTINCT DOMAINS OF THE GLUCAGON-LIKE PEPTIDE-1 RECEPTOR CONTROL PEPTIDE-MEDIATED BIASED AGONISM 164

APPENDIX IV: GLUCAGON-LIKE PEPTIDE-1 RECEPTOR INTERNALISATION CONTROLS SPATIOTEMPORAL SIGNALLING MEDIATED BY BIASED AGONISTS 165

APPENDIX V: ACTIVATION OF THE GLP-1 RECEPTOR BY A NON-PEPTIDIC AGONIST 166

List of Acronyms

5-HT: 5 hydroxy tryptamine

AC: Adneylate cyclase

ADRM: Adrenomedullin

Ask: Apoptosis signal-regulating kinase 1

ATP: Adenosine triphosphate

BAD: Bcl associated death promoter

cAMP: Cyclic adenomonophosphate

CHO: Chinese hamster ovary

CLR: Calcitonin receptor-like receptor

CRF1-R: Corticotrophin releasing factor 1 receptor

CRF1: Corticotrophin releasing factor 1

CRF2-R: Corticotrophin releasing factor receptor

CRF2: Corticotrophin releasing factor 2

CryoEM: cryogenic electron microscopy

CTR: Calcitonin receptor

DAG: Diacylglycerol

DEER: Double electron electron resonance

DMEM: Dulbecco's modified eagle medium

DMSO: Dimethyl sulfoxide

DNA: Deoxyribonucleic acid

DPPIV: Dipeptidyl peptidase 4

ECD: Extracellular domain

ECL: Extracellular loop

EPAC: Exchange protein activated by cAMP

FBS: Fetal Bovine Serum

FDA: Federal drug administration

GCGR: Glucagon receptor

GDP: Guanine diphosphate

GHRHR: Growth hormone releasing hormone receptor

GI: Gastrointestinal

GIP: Gastric inhibitory protein

GIPR: Gastric inhibitory protein receptor

GLP-1: Glucagon-like peptide 1

GLP-1R: Glucagon-like peptide 1 receptor

GPCR: G protein-coupled receptor

GRK: G-protein regulatory kinase

GTP: Guanosine triphosphate

HEK: Human embryonic kidney

ICL: Intracellular loop

IP_3: Inositol triphosphate

JNK: c-Jun N-terminal kinase

MD: Molecular dynamics

MEK : Mitogen-activated protein kinase

NMR: Nuclear magnetic resonance

PAC-1: First procaspase activating compound

PAC-1R: First procaspase activating compound receptor

PBS: Phosphate buffer solution

pERK: Phosphorylated extracellular signal-related kinase

PI3K: Phosphoinositide 3-kinase

PKA: Protein Kinase A

PKC: Protein kinase C

PLC: phospholipase C

PTH-R: Parathyroid hormone receptor

PTH: Parathyroid hormone

Raf: Rapidly Accelerated Fibrosarcoma

RAMP: Receptor activity modifying protein

RNA: Ribonucleic acid

SCTR: Secretin receptor

T2DM: Type 2 diabetes mellitus

TM: Transmembrane domain

VPACR: Vasoactive intestinal peptide receptor

WT: Wild type

Chapter 1:
General Introduction

1.1 G-protein coupled receptors

1.1.1 General Introduction

G protein-coupled receptors (GPCRs) are a superfamily of cell membrane spanning proteins that account for approximately 4% of the human genome comprising of about 800 genes (Fredriksson et al. 2013). They are the largest known class of membrane spanning proteins and are responsible for mediating a host of physiological effects through transmission of signal from extracellular stimuli across the cell membrane. They are ubiquitously across all tissue types. These factors have led to GPCRs being the target for around 40% of therapeutics on the market today (Lagerström & Schiöth, 2008).

All GPCRs share similar physical characteristics, an extracellular N-terminus (ECD), seven α helical transmembrane (TM) domains connected by three intracellular loops (ICLs) and three extracellular loops (ECLs) and a cytosolic tail, also referred to as helix 8. It is the specific sequence and folding of these proteins that allows for specificity for ligands and transducers leading to activation of specific pathways leading to downstream physiological responses (Venkatakrishnan et al., 2016).

In a simplistic model, GPCRs exist in a natural equilibrium between multiple receptor conformations that include both active and inactive states, providing a basal level of constitutive activity towards signalling due to the proportion of receptors in the active state (Leff, 1995). Ligand binding shifts this equilibrium, promoting conformational changes in receptor structure that result in ligand-induced changes in the ability to recruit and activate signalling partners. There are currently three very broad general classification of ligands; agonists, which shift the equilibrium toward the active state, enhancing transducer coupling; antagonists, which have little effect on the equilibrium between inactive and active receptors, and therefore do not promote (or alter constitutive) signalling; inverse agonists, which alter the equilibrium by pushing it towards the inactive state, reducing any basal activity due to reducing transducer coupling (reviewed in Kenakin, 2004). The understanding of GPCR states has evolved, now recognising multiple states of activation between the inactive and final active state of the receptor complex (Manglik et al 2015)

1.1.2 GPCR Classification

There are three major families of GPCRs, class A or rhodopsin-like receptors, which account for almost 85% of all GPCRs, class B receptors and class C (reviewed in (Cobanoglu, et al. 2011)). These families consist of further subfamilies, for example, class A contain 19 subfamilies and class B, 2 subfamilies. Receptors belonging to these subclasses have been separated based on evidence of evolutionary relationships, with each family sharing distinct signatures. For example, class A GPCRs contain an array of conserved motifs, class B GPCRs all share a large extracellular ECD of above 150 residues and class C GPCRs also contain a large ECD, but exist as obligate dimers (reviewed in (Cobanoglu et al., 2011)). A phylogenetic tree for a subset of receptors within these families and for where structural data is available is depicted in Figure 1.1).

1.1.3 G protein mediated signalling

As their name suggests, GPCRs canonically signal through the activation of heterotrimeric G proteins. GPCR mediated G protein recruitment and activation promotes downstream signalling cascades, typically through an accumulation of second messengers that promote activation of further downstream signalling pathways. G proteins contain three subunits, an alpha (α), beta (β) and gamma (γ) subunit. In the inactive state G proteins exists as a heterotrimer and are rendered inactive by bound guanosine diphosphate (GDP). Upon recruitment to an activated GPCR, due to ligand interaction or constitutive activity, the Gα protein undergoes a conformational transition, releasing GDP. This allows guanosine triphosphate (GTP) (which is present at high concentrations within the cell) to bind to the nucleotide binding site on the α subunit leading to dissociation of the α subunit from the β and γ subunits. These subunits then interact with a host of signalling proteins or with certain ion channels to promote downstream signalling. The signalling pathways activated depend on the type of G protein (Figure 1.2). The G protein is inactivated when bound GTP is converted to GDP by the GTPase activity on the Gα pathways activated depend on the type of G protein. The G protein is inactivated when bound GTP is converted to GDP by the GTPase activity on the Gα protein promoting the reassociation of the α, β and γ subunits for the next round of G protein activation. There are multiple isotypes of each G protein subunit, which allows for the formation of a plethora of diverse signalling complexes. There are 14 Gα subunits that can be

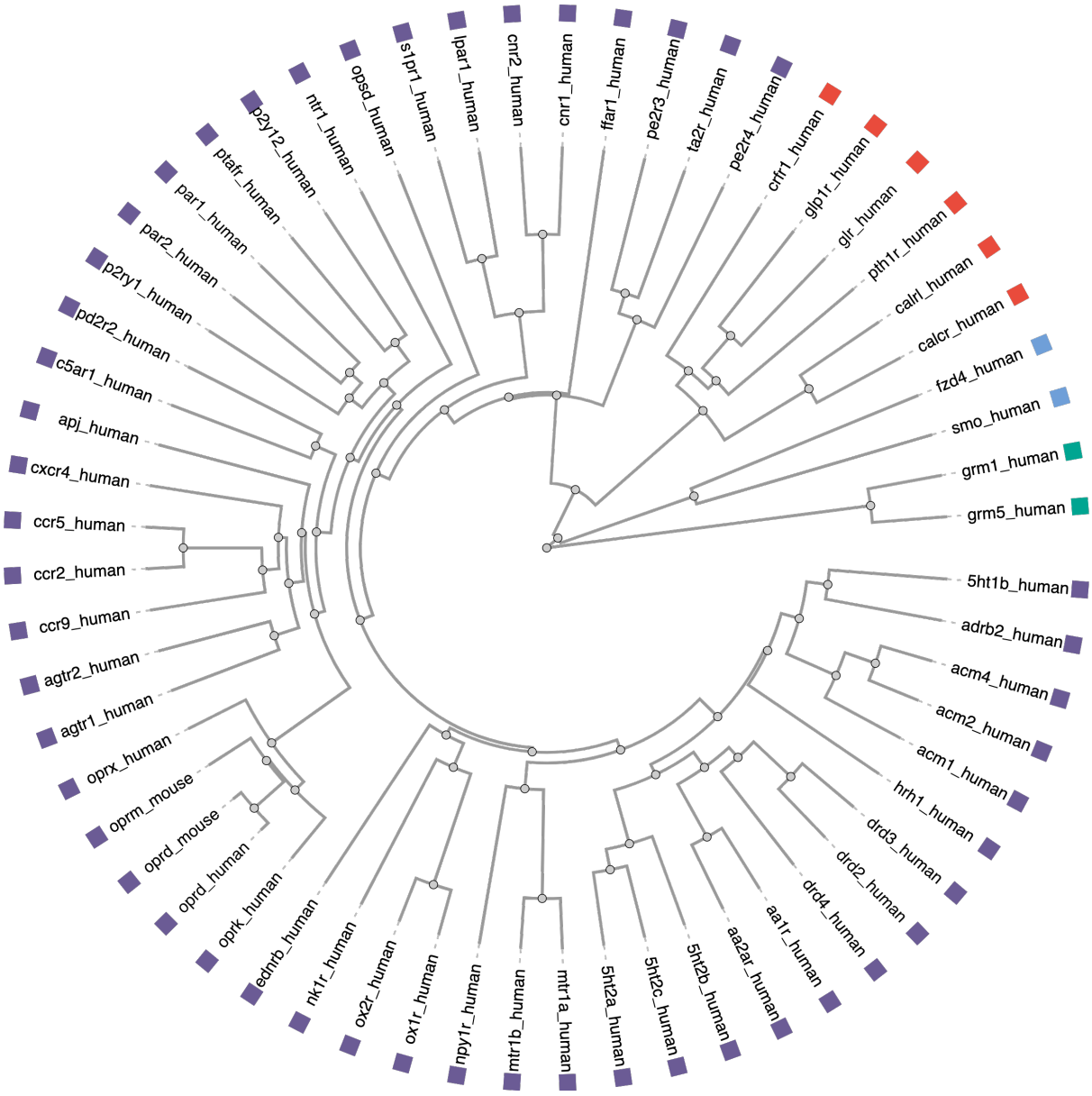

Figure 1.1) Phylogenetic tree of a subset of GPCRs with available structures which have been grouped based on structural homology. Class A (purple) Class B (red) Class C (blue) and Frizzled (green) are represented. Sourced using data and code from GPCRdb.org.

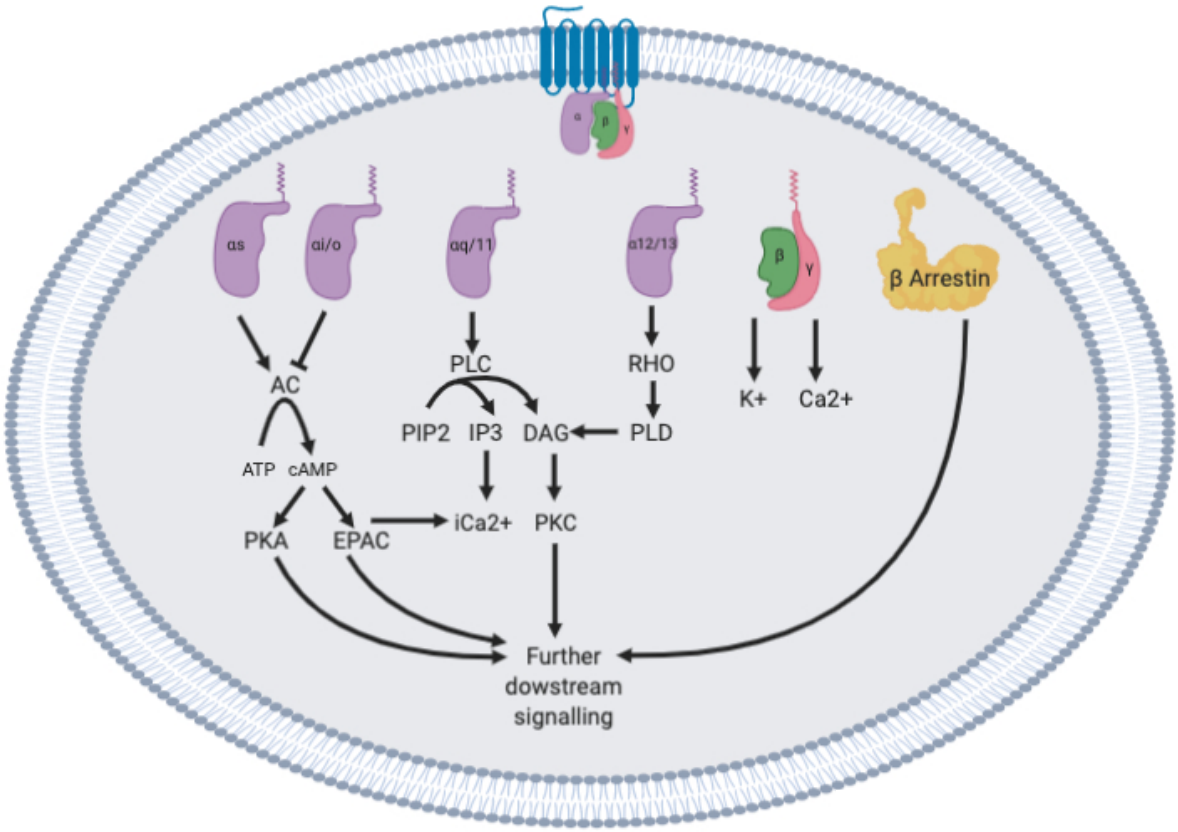

Figure 1.2: Downstream effects of G-protein activation through different signalling effectors.

broadly divided into four distinct subclasses of Gα subunits, each with distinct functions (reviewed in Hanlon & Andrew, 2015). These are classified as Gαs/olf, Gαi/o, Gαq/11 and Gα12/13. Gαs/olf interact with and activate adenylate cyclase, promoting the production of cyclic adenosine monophosphpate (cAMP) from ambient ATP. cAMP binds to and activates protein kinase A (PKA) and exchange protein activated by cAMP (EPAC), both of which affect many downstream signalling and effector molecules. Gαi/o opposes the actions of Gαs by inhibiting the adenylate cyclase, reducing cAMP production. Gαq/11 activates phospholipase C (PLC) causing the downstream production of inositol triphosphate (IP3) and diaglycerol (DAG). IP3 plays a role in mobilization of intracellular calcium from the endoplasmic reticulum, while DAG activates protein kinase C (PKC). Gα12/13 activates Rho proteins, which play a role in cellular and membrane structure (reviewed in Syrovatkina et al., 2016). Multiple classes of β and γ subunits also exist and can have effects independently of the Gα subunit, such as PLC activation, ERK1/2 phosphorylation, PI3 kinase mediated pathways and regulation of potassium and calcium channels. Although it is widely accepted that receptor activation promotes dissociation of the α subunit from the βγ subunits to promote signalling, there is also some evidence to suggest that these subunits do not always dissociate and can function as a heterotrimer (reviewed in Khan et al., 2013).

1.1.4 Regulation of GPCR signalling

The longevity of GPCR signals are managed in multiple ways. The activation of a GPCR by an agonist can result in desensitisation of the receptor, which can happen at three distinct levels; at the receptor itself, the G protein or the effector protein. Desensitisation is triggered by prolonged receptor exposure to an agonist leading to recruitment of G protein receptor kinases (GRK) that phosphorylate the receptor at the C-terminus or intracellular loops. This phosphorylation raises the affinity of the receptor for β arrestin binding. β arrestins are recruited to the receptor blocking the binding site for G protein, thereby terminating G protein mediated signaling. β arrestins also link the receptor to internalization machinery such as clathirin, that result in internalization of the receptor away from the plasma membrane into early endosomes (reviewed in Syme, Zhang, & Bisello, 2006). From there the receptor can either be trafficked into late endosomes and degraded in lysosomes or into recycling endosomes where the receptor will be recycled back to the cell surface where it can be activated again (Figure 1.3) (reviewed in Von Zastrow & Hanyaloglu, 2008).

1.1.5 Non-canonical signalling

While the canonical role of β arrestins and GRKs is in regulatory processes of GPCRs, over the last decade, a growing body of evidence has emerged highlighting that β arrestins can also promote intracellular signalling directly through scaffolding various signalling proteins. While β arrestin-dependent signalling is now widely accepted (reviewed in Ma & Pei 2007), there is still controversy in the field as to whether this can occur independently of G protein activation, albeit there is evidence that this may be the case for some receptors (Grundmann et al., 2018). There is also evidence that different ligand-receptor interactions can result in different receptor conformations that induce distinct phosphorylation patterns on the intracellular face of the receptor by GRKs and protein kinases, which is speculated to act as a 'bar code' for arrestin-specific conformational changes. This then dictates the interaction of these proteins with downstream signalling partners, such as ERK1/2 and JNK3 (that are well characterised in their interaction with arrestins), Raf, MEK1, Ask1, MKK and that have also been implicated in interacting with β arrestin scaffolds (reviewed in Tobin, Butcher, & Kong, 2008). Recent evidence shows that specific phosphorylation patterns cause by GRKs are important for specific downstream effects of β arrestins after binding to a GPCR to influence conformation and downstream signalling of the arrestin (Mayer et al. 2019)

1.1.6 Biased agonism

GPCRs can be classified based on the preferential G protein and signalling pathway that they couple to in order to mediate physiological actions. However, many GPCRs are pleiotropically coupled, meaning they can couple to more than one transducer and activate multiple intracellular signalling cascades (reviewed in Wang, Qiao & Li, 2018). This pleiotropic coupling to multiple G protein and non-G protein-dependent signalling pathways allows for activation of a plethora of downstream effects and these are dependent on the bound ligand. Importantly, these differential signalling pathways can lead to different physiological responses from the cell. Therefore, the relative efficacy for which these receptors signal to each of these signalling pathways determines the overall combined physiological response that the receptor displays. However, not all ligands acting at the same GPCR are able to stimulate the full signalling repertoire associated with that GPCR. Different ligands activating the receptor can

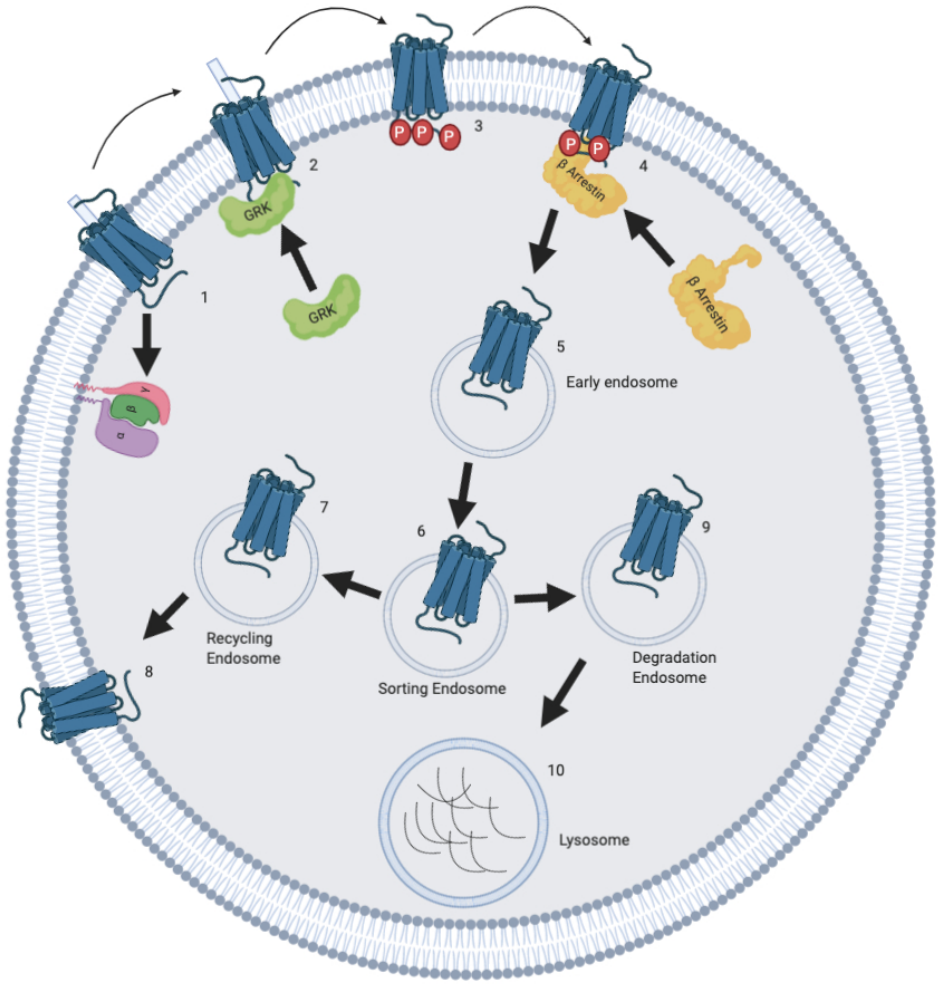

Figure 1.3: Regulation of GPCRs: Activated GPCRs, promote G protein dissociation (1). They also recruit GRKs (2) that phosphorylate the receptor (3), promoting the recruitment of β arrestins (4). Arrestin-bound GPCRs are internalised into early endosomes (5) and then shunted into sorting endosomes (6) where they are either recycled back to the cell membrane (7-8) or targeted to lysosomes for degradation (9-10).

therefore promote distinct signalling of the receptor in a phenomenon known as ligand-mediated signal bias or biased agonism (Figure 1.4) (reviewed in Kenakin & Christopoulos, 2013).

Biased agonism arises due to the ability of distinct ligands promoting different conformational changes within the receptor, which alters the way it couples to certain signalling effectors (reviewed in Wootten et al 2018). There are multiple examples of such ligands such as TRV027 at the Angiotensin II receptor that activates β arrestin 2 mediated signalling events, without coupling to G proteins (Violin et al., 2010). Despite this, this ligand exerts the same physiological effects as the native ligands in decreasing blood pressure and increasing cardiac contractility. It has therefore been suggested that for this receptor activation arrestin-mediated signalling pathways leads to the desired therapeutic effect (Violin et al., 2010).

As biased agonists are able to alter the relative strength to which each signalling pathway is activated, this opens up the possibility that ligands may be identified for a particular receptor that preferentially couple the receptor to certain signalling pathways at the exclusion of others, altering the physiological response of the cell to provide a better therapeutic output. This may be due to activation of signalling that leads to therapeutically beneficial effects of the receptor response, while avoiding effects down pathways that lead to the side effects seen with some drugs. Some clinically used β blockers, such as carvedilol, which are used as a first line treatment for hypertension, were previously characterised as antagonists at β adrenoreceptors (reviewed in Thanawala et al 2014). Later studies revealed that the most effective β blockers (for example, carvedilol and nebivolol) were in fact biased ligands that do not activate canonical G protein signalling pathways but are agonists of β arrestin mediated signalling (Erickson et al., 2013)(Wisler et al., 2007). Evidence is also available for beneficial effects of biased ligands at the μ-opioid receptor, a popular target for pain medication, where a ligand that recruits and activates G-protein mediated pathways as opposed to arrestin scaffolding promotes greater analgesia, with β arrestins promoting side effects (DeWire et al., 2013). However, more recent data has shed light on this theory for opioid receptors (Yudin & Rohacs, 2019), and instead suggest that perhaps efficacy rather than bias may be important for therapeutic efficacy devoid of side effects. This highlights the need to better understand biased agonism. The concept of biased agonism has potential to fine-tune receptor signalling. However, the challenge in drug discovery is that currently for most receptors and disease states the relationship between individual signalling pathways and physiological efficacy is not

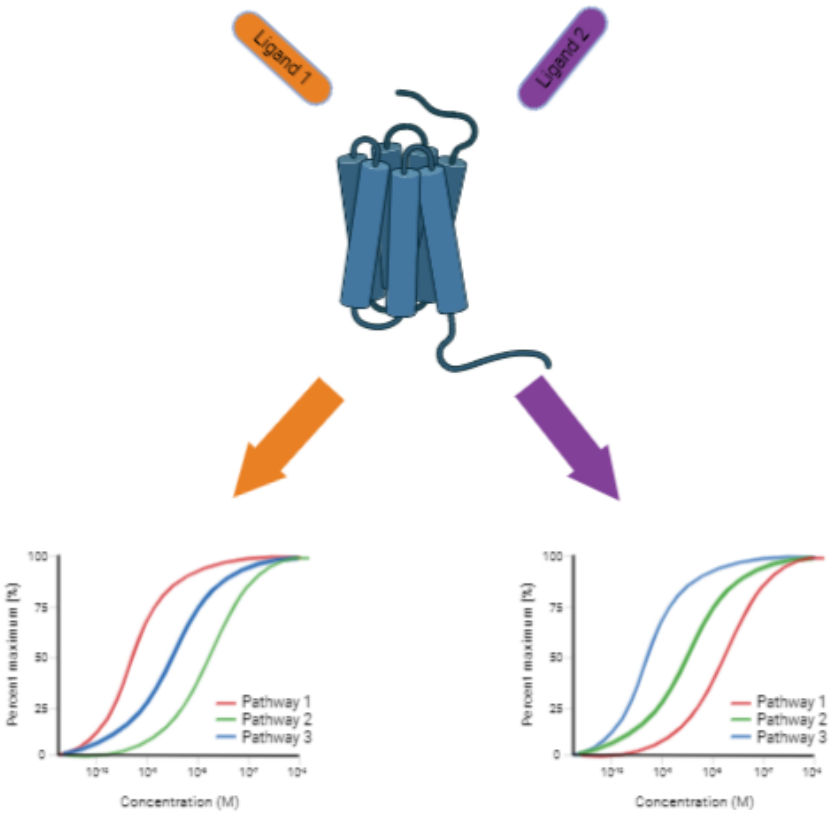

Figure 1.4: Basic illustration of biased agonism where two ligands acting at the same receptor can have distinct signalling outcomes. This is often visualised by comparing concentration response curves for different signalling pathways. In the example here, ligand 1 is more potent at activating pathway 1 and 3 over pathway 2, whereas ligand 2 is more potent towards activation of pathway 3 over pathways. 1 and 2.

understood. Therefore, more basic research is required in order to understand which cellular efficacies may lead to therapeutic success. In addition, to rationally design drugs that display biased agonism requires understanding of GPCR structure and how this relates to biased agonism.

1.1.7 Analytical models to quantify GPCR activity and biased agonism

The easiest way to view biased signalling in pharmacology is to perform concentration response curves to assess activation of multiple signalling pathways by different ligands to identify reversals in the relative potency, or maximal signal between ligands in different pathways (Figure 1.4). Currently physiological outcomes of signal bias are not fully understood for the majority, if not all GPCRs, however to exploit biased signalling for drug discovery, it is important to be able to quantify this behaviour. There are a number of methods that have been used to determine ligand bias, however the most common model for this is the Black/Leff operational model (Black, Leff, Shankley, & Wood, 1985), which allows the determination of two factors. K_A describes the affinity of the ligand when coupled to a particular signalling pathway and the term tau τ is used to describe the intrinsic efficacy and the sensitivity of the response from the system. When combining these two factors a single number can be derived, Log (τ/K_A) the transduction ratio, which describes the intrinsic efficacy of a ligand for an individual pathway. These two factors, efficacy (τ) and functional affinity (K_A) can be isolated using the Black-Leff operational model fitted to concentration response data to derive a single number (the transduction ratio) that allows the determination of exactly how well a ligand is activating a given pathway (Kenakin, et al. 2012). Different ligands interacting with different signalling pathways can give individual transduction ratios for each pathway, which when normalised against a reference ligand and reference signalling pathway, provide a scale to statistically evaluate differences in signalling bias between ligands in a way that can inform structure activity relationships in drug discovery programs (Kenakin et al., 2012). Other methods have been used including (i) bias plots that qualitatively identify biased ligands by plotting concentration response data for pathway one on the axis and pathway 2 on the y axis and comparing differences in the curves from a referene ligand (Gregory et al., 2010) and (ii) equiactive comparison method, which uses the EC50 and Emax of one ligand across two pathways compared to a reference ligands response to the same two pathways (Rajagopal et al. 2011).

1.1.8 GPCR structural biology

Prior to 2017, the majority of projects aimed at understanding and resolving the structure of GPCRs were predominantly focused on class A GPCRs. For many years the only information on the 7TM structure of GPCRs was from projection structure of Rhodopsin (Schertler, Villa & Henderson 1993). The first crystal structure of a mammalian GPCR was of the bovine rhodopsin in the year 2000 (Palczewski et al., 2000). The first x-ray structure of a non-visual receptor was solved in 2007 and since this time there has been an fast increase in the number of receptor structures solved by x-ray crystallography, with structures for more than 60 unique receptors now available (Figure 1.5). The majority of these are solved in an inactive conformation with structures of single receptors in complex with different ligands with various actions (agonists, antagonists etc.). To enable crystallisation, receptors have required multiple receptor modifications, including mutations and fusion proteins to enhance the thermostability (hence reducing conformational variance and flexibility) (Vaidehi, Grisshammer, & Tate, 2016) or to provide greater surfaces for crystal packing (Griffin & Lawson, 2011). These limit interpretation of these structures as the receptors are often highly modified.

More recently, x-ray crystallography has been used to solve structures of class A receptors in active conformations, however, to date only one of these is coupled to a full heterotrimeric G protein (Rasmussen et al., 2011). Methods that have been used to stabilise active state conformations of receptors include either nanobodies that mimic G protein interaction (Griffin and Kawson, 2011) or complexing with a modified G protein a subunit coined mini-G (Nehmea et al., 2017). The structure of the full heterotrimeric receptor also required the use of nanobody 35 to stabilise the complex for crystallisation (Steyaert & Kobilka, 2011). In recent years, advances in cryogenic electron microscopy has made it possible to solve full-length active structures of GPCR coupled to ligand and heterotrimeric G-proteins. This includes receptors from class A (e.g. García-Nafría, et al. 2018), B (e.g Liang et al., 2017) and C families (e.g Doré et al., 2014), coupled to Gαs (e.g Liang et al., 2017) and Gαi (e.g Draper-Joyce et al., 2018) proteins and more recently Class A coupled to β arrestins (e.g Kang et al., 2015). Dominant negative Gα proteins have been engineered to facilitate this. These proteins are have lower affinity for nucleotide and have been used to trap the receptor: G protein complex in a nucleotide bound state, trapping the active receptor conformation (Liang et al., 2018a). Nanobodies (Nb35) and short chain antibodies (ScFv16) have also been used to stabilise the nucleotide bound state (Maeda et al., 2018). Engineered mini G-proteins have also been used

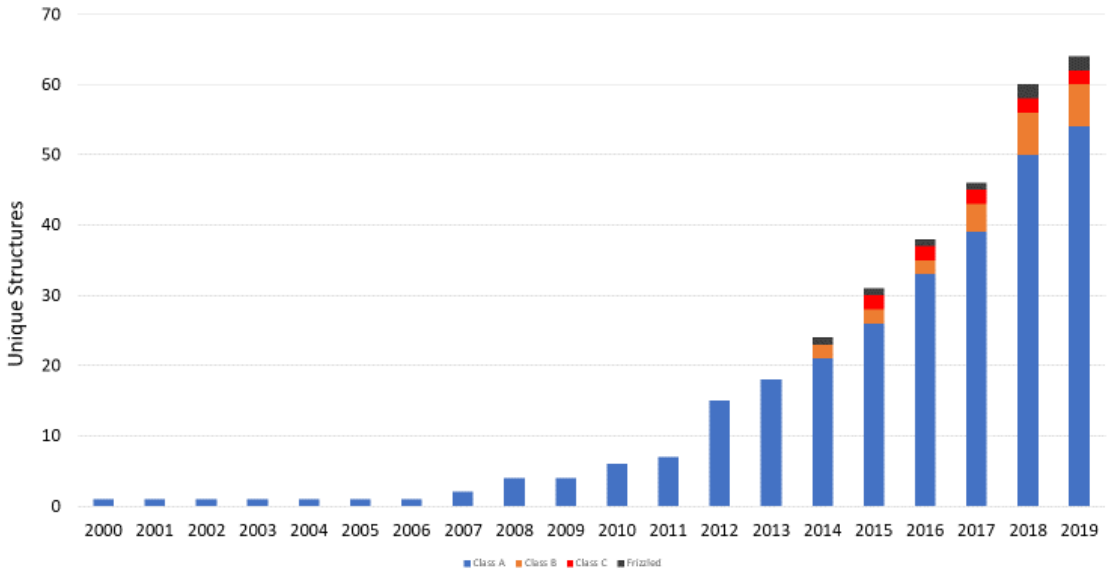

Figure 1.5: The growth of available unique structures of GPCRs. Adapted from the GPCRdb

to solve GPCR structures including mini Gαo complexed with rhodopsin and $5HT_{1B}$ receptor (García-Nafría, et al. 2018).

Comparing crystal structures of receptors in the active versus inactive state or with different ligands bound has revealed some details into how ligands can stabilise different conformations of the same receptor. Multiple structures are available of the $\beta_2$adrenoreceptor (Rasmussen et al., 2011), acetylcholine muscarinic receptors (Thal et al., 2016) as well as members of the opioid receptor (Shang & Filizola, 2015). In inactive and active states. These studies all show similar large scale conserved movements upon activation, including a large outward movement of TM6 and an inward shift of TM7 at the intracellular face. From the crystal structure data of the β2 adrenoreceptor in complex with Gαs there is also a large structural rearrangement of TM5 which forms key interactions with the G-protein. Comparison of active and inactive crystal structures for these three class A GPCRs also showed the importance of core residues in TM3, which have interhelix interactions that need to be either broken or formed to transition between the inactive and active state of the receptor (Rasmussen et al., 2011). The more recent arrestin-bound class A GPCRs revealed a similar shift within the TM bundle when comparing the inactive state to that observed with G protein, albeit TM6 appears to have a much more pronounced movement when G protein is bound relative to arrestin (Kang et al., 2015).

In recent years, advances in cryo-electron microscopy have had a major impact on GPCR structural biology, particularly in the ability to solve active state GPCRs complexes bound with transducers. This has enabled the determination of the active state of full length class B and C (Mao et al 2020) GPCRs as well as Class A GPCRs. For class A and B receptors, there are now numerous GPCR structures solved in complex with Gs (Liang et al 2017)(Liang et al 2018a)(Liang et al 2017b)(Zhao et al 2020) and Gi proteins (Draper-Joyce et al 2018)(Garcia-Nafria et al 2018). More recently, class A GPCRs structures have been determined in complex with G11 proteins(Maeda et al 2019) and β-arrestins (Yin et al 2019)(Staus et al 2020).

Active state structures of class B receptors, revealed similar large outward movement of TM6 seen in class A receptors, which accommodates the coupling of the G protein α5 helix. Comparison of class A structures reveal differences in the extent of movement of helix 6 (TM6). Similar G proteins Gαi and Gαo have an inhibitory effect on adenylate cyclase however produce a smaller conformational change in TM6 compared to Gαs structures. TM6 in class B

GPCRs all have a distinctive kink within the centre of the helix not seen in class A GPCRs, which may be due to the added size of ligands that bind class B GPCRs resulting in a more open binding pocket within the extracellular face. This requires TM6 to move out at both the extracellular and intracellular face upon ligand and G protein binding, hence inducing the extreme kink within the helix. Interestingly, while in class A GPCRs TM6 appears to open to a different extent depending on whether bound to Gαs or Gαi, recent data revealed a similar movement within the intracellular face of class B GPCRs when coupled to either Gαs or Gi (Van Eps, et al .2018).

These structural studies in combination with multiple biophysical studies have also revealed that different ligands can induce and stabilise different conformations of a receptor. Studies on both class A and class B GPCRs have also revealed differential rearrangement of distinct networks of amino acids within these receptors occurs in the presence of distinct biased ligands, giving some insights into how different ligands may induce biased agonism (Manglik et al., 2015)(Wingler et al., 2019).

1.1.9 Biophysical methods to study conformation and dynamics of GPCRs

Structural information is important for understanding how ligands and transducers interact with their receptors and alter receptor structure, however these are static structures that capture a snapshot of a metastable conformation. GPCRs are highly dynamic proteins. It is believed to be this dynamic behaviour that biased ligands are able to exploit to be able to create different patterns of activation and conformation that lead to the ability of receptors to couple to multiple transducers, to promoted differential activation (ie full vs partial agonism), and for ligands to promote differing signalling profiles (biased agonism). Studies assessing receptor dynamics and conformation associated with different classes of ligands has been explored most extensively for class A GPCRs. Around the turn of the century, the Kobilka group was using fluorescent spectroscopy with thiol reactive, environmentally sensitive probes to demonstrate how ligand activation results in movements of TM6 as well as movements in TM3 (Gether et al., 1997). Further studies using this technique determined ligand-specific conformations for the β2 adrenoreceptor (Seifert et al. 2001).

Studies in multiple class A GPCRs have shown through NMR methods that an active state of a receptor can only be stabilised in the presence of both a G protein or G protein mimicking nanobody and a ligand. In complex with the ligand alone, the receptor adopts an intermediate state (reviewed in Sounier et al., 2015). Other techniques such as DEER spectroscopy (Manglik

et al, 2015) and single molecule FRET (Gregorio et al. 2018) have also been able to distinguish multiple GPCR states. For example during activation b2 adrenoreceptors can adopt three, potentially four different states of activation between the active and inactive state (Liu, et al. 2013). These same approaches have been applied to many class A receptors including members of the 5-HT family (Shan, Khelashvili, Mondal, et al, 2012), α_{2A} adrenoreceptor (Zurn et al., 2009) and the μ opioid receptor (Sounier et al., 2015) to name a few. A recent study using DEER spectroscopy by Wingler et al. in 2019 used probes in multiple positions of the AngII receptor to explore the conformational signature adopted within the receptor in the presence of a suite of biased ligands. They revealed four major conformational states induced in this receptor including a 'closed' inactive state, an 'open' active state and two intermediate states in which TM6 is not fully open to allow full opening of the G-protein binding cavity within the receptor, which they termed 'occluded' 1 and 2. Antagonists mostly occupied the closed state, G-protein biased agonists mostly occupied the open state, while arrestin biased ligands occupied mostly one of the occluded states. This is consistent with the recent arrestin-bound structures that exhibit a TM6 conformation that was not closed but not as open as the G protein-bound state (Kang et al 2015). Single molecule FRET technology has also shown that the extent to which TM6 shifts correlates with efficacy (Gregorio et al 2017).

Evidence is also emerging for TM7 as a key area for arrestin interaction and potentially a key mediator in biased signalling. Recent structures of GPCRs in complex with arrestin's confirmed key interactions between the finger loop of the arrestin and TM7 of the receptor. Earlier NMR data assessing arrestin biased ligands at the β2 Adrenoreceptor revealed the importance of movements in this helix for arrestin recruitment for ligands biased in favour of arrestin recruitment (Kang et al., 2015). H8 and the C-terminus of GPCRs have also been demonstrated to be key in arrestin binding (Kirchberg et al., 2011) and NMR data from the μ-opioid receptor has also been used to demonstrated movements in H8 are part of a fully active receptor complex and are also required for arrestin coupling (reviewed in Sounier et al., 2015).

1.2 Class B GPCRs

Class B GPCRs, also known as secretin/adhesion like receptors, are the second largest class of GPCRs and contain two subclasses of receptors. Of the mammalian family, 33 receptors are adhesion-like and 15 are secretin-like. Class B GPCRs are recognisable by their large glycosylated ECD, which plays a major role in the recognition and binding of peptide ligands.

These receptors are activated endogenously by large peptide hormones (Bjarnadóttir, Fredriksson, & Schiöth, 2007).

1.2.1 Secretin-like receptors

Class B secretin-like receptors include; calcitonin and calcitonin receptor-like receptors (CALCR, CALCRL); corticotrophin-releasing factor receptors (CRFR1, CRFR2); the glucagon receptor (GCGR); the gastric inhibitory polypeptide receptor (GIPR); the glucagon-like peptide receptors (GLP-1R, GLP-2R); the growth-hormone-releasing hormone receptor (GHRHR); the adenylate cyclase activating polypeptide receptor (PAC1/ADCYAP1R1); the parathyroid hormone receptors (PTHR1, PTHR2); the secretin receptor (SCTR) and the vasoactive intestinal peptide receptors (VPAC1R/VPAC2R) (reviewed in Poyner & Hay, 2012). Class B receptors bind peptide hormones and mediate a large range of physiological effects, such as bone maintenance, and glucose homeostasis, body weight, appetite, neurological effects (reviewed in Poyner & Hay, 2012). These receptors are characterised by a long N-terminus that forms a structured ECD containing six conserved cysteine residues, that form three disulphide bonds. These are essential for correct folding that allow binding of their large peptide ligands (Bazarsuren, et al. 2002). Due to their wide range of important physiological effects, this subclass of class B receptors are promising targets for development of novel therapeutics for many diseases, including neurodegenerative disorders and inflammation (VPAC1R, PAC1R), type II diabetes mellitus (GLP-1R, GCCR) and bone disease (PTHR, CTRs). For the purpose of this thesis, class B GPCRs will refer to secretin-like receptors.

1.2.2 Class B GPCR ligand binding

In solution, native class B GPCR peptide ligands do not contain secondary structure, however they adopt secondary structure upon binding to their receptor. These peptides adopt helical structures as observed in crystal and cryo-EM structures of peptides bound to either isolated ECDs or full-length structures of their respective class B GPCR (Liang et al., 2017)(Liang et al., 2018b). A key feature of class B GPCR function is their two-domain mode of binding peptide ligands. (Figure 1.6)(reviewed in Hoare, 2005). Initially, the C-terminus of the ligand forms a high affinity interaction with the ECD of the receptor creating an affinity trap to tether the ligand in place, which then allows the N-terminus of the ligand to interact with the upper portion of the receptor TM domain. The interaction between the peptide ligand and TM domain is of vital importance for activation of the receptor by full-length peptides ligands (Pal,

Melcher, & Xu, 2012). A deep cavity located at the extracellular surface of the TM bundle is the pocket that engages of the N-terminus of the ligand. This pocket was first visualised in crystal structures of the inactive TM bundle of these receptors, and has been confirmed in recent full length active CryoEM structures (Liang et al., 2017)(Liang et al., 2018). Molecular modelling and structural studies of activated Class B GPCRs, along with photoaffintiy and mutagenesis studies (Yang et al., 2016), have determined that the N-terminus of peptide ligands bind within this cavity, with the highly conserved histidine residue at position one of class B GPCRs lignads binding deep within this pocket (Lee, Booe, & Pioszak, 2015). However, to date, the importance of the residues within this pocket have not been fully explored. There have been a limited number of small molecule ligands identified for class B GPCRS. Those that are available are limited to a few receptors, including agonists for the GLP-1R (Chen et al., 2007)(Freeman et al., 2016)(Thompson, et al. 2016) and antagonists for the GCGR (Sammons & Lee, 2015), CGRP (Doods et al., 2000), ADMR (Ochoa-Callejero et al., 2017) and GLP-1R (Nance et al., 2017). For a number of receptors there have also been allosteric ligands identified (GLP-1R, GCGR and CTR)(Hoare 2007).

1.2.3 Class B GPCR signalling and regulation of activity

Class B GPCRs predominantly signal through Gαs to promote cAMP signalling. However, these receptors are also promiscuous and are capable of coupling to other classes of Gα proteins including; Gαq/11, Gαi/o/z and Gα12/13 as well as coupling to non-visual arrestins, β arrestins 1 and 2 (reviewed in Karageorgos et al., 2018). Because of this ability to couple to multiple signalling effectors this class of receptor is highly susceptible to biased agonism. The majority of class B GPCRs are capable of recruiting arrestins. Most class B GPCRs have also been reported to undergo internalisation and many have also been shown to exhibit endosomal signalling (Ismail et al., 2016).

1.2.4 Class B GPCR structural information

Until recently structural information for class B GPCRs has been limited. Crystal structures have been solved for the extracellular domain of many class B GPCRs, many in complex with peptide ligands (e.g. Underwood et al., 2010)(e.g. ter Haar et al., 2010). These structures revealed how peptides interact with their respective receptor ECDs, with the C-terminus of the

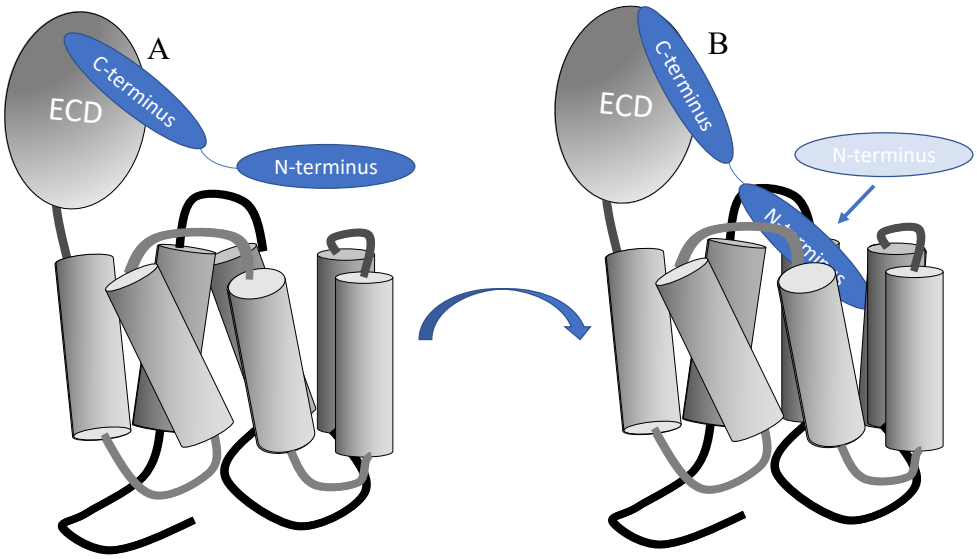

Figure 1.6: The two domain binding mode of class B GPCRs where the C-terminus binds first to the ECD (**A**) allowing engagement of the peptide N-terminus with the top of the TM bundle (**B**). (adapted from Hoare 2007)

peptides engaged in a conserved cavity and the N-terminus sitting below the isolated ECD not forming any interactions. In 2013 crystal structures of the isolated TM domains of the glucagon receptor (GCGR) (Siu et al., 2013) and the corticotrophin releasing factor 1 receptor (CRF1R) (Hollenstein et al., 2013) in their inactive states were solved. There are now x-ray structures of full-length class B GPCRs bound to antagonist antibodies (GCGR) (Jazayeri et al., 2016) and peptide agonists (PTH1R, GCGR and GLP-1R), albeit these receptors are stabilised in predominantly inactive conformations (Jazayeri et al., 2017)(Ehrenmann, et al., 2019)(Siu et al 2013)

The use of single particle cryogenic electron microscopy (Cryo-EM) has recently allowed full length fully active (with ligand and heterotrimeric Gs-protein) structures to be solved for class B GPCRs. The first of these structures was published in 2017, that of the calcitonin receptor (CTR) coupled to salmon calcitonin and Gαsβ1γ2 (Liang et al., 2017). This receptor was essentially wildtype, with the exception of cleavable affinity tags required for purification. Stabilisation of the complex was achieved by using nanobody 35 to stabilises the nucleotide free form of the G protein bound to the receptor. In addition to the CTR structure, there are now published structures of the GLP-1R bound to two different peptides (Y. Zhang et al., 2017)(Liang et al., 2018a) and one to a small molecule agonist (Zhao et al., 2020), the calcitonin receptor-like receptor (CLR) with an accessory protein, receptor activity modifying protein (RAMP) (Liang, et al., 2018c), the CRF1 and CRF2 receptors, GCGR and the PAC1 receptor (Wang et al., 2020). These are all in complex with heterotrimeric Gαs and combined with the inactive structures reveal a common activated pose for this class of receptors.

1.2.4.1 Class B GPCR structure comparison

The recent expansion of class B GPCR structures has also allowed investigation of similarities in active state class A and class B GPCRs. Due to the key difference in ligand properties and the large extracellular domain found in class B GPCRs, but not in the Class A GPCRs where structures have been solved, there are many conformational differences in the extracellular surfaces of the receptors that are linked to the types of ligand that they interact with. However, at the intracellular surface, there are structural similarities between the two classes with TMs 1-3 and 5-7 all adopting similar positions when coupled to G protein. TM5 extends further into the cytoplasm in the class A structures relative to class B GPCRs. In contrast, the class B

structures have an extended helix 8 which forms interactions with the β subunit of the heterotrimeric G protein that was not evident in the class A structures. There is a difference in the relative positioning of TM4, which is the dimerization site for class B GPCRs and mutations to residues in this domain impact the g-protein mediated signalling. Similarly, activation of both classes of receptors is associated with an outward shift at the intracellular face of TM6. In class A GPCRs this is associated with a pivot around a conserved proline motif where the top of TM6 moves in and the bottom moves out. In contrast, in class B GPCRs, TM6 moves outwards at both the extracellular face (required to accommodate peptide agonists) and the intracellular face. This is facilitated by a partial unwinding the highly conserved PXXG motif, which leads to a very sharp kink in the middle of TM6 (Figure 1.7).

There are conserved motifs in the peptide binding site within the TM of class B GPCRs, but large differences in the conformation of the ECD. This suggests an evolutionary link between the activation by peptide ligands for class B GPCRs (via their interaction with their respective TM bundles), but their specificity may be determined by interactions of the C-terminus of the ligand with the receptor ECD (reviewed in Pal, Melcher and Xiu, 2013). Comparisons between different class B GPCR structures revealed there are a number of important structural differences in these receptors. This includes differences in the location of the ECD, TM1, ECL1, TM6-ECL3, TM7 and in the arrangement of ICL-2. There is one structure of the GLP-1R bound to an 11mer peptide (Jazayeri et al., 2017). This receptor displays a much less pronounced kink in TM6 compared to inactive structures that could potentially due to accommodating a smaller ligand, however this was a modified receptor with mutations in TM6 that likely contributed to these differences.

The G protein binding site and residues important for receptor activation appear to be conserved between class B GPCRs (but not class A) suggesting a universal mechanism of action for receptor activation and coupling of G-protein by this receptor class. However, despite class B GPCRs binding preferentially to Gαs there is not an absolute conservation of the space in which the G-protein couples or the residues that interact with the G-protein when comparing available structures.

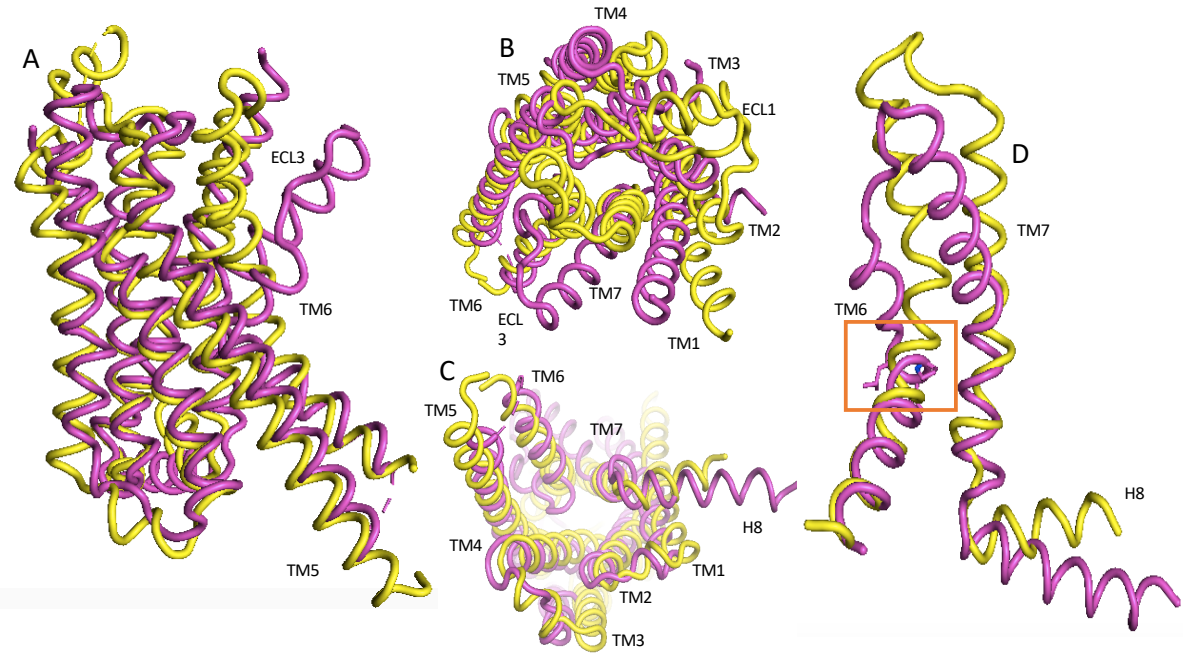

Figure 1.7: An overlay of the active β2 adrenoreceptor (yellow) and active calcitonin receptor (purple) (**A**) highlighting differences in the kink in TM6, and arrangement of TM5 and ECL3. An extracellular view (**B**) highlights extensive conformational differences within the extracellular face of these receptors, due to the nature of the different ligands that they bind (ie small molecules vs large peptides). Intracellular view (**C**) reveals a similar overall intracellular arrangement of the TM helices, however there is an extended helix 8 in the calcitonin receptor relative to the β2 adrenoreceptor, as well as differences in the conformations of the intracellular loops between the two structures. The kink in TM6 (**D**) is more pronounced in the class B structure due to the unwinding of the PXXG motif (in the red box).

1.2.5 Structure function studies of class B GPCRs

Understanding how ligands dock into their receptor has been the focus of many groups to elucidate the structural mechanisms underlying receptor activation in class B GPCRs. Techniques such as photoaffinity labelling, mutagenesis and receptor chimeras have been used to probe ligand interaction with their receptors for a large range of class B GPCRs such as the secretin receptor (Dong et al. 2012)(Te et al. 2012)(Dong et al. 2020) vasoactive intestinal peptide 1 (VPAC1) receptor (Chugunov et al. 2010), the calcitonin receptor (Dal Maso et al 2018)(Dal Maso et al 2019), calcitonin gene related peptide receptor (Booe et al 2015)(Qi et al. 2018)(Conner et al. 2015)(Vohra et al. 2013)(Qi et al. 2010)(Wolley et al. 2013), adrenomedullin receptors (Qi et al 2008)(Watkins et al 2013), as well as the GCGR (Yang et al 2016) and GLP-1R (Dong et al. 2014). Collectively, combined with molecular modelling and docking studies, these data revealed class B peptide agonists bind to a similar pocket within their respective receptors. This binding site was identified to extend deep into the receptor core to accommodate the N-terminal activation domain of the respective ligands, where they form interactions with common receptor residues (albeit the specific nature of some of these side chains differ with different receptors) within TM1, TM2, TM3, TM5 and TM7, as well as ECL2 and ECL3. Emerging structures of many of these receptors in recent years have confirmed many of these predicted interactions (Liang et al 2017)(Liang et al 2018a)(Liang et al 2018b)(Zhang et al. 2017)(Zhang et al 2018)(Liang et al 2020)(Ma et al 2020)(Zhao et al 2020)(Dong et al 2020).

Cysteine cross linking studies have also been employed for probing secretin interactions with its receptor, specifically the extracellular loops (ECLs) (Dong et al., 2014). These studies identified strong interactions between residues in the N-terminus of the ligand and ECLs 2 and 3 and additional weaker interactions that potentially arise due to transient interactions that could be responsible for intermediate conformations between ligand and receptor, similar to those observed in Class A GPCRs (Dong et al., 2016). Work on the CRF1R receptor using photo crosslinking showed agonist activity could also be linked to bends in helices six and seven (Siedel et al 2017), which recently confirmed in cryo-EM structures of these receptors.

The GLP-1R has been by far the best studied of the class B family when it comes to probing receptor-ligand interactions and receptor activation by mutagenesis (reviewed in de Graaf et

al., 2016). This receptor is the focus of this thesis and the literature around this is discussed more extensively in later sections.

Unlike Class A GPCRs, comparatively little work has been performed in class B GPCRs to understand conformational dynamics/changes upon ligand activation. There have been limited molecular dynamics studies performed on the GCGR and GLP-1R that show an interaction between the receptor extracellular domain and the top of the TM that maintain the receptor in an inactive state (J. Zhang et al., 2016) and more recently these methods have been used to compare peptide and non-peptide receptor activation of the GLP-1R (discussed in further detail below).

1.3 The Incretin System

1.3.1 Glucose homeostasis and the incretin system

Glucose homeostasis in humans is tightly regulated and involves peptide incretin hormones that are produced in the L cells of the ileum and colon, and act on receptors in the pancreas. Upon meal ingestion blood glucose is increased promoting glucose-dependent release of insulin from the pancreas, which acts at various tissues around the body (reviewed in Holst, Vilsbøll, & Deacon, 2009). Insulin promotes an increase in glucose uptake in adipose tissue and muscle, while decreasing glucose production in the liver. These effects combined lead to a decrease in plasma glucose. The amount of insulin released upon an oral glucose load is considerably larger than an intravenous glucose load (Lindgren et al., 2011). This implies that glucose sensing within the gastrointestinal tract results in potentiated insulin secretion (Lindgren et al., 2011). This effect was shown to occur due to gut-derived hormones, known as incretins that are secreted in response to a meal and make a significant contribution to postprandial insulin release. This is termed the incretin effect, which is caused by two hormones, Gastric Inhibitory Peptide (GIP) and Glucagon-Like Peptide 1 (GLP-1) (reviewed in Holst et al., 2009).

1.3.2 Glucagon-Like Peptide 1

The glucagon-like peptide 1 (GLP-1) is an incretin hormone released from the gastrointestinal tract upon ingestion of nutrients and travels along the entero-insular axis where it acts on the β cells of the pancreas to causes an increase in insulin biosynthesis and secretion, while also stimulating β cell proliferation and promoting β cell survival (Edwards et al, 1999). It also decreases glucagon secretion, which results in the reduction of glucose production in the liver. All of these effects help to decrease plasma glucose but importantly only occur in the presence of high glucose. GLP-1 also has effects outside of the pancreas that lead to decreases in blood glucose (Edwards et al, 1999). The vagal nerve controls gastric emptying and GLP-1 is expressed in vagal neurons and is known to decrease gastric emptying (Lu et al., 2018). Up to 50% of GLP-1's ability to control glucose homeostasis has been linked to the hormone's capability to decrease gastric emptying (Moore et al, 2013) limiting the release of carbohydrates into the small intestine and slowing glucose uptake into the blood. In addition, GLP-1 also decreases appetite, increasing satiety, which may occur through centrally mediated mechanisms (reviewed in Drucker 2018). Due to its short half-life in the blood, it is unclear how GLP-1 released from the gut mediates these functions. One proposed mechanism of action is that this occurs via vagal nerve innervation (Krieger et al 2016). GLP-1 also has effects outside the control of glucose homeostasis; it can reduce weight (e.g. Dar, Tahrani, & Piya, 2015) and has neuroprotective effects (e.g. Gault & Hölscher, 2018). GLP-1 also has cardioprotective effects in the heart (e.g. Boyle, Livingstone, & Petrie, 2018) (Figure 1.8). All of the these effects of GLP-1 are caused through its binding to the GLP-1 receptor (GLP-1R).

1.3.2 Targeting the GLP-1 system in disease

Due to its role in controlling blood glucose, the GLP-1R is a major therapeutic target for Type II diabetes mellitus. Also referred to as non-insulin dependent diabetes, Type II diabetes mellitus is characterised by impaired function of β cells in the pancreas, desensitisation of peripheral tissues to insulin and a high level of plasma glucose. Type II diabetes affects approximately 340 million people worldwide and the World Health Organisations attribute 1.5 million deaths yearly to diabetes (I & II) (WHO, 2017). Current treatments for diabetes include insulin mimetics such as Sulfonylureas that target the insulin receptor and other drugs such as Metformin and Thiazolidinedione (TZD's) that target sensitivity to insulin in peripheral tissues

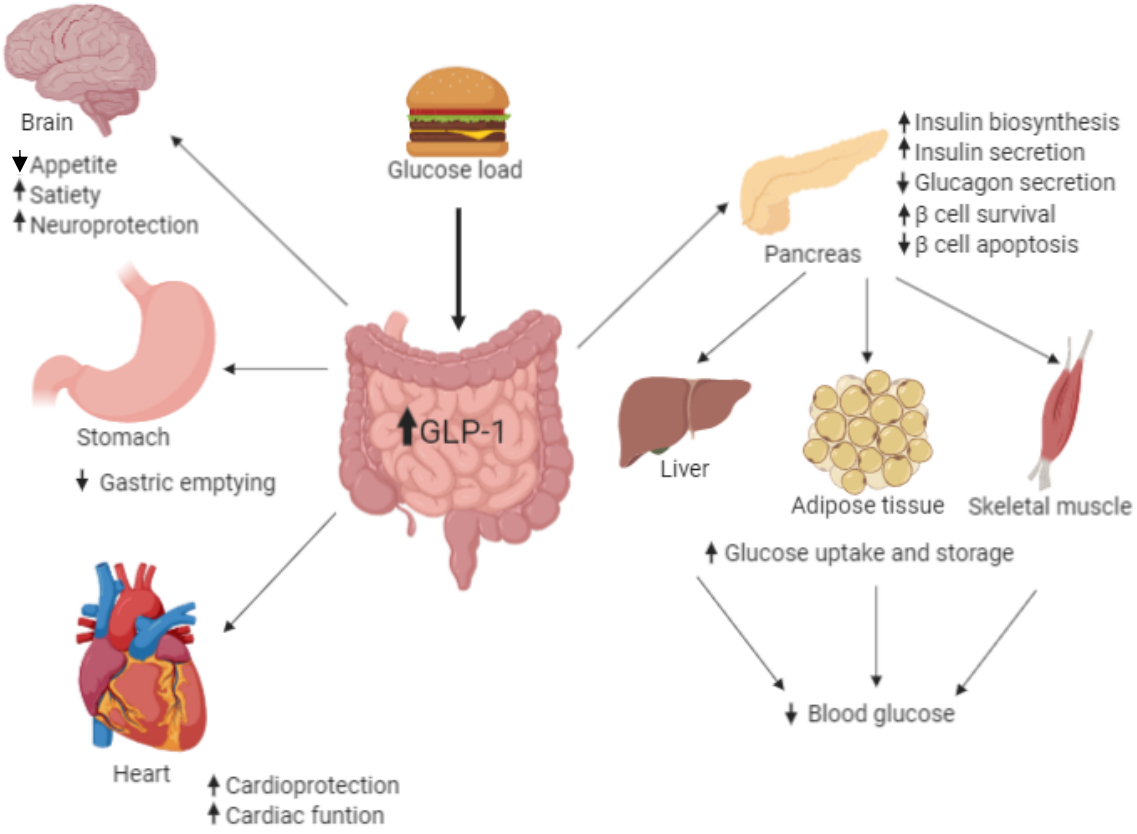

Figure 1.8: Physiological effects of GLP-1 on various tissues throughout the body (adapted from Drucker et al 2012)

and drugs that target the GLP-1 system (reviewed in Drucker, Habener, & Holst, 2017). Although GLP-1 injections can restore normal glucose levels in diabetic patients, its therapeutic potential is limited due to its short half-life (<2 mins in plasma). Available clinical options for treatment of diabetes that target the GLP-1 system include dipeptidyl dipeptidase IV (DPPIV) inhibitors, which extend the plasma half-life of GLP-1 by inhibiting its breakdown by DPPIV, and GLP-1 mimetics, which are analogues of GLP-1 that have an extended half-life due to their resistance to be degraded by DPPIV (reviewed in Drucker et al., 2017). To date, a number of GLP-1 based drugs have been approved for clinical use, with many more in clinical trials. There are now 6 FDA approved drugs that target the GLP-1R for type 2 diabetes, with one also being approved for treatment of obesity. Some of these approved therapies are also undergoing trials for neurological disorders including Alzheimer's and Parkinson's diseases (reviewed in Drucker et al., 2017).

Approved (by FDA) GLP-1R targeting peptides include exendin (half-life 2hrs), lixisenatide (4 hours), liraglutide (half-life 10hrs), dulaglutide (4.7 days) and semaglutide (7 days). Long acting Exendin-4 has also been developed extending the half-life of the therapeutic to 7 days (reviewed in Sharma, et al. 2018). While these are used both in monotherapy and in combination therapy in conjunction with other diabetic treatments, their route of administration (subcutaneous injection) has led screening programs to pursue small molecule drug development that can be used orally. To date, at least three small molecule ligands are in clinical trials targeting the receptor for the treatment of Type II diabetes mellitus (Willard, Beuno and Sloop 2020).

Approved GLP-1R peptide mimetics have been associated with adverse gastrointestinal symptoms, however therapeutics with longer half-lives requiring fewer administrations have less reported side-effect profiles. While this led to the hypothesis that nausea and GI effects were associated with their route of administration, Semaglutide available in an oral formulation has similar gastroinestinal (GI) effects to the injectable form of the same peptide, suggesting these are on target side effects (Davies et al., 2017). There are also a number of concerns regarding the long-term use of incretin mimetics, as they have been reported to be associated with serious side effects, such as an increased risk of pancreatitis and various cancers (including pancreatic and thyroid cancers) (reviewed in Filippatos et al. 2014). However, the general consensus is that these reported side effects are not well-supported in the patient data, albeit the longer term implications of these drugs are yet to be realised. In addition, diabetes itself is

a risk factor for pancreatitis and pancreatic cancer so the incidence of these might be linked to the disease rather than the treatment (reviewed in Filippatos et al., 2014).

The GLP-1 mimetic liraglutide was recently approved in Europe as a weight loss agent (Mehta, Marso, & Neeland, 2017) and is also currently in clinical trials for both neurodegenerative diseases and cardiovascular diseases (Clinical trial NCT01843075), however, the signalling mechanisms through which GLP-1R activation mediates these actions in the brain and heart are currently unclear. Knowledge of how the GLP-1R signals in these different tissue types is important to understanding how incretin mimetics may mediate their therapeutic actions and how to avoid the side effects associated with these treatments in the same way it is important for research into GLP-1s action in diabetes.

1.4 The Glucagon-Like Peptide 1 Receptor

The GLP-1R is a GPCR that belongs to the class B subfamily. It contains the characteristic seven transmembrane α helices and a large ECD, and there are a large array of peptide agonists that have been developed for this receptor, all of which are predicted to engage the TM domain of the receptor to promote activation. This receptor also has a few non-peptide agonists identified and a number of allosteric ligands, which bind at a topographically distinct sites to peptide agonists within the TM domain.

1.4.1 GLP-1R Ligands

Endogenous ligands of the GLP-1R are derived from the pre-proglucagon gene from which glucagon is also derived. There are multiple endogenous ligands that can activate the GLP-1R including 4 variants of GLP-1; the predominant form GLP-1(7-36)NH_2, as well as GLP-1(1-37), GLP-1(1-36)NH_2, GLP-1(7-37). Oxyntomodulin, which is derived from the same gene as GLP-1 and is structurally very similar, acts predominantly at the GLP-1R but also has activity at the glucagon receptor. Multiple peptides have also been developed as therapeutic ligands for the GLP-1R (Figure 1.8). The first developed was exendin-4, derived from the saliva of the gila monster. Since then a series of peptides based on the endogenous peptide with various alterations to extend the half-life have been developed including; liraglutide, lixisenatide, albiglutide, dulaglutide and semaglutide (Figure. 1.9). Taspoglutide was also in clinical trials

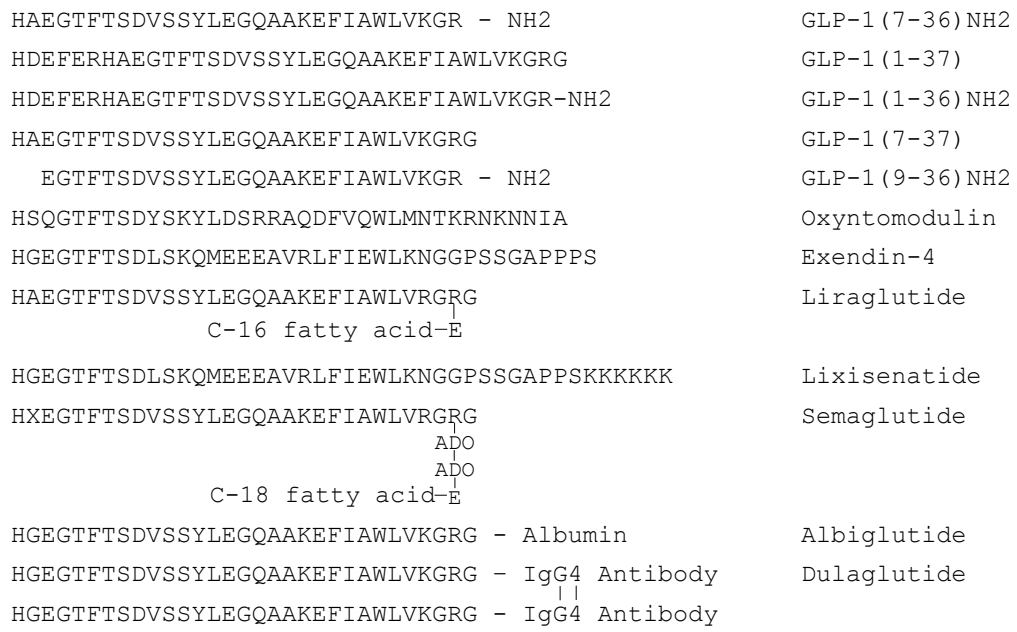

Figure 1.9: Endogenous and therapeutically used peptide ligands of the GLP-1R.

as a potential therapeutic, however failed due to unacceptable side effect profiles. There are also a number of other peptides in clinical development, some that solely act on the GLP-1R, while others are being developed to co-target the GLP-1R and the GIPR and/or GCGR, as dual agonism at these receptors is proposed to have therapeutic advantages over activation of the GLP-1R alone (Usui, Yabe and Seino 2019).

The metabolite of GLP-1, GLP-1(9-36)NH_2, which was previously thought to be biologically inactive, has some weak biological action at the GLP-1R (Wootten, Reynolds, Smith, et al., 2016) and can be modulated by positive allosteric modulators of the
receptor (Nolte et al., 2014). Also, GLP-1(28-36) (produced as a result of neutral endopeptidase 24.11) has also been shown to have biological effect however it may be via receptor independent mechanisms (Li et al., 2019).

11mer peptides based on the N-terminus of the native GLP-1 peptide are being explored for their ability to activate the GLP-1R, several being developed and having efficacy at the receptor despite only interacting with the top of the TM domain (Haque et al., 2010)(Hoang et al., 2015). Several small molecule ligands have also been developed for the receptor, some of which bind in an overlapping site to that of peptides, others that bind at an allosteric site. These have an

allosteric effect while also having intrinsic efficacy for GLP-1R, including compound 2 (6,7-dichloro-2-methylsulfonyl-3-N-tert-butylaminoquinoxaline) and 4-(3-benzyloxyphenyl)-2-ethylsulfinyl-6-(trifluoromethyl) pyrimidine (BEPT) (Nolte et al., 2014), which binds at an intracellular site at the bottom of TM6 on the receptor (Knudsen 2007). Newer small molecule ligands are now in clinical development, such as Transtech pharma compound 273, OWL33 from Chugai and Eli Lilly and a series of small molecules from Pfizier (Willard, Beuno and Sloop 2020). These are predicted to bind to residues which overlap with the peptide orthosteric site.

1.4.2 GLP-1R signalling

The GLP-1R binds preferentially to Gαs proteins promoting the production of cAMP, however it is pleiotropically coupled and can bind and activate, to a lesser extent, Gαi/o, Gαq and Gα12/13 proteins. Activated G proteins and/or β arrestins promote the generation of second messengers such as cAMP, Ca2+ or phosphoinositides and the phosphorylation of MAP kinase

pathways, but the relative contributions of each individual effector to many of these signalling pathways is not well understood. The receptor can also recruit regulatory proteins, such as GRKs and β arrestins that also promote and influence downstream cellular signalling (reviewed in Pabreja et al., 2014).

GLP-1R mediated signalling and the downstream physiological consequences have been most extensively studied in pancreatic β cells (Figure 1.10). Activation of Gαs by the GLP-1R stimulates adenylate cyclase to increase cAMP levels, promoting activation of protein kinase A and exchange protein activated by cAMP (EPAC) (Fletcher et al., 2016). In the pancreatic β cells, this is directly involved in the transcription of the proinsulin gene and its subsequent secretion (reviewed in Fletcher et al., 2016). PKA, once activated, can also inhibit K^+ATP channels, which increases cytosolic Ca^{2+} and subsequent membrane depolarisation, resulting in the exocytotic release of insulin. A number of additional signalling mechanisms can also contribute insulin secretion, including roles for pERK1/2 and β arrestins (e.g. Sonoda et al., 2008).

A number of cellular signalling pathways also contribute to observed effects of GLP-1 on β cell proliferation, survival and differentiation. This includes CREB activation downstream of cAMP accumulation which promotes Bcl-2 and Bcl-xl leading to proliferation, and activation by PKA downstream of cAMP which promotes activation of MAP kinases linked to neogenesis . Inhibition of caspase activity, NFκB and Fox1 by pAkt contributes to protection against β cell apoptosis (reviewed in Fletcher et al., 2016). ERK 1/2 activation has also been implicated in β cell proliferation and differentiation. β arrestin-1 is also important in the activation of ERK1/2 and CREB related gene transcription that leads to β cell survival (reviewed in Pabreja et al 2014) (Figure 1.10).

1.4.3 GLP-1R and biased agonism

Like all GPCRs, distinct ligands activating the GLP-1R can give rise to different receptor conformations that eventuate in differential signalling profiles. Of all the GLP-1R ligands assessed for biased agonism behaviour to date all are able to promote secretion of insulin from β cells, albeit some are not as efficacious as others. To date, the evidence suggests that all ligands differentially activate various signalling pathways downstream of GLP-1R activation, albeit with the evidence to hand, some profiles are only subtly different to that of the primary endogenous ligand GLP-1(7-36)NH_2 (reviewed in Koole et al., 2013).

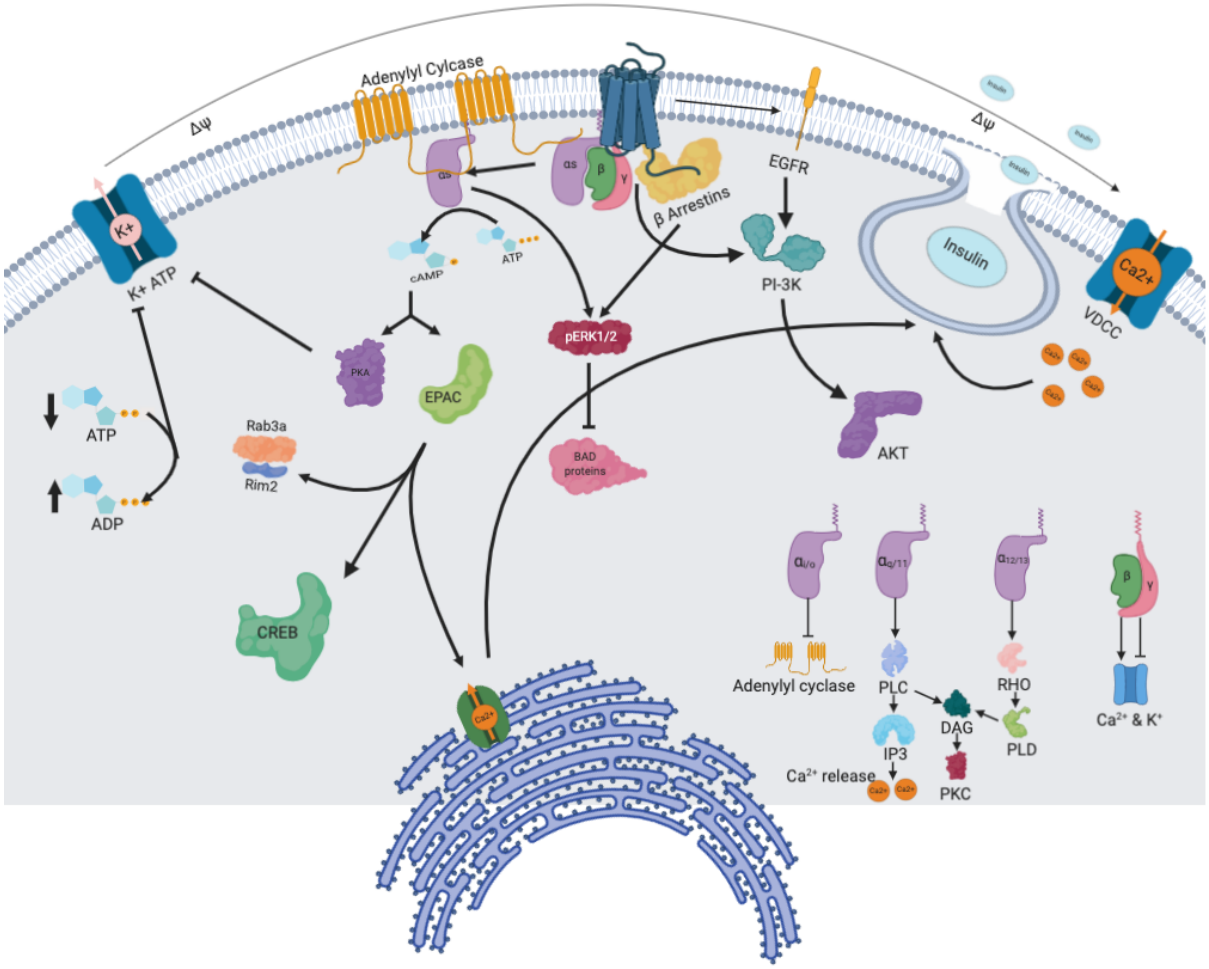

Figure 1.10: Basic overview of signalling of the GLP-1R in a beta cell (adapted from Pabreja et al 2016)

For the GLP-1R, biased signalling has been routinely studied across five major signalling pathways that are activated post receptor activation; cAMP, pERK1/2, iCa^{2+} and recruitment of the two regulatory proteins β arrestin-1 and β arrestin-2. When compared to the native GLP-1 ligand, the endogenous agonist oxyntomodulin preferentially activates pERK1/2 as well as recruitment of regulatory proteins over the cAMP pathway (reviewed in Koole et al., 2013). Therapeutic ligands such as exendin-4 and liraglutide are also biased ligands but to a lesser extent than oxyntomodulin (reviewed in Fletcher et al., 2018). Similar to oxyntomodulin, exendin 4 is biased towards regulatory protein recruitment compared to cAMP, however it has a similar profile to GLP-1 when accessing MAP kinases. Liraglutide preferentially activates pERK1/2 over cAMP compared to GLP-1, however is biased away from regulatory protein recruitment. Small molecule ligands of the GLP-1R, including BETP and Compound 2 are also biased ligands at the receptor in comparison to GLP-1 (Fletcher et al., 2018). For these ligands, relative to equivalent amounts of cAMP, β arrestin recruitment was much more heavily favoured in comparison to the primary endogenous ligand GLP-1(7-36)NH_2 (Koole et al., 2013). Looking to delve further into the role bias might play in a therapeutic setting, novel ligands with unique chemistries have been synthesised with the express purpose of inducing bias in full length ligands. The substitution of β amino acids into the native GLP-1 sequence induced various ways different biased agonism profiles relative to GLP-1 that were dependent on the unnatural amino acid introduced and the position of the substitution within the peptide (Hager et al. 2017). This included both G protein biased and arrestin biased peptides. Additional studies describe the development of biased agonists that favour G protein (Gαs and Gαq) activation over β arrestin recruitment. These include exendin P5 and exendin-Phe1. Exendin-P5 is a novel biased agonist that was synthesised based on C-terminal sequence of exendin-4, (Ex4(9-39), but with a 10 amino acid N-terminus that was distinct from the parental peptide. This peptide had differential in vitro signalling compared to the exendin-4 where it was biased towards G protein signalling over arrestins (Zhang et al. 2015). Interestingly, in vivo, it was a weaker insulin secretagogue then exendin-4, but had greater efficacy in correcting blood glucose. It also displayed increased adipogenesis (but decreased adipocyte size) relative to exendin-4 (Zhang et al 2015). Collectively this data suggests a novel mechanism by which this peptide controls blood glucose levels in the absence of raising insulin levels.

A second modified exendin-4 peptide, exendin–Phe1, contains a substitution of the N-terminal histindine residue at position 1 with phenylalanine. This peptide did not recruit arrestins as strongly as exendin-4, but was able to promote cAMP accumulation to a similar extent,

therefore relative to exendin-4 was classified as a G protein biased agonist (Jones et al., 2018). The trafficking of the exendin-Phe1 peptide was also reduced significantly compared to exendin-4 and a higher percentage of those receptors that were internalised, were then recycled back to the cell surface. In vivo profiling in repeat glucose tolerance tests revealed Exendin-Phe1 was able to maintain glucose control up to 8 hours after injection in response to a glucose challenge, compared with exsendin-4 which displayed a less prolonged response, and this was also correlated with higher insulin levels. This study suggested that a ligand that spends more time at the plasma membrane (by undergoing less internalisation and greater recycling) may provide greater therapeutic output with respect to glucose control compared to other ligands (Jones et al., 2018).

These studies highlight the potential to exploit biased agonism to provide therapeutic advantages, where new GLP-1R therapies could be developed that have a different mechanism to existing therapies and may offer greater efficacy, as well as the potential to reduce on-target side effects. However, to exploit biased agonism requires a full understanding of the ideal profile of activation to provide the best in vivo profile. To establish this will require a large library of compounds with novel bias to be able to elucidate which bias profiles are most beneficial in a therapeutic setting.

1.4.4 Structural studies on the GLP-1R

There are now multiple structures of the GLP-1R, including both active and inactive states. The first structure of the TM domain was an inactive structure of the isolated TM domain with various changes made to stabilise the construct (Song et al. 2017) with many thermostabilising mutations. Later, there was also a full-length crystal structure of the receptor bound to an 11mer ligand (named Heptares P5) but without G-protein present (Jazayeri et al., 2017). This receptor was also heavily modified by mutations. More recently three full length fully active structures were published, one bound to the native ligand, GLP-1 (Y. Zhang et al., 2017), one to a biased agonist, Exendin-P5 (Liang et al., 2018b) and one to a small molecule non-peptide agonist TTP-OAD2 (Zhao et al., 2020), all in complex with Gαs. The three peptide bound structures contained many similarities while the small molecule bound structure had more differences (Figure 1.11).

Figure 1.11: Overlay of 4 active GLP-1R structures bound to GLP-1 (Orange) (Zhang et al 2018), Exendin-P5 (Purple) (Liang et al 2018b) and Heptares-P5(light Green) (Jayazera et al 2018), small molecule agonist TT-OAD2 (Teal) (Zhao et al 2020).

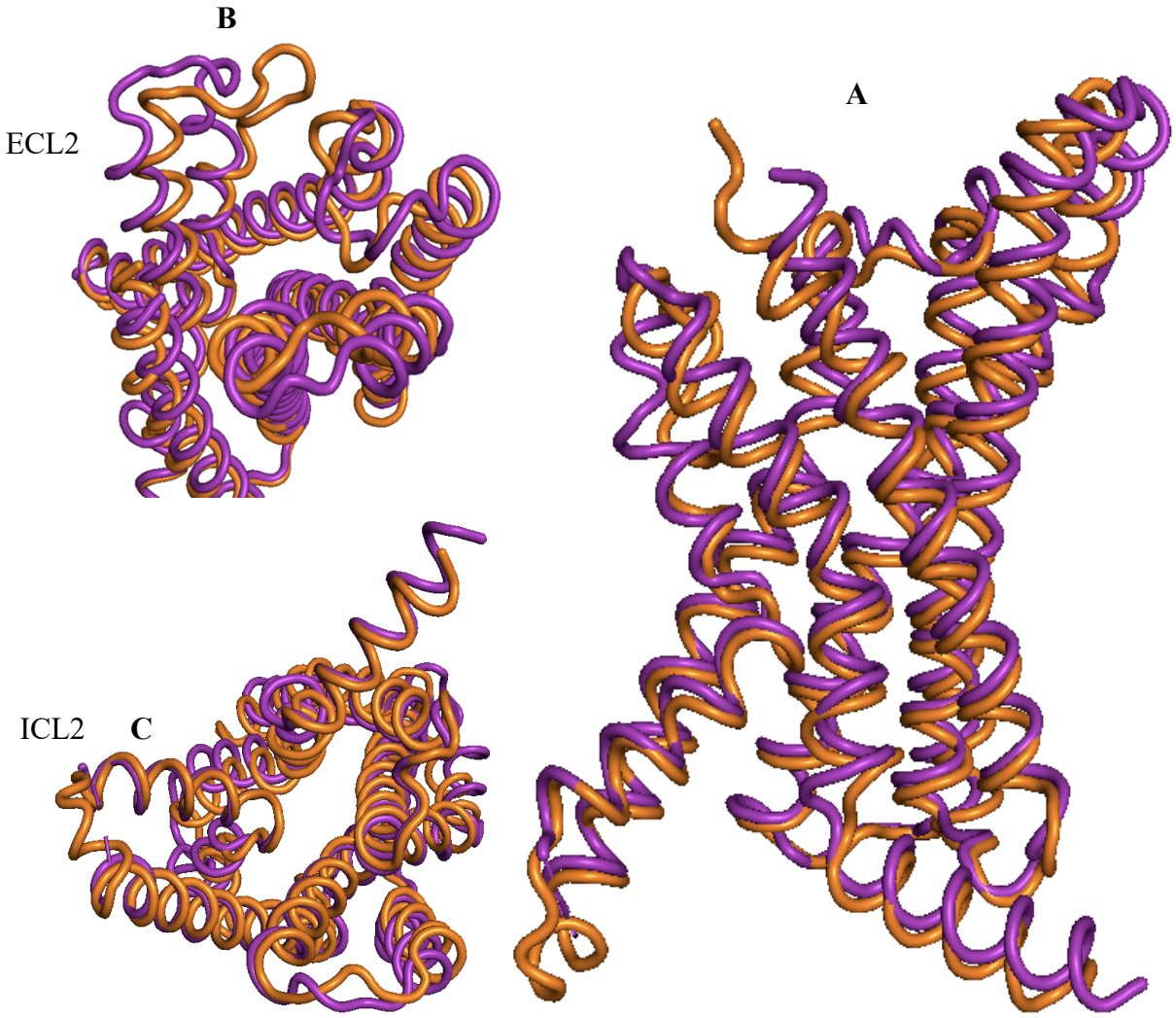

Figure 1.12: Overlay of the active GLP-1R structure bounds to GLP-1 (orange) (Zhang et al 2018) and Exendin-P5 (purple) (Liang et al 2018b) (**A**) highlighting differences in ECL2 (**B**) and ICL2 (**C**)

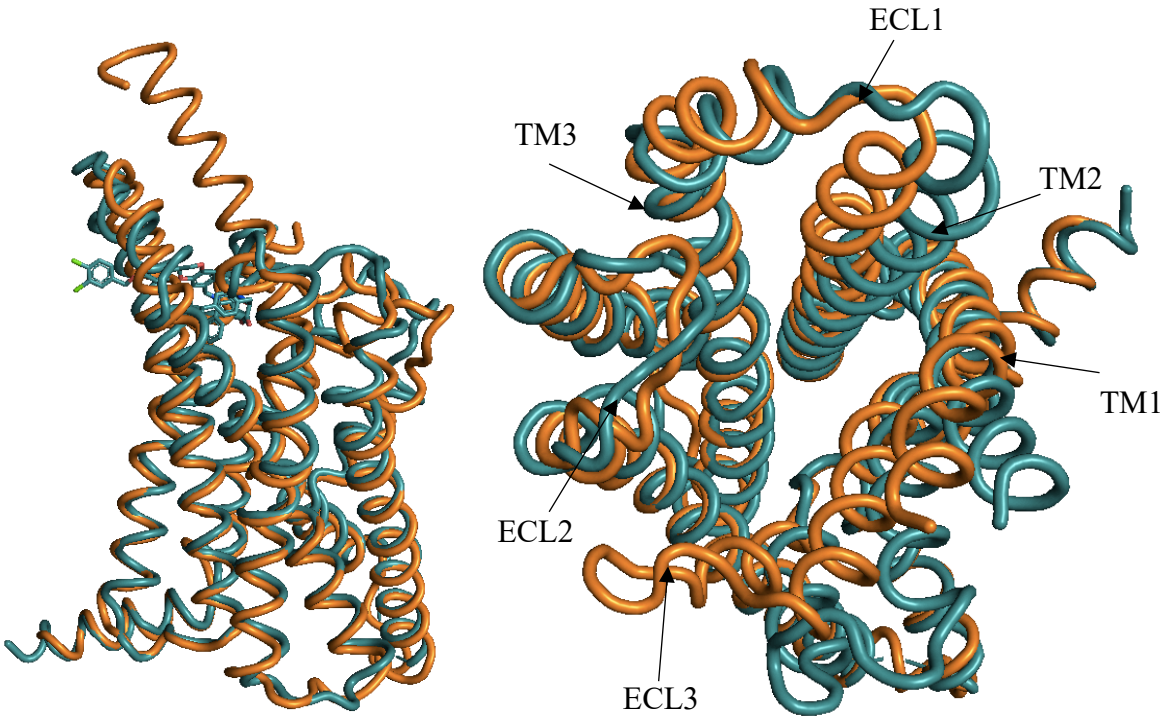

Figure 1.13: Comparison of the GLP-1 bound GLP-1R (orange) (Zhang et al 2018) to the TT-OAD2 bound structure (teal) (Zhao et al 2020) showing differences in ligand orientation (**A**) and the extracellular surface (**B**).

Comparison of the two full length unmodified receptor structures that contain full-length peptides revealed little difference in the position of the ligand, N-terminal domain, ECD or the G-protein binding site. However, large conformational differences were observed in the arrangement of the tops of TM1, TM6, TM7, as well as ECL3 and ICL3 on the exendin-P5 bound structure compared to the GLP-1 bound structure (Liang et al 2018b)(Figure 1.12).

The non-peptide (TTP-OAD2) bound GLP-1R structure bound to Gαs revealed limited overlap between the TTP-OAD2 and the peptide binding site. The non-peptide bound high up in the TM bundle in a pocket where it forms multiple interactions with residues in TM1, TM2, TM3, ECL1 and ECL2, as well as extending to form interactions with the bilayer (Zhao et al. 2020)(Figure 1.13). This ligand induces a very distinct profile of signalling to peptide ligands, inducing only cAMP signalling with very different kinetics to that of peptide ligands (Zhao et al 2020). This ligand induced similar conformational transitions in the intracellular face of the GLP-1R that interacts with Gαs, but very different conformations at the extracellular face, including differences in the ECD conformation, TM1-3, TM6-7 and all three extracellular loops (Zhao et al 2020)(Figure 1.13).

1.4.5 Structure-function studies on the GLP-1R

Extensive mutagenesis studies have been performed on the GLP-1R to understand how the residues on the extracellular surface of TM bundle interact with agonists. The majority of data has focussed on the main endogenous peptide GLP-1, however there is also extensive profiling of oxyntomodulin and exendin-4 characterising residues within the ECLs (Lei et al 2018)(Wootten et al 2016)(Yang et al 2015)(Coopman et al 2011)(Dodds & Donnelly 2015). These data revealed the importance specific residues of the receptor in influencing receptor signalling by these agonists. Included in this data is a full alanine scan of the ECLs characterising GLP-1(7-36)NH_2 (the native ligand), oxyntomodulin and exendin-4 that revealed the global importance of regions within the extracellular surface for pathway specific efficacies, with ECL2 being important for intracellular Ca^{2+} mobilisation and cAMP signalling and ECL3 important for pERK1/2 signalling (Wootten, et al. 2016). However, there are also residues within these domains responsible for ligand-specific differences in peptide binding and transmission of efficacy, for example E387 had no significant impact on ligand binding for those assessed but selectively reduced cAMP efficacy for exendin 4 with no significant effect on GLP-1 or oxyntomodulin. In addition, a cluster of polar residues that lie deep within the TM bundle, at the base of the peptide ligand binding site are integral for transmission of signalling

and biased agonism (Wootten et al., 2015). Mutation of these important amino acids to alanine revealed key residues within this network for binding GLP-1 and exendin-4, but not oxyntomodulin (Wootten et al., 2015). In addition, these mutations altered GLP-1(7-36)NH_2 and exendin-4 efficacy differentially to that of oxyntomodulin. For example, GLP-1(7-36)NH_2 and exendin-4 cAMP and Ca^{2+} signalling, and to a lesser extent pERK1/2 signalling was negatively affected by mutation of arginine at position 190, conversely oxyntomodulin cAMP efficacy was improved and iCa2+ and pERK1/2 unaffected by this mutation (Wootten et al., 2015). This difference in response was attributed to variance in ligand sequence at position nine (position 3 of the mature peptide). GLP-1(7-36)NH_2 and exendin-4 have a negatively charged glutamic acid at this location, which forms a salt bridge interaction with arginine 190 upon its binding, disrupting the inactive receptor hydrogen bond network, potentially allowing for rearrangement of TM6 and receptor activation. Oxyntomodulin, however, has a neutral charged glutamine residue at this position that is not required for oxyntomodulin affinity, yet disruption of ground state interactions upon agonist binding could account for the increased efficacy of the mutation. Chimeric peptides with swaps at residue 9 between GLP-1(7-36)NH_2 and oxyntomodulin reverses the profile of the two peptide ligands, such that R190 becomes a crucial residue for the affinity and signalling of oxyntomodulin with glutamic acid at position 9, but not for GLP-1(7-36)NH_2 with glutamine at position 9 (Wootten, et al. 2016). Polar residues near the intracellular surface of the receptor have also been shown to have key roles in stabilising the ground state of the receptor, where alanine mutations either induced constitutive activity or enhanced cAMP potency (Wootten, et al. 2016). These residues could also impact effector specificity, which has the potential to alter ligand bias profiled. Residues at the top of TM1 have also been found to be important in both binding and signalling in a ligand specific manner (Lei et al 2018). Mutagenesis data, combined with novel structural information is beginning to provide unique insights into how biased agonism occurs at the structural level. However, there is still additional information required to fully understand how this occurs and how distinct ligands engage and activate this receptor.

1.5 Scope of thesis

While many biased ligands for the GLP-1R have been identified, there are many potential signalling complements possible from activation of this receptor. To ultimately be able to understand the biased profiles of ligands and relate to their physiological requires a wide range of ligands with unique bias profiles and to be able to identify mechanistically how these profiles

arise. My thesis is focuses at generating a greater understanding of the mechanistic basis for which bias arises at this receptor.

To attempt to identify ligands with more extreme bias profiles than those previously assess, the first part of my project focuses on profiling a range of novel ligands and assessing their how their differing structures activate the GLP-1R, in terms of efficacy and biased agonism. To address this a series of novel 11mer ligands with distinct chemistry were synthesised based on the N-terminus of the native peptide (GLP-1(7-36)NH_2) with the intention of creating a smaller ligand still capable of acting at the GLP-1R, but with more limited engagement with the ECD were selected for the study. These ligands were tested in a CHO FlpIn cell system for a series of pharmacological assays that are associated with signalling that is important for the physiological outputs mediated by the GLP-1R.

In the second results chapter of my thesis, I have utilised HEK293 cells where individual effector proteins have been deleted (via CRISPR/Cas9) to understand the contribution of individual G protein subtypes or beta arrestins1 and 2 to signalling mediated by both full length biased agonists and biased 11mer peptides (relative to GLP-1).

The last section of my thesis uses a large scale alanine mutagenesis to explore the role of individual residues within the deep TM binding pocket to understand the importance of these residues in peptide affinity and efficacy for a range of biased agonists. With the availability of new structural data, this data is beginning to explain which receptor-ligands interactions drive affinity, which drive efficacy and how these differ between ligands with different efficacies and bias profiles.

Chapter 2:
Methods

2.1 Reagents

Peptide ligands - GLP-1(7-36)NH_2, Exendin-4, Oxyntomodulin and Exendin-P5 were all purchased from China Peptides (Hangzhou, China), Liraglutide was purchased from Bachem (Bubendorf, Switzerland). Exendin(9-39) was purchased from Mimotopes. 11mer peptides 1B, 3 and 14 were synthesised by Phil Thompson's group within the medicinal chemistry department at the Monash Institute of Pharmaceutical Sciences. Heptares P5 was a gift from Heptares and the remaining 11mer peptides and GLP-1 A^{13} were synthesised in collaboration with Pfizer solubilised in DMSO to a stock concentration of .

General Reagents – Dulbecco's Modified Eagle Media (DMEM – low glutamate no sodium pyruvate), Fluo8 acetylmethylester (fluo8 AM), coelenterazine h and hygromyocin B were purchased from Invitrogen (Carlsbad, CA, U.S.A). Fetal bovine serum (FBS) was purchased from the Thermo Electric company (Melbourne, Vic, Australia). LANCE cAMP assay and 384 well optiplates were purchased from PerkinElmer Analytical sciences (Walthorn, MA, U.S.A). Surefire^{TM} ERK1/2 reagents were obtained from TGR Biosciences (Adelaide, SA, Australia). I^{125} Mono-iodinated Bolton-Hunter reagent was purchased from Perkin Elmer Life Science (Walthorn, MA, U.S.A). SigmaFast o-phenylenediamine dihydrochloride tablets (Catalogue # and antibodies were purchased from Sigma-Aldrich (St. Louis, MO). CRISPR KO HEK293 cells were a gift from Dr. Asuka Inoue (Tokyo University).

2.2 Cell Culture

Cell culture was performed in PS2 laminar flow hoods under sterile conditions. Chinese Hamster Ovary FlpIn, (CHOFlpIn) cells with a stable expression of the human (or mutant) GLP-1R or HEK293 cells (parental WT and CRISPR KO) were maintained at 37°C and in 5% CO2 in (DMEM) supplemented with 1 mM sodium pyruvate, 2.5mM d-glucose and 4mM L-glutamine, containing 10% (v/v) Fetal Bovine Serum. When cells reached confluency, they were washed with Phosphate Buffered Saline (PBS) and detached from the flask using the chelating agent, versene (0.53 mM EDTA in PBS), pelleted by centrifugation at 350g for 3 min and the supernatant removed. Cells were resuspended in DMEM and either seeded to a new flask to maintain the cell line or counted and seeded for assays. For cell counting, 20µl of the suspension was added to 160µl of DMEM and 20µl of trypan blue giving a 1:10 dilution of cells and cells were counted using a hemocytometer.

2.3.1 Transient transfections

HEK293 CRISPR cells were incubated in T75 cell culture flasks with 5ug 2xcMychGLP-1R or 2.5µg 2xcMychGLP-1R-Rluc8 and 2.5µg β arrestin-1-YFP prepared in sterile 150mM NaCl. 30 µg of PEI was prepared in sterile 150mM NaCl, combined with DNA and co-incubated for 15 minutes and then added dropwise to the cells. 24 hours later the cells were seeded in 96 well plates at 30,000 per well. Experiments were performed 24 hours later (48 hours post transfection).

2.3.2 Generation of stable cell lines

Parental CHOFlpIn cells were seeded in T25 cell culture flasks in 10% FBS DMEM + 600µg of zeocin and allowed to reach ~80% confluence. 0.5µg of WT or mutant 2xcMychGLP-1R and 4.5ug of pOG44 was made up in 250µl of sterile 150mM NaCl. 30µl of PEI (1mg/ml) was diluted to 250ul of sterile 150mM NaCl. DNA and PEI solutions were combined and incubated for 15 mins. This solution was added dropwise cells and incubated for 48 hours. After 48 hours the media was removed and replaced with selection media (DMEM, 10%FBS, 600µg/ml Hygromyocin) (a no DNA negative control was also included to ensure untransfected cells were killed by the treatment). After 48 hours cells were detached and reseeded back to the same flasks. Some cell lines used in chapter 5 were generated by Wootten et al 2016 using the same method

2.3 Cell based assays

To minimise any systematic errors in cell based assays, the plate layout was varied with a different plate layout used for each independent experimental repeat, in terms of the location of mutant vs wildtype cell lines (Chapters 3 and 5) and in the location of different drug concentrations and controls. For chapter 5, where >50 cell lines were used, only WT and 5 other cell lines were in culture at any one time to ensure there was no cross contamination of cell lines due to handling too many different lines in each subsets of experiments. All mutant receptor studies included a wildtype control.

2.3.1 cAMP accumulation

All cAMP studies were performed using a LANCE-cAMP assay kit with a modified protocol to the manufacturers' recommendations (PerkinElmer life sciences, Melbourne). CHO FlpIn-GLP-1R cells were seeded in Falcon clear 96 well flat bottom plates at a density of $3x10^4$ cells per well in DMEM, 10 % FBS and incubated overnight at 37°C in 5% CO2. Media was removed from cells and replaced with 90µl pre- warmed stimulation buffer (phenol red free DMEM, 0.1% (w/v) bovine serum albumin (BSA) and 0.5mM IBMX, pH 7.4). Cells were incubated at 37°C and 5% CO_2 for 30 min. Cells were stimulated with 10µL of increasing concentrations of ligand from 1pM to 10µM (depending on ligand). Vehicle (stimulation buffer) was used for a negative control and forskolin (100 µM) for a positive control. Cells were incubated for 30min at 37°C in 5% CO2 following ligand addition. This reaction was quickly terminated by rapid removal of stimulation buffer and addition of 50µl of ice cold 100% ethanol. Ethanol was evaporated off and replaced with 75µl lysis buffer (0.3% Tween20 (v/v), 5mM HEPES and 0.1% BSA(w/v) pH7.4). Lysates were frozen and thawed to increase cell lysis. 5µl of lysate was added to a corresponding well in a 384 well optiplate (Perkin Elmer, life and analytical sciences). A cAMP standard curve was prepared in the range 0.1nM-10µM and added to additional wells of the 384 well plate. 5µl of Alexa anti-cAMP antibody mixture (0.5% Alexa fluor-647 anti cAMP in detection buffer supplied by the manufacturer) was added to each of the wells in the optiplate containing lysate or cAMP standard and incubated for 30 min at RT in reduced lighting conditions. 10µl of Eu-SA and biotinylated cAMP mix (0.02% (v/v) EuW8044 labelled streptavidin (Eu-SA) and 0.07% biotinylated cAMP (v/v) diluted in kit detection buffer and pre-incubated for a minimum of 15 min) was added to each well and incubated at RT for 1 hr before detection of HTRF using a top read on the Envision plate reader system. Raw RFU values were then converted using the standard curve to give absolute cAMP levels. All data was normalised either to forskolin or to the GLP-1(7-36)NH_2 response, performed in parallel in all experiments. Plate layout was randomised in each experiment to control for plate effect. All experiments were initially normalised to forskolin as an internal control and then to a reference ligand/cell line

2.3.2 pERK1/2 assays.

All ERK1/2 phosphorylation studies were performed using an ALPHAscreen Surefire ERK1/2 phosphorylation kit with ALPHAscreen anti-ERK acceptor beads and streptavidin donor beads. CHO FlpIn cells were seeded in Falcon clear 96 well flat bottom plates at a density of $3x10^4$ cells per well in DMEM, 10% FBS and placed in an incubator at 37°C in 5% CO_2 overnight.

Media was removed carefully and replaced with 90 µl FBS free DMEM and incubated at 37°C in 5% CO2 for a minimum of six hours before experiments were performed.

Initially, for each peptide, pERK1/2 reverse timecourse experiments were performed by adding 10 µl of ligand, to give a final concentration of 1 µM. Cells were stimulated for 0, 1, 2, 4, 6, 8, 10, 15, 30, 45 or 60 min in separate wells of a 96-well plate. Vehicle was added as negative control and 10% FBS was added to separate wells at 7 minutes as positive control (the FBS pERK1/2 response is known to peak around 6 minutes and stay sustained). Reactions were terminated by removal of media and addition of 50µl surefire lysis buffer. Lysates were frozen and thawed before pERK1/2 was detected.

For pERK1/2 detection, 5µl of lysate was transferred from each well in the 96 well to corresponding wells in a 384 well OptiPlate. Detection solution was prepared containing 60 parts surefire reaction buffer, 10 parts Surefire activation buffer, 0.3 parts Protein A acceptor bead and 0.3 parts Steptavidin coated donor bead. 8.5µl of this solution was added to each well containing lysate in reduced light conditions. Lysates with detection mix were incubated for 1 hr at 37°C. Plates were then rested for 15 minutes after removal from the incubator to allow the reactions to calibrate to room temperature. Plates were read using a top read on the Envision plate reader using the ALPHAscreen protocol with excitation filter 485/20 and emission filter 532/25.

Following initial time course experiments, data were analysed and the peak response time was identified. This timepoint was used to generate full concentration response curves for each peptide ligand. Cells and assays were prepared in the same way as above, however, cells were stimulated with 10µl of increasing concentration of ligand from 10pM to 1µM in full log units. Vehicle was used for a negative control and FBS as a positive control. Cells were incubated for the relevant time determined in timecourse experiments before being lysed and pERK1/2 detected. Data was normalised to positive control as an internal control and then to a reference ligand.

2.3.3 iCa2+ mobilisation assay.

The Flexstation Ca^{2+} mobilisation assay (Molecular Devices) is a fluorimetric assay that quantifies the elevation of intracellular calcium concentration in response to receptor agonists. It is a real time, live in vitro assay using a Ca^{2+} sensitive fluorescent dye to report the calcium concentration within the cell. CHO FlpIn GLP-1R or transiently transfected HEK293 cells were plated in Falcon clear 96 well flat bottom plates at a density of $3x10^4$ cells per well in DMEM, 10% FBS and incubated at 37°C in 5% CO_2 overnight. Media was removed and replaced with 90µl of pre-warmed iCa^{2+} buffer (150nmM NaCl, 2.6mM KCl, 1.18mM $MgCl_2.6H_2O$, 10mM D-Glucose, 10mM HEPES, 2.2mM $CaCl_2.2H_2O$, 0.5%w/v BSA 4mM Probenecid, pH7.4) supplemented with 1µM Fluo-8 AM in light sensitive conditions. Cells were incubated for 1hr at 37°C without CO_2. Receptor-mediated calcium mobilisation was determined in a Flexstation where increasing concentrations of ligand were added in the instrument. Fluorescence was determined throughout the entire read in the Flexstation. The plates were read in the Flexstation with a 14 second baseline read before ligand addition. Ligand concentration ranged from 10nM to 10µM in full log units, and subsequent reads every 1.36 seconds for 120 seconds. Cells were excited at 485 nm and the corresponding response was recorded at 525nm. A curve was created using a 9 point smoothing. As all peptide ligands assessed in the study displayed similar kinetic profiles, the peak response was recorded for each concentration of peptides. Ligands were prepared in iCa^{2+} buffer, vehicle was used as a negative control and 100µM ATP was used as a positive control in CHO studies and 1µm of Ionomycin for HEK293 studies. Data was normalised to the positive control and then normalised to the WT response for each ligand. The data was normalised to the positive control as 100% as an internal control and then to a reference ligand/cell line.

2.3.4 Bioluminescence Resonance Energy Transfer

CHO FlpIn expressing transiently expressing GLP-1R-Rluc8 and β arrestin 1-venus or β arrestin 1-YFP were seeded in Falcon clear 96 white flat bottom plates at a density of $3x10^4$ cells per well in DMEM and incubated at 37°C in 5% CO_2 and left overnight. Media was removed, cells were washed and replaced with 80µl 1X Hanks balanced salt solution (HBSS) with 0.1%(w/v) BSA, pH 7.4 and incubated at 37° for 30 min. 10µM of the Rluc8 substrate Coelenterazine h (final concentration 5µM) was added in reduced lighting coniditions to each well and incubated for a further 10 mins. Plates were read in a Lumistar (Omega), which allows

for simultaneous reading of signals at 475nm (Rluc8) and 535nm (venus). Wells were read for 4 cycles before addition of 10µl of ligand (final concentration 1µM) or negative control (vehicle) and read for a further 12 min with a 10 second delay in each read. The BRET signal for each time point measured, was calculated by dividing ratio of 535 by 475. The vehicle ratio was then subtracted to give the ligand-induced BRET signal. From these time course experiments, the time to reach a peak response was calculated. Concentration response curves were generated at this time point. For these, cells were prepared in the same way, however after addition of coelenterazine h but before collection of data ligand or negative control (vehicle) was added and allowed to incubate for 2.5mins prior to detection using a single read on the Omega Lumistar. Data was analysed as ratio of 535nm to 475nm and corrected for baseline values to calculate ligand induced BRET. For chapter 4 BRET data was read in a kinetic format and the total AUC was taken and then plotted as a concentration response curve. Data was normalised to maximum response of a reference ligand for analysis

2.4 Whole cell radioligand binding.

To create the tracer ligand, mono-iodinated Iodine, Bolton Hunter, was incubated with Exendin(9-39) overnight and then run through a HPLC and fractions corresponding to the labelled ligand were collected and tested to ensure ligand was still able to bind to the GLP-1R. CHO FlpIn-GLP-1R cells were seeded in Falcon clear 96 well flat bottom plates at a density of $3x10^4$ cells per well in DMEM, 10 % FBS and incubated overnight at 37°C in 5% CO_2. Cells were cooled to 4°C to minimise internalisation. Cells were then washed twice in ice cold 1x PBS and placed in 80ul of ice cold binding buffer (1x HBSS, 25mM HEPES, 0.1% BSA pH 7.4) and kept at 4°C. 10ul of tracer diluted in binding buffer was added to each well, calculated to be at ~25000 counts (approx. 25 pM) per well. 10µl of competing ligand (made up in binding buffer) was added to each well and incubated at 4°C overnight. The next day buffer was removed, then quickly washed with ice cold PBS 3 times before the addition of 50µl of ice cold 0.1M NaOH was added to each well. Contents of wells were added to 6ml poly tubes and read on wizard gamma counter (perkin-elmer)(80 % counting efficiency)(Wootten et al 2016a/b). Data was normailsed to the bottom of the curve for exendin (9-39) to determine non-specific binding.

2.5 ELISA

Receptor expressing and parental CHO-FlPIn cells were plated in a 24 well plate at a density of 250,000 cells per well, with 500µl of DMEM + 10%FBS and incubated overnight at 37ºC and 5% CO_2. Media was aspirated and cells washed three times with PBS. 250µl of 3.7% paraformaldehyde (PFA) was added to each well and incubated at 4ºC for 15mins. PFA was aspirated and then cells were washed with PBS and each cell was then 'blocked' using a solution of 2% BSA and 0.05% Tween20 and incubated at RT for 45mins. The blocking solution was removed and the 125µl of primary antibody diluted (1:2000) in PBS and 2% BSA and incubated at RT for 1hr with gentle agitation. The primary antibody was aspirated and cells were washed three times in PBS with 0.05% Tween20. Blocking mix was again applied for 15min at RT. Blocking solution was aspirated and 125µl of secondary antibody was applied at a 1:2000 dilution in PBS with 2% BSA. Plates were incubated for 1hr at RT with gentle agitation. Secondary antibody was aspirated and wells were washed three time with PBS with 2% BSA and 0.05% Tween20. Substrate was prepared (SigmaFast OPD) by dissolving 1 gold and 1 silver tablet in 20ml of water in the dark. To each well 100µl of substrate solution was added and incubated in the dark for 5 min (positive wells develop a yellow colour). 100µl of 3M HCl was added to stop the reaction, the solution was transferred to a 96 well plate and read on the Envision at 492nM.

2.6 GLP-1R Mutagenesis

2.6.1 Primer generation

Using the known sequence of the hGLP-1R, primers were designed to mutate each of the residues of interest to alanine in a manner that required the least number of nuceleotide changes (1-2 nucleotides). Primers were extended up to 15 amino acids on both sides of the region of mutation and ended with cystosine or guanine. Primers were purchased from Geneworks.

2.6.2 Quikchange site directed mutagenesis

200µg of primer (both sense and anti-sense) were incubated with 50µg of 2xcMychGLP-1R template, 0.5µl of Q5 DNA polymerase (New England Biolabs), 10µl of free nucleotides (dNTPs), 2.5µl of DMSO and made up to 25µl with reaction buffer. Solution was heated to

96°C for 30 secs (to allow DNA denaturing), cooled to 55°C for 30 secs (to allow primer annealing) and then heated back to 72°C for 6 minutes (to allow extension). The reactions were cycled 18 times. At the end of the cycle, 1µl of Dpn-1 (New England Biolabs) was added to degrade the parental methylated template DNA and inclubated at 37°C overnight. Reactions were then stored at 4°C or used for transformations.

2.6.3 DNA expansion (transformation and minipreps)

3µl Newly mutated DNA (in pE5/Frt/V5 vector) was placed in a 15ml round bottom tube and incubated with 30µl of competent bacterial cells on ice for 15 mins. These cells were then heat shocked at 42°C for 45 sec and then placed back on ice for 2 min. 250µl of SOC buffer was added before being shaken for 1 hour at 37°C. After 1 hr solution was pipetted onto an ampicillin containing agar dish and left to incubate overnight at 37°C. 12 hours later single bacteria colonies were picked and placed into 5ml of LB broth containing 50µl/ml ampicillin and incubated overnight at 37°C. DNA was extracted from culture 12 hours later using the Promega Wizard Plus SV Minipreps DNA Purification System following the manufacturers instructions.

2.6.4 DNA sequencing

Purified DNA (60µg) was incubated with either a forward (T7) or backward (BGH long) sequencing primer in 12 µl total solution and supplied to Australian Genomic Research Facility for Sanger sequencing on the plasmid. Mutation was confirmed to be present using 4peaks software for mac and then the remaining sequence was confirmed using San Diego Supercomputer biology workbench compared against the known hGLP-1R sequence.

2.7 Data and statistical analysis

All data analysis was performed using GraphPad Prism 6. Concentration response curves were analysed using a three-parameter curve fit (equation 1).

Equation 1:

$$y = Bottom + \frac{(Top - Bottom)}{1 + 10^{(log(EC50) - \log[A])}}$$

where, bottom represents y value in the absence of ligand, top represents the maximal stimulation in the presence of ligand, bottom represents the basal response in the absence of ligand, [A] is the molar concentration of ligand and EC50 represents the molar concentration required to generate a response halfway between top + bottom.

To quantify signalling bias, which may be manifested as selective affinity (K_A) and/or efficacy (τ) of an agonist for a given pathway, agonist concentration curves were analysed with an operational model of agonism (Gregory et al 2007) but modified to directly calculate the ratio of τ/K_A in a manner similar to that described by Figeuro et al 2009 for each pathway using equation 2.

Equation 2:

$$y = \frac{Emax \times (\tau/K_A)^n \times [B]^n}{[B]^n \times (\tau/Ka)^n + (1 + [B]/K_B)^n}$$

Where Emax is the is the maximal possible response of the system (not the agonist), basal is the basal response in the absence of agonist (vehicle), K_B denotes the functional equilibrium dissociation constant of the agonist (B), τ is an index of the coupling efficiency (or efficacy) if the agonist and is defined as the total concentration of receptor required to elicit a given response divided by the concentration of agonist- receptor complex that yields half the maximal system response (Emax) and n is the slope of the transducer function that links occupancy to response.

τ/KA ratios were then normalised to that of a reference ligand (GLP-1(7-36)NH_2 or 1B) and a reference pathway (cAMP) to calculate $\Delta\Delta\tau/K_A$ ratios for comparison of signalling bias from novel peptide ligands and liraglutide relative to GLP-1(7-36)NH_2.

Inhibition binding data were fitted to the three parameter logistic equation in equation 3.

Equation 3.

$$y = Bottom + \frac{(Top - Bottom)}{1 + 10^{(\log [A]) - \log IC50)}}$$

Where bottom is binding of the radioligand in the presence of a saturating concentration of competition ligand that is equivalent to non-specific binding, Top is the specific binding of the radioligand in the absence of any competing ligand, [A] is the molar concentration of the competing unlabelled ligand and IC50 is the molar concentration of the unlabelled ligand that generates a response halfway between Top and Bottom.

The Black-Leff operational model of agonism (equation 4) was also applied to concentration response data in chapter 5 to determine functional affinity and efficacy.

Equation 4.

$$\mathrm{Y} = \mathrm{Bottom} + \frac{\mathrm{E_m} - \mathrm{Bottom}}{1 + \frac{10^{\log \mathrm{K_A}} + 10^{\log [\mathrm{A}]}}{10^{\log \tau + \log [\mathrm{A}]}}}$$

where Bottom represents the y value in the absence of ligand(s), E_m represents the maximal stimulation of the system, K_A is the agonist-receptor dissociation constant in molar concentration, [A] is the molar concentration of ligand and τ is the operational measure of efficacy in the system, which incorporates signalling efficacy and receptor density. All estimated τ values were then corrected to cell surface expression (τ_c) determined by whole cell ELISA as previously reported .

Equation 5.

$$\sqrt{((S.E.M1)^2 + S.E.M2)^2)}$$

To determine propagated error of the $\Delta\Delta\tau/K_A$ ratios, S.E.M1 refers to the standard error of the mean of ligand 1 and S.E.M2 refers to the standard error of the mean of ligand 2

2.8 Statistical tests

All data/estimated parameters were assessed by one way analysis of variance with a Dunnett's post hoc test was used to assess significance of ligands relative to the control ligand GLP-1(7-36)NH_2, or mutant receptors relative to the wildtype receptor. Statistical significance was accepted at $p<0.05$. Normalised data was analysed for statistical difference

2.9 Graphical Software

Figures were created in either Biorender (Biorender.com), PyMol or Graphpad Prism.

Chapter 3:
Assessing the bias of novel 11mer ligands at the glucagon-like peptide 1 receptor.

3.1 Introduction

The GLP-1R is an important target in the treatment of type 2 diabetes mellitus with multiple approved therapeutics targeting the receptor available. However, these therapeutics are associated with side effects, the most common of which is gastrointestinal discomfort and nausea, which has caused some patients to cease treatments with these therapeutics (Aroda, 2018)

The GLP-1R is a pleiotropically linked receptor that couples to multiple canonical and non-canonical signalling transducers, and thus is particularly prone to biased agonism, a phenomenon that describes the ability of a ligand to preference one signalling pathway over another relative to a reference agonist (e.g Koole et al., 2013). The GLP-1R has many known biased ligands, including the endogenous peptide oxyntomodulin as well as therapeutics such as exendin-4 and liraglutide, which display differing levels of bias relative to the native GLP-1 peptide and also relative to each other (Koole et al., 2013). Similar to other therapeutics that benefit from biased agonism (Whalen, Rajagopal, & Lefkowitz, 2011), there is potential that biased agonism could provide an answer to overcoming the side effect profiles of current GLP-1R agonists. By being able to link certain physiological effects to distinct signalling pathways, it may be possible to develop therapeutics that target the pathways that give the desired therapeutic outcomes while avoiding those which lead to side effects. To be able to determine which pathways are beneficial and which are detrimental, a greater range of ligands with novel bias profiles are needed to be able to test the physiological implications of biased agonism at the GLP-1R.

The potential of GLP-1R biased agonism was highlighted by the agonist exendin-P5, a recently identified biased ligand with a scaffold related to exendin-4, whereby it exhibits the same C-terminal sequence but a different N-terminal sequence (Zhang et al., 2015). Relative to exendin-4, this peptide favours G protein-mediated signalling events over β arrestin recruitment in cell-based studies, and when compared *in vivo* had a greater ability to correct hyperglycaemia while being a less efficacious insulin secretagougue, relative to exendin-4 in diabetic rodent models (Zhang et al., 2015). Moreover, it displayed enhanced adipogenesis. This data shows the potential a biased therapeutic can have in a disease setting. However, more

work is required to optimise this kind of ligand and also to explore how to develop such compounds to limit side effects while maximising positive effects.

Recent cryo-EM structures solved with various ligands bound to the GLP-1R (Liang et al., 2018b; Zhang et al., 2017) revealed that the first nine residues of these peptides reside in a binding pocket that extends relatively deep within the TM core of the receptor (coined the deep TM binding pocket). Coupled with the knowledge that the interaction between the N-terminus of the ligand and the extracellular portion of the TM core is critical for receptor activation (Hoare, 2005), short 11mer peptides were developed to specifically target the TM helical bundle of the receptor. These 11mer peptides containing a range of hydrophobic substitutions, designed to increase interaction with the TM core of the receptor. In addition, constraints to induce cyclisation were introduced to some of these peptides; modifications that can potentially enhance peptide stability, alter peptide absorption and/or enhance affinity and/or efficacy at the target receptor.

17 peptides were synthesised based on the first 11 residues of the native peptide with a linker inducing cyclisation between different substituted residues and various distances along the sequences (Hoang et al., 2015). This resulted in a vast diversity in affinity and cAMP potency. Only three of those peptides had affinity under 100nM and six with cAMP EC_{50}'s under 100nM with these being overlapping peptides. Of this subset, two of the peptides showed pharmacological properties most similar to GLP-1; peptide #3 had both affinity and cAMP potency approximately 10 fold less than the native GLP-1 peptide, and peptide #14, which had affinity approximately 30 fold lesser and equipotent cAMP response (Hoang et al., 2015). A series of 11mer peptides were also developed by Heptares in an effort to aid crystallisation of the GLP-1R (Jazayeri et al., 2017). The peptide used for structure, "Heptares P5", had reduced affinity compared to the native peptide GLP-1, but similar cAMP response. These publications on GLP-1R 11mer peptides showed it was feasible to create a shorter peptide with full receptor agonism even if they exhibited lower affinity in competition binding assays. In collaboration with Pfizer, a more extensive series of 11mer peptides, built around the scaffold 1B from the original paper (Hoang et al., 2015), were synthesised and these contained a range of additional hydrophobic substitutions within the sequence in and attempt to increase affinity for the receptor.

Given that a range of biased profiles have been observed with GLP-1R full length agonists, and the likelihood that the nature of the 11mer interactions with the GLP-1R differ significantly from that of full length peptides, it is also very likely that these types of ligands will induce significant bias relative to GLP-1 and to each other. Within this chapter, two cyclised peptides from Hoang et al., 2015 (3 and 14) and the range of 11mers developed by Pfizer, all based on the 1B scaffold, were screened in ligand competition binding assays and a range of common signalling pathways required for the actions mediated by the GLP-1R. 11mers were separated by either cyclisation/linearity or the composition of their first residue, which had three forms; the native histidine, a double aromatic with the same charge distribution as histidine or an aromatic with an altered charge distribution (Figure 3.1). The extensive characterisation of these 11mers described in this chapter will inform creation of further short, peptides with potentially improved bioavailability, for therapeutic use. In this context, we discovered novel biased agonism amongst these chemically distinct peptides and these may be useful tools to further dissect the physiological implications of biased agonism.

3.2 Results and discussion:

This study utilised an immortalised CHO FlpIn cell line stably expressing the GLP-1R (as is standard in the field for profiling novel ligands). For all ligands, concentration response curves were generated for cAMP accumulation, pERK1/2, intracellular calcium mobilisation and β arrestin recruitment. Historical data in testing bias for GLP-1 ligands has revealed similar profiles for numerous ligands when assessing β arrestin1 and β arrestin2 recruitment (Koole et al 2013). In this study, we decided to focus on β arrestin 1 recruitment to the GLP-1R, as it is known to have a role in GLP-1R mediated insulin secretion and β cell survival (Sonada et al 2014).

Due to the nature of the assays, calcium was captured in real time kinetic format, whereas pERK and β arrestin recruitment were determined as an endpoint assay at the peak response time for each ligand. To determine the appropriate time point, time-courses for pERK1/2 phosphorylation or β arrestin recruitment were first generated at a single concentration of peptide to assess if the kinetics for pERK1/2 and β arrestin recruitment differed from full length peptides, and to determine the appropriate time-point for generation of concentration response data (Figs S1 & S2). All peptides peaked between 6-8 mins for pERK1/2 and 2-3 mins for β

GLP-1(7-36)NH_2
HAEGTFTSDVSSYLEGQAAKEFIAWLVKGRG

Scaffold ligand
1B: H(Aib)EGT$X_{6.1}$TSD$X_{10}X_{11.2}$

H^1
453: H(Aib)EGT$X_{6.1}$TSDX_{10}Y
787: H(Aib)EGT$X_{6.1}$TSD$X_{10}X_{11.1}$
$X_{1/3}{}^1$
052: X_1(Aib)EGT$X_{6.2}$TSD$X_{10}X_{11.2}$
820: X_1(Aib)EGT$X_{6.2}$TSD$X_{10}X_{11.3}$
009: X_3(Aib)EGT$X_{6.1}$TSD$X_{10}X_{11.2}$
$X_2{}^1$
646: X_2(Aib)EGT$X_{6.1}$TSD$X_{10}X_{11.2}$
551: X_2(Aib)EGT$X_{6.1}$TSD$X_{10}X_{11.3}$
667: X_2(Aib)EGT$X_{6.3}$TSD$X_{10}X_{11.2}$
Cyclised

3: H(Aib)EGK$X_{6.1}$TSE$X_{10}X_{11.2}$

14: H^hCEG^{h}C$X_{6.1}$TSD$X_{10}X_{11.2}$

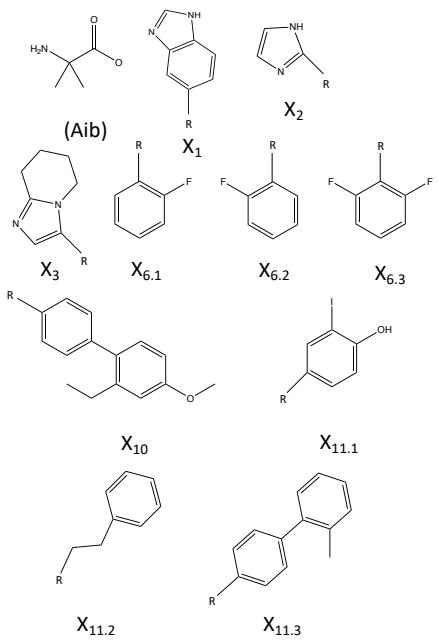

Figure 3.1: Structure of 11mer ligands. Aib = 2-aminoisobutyric acid, X1 = 3-Ethyl-5,6,7,8-tetrahydroimidazol[1,2-a]pyridine X2 = 2-Ethylimidazole, X3 = 5-Methyl-1H-benzimidazole X6.1 = αmethyl-2fluro-phenylalanine, X6.2 = αmethyl-5fluro-phenylalanine, X6.3 = αmethyl-2,5fluro-phenylalanine, X10 = biphenyl, X11.1 3-I-Y, X11.2 homo homo phenylalanine, 11.3 = 2-methylbiphenyl. 'R' is used to indicate attachment point to peptide backbone

arrestin recruitment, and therefore concentration response curves were generated at the same time-point (7mins) for all peptides assessed. Only β arrestin was assessed for recruitment as this is the arrestin shown to have physiological effects (Sonada et al 2014) and historical data in testing bias for GLP-1 ligands shows the two β arrestins are recruited similarly (Koole et al 2013).

3.2.1 Comparison of GLP-1 full length peptide vs scaffold 11mer 1B

In studying the structure activity relationship of the peptides it was observed that alanine substitutions to positions 1-9 (equivalent to 7-16 in GLP-1(7-36)NH_2) was particularly detrimental to cAMP accumulation (Adelhorst et al. 1994). To more explicitly explore the role of those first 9 residues have in activation of the GLP-1R a series of 11 amino acid peptides (11mers) were synthesised where the first 9 residues were identical to GLP-1 but the C-terminal 21 amino acids in the native peptide were replaced by two large hydrophobic aromatic residues. From this initial backbone, additional peptides were synthesised where an amino-isobutryic acid was substituted into position 2 to prevent DPPIV hydrolysis and thus extend plasma half-life for in vivo studies, and others that included substitution with a fluoridated aromatic at position 6 to induce helicity in the peptide (Mapelli et al., 2009)(Haque et al., 2010). This latter peptide was equipotent with GLP-1 in cellular assay of cAMP accumulation and had similar efficacy to exendin-4 in promotion of insulin secretion and control blood glucose in obese mice (Mapelli et al., 2009). This peptide (1A) was then further modified at the C-terminal residue, which replaced with a smaller aromatic residue yielding peptide (1B) that had slight improvements in affinity and potency in cAMP accumulation assays (Hoang et al., 2015). In the current study, 1B had lower affinity than GLP-1 (Figure 3.2A), likely due to less contacts between the peptide and receptor. 1B was also a full agonist in all pathways with no significant differences in the maximal responses measured between the two ligands (Figure 3.2C, 3.2E; Table 3.1) Equally, 1B had lower potency in all pathways relative to GLP-1, consistent with its lower affinity (Figure 3.2B, 3.2D; Table 3.1).

While the derived potency value for 1B in cAMP in this study is similar to that described in Hoang et al., 2016 (0.4nM vs 0.12nM), the derived binding inhibition values between the two studies are drastically different (approximately 500-fold). In this current study an antagonist probe was used for the binding studies, which will preferentially label the non-transducer bound state, whereas an agonist probe was used in Hoang et al., 2016, therefore preferentially

labelling the active state that will couple to transducer. The vast differences in observed pIC50/pKi values between the two studies suggests that the 11mer peptide has a higher affinity for the active state than the inactive state of the receptor. It also suggests that G proteins (ie Gs) are likely to greatly enhance the affinity of the 11mer peptide through allosteric coupling, as has been observed for multiple class A GPCRs (eg, Devree et al., 2016), although further studies will be required to confirm this. This is also likely to also be true for GLP-1, where studies using an antagonist probe generally provide lower affinity estimates with pKi values of 3-10 nM, compared to those using an agonist probe (0.1-1nM) (eg Wootten et al, vs 2016, Yang et al., 2016). Other differences in the assay format could also affect the apparent affinity of 1B in the two different studies. While the assay used in this chapter was performed in whole cells, the previous study was performed using membrane preparations. In addition, the antagonist probe used here can also bind extensively within the ECD, whereas the probe used in the published study was an 11mer peptide, assumed to bind predominantly to the transmembrane bundle. It may therefore be more difficult for an 11mer peptide to displace the probe in this current study as the probe will only partially overlap with the assumed binding site of the 11mer. This could therefore impact on the observed pIC50/pKi values in a competition binding assay.

Nonetheless, Peptide 1B was the base scaffold peptide for the remaining 11mers used in this study and therefore provides the reference peptide used throughout the remainder of the chapter.

3.2.2 1B scaffold modifications retaining linearity and H^1 at the N-terminus

Histidine is the native amino acid in the first position of endogenous GLP-1R agonists and for the majority of other native peptide ligands for class B GPCR peptides (Hollenstein et al., 2014). The two 11mer ligands 453 and 787, are based on the scaffold of 1B, each retaining histidine at position 1, all with residue 2 substituted by Aib. In addition, peptide 453 has a tyrosine in position 11 and 787 has an iodinated tyrosine in position 11 (Figure 3..1).
Both peptides had comparable affinities in competition for ^{125}I-exendin(9-39) binding, and potencies for stimulation of cAMP, iCa^{2+} and pERK1/2 pathways, and the potencies in these assays were similar to those observed with 1B (Figure 3.2A-3.2D).

		Affinity	cAMP		pERK1/2		iCa^{2+}		β-Arr1 recruitment	
		pIC50	pEC_{50}	E_{max}	pEC_{50}	E_{max}	pEC_{50}	E_{max}	pEC_{50}	E_{max}
NATIVE LIGAND	GLP-1(7-36)NH_2	8.27±0.09	10.39±0.16	100.00±4.90	8.82±0.12	100.00±4.07	7.43±0.10	100.00±4.70	7.70±0.15	100.00±5.69
SCAFFOLD LIGAND	1B	6.53±0.17*	9.33±0.19*	110.80±8.23	7.90±0.12*	129.90±6.99	5.99±0.14*	114.90±13.88	6.03±0.26*	96.10±19.17
CYCLISED LIGANDS	3	7.16±0.13*	7.19±0.22*$^{+}$	124.90±21.85	7.10±0.22*$^{+}$	71.93±8.79*$^{+}$	ND	ND	ND	ND
	14	5.66±0.19*	8.10±0.20*$^{+}$	97.62±10.33	7.60±0.16*$^{+}$	95.03±6.85^{+}	5.84±0.15*	128.20±21.26	ND	ND
H	453	6.07±0.23*	9.28±0.22*	94.57±8.34	7.79±0.10*	94.05±4.15^{+}	6.24±0.15*	101.00±10.43	ND	ND
	787	6.80±0.25*	9.56±0.28	64.86±6.12*$^{+}$	7.52±0.19*	124.2±10.26	6.31±0.11*	107.70±7.40	ND	ND
X1/3	052	5.66±0.28*	9.43±0.26	83.40±8.01	7.68±0.12*	95.92±5.21^{+}	6.25±0.14*	107.60±10.25	ND	ND
	820	5.99±0.25*	9.01±0.22	78.91±7.59	7.22±0.16*	105.30±8.61	6.06±0.12*	115.50±11.06	ND	ND
	009	6.37±0.23*	10.17±0.21	89.77±6.72	7.83±0.13*	114.90±6.56	6.88±0.09*	115.80±4.81	7.19±0.19	82.19±8.23
X2	646	5.42±0.49*$^{+}$	8.30±0.28*	83.02±10.95	7.22±0.29*$^{+}$	70.14±10.80*$^{+}$	ND	ND	ND	ND
	551	5.14±0.50*$^{+}$	7.99±0.19*$^{+}$	102.2±10.57	7.27±0.17*$^{+}$	78.72±6.76^{+}	ND	ND	ND	ND
	667	6.87±0.29*	8.17±0.21*	93.44±9.73	7.44±0.14*	79.06±5.36^{+}	6.41±0.66	24.67±12.87*	ND	ND

Table 3.1: Affinity and activity data derived from three parameter analysis to concentration response data for radioligand binding, cAMP accumulation, ERK1/2 phophorylation, iCa^{2+} mobilization and β-arrestin 1 recruitment, for 11mer ligands and GLP-1 at the GLP-1R. All experiments were performed in FlpIn CHO cells stably expressing the human GLP-1R. Data is normalised to the maximum response of GLP-1 in each assay and analysed using a three-parameter logistic equation. IC50 is the concentration of drug that inhibits 50 % of the bninding of the radioligand ^{125}Iexendin(9-39) and is representative of the affinity for the receptor. pEC_{50} is the negative algorithm of the concentration of ligand required to elicit 50% of the maximum response and E_{max} represents the maximum response of the ligand, expressed as a % of the response elicited by GLP-1. Values are mean±s.e.m and are representative of 3-4 independent experiments performed in duplicate. Maximum responses from incomplete curves are predicted from curve fitting (where possible). *Statistical significantly different from GLP-1 as determined by one-way analysis of variance with a Dunnetts post-test ($p < 0.05$). ND = not determined due to incomplete curves or no detectable response. $^{+}$Statistically different from 1B, using a one-way analysis of variance followed by Dunnett's post-test

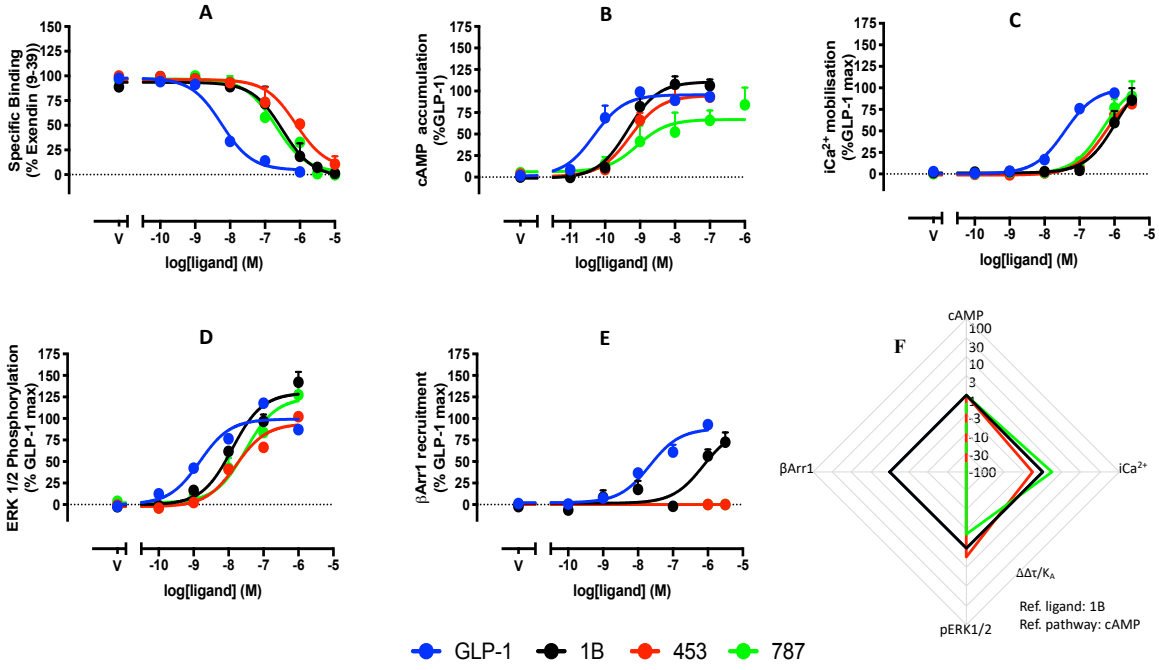

Figure 3.2: Signalling assays for 11mer ligands with histidine at position 1 (453 in red, 787 in green) with GLP-1 (blue) and 1B (black) for reference. ^{125}I-exendin(9-39) radioliagnd competition binding (**A**), cAMP accumulation (**B**), iCa^{2+} mobilisation (**C**), ERK1/2 phosphorylation (**D**), β Arrestin 1 recruitment (**E**) and web of bias (**F**) with $\Delta\Delta\tau/K_A$ values derived from operational fitting of the concentration response data and normalsed to 1B (ligand) and the cAMP accumulation (pathway). Dashed lines represent no bias detected at that pathway. Radioligand binding normalised to specific binding minimum and signalling normalised to GLP-1 Emax. **A-E** are mean + S.E.M and representative of 3-4 independent experiments performed in duplicate. Solid data points on **F** represent significant bias assessed by One Way ANOVA with Dunnetts post-test ($p<0.05$) compared to the 1B cAMP value

However, neither 453 nor 787 recruited β arrestins in the concentration range tested. Not surprisingly, when calculating bias there was little difference between the three 11mers and 1B for iCa^{2+} mobilisation and pERK1/2 compared to cAMP accumulation. As 453 and 787 did not recruit arrestin but were equipotent in all other pathways, these 11mer are biased away from β arrestin recruitment towards each of the second messenger pathways, however, this bias could not be quantified as a β-arrestin recruitment concentration-response curve could not be established for 453 and 787 (Figure 3.2; Table 3.1).

Considering the similarity within these peptide sequences this difference in ability to recruit β arrestins is extremely interesting; the three ligands differ only in the final (11th) residue where 1B has a homo homo phenylalanine (hhf), 453 has a tyrosine and 787 has a tyrosine with an iodinated third carbon (Figure 3.1). In contrast to these peptides, the Heptares P5 11mer promotes arrestin recruitment with very similar potency to the native GLP-1 peptide and 1B. Interestingly, this peptide contains a residue similar to the hhf in peptide 1B. In the solved X-ray crystal structure of Heptares P5 bound to the GLP-1R (Jazayeri et al., 2017), the C-terminus of the peptide is located within a hydrophobic pocket between TM1 and the TM2 ECL-1 boundary, but may also form interactions with the lipid bilayer. Both the 1B and Heptares P5 11mers have an extended 3 carbon linker between the aromatic ring at this position and the peptide backbone, whereas the two tyrosine-containing 11mers only have a single carbon linker. Interestingly, in the Heptares P5 11mer bound GLP-1R crystal structure, the additional length of this linker places the aromatic headgroup in close proximity to ECL1, ECL2 and the N-terminal helix of the GLP-1R extracellular domain, where it forms interactions with residues in each of these domains, thus stabilising these
regions (Jazayeri et al., 2017) (Figure 3.3). In contrast, a shorter linker would place the tyrosine in a distinct position where it would be unable to form interactions with all
three domains. 11mers with the shorter linker would therefore stabilise a distinct conformation of the bundle and ECD relative to those with the longer linkers, such that the receptor can still efficiently activate Gαs recruitment, but has impaired arrestin recruitment. Interestingly, GLP-1 and exendin-P5 peptides have a serine, a small uncharged sidechain, in the equivalent position (amino acid 11) of their sequences that forms multiple contacts with the extracellular domain and extracellular loops, as observed in the recent exendin-P5 cryo-EM structure (Liang et al., 2018b). However, exendin-P5 and GLP-1 are full-length peptides that form extensive interactions with the ECD, ECL1 and ECL2 stabilising these domains and the biased agonism

that occurs between these peptides is likely to be driven by a distinct mechanism to the biased agonism of 453 and 787.

3.2.3 Cyclised peptides.

Peptides 3 and 14 (Figure 3.1) were first reported in Hoang et al., 2016. These peptides were built upon the scaffold 1B but have different primary sequences to each other. Cyclisation to further induce tertiary structure in the peptides was induced either by adding a lactam bridge between a lysine at position 5 and a glutamic acid at position 9 in the 11mer peptide 3, or a disulphide bond between two homo-cysteines substituted at positions 2 and 5 in the 11mer, peptide 14 (Figure 3.1). These peptides, as well as the scaffold 11mer peptide 1B have previously been published with parameters reported for affinity and cAMP signalling (Hoang et al., 2015). In concordance with the original paper, the scaffold peptide 1B displayed nM potency for cAMP production despite only having an affinity of ~300nM (Figure 3.2A, Table 3.1). Both peptide 3 and peptide 14 displayed lower potency for cAMP accumulation than the scaffold 1B (Figure 3.4 Table 3.1). Interestingly, peptide 3 displayed a 3-fold higher affinity than 1B, but was 100-fold less potent in inducing cAMP signalling. In contrast, peptide 14 displayed ~10-fold reduced affinity and cAMP potency, relative to 1B (with no significant change in Emax) (Figure 3.4A, 3.4B; Table 3.1). Interestingly, while peptide 14 was approximately 10-fold more potent in cAMP accumulation assays than peptide 3, it displayed 10-fold lower affinity. The rank order of potency in cAMP accumulation assays, 1B>14>3, was the same as described in the original paper, however, the rank order of affinity was distinct from that reported in the original article (1B>3>14) compared to our data (3>1B>14) but the difference may be due to a difference in radioligand used in the Hoang et al paper they use a radiolabelled 11mer agonist. . The distinction in affinity-cAMP potency ratio between peptide 3 and peptide 14 suggests that peptide 14 has much higher efficacy for the cAMP pathway compared to peptide 3. Extending the analysis beyond that in the published paper, the profiles of these peptides were assessed using other signalling endpoints (Figures 3.4C-E). While the scaffold ligand 1B was able to promote calcium mobilisation and recruit β arrestin-1 with a similar potency to its observed affinity, neither cyclised 11mer was able to recruit β arrestins, and peptide 3 was also unable to stimulate intracellular calcium mobilisation at the concentration range tested (Figure 3.4C).

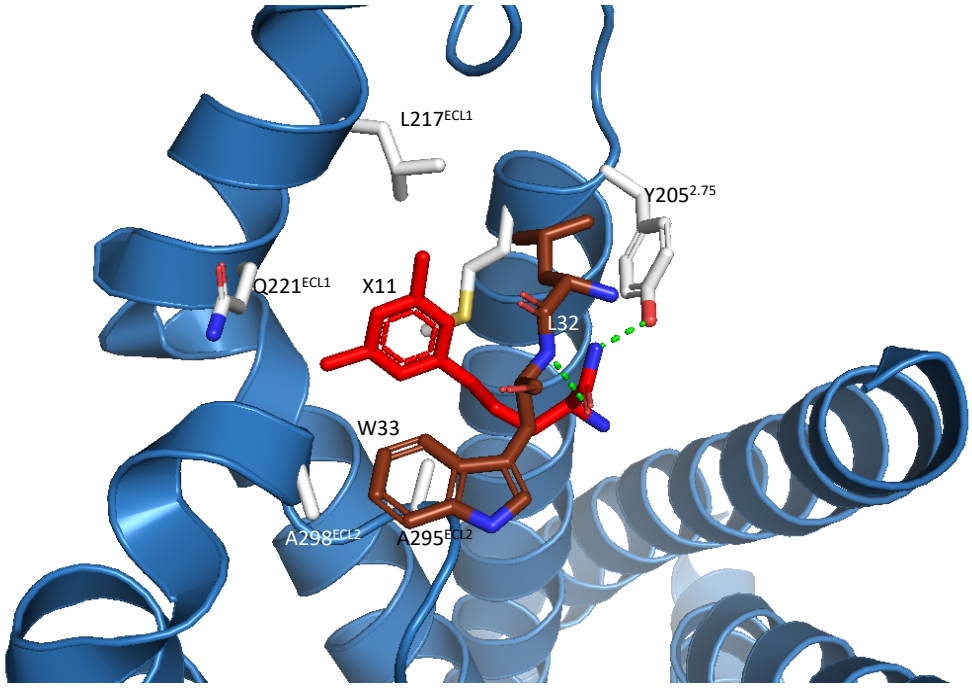

Figure 3.3: Binding pose of the X11 residue of the Heptares P5 modelled into a crystal structure of the GLP-1R bound to the 11mer ligand and the residues that are within 5 Å of the X11 residue. Side chains of the receptors are shown in white, the ligand is in red. Hydrogen bonds formed between the ligand and receptor are shown in green. Residues in the ECD are shown in brown as they are not part of the original structure but part of the ECD crystal structure solved by Underwood et 2011 modeled onto the crystal structure by Jazayeri et al., 2017.

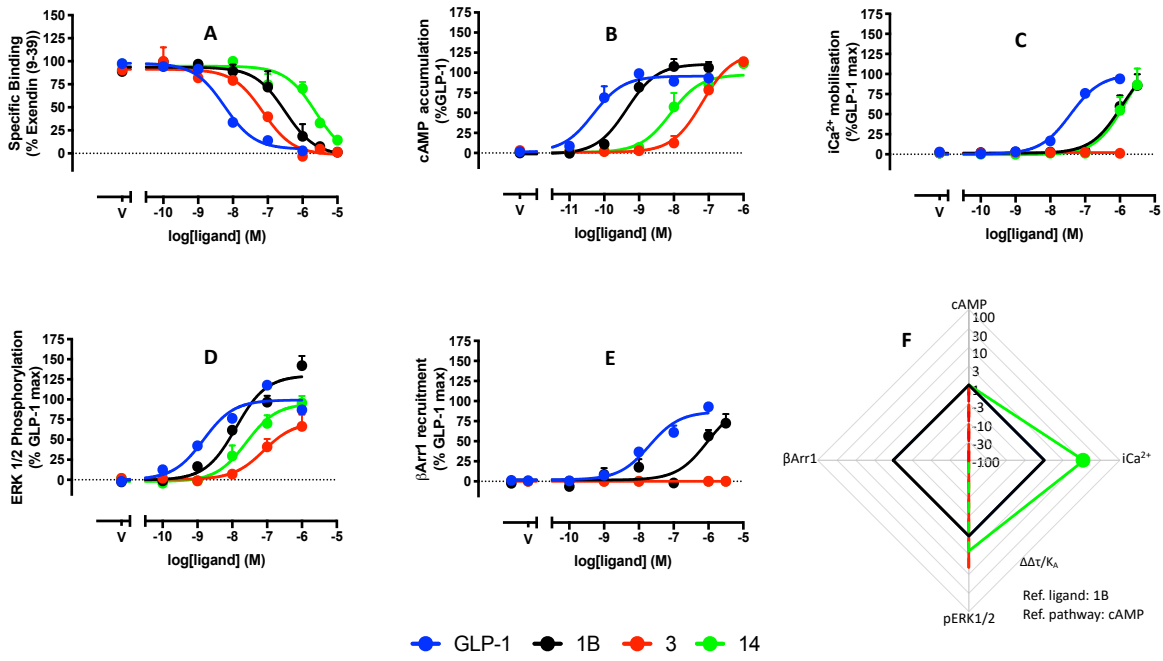

Figure 3.4: Signalling assays for 11mer ligands with cyclic constraints (3 in red, 14 in green) with GLP-1 (blue) and 1B (black) for reference. ^{125}I-exendin(9-39) radioliagnd competition binding (**A**), cAMP accumulation (**B**), iCa^{2+} mobilisation (**C**), ERK1/2 phosphorylation (**D**), β Arrestin 1 recruitment (**E**) and web of bias (**F**) with $\Delta\Delta\tau/K_A$ values derived from operational fitting of the concentration response data and normalsed to 1B (ligand) and the cAMP accumulation (pathway). Dashed lines represent no bias detected at that pathway. Radioligand binding normalised to specific binding minimum and signalling normalised to GLP-1 Emax. **A-E** are mean + S.E.M and representative of 3-4 independent experiments performed in duplicate. Solid data points on **F** represent significant bias assessed by One Way ANOVA with Dunnetts post-test ($p<0.05$) compared to the 1B cAMP value

In contrast, peptide 14 was able to stimulate intracellular calcium, with an EC_{50} equivalent to 1B (Figure 3.4C, Table 1). All 3 11mers stimulated ERK1/2 phosphorylation with the same rank order of potency to that observed in cAMP accumulation assays (1B>14>3) (Figure 3.4D versus 3.4B, Table 3.1).

As both the 1B scaffold and peptide 14 are full agonists in cAMP, pERK1/2 and calcium mobilisation assays, comparison of their EC_{50} and IC_{50} values provide an indication of their efficacy in each pathway. Comparisons of these parameters suggest that while 1B may be more efficacious in promoting cAMP accumulation than peptide 14 (ratios of 1:75 and 1:250, respectively), peptide 14 is more efficacious in pERK1/2 and iCa^{2+} mobilisation assays (ratios of 33:1 and 1:2, and 10:1 and 1:1, respectively) (Table 3.1). This suggests that peptide 14 is a biased agonist relative to 1B. Application of the operational model to the concentration response data enabled the $\Delta\Delta\tau/Ka$ that describes the relative bias relative to 1B and the cAMP accumulation assay to be derived. This analysis confirmed that peptide 14 had significant bias towards iCa^{2+} mobilisation and showed a trend in bias towards the pERK1/2 pathway, relative to 1B and cAMP response (Figure 3.4F and Table 3.2).

While the peptide 3 11mer clearly has lower efficacy (despite higher affinity) across all pathways relative to 1B and peptide 14, when comparing the two pathways where peptide 3 was able to induce a robust response (cAMP and pERK), the peptide pEC_{50} values were similar to its measured affinity (approx. 100nM). Interestingly, this ligand was a full agonist for cAMP signalling where the maximal response measured was not significantly different to 1B, but in contrast, it was a partial agonist for pERK1/2 where the maximal response for pERK1/2 was significantly lower for peptide 3 relative to 1B (Table 3.2). This suggests that peptide 3 is a more efficacious cAMP agonist than it is for pERK1/2. Nonetheless, this is also true for 1B and peptide 14, and calculation of bias factors revealed that peptide displays bias towards ERK phosphorylation relative to cAMP accumulation when compared with the scaffold ligand 1B, and this bias is larger than that observed with peptide 14, albeit that it did not reach statistical significance (Figure 3.4F, Table 3.2). Neither peptide 3 or peptide 14 were able to recruit arrestin in the concentration range tested so the potential for bias at this pathway could not be quantified.

It is known that the first five residues of GLP-1R full length peptide agonists sit deep within the transmembrane bundle. But given the added bulk of the cyclised peptides in this N-terminal

segment, it is unlikely these peptides would fit inside the same cavity on the GLP-1R structure. The loss of affinity is most likely explained by a reduction in interactions between ligand and receptor compared to full length peptides. There are multiple ligands for class B GPCRs that have a 'cyclised' N-terminus, such as calcitonin, and structures of this (Liang et al., 2017) and other ligands with novel N-terminal chemistry (exendin-P5) (Liang et al., 2018b) have revealed a larger cavity in the extracellular surface of the receptor relative to other Class B GPCR structures which allows these ligands to bind to equivalent depth in the pocket (Liang et al., 2020). The 2018 Liang et al paper detailing the exendin-P5 structure revealed a difference in conformation of ECL3 compared to GLP-1 that led to the larger binding pocket. A similar outwardly shifted conformation of ECL3 was also seen in the structure of GLP-1R bound to small molecule agonist TT-OAD2 (Liang et al. 2020) and interestingly this ligand also exhibits poor arrestin recruitment. This could imply that conformation of, or interactions with ECL3, are important for arrestin recruitment and generation of the bias profile for these and other peptides. Similarly, calcitonin, which does not promote recruitment of arrestins (Dal Maso et al., 2018) has a cyclised cap at the N-terminus, and in solved structures with its receptor there is a more open helical bundle (dal Maso et al., 2019). These ligands bind deep within the bundle similar to non-cyclised peptides (Liang et al., 2020) but also alter the conformation of the TM6/ECL3/TM7 region, which could explain the poor arrestin coupling. Peptide 14's ability to activate iCa^{2+} with comparable potency to 1B indicates a potentially shared mode of receptor interaction between the two peptides that is linked to G protein coupling. Given the differences in bulkiness and sequence between 1B and peptide 14 in the N-terminus of the peptides, it is possible that shared interactions in the C terminus could contribute to this conserved mode of signalling. However, by analogy to the Heptares P5 11mer-GLP-1R crystal structure these interactions would be primarily with ELC3, which in mutagenesis studies has limited impact for iCa^{2+} signalling, relative to mutation of the TM2/ECL1 boundary or ECL2 (Wootten et al., 2016b). As such, this may imply that the 11mer peptides form a less stable position in the pocket, as indexed by their lower binding affinity, and consequently may make more transient

	Ligands					
			Cyclised		H[1]	
pathway 1:	GLP-1(7-36)NH_2	1B	3	14	453	787
pathway 2:						
pERK1/2						
cAMP	0±0.2(1)	0.31±0.20(0.43)	1.13±0.30(13.61)*	0.71±0.28(5.08)	0.05±0.26(1.12)	-0.19±0.28(0.65)
iCa^{2+}	0±0.14(1)	0.63±0.14(4.26)*	ND	-0.02±0.23(0.95)	0.21±0.21(1.60)	-0.02±0.15(0.95)
β-Arr1	0±0.24(1)	-0.58±0.32(0.26)	ND	ND	ND	ND
iCa^{2+}						
cAMP	0±0.19(1)	-0.32±0.21(0.47)	ND	0.73±0.26(5.33)*[+]	-0.16±0.24(0.7)	-0.16±0.28(0.69)
pERK1/2	0±0.14(1)	-0.63±0.14(0.23)*	ND	0.02±0.23(1.05)	-0.21±0.21(0.63)	0.02±0.15(1.05)
β-Arr1	0±0.23(1)	-0.05±0.4(0.9)	ND	ND	ND	ND
β-Arr1						
cAMP	0±0.27(1)	-0.28±0.19(0.53)	ND	ND	ND	ND
pERK1/2	0±0.24(1)	0.58±0.32(0.26)	ND	ND	ND	ND
iCa^{2+}	0±0.23(1)	0.05±0.4(1.11)	ND	ND	ND	ND

	Ligands						
		X_1/X_2[1]				X_3[1]	
pathway 1:	GLP-1(7-36)NH_2	052	820	009	646	551	667
pathway 2:							
pERK1/2							
cAMP	0±0.2(1)	-0.48±0.31(1.11)	-0.19±0.31(0.76)	-0.61±0.23(0.25)	0.48±0.32(3.02)	0.68±0.23(4.73)	0.58±0.26(3.78)
iCa^{2+}	0±0.14(1)	-0.27±0.23(0.54)	-0.19±0.23(0.64)	-0.3±0.21(0.50)		ND	ND
β-Arr1	0±0.24(1)	ND	ND	-0.08±0.28(0.84)	ND	ND	ND
iCa^{2+}							
cAMP	0±0.19(1)	-0.21±0.27(0.62)	0.08±0.3(1.19)	-0.31±0.31(0.59)	ND	ND	ND
pERK1/2	0±0.14(1)	0.27±0.23(1.85)	0.19±0.23(1.56)	0.3±0.21(2)	ND	ND	ND
β-Arr1	0±0.23(1)	ND	ND	0.22±0.28(1.66)	ND	ND	ND
β-Arr1							
cAMP	0±0.27(1)	ND	ND	-0.53±0.34(0.3)	ND	ND	ND
pERK1/2	0±0.24(1)	ND	ND	0.08±0.28(1.2)	ND	ND	ND
iCa^{2+}	0±0.23(1)	ND	ND	-0.22±0.28(0.60)	ND	ND	ND

Table 2: Bias factors derived from (τ/K_A) values normalised to GLP-1 values to give ($\Delta\tau/K_A$) values for 11mers to give value to the bias between pathways; cAMP against pERK1/2, cAMP against iCa^{2+}, cAMP against β-arrestin 1 recruitment, pERK1/2 against iCa^{2+}, pERK1/2 against β-arrestin 1 recruitment, and iCa^{2+} against β-arrestin 1 recruitment. Values are the mean ± SEM of three to four individual experiments, conducted in duplicate. *Statistically significantly different from GLP-1, $^{+}$Statistically different from 1B, using a one-way analysis of variance followed by Dunnett's post-test

or have fewer interactions with the extramembranous portion of the receptor resulting in a lower iCa^{2+} response relative to full-length peptides. Reduced calcium signalling for these 11mer ligands as a whole may be due to a paucity of interactions with ECL2.

3.2.4 1B scaffold with X^1/X^3 substitutions at position 1

11mers in this subset (052, 820, 009) all have an extended aromatic in the first position with a double aromatic ring, that includes the imidazole ring present in histidine. 052 and 820 contain the same group (3-Ethyl-5,6,7,8-tetrahydroimidazol[1,2-a]pyridine), whereas 009 contains a slightly different group (5-Methyl-1H-benzimidazole), the difference between X^1 and X^3 being the location of the imidazole ring either on the lower aromatic (X^1) or upper aromatic (X^3) in the structure (Figure 3.1).

11mer 009 is essentially the same as 1B, but with the aforementioned aromatic substitution at position 1. This peptide had a similar affinity and pERK1/2 signalling profile to 1B but was greater than 10-fold more potent for cAMP accumulation, iCa^{2+} mobilisation and β-arrestin recruitment, achieving a similar potency to the native GLP-1 peptide, albeit with lower affinity than GLP-1 (Figure 3.5). In the overall bias profile this therefore presents as a trend towards bias away from the pERK1/2 pathway relative to cAMP accumulation (Figure 3.5F), but the bias away from pERK is also true relative to iCa^{2+} mobilisation and β-arrestin recruitment, which have the same enhanced potency for 009 relative to 1B that is observed with cAMP accumulation assay.

The histidine in the native GLP-1 peptide sits in a pocket formed by $Q234^{3.37}$ $V237^{3.40}$, $Y241^{3.44}$, $W306^{5.36}$ and $I313^{5.43}$ (Figure 3.6), with molecular dynamic studies showing the histidine to be relatively mobile in the binding pocket (Yang et al., 2016). Interestingly, the cap motif for the Heptares P5 11mer is similar to histidine, however, assumes a different position compared to histidine in the native ligand, sitting deeper within the bundle then GLP-1 (Jazayeri et al., 2017). This may be due to the extended linker of the first residue, and larger second residue of Heptares P5, altering the interactions in the pocket. The N-terminus of the 11mers assessed in this study (excluding 11mer peptide 14) are generally more similar to GLP-1, so the position of the first residue is more likely to mimic the position of the native ligand. While the originally published GLP-1-GLP-1R cryo-EM structure had ambiguous density for

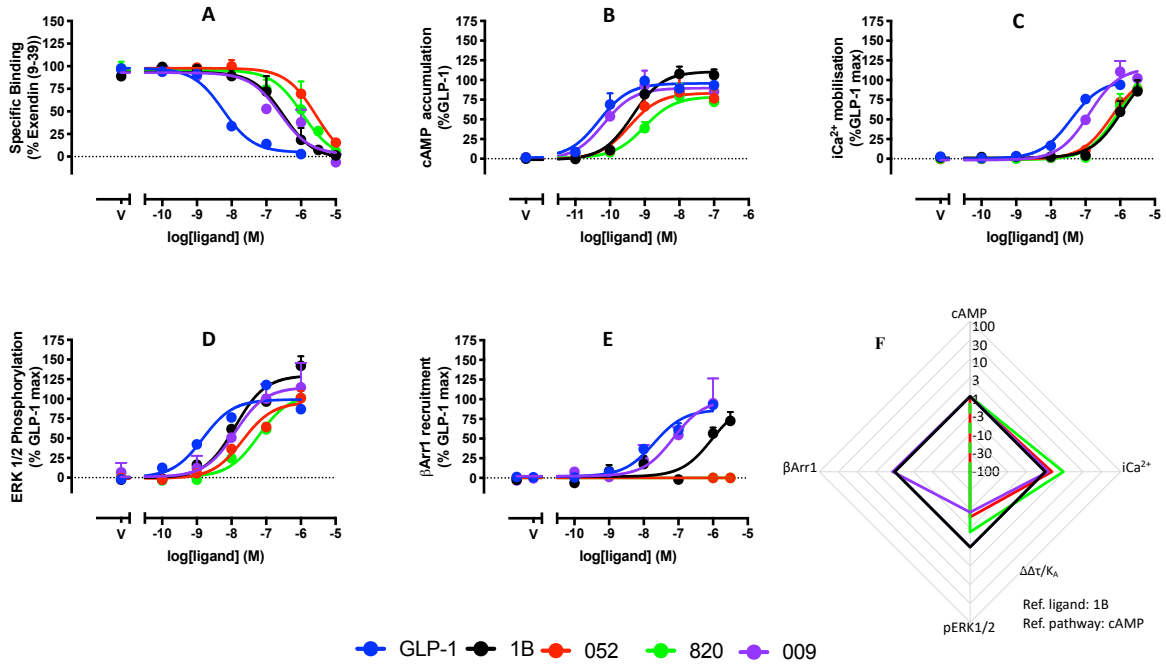

Figure 3.5: Signalling assays for 11mer ligands with amino acid X^{1}/X^{3} at position 1 (052 in red, 820 in green and 009 in purple) with GLP-1 (blue) and 1B (black) for reference. ^{125}I-exendin(9-39) radioliagnd competition binding (**A**), cAMP accumulation (**B**), iCa^{2+} mobilisation (**C**), ERK1/2 phosphorylation (**D**), β Arrestin 1 recruitment (**E**) and web of bias (**F**) with $\Delta\Delta\tau/K_A$ values derived from operational fitting of the concentration response data and normalsed to 1B (ligand) and the cAMP accumulation (pathway). Dashed lines represent no bias detected at that pathway. Radioligand binding normalised to specific binding minimum and signalling normalised to GLP-1 Emax. **A-E** are mean + S.E.M and representative of 3-4 independent experiments performed in duplicate. Solid data points on **F** represent significant bias assessed by One Way ANOVA with Dunnetts post-test ($p<0.05$) compared to the 1B cAMP value

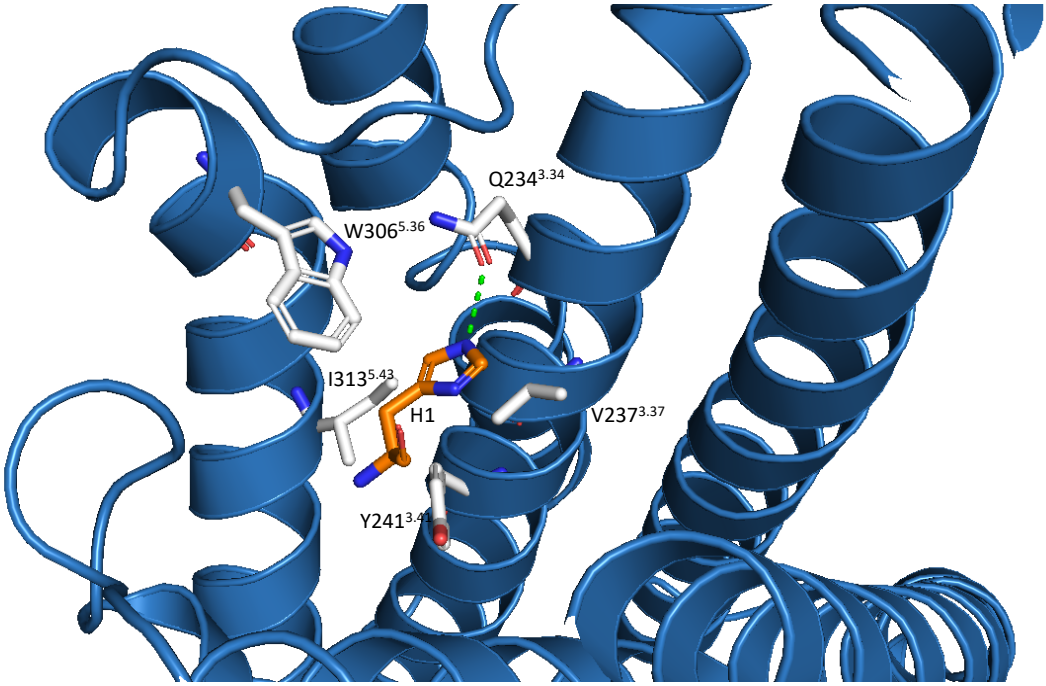

Figure 3.6: Binding pocket of the histidine in position 1 modelled into a Cryo-EM structure of the GLP-1R bound to the native peptide and the residues that are within 5 Å of the histidine. Side chains of the receptors are shown in white, the ligand is in orange. Hydrogen bonds formed between the ligand and receptor are shown in green (Jayazera et al 2017).

the N-terminal peptide histidine (Zhang et al., 2017), new structures solved in our laboratory enable confident placement of this residue within density (Figure 3.5). There is the potential that, by adding bulk to the residue at the first position in the 11mer peptide 009, but maintaining the aromatic nature of the side-chain, similar interactions within the deep helical binding site occur, but that the greater bulk of this residue may limit some of its mobility. This, in turn, could lead to increased signalling for the peptide in cAMP, calcium and arrestin pathways. Interestingly, this single substitution, did not have any effect on the peptides ability to signal through the pERK1/2 pathway relative to 1B, (Figure 3.5D and Table 3.1). This indicates that pERK1/2 signalling may be dictated through other ligand-receptor interactions. Interactions in extracellular loop 3 has been shown to be important for linking the receptor to pERK signalling. In the GLP-1R X-ray structure with the Heptares P5 11mer agonist, ECL3 residue D372 formed interactions with the T11 residue in the peptide and D15
formed an interaction with R380, which sits in the TM7-ECL3 interface (Jazayeri et al., 2017) and this is similar to interactions seen between ECL3 and equivalent peptide residues in the exendin-P5 bound GLP-1R structure (Liang et al., 2018b). Mutagenesis studies where these residues were substituted with alanine had a negative impact of pERK1/2 efficacy, with limited effect on cAMP and calcium responses for full length ligands including GLP-1, exendin-4 and oxyntomodulin (Wootten et al., 2016b). Both T11 and D15 are also conserved in 009 and 1B and thus similar interactions of these peptide 11mers with ECL3, to those seen in the Heptares P5 structure, could provide an explanation for their similar pERK1/2 signalling.

11mers 052 and 820 that both contain the X^1 residue substitution have very similar behaviour. They have reduced affinity and efficacy for cAMP and pERK1/2 responses but are equipotent in the iCa^{2+} pathway, when compared to 1B. Neither of these peptides were able to recruit arrestins in the concentration range tested. These X^1 substituted peptides differed from 009 by both the residues at position 1, and the location of the fluorine group on the aromatic ring on residue 6 (Figure 3.1). 052 and 820 differed in the residue at position 11, where 052 was hhf the same as the parent scaffold and 009, whereas 820 has a 2-methybiphenyl (2'-MeBip), which is two benzene rings connected by a carbon linker. This change resulted in a small decrease in the ligand affinities, but very little difference (no significant change) to cAMP,
calcium or pERK1/2 signalling compared to each other, or compared to 1B, where both were full agonists with potencies within 3 fold of 1B, and this is reflected in the web of bias (Figure 3.5F) where no bias for these pathways was observed. In contrast, neither 052 or 820 were able

to recruit β arrestins to the GLP-1R (Figure 3.5E). This could reflect the small loss in affinity relative to 1B that itself is a low potency agonist, and higher concentrations of agonist may be required to generate a response. Nonetheless, as these ligands were equipotent to 1B in cAMP and calcium, this suggests that these peptides are biased away from β arrestin recruitment relative to these pathways as the β arrestin potency would be greate”r than 10-fold reduced to relative to 1B, however we could not quantify the extent of bias due to lack of response in the β arrestin recruitment assay.

3.2.5 1B scaffold with X^2 substitutions at position 1

The ligands in the X^2 (2-Ethylimidazole) class each contain an altered imidazole group in position 1, where the position of the nitrogen is altered relative to histidine (Figure 3.1). Aside from the residue in this position, the remainder of 646 is identical to 1B. 551 differs from 646 in its 11^{th} residue, where the 2'-MeBip group is replaced by hhf, whereas 667 differs from 646 in its 6^{th} position where the benzyl fluorine contains an additional fluorine group (Figure 3.1). The ligands in this class had the lowest activity of any of the ligand classes assessed. They all had lower affinity (10-fold) than the scaffold ligand (Figure 3.7A) and this was also reflected in lower potency in every pathway where a response could be detected (cAMP and pERK1/2) (Figure 3.7A-E). The lack of response in iCa^{2+} mobilisation or β arrestin recruitment in the concentration range tested may also be reflective of the lower affinity. As such, relative to 1B, there was no significant bias, however as β arrestin recruitment and calcium mobilisation responses could not be quantified, there is the possibility that some bias occurs.

Collectively, these results demonstrate the relative importance the first residue in GLP-1R peptide agonists. Merely altering the position of the nitrogen in the imidazole ring, as observed for 646, alters the ability of these peptides to engage the receptor and promote signalling, likely through altering the way that residue sits in the binding pocket. Speculatively, it is likely that hydrogen bonding of peptide ligands with polar residues within the peptide binding pocket, such as $Q234^{3.37}$ play a role in peptide mediated receptor affinity and activation, as mutation to these residues resulted in a cAMP potency shift to peptide agonists at the GLP-1R similar to the shift observed in the potency of these ligands relative to the scaffold shown by data in chapter 5. Ligands with X^1 at position 1 have similar affinity to ligands with X^3 but they still have comparable potency to 1B and are able to promote iCa^{2+} signalling, indicating that

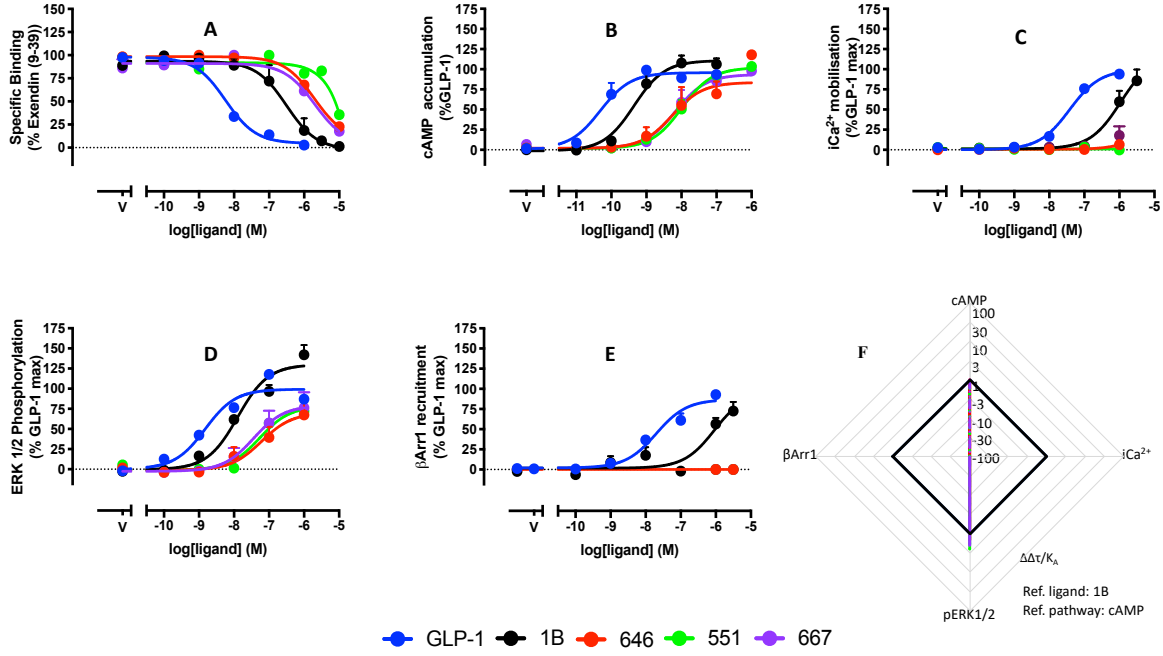

Figure 3.7: Signalling assays for 11mer ligands with amino acid X^{2} at position 1 (646 in red, 551 in green and 667 in purple) with GLP-1 (blue) and 1B (black) for reference. ^{125}I-exendin(9-39) radioliagnd competition binding (**A**), cAMP accumulation (**B**), iCa^{2+} mobilisation (**C**), ERK1/2 phosphorylation (**D**), β Arrestin 1 recruitment (**E**) and web of bias (**F**) with $\Delta\Delta\tau/K_A$ values derived from operational fitting of the concentration response data and normalsed to 1B (ligand) and the cAMP accumulation (pathway). Dashed lines represent no bias detected at that pathway. Radioligand binding normalised to specific binding minimum and signalling normalised to GLP-1 maximum. **A-E** is mean + S.E.M and representative of 3-4 independent experiments performed in duplicate. Solid points on **F** represent significant bias assessed by One Way ANOVA with Dunnetts post-test ($p<0.05$).

reduced affinity is not the only factor in reducing the ability of these ligands to signal. It is likely that a specific set of interactions are required to promote receptor activation, and that switching the position of the polar atom within this residue alters the receptor interaction pattern resulting in a less efficacious ligand than is observed with the X^3 substitutions. With less stable/fewer interactions in the binding pocket, reduced residency time could contribute to lower signalling, particularly through the iCa^{2+} pathway. There is evidence of this with other GPCRs, including the class A NK1 receptors, B2 adrenoceptor and endothelin receptors, where altered ligand residency is linked to changed signalling profiles (McCorvy et al., 2017), and within class B GPCRs there is evidence of different kinetics affecting signalling for the PTH receptor therapeutics (Vilardaga et al, 2011).

3.2.6 Overall comparisons to GLP-1

When comparing these 11mer peptide ligands to the native GLP-1 peptide as the reference, similar trends for biased agonism are observed to calculated with peptide 1B as the reference (Figure 3.8), however, the extent of biased agonism is greater relative to GLP-1 and this is most likely due to GLP-1's more potent activity in the cAMP pathway compared to 1B. For example, peptide 3 is significantly biased towards pERK1/2 compared to cAMP with GLP-1 as the reference peptide, whereas the bias did not achieve statistical significance with 1B as the reference (Figure 3.8 versus 3.4F). Interestingly, the pattern of biased agonism observed for the 11mer peptides in the current study was distinct from the published biased agonism profile of other GLP-1R agonists. The two most studied ligands, the endogenous peptide oxyntomodulin and the therapeutic agonist, exendin-4, are both biased towards β arrestin 1 recruitment, and oxyntomodulin is also biased towards pERK1/2, relative to GLP-1 and cAMP accumulation (Pabreja et al., 2014). Another therapeutic, liraglutide, is also biased towards pERK1/2 (Fletcher et al., 2018). In another study, a series of full length ligands with altered amino acids in various places along the peptide were synthesised with intent to examine their potential to exhibit altered signaling bias. Indeed, various different biased agonists were identified, with some peptides biased towards pERK1/2 and β arrestin recruitment, relative to GLP-1 and cAMP accumulation, similar to oxyntomodulin (Hager et al., 2017). However, one peptide was biased towards β arrestin recruitment and away from iCa^{2+} mobilisation, relative to the reference ligand. 11mer peptide 14 had novel biased agonism relative to any other peptide that has been assessed, exhibiting bias towards iCa^{2+} mobilisation relative to GLP-1. Peptide 3 is also an interesting case, with no observable signal for either iCa^{2+} mobilisation or β arrestin

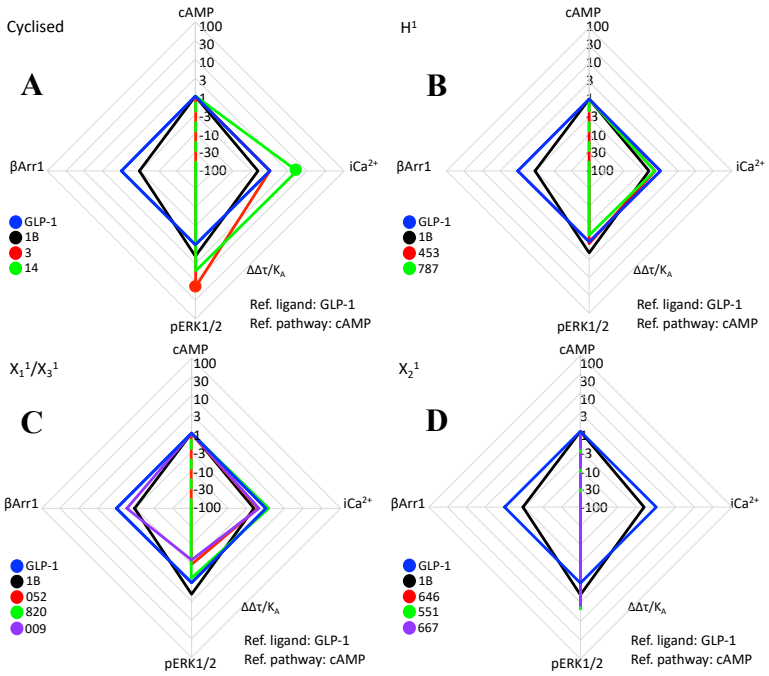

Figure 3.8: Web of bias for 11mer peptide agonists relative to GLP-1. (**A**) cyclised ligands (1B, 3 and 14) (**B**) H^1 ligands (1B, 453 and 787) (**C**) X_1/X_3^1 (1B, 052, 820 and 009) and (**D**) X_2^1 (1B, 646, 551 and 667) The τ/KA ratio extracted from standard concentration-response data using operational modeling is used to calculate bias factors (ΔΔ(τ/KA) through normalization of the transduction coefficient (τ/KA) to a reference ligand (GLP-1) and reference pathway (cAMP accumulation). Circles represent data that are significantly different by One Way ANOVA, with Dunnetts post-hoc test. $P<0.05$ was considered significant. Quantitative data are shown in Table 3.2.

recruitment but a significant bias towards pERK1/2. These peptides may be useful to probe the role of pERK1/2, with limited influence from other pathways, although other differences in signalling from pathways not assessed in the current study are possible. It is important that the recombinant expression system used to profile the peptides in the current study is not a cell line relevant to GLP-1 physiology. Nonetheless, there is some evidence to suggest that pERK1/2 bias can be translated from CHO cells to INS-1 cells (rat β cell insulinoma cells) (Wootten et al., 2016), but if, and how, it transfers into human tissue is unknown. Newer data suggests that the conformation of the ECD and TM6&7 play a role in generation of different bias (Wootten et al 2016a), and, as mentioned above, other GLP-1 peptides with a unique N-terminus can have more open bundles arising from different conformations of TM 6 and 7, and similar signalling profiles to some of the 11mer peptides; relatively strong cAMP response with weak iCa^{2+} mobilisation and arrestin recruitment. Therapeutically, 11mers could provide distinct advantages over full length ligands. As seen in the current data they can have unique signalling, and they are likely to have higher oral bioavailability and lower cost to manufacture than full length peptides. Moreover, they appear to better recapitulate cAMP signalling than currently described small molecule ligands (Freeman et al., 2016)(Thompson et al. 2016)(Nolte et al., 2014)(Chen et al., 2007).

Nonetheless, the potential of such 11mer peptide ligands as therapeutics is dependent on the amino acid substitutions being tolerated in humans. Furthermore, the inclusion of bulky hydrophobic residues would likely alter the volume of distribution compared to full-length peptides (Datta-Mannan 2019), and thus the delivery and bioavailability would need to be empirically determined and optimised. For research purposes, the difference in chemistry for these ligands compared to other ligands and the novel biased agonism displayed by some of these peptides, makes them interesting tools for understanding receptor structure-function, including how residence time at the receptor affects the kinetics of signalling, and in understanding of peptide-receptor interactions that can lead to bias and eventually the role of bias in physiological settings. Thus, these tools serve an important purpose in the eventual goal of rational drug design for the GLP-1R, harnessing biased agonism for therapeutic advantage.

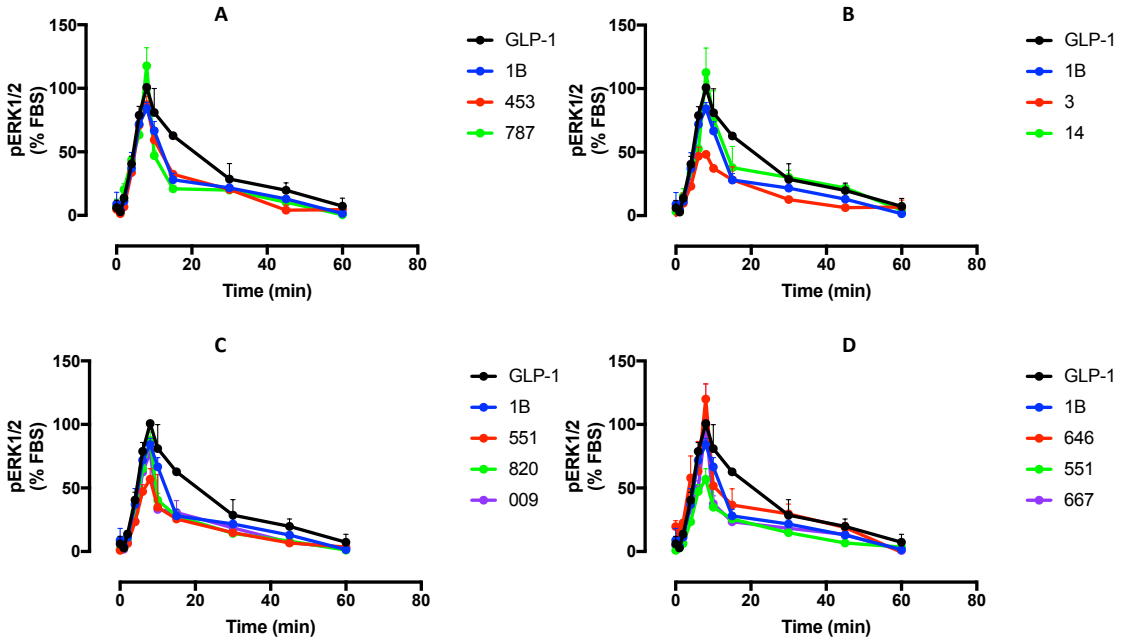

Figure S3.1: pERK1/2 time-course experiments for 11mer ligand classes, with GLP-1 and scaffold ligand 1B on each graph as reference, H^1 (**A**, 453, 787), Cyclised (**B**, 3, 14), X^1/X^3 (**C**, 052, 820, 009), X^2 (**D**, 646, 551, 667). 1uM of ligand was used for all experiments. **A-D** is mean + SEM of 3 independent experiments

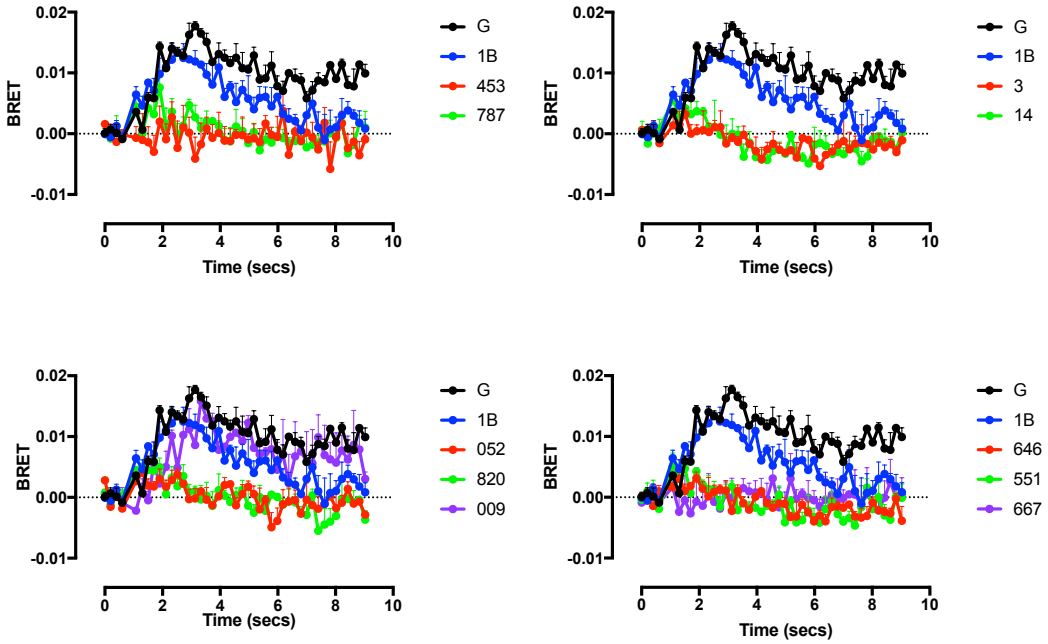

Figure S3.2: β arrestin recruitment time-course experiments for 11mer ligand classes, with GLP-1 and scaffold ligand 1B on each graph as reference, H^1 (**A**, 453, 787), Cyclised (**B**, 3, 14), X^1/X^3 (**C**, 052, 820, 009), X^2 (**D**, 646, 551, 667). 1uM of ligand was used for all experiments. **A-D** is mean + SEM of 3 independent experiments

Chapter 4:
Assessing the role of different signalling effectors in G protein and β arrestin deficient cell lines for GLP-1R ligands.

4.1 Introduction

The GLP-1R is a therapeutic target for type 2 diabetes mellitus with multiple approved drugs targeting the receptor. Canonically the GLP-1R couples to Gαs protein, promoting the production of cAMP. The receptor however, promiscuously couples to other Gα proteins, including Gαq/11, Gαi/o and Gα12/13, as well as regulatory proteins, β arrestins, which can influence both G protein signalling and signal in their own right (reviewed in Pabreja et al. 2014).

Different signalling effectors are responsible for distinct signalling outputs within the cell. The degree to which individual ligands induce receptor engagement with each signalling effectors and how these interactions promote activation of cellular signalling mediated by those transducers, may in part explain the biased agonism that has been observed for ligands at the GLP-1R. Previous work in the area used pharmacological tools to silence downstream targets of G protein activation (Wootten et al., 2016a). These types of studies revealed individual ligands for the GLP-1R have different requirements for different G proteins to mediate downstream signalling events. Inhibition of adenylate cyclase using ddAdo, and KH7 and PKA using H98 and KT5720, as a proxy for Gαs inhibition, as expected heavily impaired cAMP production mediated by exendin-4, GLP-1 and oxyntomodulin (Wootten et al., 2016). Surprisingly, overnight pertussis toxin treatment, alters the Gαi protein so it is no longer available for activation, also revealed a positive Gαi contribution to cAMP production, which is contrary to the canonical role of Gαi/o in inhibition of adenylate cyclase (Dessauer, Chen-Goodspeed, & Chen, 2002). Inhibition of G protein βγ subunits with gallein and Gαq/11 blockage with the inhibitor UBO (Schrage et al., 2015) had no effect on cAMP accumulation, however, they significantly impaired calcium signalling. In addition, blockage of other Gα protein subfamilies using pharmacological inhibitors also modulated calcium signalling, although the effect varied in a ligand-dependent manner (Wootten et al., 2016a). Using pertussis toxin or gallein also revealed a global effect of Gαi/o and Gβγ on inhibition of pERK1/2, as well a ligand-specific Gαq/11 component (UBO-sensitive) for pERK, for GLP-1 and exendin-4, but not oxyntomodulin. In addition, silencing of β-arrestins using transfection of a dominant negative mutant version of β-arrestins 1 or 2, reduced pERK1/2 signalling universally for the three ligands (Wootten et al., 2016a). These studies provide useful insights into the role of G proteins and β-arrestins in downstream signalling mediated by the GLP-1R,

however, the pharmacological inhibition approach employed has limitations for interpretation of results, either due to non-specific actions of some of the inhibitors (i.e. H98 and KT5720 used to inhibit functions downstream of Gαs, and UBO, which has been also shown to inhibit Gβγ signalling (Zhan-Guo & Jacobson, 2016)) or incomplete inhibition of signalling using these methods (i.e. some Gαi/o family members are insensitive to pertussis toxin) (Chan et al, 2002), as well as other limitations associated with currently available inhibitors. For example, the use of gallein for inhibition of Gβγ function is limited as these subunits have multiple interaction faces that are distinctly used to interact with different proteins and it is unclear if gallein is able to inhibit all actions meditated by these proteins (Sanz 2017). Furthermore, indirect inhibitors of G protein function (in the case of downstream inhibitors H98 and KT5720) leave open the potential for G proteins to exert influences in ways beyond direct action on the adenylate cyclase pathway. To be able to extract the diversity of roles that each transducer plays in distinct signalling outcomes, a model that directly silences the transducer being assessed, with no off-target effects, would be ideal. Using dominant negative versions of the G protein or siRNA provide options for this, however these models may suffer from limits in the efficiency of delivery and are not always able to fully eliminate the native protein of interest.

In this chapter I have further assessed the role of different G protein families and β-arrestins in downstream signalling by biased GLP-1R agonists, using a series of HEK293 cells that were engineered to remove families of signalling effectors using CRISPR/CAS9 technology (developed by Dr. Asuka Inoue, Tohoku University, Japan). This included cells that lacked Gαs/olf (ΔGαs), Gαq/11, (ΔGαq/11) all subtypes of Gαi/o (ΔGαi/o), Gα12/13 (ΔGα12/13) as well as a complete Gα knockout line (ΔGall), in addition to cells with both β arrestins knocked out (Δβarr1/2). These present a 'cleaner' way to investigate the potential role that different transducers may contribute to individual signalling outputs and have been used by other groups, for example to show lack of arrestin signalling in absence of active G protein (Grundmann et al. 2018) and the role of active Gαq/11 signalling for a full pERK response at the free fatty acid receptor 4 (Alvarez-Cuerto et al. 2016). As HEK293 cells do not endogenously express the receptor of interest, each cell line was transiently transfected with 2xcMychGLP-1R for each experiment, and these cells underwent parallel assessment of multiple assay endpoints. The basic complement of GLP-1R ligands that were tested in the previous inhibitor study (GLP-1, exendin-4 and oxyntomodulin) were assessed (Wootten et al, 2016a), as well as a

series of additional novel biased ligands. This included exendin-P5, reported to display bias towards G protein mediated signalling over arrestin (and with a unique in vivo profile) (Zhang et al., 2015). The previous inhibitor study assessed a limited number of signalling endpoints in CHO cell lines, however the biased signalling profiles of these ligands has been demonstrated in multiple cell backgrounds (Wootten et al., 2016). This is also true for ExP5 which has demonstrated similar biased agonism profiles in CHO and HEK cells (Liang et al., 2018, Zhang et al., 2015).

The contribution of different effectors to the cAMP profile of select 11mer peptide agonists identified in the previous chapter were also assessed, These were selected for their interesting cAMP profiles (in comparison to their affinities) relative to GLP-1 and for their particular chemistry. 009 was selected as as it displayed low affinity relative to GLP-1, but similar ability to activate the cAMP pathway suggesting this ligand is more efficacious than GLP-1 in this pathway. This is despite it containing a substitution of the first amino acid that was previously thought to be crucial for peptide activity at the GLP-1R. 1B was chosen as this was the scaffold peptide in the previous chapter and also has a biased profile away from β arrestin recruitment relative to GLP-1. 14 and 3 were selected as these are constrained cyclic peptides that are constrained in different positions and exhibited very interesting cAMP profiles. Peptide 3 had a 3-fold higher affinity than 1B, yet much lower pEC50 value (100-fold lower) in cAMP production, whereas peptide 14 had increased affinity (30-fold) relative to peptide 3, yet exhibited a 10-fold more potent cAMP response. Investigating the role that individual signalling mediators play in the overall signalling complement for biased ligands may lead to a greater understanding of the proximal events in the GLP-1R signalling cascade that ultimately lead to biased agonism profiles in downstream signalling and regulation.

4.2 Results

4.2.1 GLP-1R expression profiles in different HEK293 cell lines

For all experiments, transfected hGLP-1R was tagged with Rluc8 at its intracellular C-terminus. This construct has been previously assessed in our lab relative to the untagged GLP-1R; the addition of Rluc8 does not alter the pharmacology of the GLP-1R assessed over multiple signalling endpoints (Hager et al., 2017). Overall GLP-1R expression was measured through comparison of the luminescence signal upon the addition of the substrate

coelenterazine. These data are presented in Figure 4.1 as a % of that of the receptor in the WT cell line, grouped across multiple transfections. Compared to WT, the ΔGαs, ΔGαq/11 and ΔGαi/o all had higher receptor expression, while ΔGα12/13, ΔGall and Δβarr1/2 had equivalent expression of the receptor (Fig. 4.1)

4.2.2 GLP-1R cAMP accumulation profiles in the absence of distinct G protein families or β arrestins

Assessment of cAMP accumulation was performed in WT and each of the knockout cell lines following transfection with the GLP-1R. All responses for each of the individual ligands in the KO cell lines were normalised to that of the same ligand at the WT receptor for comparison across the ligands on the contribution of individual transducer proteins to cAMP signalling (Figure 4.2 & 4.3). Concentration response data was analysed using a three-parameter logistic equation to derive pEC50 and Emax values (Table 4.1). It should be noted all ligands were full agonists reaching similar levels of cAMP response as a percentage of positive control forskolin (Table 4.1.1). Assessment of all ligands revealed some universal trends across the cell lines. As expected, the presence of Gαs was absolutely required to initiate cAMP accumulation, with none of the ligands able to produce a response in either the ΔGαs or complete ΔGα protein KO cells. Potencies of all ligands in the ΔGαq/11 cell line were similar to the WT cells, however, maximal responses were increased for exendin-4, oxyntomodulin and 11mers 14, 1B and 009 albeit statistical significance was only reached for 1B and 009 (Table 4.1). In the Gαi/o line there was a ligand-dependent effect on the cAMP potency, with reduced pEC50 for GLP-1 and exendin-P5 only. In terms of maximum response Gαi/o KO induced a modest enhancement in maximal response for exendin-4, however a large, statistically significant, enhancement was observed for oxyntomodulin (Figure 4.2, Table 4.1 & 4.1.1). Little effect was observed on the remaining agonists. Gα12/13 KO had little to no impact on the pEC50 of ligands but did have a ligand-specific effect on Emax, lowering the maximum response for GLP-1, oxyntomodulin, 1B, 14, Exendin P5 and 009, albeit that only for the latter two ligands did the effect achieve statistical significance. Interestingly there was minimal effect of Gα12/13 on exendin-4 cAMP responses. β arrestin KO had very little effect on cAMP accumulation for most ligands, however maximum response was slightly enhanced for 11mer 009. Limited conclusions can be drawin for peptide 3 and the importance of GαI, Gα12/13 and Gαq/11 and their influence on

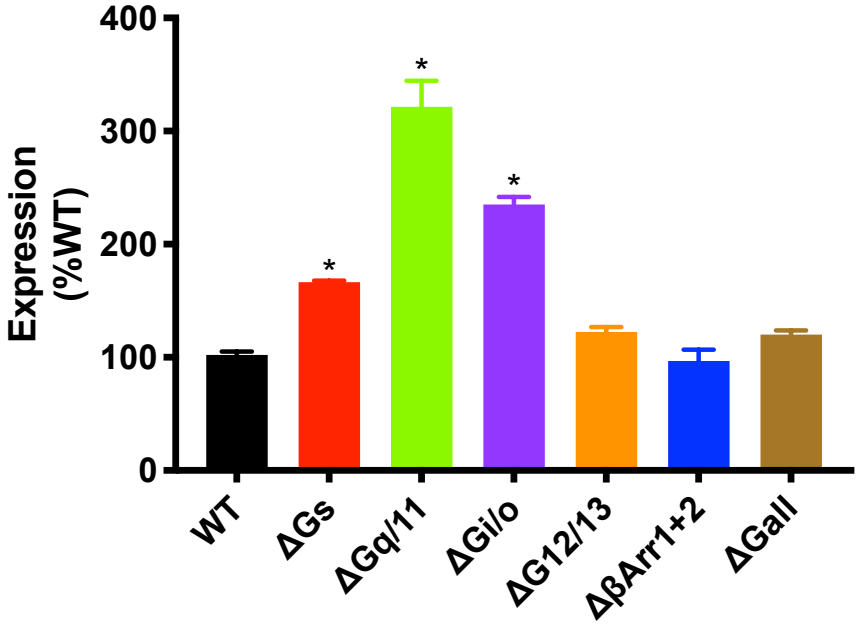

Figure 4.1: **Expression of GLP-1R in signaling molecule deficient HEK293 cells.** Transiently transfected HEK293 cells were assessed for expression of GLP-1R-Rluc8 measured via luminescence signal following coelenterazine addition. N=3. *Statistically different from expression in WT cells using One Way ANOVA with a Dunnett's post test ($p<0.05$).

	WT		Gαs		Gαq/11		Gαi/o		Gα12/13		Gαcomplete		βArrestin1/2	
LIGANDS	**pEC_{50}**	**Emax**	**pEC_{50}**	**Emax**	**pEC_{50}**	**Emax**	**pEC_{50}**	**Emax**	**pEC_{50}**	**Emax**	**pEC_{50}**	**Emax**	**pEC_{50}**	**Emax**
GLP-1(7-36)NH_2	**9.97±0.28**	**100±8.06**	**ND**	**ND**	**9.94±0.21**	**85.48±5.69**	**8.89±0.39**	**111.1±15.03**	**9.84±0.52**	**65.14±8.72**	**ND**	**ND**	**9.74±0.33**	**99.87±10.17**
EXENDIN 4	**10.76±0.35**	**100±7.64**	**ND**	**ND**	**10.52±0.16**	**125.7±4.85**	**10.51±0.53**	**142.4±16.23**	**10.8±0.39**	**94.2±18.13**	**ND**	**ND**	**10.37±0.31**	**137.8±10.62**
OXYNTOMODULIN	**9.13±0.3**	**100±10.1**	**ND**	**ND**	**9.07±0.19**	**138.6±9.94**	**8.83±0.27**	**187.3±16.28***	**9.12±0.34**	**58.98±6.87**	**ND**	**ND**	**8.62±0.19**	**109.4±8.98**
EXENDIN P5	**9.56±0.32**	**100±9.41**	**ND**	**ND**	**9.13±0.24***	**84.95±7.54**	**8.16±0.39**	**128.2±17.22**	**9.26±0.24**	**48.83±3.5***	**ND**	**ND**	**8.88±0.25**	**95.74±9.61**
1B	**8.83±0.27**	**100±8.82**	**ND**	**ND**	**9.85±0.25**	**155.2±12.64***	**8.99±0.4**	**114.4±14.81**	**8.43±0.46***	**73.38±10.63**	**ND**	**ND**	**8.88±0.19**	**110.4±7.27**
009	**9±0.35**	**100±10.97**	**ND**	**ND**	**9.27±0.19**	**147±8.83***	**9.01±0.29**	**124.3±12**	**9.51±0.45**	**47.8±6***	**ND**	**ND**	**8.81±0.29**	**147.3±13.88***
3^	**ND**	**100±13.97**	**ND**	**ND**	**ND**	**70.12±32.83**	**ND**	**77.18±29.49**	**ND**	**40.39±25.27**	**ND**	**ND**	**ND**	**64.01±27.29**
14	**7.57 ±0.51**	**100 ±22.24**	**ND**	**ND**	**7.62±0.28**	**137.7±16.38**	**7.43±0.17**	**95.32±8.37**	**7.99±0.36**	**49.84±8.45**	**ND**	**ND**	**8.04±0.36**	**79.94±11.97**

Table 4.1) **cAMP accumulation data for GLP-1R agonists in HEK293 cells with signalling molecules removed by CRISPR/CAS9** pEC50 and Emax (expressed as a % of the response in the WT cell line) for cAMP accumulation for both full length and 11mers GLP-1R ligands in transiently transfected HEK293 WT and signalling molecule deficient cells. Values are the mean ± SEM of 3-4 independent experiments. Statistical significance was assessed with one way analysis of variance (ANOVA) with Dunnett's post-test (*p<0.05). ^ 11mer peptide 3 curves were not dully defined so curve fitting could not confidently predict potency and Emax values. The Emax values are reported at % response at 1μM of peptide.

WT EMAX (%FSK)	GLP-1	EXENDIN 4	OXYNTOMODULIN	EXENDIN P5	1B	009	3^	14
	35.42±3.206	**35.88±2.05**	**31.37±2.66**	**35.18±3.22**	**31.82±2.70**	**29.24±3.09**	**32.23±4.24**	**27.7±7.08**

Table 4.1.1) **Un-normalised cAMP EMAX response in HEK293 cells with signalling molecules removed by CRISPR/CAS9** Emax (expressed as a % of the FSK response) for cAMP accumulation for both full length and 11mers GLP-1R ligands in transiently transfected HEK293 WT and signalling molecule deficient cells. Values are the mean ± SEM of 3-4 independent experiments. Statistical significance was assessed with one way analysis of variance (ANOVA) with Dunnett's post-test (*p<0.05) where the WT cell line was used as the control. ^11mer 3 maximum response is response to 1μM of peptide as curve couldn't be determined

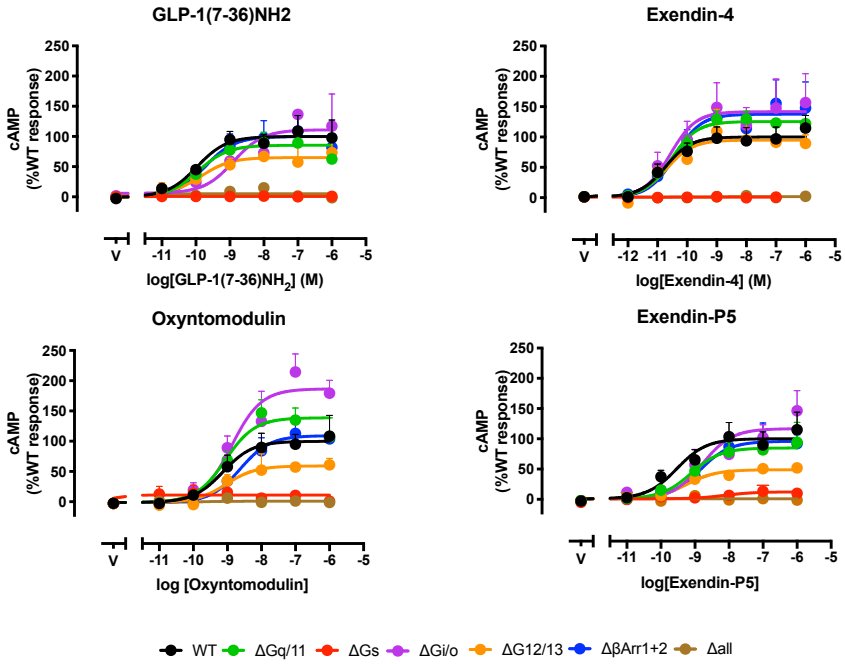

Figure 4.2: **cAMP accumulation in signaling molecule deficient HEK293 cells.** Transiently transfected HEK293 cells were assessed for cAMP accumulation with a series of full length GLP-1R agonists in a WT (black), ΔGs (red), ΔGq/11 (green), ΔGi/o (purple), ΔG12/13(orange), ΔβArrestin 1&2 (blue) and ΔGall (brown). All data is normalised to the response in the WT cell line for each ligand. Data is shown as mean + S.E.M of 3-4 individual experiments, each performed in triplicate.

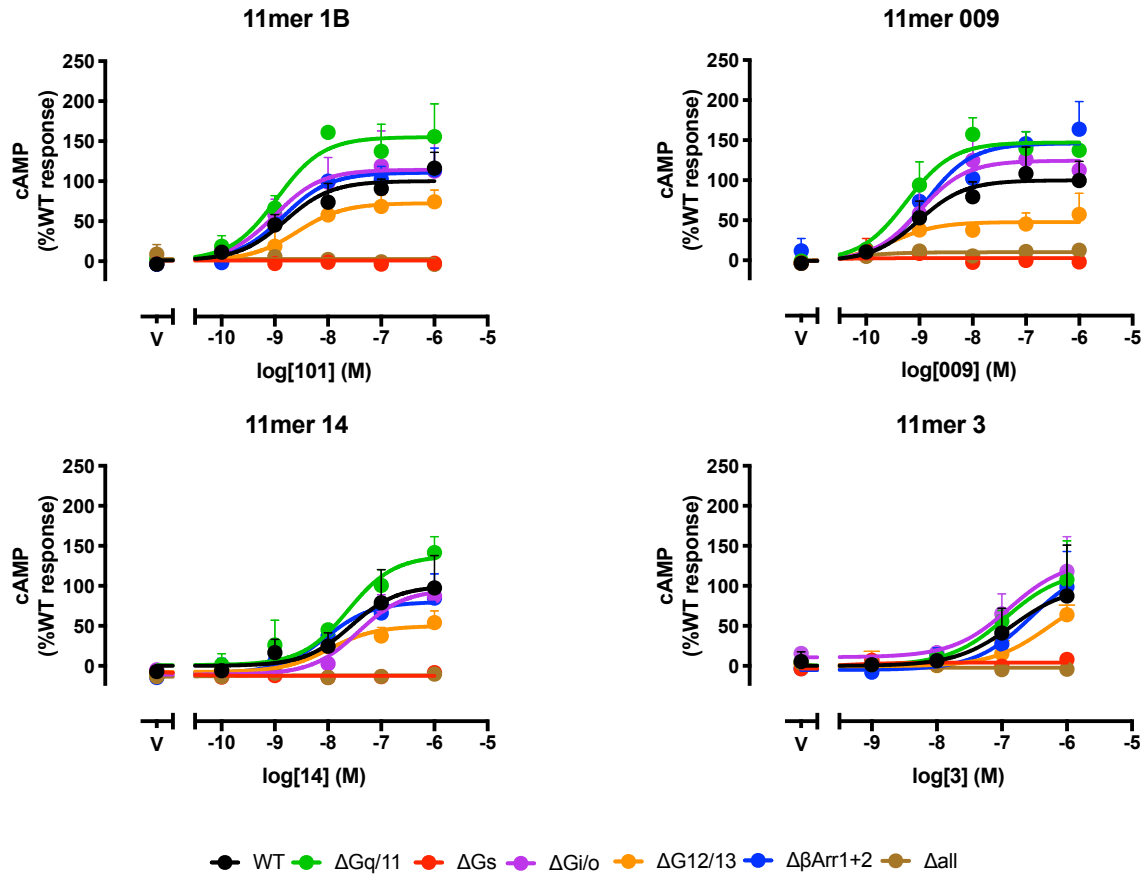

Figure 4.3: **cAMP accumulation in signaling molecule deficient HEK293 cells.** Transiently transfected HEK293 cells were assessed for cAMP accumulation with a series of 11mer GLP-1R agonists in WT (black), or ΔGs (red), ΔGq/11 (green), ΔGi/o (purple), ΔG12/13(orange), ΔβArrestin 1&2 (blue) and ΔGall(brown) cells. All data is normalised to the response in the WT cell line for each ligand. Data is shown as mean + S.E.M of 3-4 individual experiments, each performed in triplicate.

cAMP as the top of the curves for these were not clearly defined within the concentration range assessed and this will require further investigation.

4.2.3 GLP-1R calcium mobilisation profiles in the absence of distinct G protein families or β arrestins

Assessment of intracellular calcium mobilisation was also performed in WT and each of the knockout cell lines following transfection with the GLP-1R. All responses for each individual ligand in the KO cell lines were normalised to that of the same ligand at the WT receptor allowing for a direct comparison across the ligands on the contribution of individual signalling molecules to calcium signalling (Fig. 4.4). Concentration response data was analysed using a three-parameter logistic equation to derive pEC50 and Emax values (Table 4.2). iCa2+ was only assessed for the full-length ligands, as the 11mer ligands had very weak calcium responses (Figure 4.4 and Figures from Chapter 3). Gαq/11 was absolutely required for iCa2+ mobilisation as no ligand was able to elicit a response in either the ΔGαq/11 or complete ΔG protein KO cells. Universally, in the ΔGαi/o cell line only minimal differences on the peak iCa2+ response were observed compared to the WT cells. However, there trends towards an enhancement of potency for exendin-4, and a small attenuation of potency for exendin-P5 in the ΔGαi/o cell line compared to WT cells (Figure 4.4, Table 4.2). Both Gαs and Gα12/13 KO had deleterious effects on both the potency and maximum peak response mediated by all ligands assessed when compared to WT cell line. Knockout of β arrestins had a ligand-specific effect, with deletion of β arrestin enhancing the potency of the peak iCa2+ response for both GLP-1 and exendin P5 (~10 fold). No effect was observed for oxyntomodulin, however, a significant reduction (>40 %) in the maximum response was observed for exendin-4 (Figure 4.4, Table 4.2).

4.3.4 GLP-1R β arrestin-1 recruitment profiles in the absence of distinct G protein families or β arrestins

Similar to assay of calcium mobilisation, β arrestin recruitment was only assessed for full length ligands in WT and each of the knockout cell lines following transfection with the GLP-1R. All experiments were conducted using full kinetic traces (Figure S4.1) and the AUC (0-8min) was calculated for each ligand concentration, and responses for each individual ligand in the KO cell lines were normalised to that of the same ligand at the WT receptor allowing for

a direct comparison across the ligands on the contribution of individual signalling molecules to β arrestin recruitment (Fig. 4.5). Concentration response data was analysed using a three-parameter logistic equation to derive pEC50 and Emax values (Table 4.3). Maximum response in the recruitment assay, compared to WT cell background, was increased in ΔGαq/11, and ΔGα12/13 cells for all peptides except oxyntomodulin, whereas Emax was increased for all peptides except exendin-P5 in the ΔGαall cells. In contrast, the maximal response to peptides in the ΔGαi/o cells was not significantly different from WT cells. Interestingly, the maximal β-arrestin-1 recruitment was either unchanged (exendin 4), or reduced in the ΔGαs cell line, with no measurable response detected when exendin-P5 was used as the agonist (Figure 4.5, Table 4.3). Knockout of the Gα subunits had minimal effect on peptide potency, with the exception of exendin-P5 that exhibited lower potency in the ΔGαi/o, ΔGαq/11, and ΔGα12/13 cells, while in the ΔGαs cells the lack of response precluded interpretation of effects on potency. Intriguingly, in contrast to the cells with selective knockout of Gα protein families, in the ΔGαall cells, exendin-P5 displayed similar potency compared to WT cells, albeit with lower Emax as noted above (Figure 4.5, Table 4.3).

4.3 Discussion

The GLP-1R is a pleiotropically coupled receptor (reviewed in Fletcher et al., 2016), meaning it can recruit and activate a broad range of signalling effectors, including all those assessed in this chapter using CRISPR engineered cell lines. Gαs is the most readily recruited Gα protein and subsequently cAMP is the most potently activated signalling pathway. GLP-1R can couple to Gαq/11 to promote iCa^{2+} mobilisation as well as Gαi/o proteins, which canonically inhibit cAMP response but can also contribute positively to cAMP signalling for some ligands of the GLP-1R (Wootten et al., 2016a). β arrestins also interact with the GLP-1R and have been shown to play a role in internalisation of the receptor as well as signalling through the pERK1/2 pathway (Wootten et al., 2016a). There is also evidence that shows multiple signalling effectors can play a role in the same signalling pathway (Wootten et al., 2016a). In this chapter, assessment of signalling complexity using signalling molecule deficient cell lines revealed that there is a multifarious interplay of roles of different effectors in the overall signalling complement mediated by the GLP-1R.

	WT		Gαs		Gαq/11		Gαi/o		Gα12/13		Gαcomplete		βArrestin1/2	
LIGANDS	**pEC_{50}**	**Emax**	**pEC_{50}**	**Emax**	**pEC_{50}**	**Emax**	**pEC_{50}**	**Emax**	**pEC_{50}**	**Emax**	**pEC_{50}**	**Emax**	**pEC_{50}**	**Emax**
GLP-1(7-36)NH_2	**8.82±0.16**	**100±5.31**	**8.18±0.24**	**58.44±5.15***	**ND**	**ND**	**8.70±0.50**	**108.7±16.22**	**7.3±0.47**	**43.6±8.14***	**ND**	**ND**	**9.95±0.34**	**88.29±6.64**
EXENDIN 4	**9.05±0.34**	**100±10.73**	**8.43±0.16**	**44.63±2.3***	**ND**	**ND**	**9.66±0.34**	**97.89±7.87**	**8.8±0.72**	**22.61±18.13***	**ND**	**ND**	**9.21±0.32**	**58.75±5.02***
OXYNTOMODULIN	**7.92±0.11**	**100±4.43**	**7.31±0.45**	**63.06±13.01**	**ND**	**ND**	**7.67±0.18**	**133.5±9.52**	**6.61±0.46**	**44.29±13.63**	**ND**	**ND**	**8 ±0.25**	**84.3±7.23**
EXENDIN P5	**7.85±0.22**	**100±9.15**	**7.69±0.49**	**54.72±10.61**	**ND**	**ND**	**7.06±0.26**	**123.5±17.53**	**ND**	**ND**	**ND**	**ND**	**8.88±0.25**	**95.74±9.61**

Table 4.2) **iCa2+ mobilisation data for GLP-1R agonists in HEK293 cells with signalling molecules removed by CRISPR/CAS9** pEC50 and Emax ((expressed as a % of the response in the WT cell line) for iCa2+ mobilisation for full length GLP-1R ligands in transiently transfected HEK293 WT and signalling molecule deficient cells. Values are the mean ± SEM of 3-4 independent experiments. Statistical significance was assessed with one way analysis of variance (ANOVA) with Dunnett's post-test (*p<0.05)

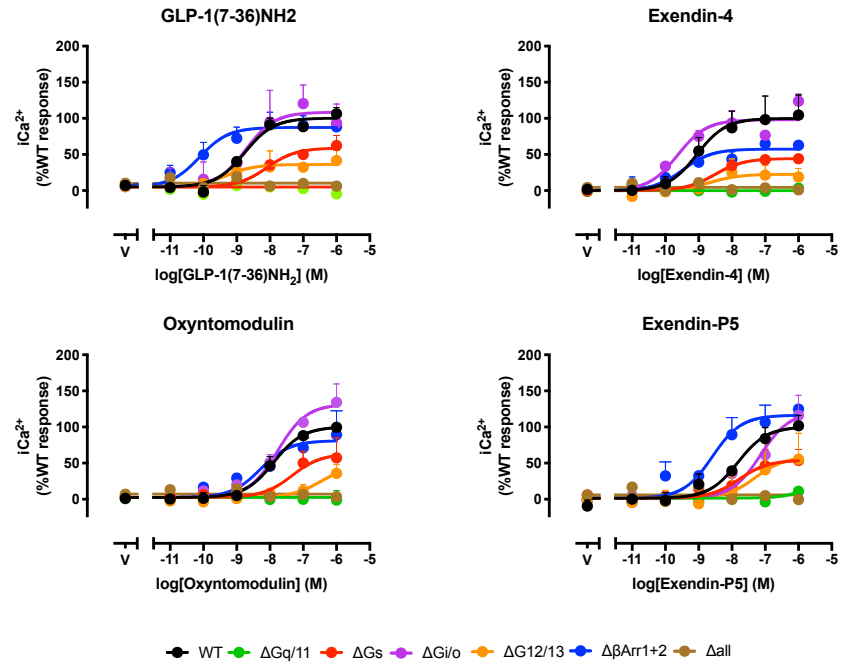

Figure 4.4: **iCa^{2+} accumulation in signaling molecule deficient HEK293 cells.** Transiently transfected HEK293 cells were assessed for iCa^{2+} accumulation with a series of full length GLP-1R agonists in WT (black), or ΔGs (red), ΔGq/11 (green), ΔGi/o (purple), ΔG12/13(orange), ΔβArrestin 1&2 (blue) or ΔGall(brown) cell. All data is normalised to the response in the WT cell line for each ligand. Data is shown as mean + S.E.M of 3-4 individual experiments, each performed in triplicate.

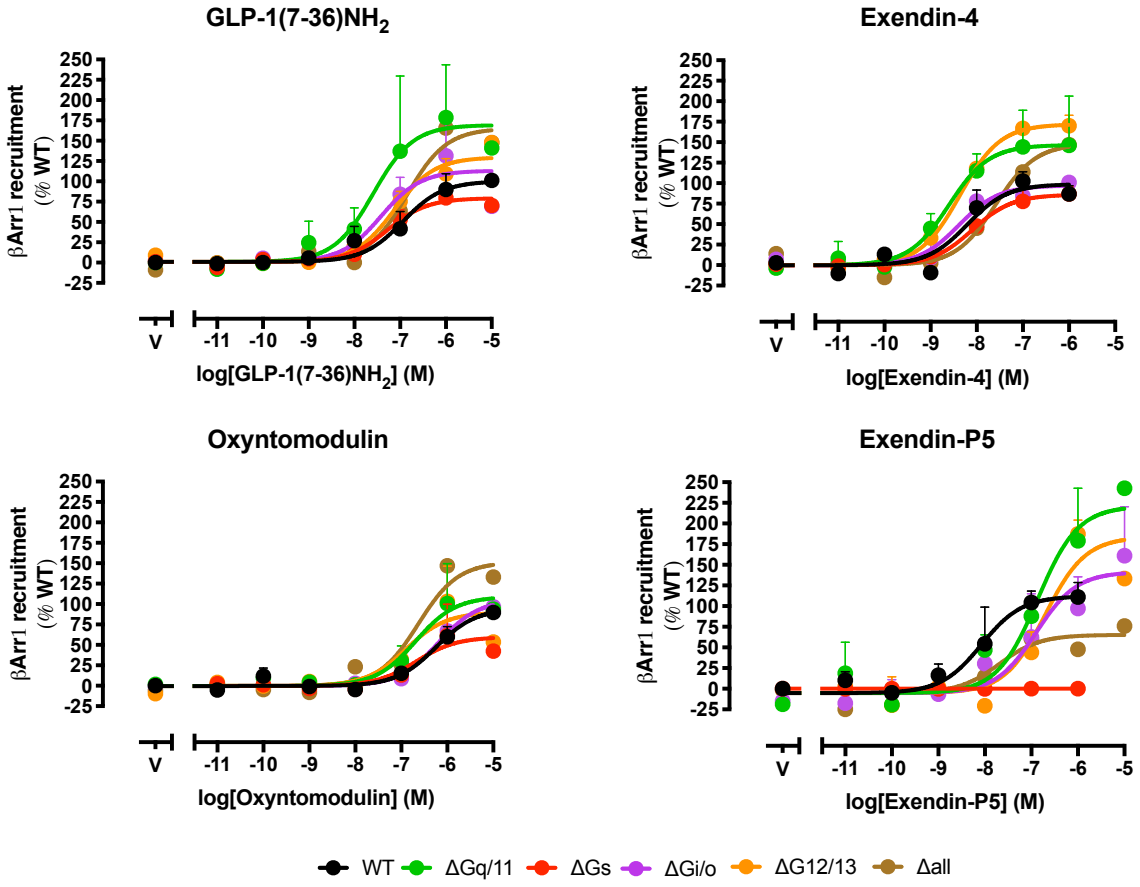

Figure 4.5: **βArrestin 1 recruitment in signaling molecule deficient HEK293 cells.** Transiently transfected HEK293 cells were assessed for βArrestin-1 recruitment with full-length GLP-1R agonists in WT (black) cells, or ΔGαs (red), ΔGαq/11 (green), ΔGαi/o (purple), ΔGα12/13 (orange) and ΔGαall (brown). All data is normalised to the response in the WT cell line for each ligand. Data is shown as mean + S.E.M of 3-4 individual experiments, each performed in triplicate.

	WT		Gαs		Gαq/11		Gαi/o		Gα12/13		Gαcomplete	
LIGANDS	**pEC_{50}**	**Emax**	**pEC_{50}**	**Emax**	**pEC_{50}**	**Emax**	**pEC_{50}**	**Emax**	**pEC_{50}**	**Emax**	**pEC_{50}**	**Emax**
GLP-1(7-36)NH_2	**6.88±0.25**	**100±11.86**	**7.3±0.18**	**79.16±6.18**	**7.59±0.45**	**169.3±29.16**	**7.12±0.16**	**129.8±9.16**	**7.44±0.37**	**112.9±16.22**	**6.87±0.18**	**165.1±12.59**
EXENDIN 4	**8.22±0.23**	**100±7.64**	**8.09±0.19**	**86.07±6.45**	**8.61±0.37**	**146.6±18.22**	**8.37±0.25**	**97.27±8.6**	**8.35±0.07**	**172±4.79**	**7.6 ±0.17**	**148.2±11.06**
OXYNTOMODULIN	**6.24±0.18**	**100±10.15**	**6.71±0.54**	**59.59±16.85**	**6.66±0.38**	**109.6±20.69**	**6.19±0.09**	**105.3±6.11**	**6.9±0.41**	**89.95±18.2**	**6.64±0.25**	**151.3±17.24**
EXENDIN P5	**7.98±0.26**	**100±12.24**	**ND**	**ND**	**6.89±0.28**	**221.9±31.56**	**6.86±0.41**	**142.3±25.69**	**6.76±0.26**	**183.2±26.18**	**7.79±0.36**	**64.83±9.17**

Table 4.3) **β Arrestin 1 recruitment data for GLP-1R agonists in HEK293 cells with signalling molecules removed by CRISPR/CAS9** pEC50 and Emax (expressed as a % of the response in the WT cell line) for Arrestin 1 for full length GLP-1R ligands in transiently transfected HEK293 WT and signalling molecule deficient cells. Values are the mean ± SEM of 2-4 independent experiments. Statistical significance assessed with one way analysis of variance (ANOVA) with Dunnett's post-test (*p<0.05)

Looking at the most studied signalling transducers, Gαs and Gαq, and the pathways that they are most associated with these proteins, cAMP and iCa2+ respectively, these effectors are absolutely required to initiate any signalling response for these pathways. However, more subtle effects were seen on these pathways in the selective absence of other G proteins or β arrestins, suggesting that there is cross-talk across pathways and that co-activation of multiple transducers influences the "texture" of response for any individual pathway. Therefore, it appears that while (Gαs and Gαq are essential for the activation of cAMP-dependent or intracellular calcium-dependent signalling pathways respectively, other signalling effectors are responsible for fine-tuning these responses.

For cAMP production both GLP-1 and Exendin-P5 displayed a rightward shift in their concentration response curves when Gαi/o was depleted, suggesting there is a positive role of Gαi/o in production of cAMP mediated by these peptides. While this may be at odds with the usual role Gαi/o plays in negatively regulating adenylate cyclase, the current result is consistent with previous data performed in CHO cell lines that revealed a positive Gαi/o component to cAMP output from the GLP-1R (Wootten et al., 2016a). Interestingly, deletion of Gαi/o also increased the maximum response for all full-length ligands and 11mer peptides to varying degrees (Figure 4.2 & 4.3), but not for the 11mer peptide 3. This is more consistent with the canonical view of cAMP regulation where activation of Gαi/o inhibits adenylate cyclase, and for the GLP-1R, this occurs at high concentrations of ligand (Zhao et al 2020). Thus, in the absence of Gαi/o, this inhibitory effect is removed resulting in an overall higher response. 11mer ligands may not be able to promote a response from Gαi/o either due to bias away from this pathway relative to the response of GLP-1, or an inability to reach an adequate peptide concentration within the practical confines of the assay due to the lower affinity of these peptides. In the iCa^{2+} mobilisation pathway knocking out Gαi/o had a ligand specific effect, raising the maximum peak response for oxyntomodulin and exendin P5 (Figure 4.4). In addition, in β arrestin recruitment, all ligands had an increased maximum response in the absence of Gαq/11.

Although the data may be confounded by the higher level of total GLP-1R that occurs in the absence of Gαi/o, it is likely that Gαi/o plays both a positive, and negative role in cAMP signalling and also a positive role on calcium signalling and β arrestin recruitment, albeit in a

ligand-dependent manner (i.e. for those ligands where no effect was observed in the Emax for one but not the other). This would be consistent with the known spectrum of effects that may occur via Gαi/o-dependent βγ-mediated signalling (Zamponi & Currie, 2013). To definitely determine the effect of Gαi/o in the signalling pathways assessed in the current study, more sophisticated measures of GLP-1R cell surface expression in each of the cell lines, will be required. While the Rluc8 signal (Figure 4.1) provides a measure of expression in each cell line, these receptors are not necessarily expressed at the cell surface where they could be activated by peptide ligands. This could be addressed by using an ELISA or FACS based method, with antibodies to extracellular epitopes on the receptor, that solely measure cell-surface expression.

Decreased second messenger signalling that was observed for select ligands in the absence of Gα12/13 was a novel and interesting finding for the GLP-1R. While it was known that the GLP-1R could couple to Gα12/13 proteins (Luciani et al., 2010), their contribution to these major signalling pathways had not been explored previously. Decreased maximum responses were observed in cAMP accumulation assays for GLP-1, oxyntomodulin, exendin P5, 1B, 009 and 14, and these observations highlight an unexpected importance of these Gα proteins in the generation of cAMP responses (Figures 4.2 & 4.3). However, it also emphasises that the importance of these G proteins depends on the activating ligand. Interestingly, while there was a suppression of maximum cAMP response, there was no change to potency of the peptides assayed, except for 1B. Gα12/13 can interact with class seven of the adenylate cyclase family of proteins (AC-VII) and deletion of AC-VII can result in decreased cAMP response mediated by Gα12/13 linked receptors (Jiang, Collins, Davis, Fraser, & Sternweis, 2008). The HEK293 cells used for this study express 7 of 9 classes of AC, including ACVII (Atwood, Lopez, Wager-Miller, Mackie, & Straiker, 2011). The effect of Gα12/13 knockdown on GLP-1R-mediated activation of cAMP, suggests that the peptide ligands affected may promote stimulation of AC-VII by this non-canonical mechanism, albeit that further studies will be required to test this hypothesis. Interestingly, exendin 4 did not show a reduced cAMP response when Gα12/13 was deleted. Exendin 4 is a more potent activator of the cAMP pathway compared to other ligands and this is observed in both WT and Gα12/13 KO cells. One potential explanation for this is a stronger, more sustained interaction with Gαs proteins compared to other ligands, which reduced the ability of the activated receptor to drive

Gα12/13-ACVII mediated cAMP production, thus negating the influence of this pathway in the observed maximum response.

In addition to altering the cAMP pathway, Gα12/13 KO also reduced both the maximum response and potency for the subset of ligands tested in the iCa2+ assay suggesting a role for Gα12/13 in this pathway, though only two reached statistical significance. In addition, although exendin-4 does not require Gα12/13 activation for a full cAMP response, the influence of removing these Gα proteins on the exendin-4 mediated calcium response reveals that this ligand may still promote coupling of the GLP-1 receptor to this G protein family (Table 4.2). Gα12/13 is known to interact with PLC epsilon, which differs to the isoform activated by Gαq/11 proteins, which interact with the β isoform of PLC (Taylor, Chae, Rhee, & Exton, 1991). This data suggests that the activation of Gα12/13 and subsequently PLC epsilon may be important in the development of the iCa2+ responses mediated from the GLP-1R, but again the extent to which this transducer family is involved is peptide-dependent.

In addition to abrogating cAMP accumulation, Gαs KO reduced both potency and maximum responses for all ligands in the iCa2+ pathway for the subset tested. Mechanisms for Gαs mediated iCa2+ responses have been described previously for the GLP-1R through the AC-PKA-EPAC pathway (Meloni, Deyoung, Lowe, & Parkes, 2013). In contrast to Gαq/11 and Gα12/13, which interact with PLC isoforms to create DAG and IP3 to release intracellular calcium, Gαs can also influence calcium signalling through EPAC2 phosphorylation downstream of PKA, promoting the release of calcium from intracellular stores (Meloni et al., 2013). The major physiological outcome of GLP-1R activation is the promotion of insulin release from pancreatic β cells. Calcium mobilisation is absolutely essential for insulin secretion and this does not occur in the absence of cAMP (Meloni et al., 2013), and therefore it is perhaps no surprise that the most potently activated G protein (Gαs), by the GLP-1R, leads to cAMP that can play a major role in calcium signalling, independent of Gαq/11 driven changes to intracellular calcium. This known intersection of Gαs and calcium mobilisation may further explain why cAMP production plays a major role in this insulin secretory response upon GLP-1R activation.

Deletion of β arrestins also had signalling pathway and ligand-specific effects on GLP-1R function. While there was little impact on cAMP accumulation, there were differing effects between ligands when exploring the calcium mobilisation pathway where there was a decrease in maximum response for exendin 4, increased potency for GLP-1 and exendin P5, and an unaltered response for oxyntomodulin (Figure 4.5). These ligands exhibit differences in their ability to recruit β arrestins and β arrestins have been implicated in many aspects of cellular signalling and regulation (Jones et al., 2018). Exendin P5 is biased away from β arrestin recruitment relative to cAMP, although more recent thinking is that this bias arises due to similar coupling to β arrestin but with more efficient Gαs coupling relative to GLP-1 (Liang et al., 2018b). Previous studies have identified that the GLP-1R can continue to signal following internalisation to endosomal compartments (Fletcher et al., 2018) and that blocking internalisation alters GLP-1R signalling, reducing both cAMP production and pERK (Fletcher et al., 2018). While GLP-1R internalisation can occur independently of β arrestin recruitment, there are also reports that the GLP-1R can undergo β arrestin-mediated internalisation (Thompson & Kanamarlapudi, 2015) so the inability to couple to β arrestin, may alter internalisation and trafficking of the receptor, that in turn may alter the signalling profile. In deleting β arrestins we saw how it can impact different signalling pathways in that it can increase cAMP maximum response for certain ligands and increase iCa^{2+} potency for some ligands.

Deletion of different G protein transducers had very little effect on the potency of most peptides tested for β arrestin recruitment, including the full Gα KO. This shows that Gα protein interactions are not necessarily required for the recruitment of β arrestin, however, as this study only measures recruitment of β arrestins to the receptor, it remains to be seen whether G protein recruitment/activation are required for activation of β arrestin-mediated signalling events. Studies of other receptors using the same cell lines have shown that Gα protein recruitment is not required for recruitment of GRK to the dopamine receptor (Pack, Orlen, Ray et al, 2018). While recruitment of GRK and subsequent β arrestin recruitment are not automatically linked, the two do commonly follow each other. The two occurring in the absence of G protein suggests that a ligand-bound receptor conformation that supports GRK/β arrestin regulatory protein recruitment can occur without the receptor accessing conformations required for G protein recruitment.

While we can infer mechanisms from the use of CRISPR engineered cell lines, there are a number of limitations to their use in studies such as the one described in this chapter. We know the specific changes that were made to the cell via CRISPR/Cas9 technology in the deletion of the transducers, but it is more difficult to determine the adaptive change these cells may have undergone after the deletion of different signalling molecules. For example, it is possible that other signalling transducers are up or downregulated or other adaptive changes to these cells, such as changes to other transducers or to protein trafficking/recycling machinery, may occur over time. For example, the deletion of one Gα protein may increase the concentration of other G proteins, and also allow association of other Gα proteins with the receptor that may not occur as readily when a higher affinity G protein is present. Trafficking of the receptor may also be affected by the deletion of certain signalling transducers changing the way that receptors move within the plasma membrane and/or internalise to intracellular locations, and/or the rate or extent of recycling back to the plasma membrane occurs. Moreover, such changes could alter signalling from certain endosomal environments and therefore have effects that are not as a direct result of the transducer that was depleted.

The results presented in the current chapter show that there is a complex interplay between signalling effectors that converge to the overall signalling response associated with activation of the GLP-1R. We have seen how cAMP production and iCa^{2+} mobilisation have an absolute requirement for Gαs and Gαq/11, respectively, as was expected from the canonical understanding of G protein mediated signalling. However, unexpectedly, a substantial role for Gα12/13 in fine-tuning both cAMP and iCa^{2+} signalling was also observed. In addition, there are differences in interaction between β arrestin and ligand bound receptor that occur in a ligand-dependent manner, which also has the potential to alter signalling outcomes. Although there has been much recent discussion on the extent of G protein-independent, arrestin-dependent signaling (Grundmann et al., 2018), there does not appear to be the requirement for Gα protein activation of the GLP-1R for the recruitment of β arrestins.

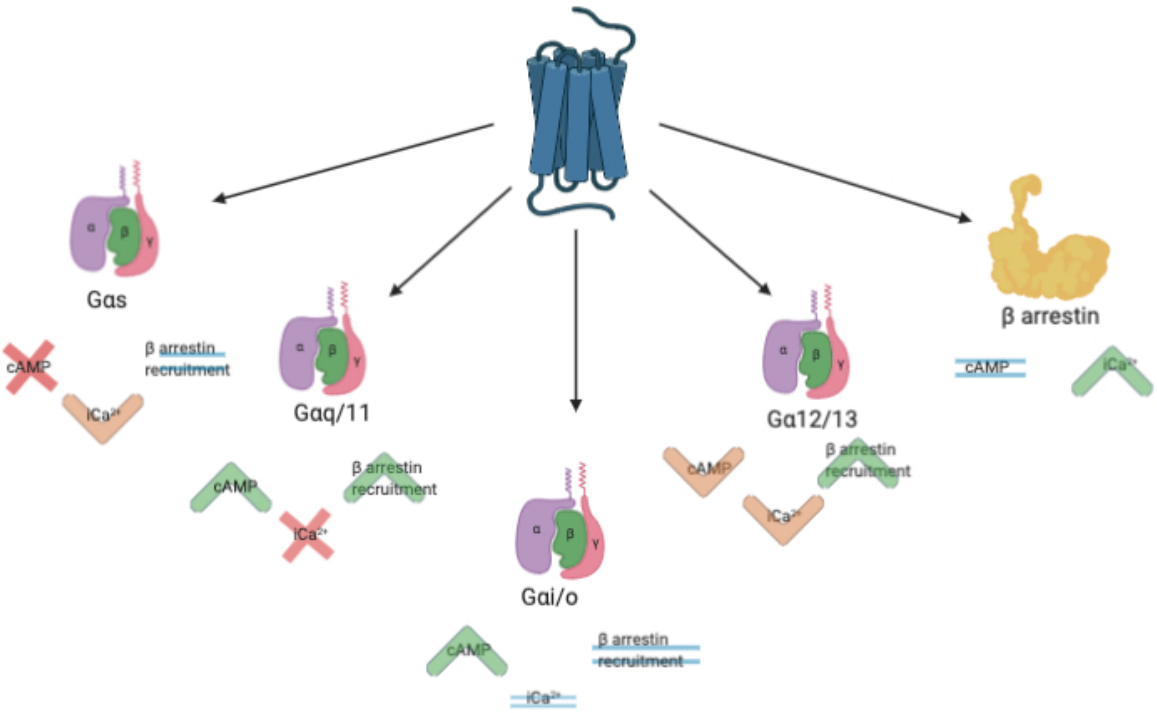

Figure 4.6: A diagram showing the trends in signaling seen globally across the peptides when individual G protein's were deleted via CRISPR/CAS9. Red cross indicates no signaling, green arrow indicates a trend towards increase in signallings, orange arrow indicates a trend towards lower singalling, blue equals sign indicates no trends in signaling either way.

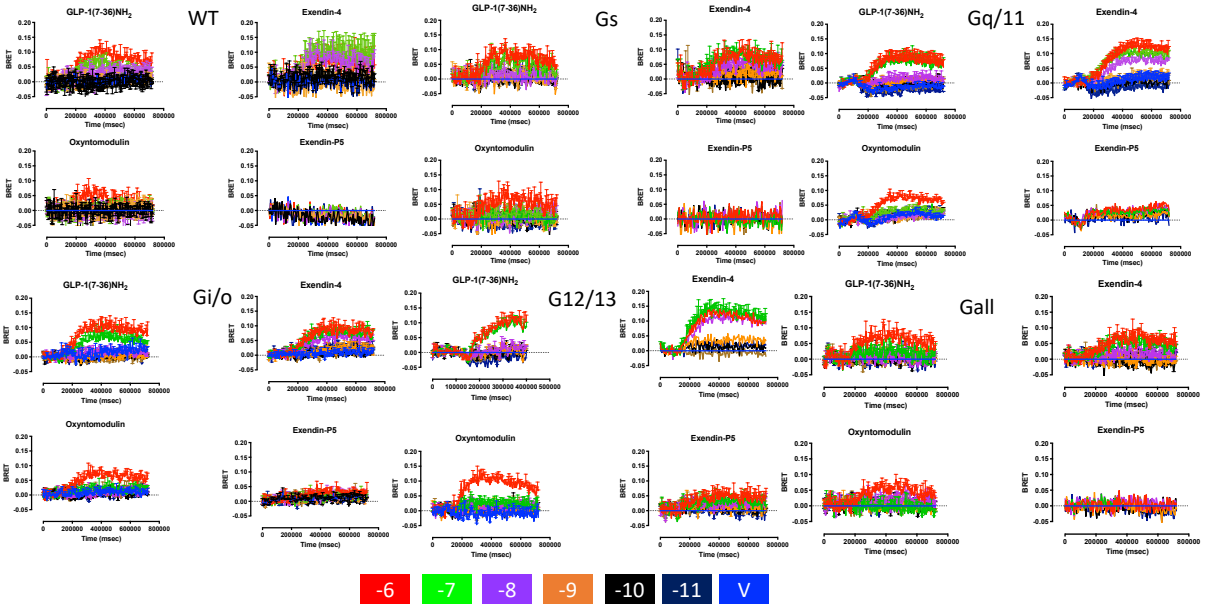

Figure S4.1: Representative traces of β arrestin recruitment in signalling effector deficient HEK293 cells

Chapter 5:
The role of individual residues of the extracellular surface in affinity and cAMP efficacy for ligands at the GLP-1R

5.1 Introduction

Biased agonism describes the ability of a ligand acting at the same target to promote a distinct signalling output relative to a reference agonist (Rankovic, Brust, & Bohn, 2016). This phenomenon is evident at the GLP-1R with all ligands that have been assessed displaying some form of bias compared to the native peptide, GLP-1 (Koole et al., 2013)(Hager et al., 2017)(H. Zhang et al., 2015). Biased agonism holds promise for drug discovery and the recent discovery of ligands such as exendin-P5 and exendin-Phe1 revealed potential for therapeutic benefits from GLP-1R biased agonism (H. Zhang et al., 2015)(Jones et al., 2018). However, to harness biased agonism for therapeutic development requires knowledge around the desired signalling profile and how biased agonism arises at the level of the receptor:ligand interaction.

Class B GPCR peptide agonists bind the receptor in a two-domain mode (Pal, Melcher, & Xu, 2012). The peptide C-terminus binds to the extracellular domain of the receptor, while the N-terminus of the ligand binds within the top of the transmembrane bundle. It is this later interaction between the ligands N-terminus and transmembrane bundle that is responsible for receptor activation. The specifics of peptide interactions with residues within the GLP-1R TM bundle has been explored by single alanine substitutions but, with the exception of GLP-1, this has been limited to studies of the extracellular loops and polar core of the GLP-1R using a limited subset of ligands (Lei et al., 2018) (Wootten, et al., 2016a) (Yang et al., 2016)(Coopman et al., 2011)(Dods & Donnelly, 2015). Additional published work from our group revealed distinct residues within the TM bundle that globally drive receptor activation and signalling as well as residues that display ligand-dependent and/or pathway dependent effects on receptor function (Wootten, et al., 2016a)(Wootten et al., 2015). These studies concluded that ligand interactions with residues in ECLs 1&2 were crucial for cAMP production and iCa^{2+} mobilisation, and while residues within ECL3 were also important for these pathways, they played a less significant role, but were more important for pERK1/2 signalling (Wootten, et al., 2016a).

The most well-described mechanism for biased agonism is due to differential transducer coupling to the receptor in the presence of different ligands. GLP-1R ligands, such as exendin-4 and oxyntomodulin, display a similar ability as GLP-1 to couple to G protein, yet enhanced preference for coupling to arrestins (Koole et al., 2013). In contrast, exendin-P5 has G protein bias, and this arises due to a similar ability to recruit arrestins, but higher efficacy for activation

of cAMP, presumably through enhanced activation of Gαs (H. Zhang et al., 2015). Therefore, in these cases, bias is predicted to arise due to differential efficacy that is induced from differential abilities to activate the Gαs transducer (Liang et al., 2018c).

Recent advances in cryo-electron microscopy (cryo-EM) have made it possible to solve the structure of full-length peptide bound class B GPCRs. To date, two peptide bound full length GLP-1R structures have been published, a low resolution GLP-1 bound (Y. Zhang et al., 2017) and biased agonist exendin P5 bound (Liang et al., 2018b), where, in both cases, the receptor is in a fully active conformation in complex with the transducer Gαs. Our group have now solved a high resolution GLP-1-bound GLP-1R structure coupled to Gαs (2.1Å resolution), as well as two previously unsolved peptide bound:GLP-1R:Gαs structures; exendin 4 and oxyntomodulin. In the case of the GLP-1-, oxyntomodulin- and exendin-P5-bound structures, residues within the peptide and TM binding pocket, side chains were well resolved in the cryo-EM maps, however, the exendin 4 structure had poor peptide-side chain resolution. These four structures revealed a common binding pocket shared by all ligands but there were clear differences in the conformation of the extracellular region of the TM bundle in the consensus cryo-EM density maps.

In this chapter of my thesis, I have expanded on our previous mutagenesis dataset(s) to study residues within the deep TM binding pocket of the GLP-1R that accommodates the extreme N-terminus of peptide ligands in their final metastable binding pose. To assess the importance of individual residues within this binding site to ligand affinity and Gαs efficacy, a variety of GLP-1R peptide ligands that display differential efficacy for cAMP production were assessed. Each residue lining this pocket was mutated to alanine or guanine and stable cell lines expressing these receptors were generated. In addition, residues within the ECLs that made contact with any ligand were also included. GLP-1 and biased agonists exendin 4, oxyntomodulin and exendin P5 were tested at wildtype and each mutant receptor cell line to assess ligand affinity and their ability to promote cAMP accumulation. These data were analysed in context of the now available cryo-EM structures of each of these peptides bound to the GLP-1R that have recently been solved by other members of our laboratory. Adding to the large datasets of receptor mutants already published (mainly for GLP-1, oxyntomodulin and exendin-4), this information reveals topographical areas of the receptor important for

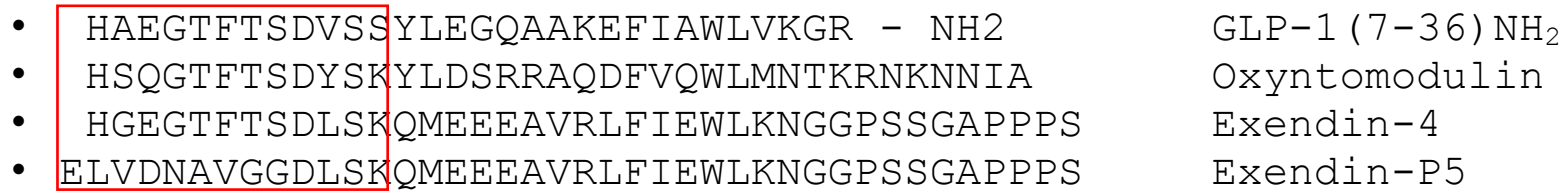

Figure 5.1: Sequence of peptide ligands used in mutagenesis experiments with a box to show the N-terminus of the ligands

affinity and ligand efficacy, which will aid in the rational design of peptide ligands and potentially biased agonists, when an ideal bias profile is determined.

5.2 Results

5.2.1 Effects of alanine mutations on receptor expression

Stable cell lines expressing either the WT GLP-1R or single Ala mutations to residues in either the ECLs or the conserved central polar network were generated previously with receptor expression characterized and published. Those that form crucial interactions with peptide ligands are included in this thesis, as additional ligands were assessed in this chapter to that published previously. From these published data, E139$^{1.34}$A, L144$^{1.39}$A, R190$^{2.60}$A, Y205$^{2.75}$A, W297^{ECL2}A, H363$^{6.52}$A, E364$^{6.53}$A, R380$^{7.35}$A, K383$^{7.38}$A and L384$^{7.39}$A all had significantly decreased cell surface expression relative to WT (Lei et al., 2018)(Koole et al., 2012)(Wootten, et al., 2016a). Cell lines that had increased expression included E138$^{1.33}$A, L141$^{1.36}$A, N300^{ECL2}A and L388$^{7.43}$A, though only E138$^{1.33}$A and N300^{ECL2} was significant (Table 5.1). No cell surface expression was detectable for W306$^{5.36}$A. With the exception of the cell lines noted above, all other mutant cell lines were generated specifically for this study using the FlpIn isogenic expression system. CHO FlpIn cells expressing mutant GLP-1R constructs were tested for expression using a cell surface ELISA to detect the cMyc epitope tag located at the N-terminus of the each GLP-1R construct. All mutants were normalized to WT GLP-1R expression levels with parental CHO FlpIn cells serving as a negative control to detect any non-specific signal from non-specific binding of antibodies. A one-way ANOVA with a Dunnett's post-test was performed to assess significant difference from WT expression. No significant differences from WT receptor expression were noted in the expression of any of the newly generated mutant receptors (Figure 5.2, Table 5.1).

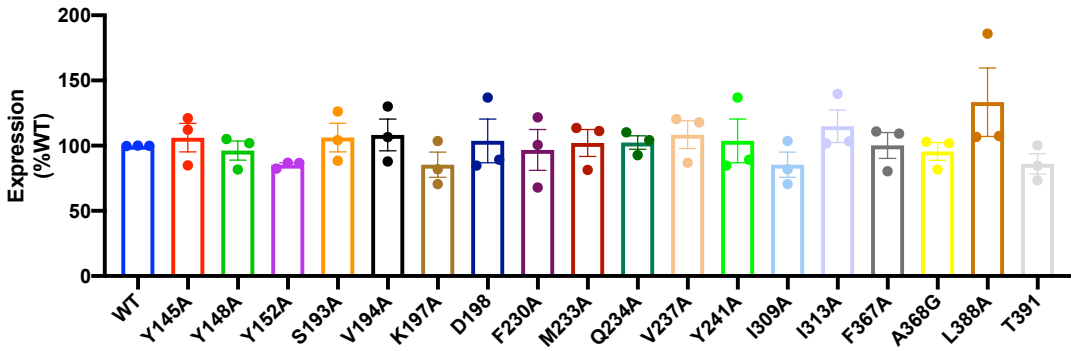

Figure 5.2). Cell surface expression of unpublished mutant GLP-1R cell lines assessed by ELISA and normalized to WT expression. Data is representative of mean ± SEM of 3 independent experiments

		GLP-1(7-36)NH_2	Exendin 4	Oxyntomodulin	Exendin P5	Exendin (9-39)
	Expression %	**pIC50**	**pIC50**	**pIC50**	**pIC50**	**pIC50**
WT	100±2	8.56±0.03	9.09±0.02	7.73±0.04	7.19±0.05	8.08±0.02
P137$^{1.32}$A	*102±14*	7.39±0.06*	8.63±0.04*	7.13±0.08*	6.36±0.14*	7.34±0.04*
E138$^{1.33}$A	*164±13**	8.16±0.07*	9.16±0.06	7.34±0.05	7.22±0.07	8.17±0.05
E139$^{1.34}$A	*37±8**	ND	ND	ND	ND	ND
L141$^{1.36}$A	*136±8*	7.85±0.07*	8.60±0.05*	6.22±0.07*	6.99±0.09	7.56±0.06*
L142$^{1.37}$A	*94±11*	7.97±0.05*	9.18±0.05	7.09±0.07**	6.27±0.17*	7.98±0.05
L144$^{1.39}$A	*25±6**	7.96±0.09*	9.31±0.11	7.28±0.11	6.59±0.11*	8.32±0.05
Y145$^{1.40}$A	106±10	8.21±0.06	9.26±0.08	7.61±0.06	7.36±0.08	7.96±0.05
Y148$^{1.43}$A	96±7	7.55±0.10*	7.42±0.07*	6.46±0.09*	6.87±0.09	8.04±0.05
Y152$^{1.47}$A	85±2	7.26±0.26*	6.50±0.12*	6.85±0.32*	7.19±0.09	6.95±0.09*
R190$^{2.60}$A	*53±3**	6.99±0.09*	6.60±0.12*	7.77±0.10	ND	6.98±0.09*
S193$^{2.63}$A	106±11	8.29±0.06	8.92±0.10	7.83±0.10	7.12±0.11	8.22±0.11
V194$^{2.64}$A	108±9	8.21±0.07	8.02±0.09*	7.11±0.08*	6.74±0.09*	8.14±0.20
K197$^{2.67}$A	85±10	6.20±0.11*	7.64±0.10*	5.81±0.07*	ND	6.01±0.12*
D198$^{2.68}$A	104±16	6.81±0.07*	6.85±0.07*	6.15±0.13*	6.72±0.13*	7.68±0.35*
L201$^{2.71}$A	*94±2*	7.41±0.08*	8.61±0.10*	6.97±0.10*	6.60±0.09*	7.91±0.06
K202$^{2.72}$A	*94±3*	8.22±0.08	8.80±0.09	6.72±0.05*	6.77±0.12*	7.77±0.13
M204$^{2.74}$A	*99±2*	7.10±0.12*	7.80±0.07*	6.13±0.06*	7.17±0.10	7.99±0.08
Y205$^{2.75}$A	*68±5**	8.51±0.07	8.06±0.03*	7.44±0.07	7.16±0.12	8.07±0.06
S206$^{2.76}$A	*111±6*	8.310.07	8.74±0.06	7.78±0.06	6.56±0.09*	8.01±0.05
Q210^{ECL1}A	*88±4*	8.55±0.07	8.71±0.07	7.18±0.09*	6.30±0.08*	8.02±0.05
Q211^{ECL1}A	*112±5*	8.63±0.07	8.47±0.11*	7.71±0.09	6.62±0.17*	8.06±0.01
H212^{ECL1}A	*103±3*	8.91±0.05	9.35±0.09	7.89±0.08	6.55±0.18*	8.15±0.06
W214^{ECL1}A	*99±5*	8.28±0.05	8.80±0.07	7.37±0.07	6.85±0.08	7.90±0.08
F230$^{3.33}$A	97±15	7.33±0.16*	7.68±0.08*	7.53±0.21	6.87±0.10	8.23±0.10
M233$^{3.36}$A	102±10	7.19±0.07*	7.76±0.04*	6.63±0.11*	6.91±0.18	8.45±0.07*
Q234$^{3.37}$A	102±5	6.94±0.08*	7.84±0.07*	6.25±0.08*	7.18±0.10	7.81±0.07
V237$^{3.40}$A	108±11	8.02±0.05*	8.86±0.11	7.43±0.12	7.06±0.11	8.87±0.12
N240$^{3.43}$A	86±3	7.83±006*	8.72±0.05*	8.01±0.10	7.32±0.13	8.06±0.22
Y241$^{3.44}$A	103±17	ND	ND	ND	ND	ND
W297^{ECL2}A	*60±6**	6.47±0.08*	7.66±0.08*	7.39±011	5.95±0.15*	8.10±0.08
T298 ^{ECL2}A	*85±6*	8.85±0.06	9.47±0.05	8.24±0.05*	7.06±0.07	8.19±0.05
R299 ^{ECL2}A	*94±5*	7.35±0.08*	7.49±0.13*	6.26±0.18*	6.97±0.07	7.48±0.08
N300 ^{ECL2}A	*130±6**	7.02±0.07*	7.50±0.06*	6.49±0.12*	6.47±0.06*	7.95±0.04
W306$^{5.36}$A	*ND*	ND	ND	ND	ND	ND
I309$^{5.39}$A	85±10	8.05±0.15*	8.50±0.14*	7.29±0.17*	7.47±0.15	8.35±0.10*

		GLP-1(7-36)NH_2	Exendin 4	Oxyntomodulin	Exendin P5	Exendin (9-39)
	Expression %	**pIC50**	**pIC50**	**pIC50**	**pIC50**	**pIC50**
R310$^{5.40}$A	103±5	6.93±0.08*	7.42±0.11*	6.17±0.07*	7.14±0.14	8.38±0.06*
I313$^{5.43}$A	115±12	7.52±0.11*	7.95±0.10*	7.05±0.12*	6.81±0.11	8.16±0.09
H363$^{6.52}$A	*59±4**	7.02±0.06*	6.96±0.06*	6.42±0.08*	7.11±0.14	8.25±0.18
E364$^{6.53}$A	*41±4**	6.77±0.13*	7.06±0.16*	8.06±0.25	6.16±0.11	7.50±0.10*
F367$^{6.56}$A	100±10	8.89±0.16	ND	ND	ND	6.81±0.05*
A368$^{6.57}$G	96±7	8.04±0.11*	8.54±0.08*	7.28±0.07*	6.98±0.08	8.13±0.08
D372 ^{ECL3}A	*86±4*	7.23±0.08*	7.93±0.05*	7.21±0.11*	7.19±0.08	7.92±0.06
R380$^{7.53}$A	*73±5**	7.17±0.06*	7.68±0.06*	7.04±0.07*	6.85±0.05	8.02±0.04
F381$^{7.55}$A	*92±5*	8.54±0.05	8.97±0.05	6.39±0.05*	6.85±0.08	7.61±0.09*
K383$^{7.57}$A	*78±4**	7.81±0.05*	8.07±0.10*	6.23±0.10*	7.19±0.09	7.82±0.09*
L384$^{7.58}$A	*74±7**	7.63±0.10*	8.02±0.06*	6.27±0.11*	7.11±0.07	7.93±0.08
F385$^{7.59}$A	*110±7*	8.82±0.06	9.00±0.08	7.25±0.06*	7.61±0.12	8.17±0.07
E387$^{7.61}$A	*104±6*	7.87±0.06*	8.77±0.06	6.82±0.60*	6.02±0.14*	7.95±0.07
L388$^{7.62}$A	133±26	7.51±0.20*	7.93±0.27*	6.91±0.27*	6.69±0.17*	8.42±0.13*
T391$^{7.65}$A	96±8	7.90±0.01*	8.59±0.10*	8.34±0.12*	7.36±0.13	7.46±0.07*
Q394$^{7.68}$A	*103±3*	8.20±0.06*	8.71±0.08*	7.55±0.07	6.96±0.07	8.20±0.07

Table 5.1: Expression and pIC50 data for mutants of the deep binding pocket, extracellular loops and polar network for GLP-1(7-36)NH_2 , exendin 4, oxyntomodulin, exendin P5 and exendin (9-39). Expression measured via ELISA and normalised to the expression of the WT cell line, binding measured by radioligand competition binding using 125 I Exendin(9-39). Statistics used was One Way ANOVA with Dunnets post-test compared to the WT expression or pIC50 (*=$p<0.05$). Values in italics are taken from either Wootten et al. 2015, Wootten et al. 2016, Koole et al. 2012, Koole et al. 2013 and Lei et al 2018. Data obtained for GLP-1 was pooled with data from above papers, data for exendin 4 and oxyntomodulin was taken from papers above with authors permission

5.2.2 Effects of alanine mutations on ligand binding affinity

Binding affinity for GLP-1, Exendin-4, Oxyntomodulin and Exendin-P5 was assessed using a radiolabeled competition binding. I^{125}Exendin(9-39) was used as the tracer and non-specific binding was determined by using a saturating concentration of unlabeled exendin(9-39). For Y241$^{3.44}$A and E139$^{1.33}$A, ligand affinity could not be assessed, as these mutant receptors did not bind the iodinated tracer. Unsurprisingly, W306A (that displayed undetectable cell surface expression) did not bind the iodinated tracer ligand. All other mutant GLP-1R cell lines were able to bind I^{125}Exendin(9-39) and therefore competition binding curves were generated with GLP-1(7-36)NH_2, Exendin-4, Oxyntomodulin and Exendin-P5. These are presented in Figure 5.3. A one-site three parameter inhibition binding curve was fit to the grouped data using Prism and pIC50 values determined (Table 5.1). The difference between pIC50 values of WT and mutant GLP-1Rs are plotted as bar graphs (Figure 5.4) and colour-coded dependent on the degree to which the mutation affected affinity. This provides a visual representation to easily compare similarities and differences in the patterns observed across the whole dataset between ligands. As a whole, mutations to residues in the extracellular surface of the receptor had a greater impact on the binding affinity of GLP-1(7-36)NH_2, Exendin-4 and Oxyntomodulin compared to Exendin-P5 (Table 5.1, Figures 5.3&4).

34 residues when mutated to Ala significantly altered affinity of GLP-1 with 21 of these having greater than 10 fold effect (P137$^{1.32}$A, Y148$^{1.43}$A, Y152$^{1.47}$A, R190$^{2.60}$A, D198$^{2.68}$A, L201$^{2.71}$A, K202$^{2.72}$A, Y205$^{2.73}$A, M233$^{3.36}$A, Q234$^{3.37}$A, V237$^{3.40}$A, W297^{ECL2}A, R299^{ECL2}A, N300^{ECL2}A, R310$^{5.40}$A, I313$^{5.43}$A, H363$^{6.52}$A, E364$^{6.53}$A, D372^{ECL3}A, R380$^{7.35}$A, L388$^{7.43}$A). A similar pattern for mutation of these residues was observed for Exendin-4 where 31 mutations in total significantly altered affinity, 21 reducing affinity greater than 10-fold (Y152$^{1.47}$A, R190$^{2.60}$A, V194$^{2.64}$A, D198$^{2.68}$A, L201$^{2.71}$A, Y205$^{2.73}$A, Q211^{ECL2}A, F230$^{3.33}$A, M233$^{3.36}$A, Q234$^{3.37}$A, V237$^{3.40}$A, W297^{ECL2}A, R299^{ECL2}A, N300^{ECL2}A, R310$^{5.40}$A, I313$^{5.43}$A, H363$^{6.52}$A, E364$^{6.53}$A, D372^{ECL3}A, R380$^{7.53}$A, L388$^{7.43}$A). While many of these overlapped with GLP-1 (Figure 5.3), the magnitude of effect sometimes differed. There were a couple of exceptions where effects of mutations differed between GLP-1 and Exendin-4. V194$^{2.64}$A, S205$^{2.74}$A and H211^{ECL2}A significantly altered Exendin-4 affinity with no effect on GLP-1 whereas L144$^{1.39}$A, Y145$^{1.40}$A, V237$^{3.40}$A and N240$^{3.44}$A selectively reduce GLP-1 affinity with little effect on exendin-4 (Table 5.1, Figure 5.3).

While there was also overlap with residues that altered affinity of Oxyntomodulin when mutated to Ala, overall a different pattern was observed (relative to GLP-1 and Exendin-4), when comparing the data as a whole (Figure 5.3). 28 residues in total significantly reduced Oxyntomodulin affinity, however only 16 residues (L141$^{1.36}$A, Y148$^{1.43}$A, Y152$^{1.47}$A, K197$^{2.67}$A, D198$^{2.68}$A, L201$^{2.71}$A, K202$^{2.72}$A, M204$^{2.74}$A, M233$^{3.36}$A, Q234$^{3.37}$A, R299^{ECL2}A, N300^{ECL2}A, R310$^{5.40}$A, F381$^{7.41}$A, K383$^{7.43}$A, L384$^{7.33}$A) impacted greater than 10-fold. In contrast to GLP-1 and Exendin-4, mutations to residues within TM1 (L141$^{1.36}$ and Y158$^{1.47}$) and the top of TM7 (K381-F385) have a greater impact on Oxyntomodulin affinity. Interestingly, W297^{ECL2}A within ECL2, M233$^{3.36}$A and residues within TM2 (R190$^{2.60}$A, S193$^{2.63}$A, V194$^{2.64}$A) had a large impact on GLP-1 and Exendin-4, however little impact on Oxyntomodulin affinity. In addition, 2 residues (T391$^{7.46}$A and T298^{ECL2}A) when mutated significantly increased affinity of Oxyntomodulin. While T298^{ECL2}A had a similar trend for GLP-1 and Exendin-4, the opposite effect (reduced affinity) was observed for these ligands for T391$^{7.46}$A, highlighting different roles of this residue depending on the bound ligand (Figure 5.4).

While residues within the TM binding pocket play an important role in driving ligand affinity for GLP-1, Oxyntomodulin and Exendin-4, they play a much smaller role for Exendin-P5 (Figure 5.4). Only 3 out of the 51 residues assessed (W297^{ECL2}A, E364$^{6.52}$A and E387$^{7.42}$A) negatively impacted Exendin-P5 binding greater than 10-fold (with all of these also being crucial for the other 3 ligands). However, there were 13 that had a smaller yet significant impact on Exendin-P5 affinity (P137$^{1.33}$A, L142$^{1.38}$A, L144$^{1.40}$A, K197$^{2.67}$A, L201$^{2.71}$A, M204$^{2.74}$A, Q210^{ECL2}A, Q211^{ECl2}A, H212^{ECL2}A, W214^{ECL2}A, W306$^{5.36}$A, L388$^{7.43}$A), most of which also affected the other agonists, albeit often to a greater degree than Exendin-P5. Interestingly, the residues in ECL1 (Q210-W214) all had an impact of on Exendin-P5 affinity, with little effect on the other agonists assessed (Figure 5.4). All pIC50 results (as fold change from WT) were heat mapped onto ligand bound GLP-1R models generated from modelling into the cryo-EM maps generated by our laboratory.

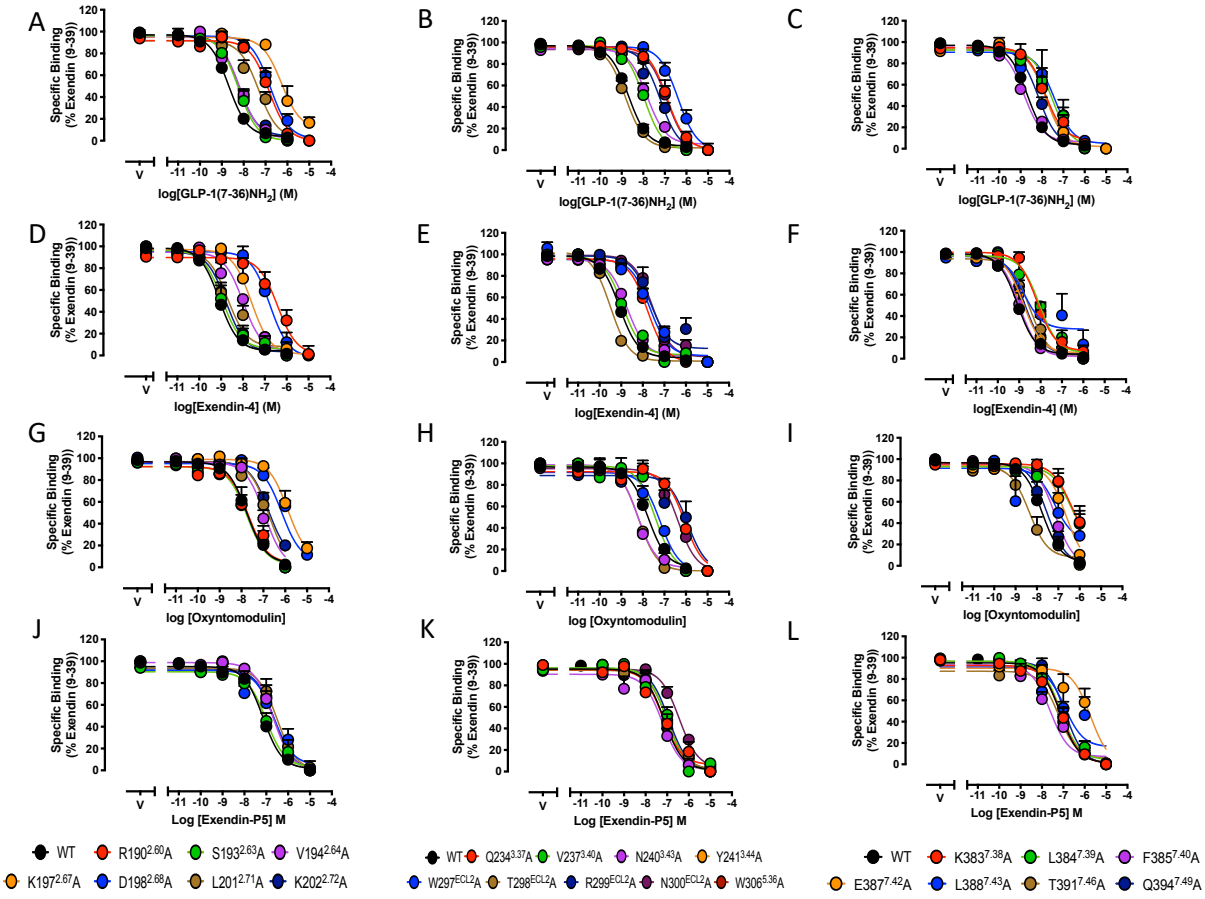

Figure 5.3.1). Competition binding studies for WT and alanine mutant GLP-1 receptors showing the ability of GLP-1(7-36)NH_2 (**A-C**), Exendin-4 (**D-F**), Oxyntomodulin (**G-I**) and Exendin-P5 (**J-L**) to compete with the tracer, I^{125} Exendin(9-39). Data are expressed as % specific binding by normalizing to the value for I^{125} Exendin(9-39) binding in the absence of unlabeled ligand (100 %) and in the presence of a saturating concentration of unlabeled Exendin(9-39). Data were fit to a one-site inhibition binding curve. All values are grouped data showing the mean ± SEM of 3-4 independent experiments performed in duplicate.

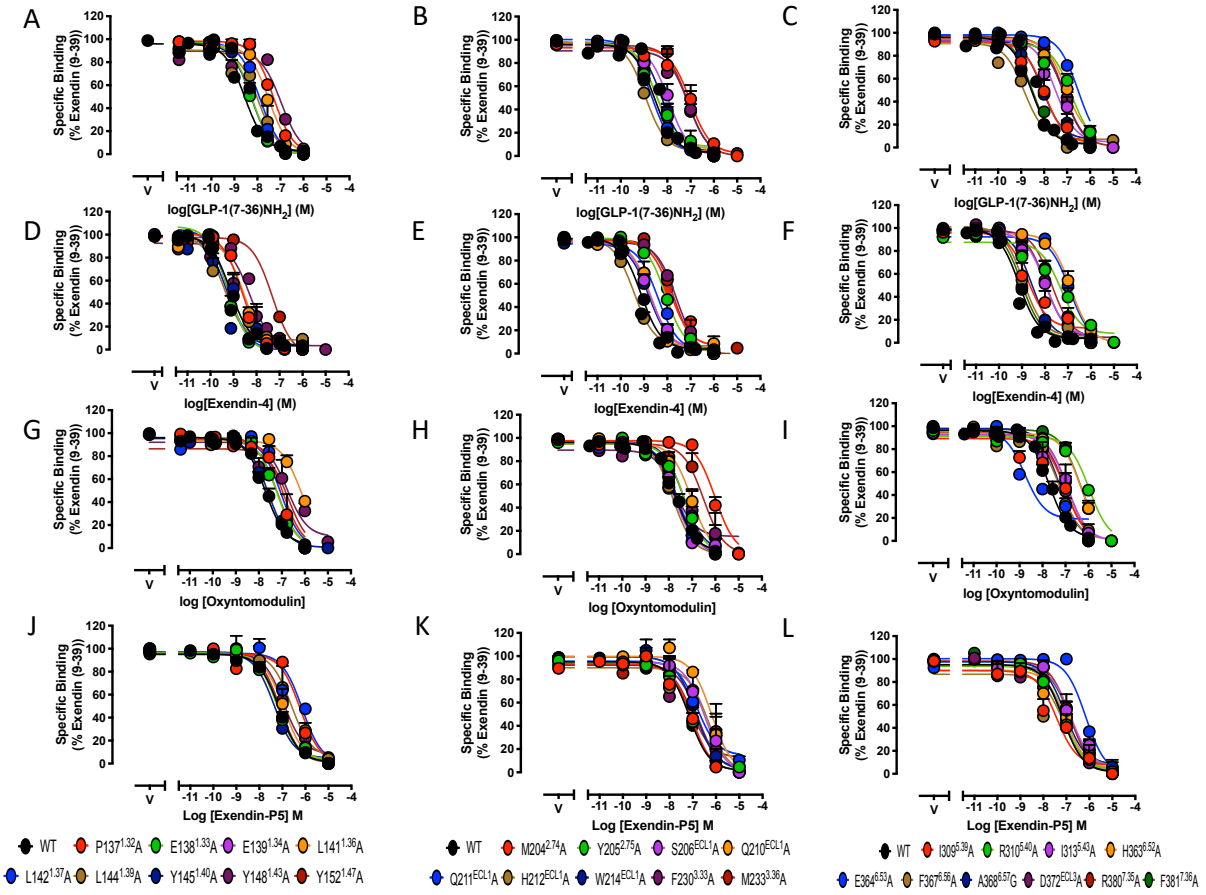

Figure 5.3.2). Competition binding studies for WT and alanine mutant GLP-1 receptors showing the ability of GLP-1(7-36)NH_2 (**A-C**), Exendin-4 (**D-F**), Oxyntomodulin (**G-I**) and Exendin-P5 (**J-L**) to compete with the tracer, I^{125} Exendin(9-39). Data are expressed as % specific binding by normalizing to the value for I^{125} Exendin(9-39) binding in the absence of unlabeled ligand (100 %) and in the presence of a saturating concentration of unlabeled Exendin(9-39). Data were fit to a one-site inhibition binding curve. All values are grouped data showing the mean ± SEM of 3-4 independent experiments performed in duplicate.

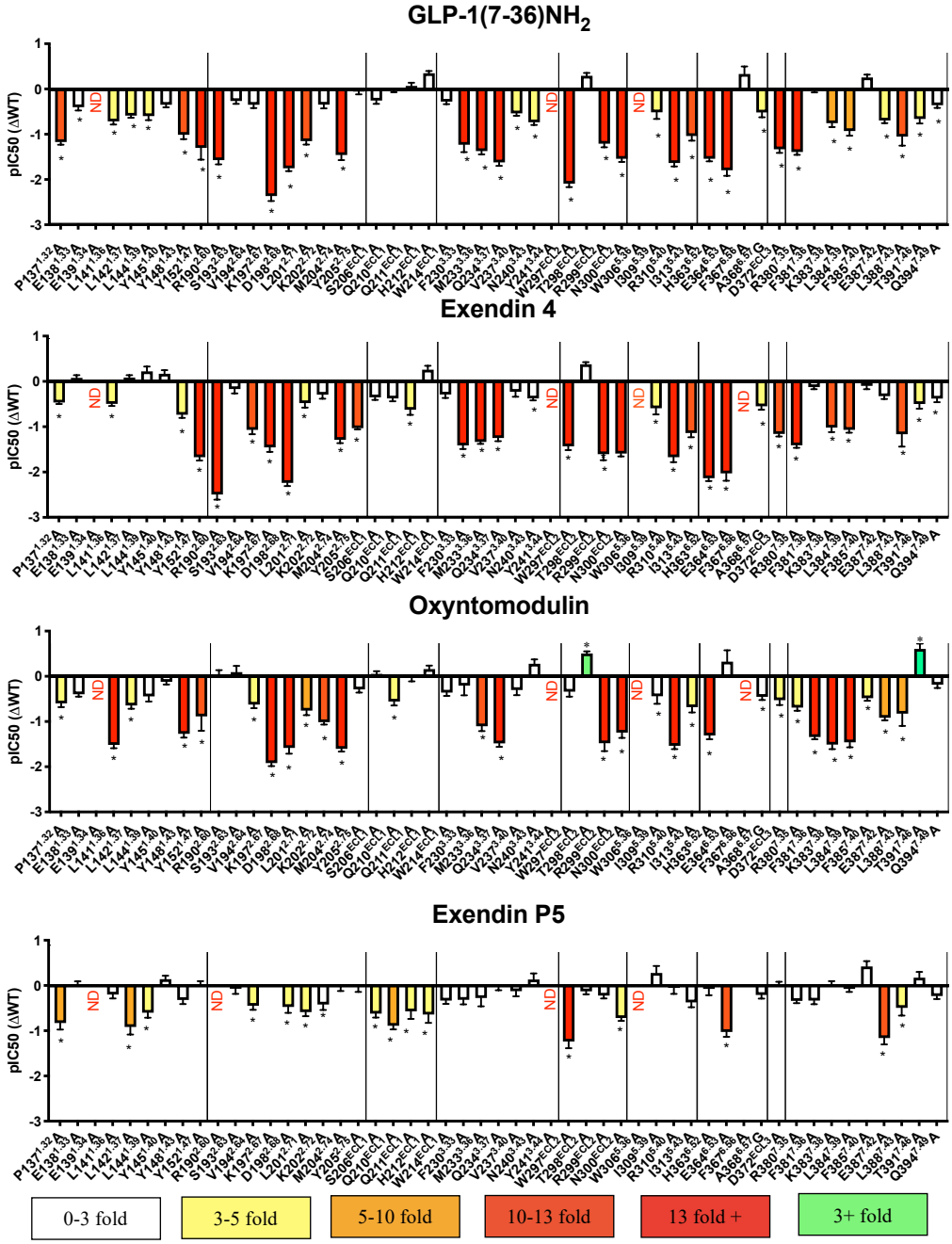

Figure 5.4) Difference in ligand binding (pIC50) of GLP-1R mutants compared to the WT for GLP-1 (top), Exendin-4 (second from top), Oxyntomodulin (third from top) and Exendin-P5 (bottom). Statistical significance of changes in binding affinity was determined by one-way analysis of variance and Dunnett's post-test, with those that are significantly different from WT indicated with an asterisk (*$p < 0.05$). Data coloured based on the direction (yellow-red = reduced affinity, green = enhanced affinity) and the extent of effect. All values are ± SEM of 3-6 independent experiments, conducted in duplicate. ND indicates no response was measurable in concentration range tested.

These were coloured according to the magnitude of effect of alanine mutation from each residue using the same colour scheme used in Figure 3, to give a stronger visual representation of the effect these mutations had on affinity relative to their locations in the TM binding site (Figure 5.5)

5.2.3 Effects of alanine mutations on ligand-induced cAMP signalling

WT and mutant receptors were assessed for their ability to signal to the cAMP pathway. Concentration response curves were generated for the four peptides GLP-1, Oxyntomodulin, Exendin-4 and Exendin-P5 and data was normalised to the maximum response of the WT receptor (Figure 5.6). pEC50 and Emax values were determined using a three-parameter curve fit. These are presented in Table 5.2. For all four ligands there was a universal decrease in both EC50 and/or Emax values for the majority of mutants assessed, when compared to the WT receptor (Figure 5.6, Table 5.2).

While EC50 and Emax values are useful to assess the ability of different mutant receptors to signal, there are a number of factors that contribute to the information obtained in these values. EC50 values are composite of the functional affinity (the affinity of the agonist when coupled to the particular pathway being assessed), efficacy (the ability of the ligand to activate the pathway) and the number of receptors present at the cell surface, whereas Emax values are a composite of efficacy and the number of receptors present in the cell. These numbers are therefore influenced by differing receptor expression levels of mutant receptors relative to WT. Operational fitting of concentration response data can separate functional affinity (K_A) and efficacy (τ). As efficacy values (but not functional affinity) are influenced by receptor expression levels, the operational measure of tau can be corrected for differences in expression levels between WT and mutant receptors to provide a measure of efficacy that is independent of expression differences (tau_c (τ_c)) and allows for direct comparisons between cell lines expressing different receptor variants (Wootten et al 2016a). These values, derived from operational fitting to concentration response data are presented in Table 5.2. The change in pK_A and $Log\tau_c$ values between WT and each mutant receptor are plotted as bar graphs in Figures 5.7 and 5.8, respectively, and coloured according to their level of effect.

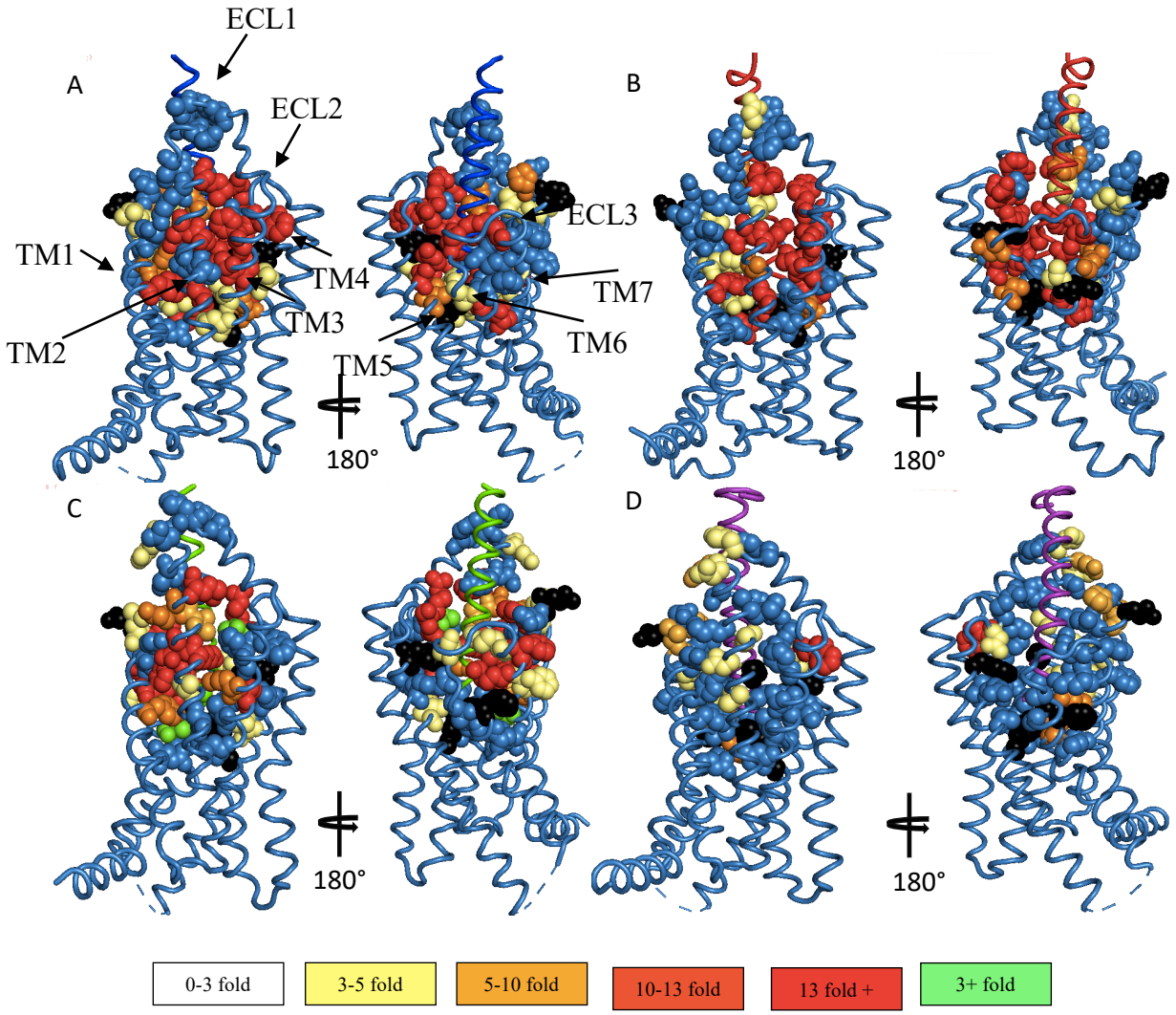

Figure 5.5) Cryo-EM strucutres of the active GLP-1R bound to GLP-1R (**A**), Exendin-4 (**B**), oxyntomodulin (**C**) and Exendin-P5 (**D**) with pIC50 values heat mapped onto each assessed residue to show affect of mutants on ligand affinity. Residues which had neutral impact are shaded in blue, reductions between 3-5 fold in yellow. 5-10 fold in light orange, 10-15 in dark orange, 15+ fold in red and any positive changes are in green. Residues where no radioligand binding was detected were are shaded black. Ligand colours are GLP-1 (blue), exendin 4 (red), oxyntomodulin (green) and exendin P5 (purple)

Similar to affinity values, these were also mapped onto receptor models (cryo-EM structures) of the individual ligand-bound GLP-1Rs (Figures 5.9 and 5.10).

5.2.3.1 Effects of alanine mutations on pKA

pKA values derived from the operational analysis closely trend with pEC50 values for cAMP. For GLP-1, Oxyntomodulin and Exendin-4, these values also closely correlate (qualitatively) with the measured affinity values. The derived pKA value for GLP-1 was significantly reduced for 29 mutations relative to the WT receptor, of which 24 (Y152$^{1.47}$A, R190$^{2.60}$A, S193$^{2.63}$A, V194$^{2.64}$A, L201$^{2.71}$A, K202$^{2.72}$A, M204$^{2.74}$A, F230$^{3.33}$A, M233$^{3.36}$A, Q234$^{3.37}$A, V237$^{3.40}$A, N240$^{3.43}$A, Y241$^{3.44}$A, W297^{ECL2}A, R299^{ECL2}A, N300^{ECL2}A, I309$^{5.39}$A, R310$^{5.40}$A, I313$^{5.43}$A, D372^{ECL3}A, K383$^{7.38}$A, L384$^{7.39}$A, F385$^{7.40}$A, L388$^{7.43}$A) were greater than 10-fold. A similar pattern was observed with Exendin-4 where a total of 25 residues displayed altered functional affinity, all of which were greater than 10-fold (L141$^{1.36}$A, Y145$^{1.40}$A, Y152$^{1.47}$A, R190$^{2.60}$A, S193$^{2.63}$A, L201$^{2.71}$A, K202$^{2.72}$A, M204$^{2.74}$A, Y205$^{2.75}$A, S206$^{2.76}$A, Q210^{ECL1}A, M233$^{3.36}$A, Q234$^{3.37}$A, V237$^{3.40}$A, Y241$^{3.44}$A, W297^{ECL2}A, R299^{ECL2}A, I309$^{5.39}$A, R310$^{5.40}$A, I313$^{5.43}$A, F367$^{6.56}$A, A368$^{6.57}$G, D372^{ECL3}A, K383$^{7.38}$A, L384$^{7.39}$A, L388$^{7.43}$A) and 16 were shared (Y145$^{1.40}$A, R190$^{2.60}$A, S193$^{2.63}$A, L201$^{2.71}$A, K202$^{2.72}$A, Q234$^{3.37}$A, V237$^{3.40}$A, W297^{ECL2}A, R299^{ECL2}A, I309$^{5.39}$A, R310$^{5.40}$A, I313$^{5.43}$A, A368$^{6.57}$G, D372^{ECL3}A, K383$^{7.38}$A, L384$^{7.39}$A, L388$^{7.43}$A). Interestingly, while the mutations that reduce affinity overlap, generally there is a greater effect of mutation on GLP-1 functional affinity than Exendin-4 for the majority of these mutations (Figures 5.7 and 5.8)

Similar to observed in the overall affinity measures, a large number of mutations also altered Oxyntomodulin functional affinity, and while the majority of these overlapped with those that altered GLP-1 and Exendin-4, the overall pattern of effect differed (Figure 5.7). While 27 mutations statistically reduced functional affinity, only 13 of these reduced the KA by greater than 10-fold (P137$^{1.32}$A, L142$^{1.37}$A, L144$^{1.39}$A, Y145$^{1.40}$A, R190$^{2.60}$A, L201$^{2.71}$A, K202$^{2.72}$A, M204$^{2.74}$A, Y205$^{2.75}$A, S206$^{2.76}$A, Q211^{ECL1}A, H212^{ECL1}A, F230$^{3.33}$A, M233$^{3.36}$A, V237$^{3.40}$A, Y241$^{3.41}$A, R299^{ECL2}A, N300^{ECL2}A, I309$^{5.39}$A, R310$^{5.40}$A, I313$^{5.41}$A, E364$^{6.53}$A, D372^{ECL2}A, R380$^{7.35}$A,

	GLP-1(7-36)NH_2				Exendin 4				Oxyntomodulin				Exendin P5			
	pEC50	EMAX	pKA	τ_c	pEC50	EMAX	pKA	τ_c	pEC50	EMAX	pKA	τ_c	pEC50	EMAX	pKA	τ_c
WT	9.91±0.03	100±1	9.23±0.07	0.85±0.03	10.48±0.05	100±1	9.80±0.07	0.75±0.03	8.24±0.05	100±1	7.99±0.05	0.72±0.03	9.12±0.04	100±1	8.39±0.07	0.83±0.04
P137$^{1.32}$A	9.73±0.21	69±4*	9.32±0.20	0.71±0.07	10.45±0.29	89±7	9.83±0.20	0.64±0.11	7.66±0.20	78±5	7.43±0.16	0.46±0.09	9.30±0.29	42±4*	9.05±0.27	-0.09±0.08*
E138$^{1.33}$A	9.86±0.16	81±4	9.35±0.21	0.49±0.05	10.26±0.09	103±3	9.38±0.23	0.79±0.15	7.84±0.14	101±5	7.56±0.10	0.71±0.1	10.06±0.40	54±6*	9.71±0.29*	-0.11±0.07*
E139$^{1.34}$A	10.25±0.25	52±5*	10.01±0.57	0.56±0.26	10.90±0.51	28±4*	10.73±0.51	-0.11±0.27*	8.16±0.33	34±3*	8.08±0.31	0.22±0.26*	6.67±0.36*	35±5*	6.90±0.63*	0.19±0.11*
L141$^{1.36}$A	9.69±0.14	95±4	9.00±0.37	0.63±0.07	10.43±0.12	113±4*	9.18±0.37	1.28±0.31*	7.25±0.16	105±7	6.93±0.13*	0.89±0.18	8.92±0.16	84±4	8.38±0.12	0.42±0.06
L142$^{1.37}$A	9.78±0.19	62±4*	9.47±0.20	0.25±0.07*	10.79±0.27	77±6	10.3±0.20	0.27±0.09*	7.44±0.20	72±5*	7.24±0.18	0.39±0.09	5.39±0.53*	97±5	8.93±0.40	-0.23±0.1*
L144$^{1.39}$A	8.68±0.16*	64±4*	8.37±0.23	0.64±0.42	8.79±0.14*	69±4*	8.41±0.23*	0.73±0.43	6.22±0.21*	37±4*	6.12±0.31*	0.23±0.43*	8.37±0.21	76±5*	7.93±0.18	1.03±0.22
Y145$^{1.40}$A	9.51±0.13	96±4	8.79±0.12	1.09±0.06	10.31±0.09	94±2	9.63±0.12	0.74±0.07	7.93±0.08	105±3	7.61±0.07	1.02±0.09	8.53±0.12	99±4	7.76±0.13	0.86±0.08
Y148$^{1.43}$A	8.57±0.11*	85±3	8.03±0.14*	0.77±0.06	9.50±0.20*	93±6	8.86±0.14*	0.83±0.08	7.33±0.30*	50±5*	7.27±0.17*	0.31±0.06	7.87±0.18*	38±3*	7.73±0.24	-0.05±0.07*
Y152$^{1.47}$A	8.14±0.17*	61±4*	7.80±0.19*	0.16±0.07*	9.00±0.21*	60±4*	8.74±0.19*	0.33±0.07*	7.41±0.23	59±5*	7.25±0.19*	0.32±0.07	6.85±0.24*	12±1*	6.61±1.34*	-0.84±0.26*
R190$^{2.60}$A	7.19±0.12*	69±4*	6.89±0.12*	0.11±0.08*	8.69±0.14	79±4*	8.32±0.12*	0.54±0.07	9.10±0.09*	87±2	8.87±0.07*	1±0.06	7.57±0.48*	20±4*	7.53±0.62*	-0.26±0.15*
S193$^{2.63}$A	9.22±0.13	110±5	8.11±0.22	1.31±0.26	10.18±0.35	82±8	9.68±9.22	0.55±0.09	8.44±0.24	96±8	8.15±0.14	0.83±0.11	8.50±0.12	95±4	7.78±0.24	0.81±0.14
V194$^{2.64}$A	8.71±0.27*	64±6*	8.42±0.25	0.27±0.08*	9.64±0.29*	64±5*	9.34±0.25	0.26±0.08*	7.94±0.15	55±3*	7.78±0.21	0.14±0.07*	7.25±0.30*	62±9*	6.94±0.30*	0.23±0.13*
K197$^{2.67}$A	8.65±0.62*	25±6*	8.50±0.68	-0.25±0.2*	10.18±0.50	24±3*	10.01±0.68	-0.08±0.14*	8.71±0.71	27±5*	8.69±0.54	0±0.11*	ND	ND	ND	ND
D198$^{2.68}$A	6.19±0.13*	88±9	5.68±0.23*	0.73±0.32	7.90±0.11*	84±4	7.37±0.23*	0.69±0.12	6.54±0.19*	52±4*	6.18±0.25*	0.2±0.09*	7.13±0.34*	10±1*	7.09±1.53	-0.76±0.27*
L201$^{2.71}$A	8.09±0.08*	91±3	7.54±0.19*	0.40±0.09*	9.30±0.13*	90±2	8.70±0.19*	0.48±0.1	6.54±0.15*	61±2*	6.41±0.6*	-0.17±0.07*	8.38±0.15	92±5	7.73±0.16	0.74±0.08
K202$^{2.72}$A	8.62±0.12*	88±4	8.10±0.26*	0.36±0.07*	9.71±0.08	90±2	9.03±0.26	0.51±0.12	7.33±0.07*	80±2*	7.09±0.12*	0.52±0.06	7.98±0.19*	97±7	7.30±0.20	0.84±0.13
M204$^{2.74}$A	7.94±0.09*	83±3	7.44±0.25*	0.55±0.09	9.61±0.07	96±2	8.98±0.25	0.78±0.13	6.73±0.08*	78±3*	6.49±0.13*	0.46±0.06	8.03±0.16*	71±5*	2.61±0.31	0.36±0.12*
Y205$^{2.75}$A	9.07±0.31	65±6*	8.83±0.36	0.22±0.07*	9.32±0.24*	42±3*	9.10±0.36	0.09±0.09*	7.32±0.20*	51±4*	7.16±0.17*	0.08±0.07*	8.64±0.26	86±7	8.23±0.16	0.75±0.09
S206$^{2.76}$A	9.97±0.10	107±3	9.02±0.26	1.05±0.1	9.64±0.27	104±7	8.93±0.26	0.95±0.17	7.83±0.07	99±3	7.52±0.10	0.83±0.09	8.85±0.10	96±3	8.15±0.13	0.74±0.07
Q210^{ECL1}A	9.83±0.14	74±3*	9.38±0.19	0.46±0.06	10.79±0.10	88±3	10.19±0.19	0.68±0.08	7.22±0.10*	89±3	6.94±0.12*	0.71±0.07	9.29±0.23	64±4*	8.91±0.30	0.31±0.09*
Q211^{ECL1}A	9.46±0.11	85±3	8.97±0.17	0.53±0.05	10.51±0.11	92±2	9.85±0.17	0.68±0.08	7.54±0.08	84±2	7.28±0.10*	0.31±0.05	9.67±0.26	84±6	9.12±0.25	0.51±0.1
H212^{ECL1}A	10.26±0.10	90±3	9.67±0.17	0.66±0.06	10.44±0.08	86±2	9.90±0.17	0.59±0.07	8.00±0.10	100±2	7.77±0.10	0.47±0.05	9.36±0.14	91±3	8.73±0.24	0.68±0.07
W214^{ECL1}A	9.24±0.11*	84±3	8.71±0.22	0.36±0.06*	10.30±0.14	93±4	9.62±0.22	0.74±0.11	7.53±0.12	71±3*	7.32±0.13*	0.16±0.05*	8.00±0.17*	54±4*	7.69±0.38	0.11±0.12*
F230$^{3.33}$A	8.18±0.16*	96±6	7.47±0.25*	0.77±0.2	9.35±0.28*	75±7	8.92±0.25	0.59±0.15	7.60±0.16	90±6	7.32±0.15	0.85±0.16	8.15±0.09*	98±4	7.38±0.26	1.03±0.21
M233$^{3.36}$A	8.32±0.18*	91±7	7.70±0.24*	0.84±0.13	9.18±0.34*	80±9	8.73±0.24*	0.64±0.11	8.01±0.25	92±9	7.72±0.14	0.87±0.11	8.05±0.22*	85±9	7.48±0.25	0.73±0.14
Q234$^{3.37}$A	7.93±0.12*	98±5	7.20±0.21*	0.82±0.14	9.14±0.15*	88±5	8.57±0.22*	0.61±0.11	6.92±0.12*	84±4	6.70±0.14*	0.55±0.08	9.19±0.15	94±5	8.50±0.19	0.73±0.1
V237$^{3.40}$A	8.35±0.10*	95±4	7.68±0.24*	0.61±0.14	8.95±0.23*	95±8	8.30±0.24*	0.62±0.14	7.48±0.12	112±6*	7.11±0.13*	1.23±0.36	8.08±0.09*	107±4	7.06±0.26	0.99±0.28
N240$^{3.43}$A	9.02±0.11*	80±3	8.61±0.14	0.25±0.08*	10.54±0.11	84±2	10.00±0.14	0.62±0.06	8.71±0.09	89±2	8.48±0.09	0.7±0.05	7.06±0.13*	89±5	6.49±0.29*	0.71±0.15
Y241$^{3.44}$A	9.59±0.15	105±5	8.66±0.26	0.95±0.18	9.45±0.14	89±4	8.84±0.26	0.67±0.11	6.36±0.14*	82±5	6.10±0.22*	0.55±0.11	7.31±0.12*	53±3*	7.13±0.48	0.1±0.16*
W297^{ECL2}A	6.82±0.15*	48±5*	6.57±0.14*	0.03±0.13*	7.90±0.17*	75±6*	7.51±0.14*	0.24±0.1*	ND	ND	ND	ND	7.93±0.14*	67±4*	7.54±0.15	0.51±0.09*

T298 ^{ECL2}A	10.15±0.12	80±3*	9.65±0.17	0.36±0.06*	10.50±0.16	69±3*	10.15±0.17	0.2±0.06*	7.98±0.14	96±4	7.83±0.16	0.85±0.12	9.15±0.18	75±4*	8.74±0.13	0.49±0.06
R299 ^{ECL2}A	8.09±0.14*	61±4*	7.77±0.18*	0.03±0.06*	9.92±0.25	56±4*	9.63±0.18	0.16±0.05*	6.90±0.13*	47±2*	6.78±0.23*	0.04±0.07*	7.90±0.14*	78±5*	7.41±0.15*	0.5±0.07
N300 ^{ECL2}A	6.88±0.10*	62±4*	6.54±0.13*	-0.1±0.09*	8.70±0.14*	75±4*	8.28±0.14*	0.21±0.06*	6.77±0.29*	21±1*	7.48±0.61	-0.66±0.11*	8.20±0.11*	82±4*	7.69±0.13	0.42±0.06*
W306$^{5.36}$A	ND	ND	ND	ND	ND	ND	ND	ND	ND	ND	ND	ND	ND	ND	ND	ND
I309$^{5.39}$A	8.64±0.17*	109±7	7.62±0.24*	1.11±0.25	9.25±0.30*	97±10	8.57±0.24*	0.93±0.15	7.78±0.13	104±6	7.45±0.13	1.15±0.18	7.21±0.11*	66±4*	6.86±0.37*	0.4±0.19*
R310$^{5.40}$A	7.90±0.43*	26±4*	8.05±0.28*	0.4±0.4	8.17±0.18*	48±4*	8.00±0.28*	0.52±0.24	6.57±0.21*	60±5*	6.46±0.18*	0.71±0.39	5.68±0.18*	70±11*	5.43±0.43*	0.82±0.47
I313$^{5.43}$A	8.40±0.15*	84±4	7.91±0.20*	0.53±0.08	9.76±0.20*	66±4*	9.41±0.20	0.26±0.06*	7.66±0.20	75±5*	7.46±0.15	0.39±0.06	8.17±0.14*	88±5	7.60±0.17	0.61±0.09
H363$^{6.52}$A	9.71±0.21	28±2*	9.59±0.36	-0.11±0.08*	10.16±0.29	34±3*	10.02±0.36	-0.09±0.09*	8.15±0.17	32±2*	8.15±0.31	-0.03±0.08*	7.88±0.47*	22±4*	8.07±0.64	-0.25±0.14*
E364$^{6.53}$A	8.89±1.56	8±3*	8.87±2.4	-0.57±0.2*	9.17±0.84*	11±2*	9.32±2.4*	0.02±0.26*	7.10±0.32	52±6*	6.99±0.38*	0.65±0.16	7.27±1.15	7±2*	9.01±3.70	-0.71±0.23*
F367$^{6.56}$A	8.92±0.17*	93±5	8.25±0.22	0.78±0.11	9.35±0.26*	68±4*	9.04±0.22	0.35±0.26	7.90±0.12	91±4	7.64±0.12	0.73±0.09	6.16±0.27*	26±5*	6.22±1.13*	-0.4±0.42*
A368$^{6.57}$G	9.05±0.20*	84±5	8.50±0.19	0.64±0.07	10.02±0.21	65±4*	9.66±0.19	0.33±0.07*	7.98±0.18	61±4*	7.82±0.16	0.27±0.06	7.16±0.17*	84±7	6.71±0.21*	0.61±0.12
D372 ^{ECL3}A	7.80±0.08*	80±3*	7.36±0.17*	0.36±0.07*	9.15±0.11*	96±3	8.47±0.19*	0.86±0.1	6.70±0.22*	61±6*	6.67±0.21*	0.28±0.08	8.82±0.10	106±3	7.98±0.15	1.14±0.11
R380$^{7.53}$A	6.78±0.08*	81±4*	6.33±0.16*	0.44±0.11*	8.03±0.15*	78±4*	7.65±0.16*	0.19±0.08*	6.54±0.33*	43±6*	6.43±0.30*	-0.12±0.1*	7.16±0.09*	96±4	6.55±0.15*	0.92±0.1
F381$^{7.55}$A	9.85±0.10	77±2*	9.40±0.18	0.28±0.05*	10.48±0.12	79±2	9.99±0.18	0.51±0.06	7.99±0.19	66±4*	7.80±0.20	0.31±0.07	8.83±0.10	96±3	8.13±0.14	0.84±0.08
K383$^{7.57}$A	6.90±0.10*	93±6	6.30±0.25*	0.62±0.18	8.74±0.24*	62±5*	8.41±0.25*	0.14±0.08*	7.27±0.28*	26±3*	7.25±0.45*	-0.48±0.1*	8.70±0.13	121±4*	ND	ND
L384$^{7.58}$A	8.47±0.13*	81±4	8.00±0.22*	0.44±0.09	10.01±0.13	67±2*	9.62±0.22	0.33±0.08	7.38±0.17	76±5*	7.23±0.14*	0.16±0.08*	7.09±0.15*	104±8	6.30±0.27*	1.11±0.21
F385$^{7.59}$A	9.47±0.14	87±3	8.93±0.21	0.27±0.06*	10.31±0.13	74±3*	9.83±0.21	0.16±0.07*	7.84±0.12	85±4	7.62±0.13	0.34±0.07	8.99±0.11	111±4	7.92±0.23	1,21±0.18
E387$^{7.61}$A	9.86±0.08	91±2	9.24±0.21	0.67±0.07	10.30±0.11	90±3	9.66±0.21	0.67±0.09	7.43±0.29	55±6*	7.28±0.20	0.09±0.09*	7.20±0.18*	74±7*	6.81±0.20*	0.38±0.09*
L388$^{7.62}$A	7.64±0.18*	98±8	6.91±0.21*	0.78±0.18	9.12±0.21*	79±6	8.64±0.21*	0.41±0.09	6.90±0.15*	90±6	6.72±0.15*	0.6±0.11	7.83±0.11*	95±4	7.16±0.21*	0.7±0.13
T391$^{7.65}$A	9.36±0.25	76±5*	8.91±0.21	0.6±0.08	10.86±0.25	62±4*	10.50±0.21	0.4±0.08	8.15±0.17	70±4*	7.98±0.14	0.52±0.08	7.81±0.13*	83±4	7.29±0.18*	0.73±0.11
Q394$^{7.68}$A	9.57±0.13	87±3	9.02±0.14	0.3±0.06*	10.44±0.17	86±4	9.93±0.14	0.58±0.06	8.02±0.08	95±2*	7.77±0.09	0.55±0.07	7.77±0.16*	73±5*	7.37±0.15*	0.38±0.06*

Table 5.2: Parameters derived from cAMP accumulation data (pEC50, Emax, pKA and Logτ_c) for mutants within the GLP-1R TM peptide binding site, for GLP-1(7-36)NH_2, Exendin 4, Oxyntomodulin and Exendin P5. Emax and pEC50 values are mean ± SEM of 3-4 independent experiments. pKA and τ values and S.E.M were calculated from operational curve-fitting to grouped data (n=3-4). τ values were corrected for differences in expression between WT and mutant receptors and errors propagated to provide τ_c ± S.E.M. ND is reported where experimental values could not be defined, either because no response was observed, or in some cases where responses were observed, but the top of the concentration response curve was not defined within the concentration range assessed.

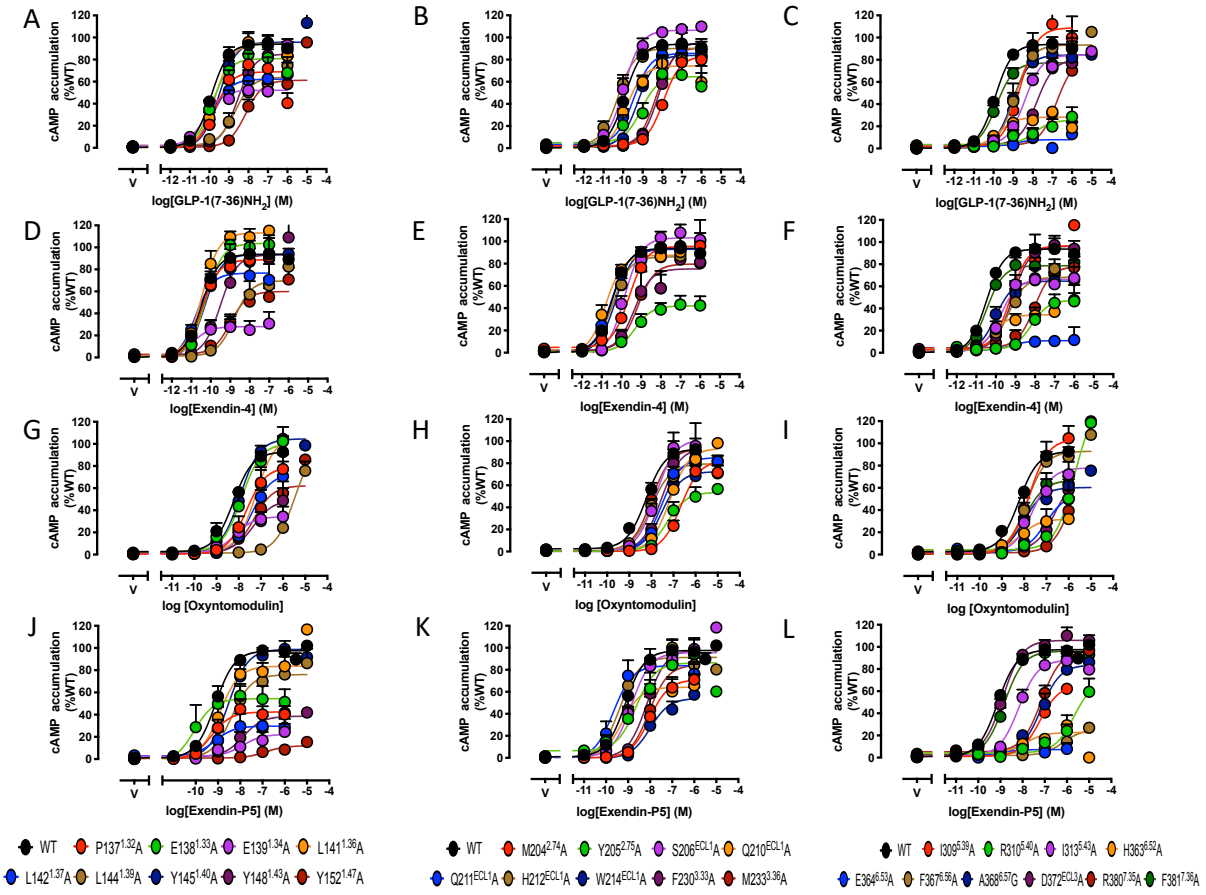

Figure 5.6.1) cAMP concentration response curves for WT and single alanine mutant GLP-1 receptors for GLP-1(7-36)NH_2 (**A-C**), Exendin-4 (**D-F**), Oxyntomodulin (**G-I**) and Exendin-P5 (**J-L**). Mutant receptor response was normalized to WT receptor response for each ligand. Curve was fitted using the operational model of agonism with the hill slope constrained to 1. Data is representative of the mean ± SEM of 3-4 independent experiments performed in duplicate.

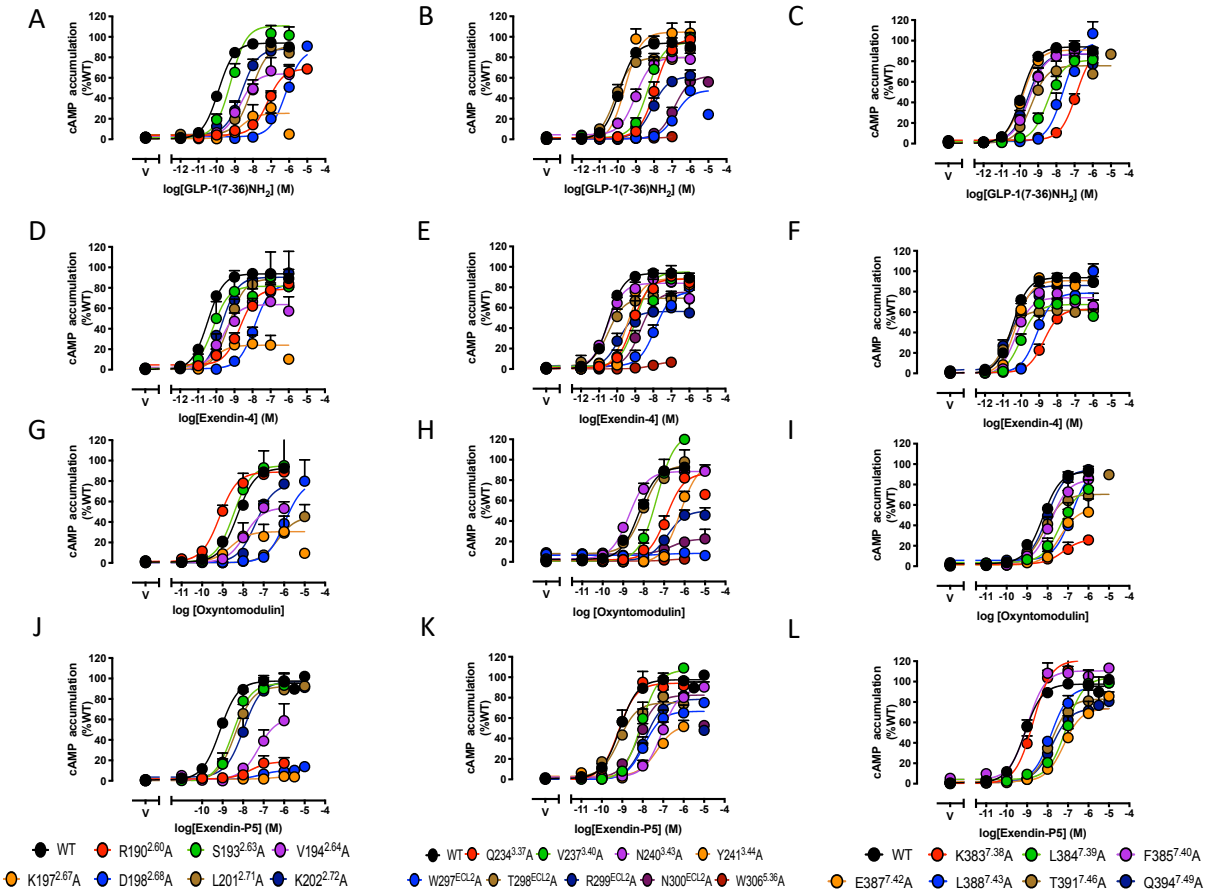

Figure 5.6.2) cAMP concentration response curves for WT and single alanine mutant GLP-1 receptors for GLP-1(7-36)NH_2 (**A-C**), Exendin-4 (**D-F**), Oxyntomodulin (**G-I**) and Exendin-P5 (**J-L**). Mutant receptor response was normalized to WT receptor response for each ligand. Curve was fitted using the operational model of agonism with the hill slope constrained to 1. Data is representative of the mean ± SEM of 3-4 independent experiments performed in duplicate.

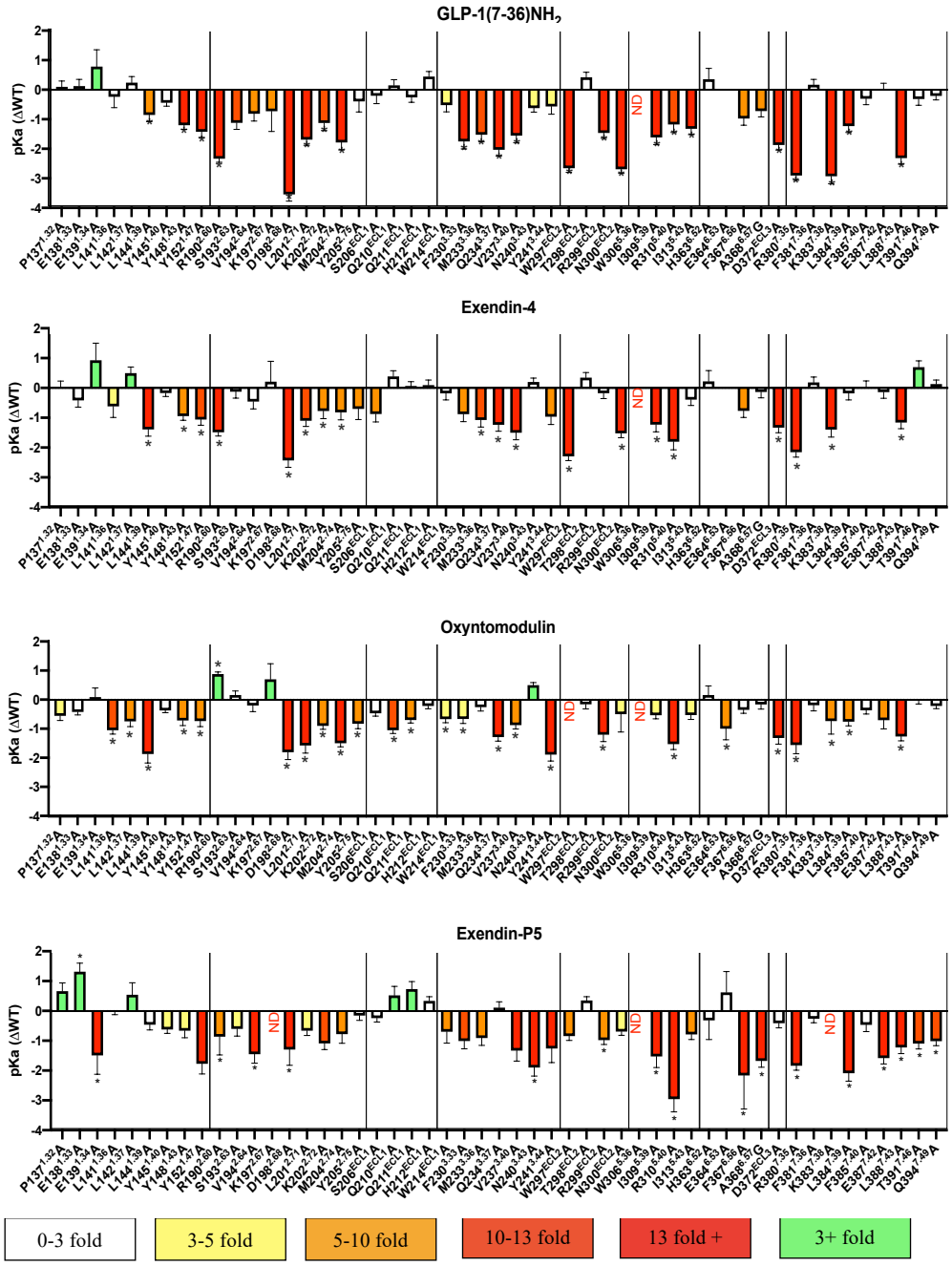

Figure 5.7) Difference in functional affinity for the cAMP pathway (pKA) for single Ala GLP-1R mutants, compared to the WT receptor values for GLP-1 (top), Exendin-4 (second from top), Oxyntomodulin (third from top) and Exendin-P5 (bottom). One-way analysis of variance and Dunnett's post-test was performed to compare pKA values from mutants relative to the WT receptor. Values indicated with an asterisk were statistically different from WT (*$p < 0.05$). Data that are statistically significant are colored based on the direction (yellow-red = reduced, green = enhanced) and extent of effect. All values are ± SEM of 3-4 independent experiments, conducted in duplicate.

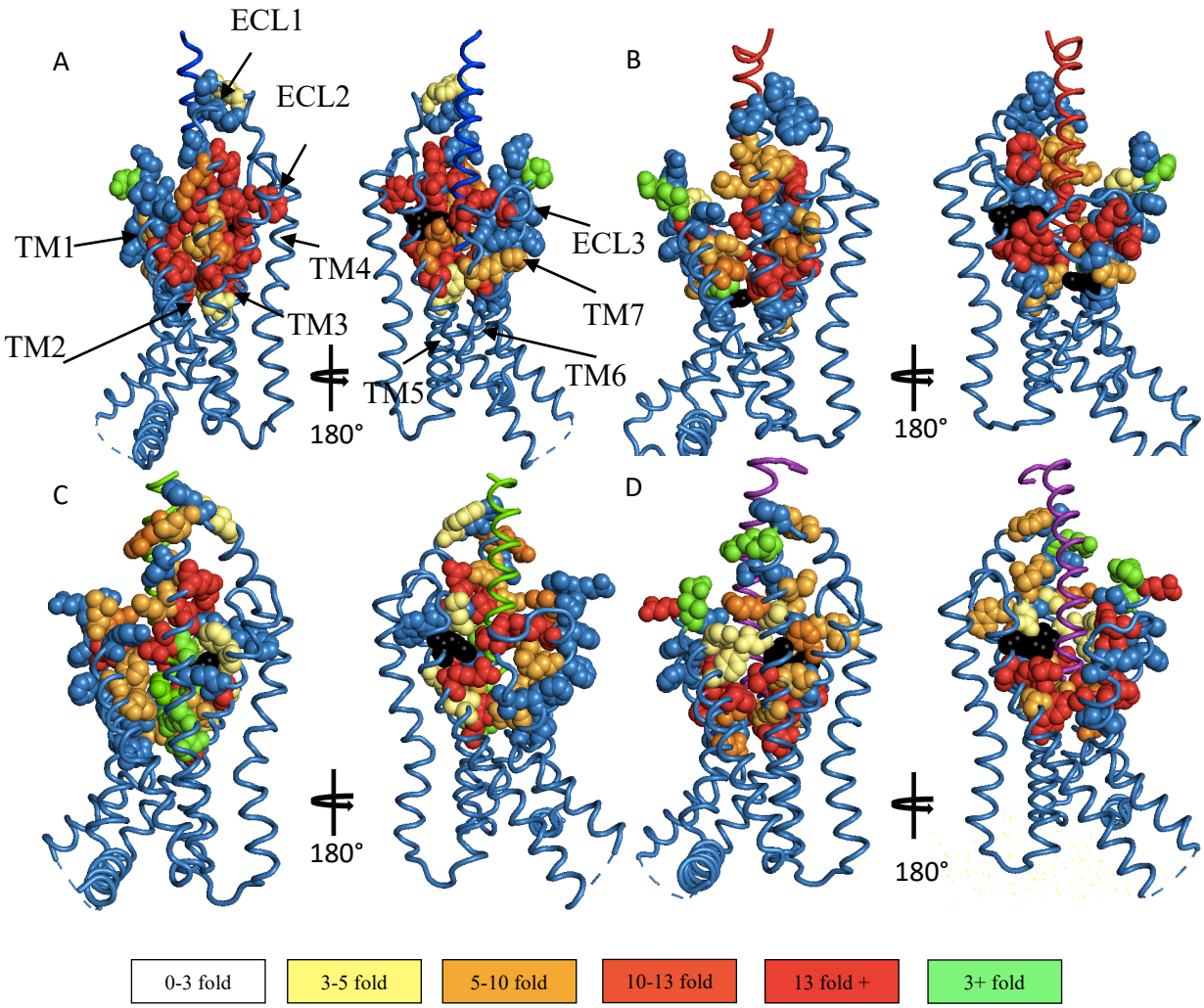

Figure 5.8) Cryo-EM structures of the active GLP-1R bound to GLP-1 (**A**), Exendin-4 (**B**), Oxyntomodulin **(C)** and Exendin-P5 (**D**). Fold differences in pKA values for alanine mutation of individual residues relative to the WT are heat mapped onto each assessed residue to show effect of mutants on pKA. Residues which had neutral impact are shaded in blue, 3-5 fold reduced pKA in yellow, 5-10 fold reduced pKA in light orange, 10-13 reduced pKA in dark orange, 13+ fold reduced pKA in red, whereas those that enhanced pKA are in green. Residues where no response was detected are shaded black. Ligand colours are GLP-1 (blue), exendin 4 (red), oxyntomodulin (green) and exendin P5 (purple)

K383$^{7.38}$A, L384A, E387$^{7.42}$A, L388$^{7.43}$A). Interestingly, residues in ECL1 had a ligand specific negative effect on Oxyntomodulin, whereas residues in TM1 increased pKA for the other agonists assessed, but not for oxyntomodulin (Figures 5.7 and 5.8).

Interestingly, despite only a few residues altering the overall affinity of Exendin-P5 (as measured in a radioligand binding assays (Figure 5.4), the functional affinity determined by operational modelling was significantly reduced for 33 of the mutated residues, relative to the WT receptor, with 21 of these reducing the functional affinity by greater than 10-fold (E139$^{1.33}$A, R190$^{2.60}$A, K197$^{2.67}$A, L201$^{2.71}$A, K202$^{2.72}$A, M204$^{2.74}$A, M233$^{3.36}$A, N240$^{3.40}$A, Y241$^{3.41}$A, I309$^{5.39}$A, R310$^{5.40}$A, F367$^{6.56}$A, A368$^{6.57}$G, R380$^{7.35}$A, K383$^{7.38}$A, L384$^{7.39}$A, E387$^{7.42}$A, L388$^{7.43}$A, T391$^{7.46}$A, Q394$^{7.49}$A) (Figure 5.7 and Figure 5.8). Residues within TM7 had a greater impact on pKA for Exendin P5 compared to other ligands.

5.2.3.2 Effects of alanine mutations on efficacy (τ)

In contrast to effects on affinity and functional affinity, much smaller effects of GLP-1R peptide binding site mutations were observed on the efficacy of GLP-1, Exendin-4 and Oxyntomodulin. While GLP-1 was significantly impacted by alanine mutation to 21 residues, only 3 residues (K197$^{2.67}$A, H363$^{6.52}$A, E364$^{6.53}$A) reduced efficacy by greater than 10-fold (Figure 5.8, Table 5.2). Similarly, Oxyntomodulin and Exendin-4 efficacy was reduced by mutation to 16 and 17 residues respectively though all of these displayed a less than a 10-fold effect (Figure 5.9).

In contrast, Exendin-P5 cAMP efficacy was more greatly affected by mutations to these residues (Table 5.2, Figures 5.9 and 5.10). Of the mutations tested, 22 significantly reduced cAMP efficacy with 8 of these (L141$^{1.36}$A, Y152$^{1.47}$A, R190$^{2.60}$A, K197$^{2.67}$A, D198$^{2.68}$A, H363$^{6.52}$A, E364$^{6.53}$A, F367$^{6.57}$A, K384$^{7.38}$A) reaching greater than 10-fold. These residues reside within three regions within the receptor, the tops of TM1, TM2 and TM6. K197$^{2.67}$A had a universal negative impact on cAMP all ligands, as did mutations within ECL2 (Figures 5.9 and 5.10, Table 5.2). Residues mutated at the top of TM1 had a greater impact on Exendin P5 accumulation compared with all other agonists assessed. Exendin 4, Exendin P5 and GLP-1 shared a greater loss of function with mutations to residues in TM6, whereas this was not observed with Oxyntomodulin (Figures 5.9 and 5.10, Table 5.2). Mutations to residues in TM2 also had a greater impact on GLP-1, Oxyntomodulin and exendin P5 compared to exendin 4. Interestingly, TM7 played a role in transmission of efficacy for GLP-1, exendin 4 and Oxyntomodulin, but played little role in efficacy for exendin P5, despite altering functional affinity (Figures 5.7 and 5.9)

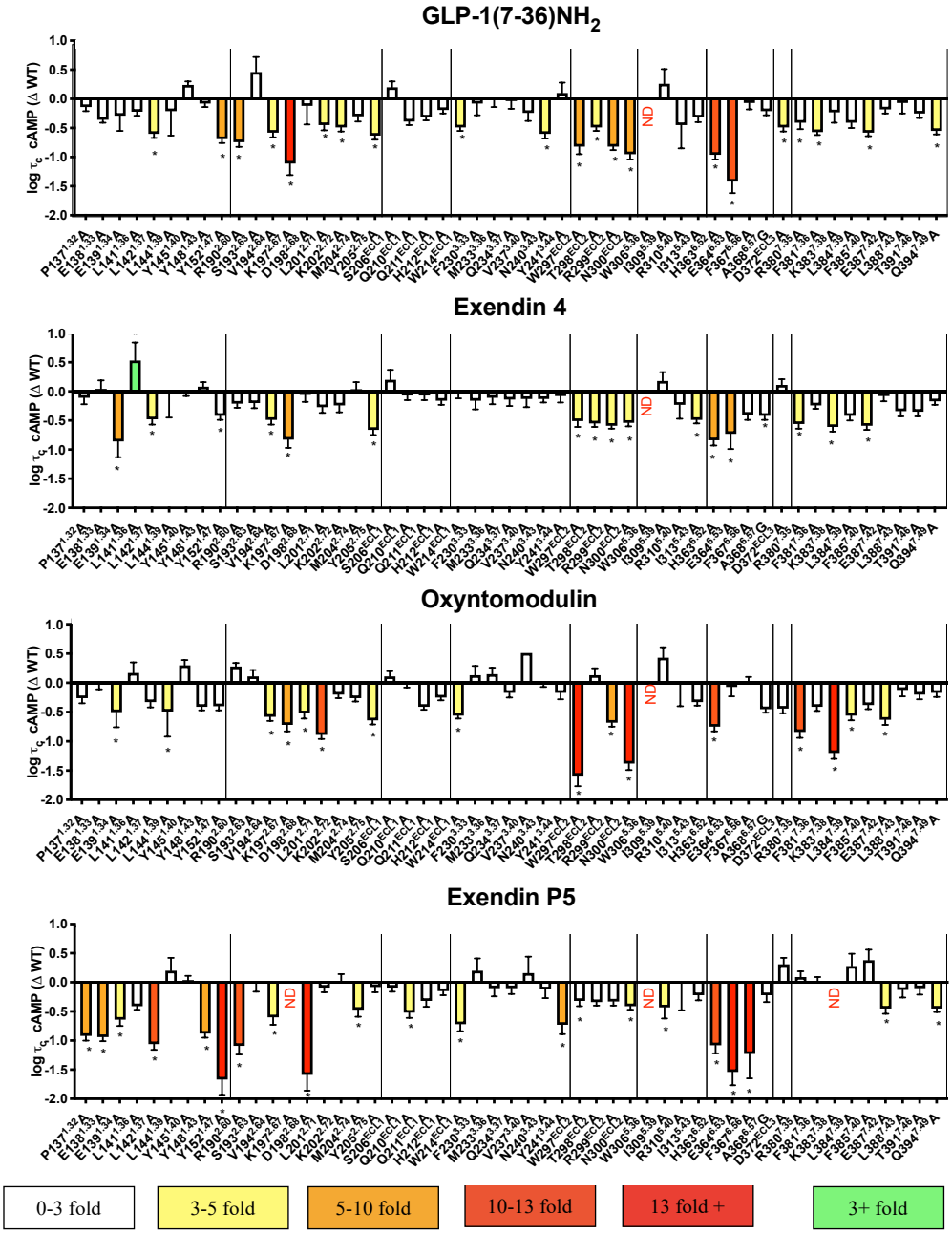

Figure 5.9) Difference in efficacy ($\log\tau_c$) of GLP-1R mutant receptors compared to the WT receptor for GLP-1 (top), Exendin-4 (second from top), Oxyntomodulin (third from top) and Exendin-P5 (bottom). A one-way analysis of variance and Dunnett's post-test was performed on $\log\tau_c$ values, and values indicated with an asterisk are statistically different from the WT values (*$p < 0.05$). Data that are statistically significant are colored based on the direction (yellow-red = reduced, green = enhanced and extent of effect. All values are $\log\tau_c \pm$ SEM of 3-4 independent experiments, conducted in duplicate. ND indicates no response was measurable in concentration range tested for that mutant receptor.

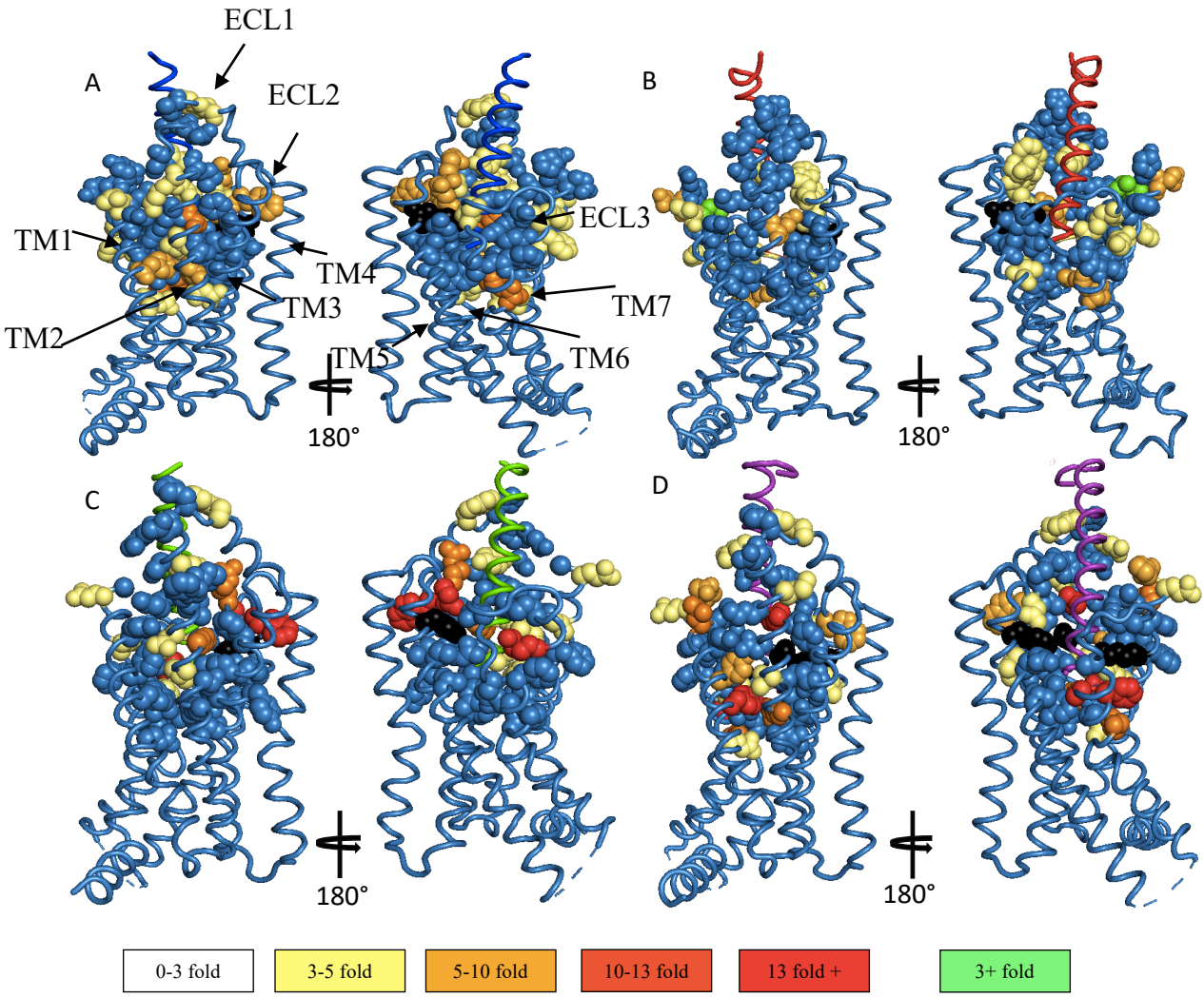

Figure 5.10) Cryo-EM structures of the active GLP-1R bound to GLP-1 (**A**), Exendin-4 (**B**), Oxyntomodulin (**C**) and Exendin-P5 (**D**) with fold-changes in logτ_c values (of Ala mutants to individual residues relative to WT) are heat mapped onto each assessed residue to show the effect of mutants on cAMP efficacy. Residues which had neutral impact are shaded in blue, 3-5 fold reduced efficacy in yellow, 5-10 fold reduced efficacy in light orange, 10-13 fold reduced efficacy in dark orange, 3+ fold reduced efficacy in red and enhanced efficacy are in green. Residues where no response was detected are shaded black. Ligand colours are GLP-1 (blue), exendin 4 (red), oxyntomodulin (green) and exendin P5 (purple)

5.3 Discussion

The ECLs of the GLP-1R are important for both the affinity and functional activity of peptide ligands. Residues within the ECLs, as well as residues located within the TMs of the TM bundle, line the peptide binding site as revealed by recent structures of the GLP-1R (Liang et al, 2017)(Liang et al, 2018b)(Zhang et al, 2018). This chapter extended previous mutational analysis on this receptor to explore all residues that line this deep TM binding pocket that accommodates the N-termini of peptide agonists. A full mutational analysis of this pocket revealed the importance of individual residues required for affinity and cAMP activity mediated by four agonists, GLP-1(7-36)NH_2, Exendin 4, Oxyntomodulin and exendin-P5, expanding our understanding of how distinct (biased) peptide ligands activate the GLP-1R, promoting cAMP signalling. This work revealed striking differences in the requirements for affinity and cAMP efficacy between exendin-P5 and the other three ligands (GLP-1, Oxyntomodulin and exendin-4) assessed, with more subtle differences present between GLP-1, exendin-4 and Oxyntomodulin in their requirements for activating the GLP-1R.

The C-terminal region of exendin-4 and exendin P5 is identical to exendin(9-39). While exendin (9-39) is an antagonist, exendin 4 and exendin P5 have extended N-terminal sequences that engage within the receptor TM core to activate the GLP-1R. Consistent with published data, exendin-P5 had approximately 10-fold lower affinity, whereas, exendin 4 had approximately 10-fold higher affinity, than exendin(9-39). This suggests that interactions within this TM core enhance the affinity of exendin 4 through the formation of additional contacts between the receptor and the ligand. In contrast, exendin P5 interactions within the TM bundle do not contribute much to the overall affinity of the ligand (in fact, they appear to destabilize the interactions formed by the 9-39 region as this ligand has lower affinity than exendin(9-39). This is supported by the mutagenesis data where overall the TM binding pocket mutations had limited impact on the affinity of exendin P5 when assessed using an antagonist probe (that should predominantly measure the affinity of the non-transducer coupled receptor).

Exendin-P5 has a unique N-terminal sequence when compared to the other three agonist ligands, which all share a high degree of sequence homology (Figure 5.1). Despite its much lower binding IC50, it only displayed 25-fold lower cAMP EC50 than exendin 4. The ratio of affinity (pIC50) to potency (pEC50) can be used as a measure of efficacy when all agonists are

full agonists (as is the case here at the WT receptor). This ratio is greater for exendin P5 than exendin 4 (as well as GLP-1 and Oxyntomodulin) suggesting exendin P5 is a more efficacious ligand (Liang et al, 2018b). Therefore, despite the bulky N-terminus reducing the affinity of this ligand, it plays a significant role in determining the functional activity of the peptide. This is also evident when assessing the cAMP data using operational modelling, where the calculated functional affinity of exendin P5 at the WT receptor was only 10-fold lower and its efficacy (tau) was higher than that of exendin 4 (Table 5.2, Figure 5.6).

Affinity (pIC50) is a composite value, where the equilibrium between multiple 'micro' affinity states will contribute to the value determined. In contrast, the functional affinity (pK_A) is the affinity of the receptor in the receptor state in which cAMP is produced (active state of the receptor coupled to Gαs). The measures of affinity and functional affinity at the wildtype receptor suggests that Exendin-P5 affinity is enhanced in the presence of Gαs (pK_A), however that Gs contributes less towards the overall affinity of the ligand itself (pIC50). In addition, many of the assessed TM binding site mutations had a large and significant impact on the functional affinity of Exendin-P5 (affinity for the Gαs occupied receptor) and its efficacy for generation of cAMP, yet only minimal effect on the global affinity measure. This suggests that interactions of Exendin-P5 within the TM pocket are crucial to couple the receptor to the cAMP signaling pathway and for the enhanced affinity of exendin P5 when coupled to this pathway. In particular, the mutational analysis revealed that interactions of exendin P5 with TM1, TM2 and TM6 were crucial for the high efficacy of exendin P5. It is interesting to note that TM1 has been previously implicated as a crucial domain that contributes to biased agonism (Lei et al., 2018).

In contrast to exendin P5, the other three peptides assessed in this study had similar values in their measured affinity via radioligand binding using an antagonist tracer, and their functional affinity when coupled to Gαs-mediated cAMP, and these two parameters were also similarly negatively affected by the majority of mutations. This suggests that the high affinity of these ligands is likely driven by a greater overall contribution of Gs (relative to other effectors that may couple at the intracellular face of the receptor) to their overall measured affinity. The mutagenesis data also suggests that these ligands form strong interactions with residues within the TM bundle that contribute to their observed affinity. In contrast to Exendin-P5, with the exception of a few residues, the impact on efficacy was much smaller for GLP-1,

Oxyntomodulin and Exendin-4, suggesting a smaller role of ligand-receptor interactions within this pocket in driving efficacy. These observations highlight that while the ligand N-terminus of peptides are very important in agonism of the GLP-1R, even for a single pathway, the way the ligand engages can have distinct functional implications that will influence biased agonist profiles.

Recent cryo-EM structures from our group revealed the binding pose of GLP-1, Exendin-4 (unpublished), Exendin-P5 (Liang et al., 2018) and Oxyntomodulin (unpublished) bound to the GLP-1R (Figure 5.11). In these structures, the binding pocket for Exendin-P5 was more open than when the other three ligands were bound (Figure 12 B&C). This was due to a larger outward movement of TM6 and TM7 in the exendin-P5 bound structure that was essential to allow the binding of its longer and bulkier N-terminus (relative to the other three agonists) (Liang et al., 2018b). Interestingly, our collaborators performed MD simulations on our recently solved structures of the GLP-1R bound to each of these four agonists and Gs (summarized in Figure 5.12). These highlighted that Exendin-P5 exhibits more mobility and forms more transient interactions with residues in the TM binding pocket compared to the GLP-1 and exendin 4. The difference in size of the N-termini that results in a much more open binding pocket provides these differences as the peptide has more room to move around the pocket. This supports the limited effect of any single mutation on overall affinity for exendin P5 as the peptide would readily form new/alternate interactions. When comparing specifically hydrogen bond interactions deep within the binding pocket (Figure 5.12), far fewer and shorter-lived interactions were formed with residues at the bottom of the binding pocket relative to GLP-1 and exendin-4. This also suggests that potentially ligands that form weaker interactions deep within the TM core, may more readily activate and turnover G protein therefore activating more cAMP, and this could explain the higher efficacy of exendin P5 relative to GLP-1 and exendin 4 (seen in Zhao et al., 2020). The greater effect of TM binding mutations on the operational measure of efficacy for Exendin-P5 relative to the other three ligands also supports this theory that low stability in the pocket is linked to greater cAMP efficacy.

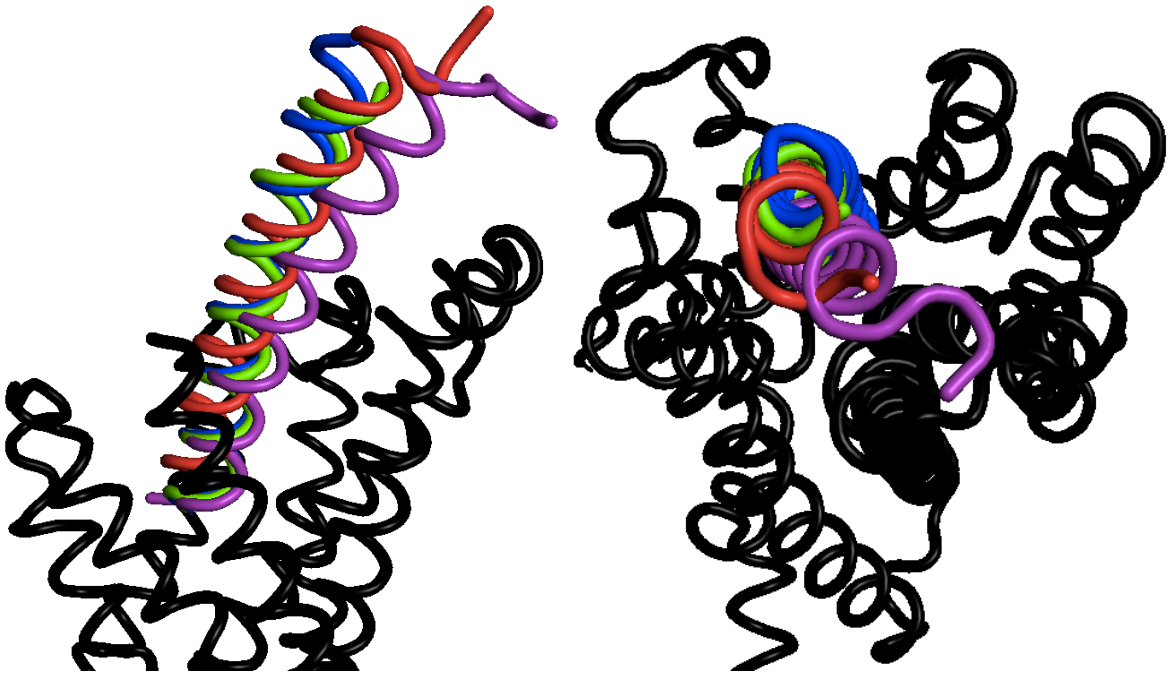

Figure 5.11: Binding pose of ligands bound on the GLP-1R. GLP-1 (blue), Exendin-4 (red), oxyntomodulin (green) and Exendin-P5 (purple)

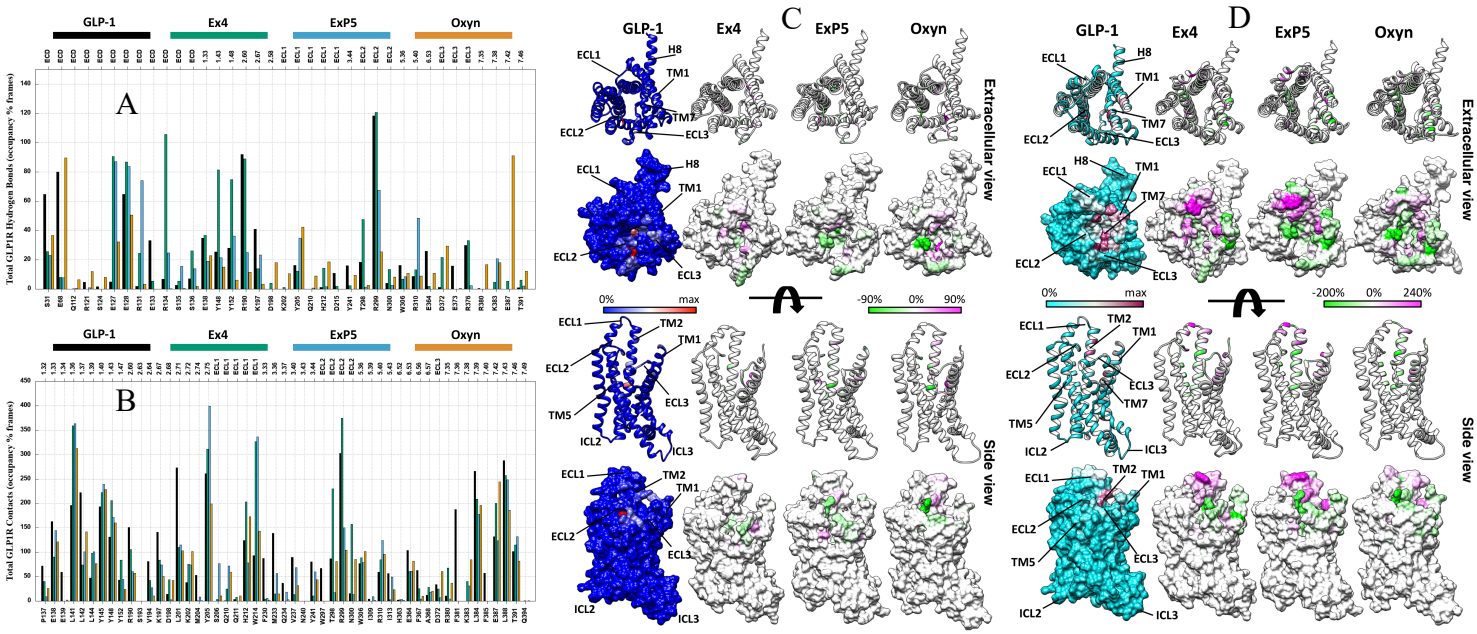

Figure 5.12: Summary of molecular dynamic studies performed on the 4 ligand bound receptors showing hydrogen bonds formed (**A**), total contacts made (**B**), and that data heat mapped onto the static structure (**C&D** respectively). MD studies performed by Guiseppe Deganutti as part of a collaboration with the Chris Reynolds laboratory.

Our mutagenesis study supports distinct roles of individual residues or regions within the GLP-1R binding pocket for signaling of peptide agonists that may be linked to their differential efficacies and biased agonism profiles. ECL2 has previously been implicated in controlling GLP-1R signalling, including cAMP production (Koole et al., 2012, Wootten et al., 2016a). Mutations to this region impacted the function of all four peptides confirming the importance of this domain in peptide function, however the impact of individual residues and magnitude of effects differed between ligands. When looking at the static structures, the conformation of ECL2 for GLP-1, Oxyntomodulin and Exendin P5 was very similar. W297 ^{ECL2}, an absolutely conserved residue across class B GPCRs, was has a role receptor function for all four ligands. In addition, residues R299^{ECL2} and N300^{ECL2} were also important for all four peptides. While ala mutations to all 3 of these residues altered either affinity, functional affinity or both for all peptides, these effects were smaller for Exendin-P5. In addition, all three mutations reduced efficacy for GLP-1, Oxyntomodulin and exendin 4, with little effect on the efficacy of Exendin P5, suggesting a differential requirement for these residues for different agonists. The MD analysis showed prolonged contacts between exendin 4, GLP-1 and Oxyntomodulin between these residues, but weaker and less prolonged interactions between Exendin-P5 and ECL2, which is consistent with the molecular pharmacology data.

Within the static cryo-EM structures, there are differences in backbone and side chain interactions formed by residues in ECL1 (Figure 5.13B), however it should be noted that the cryo-EM density in this region was relatively poor for most of the ligands. This suggests a highly dynamic area of the receptor in the active state. Interestingly, the region of this loop between Q210-W214 was one of the few regions important for Exendin-P5 affinity. Molecular dynamic simulations revealed an increased level of contacts between this region of the receptor and ligand for Exendin-P5 relative to GLP-1 (Figure 5.12). Interestingly Exendin 4 also displayed enhanced contacts in this region in the MD simulations, with no effect of mutations in this region on its affinity. These differences could be due to Exendin-4 forming many additional strong interactions in the core, such that the loss of these contacts has more limited effect on its affinity.

The largest difference in conformation in the static structures when comparing GLP-1R:Gαs complex bound by the four different peptide agonists occurred within the TM6-ECL3-TM7 (Figure 5.13A) domain. The importance of this region has previously been implicated in biased

agonism, with greater effects of mutations in this region on pERK (potentially arrestin mediated) than second messenger signaling (G protein mediated)(Wootten et al. 2016a). Interestingly, the mutagenesis study revealed residues within the top of TM6 and TM7 were important for affinity and cAMP functional affinity and efficacy of GLP-1, Exendin-4 and Oxyntomodulin. These regions were also important for Exendin-P5, however, the effects manifested only in functional affinity and efficacy, highlighting common roles of these regions in activation of Gαs (albeit there were distinctions in importance of individual residues within these regions that differed in their magnitude of effect between ligands). In the static structures and MD simulations, GLP-1, Exendin-4 and Oxyntomodulin all form direct interaction with residues within the top TM6 that are not seen in the Exendin-P5 structure, while all ligands form interactions with TM7. This can be explained by the structural data, once again comparing the GLP-1 and Exendin-P5 structures where the conformation of the backbone of TM6/ECL3 in the region of D372^{ECL3} is the most different. D372 ^{ECL3} at the TM6/ECL3 boundary forms key interactions with charged residues either within TM5 or the ligand itself when GLP-1, Oxyntomodulin or Exendin-4 are bound, but no interactions when Exendin-P5 is bound. The lack of this interaction can account for the more outward movement of TM6/ECL3 boundary in the presence of Exendin-P5 as interactions of charged residues with D372 ^{ECL3} in the other structures limits this outward movement. These differences may explain the effect of mutation to D372 ^{ECL3} (D372 ^{ECL3}A) which played no role in ExP5, but was crucial for all other ligands, reducing their affinity to an extent that closely matched that of Exendin-P5.

Interestingly, F367$^{6.56}$ is located deeper within TM6. This residue when mutated to alanine had the opposite effect when mutated to alanine, resulting in a large reduction in both the functional affinity and the efficacy of Exendin P5, but with much smaller effects with the other agonists assessed. This may be a consequence of the limited interactions of the Exendin P5 peptide with regions higher up in TM6 that are important for interactions with the other ligands, such that resides that reside deeper in the bundle within TM6 have a greater role for this peptide than the other agonists.

Consistent with published work, residues located deep within the GLP-1R binding site that form part of a highly conserved polar network in class B GPCRs (R190$^{2.60}$, N240$^{3.43}$, E364$^{6.53}$ and Q394$^{7.49}$), play a much smaller role in the affinity and efficacy of Oxyntomodulin, but were crucial for the behavior of the other peptide agonists, including Exendin-P5. Analysis of the

static structure revealed differences in the conformation of residues within this network in the oxyntomodulin-bound structure compared to the other three structures (Figure 5.14). R190$^{2.60}$ forms direct interactions with all ligands in the static structures, which presumably disrupts ground state interactions that trigger rearrangement of the polar network that is crucial to allow the receptor to adopt an active state and allosterically transmit signals to the intracellular face. Interestingly interactions of GLP-1, Exendin-4 and Exendin-P5 are via a negative charged glutamic acid whereas Oxyntomodulin forms a weaker interaction through a glutamine residue. Chimeric peptides between GLP-1 and oxyntomodulin when tested at the R190$^{2.60}$A mutation, switched the mutagenesis profile with Q9 GLP-1 resembling WT oxyntomodulin and E3 oxyntomodulin resembling WT GLP-1 (Wootten et al., 2016). This set of data reveals how different ligands can have vastly different requirements for this residue within the TM bundle for receptor activation and signalling, albeit despite this, in all cases this network still undergoes a reorganisation to allow activation. The differences in how this network reorganizes may account for some of the biased agonism profiles observed between different peptide ligands.

E364$^{6.53}$ within this central polar network has a particularly interesting binding profile for exendin P5 that is not seen for the other peptides. In the peptide bound structures, this residue does not directly contact the peptide ligands, but instead forms extensive hydrogen-bond interactions that stabilise this central polar network. Interestingly Ala mutation of this residue had little effect on the pIC50 calculated from a three-parameter curve fit for any of the ligands. However, for exendin P5 (but not the other ligands), the inhibition curve is clearly biphasic and the data does not fit well to the three-parameter curve fit (and as such the reported pIC50 from the global analysis, does not capture this effect). The “high affinity” phase of this curve clearly has a higher pIC50 value than the one estimate from the three-parameter fit, however a biphasic model could not be fit to the data as this would require more data points (ie half log concentrations). This suggests upon binding of exendin P5 to this mutant receptor, the receptor more readily adopts an active state, relative to when the standard peptide ligand is bound. This is likely due to the influence of this residue on the conformation of TM6 and TM7, which in exendin P5 bound structure adopts a distinct conformation relative to when the other peptides are bound. There is also the potential this is due to enhanced allosteric influence of G protein binding to exendin P5 affinity at this mutant receptor relative to the other peptides suggesting that this side chain is important for allosteric communication between the G protein and agonist binding site and that its influence differs in a peptide dependent manner. Further experiments

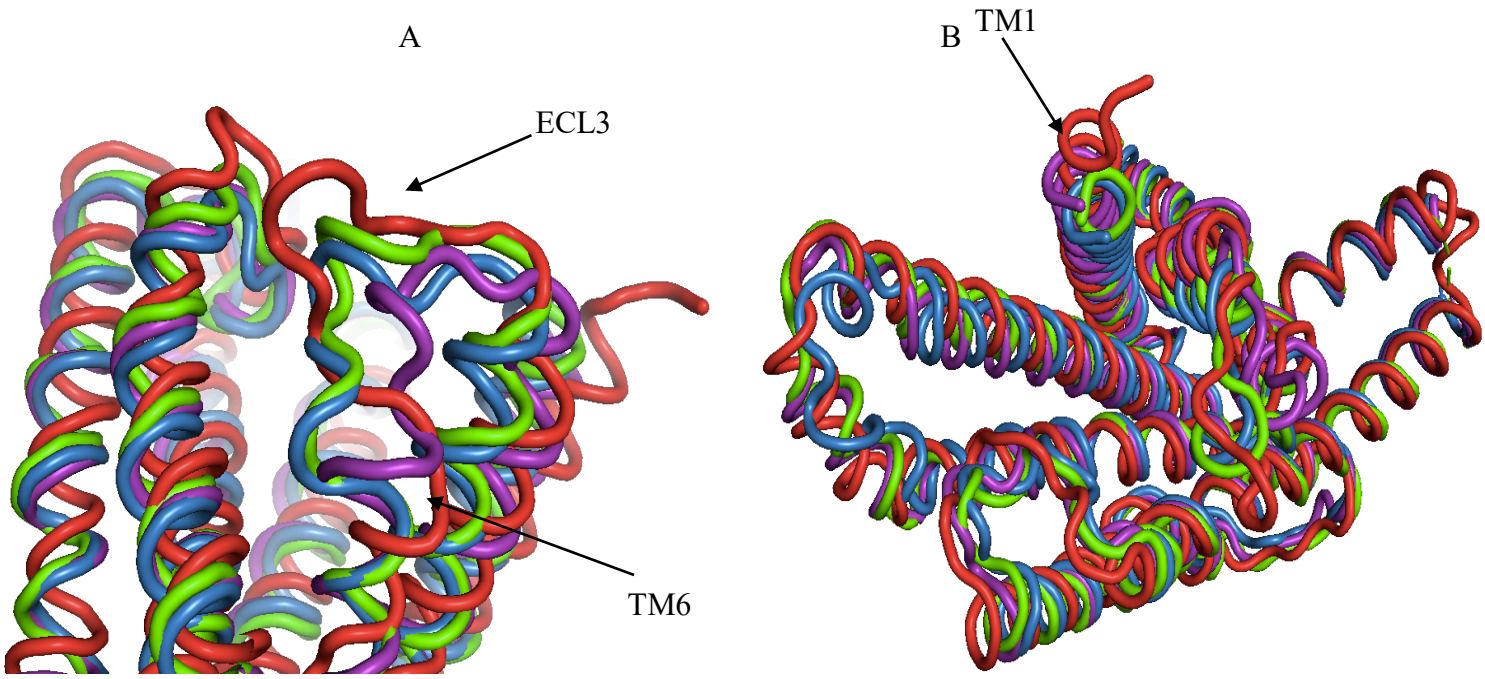

Figure 5.13: Overlay views of the active GLP-1R bound to GLP-1 (blue), oxyntomodulin (green), exendin-P5 (purple) and exendin-4 (red) highlighting differences in, TM6-ECL3 (**A**) and The extracellular face.(**B**)

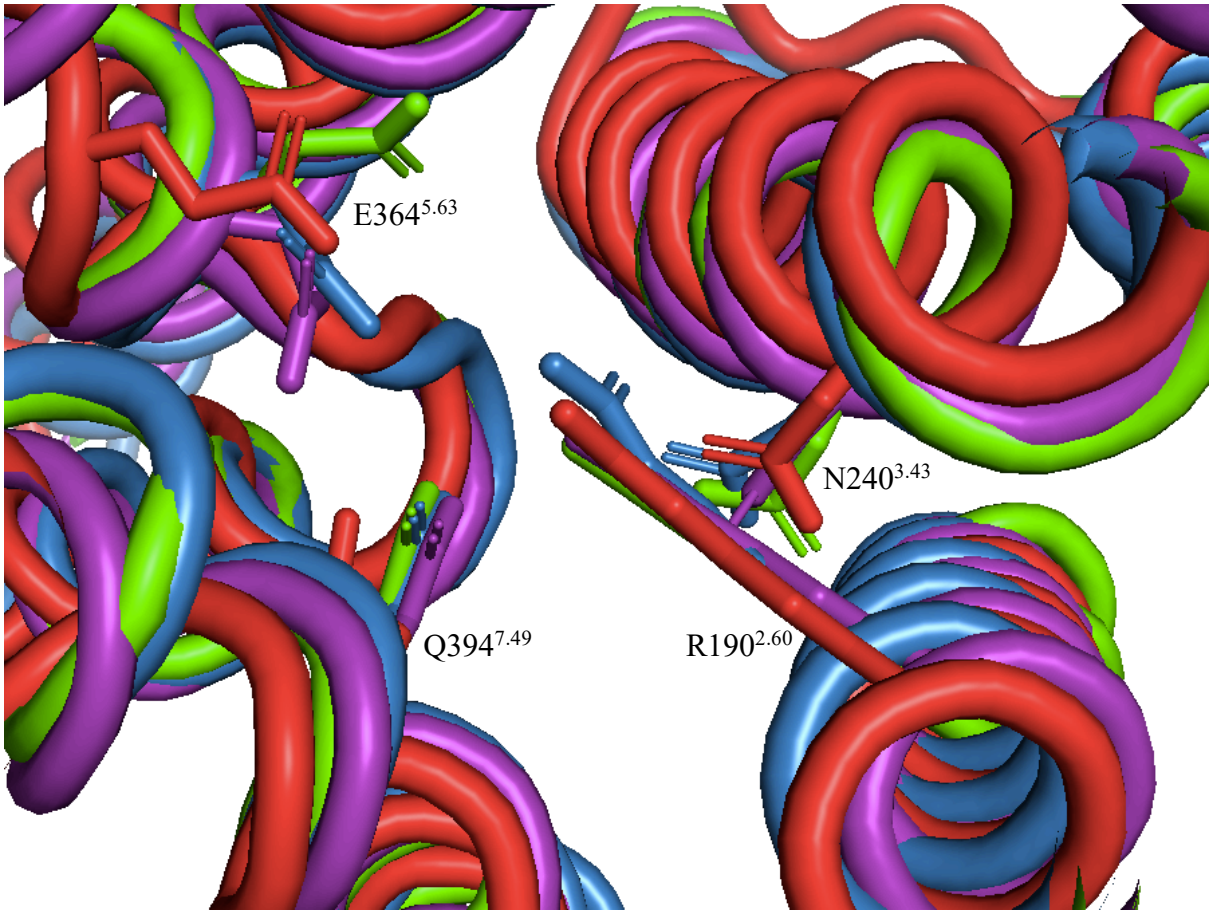

Figure 5.14: Polar network of residues at base of the GLP-1R binding pocket when bound by GLP-1 (blue), Oxyntomodulin (green), Exendin-P5 (purple) and Exendin-4 (red) highlighting a different rearrangement of this network in the oxyntomodulin bound structure.

with more concentrations of agonist, as well binding studies in the absence and presence of G protein would be required to fully discern this. Two further residues, Y152$^{1.47}$ and Y241^{343} also participate in stabilising the polar network at the base of the GLP-1R binding pocket in all four cryo-EM structures described in this study, and this observation has not be reported previously. Mutation of these residues to alanine affected the pharmacology of all 4 peptide agonists highlighting the importance of these residue in the stabilization of the important polar network in core of the receptor (Wootten et al., 2013)(Wootten et al., 2016). Interestingly, Y241$^{3.43}$A reduced the affinity for all agonists but only reduced the efficacy for Exendin P5. In contrast, Y152$^{1.47}$A had a large influence on affinity for GLP-1, Oxyntomodulin and Exendin-4, but not Exendin P5. However, similar to Y241$^{3.43}$A, this mutation only altered functional affinity of Exendin P5. This is consistent with the overall observations that only transient interactions are formed with this peptide with individual residues, but that these are important for functional coupling to the cAMP pathway. Y152$^{1.47}$ is also crucial for efficacy for all ligands as its removal by mutation to alanine reduced efficacy for all ligands, albeit the importance was greater for exendin-P5 efficacy relative to the other peptides. This highlights that stabilization of the central polar network is crucial for the function of all agonists, however it has a much smaller influence of Exendin P5 affinity compared to the other ligands. In contrast, the stabilisation of the polar network is critical for Exendin P5 efficacy.

Key residues located 2 turns above residues that form this polar network within TM2 also play key roles in receptor function. K197$^{2.67}$ forms direct interactions with all 4 peptides in the cryo-EM structures and not surprisingly, its mutation to alanine dramatically reduces the affinity of all four peptides (>70-fold for GLP-1, Oxyntomodulin and Exendin-4 and undetectable for Exendin P5). This residue has a smaller role in efficacy, nonetheless was also important for efficacy for all 4 ligands. Within the structures, it was also evident that the side chain of K197$^{2.67}$ was stabilised by a salt bridge interaction with D198$^{2.68}$. In accordance, mutation of this side chain to alanine resulted in similar (albeit effect sizes were smaller) patterns of response to mutation of K197$^{2.67}$ and highlighting the key roles of these two residues in receptor function.

Another key and interesting residue assessed in this thesis for the first time was that if Q234$^{3.37}$, also located 2 helical turns above the conserved polar network. Within the cryo-EM structures, this residue forms hydrogen bond interactions with the N-terminal Histidine of GLP-1, Oxyntomodulin and Exendin-4 and accordingly, mutation of Q234$^{3.37}$ resulted in reduction of

affinity. In contrast, Exendin P5, which lacks a histidine residue at its N-terminus did not form any direct interactions with Q234$^{3.37,}$ consistent with the lack of effect of mutation on its pharmacological profile.

This mutagenesis study, in combination with accompanying structures and molecular dynamics studies have revealed key differences in the role the residues within the TM peptide binding site of the GLP-1R in affinity and cAMP efficacy. Exendin-P5 is a much lower affinity peptide than GLP-1, Exendin-4 and Oxyntomodulin, and this is reflected in the mutagenesis data where the TM binding pocket contributed little to its overall affinity, however the role of residues in this pocket on cAMP functional affinity and efficacy revealed the requirement for the N-terminus of this ligand to engage the bundle for promoting downstream signalling. There were also distinctions in the regions of the receptor important for affinity and activation between the four different agonists that can link their different pharmacological profiles. The extracellular surface has already been shown to be important in the generation of signaling and biased agonism but combined with new structural information, we can begin to see how specific interactions or interactions with distinct topographical areas of the receptor can contribute to differences in receptor pharmacology. Harnessing this information can lead to more rational drug design targeting areas from which certain signaling profiles arise if a physiologically beneficial profile can be determined.

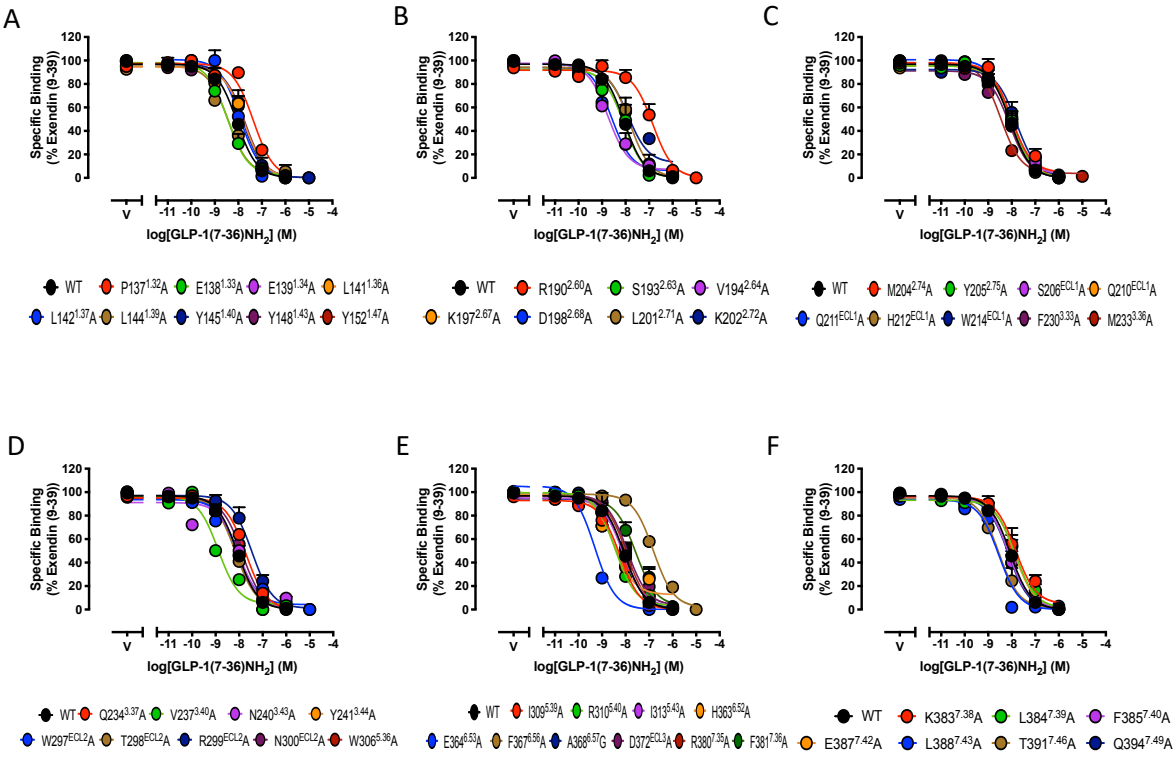

Figure S5.1). Competition binding studies for WT and alanine mutant GLP-1 receptors showing the ability of unlabelled Exendin (9-39) (**A-F**), to compete with the tracer, I^{125} Exendin(9-39). Data are expressed as % specific binding by normalizing to the value for I^{125} Exendin(9-39) binding in the absence of unlabeled ligand (100 %) and in the presence of a saturating concentration of unlabeled Exendin(9-39). Data were fit to a one-site inhibition binding curve. All values are grouped data showing the mean ± SEM of 3-4 independent experiments performed in duplicate.

Chapter 6:
Summary and Future Directions

My thesis project continued the extensive work performed by our laboratory, and others, to understand biased profiles of novel GLP-1R agonists, the contribution of individual transducers to GLP-1R downstream signalling and to use mutagenesis studies to understand structure-function relationships and how distinct residues within the GLP-1R contribute to binding, signalling and biased agonism for different ligands. Numerous studies have been reported that identify biased ligands for the GLP-1R, however, the majority of these have focused on generating and characterising the behaviour of novel full-length peptides (Koole et al., 2013)(Hager et al. 2017). More recently, smaller peptides have emerged that were designed to predominantly engage the TM domain of the GLP-1R (Hoang et al., 2015). The work in chapter 3 of this thesis builds on the work of others in the field, reporting the characterisation of a series of novel 11mer GLP-1R peptide agonists that were generated by our collaborators at Pfizer.

Recent work exploring the structure and pharmacology of the GLP-1R (and other class B GPCRs) suggest that the conformation and dynamics of the GLP-1R ECD in the presence of different ligands may be linked to biased agonism profiles (Lei et al., 2018). 11mer peptides designed to mimic the N-terminus of full-length peptides are predicted to form only limited engagement with the GLP-1R ECD and would therefore be expected to induce different GLP-1R ECD conformations or dynamics to that stabilised by full length ligands. In turn, it would be expected that unique pharmacological profiles might be observed from these types of agonists relative to full length peptides. While the affinity of the 11mer peptides characterised in this thesis were lower than full length GLP-1, which was expected given that they form fewer contacts with the receptor, surprisingly, some of the 11mer peptides, including 1B displayed remarkedly similar bias profiles to GLP-1. Nonetheless modifications within the parent 11mer scaffold (1B) resulted in a range of 11mer peptides with quite distinct signalling profiles, which included changes in signalling to beta arrestin, pERK1/2 and/or calcium mobilisation relative to cAMP production. Therefore, this study revealed how small changes between similar peptides can lead to divergent signalling and biased agonist profiles.

Within the 11mer study, a range of peptide ligand SAR was performed around the parent scaffold 1B, where a wide range of changes were made within a select few positions including positions 1, 6, 10 and 11. This study found that alterations to the first residue of the peptide (a histidine in native GLP-1) was the biggest determinant in how well a ligand would bind and subsequently signal. This was not surprising as for the majority of class B GPCRs (including the GLP-1R) modifications to the N-terminal His in their native peptides, often result in

reduced affinity, altered efficacy or non-functional ligands. Alterations to other locations in the 1B 11mer scaffold (6, 10 or 11) induced more subtle changes in ligand signalling profiles, and these effects differed depending on the composition of the residue in the first position.

Two cyclised 11mers, 3 and 14, were also generated around the 1B scaffold incorporating cyclic constraints between position 5 and 9 (3) by the addition of a lactam bridge and positions 2 and 5 (14) by a di-sulphide bond. 11mer 14 was a poor binder but was relatively better at signalling (relative to its affinity), however 11mer 3 had higher affinity than 1B, but reduced ability to signal. Given the open binding pocket observed in class B GPCR structures, it is unlikely that the constrained peptides were too bulky to engage the receptor TM core, however, it is more likely that they were constrained into a conformation that either altered the ability of the peptide to engage in an optimal conformation for high affinity (11mer 14) or that enabled efficient binding within the receptor but had limited flexibility to enable full receptor function (11mer 3).

While this study revealed promise in the use of short peptides as an avenue for generating novel ligands, there are a range of future studies that would be interesting to explore. In continuing experiments on this set of peptides, it would be interesting to investigate a more thorough examination of pathways that the GLP-1R is capable of activating, including additional MAP kinase pathways that are important for GLP-1R function. Investigating the ligand binding kinetics would also be beneficial to determine how these alterations affect residence time and how that might relate to changes in signalling output. Finally, understanding how the receptor is trafficked post activation by these 11mer ligands would be incredibly pertinent information given the potential for internalised GLP-1Rs to signal from endosomes, and for the location of the activated receptor within the cell to alter the profile of signalling through the generation of compartmentalised signals (Fletcher et al., 2018). Beyond experiments in a recombinant systems, taking these novel ligands into more physiologically relevant cell lines (for example INS-1/823) or primary cells would be important to see how they change signalling in more native systems, for example in promoting insulin secretion. The exploration of some of these peptides in *in vivo* models of diabetes would also be exciting, to determine the potential of some of these novel biased profiles to provide therapeutic advantages. A toolbox of ligands with distinct chemistries and pharmacologies are important for developing concepts such as biased agonism so that they can be exploited for therapeutic advantage. Novel tools widen the scope of available ligands targeting this receptor enabling a wider exploration of chemical and

conformational space that can be explored in in vivo studies to understand the implications of biased agonism for this important therapeutically relevant GPCR.

The fourth chapter within this thesis explored a range of peptide agonists in series of HEK-293 cells where Gα proteins or β arrestin's were deleted via CRISPR/Cas9 technology (Alvarez-Curto et al., 2016). These were used to assess the role that each subfamily of signalling effectors had on the contribution to individual signal pathways produced by distinct biased agonists. Using GLP-1(7-36)NH_2, oxyntomodulin, Exendin-4, Exendin-P5 and 11mers with interesting pharmacology identified from chapter 3 of this thesis, I assessed the role of select transducer subfamilies for GLP-1R-mediated cAMP accumulation, iCa^{2+} mobilisation and β arrestin recruitment. As expected, the cognate Gα protein for each of the relevant pathways was absolutely required for the initiation of cAMP (Gαs) and iCa^{2+} (Gαq/11). Despite the absolute requirement of the canonical G protein, there was also involvement of other signalling effectors that occurred in a ligand-dependent manner. For cAMP accumulation there was a ligand-dependent requirement of Gαi/o for production of cAMP, which is in contrast to the canonical role of Gαi/o but consistent with previous reports for the GLP-1R (Wootten et al., 2016a). Interestingly, Gα12/13 played a role in cAMP accumulation and also modulated the amount of iCa^{2+} mobilisation observed, while deletion of Gαs decreased both potency and maximum Ca^{2+} response suggesting a positive modulation of this pathway by Gαs. Surprisingly, β arrestin deletion increased potency for the Ca^{2+} mobilisation pathway when activated by GLP-1 and Exendin-P5, with no effect on exendin-4 and oxyntomodulin. β arrestins can play multiple roles in GLP-1R signalling, one of which is ligand-induced receptor internalisation. There is the potential that β arrestin-mediated receptor movement from the plasma membrane is required for full iCa^{2+} signalling for select ligands. However, GLP-1R internalisation is reported to only be partially dependent on β arrestins and the β arrestin biased agonists exendin-4 and oxyntomodulin were less impacted by deletion of these proteins (relative to GLP-1 and Exendin-P5). Interestingly, we also revealed that recruitment of β arrestin to the GLP-1R was not dependent on G protein recruitment and activation as the deletion of all G alpha proteins resulted in enhanced ligand-dependent recruitment of β arrestin.

Future directions to expand on the work presented in chapter 4 include expanding the pathways assessed in the CRISPR engineered cell lines to include pERK1/2 and other MAP kinases. Including more ligands in this study would also be informative, including producing a complete set of data for the 11mer ligands, additional peptides that are used as approved therapeutics, other ligands with novel bias and small molecule ligands. Investigating the receptor

internalisation and trafficking in the absence of different signalling effectors would provide additional information on the role of transducer in promoting ligand-induced receptor trafficking. There are many often contradictory reports in the literature regarding the mechanism by which the GLP-1R internalises, including via β arrestin-dependent and Gαq/11-dependent mechanisms. These cell lines provide a mechanism to assess this further, however, the caveats that CRISPR modified cell lines may undergo adaptive changes to the WT cells also need to be taken into account when interpreting data from these systems.

Chapter 5 of my thesis was an extension of a larger mutagenesis project within the laboratory, which includes mapping of residues throughout the GLP-1R for their role in peptide ligand binding, activation and cellular signalling. My study explored the role of residues that line the peptide agonist binding site within the GLP-1R to determine their importance in peptide affinity and cAMP signalling. Simultaneously to this, structural biology efforts in our laboratory have led to the determination of multiple structures for the GLP-1R, bound with different ligands and coupled with Gαs. This included our recently published exendin P5 bound GLP-1R structure (Liang et al., 2018b) a higher (2.1A) resolution GLP-1 bound structure that addressed many modelling errors within the previously solved structure by the Skiniotis group, in addition to an exendin-4 and oxyntomodulin bound structure. Using large scale mutagenesis data, in combination with mutational data and MD simulations, allowed for detailed interpretation of the role of residues that directly contact ligands within the GLP-1R peptide binding site. Overall, we confirmed the importance of individual residues in the affinity and activation (for cAMP) for individual peptide agonists providing detailed maps for the role of individual residues for different parameters of receptor function. Interestingly, we could link the more open bundle in the static structure of the exendin P5-bound GLP-1R (relative to other peptide ligands) with the mutagenesis and MD data to identify that exendin P5 formed more transient interactions than the other peptides, likely due to the increased space in the bundle. This resulted in a smaller requirement of any one residue for ligand affinity. However, while this was true for affinity, interactions formed by these residues were crucial for coupling ligand binding to the cAMP pathway. Similar to the other agonists, the pKa of exendin-P5 was impacted heavily by mutations to residues in this extracellular facing pocket. This was in stark contrast to affinity values for exendin P5 which suggests that multiple states (not just the Gαs bound state) contribute to the overall affinity of exendin P5.

The potency of the cAMP response of exendin P5 was very similar to the response of the native peptide, which was surprising, especially when compared to its affinity, which was 100-fold lower than GLP-1. This suggests that ligands that form more transient interactions deep within the bundle result in higher efficacy within the cAMP pathway. This may arise because peptides (such as GLP-1) that form tighter, more sustained interactions with the receptor may couple more strongly to the Gs protein, but promote less turnover due to the tighter interactions allowing less flexibility. This would be consistent with the higher affinity for these ligands in overall affinity measures also correlating with their functional affinity measurement but having lower efficacy (i.e. they couple more strongly to Gαs, but turnover less G protein). In contrast, those that form weaker interactions promote weaker engagement of the G protein that allow for faster activation (as this requires G protein dissociation), hence resulting in higher overall efficacy. This phenomenon has been observed previously with the calcitonin receptor where lower affinity agonists are more efficacious ligands (Furness et al., 2016).

Differences in the GLP-1R conformation were observed in the static cryo-EM structures that may be linked to differential efficacies and biased agonism of the GLP-1 receptor. The TM6-ECL3-TM7 region was the area of the receptor where the largest conformational differences were observed with the different ligands bound. Interestingly, this is a key region within the GLP-1R that has been previously linked to biased agonism (Wootten et al., 2016a) Cysteine cross linking studies performed in the related secretin receptor show that a receptor occupies many transient states as the ligand binds the receptor and that ECL3 is a key region for maintenance of the ground state and transition to an active state or states (Dong et al., 2016). Mutations within ECL3 may interrupt receptor contacts made in the transient inactive states and impede or alter the ability of ligands to transition the receptor to active state(s). This would result in mutant receptors that occupy different active conformations that change the ability of the receptor to couple to the cAMP pathway, however the ability to see ligand-dependent differences in the mutation profiles from this region, further confirm the importance of this region in defining the biased profiles of different agonists.

There are many additional studies that could be performed to extend the work presented in chapter 5. Firstly, the number of signalling pathways that were assessed could be increased to include other signalling pathways including iCa^{1+}, pERK1/2 and other MAP kinases and arrestin recruitment. Determination the functional importance of diverse ligand-receptor interactions to different signalling outputs will provide unprecedented information on the role

of distinct peptide contacts with different regions of the receptor that contribute to activation of unique pathway combinations and also how different ligands can promote individual activation profiles. Testing additional ligands in our panel of mutant receptor cell lines, for their ability to bind to and signal through these mutant receptors will expand knowledge of how different classes of ligands commonly or uniquely engage the TM domain. This could include the 11mers that were characterised in the first part of my thesis or other therapeutically relevant ligands for the GLP-1R that we have access to (i.e; Liraglutide, Lixisenatide etc.), as well as other biased ligands that have been identified for the GLP-1R. Other interesting ligands that have been assessed in our lab in structural studies include non-peptide agonists with very unique signalling profiles and that bind in distinct manners to the receptor relative to peptide agonists, such as TT-OAD2 (Zhao et al., 2020). Studies assessing kinetics of ligands on select mutations would also be informative as we attempt to understand the mechanism through which ligands reach their final binding pose. Finally, some understanding of how these altered signalling outputs are linked to coupling to effector proteins, and how mutations within the receptor impact this could be explored using the HEK239 CRISPR KO cells that I utilised in chapter 4 of this thesis.

Overall my thesis has extended knowledge on biased agonist profiles and the mechanisms for which these arise for a toolbox of ligands for the GLP-1R. Novel ligands with unique biased profiles provide additional tool compounds that could be used to increase our understanding of the ideal biased profiles to target for the best therapeutic outcomes for future drug development (ie through future correlation to in vivo studies). Understanding mechanistic details of how these biased profiles arise both at the cellular and structural level will facilitate structure-based drug development of novel therapeutics with specific biased profiles that can be used in future development programs to design better and improved agonists to target the GLP-1R system.

Chapter 7:
Bibliography

Adelhorst, K., Hedegaard, B. B., Knudsen, L. B., & Kirk, O. (1994). Structure-activity studies of glucagon-like peptide-1. *The Journal of Biological Chemistry*, *269*(9), 6275–6278. Retrieved from http://www.ncbi.nlm.nih.gov/pubmed/8119974

Alvarez-Curto, E., Inoue, A., Jenkins, L., Raihan, S. Z., Prihandoko, R., Tobin, A. B., & Milligan, G. (2016). Targeted elimination of G proteins and arrestins defines their specific contributions to both intensity and duration of G protein-coupled receptor signaling. *Journal of Biological Chemistry*, *291*(53), 27147–27159. https://doi.org/10.1074/jbc.M116.754887

Aroda, V. R. (2018). A review of GLP-1 receptor agonists: Evolution and advancement, through the lens of randomised controlled trials. *Diabetes, Obesity and Metabolism*, *20*(November 2017), 22–33. https://doi.org/10.1111/dom.13162

Atwood, B. K., Lopez, J., Wager-Miller, J., Mackie, K., & Straiker, A. (2011). Expression of G protein-coupled receptors and related proteins in HEK293, AtT20, BV2, and N18 cell lines as revealed by microarray analysis. *BMC Genomics*, *12*(1), 14. https://doi.org/10.1186/1471-2164-12-14

Bazarsuren, A., Grauschopf, U., Wozny, M., Reusch, D., Hoffmann, E., Schaefer, W., … Rudolph, R. (2002). In vitro folding, functional characterization, and disulfide pattern of the extracellular domain of human GLP-1 receptor. *Biophysical Chemistry*, *96*(2–3), 305–318. https://doi.org/10.1016/S0301-4622(02)00023-6

Bjarnadóttir, T. K., Fredriksson, R., & Schiöth, H. B. (2007). The Adhesion GPCRs: A unique family of G protein-coupled receptors with important roles in both central and peripheral tissues. *Cellular and Molecular Life Sciences*, *64*(16), 2104–2119. https://doi.org/10.1007/s00018-007-7067-1

Black, J. W., Leff, P., Shankley, N. P., & Wood, J. (1985). An operational model of pharmacological agonism: the effect of E/[A] curve shape on agonist dissociation constant estimation. 1985. *British Journal of Pharmacology*, *160 Suppl*, 561–571. https://doi.org/10.1111/j.1476-5381.2010.00855.x

Booe, J., Walker, C., Barwell, J., Kuteyi, G., Simms, J., Jamaluddin, M., Warner, M., … Pioszak, A. Structural basis for receptor activity modifying protein-dependent selective peptide recognition by a g-protein coupled receptor. *Molecular Cell.* 58, 1040-1052

Boyle, J. G., Livingstone, R., & Petrie, J. R. (2018). Cardiovascular benefits of GLP-1 agonists in type 2 diabetes: A comparative review. *Clinical Science*, *132*(15), 1699–1709. https://doi.org/10.1042/CS20171299

Chan, J. S. C., Yung, L. Y., Lee, J. W. M., Wu, Y.-L., Pei, G., & Wong, Y. H. (2002). Pertussis Toxin-Insensitive Signaling of the ORL1 Receptor: Coupling to Gz and G16 Proteins. *Journal of Neurochemistry*, *71*(5), 2203–2210. https://doi.org/10.1046/j.1471-4159.1998.71052203.x

Chen, D., Liao, J., Li, N., Zhou, C., Liu, Q., Wang, G., … Wang, M. W. (2007). A nonpeptidic agonist of glucagon-like peptide 1 receptors with efficacy in diabetic db/db mice. *Proceedings of the National Academy of Sciences of the United States of America*, *104*(3), 943–948. https://doi.org/10.1073/pnas.0610173104

Chugunov, A., Simms, J., Poyner, D., Dehouck, Y., Rooman, M., Gills, D., Langer, I., (2010) Evidence that interactions interactions between conserved residues in transmembrane helices 2,3 and 7 are crucial for human VPAC1 receptor activation. *Molecular Pharmacology.* 78(3)394-401

Cobanoglu, M. C., Saygin, Y., & Sezerman, U. (2011). Classification of GPCRs using family specific motifs. *IEEE/ACM Transactions on Computational Biology and Bioinformatics*, *8*(6), 1495–1508. https://doi.org/10.1109/TCBB.2010.101

Conor, A., Hay, D., Simms, J., Howitt, G., Schindler, M., Smith, D., Wheatley, M., Poyner,

D. (2005) A key role for transmembrane prolines in calcintonin receptor-like receptor agonist binding and signalling; implications for family B G-Protein Couples Receptors. *Molecular Pharmacology.* 67 20-31

Coopman, K., Wallis, R., Robb, G., Brown, A., Wilkinson, G., Timms, D., & Willars, G. B. (2011). Residues within the Transmembrane Domain of the Glucagon-Like Peptide-1 Receptor Involved in Ligand Binding and Receptor Activation : Modelling the Ligand-Bound Receptor. *Molecular Endocrinology*, *25*(October), 1804–1818. https://doi.org/10.1210/me.2011-1160

Dal Maso, E., Glukhova, A., Zhu, Y., Garcia-Nafria, J., Tate, C. G., Atanasio, S., … Sexton, P. M. (2019). The Molecular Control of Calcitonin Receptor Signaling. *ACS Pharmacology & Translational Science*, *2*(1), 31–51. https://doi.org/10.1021/acsptsci.8b00056

Dal Maso, E., Zhu, Y., Pham, V., Reynolds, C. A., Deganutti, G., Hick, C. A., … Wootten, D. (2018). Extracellular loops 2 and 3 of the calcitonin receptor selectively modify agonist binding and efficacy. *Biochemical Pharmacology*, *150*(December 2017), 214–244. https://doi.org/10.1016/j.bcp.2018.02.005

Dar, S., Tahrani, A. A., & Piya, M. K. (2015). The role of GLP-1 receptor agonists as weight loss agents in patients with and without type 2 diabetes. *Practical Diabetes*, *32*(8), 297-300b. https://doi.org/10.1002/pdi.1978

Datta-Mannan, A. (2019) Mechanism influencing the pharmacokinetics and disposition of monoclonal antibodies and peptides. *Drug Metabolism and Disposition.* 47(10) 1100-1110

Davies, M., Pieber, T. R., Hartoft-Nielsen, M. L., Hansen, O. K. H., Jabbour, S., & Rosenstock, J. (2017). Effect of oral semaglutide compared with placebo and subcutaneous semaglutide on glycemic control in patients with type 2 diabetes a randomized clinical trial. *JAMA - Journal of the American Medical Association*, *318*(15), 1460–1470. https://doi.org/10.1001/jama.2017.14752

de Graff, C., Donnelly, D., Wootten, D., Sextin, P., Miller, L., Ahn, J., … Wang, M. (2016) Glucagon-Like Petide-1 and it Class B G-Protein Coupled Receptors: A long march to therapeutic success. *Pharmacological Reviews.* 68(4) 954-1013

Della Rocca, G. J., Maudsley, S., Daaka, Y., Lefkowitz, R. J., & Luttrell, L. M. (1999). Pleiotropic coupling of G protein-coupled receptors to the mitogen- activated protein kinase cascade: Role of focal adhesions and receptor tyrosine kinases. *Journal of Biological Chemistry*, *274*(20), 13978–13984. https://doi.org/10.1074/jbc.274.20.13978

Dessauer, C. W., Chen-Goodspeed, M., & Chen, J. (2002). Mechanism of Galpha i-mediated inhibition of type V adenylyl cyclase. *The Journal of Biological Chemistry*, *277*(32), 28823–28829. https://doi.org/10.1074/jbc.M203962200

DeWire, S. M., Yamashita, D. S., Rominger, D. H., Liu, G., Cowan, C. L., Graczyk, T. M., … Violin, J. D. (2013). A G protein-biased ligand at the μ-opioid receptor is potently analgesic with reduced gastrointestinal and respiratory dysfunction compared with morphine. *The Journal of Pharmacology and Experimental Therapeutics*, *344*(March), 708–717. https://doi.org/10.1124/jpet.112.201616

Dods, R., & Donnelly, D. (2015). The peptide agonist-binding site of the glucagon-like peptide-1 (GLP-1) receptor based on site-directed mutagenesis and knowledge-based modelling. *Bioscience Report*, *1*, 1–13. https://doi.org/10.1042/BSR20150253

Dong, M., Koole, C., Wootten, D., Sexton, P. M., & Miller, L. J. (2014). Structural and functional insights into the juxtamembranous amino-terminal tail and extracellular loop regions of class B GPCRs. *British Journal of Pharmacology*, *171*(5), 1085–1101. https://doi.org/10.1111/bph.12293

Dong, Maoqing, Lam, P. C., Orry, A., Sexton, P. M., Christopoulos, A., Abagyan, R., &

Miller, L. J. (2016). Use of cysteine trapping to map spatial approximations between residues contributing to the helix N-capping motif of secretin and distinct residues within each of the extracellular loops of its receptor. *The Journal of Biological Chemistry*, 1–25. https://doi.org/10.1074/jbc.M115.706010

Dong, M., Deganutti, G., Piper, S., Liang, L., Khoshouei, M., Belousoff, M., … Miller, L. (2020) Structure and dynamics of the active Gs-coupled human secretin receptor. *Nature Communications.* 11(4317) 2020.

Dong, M., Xu, X., Ball, A., Makhoul, J., Lam, P., Pinon, D., … Miller, L. (2012) Mapping spacial approximations between the amino terminus of secretin and each of the extracellular loops of its receptor using cysteine trapping. *The FASEB Journal.* 26 5092-5105.

Doods, H., Hallermayer, G., Wu, D., Entzeroth, M., Rudolf, K., Engel, W., & Eberlein, W. (2000). Pharmacological profile of BIBN4096BS, the first selective small molecule CGRP antagonist. *British Journal of Pharmacology*, *129*(3), 420–423. https://doi.org/10.1038/sj.bjp.0703110

Doré, A. S., Okrasa, K., Patel, J. C., Serrano-Vega, M., Bennett, K., Cooke, R. M., … Marshall, F. H. (2014). Structure of class C GPCR metabotropic glutamate receptor 5 transmembrane domain. *Nature*, *511*(7511), 557–562. https://doi.org/10.1038/nature13396

Draper-Joyce, C. J., Khoshouei, M., Thal, D. M., Liang, Y. L., Nguyen, A. T. N., Furness, S. G. B., … Christopoulos, A. (2018). Structure of the adenosine-bound human adenosine A1 receptor-Gi complex. *Nature*, *558*(7711), 559–565. https://doi.org/10.1038/s41586-018-0236-6

Drucker, D. J., Habener, J. F., & Holst, J. J. (2017). Discovery, characterization, and clinical development of the glucagon-like peptides. *Journal of Clinical Investigation*, *127*(12), 4217–4227. https://doi.org/10.1172/JCI97233

Ehrenmann, J., Schöppe, J., Klenk, C., & Plückthun, A. (2019). New views into class B GPCRs from the crystal structure of PTH1R. *FEBS Journal*, *286*(24), 4852–4860. https://doi.org/10.1111/febs.15115

Erickson, C. E., Gul, R., Blessing, C. P., Nguyen, J., Liu, T., Pulakat, L., … Andresen, B. T. (2013). The β -blocker Nebivolol Is a GRK/ β -arrestin Biased Agonist. *PLoS ONE*, *8*(8). https://doi.org/10.1371/journal.pone.0071980

Figueroa, K., Griffin, M., Ehlert, F. (2009) Selectivity of agonists for the active state of the M1 to M4 muscarinic reecptor subtypes. *The Journal of Pharmacology and Experimental Therapeutics.* 328(1)331-342

Filippatos, T. D., Panagiotopoulou, T. V., & Elisaf, M. S. (2014). Adverse Effects of GLP-1 Receptor Agonists. *The Review of Diabetic Studies : RDS*, *11*(3–4), 202–230. https://doi.org/10.1900/RDS.2014.11.202

Fletcher, M. M., Halls, M. L., Christopoulos, A., Sexton, P. M., Wootten, D., Lagerstrom, M. C., … Carpino, P. A. (2016). The complexity of signalling mediated by the glucagon-like peptide-1 receptor. *Biochemical Society Transactions*, *44*(2), 582–588. https://doi.org/10.1042/BST20150244

Fletcher, M. M., Halls, M. L., Zhao, P., Clydesdale, L., Christopoulos, A., Sexton, P. M., & Wootten, D. (2018). Glucagon-like peptide-1 receptor internalisation controls spatiotemporal signalling mediated by biased agonists. *Biochemical Pharmacology*, *156*(July), 406–419. https://doi.org/10.1016/j.bcp.2018.09.003

Fredriksson, R., Lagerstrom, M. C., Lundin, L.-G., & Schiöth, H. B. (2003). The G-Protein-Coupled Receptors in the Human Genome Form Five Main Families . Phylogenetic Analysis , Paralogon Groups , and Fingerprints. *Molecular Pharmacology*, *63*(6), 1256–1272.

Freeman, J., Weaver, S., Davis, S., Rao, M., Quada, J., Santhosh, K., … Valcarce, C. (2016). TTP273 : Oral , G protein Pathway Selective In silico modeling suggests vTv GLP-1R Agonists Bind to an Allosteric Site.

Furness, S. G. B., Liang, Y., Nowell, C. J., Christopoulos, A., Wootten, D., George, S., … Sexton, P. M. (2016). Ligand-Dependent Modulation of G Protein Article Ligand-Dependent Modulation of G Protein Conformation Alters Drug Efficacy. *Cell*, *167*(3), 1–11. https://doi.org/10.1016/j.cell.2016.09.021

García-Nafría, J., Lee, Y., Bai, X., Carpenter, B., & Tate, C. G. (2018). Cryo-EM structure of the adenosine A2A receptor coupled to an engineered heterotrimeric G protein. *ELife*, *7*, 1–19. https://doi.org/10.7554/eLife.35946.001

García-Nafría, J., Nehmé, R., Edwards, P. C., & Tate, C. G. (2018). Cryo-EM structure of the serotonin 5-HT1B receptor coupled to heterotrimeric Go. *Nature*, *558*(7711), 620–623. https://doi.org/10.1038/s41586-018-0241-9

Gault, V. A., & Hölscher, C. (2018). GLP-1 receptor agonists show neuroprotective effects in animal models of diabetes. *Peptides*, *100*(September 2017), 101–107. https://doi.org/10.1016/j.peptides.2017.11.017

Gether, U., Lin, S., Ghanouni, P., Ballesteros, J. A., Weinstein, H., & Kobilka, B. K. (1997). Agonists induce conformational changes in transmembrane domains III and VI of the β2 adrenoceptor. *The EMBO Journal*, *16*(22), 6737–6747. https://doi.org/10.1093/emboj/16.22.6737

Gondin, A. B., Halls, M. L., Canals, M., & Briddon, S. J. (2019). GRK mediates μ-opioid receptor plasma membrane reorganization. *Frontiers in Molecular Neuroscience*, *12*(May), 1–14. https://doi.org/10.3389/fnmol.2019.00104

Gregorio, G., Masureel, M., Hilger, D., Terry, D., Juette, M., Zhao, H., Zhou, Z., …Blanchard, S. (2017) Single-molecule analysis of ligand efficacy in β_2AR-G protein activation. *Nature.*547(7661):68-73. doi:10.1038/nature22354

Gregory, K., Sexton, P., Christopolous, A. (2007) Allosteric modulators of muscarinic acetylcholine receptors. *Current Neuropharmacology*. 5(3) 157-167

Griffin, L., & Lawson, A. (2011). Antibody fragments as tools in crystallography. *Clinical and Experimental Immunology*, *165*(3), 285–291. https://doi.org/10.1111/j.1365-2249.2011.04427.x

Grundmann, M., Merten, N., Malfacini, D., Inoue, A., Preis, P., Simon, K., … Kostenis, E. (2018). Lack of beta-arrestin signaling in the absence of active G proteins. *Nature Communications*, *9*(1), 341. https://doi.org/10.1038/s41467-017-02661-3

Hager, M. V., Clydesdale, L., Gellman, S. H., Sexton, P. M., & Wootten, D. (2017). Characterization of signal bias at the GLP-1 receptor induced by backbone modification of GLP-1. *Biochemical Pharmacology*, 1–10. https://doi.org/10.1016/j.bcp.2017.03.018

Hanlon, C. D., & Andrew, D. J. (2015). Outside-in signaling - a brief review of GPCR signaling with a focus on the Drosophila GPCR family. *Journal of Cell Science*, 3533–3542. https://doi.org/10.1242/jcs.175158

Haque, T. S., Lee, V. G., Riexinger, D., Lei, M., Malmstrom, S., Xin, L., … Krupinski, J. (2010). Peptides Identification of potent 11mer Glucagon-Like Peptide-1 Receptor agonist peptides with novel C-terminal amino acids : Homohomophenylalanine analogs. *Peptides*, *31*(5), 950–955. https://doi.org/10.1016/j.peptides.2010.01.008

Hoang, H. N., Song, K., Hill, T. A., Derksen, D. R., Edmonds, D. J., Kok, W. M., … Fairlie, D. P. (2015). Short hydrophobic peptides with cyclic constraints are potent glucagon-like peptide-1 receptor (GLP-1R) agonists. *Journal of Medicinal Chemistry*, *58*(9), 4080–4085. https://doi.org/10.1021/acs.jmedchem.5b00166

Hoare, S. R. J. (2005). Mechanisms of peptide and nonpeptide ligand binding to Class B G-protein-coupled receptors. *Drug Discovery Today*, *10*(6), 417–427.

https://doi.org/10.1016/S1359-6446(05)03370-2
Hollenstein, K., De Graaf, C., Bortolato, A., Wang, M. W., Marshall, F. H., & Stevens, R. C. (2014). Insights into the structure of class B GPCRs. *Trends in Pharmacological Sciences*, *35*(1), 12–22. https://doi.org/10.1016/j.tips.2013.11.001
Hollenstein, K., Kean, J., Bortolato, A., Cheng, R. K. Y., Doré, A. S., Jazayeri, A., … Marshall, F. H. (2013). Structure of class B GPCR corticotropin-releasing factor receptor 1. *Nature*, *499*(7459), 438–443. https://doi.org/10.1038/nature12357
Holst, J. J., Vilsbøll, T., & Deacon, C. F. (2009). The incretin system and its role in type 2 diabetes mellitus. *Molecular and Cellular Endocrinology*, *297*(1–2), 127–136. https://doi.org/10.1016/j.mce.2008.08.012
Ismail, S., Gherardi, M.-J., Froese, A., Zanoun, M., Gigoux, V., Clerc, P., … Fourmy, D. (2016). Internalized Receptor for Glucose-dependent Insulinotropic Peptide stimulates adenylyl cyclase on early endosomes. *Biochemical Pharmacology*, *120*, 33–45. https://doi.org/10.1016/j.bcp.2016.09.009
Jazayeri, A., Doré, A. S., Lamb, D., Krishnamurthy, H., Southall, S. M., Baig, A. H., … Marshall, F. H. (2016). Extra-helical binding site of a glucagon receptor antagonist. *Nature*, *533*(7602), 274–277. https://doi.org/10.1038/nature17414
Jazayeri, Ali, Rappas, M., Brown, A. J. H., Kean, J., Errey, J. C., Robertson, N. J., … Marshall, F. H. (2017). Crystal structure of the GLP-1 receptor bound to a peptide agonist. *Nature*, *546*(7657), 254–258. https://doi.org/10.1038/nature22800
Jiang, L. I., Collins, J., Davis, R., Fraser, I. D., & Sternweis, P. C. (2008). Regulation of cAMP responses by the G12-13 pathway converges on adenylyl cyclase VII. *Journal of Biological Chemistry*, *283*(34), 23429–23439. https://doi.org/10.1074/jbc.M803281200
Jones, B., Buenaventura, T., Kanda, N., Chabosseau, P., Owen, B. M., Scott, R., … Bloom, S. R. (2018). Targeting GLP-1 receptor trafficking to improve agonist efficacy. *Nature Communications*, *9*(1). https://doi.org/10.1038/s41467-018-03941-2
Kang, Y., Zhou, X. E., Gao, X., He, Y., Liu, W., Ishchenko, A., … Xu, H. E. (2015). Crystal structure of rhodopsin bound to arrestin by femtosecond X-ray laser. *Nature*, *523*(7562), 561–567. https://doi.org/10.1038/nature14656
Karageorgos, V., Venihaki, M., Sakellaris, S., Pardalos, M., Kontakis, G., Matsoukas, M. T., … Liapakis, G. (2018). Current understanding of the structure and function of family B GPCRs to design novel drugs. *Hormones*, *17*(1), 45–59. https://doi.org/10.1007/s42000-018-0009-5
Kenakin, T. (2004). Principles: Receptor theory in pharmacology. *Trends in Pharmacological Sciences*, *25*(4), 186–192. https://doi.org/10.1016/j.tips.2004.02.012
Kenakin, T., & Christopoulos, A. (2013). Signalling bias in new drug discovery: detection, quantification and therapeutic impact. *Nature Reviews. Drug Discovery*, *12*(March 2013), 205–216. https://doi.org/10.1038/nrd3954
Kenakin, T., Watson, C., Muniz-Medina, V., Christopoulos, A., & Novick, S. (2012). A simple method for quantifying functional selectivity and agonist bias. *ACS Chemical Neuroscience*, *3*(3), 193–203. https://doi.org/10.1021/cn200111m
Khan, S. M., Sleno, R., Gora, S., Zylbergold, P., Laverdure, J.-P., Labbé, J.-C., … Hébert, T. E. (2013). The expanding roles of Gβγ subunits in G protein-coupled receptor signaling and drug action. *Pharmacological Reviews*, *65*(2), 545–577. https://doi.org/10.1124/pr.111.005603
Kirchberg, K., Kim, T.-Y., Möller, M., Skegro, D., Dasara Raju, G., Granzin, J., … Alexiev, U. (2011). Conformational dynamics of helix 8 in the GPCR rhodopsin controls arrestin activation in the desensitization process. *Proceedings of the National Academy of Sciences of the United States of America*, *108*(46), 18690–18695. https://doi.org/10.1073/pnas.1015461108

Knudsen, L. B., Kiel, D., Teng, M., Behrens, C., Bhumralkar, D., Kodra, J. T., … Lau, J. (2007). Small-molecule agonists for the glucagon-like peptide 1 receptor. *Proceedings of the National Academy of Sciences of the United States of America*, *104*(3), 937–942. https://doi.org/10.1073/pnas.0605701104

Koole, C., Savage, E. E., Christopoulos, A., Miller, L. J., Sexton, P. M., & Wootten, D. (2013). Minireview: Signal bias, allosterism, and polymorphic variation at the GLP-1R: implications for drug discovery. *Molecular Endocrinology (Baltimore, Md.)*, *27*(8), 1234–1244. https://doi.org/10.1210/me.2013-1116

Koole, C., Wootten, D., Simms, J., Miller, L. J., Christopoulos, A., & Sexton, P. M. (2012). Second extracellular loop of human glucagon-like peptide-1 receptor (GLP-1R) has a critical role in GLP-1 peptide binding and receptor activation. *Journal of Biological Chemistry*, *287*(6), 3642–3658. https://doi.org/10.1074/jbc.M111.309328

Kreiger, J., Arnold, M., Peterson, K., Lossel, P., Langhans, W., Lee, S. (2016) Knockdown of GLP-1 receptors in vagal afferents affects normal food intake and glycaemia. *Diabetes.* 65(1) 34-43

Lagerström, M. C., & Schiöth, H. B. (2008). Structural diversity of G protein-coupled receptors and significance for drug discovery. *Nature Reviews. Drug Discovery*, *7*(4), 339–357. https://doi.org/10.1038/nrd2518

Lee, S. M., Booe, J. M., & Pioszak, A. A. (2015). Structural insights into ligand recognition and selectivity for classes A, B, and C GPCRs. *European Journal of Pharmacology*, *763*, 196–205. https://doi.org/10.1016/j.ejphar.2015.05.013

Leff, P. (1995). The two-state model of receptor activation. *Trends in Pharmacological Sciences*, *16*(3), 89–97. https://doi.org/10.1016/S0165-6147(00)88989-0

Lei, S., Clydesdale, L., Dai, A., Cai, X., Feng, Y., Yang, D., … Sexton, P. M. (2018). Two distinct domains of the glucagon-like peptide-1 receptor control peptide-mediated biased agonism. *Journal of Biological Chemistry*, *293*(3), 9370–9387. https://doi.org/10.1074/jbc.M115.653899

Li, L., Wu, L., Xia, E., Yan, W., Cai, X., Han, J., & Sun, L. (2019). Novel nonapeptide GLP (28-36) amide derivatives with improved hypoglycemic and body weight lowering effects. *Bioorganic & Medicinal Chemistry*. https://doi.org/10.1016/j.bmc.2019.03.014

cLiang, Y.-L., Zhao, P., Draper-Joyce, C., Baltos, J.-A., Glukhova, A., Truong, T. T., … Furness, S. G. B. (2018). Dominant Negative G Proteins Enhance Formation and Purification of Agonist-GPCR-G Protein Complexes for Structure Determination. *ACS Pharmacology & Translational Science*, *1*(1), 12–20. https://doi.org/10.1021/acsptsci.8b00017

Liang, Y. L., Belousoff, M. J., Zhao, P., Koole, C., Fletcher, M. M., Truong, T. T., … Wootten, D. (2020). Toward a Structural Understanding of Class B GPCR Peptide Binding and Activation. *Molecular Cell*, *77*(3), 656-668.e5. https://doi.org/10.1016/j.molcel.2020.01.012

aLiang, Y. L., Khoshouei, M., Deganutti, G., Glukhova, A., Koole, C., Peat, T. S., … Sexton, P. M. (2018). Cryo-EM structure of the active, Gs-protein complexed, human CGRP receptor. *Nature*, *561*(7724), 492–497. https://doi.org/10.1038/s41586-018-0535-y

bLiang, Y. L., Khoshouei, M., Glukhova, A., Furness, S. G. B., Zhao, P., Clydesdale, L., … Wootten, D. (2018). Phase-plate cryo-EM structure of a biased agonistbound human GLP-1 receptor-Gs complex. *Nature*, *555*(7694), 121–125. https://doi.org/10.1038/nature25773

Liang, Y. L., Khoshouei, M., Radjainia, M., Zhang, Y., Glukhova, A., Tarrasch, J., … Sexton, P. M. (2017). Phase-plate cryo-EM structure of a class B GPCR-G-protein complex. *Nature*, *546*(7656), 118–123. https://doi.org/10.1038/nature22327

Lindgren, O., Carr, R. D., Deacon, C. F., Holst, J. J., Pacini, G., Mari, A., & Ahreń, B. (2011). Incretin hormone and insulin responses to oral versus intravenous lipid

administration in humans. *Journal of Clinical Endocrinology and Metabolism*, *96*(8), 2519–2524. https://doi.org/10.1210/jc.2011-0266

Liu, J., Horst, R., Katritch, V., Stevens, R., & Wuthrich, K. (2013). Biased signalling pathways in beta2-adrenergic receptor characterized by 19F-NMR. *Science*, *335*(6072), 1106–1110. https://doi.org/10.1126/science.1215802.Biased

Lu, K. H., Cao, J., Oleson, S., Ward, M. P., Phillips, R. J., Powley, T. L., & Liu, Z. (2018). Vagus nerve stimulation promotes gastric emptying by increasing pyloric opening measured with magnetic resonance imaging. *Neurogastroenterology and Motility*, *30*(10), 1–11. https://doi.org/10.1111/nmo.13380

Luciani, P., Deledda, C., Benvenuti, S., Cellai, I., Squecco, R., Monici, M., … Peri, A. (2010). Differentiating effects of the glucagon-like peptide-1 analogue exendin-4 in a human neuronal cell model. *Cellular and Molecular Life Sciences*, *67*(21), 3711–3723. https://doi.org/10.1007/s00018-010-0398-3

Ma, L., & Pei, G. (2006) β-arrestin signalling and regulation of transcription. *Journal of Cell Sciences*. 120, 213-218

Maeda, S., Koehl, A., Matile, H., Hu, H., Hilger, D., Schertler, G. F. X., … Kobilka, B. K. (2018). Development of an antibody fragment that stabilizes GPCR/G-protein complexes. *Nature Communications*, *9*(1), 1–9. https://doi.org/10.1038/s41467-018-06002-w

Manglik, A., Kim, T. H., Masureel, M., Altenbach, C., Yang, Z., Hilger, D., … Kobilka, B. K. (2015). Structural Insights into the Dynamic Process of β2-Adrenergic Receptor Signaling. *Cell*, *161*(5), 1101–1111. https://doi.org/10.1016/j.cell.2015.04.043

Mapelli, C., Natarajan, S. I., Meyer, J. P., Bastos, M. M., Bernatowicz, M. S., Lee, V. G., … Ewing, W. R. (2009). Eleven amino acid glucagon-like peptide-1 receptor agonists with antidiabetic activity. *Journal of Medicinal Chemistry*, *52*(23), 7788–7799. https://doi.org/10.1021/jm900752a

Mark, C. B., & Jeannie, F. (1999). Glucagon-like peptide 1 has a physiological role in the control of Postprandial Glucose in Humans. *Diabetes*, *48*(1), 86.

Mayer, D., Damberger, D., Samarasimhareddy, M., Feldmueller, M., Vuckovic, Z., … Veprintstev, D. (2019) Distinct G-protein couples receptorp phosphorylation motis modulate arrestin affinity and activation and global profile. *Nature Communications*. 10(1261) 2019.

McCorvy, J. D., Butler, K. V, Kelly, B., Rechsteiner, K., Karpiak, J., Betz, R. M., … Roth, B. L. (2017). Structure-inspired design of β-arrestin-biased ligands for aminergic GPCRs. *Nature Chemical Biology*, (december). https://doi.org/10.1038/nchembio.2527

Mehta, A., Marso, S. P., & Neeland, I. J. (2017). Liraglutide for weight management: a critical review of the evidence. *Obesity Science & Practice*, *3*(1), 3–14. https://doi.org/10.1002/osp4.84

Meloni, A. R., Deyoung, M. B., Lowe, C., & Parkes, D. G. (2013). GLP-1 receptor activated insulin secretion from pancreatic β-cells: Mechanism and glucose dependence. *Diabetes, Obesity and Metabolism*, *15*(1), 15–27. https://doi.org/10.1111/j.1463-1326.2012.01663.x

Moore, M. C., Werner, U., Smith, M. S., Farmer, T. D., & Cherrington, A. D. (2013). Effect of the glucagon-like peptide-1 receptor agonist lixisenatide on postprandial hepatic glucose metabolism in the conscious dog. *American Journal of Physiology - Endocrinology and Metabolism*, *305*(12). https://doi.org/10.1152/ajpendo.00354.2013

Nance, K. D., Days, E. L., Weaver, C. D., Coldren, A., Farmer, T. D., Cho, H. P., … Lindsley, C. W. (2017). Discovery of a novel series of orally bioavailable and CNS penetrant Glucagon-Like Peptide 1 Receptor (GLP-1R) non-competitive antagonists based on a 1,3-disubstituted-7-aryl-5,5-bis(trifluoromethyl)-5,8-dihydropyrimido[4,5- *d*

]pyrimidine-2,4(1 <i>. *Journal of Medicinal Chemistry*, *2*, acs.jmedchem.6b01706. https://doi.org/10.1021/acs.jmedchem.6b01706
Nehmea, R., Carpenter, B., Singhal, A., Strege, A., Edwards, P. C., White, C. F., … Tate, C. G. (2017). Mini-G proteins: Novel tools for studying GPCRs in their active conformation. *PLoS ONE*, *12*(4), 1–26. https://doi.org/10.1371/journal.pone.0175642
Nolte, W. M., Fortin, J.-P., Stevens, B. D., Aspnes, G. E., Griffith, D. a, Hoth, L. R., … Carpino, P. a. (2014). A potentiator of orthosteric ligand activity at GLP-1R acts via covalent modification. *Nature Chemical Biology*, *10*(8), 629–631. https://doi.org/10.1038/nchembio.1581
Ochoa-Callejero, L., García-Sanmartín, J., Martínez-Herrero, S., Rubio-Mediavilla, S., Narro-Íñiguez, J., & Martínez, A. (2017). Small molecules related to adrenomedullin reduce tumor burden in a mouse model of colitis-associated colon cancer. *Scientific Reports*, *7*(1), 1–11. https://doi.org/10.1038/s41598-017-17573-x
Pabreja, K., Mohd, M. A., Koole, C., Wootten, D., & Furness, S. G. B. (2014). Molecular mechanisms underlying physiological and receptor pleiotropic effects mediated by GLP-1R activation. *British Journal of Pharmacology*, *171*(5), 1114–1128. https://doi.org/10.1111/bph.12313
Pack, T. F., Orlen, M. I., Ray, C., Peterson, S. M., & Caron, M. G. (2018). The dopamine D2 receptor can directly recruit and activate GRK2 without G protein activation. *Journal of Biological Chemistry*, *293*(16), 6161–6171. https://doi.org/10.1074/jbc.RA117.001300
Pal, K., Melcher, K., & Xu, H. E. (2012). Structure and mechanism for recognition of peptide hormones by Class B G-protein-coupled receptors. *Acta Pharmacologica Sinica*, *33*(3), 300–311. https://doi.org/10.1038/aps.2011.170
Palczewski, K., Kumasaka, T., Hori, T., Behnke, C., Motoshima, H., Fox, B., … Miyano, M. (2000). Crystal structure of Rhodopson: A G Protein-Coupled Receptor. *Science*, *289*, 487–488. https://doi.org/10.1524/ncrs.2006.0167
Pandy-Szekeres, G., Munk, C., Tsonkov, T., Mordalski, S., Harpsoe, K., Hauser, A., Bojarski, A., Gloriam, D. (2018) GPCRdb in 2018: Adding GPCRstructure models and ligands. *Nucleic Acid Research.* 46(d1) D440-D446.
Poyner, D. R., & Hay, D. L. (2012). Secretin family (Class B) G protein-coupled receptors - From molecular to clinical perspectives. *British Journal of Pharmacology*, *166*(1), 1–3. https://doi.org/10.1111/j.1476-5381.2011.01810.x
Qi, T., Christopolous, G., Bailey, R., Christopolous, A., Sexton, P., Hay, D., (2008) Identification of N-terminal receptor activity-modifying protein residues important for calcitonin gene-related peptide, adrenomedullin and amylin receptor function. *Molecular Pharmacology.* 74(4)1059-71
Qi, T., Dong, M., Watkins, H., Wootten, D., Miller, L., Hay, D. (2013) Receptor activity-modifying protein impairment of calcitonin receptor splice variant Δ(1-47)HCT(a) function. *British Journal of Pharmacology.* 168(3)644-657
Rajagopal, S., Ahn, A., Rominger, D., Gowen-MacDonald, W., Lam, C., DeWire, S., Violin, J., Leftkowitz, R. (2011) Quantifying Ligand bias at seven-transmembrane receptors. *Molecular Pharmacology.* 80(3) 367-377
Rankovic, Z., Brust, T. F., & Bohn, L. M. (2016). Biased agonism: An emerging paradigm in GPCR drug discovery. *Bioorganic and Medicinal Chemistry Letters*, *26*(2), 241–250. https://doi.org/10.1016/j.bmcl.2015.12.024
Rasmussen, S. G. F., DeVree, B. T., Zou, Y., Kruse, A. C., Chung, K. Y., Kobilka, T. S., … Kobilka, B. K. (2011). Crystal structure of the β2 adrenergic receptor-Gs protein complex. *Nature*, *477*(7366), 549–555. https://doi.org/10.1038/nature10361
Roed, S. N., No, A. C., Wismann, P., Iversen, H., Bräuner-Osborne, H., Knudsen, S. M., & Waldhoer, M. (2015). Functional consequences of glucagon-like peptide-1 receptor

cross-talk and trafficking. *Journal of Biological Chemistry*, *290*(2), 1233–1243. https://doi.org/10.1074/jbc.M114.592436
Sammons, M. F., & Lee, E. C. Y. (2015). Recent progress in the development of small-molecule glucagon receptor antagonists. *Bioorganic and Medicinal Chemistry Letters*, *25*(19), 4057–4064. https://doi.org/10.1016/j.bmcl.2015.07.092
Sanz, G., Leray, I., Muscat, A., Acquistapace, A., Cui, T., Riviere, J., Vincent-Naulleau, S., Giandomenico, V., Mir, L. (2017) Gallein, a Gβγ subunit signalling inhibitor, inhibits metastatic spread of timour cells by expressing OR51E2 and exposed to its odorant ligand. *BMC Research Notes*. 10(1) 541
Schrage, R., Schmitz, A. L., Gaffal, E., Annala, S., Kehraus, S., Wenzel, D., … Kostenis, E. (2015). The experimental power of FR900359 to study Gq-regulated biological processes. *Nature Communications*, *6*(May), 1–7. https://doi.org/10.1038/ncomms10156
Seidel, L., Zarzycka B., Zaidi, S., Katritch, V., Coin, I. (2017) Structural insight into the activation of a class B G-protein coupled receptor by peptide hormones in live human cells. *eLife*. 6, e27711
Seifert, R., Wenzel-Seifert, K., Gether, U., & Kobilka, B. K. (2001). Functional differences between full and partial agonists: evidence for ligand-specific receptor conformations. *The Journal of Pharmacology and Experimental Therapeutics*, *297*(3), 1218–1226.
Shan, J., Khelashvili, G., Mondal, S., Mehler, E. L., & Weinstein, H. (2012). Ligand-dependent conformations and dynamics of the serotonin 5-HT2A receptor determine its activation and membrane-driven oligomerization properties. *PLoS Computational Biology*, *8*(4). https://doi.org/10.1371/journal.pcbi.1002473
Shang, Y., & Filizola, M. (2015). Opioid receptors: Structural and mechanistic insights into pharmacology and signaling. *European Journal of Pharmacology*, *763*(1), 206–213. https://doi.org/10.1016/j.physbeh.2017.03.040
Sharma, D., Verma, S., Vaidya, S., Kalia, K., & Tiwari, V. (2018). Recent updates on GLP-1 agonists: Current advancements & challenges. *Biomedicine and Pharmacotherapy*, *108*(April), 952–962. https://doi.org/10.1016/j.biopha.2018.08.088
Shenoy, S. K., & Lefkowitz, R. J. (2005). Receptor regulation : β -arrestin moves up a notch. *Nature Cell Biology*, *7*(12), 1159–1162. https://doi.org/10.1038/ncb1205-1059
Sherlter, G., Villa, C., Henderson , R. (1993) Projection structure of rhodopsin. *Nature*. 362, 770-772
Siu, F. Y., He, M., de Graaf, C., Han, G. W., Yang, D., Zhang, Z., … Stevens, R. C. (2013). Structure of the human glucagon class B G-protein-coupled receptor. *Nature*, *499*(7459), 444–449. https://doi.org/10.1038/nature12393
Song, G., Yang, D., Wang, Y., de Graaf, C., Zhou, Q., Jinag, S., Cai, X., … Stevens, S. (2017) Human GLP-1 receptor transmembrane domain in complex with allosteric modulators. *Nature.* 546, 312-315
Sonoda, N., Imamura, T., Yoshizaki, T., Babendure, J. L., Lu, J., & Olefsky, J. M. (2008). Beta-Arrestin-1 mediates glucagon-like peptide-1 signaling to insulin secretion in cultured pancreatic beta cells. *Proceedings of the National Academy of Sciences of the United States of America*, *105*(18), 6614–6619. https://doi.org/10.1073/pnas.0710402105
Sounier, R., Mas, C., Steyaert, J., Laeremans, T., Manglik, A., Huang, W., … Granier, S. (2015). Propagation of conformational changes during m-opioid receptor activation. *Nature*, *524*, 375–379. https://doi.org/10.1038/nature14680
Steyaert, J., & Kobilka, B. (2011). Nanobody stabilization of G protein coupled receptor conformational states.Pdf. *Current Opinion in Structural Biology*, *21*(4), 567–572. https://doi.org/10.1016/j.sbi.2011.06.011.Nanobody
Syme, C. a, Zhang, L., & Bisello, A. (2006). Caveolin-1 regulates cellular trafficking and

function of the glucagon-like Peptide 1 receptor. *Molecular Endocrinology (Baltimore, Md.)*, *20*(12), 3400–3411. https://doi.org/10.1210/me.2006-0178
Syrovatkina, V., Alegre, K., Dey, R., & Huang, X. (2016). Regulation, Signaling and Physiological Functions of G-proteins Viktoriya. *Journal of Molecular Biology*, *428*(19), 139–148. https://doi.org/10.1016/j.physbeh.2017.03.040
Taylor, S. J., Chae, H. zoon, Rhee, S. G., & Exton, J. H. (1991). Activation of the β1 isozyme of phospholipase C by α subunits of the Gq class of G proteins. *Nature*, *350*(April), 516–518. https://doi.org/10.1007/978-1-84882-046-3_4
Te, J., Dong, M., Miller L., Bordner, A. (2012) Predicting the effects of amino acid replacements in peptide hormones on their binding affinities for class B GPCRs and application to the design of secretin receptor antagonists. *Journal of Computer Aided Molecular Design.* 26(7)835-845
ter Haar, E., Koth, C. M., Abdul-Manan, N., Swenson, L., Coll, J. T., Lippke, J. A., … Moore, J. M. (2010). Crystal structure of the ectodomain complex of the CGRP receptor, a class-B GPCR, reveals the site of drug antagonism. *Structure*, *18*(9), 1083–1093. https://doi.org/10.1016/j.str.2010.05.014
Thal, D. M., Sun, B., Feng, D., Nawaratne, V., Leach, K., Felder, C. C., … Christopoulos, A. (2016). Crystal structures of the M1 and M4 muscarinic acetylcholine receptors. *Nature*, *531*(7594), 335–340. https://doi.org/10.1038/nature17188
Thanawala, V., Forkuo, G., Stallaert , W., Leff, P., Bouvier, M., Bond, R. (2014) Ligand bias prevent equiality among beta-blockers. *Current Opinions in Pharmacology.* 0. 50-57
Thompson, A., & Kanamarlapudi, V. (2015). Agonist-induced internalisation of the glucagon-like peptide-1 receptor is mediated by the Gαq pathway. *Biochemical Pharmacology*, *93*(1), 72–84. https://doi.org/10.1016/j.bcp.2014.10.015
Thompson, A., Stephens, J. W., Bain, S. C., & Kanamarlapudi, V. (2016a). Molecular characterisation of small molecule agonists effect on the human glucagon like peptide-1 receptor internalisation. *PLoS ONE*, *11*(4), 1–23. https://doi.org/10.1371/journal.pone.0154229
Thompson, A., Stephens, J. W., Bain, S. C., & Kanamarlapudi, V. (2016b). Molecular characterisation of small molecule agonists effect on the human glucagon like peptide-1 receptor internalisation. *PLoS ONE*, *11*(4), 1–22. https://doi.org/10.1371/journal.pone.0154229
Tobin, A. B., Butcher, A. J., & Kong, K. C. (2008). Location, location, location...site-specific GPCR phosphorylation offers a mechanism for cell-type-specific signalling. *Trends in Pharmacological Sciences*, *29*(8), 413–420. https://doi.org/10.1016/j.tips.2008.05.006
Tuteja, N. (2009). Signaling through G protein coupled receptors. *Plant Signaling and Behavior*, *4*(10), 942–947. https://doi.org/10.4161/psb.4.10.9530
Underwood, C. R., Garibay, P., Knudsen, L. B., Hastrup, S., Peters, G. H., Rudolph, R., & Reedtz-Runge, S. (2010). Crystal structure of glucagon-like peptide-1 in complex with the extracellular domain of the glucagon-like peptide-1 receptor. *Journal of Biological Chemistry*, *285*(1), 723–730. https://doi.org/10.1074/jbc.M109.033829
Usui, R., Yabe, D., Seino, Y. (2019) Twincretin as a potential therapy for the management of type 2 diabetes with obesity. *Journal of Diabete Investigation.* 10(4) 902-905
Vaidehi, N., Grisshammer, R., & Tate, G. (2016). How do mutations thermostabilize G protein-coupled receptors? *Trends in Pharmacological Sciences*, *37*(1), 37–46. https://doi.org/10.1016/j.physbeh.2017.03.040
Van Eps, N. Van, Altenbach, C., Caro, L. N., Latorraca, N. R., & Hollingsworth, S. A. (2018). G i - and G s -coupled GPCRs show different modes of G-protein binding, *115*(10), 2–7. https://doi.org/10.1073/pnas.1721896115
Venkatakrishnan, A. J., Deupi, X., Lebon, G., Heydenreich, F. M., Flock, T., Miljus, T., …

Babu, M. M. (2016). Diverse activation pathways in class A GPCRs converge near the G-protein-coupling region. *Nature*, *40*(2), 383–388. https://doi.org/10.1038/nature19107
Vilardaga, J. P., Romero, G., Friedman, P. A., & Gardella, T. J. (2011). Molecular basis of parathyroid hormone receptor signaling and trafficking: A family B GPCR paradigm. *Cellular and Molecular Life Sciences*, *68*(1), 1–13. https://doi.org/10.1007/s00018-010-0465-9
Violin, J. D., Dewire, S. M., Yamashita, D., Rominger, D. H., Nguyen, L., Schiller, K., … Lark, M. W. (2010). Selectively Engaging B-Arrestins at the Angiotensin II Type 1 Receptor Reduces Blood Pressure and Increases Cardiac Performance. *Pharmacology & Therapeutics*, *335*, 572–579. https://doi.org/10.1124/jpet.110.173005.
Vohra, S., Taddese, B., Conner, A., Poyner, D., Hay, D., Barwell, J., Reeves, P., Upton, G., Reynolds, C. (2013) Similarity between Class A and Class B G-protein couples receptors exemplified through calcitonin gene-related peptide receptor modelling and mutagenesis studies. *Interface*. 10:20120842
Wang, J., Song, X., Zhang, D., Chen, X., Li, X., Sun, Y., … Ma, Y. (2020). Cryo-EM structures of PAC1 receptor reveal ligand binding mechanism. *Cell Research*, (January), 1–10. https://doi.org/10.1038/s41422-020-0280-2
Wang, W., Qiao, Y., Li, Z. (2018) New insights into modes of GPCR activation. *Trends in Pharamcological Science.* 39(4), 367-386
Watkins, H., Au, M., Bobby, R., Archbold, J., Abdul-Manan, N., Middledicth, M., Williams, G., Brimble, M., Dingley, A., Hay, D. (2013) Identification of key residues in adrenomedullin binding to the AM1 receptor. *British Journal of Pharmacology*. 169(1)143-155.
Whalen, E. J., Rajagopal, S., & Lefkowitz, R. J. (2011). Therapeutic potential of β-arrestin- and G protein-biased agonists. *Trends in Molecular Medicine*, *17*(3), 126–139. https://doi.org/10.1016/j.molmed.2010.11.004
WHO. (2017). *Diabetes Facts*. https://doi.org/10.1097/00152193-198704000-00001
Willard, F., Bueno, A., Sloop, K. (2012) Small molecule drug discovery at the glucagon-like perptide-2 receptor. *Experimental Diabetes Research.* 2012;2012;709893
Wingler, L. M., Elgeti, M., Hilger, D., Kobilka, B. K., Hubbell, W. L., Lefkowitz, R. J., … Staus, D. P. (2019). Angiotensin Analogs with Divergent Bias Stabilize Article Angiotensin Analogs with Divergent Bias Stabilize Distinct Receptor Conformations. *Cell*, *176*(3), 468-478.e11. https://doi.org/10.1016/j.cell.2018.12.005
Wisler, J. W., DeWire, S. M., Whalen, E. J., Violin, J. D., Drake, M. T., Ahn, S., … Lefkowitz, R. J. (2007). A unique mechanism of beta-blocker action: carvedilol stimulates beta-arrestin signaling. *Proceedings of the National Academy of Sciences of the United States of America*, *104*(42), 16657–16662. https://doi.org/10.1073/pnas.0707936104
Woolley, M., Watkins, H., Taddese, B., Karakullucku, G., Barwell, J., Smith, K., … Conner, A (2013) The role of ECL2 in CGRP receptor activation: a combined modelling and experimental approach. *Interface*. 10:20130583
Wootten, D., Reynolds, C. A., Koole, C., Smith, K. J., Mobarec, J. C., Simms, J., … Sexton, P. (2015). A Hydrogen-Bonded Polar Network in the Core of the Glucagon-Like Peptide-1 Receptor is a Fulcrum for Biased Agonism: Lessons from Class B Crystal Structures. *Molecular Pharmacology*. https://doi.org/10.1124/mol.115.101246
Wootten, D., Reynolds, C. A., Smith, K. J., Miller, L. J., Christopoulos, A., & Sexton Correspondence, P. M. (2016). The Extracellular Surface of the GLP-1 Receptor Is a Molecular Trigger for Biased Agonism. *Cell*, *165*(7), 1632–1643. https://doi.org/10.1016/j.cell.2016.05.023
Wootten, D., Reynolds, C. A., Smith, K. J., Mobarec, J. C., Furness, S. G. B., Miller, L. J., …

Sexton, P. M. (2016). Key interactions by conserved polar amino acids located at the transmembrane helical boundaries in Class B GPCRs modulate activation, effector specificity and biased signalling in the glucagon-like peptide-1 receptor. *Biochemical Pharmacology*, 1–20. https://doi.org/10.1016/j.bcp.2016.08.015

Yang, D., de Graaf, C., Yang, L., Song, G., Dai, A., Cai, X., … Wang, M.-W. (2016). Structural Determinants of Binding the Seven-transmembrane Domain of the Glucagon-like Peptide-1 Receptor. *Journal of Biological Chemistry*, (Md), jbc.M116.721977. https://doi.org/10.1074/jbc.M116.721977

Yudin, Y., & Rohacs, T. (2019). The G-protein-biased agents PZM21 and TRV130 are partial agonists of μ-opioid receptor-mediated signalling to ion channels. *British Journal of Pharmacology*, *176*(17), 3110–3125. https://doi.org/10.1111/bph.14702

Zamponi, G., & Currie, M. (2013). Regulation of CaV 2 calcium channels by G protein coupled receptors. *Biochim Biophys Acta.*, *1828*(7), 1629–1643. https://doi.org/10.1038/jid.2014.371

Zastrow, M. von, & Hanyaloglu, A. C. (2008). Regulation of GPCRs by Endocytic Membrane Trafficking and Its Potential Implications. *Annual Review of Pharmacology and Toxicology*, *48*, 537–568. https://doi.org/10.1146/annurev.pharmtox.48.113006.094830

Zhan-Guo, G., & Jacobson, K. A. (2016). On the Selectivity of the Gαq Inhibitor UBO-QIC: A Comparison with the Gαi Inhibitor Pertussis Toxin. *Biochemical Pharmacology*, *176*(1), 139–148. https://doi.org/10.1016/j.physbeh.2017.03.040

Zhang, H., Sturchler, E., Zhu, J., Nieto, A., Cistrone, P. a, Xie, J., … Lerner, R. a. (2015). Autocrine selection of a GLP-1R G-protein biased agonist with potent antidiabetic effects. *Nature Communications*, *6*(May), 8918. https://doi.org/10.1038/ncomms9918

Zhang, J., Gu, S., Sun, X., Li, W., Tang, Y., & Liu, G. (2016). Computational insight into conformational states of glucagon-like peptide-1 receptor (GLP-1R) and its binding mode with GLP-1. *RSC Adv.*, *6*(16), 13490–13497. https://doi.org/10.1039/C5RA26102C

Zhang, Y., Sun, B., Feng, D., Hu, H., Chu, M., Qu, Q., … Li, S. (2017). Cryo-EM structure of the activated GLP-1 receptor in complex with a G protein. *Nature Publishing Group*, *546*(7657), 248–253. https://doi.org/10.1038/nature22394

Zhao, P., Liang, Y. L., Belousoff, M. J., Deganutti, G., Fletcher, M. M., Willard, F. S., … Wootten, D. (2020). Activation of the GLP-1 receptor by a non-peptidic agonist. *Nature*, *577*(7790), 432–436. https://doi.org/10.1038/s41586-019-1902-z

Zurn, A., Zabel, U., Vilardaga, J., Schindelin, H., Lohse, M. J., & Hoffmann, C. (2009). Fluorescence resonance energy transfer analysis of α2a-adrenergic receptor activation reveals distinct agonist-specific conformational changes. *Molecular Pharmacology*, *75*(3), 534–541. https://doi.org/10.1124/mol.108.052399.switch

Appendix I:
Characterization of signal bias at the GLP-1 receptor induced by backbone modification of GLP-1

Biochemical Pharmacology xxx (2017) xxx–xxx

Contents lists available at ScienceDirect

Biochemical Pharmacology

journal homepage: www.elsevier.com/locate/biochempharm

Characterization of signal bias at the GLP-1 receptor induced by backbone modification of GLP-1

Marlies V. Hager [a,1], Lachlan Clydesdale [b,1], Samuel H. Gellman [a,*], Patrick M. Sexton [b,*], Denise Wootten [b,*]

[a] Department of Chemistry, University of Wisconsin, Madison, WI, United States
[b] Drug Discovery Biology, Monash Institute of Pharmaceutical Sciences and Department of Pharmacology, Monash University, Parkville, Australia

ARTICLE INFO

Article history:
Received 4 February 2017
Accepted 27 March 2017
Available online xxxx

Keywords:
Glucagon-like peptide-1 receptor
G protein coupled receptor
Biased agonism
Cell signaling
Peptides

ABSTRACT

The glucagon-like peptide-1 receptor (GLP-1R) is a class B G protein-coupled receptor that is a major therapeutic target for the treatment of type 2 diabetes. Activation of this receptor promotes insulin secretion and blood glucose regulation. The GLP-1R can initiate signaling through several intracellular pathways upon activation by GLP-1. GLP-1R ligands that preferentially stimulate subsets among the natural signaling pathways ("biased agonists") could be useful as tools for elucidating the consequences of specific pathways and might engender therapeutic agents with tailored effects. Using HEK-293 cells recombinantly expressing human GLP-1R, we have previously reported that backbone modification of GLP-1, *via* replacement of selected α-amino acid residues with β-amino acid residues, generates GLP-1 analogues with distinctive preferences for promoting G protein activation versus β-arrestin recruitment. Here, we have explored the influence of cell background across these two parameters and expanded our analysis to include affinity and other key signaling pathways (intracellular calcium mobilization and ERK phosphorylation) using recombinant human GLP-1R expressed in a CHO cell background, which has been used extensively to demonstrate biased agonism of GLP-1R ligands. The new data indicate that α/β-peptide analogues of GLP-1 exhibit a range of distinct bias profiles relative to GLP-1 and that broad assessment of signaling endpoints is required to reveal the spectrum of behavior of modified peptides. These results support the view that backbone modification via α → β amino acid replacement can enable rapid discovery of peptide hormone analogues that display substantial signal bias at a cognate GPCR.

1. Introduction

Type 2 diabetes mellitus is a chronic metabolic disorder characterized by insulin resistance, decreased insulin production, and the gradual failure of pancreatic β cells [1]. These features result in consistently high glucose levels in patients [2], a condition that can lead to severe complications and premature death [1]. Current diabetes treatments include insulin-sensitizing agents [3], exogenous insulin [4], and, more recently, agonists of the glucagon-like peptide 1 receptor (GLP-1R) [5]. This receptor has garnered interest because of its role not only in regulating blood glucose levels, but also in promoting other cellular and physiological outcomes that are impaired in diabetic patients; GLP-1R agonists increase satiety, decrease gastric emptying and enhance β cell health [6]. The most potent native agonists of the GLP-1R are two closely related forms of the glucagon-like peptide-1, which are designated GLP-1(7–36) NH_2 and GLP-1(7–37). Both are generated via processing of a longer precursor. These two peptides are referred to collectively as "GLP-1" below.

Binding of GLP-1 to the extracellular surface of the GLP-1R promotes recruitment of several G proteins, including $G\alpha_s$, $G\alpha_q$, $G\alpha_i$ and $G\alpha_o$ [7–9], as well as β-arrestin-1 and β-arrestin-2, to the cytoplasmic surface of the receptor [9,10]. While Gs stimulation is principally linked to activation of adenylate cyclase and cAMP formation, the canonical driver of GLP-1-stimulated insulin secretion [6], G_s, G_q and $G_{i/o}$ proteins can each lead to mobilization of intracellular calcium and/or ERK1/2 phosphorylation, in a ligand- and cell-type-specific manner [7–9]. β-Arrestins can modulate cell proliferation and apoptosis, at least in part through activation of MAPKs such as ERK1/2 [11,12], while also playing a role in β-cell-mediated insulin secretion [11].

The pleiotropy of signaling initiated by GPCRs allows for the potential of individual ligands of a specific receptor to generate distinct profiles of response, a phenomenon termed biased agonism [13–15]. At a receptor level, bias is engendered by unique interactions between ligands and the receptor that, in turn, can stabilize

* Corresponding authors.
E-mail address: denise.wootten@monash.edu (D. Wootten).
[1] These authors contributed equally to this work.

http://dx.doi.org/10.1016/j.bcp.2017.03.018
0006-2952/

distinct ensembles of conformations that promote differential engagement with effector proteins (e.g., a G protein or a β-arrestin) [16,17]. Biased agonists have received substantial attention for their potential as tools for elucidating GPCR signaling mechanisms, and as therapeutic candidates that might exert focused physiological effects by minimizing activation of pathways other than those that offer therapeutic benefit [15,18,19].

Oxyntomodulin, a natural ligand for the GLP-1R, and the clinically approved agonist exendin-4 exhibit bias in canonical signaling pathways and for arrestin recruitment, relative to GLP-1 in recombinant expression systems [9,20,21,25] and in insulinoma cells that natively express the GLP-1R [9]. Moreover, an N-terminally modified form of exendin-4, termed exendin P5, that exhibited bias away from arrestin recruitment (i.e., G protein-biased relative to exendin-4), was better than exendin-4 at correcting hyperglycaemia in rodent models of type 2 diabetes, despite being less efficacious than exendin-4 at promoting insulin secretion. This provides evidence that biased agonists of the GLP-1R may provide novel opportunities for therapeutic intervention [23].

Exploitation of biased agonism for therapeutic development requires an understanding of the optimal signaling profile for therapeutic benefit while minimizing on-target side effect profiles. While signaling outputs, such as cAMP, calcium and β-arrestin-1 have been linked to insulin secretion and beta cell survival, little is known regarding the optimal activation of these pathways relative to one another or of signaling pathways required for other actions, such as satiety and decreased gastric emptying and glucagon secretion, that are mediated by GLP-1R activation. In addition, signaling outputs that lead to undesired outputs of GLP-1R activation are also unknown. To fully understand these processes requires a toolbox of biased agonists with distinct biased profiles that are suitable for translational *in vivo* studies.

Recently, we have begun to explore a non-traditional approach to generate new GLP-1 analogues, involving replacement of selected α-amino acid residues with β-amino acid residues (Fig. 1A) [24,26]. This backbone-modification strategy has produced "α/β-peptides" that provide resistance to degradation by proteases [36,37]; proteolysis can limit the *in vivo* efficacy of α-peptides. This approach identified β-arrestin-biased GLP-1R agonists (relative to cAMP production) in the context of HEK-293 cells recombinantly expressing the human GLP-1R [24]. Backbone modification has received relatively little attention as an approach to the design of peptide hormone analogues, but holds significant promise for generation of novel peptides [22,24,26–33].

The ability to detect bias and indeed the observed direction of bias are dependent upon the breadth of endpoints studied and the cellular system used to explore this behavior. While the proximal driver for biased agonism may be at the level of receptor conformation, the expression of this bias (the observed bias) is critically dependent upon the expression, quantity and localization of effector and regulatory proteins within each cellular context. To explore the bias relative to other well characterized biased peptides, such as oxyntomodulin and exendin-4, required profiling these ligands in the same cellular background.

The studies described below provide a new and deeper understanding of the signaling properties of **P1**–**P9** at the GLP-1R by analyzing these peptides in a different cellular context (recombinantly expressed human GLP-1R in CHO cells, in contrast to the HEK293 cells used in previous studies) and extending the pharmacological characterization of these peptides. This includes measuring peptide affinities, and broadening the range of signaling endpoints to include ERK1/2 phosphorylation and intracellular calcium mobilization. These latter endpoints are both relevant to the physiological signaling of the GLP-1R and have been characterized in this cell background in response to other biased agonists of the GLP-1R. Thus, the new data allow direct comparison of biased profiles of the α/β-peptides with bias profiles of previously studied peptides and expands the pharmacological toolbox, providing a wider range of ligands that can be used for exploring the potential of biased GLP-1R profiles for therapeutic advantage.

2. Materials and methods

2.1. Materials

Dulbecco's modified Eagle's medium (DMEM), hygromycin-B, and Fluo-4 acetoxymethyl ester were purchased from Invitrogen (Carlsbad, CA, USA). Fetal bovine serum (FBS) was purchased from Thermo Fisher Scientific (Melbourne, Victoria, Australia). AlphaScreen™ reagents, and LANCE HTRF cAMP kit were purchased from PerkinElmer Life Sciences (Waltham, MA, USA). SureFire™ ERK1/2 reagents were generously supplied by TGR Biosciences (Adelaide, South Australia, Australia). GLP-1 was purchased from Mimotopes (Victoria, Australia).

All other reagents were purchased from Sigma (St. Louis, MO, USA) or BDH Merck (Melbourne, Vic, Australia) and were of an analytical grade.

2.2. Peptide synthesis

Peptides were synthesized in house as previously described [24].

2.3. Transfections and cell culture

Wildtype GLP-1R was isogenically integrated into FlpIn-Chinese hamster ovary (FlpInCHO) cells (Invitrogen), and selection of receptor-expressing cells was accomplished by treatment with 600 μg/mL hygromycin-B as previously reported [41]. Transfected and parental FlpInCHO cells were maintained in Dulbecco's modified Eagle's medium supplemented with 5% (v/v) FBS, 600 μg/mL hygromycin-B and incubated in a humidified environment at 37 °C in 5% CO_2. FlpInCHO cells stably expressing the GLP-1R were used at passages 18–32. FlpInCHO cell lines stably expressing GLP-1 receptor-Rluc8 and β-arrestin-1-Venus were used at passages 16–35. FlpInCHO cell lines stably expressing GLP-1 receptor-Rluc8 and β-arrestin-2-Venus were used at passages 15–33.

2.4. Radioligand binding assays

GLP-1R FlpInCHO were seeded at a density of 3×10^4 cells/well into 96-well culture plates and incubated overnight at 37 °C in 5% CO_2, and radioligand binding carried out as previously described using ^{125}I-GLP-1 as the radioligand [42]. Briefly, binding assays were performed on whole cells incubated overnight at 4 °C with 0.05 nM ^{125}I-GLP-1 tracer and increasing concentrations of unlabeled peptide. Cells were washed, solubilized in 0.1 M NaOH and radioactivity determined by γ-counting. Non-specific binding was defined by the amount of ^{125}I-GLP-1 binding in the presence of saturating concentrations of unlabeled GLP-1 (1 μM). For analysis, data were normalized to the specific binding for each individual experiment.

2.5. cAMP accumulation

GLP-1R expressing FlpInCHO cells were seeded at a density of 3×10^4 cells/well into 96-well culture plates and incubated overnight in DMEM containing 5% FBS at 37 °C in 5% CO_2. Growth media was replaced with stimulation buffer (phenol red-free DMEM containing 0.1% (w/v) BSA, 5 mM HEPES and 0.5 mM 3-isobutyl-1-methylxanthine) and incubated for 30 min at 37 °C

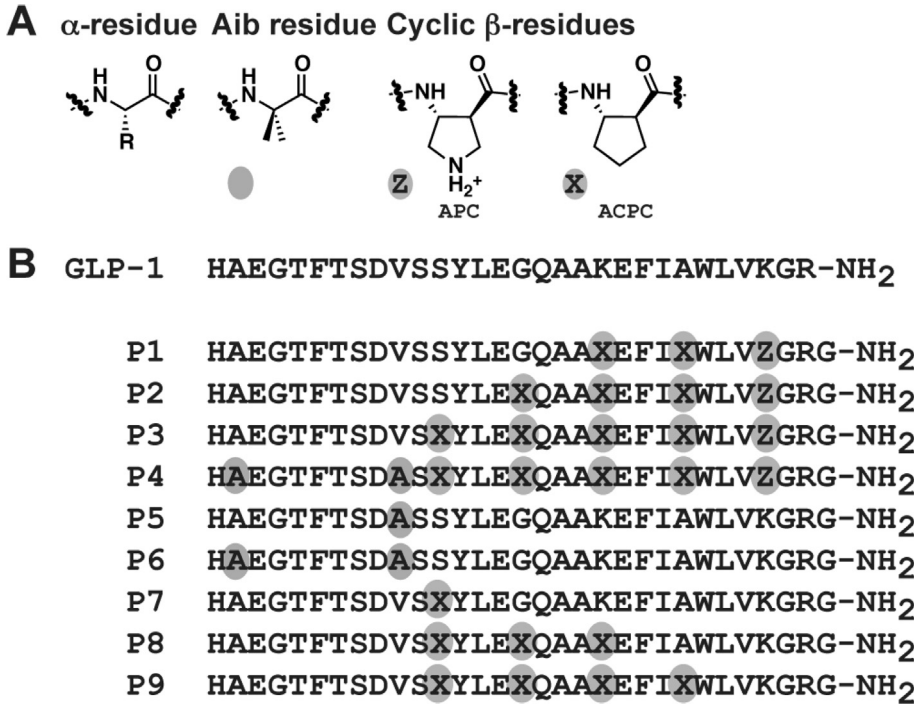

Fig. 1. A. Amino acids used in this study. Circles indicate non-natural substitutions: circles around the letter "A" represent α-residue Aib that protects peptides from degradation by DPPIV and neprilysin, and circles around the letters "X" and "Z" represent ring-constrained β-residues (X = ACPC, Z = APC). B. GLP-1(7–36)NH_2 and α/β-peptide analogues **1**–**9** (based on GLP-1(7–37)NH_2). Each peptide has a free N-terminus and a primary amide at the C-terminus.

in 5% CO_2. Cells were stimulated with increasing concentrations of peptide ligand and incubated for 30 min at 37 °C in 5% CO_2. The reaction was terminated by rapid removal of the ligand-containing buffer and addition of 50 μL of ice-cold 100% ethanol. After ethanol evaporation, 75 μL of lysis buffer (0.1% (w/v) BSA, 0.3% (v/v) Tween 20, and 5 mM HEPES, pH 7.4) was added, and 5 μL of lysate was transferred to a 384-well OptiPlate (PerkinElmer Life and Analytical Sciences).

The amount of cAMP present in each sample was determined using the Lance cAMP kit (PerkinElmer) with modifications to the manufacturers' instructions. Briefly, 5 μL of the antibody solution (100-fold dilution of Alexa Fluor 647-anti cAMP antibody solution in detection buffer) was transferred into each well containing lysates/cAMP standard in reduced lighting conditions and incubated for 30 min at room temp. 10 μl of detection mix (1:1:124 of solution 1 (2.5% v/v Eu-W8044 labeled streptavidin (Eu-SA)), solution 2 (8.75% v/v Biotin- cAMP) and detection buffer respectively) was added to each well in reduced lighting conditions, and the plate was incubated at room temperature for 1 h.

HTRF (Homogeneous Time Resolved Fluorescence) for each sample was detected using an EnVision™ plate reader with excitation at 320 nm and emission at 615 nm. cAMP was determined for all samples via conversion to concentration of cAMP using a cAMP standard curve that was detected in parallel. Data were normalized to the maximal response elicited by GLP-1, with 0% representing the concentration of cAMP in the presence of vehicle and 100% representing the concentration of cAMP in the presence of 100 nM GLP-1. 100 μM Forskolin was used as a positive control.

2.6. ERK1/2 phosphorylation

GLP-1R expressing FlpInCHO cells were seeded at a density of 3×10^4 cells/well in DMEM with 5% FBS into 96-well culture plates. The following day, the media were aspirated and the cells were washed twice with 100 μL PBS. 90 μL of serum free DMEM was then added and the cells were incubated overnight at 37 °C, 5% CO_2. Ligand-mediated pERK1/2 was determined using the AlphaScreen™ ERK1/2 SureFire™ protocol as previously described [43]. Prior to generation of concentration response curves, initial pERK1/2 timecourse experiments were performed over 1 h using high concentrations of peptide ligand (1 μM) to determine the time at which pERK1/2 was maximal after stimulation by agonists. Concentration response curves were then generated at this peak time point for each ligand. The kinetics of pERK1/2 response were similar for all ligands, peaking at 6 min. Data were normalized to the maximal response elicited by GLP-1, with 0% representing the RFU measured in the presence of vehicle and 100% representing the RFU measured in the presence of 100 nM GLP-1. 10% FBS, determined at 6 min was used as a positive control.

2.7. Intracellular calcium mobilization

GLP-1R expressing FlpInCHO cells stably were seeded in clear 96-well plates, at a density of 3×10^4 cells/well, in growth media and allowed to adhere overnight. On the day of assay, cells were washed twice with 100 μL modified Hanks buffered saline solution (HBSS containing; 150 mM NaCl, 2.6 mM KCl, 1.18 mM $MgCl_2$, 10 mM D-glucose, 10 mM HEPES, 2.2 mM $CaCl_2$, 2 mM probenecid, 0.5% (w/v) bovine serum albumin) and, in light diminished conditions, incubated for 1 h at 37 °C with the cell permeant Ca^{2+} fluorophore, Fluo-4AM (final concentration of 10 μM). After incubation, the assay plates were transferred to a Molecular Devices FlexStation (Molecular Devices, Palo Alto, CA, USA) and robotic addition of ligands was performed. Fluorescence was determined immediately after peptide addition, with an excitation wavelength set to 485 nm and an emission wavelength set to 525 nm, and readings were taken every 1.36 s for 120 s. Peak magnitude was calculated using five-point smoothing, followed by correction against basal fluorescence. The peak value was used to create concentration-response curves. Data were normalized to the maximal response elicited by GLP-1, with 0% representing the RFU measured in the presence of vehicle and 100% representing the

RFU measured in the presence of 100 nM GLP-1 100 μM ATP was used as a positive control.

2.8. β-Arrestin recruitment assays

FlpInCHO cell lines stably expressing GLP-1 receptor-Rluc8 and either β-arrestin-1- or β-arrestin-2-Venus were generated using gateway technology. These cell lines were characterized and described previously [44]. Cells were seeded in 96-well white culture plates at a density of 4×10^4 cells/well and cultured for 24 h in DMEM with 5% FBS. Cells were rinsed once with HBSS to remove traces of phenol red and incubated in fresh HBSS for further 15 min. The Rluc substrate coelenterazine-h was added to reach a final concentration of 5 μM. After a 10 min incubation, the corresponding agonist was added and bioluminescence resonance energy transfer (BRET) readings were collected using a LumiSTAR Omega instrument that allows sequential integration of signals detected in the 465–505 and 515–555 nm windows using filters with the appropriate band pass. The BRET signal was calculated by subtracting the ratio of 515–555 nm emission over 465–505 nm emission for a vehicle treated cell sample from the same ratio for the ligand treated cell sample. In this calculation, the vehicle treated cell sample represents background and results are expressed as ligand-induced BRET. This eliminates the requirement for measuring a donor only control sample. Initial time course experiments were performed over 20 min to determine the time at which β-arrestin-1 and β-arrestin-2 recruitment was maximal for each ligand. Subsequent concentration response data were collected at this peak time (2.5 min for all ligands). Data were normalized to the maximal response elicited by GLP-1, with 0% representing the RFU measured in the presence of vehicle and 100% representing the RFU measured in the presence of 100 nM GLP-1.

2.9. Data analysis

All data were analyzed using Prism 6 (GraphPad Software Inc., San Diego, CA, USA). For all analyses the data are unweighted and each y value (mean of replicates for each individual experiment) is considered an individual point. To calculate IC_{50}, EC_{50} and E_{max} values, concentration response signaling data were analyzed as previously described [41] using a three-parameter logistic equation.

Signaling bias was also quantified as previously described by analysis of concentration-response curves for functional data with nonlinear regression using an operational model of agonism modified to directly estimate the ratio of τ/K_A [24,25,41].

$$Y = \frac{E_{max} \times (\tau_c/K_A)^n \times [A]^n}{[A]^n \times (\tau_c/K_A)^n + (1 + [A]/K_A)^n} \quad (1)$$

where E_m represents the maximal stimulation of the system, K_A is the agonist-receptor dissociation constant, in molar concentration, $[A]$ is the molar concentration of ligand and τ is the operational measure of efficacy in the system, which incorporates signaling efficacy and receptor density. All estimated τ/K_A ratios included propagation of error for both τ and K_A. Changes in τ/K_A ratios with respect to GLP-1 for each novel peptide was used to quantitate bias between signaling pathways. Accordingly, bias factors included propagation of error from τ/K_A ratios of each pathway.

2.10. Statistics

Changes in peptide affinity, potency, efficacy or bias of each peptide in comparison to the GLP-1 control were statistically analyzed with a one-way analysis of variance and Dunnett's post test, and significance accepted at $p < 0.05$.

3. Results

3.1. GLP-1R agonist affinities

We assessed the affinities of GLP-1 and peptides **P1**–**P9** for the GLP-1R expressed in FlpIn CHO cells via competition with a radiolabeled antagonist, ^{125}I-exendin (9–39) (Table 1, Fig. 2A). The resulting IC_{50} values represent an averaged response arising from multiple receptor conformations that are present because individual GLP-1R molecules are presumably engaged by different intracellular partners; in this context the predominant signaling effector complex will have the most impact.

Incorporation of one (**P7**), three (**P1**, **P8**) or four (**P2**, **P9**) β amino acid residues, regardless of position, led to a ~10-fold reduction in affinity, relative to GLP-1, for the GLP-1R. Addition of a fifth β residue (**P3**, **P4**) further reduced affinity by 10-fold relative to other α/β-peptides in this set. α/β-Peptide **P4** contains two Aib substitutions, which seem to have little impact on affinity for the GLP-1R, because **P3** and **P4** are indistinguishable. This conclusion is supported by the observation that α-peptides **P5** and **P6**, which contain one or both of the Aib substitutions in **P4**, display only slightly reduced affinity for the GLP-1R relative to GLP-1.

3.2. Evaluation of cAMP production stimulated by P1–P9

We measured cAMP accumulation in response to **P1**–**P9** in FlpIn CHO cells stably expressing the human GLP-1R (Table 1, Fig. 2B). We observed a modest decline in potency arising from α → β replacement (**P1** → **P2**, **P3**), and a further decline upon Aib replacements (**P3** → **P4**). Peptides **P5**–**P7** were similar in potency to GLP-1, while **P8** and **P9** displayed substantially reduced potency relative to GLP-1. We previously assessed the activities of **P1**–**P9** in HEK293 cells transiently transfected with the human GLP-1R, using a kinetic GloSensor assay [24,45]. The cAMP potencies for **P1**–**P9** in the current study using an AlphaScreen assay are similar to those measured in HEK cells using the GloSensor assay [24]. The similarity between these two assays, involving different cell types, provides confidence that the trends are robust.

3.3. Evaluation of β-arrestin recruitment stimulated by P1–P9

We assessed β-arrestin-1 and β-arrestin-2 recruitment to the GLP-1R for **P1**–**P9** using β-arrestin-1 and β-arrestin-2 BRET assays in FlpInCHO cells stably expressing GLP-1R-Rluc8 and either β-arrestin-1 or β-arrestin-2-Venus (Table 1, Fig. 2C,D). Among α/β-peptides **P1**–**P4**, we observed substantial declines in the recruitment of β-arrestins-1 and -2 upon introduction of β residues, relative to GLP-1, with little or no β-arrestin recruitment by the maximally modified **P4**. α-Peptides **P5** and **P6** were similar to GLP-1 in terms of recruiting both β-arrestins-1 and -2 to the GLP-1R. α/β-Peptides **P7**, **P8** and **P9** exhibited substantial depressions in the maximum level of β-arrestin-1 and -2 recruited by the GLP-1R relative to GLP-1. The trends in β-arrestin recruitment are generally similar between the current set of assays and those reported previously [24], and the inter-assay differences in peptide behavior are likely due to differences in cellular background (the original BRET assays involved transfected HEK293FT cells, while the new BRET assay were conducted in transfected FlpIn CHO cells) and differential expression of regulatory proteins between the two experiments. The previous BRET assays were conducted with cells that had been co-transfected with GRK5, which enhances the affinity of β-arrestins for GLP-1R by promoting receptor

Table 1
Affinity and activity data for GLP-1 and α- and α/β-peptides **P1**–**P9** in GLP-1R binding, cAMP accumulation, Ca^{2+} mobilization, ERK1/2 phosphorylation, β-Arrestin-1 recruitment, and β-Arrestin-2 recruitment.

	Affinity	cAMP		β-Arrestin-1		β-Arrestin-2		iCa^{2+}		pERK1/2	
	*p*IC50 (M)	*p*EC_{50} (M)	E_{max}	*p*EC_{50} (M)	E_{max}	*p*EC_{50} (M)	E_{max}	*p*EC_{50} (M)	E_{max}	*p*EC_{50} (M)	E_{max}
GLP-1	8.1 ± 0.1	10.0 ± 0.1	100	7.4 ± 0.1	100	7.6 ± 0.1	100	7.5 ± 0.1	100	8.9 ± 0.1	100
P1	7.0* ± 0.1	8.8* ± 0.1	130* ± 6	6.9 ± 0.2	85 ± 7	6.9 ± 0.1	108 ± 5	7.2 ± 0.3	89 ± 8	8.3 ± 0.2	112 ± 8
P2	7.0* ± 0.1	8.2* ± 0.1	97 ± 6	6.0* ± 0.7	30* ± 20	5.9* ± 0.6	40* ± 20	6.4* ± 0.2	80 ± 10	7.9* ± 0.2	107 ± 9
P3	5.9* ± 0.1	8.3* ± 0.2	89 ± 6	6.8 ± 0.3	50* ± 7	6.4* ± 0.3	61* ± 9	5.3* ± 0.3	100 ± 30	8.1 ± 0.2	92 ± 8
P4	6.0* ± 0.1	7.6* ± 0.2	97 ± 7	N.D.	N.D.	N.D.	N.D.	5.2* ± 0.5	90 ± 40	8.3 ± 0.2	81 ± 8
P5	7.6* ± 0.1	10.0 ± 0.1	102 ± 5	8.0 ± 0.1	87 ± 4	7.1 ± 0.1	102 ± 4	7.3 ± 0.2	82 ± 6	9.2 ± 0.3	89 ± 6
P6	7.6* ± 0.1	9.9 ± 0.1	89 ± 5	7.9 ± 0.2	72 ± 4	7.4 ± 0.1	82 ± 5	7.4 ± 0.2	78 ± 5	8.9 ± 0.2	80 ± 7
P7	6.9* ± 0.1	9.6 ± 0.1	89 ± 5	7.4 ± 0.4	36* ± 6	7.0 ± 0.2	45* ± 4	7.0 ± 0.2	60 ± 5	8.9 ± 0.2	89 ± 7
P8	6.7* ± 0.1	8.5* ± 0.2	83 ± 5	7.3 ± 0.6	27* ± 9	N.D.	N.D.	5.7* ± 0.4	59* ± 7	8.2 ± 0.3	80 ± 8
P9	7.0* ± 0.1	7.7* ± 0.1	107 ± 5	6.9 ± 0.5	23* ± 6	N.D.	N.D.	N.D.	N.D.	8.0* ± 0.3	73 ± 9

All experiments were performed in FlpIn CHO cells stably expressing the human GLP-1R. Data are normalized to the maximum response elicited by GLP-1 in each assay, and analyzed using a three-parameter logistic equation. *p*EC50 values are the logarithm of the concentration of agonist that produces half the maximal response. E_{max} represents the maximal response normalized to that of GLP-1. Values are the mean ± S.E.M. of three to four individual experiments, conducted in duplicate. Maximum response values for incomplete curves are the predicted maximum derived from curve fitting. *Statistically significantly different from GLP-1 using a one way analysis of variance followed by Dunnett's test ($P < 0.05$).

phosphorylation [10,46]. In contrast, GRK5 was not employed in the current BRET assays; thus, coupling between the receptor and each β-arrestin should be weakened in the new assays relative to the original assays. A second difference is specific to the β-arrestin-2 recruitment assay. The original BRET assay employed a mutated β-arrestin-2 plasmid (R393E, R395E), which is expected to enhance the BRET signal by preventing clathrin binding and subsequent receptor internalization [10,46]. In contrast, native β-arrestin-2 was used for the current assay.

3.4. Intracellular calcium mobilization stimulated by P1–P9

To further explore how the different pathways activated by GLP-1 are affected by α → β replacements, we measured the abilities of **P1**–**P9** to promote intracellular calcium mobilization, which reports on $G\alpha_q$ and $G\alpha_s$ activation [9,47–49], in FlpIn CHO cells stably expressing the human GLP-1R (Table 1, Fig. 2E). Overall, α → β replacements led to a reduction in calcium mobilization. Incorporation of three β-amino acid residues (**P1**) into the C-terminal region of GLP-1 had the smallest impact on activity, with the decrease in activity becoming more pronounced for analogues containing additional α → β replacements extending toward the N-terminus of GLP-1 (**P2**–**P4**). Incorporation of a single β residue at position 18 (**7**) led to a slight decrease in activity; further α → β substitutions in the central region of GLP-1, to generate **P9**, essentially abolished calcium mobilization. Neither of the two Aib replacements (**P5** and **P6**) had a substantial effect on calcium mobilization in terms of potency or maximum response relative to GLP-1.

3.5. Stimulation of ERK1/2 phosphorylation stimulated by P1–P9

As a complement to characterizing the activity of analogues **1**–**9** in activating various pathways directly mediated by interaction between the GLP-1R and intracellular effector proteins (i.e. G proteins $G\alpha_s$ and $G\alpha_q$, β-arrestin-1 or β-arrestin-2), we assessed the activity of **P1**–**P9** in promoting ERK1/2 phosphorylation (Table 1, Fig. 2F). GLP-1-mediated ERK1/2 phosphorylation is dependent

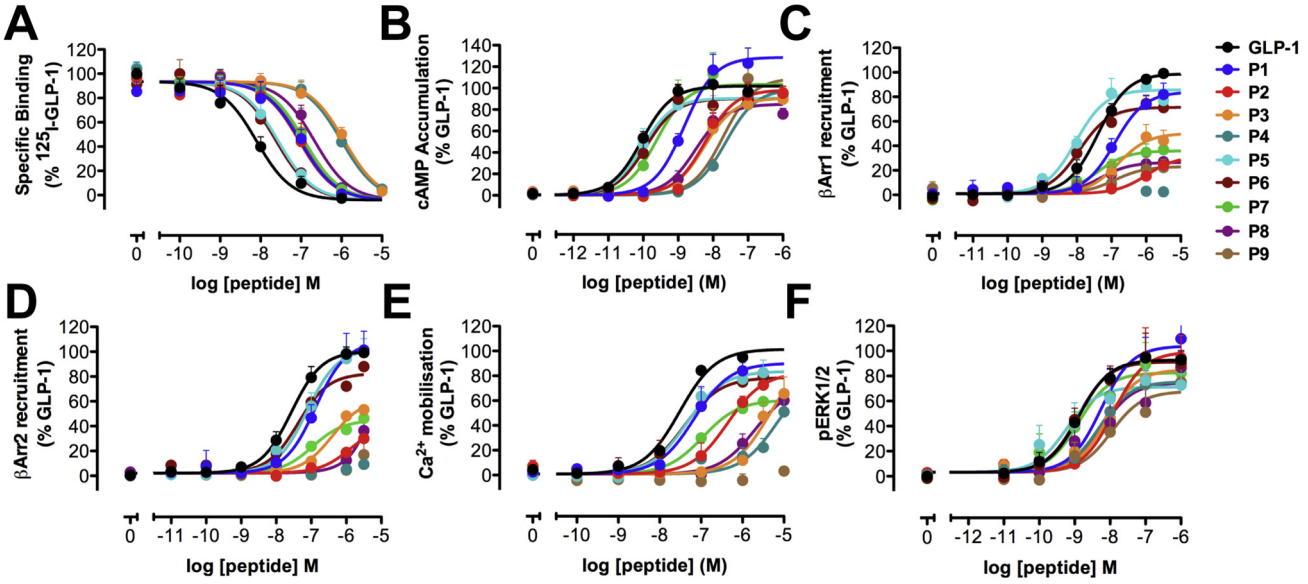

Fig. 2. Binding and signaling profiles of GLP-1 and α- and α/β-peptides **P1**–**P9** in FlpInCHO cells stably expressing the human GLP-1R. Concentration-response curves for (A) GLP-1R binding, (B) cAMP accumulation, (C) Ca^{2+} mobilization, (D) ERK1/2 phosphorylation, (E) β-Arrestin-1 recruitment, and (F) β-Arrestin-2 recruitment. Data are normalized to the maximum response elicited by GLP-1 in each assay, and analyzed using a three-parameter logistic equation. Values are the mean + S.E.M. of three to four individual experiments, conducted in duplicate.

Please cite this article in press as: M.V. Hager et al., Characterization of signal bias at the GLP-1 receptor induced by backbone modification of GLP-1, Biochem. Pharmacol. (2017), http://dx.doi.org/10.1016/j.bcp.2017.03.018

on both G protein and β-arrestin activity [9,11,12,49], which led us to explore how α → β replacement would affect signaling in this composite pathway, particularly for the β-arrestin-biased α/β-peptides **P3**, **P8** and **P9**. Our data indicate that ERK1/2 phosphorylation was less strongly affected by α → β replacements than was cAMP production, β-arrestin recruitment or calcium mobilization.

3.6. Stimulus bias induced by P1–P9

To determine whether peptides among **P1**–**P9** display signaling bias relative to GLP-1 in the expanded set of signaling pathways characterized, and to compare any bias between cAMP accumulation and β-arrestin recruitment in the CHO cell background to the β-arrestin bias we observed for α/β-peptides **P3**, **P8** and **P9** in the HEK293 cell, we analyzed the efficacy of each analogue in assays for cAMP accumulation, calcium mobilization, ERK1/2 phosphorylation, β-arrestin-1 recruitment or β-arrestin-2 recruitment using the operational model of agonism [50,51]. Transduction coefficients ($\log(\tau/K_A)$) for each analogue were extracted from concentration-response curves and compared with transduction coefficients for GLP-1 in each effector pathway. These comparisons allowed us to calculate a bias factor ($\Delta\log(\tau/K_A)$) for each peptide in terms of calcium mobilization, ERK1/2 phosphorylation, β-arrestin-1 recruitment or β-arrestin-2 recruitment relative to cAMP accumulation (Fig. 3, Table 2). We also determined bias factors for each peptide in terms of β-arrestin-1 recruitment or β-arrestin-2 recruitment relative to either calcium mobilization or ERK1/2 phosphorylation (Fig. 3, Table 2).

The bias factors summarized in Fig. 3 and Table 2 reveal that α/β-peptides **P3**, **P4**, **P7**, **P8** and **P9** manifest significant bias in at least one pathway. For example, peptides **P3**, **P7** and **P8** are weakly biased toward cAMP accumulation relative to calcium mobilization (Fig. 3A). Peptides **P3**, **P4** and **P9** are biased toward ERK1/2 phosphorylation relative to cAMP accumulation (Fig. 3B). Peptides **P3**, **P8** and **P9** are biased toward β-arrestin-1 recruitment relative to cAMP production (Fig. 3A). None among **P1**–**P9** displayed bias toward or away from β-arrestin-2 recruitment relative to cAMP accumulation (Fig. 3D); however, bias factors could not be calculated for **P4**, **P8** and **P9** due to weak β-arrestin-2 responses to these peptides (Fig. 2, Table 1). For this reason it was impossible to robustly compare β-arrestin-2 recruitment with other signaling pathways.

4. Discussion and conclusions

The characterization of **P1**–**P9** in the current study was performed in CHO cells, while our initial studies with these analogues were performed in HEK293 cells; thus, these two studies collectively allow one to assess the impact of cellular background on the manifestation of biased agonism [24]. Moreover, because the current studies evaluate bias for **P1**–**P9** in terms of a more diverse set of signaling and regulatory endpoints relative to the previous study, the data reported here allow a more complete understanding of the activity profiles of these GLP-1 analogues, and these data can be used to compare the bias profiles of **P1**–**P9** to the profiles of known agonists of the GLP-1R.

The bias factors for **P1**–**P9** in terms of β-arrestin recruitment relative to cAMP production, shown in Fig. 4 and Table 2, are consistent with those of our previous study [24], particularly for β-arrestin-1 with analogues that display strong bias, such as **P8** and **P9**, biased toward β-arrestin-1 recruitment over cAMP (either accumulation or production) in both sets of experiments and analogues with weaker bias having consistent trends (for example, **P3** is significantly biased in the CHO cell background, and trends towards bias in the HEK cells).

In our previous HEK293 studies, **P3**, **P8** and **P9** exhibited bias toward β-arrestin-2 recruitment over cAMP production [24], but in our CHO study β-arrestin-2 recruitment could not be detected for these α/β-peptides. The previous system was engineered to enhance β-arrestin-2 coupling through a combination of overexpression of GRK5 and mutation (R393E, R395E) of the arrestin that enhance the BRET signal by preventing clathrin binding and subsequent receptor internalization [10,46]. In the current assay, we examined recruitment of native β-arrestin-2, which was poorly recruited by lower-efficacy peptides. The lack of quantitative signal for these peptides makes interpretation of potential changes to signaling bias between the two cell types problematic. Overall, the pattern of bias changes in the enhanced β-arrestin-2 assay in HEK293 cells, along with the β-arrestin-1 profiles in both CHO and HEK cells, indicates fundamental differences in the properties of the **P3**, **P8** and **P9** α/β-peptides relative to GLP-1 itself. Comparing the bias profiles of **P1**–**P9** between CHO and HEK293 cells highlights that the utility of using recombinant systems lies in probing bias and in fingerprinting the activity profiles of different agonists, but not in making specific claims about the relevance of observed bias to physiological effects manifested in native cells and whole organisms.

Expanding the diversity of pharmacological parameters assessed in the current study, relative to the previous report, reveals that all of our α/β-peptides had significantly lower affinity compared to GLP-1 and more extensive bias was observed within **P1**–**P9** beyond bias toward β-arrestin recruitment over cAMP (Table 2, Fig. 3). Substitutions that only marginally altered ligand affinity (approx. 3-fold for **P5** and **P6**) did not display biased agonism, whereas α/β substituted peptides with >10-fold lower affinity than GLP-1 all had some observed bias. However, there was no correlation between the measured affinity and the biased agonism profile of these peptides.

Among **P3**, **P4**, **P7**, **P8** and **P9**, each α/β-peptide manifests significant bias in at least one pathway. **P3**, **P7** and **P8** are all weakly biased toward cAMP accumulation relative to calcium mobilization, though these analogues are only weakly active in both pathways. **P3, P4** and **P9** are biased toward ERK1/2 phosphorylation over cAMP accumulation; weak but statistically insignificant trends of this type are observed for other peptides, including **P2** and **P8**. Overall, backbone modification has only limited impact on ERK1/2 phosphorylation, leading to bias towards this pathway over those for which substantial changes in response are observed. The pathway that most closely parallels the trend in bias for ERK1/2 phosphorylation is β-arrestin-1 recruitment, toward which **P3**, **P8** and **P9** are biased over cAMP accumulation. The ERK1/2 phosphorylation signal in CHO cells is a composite of β-arrestin- and G protein- dependent signaling [9,11,12], and the correlation between ERK1/2 phosphorylation bias and β-arrestin-1 bias suggests that the arrestin pathway is predominant for **P3**, **P8** and **P9** for causing ERK1/2 phosphorylation. However, the proposed β-arrestin pathway dominance may not pertain to all α/β-peptides. Among the ERK1/2 phosphorylation-biased compounds, **P4** is the most strongly biased toward ERK1/2 phosphorylation over cAMP production, but **P4** caused no measurable signal in the β-arrestin-recruitment assays, despite the robust pERK1/2 response. Understanding the relative bias of **P4** for ERK1/2 phosphorylation versus β-arrestin recruitment will require more sensitive assays of β-arrestin recruitment.

Some among **P1**–**P9** display selective bias toward or away from either β-arrestin-1 recruitment or β-arrestin-2 recruitment when compared with various other pathways. **P6**, for example, is biased toward β-arrestin-1 recruitment over calcium mobilization, but does not favor β-arrestin-2 recruitment over calcium mobilization.

Please cite this article in press as: M.V. Hager et al., Characterization of signal bias at the GLP-1 receptor induced by backbone modification of GLP-1, Biochem. Pharmacol. (2017), http://dx.doi.org/10.1016/j.bcp.2017.03.018

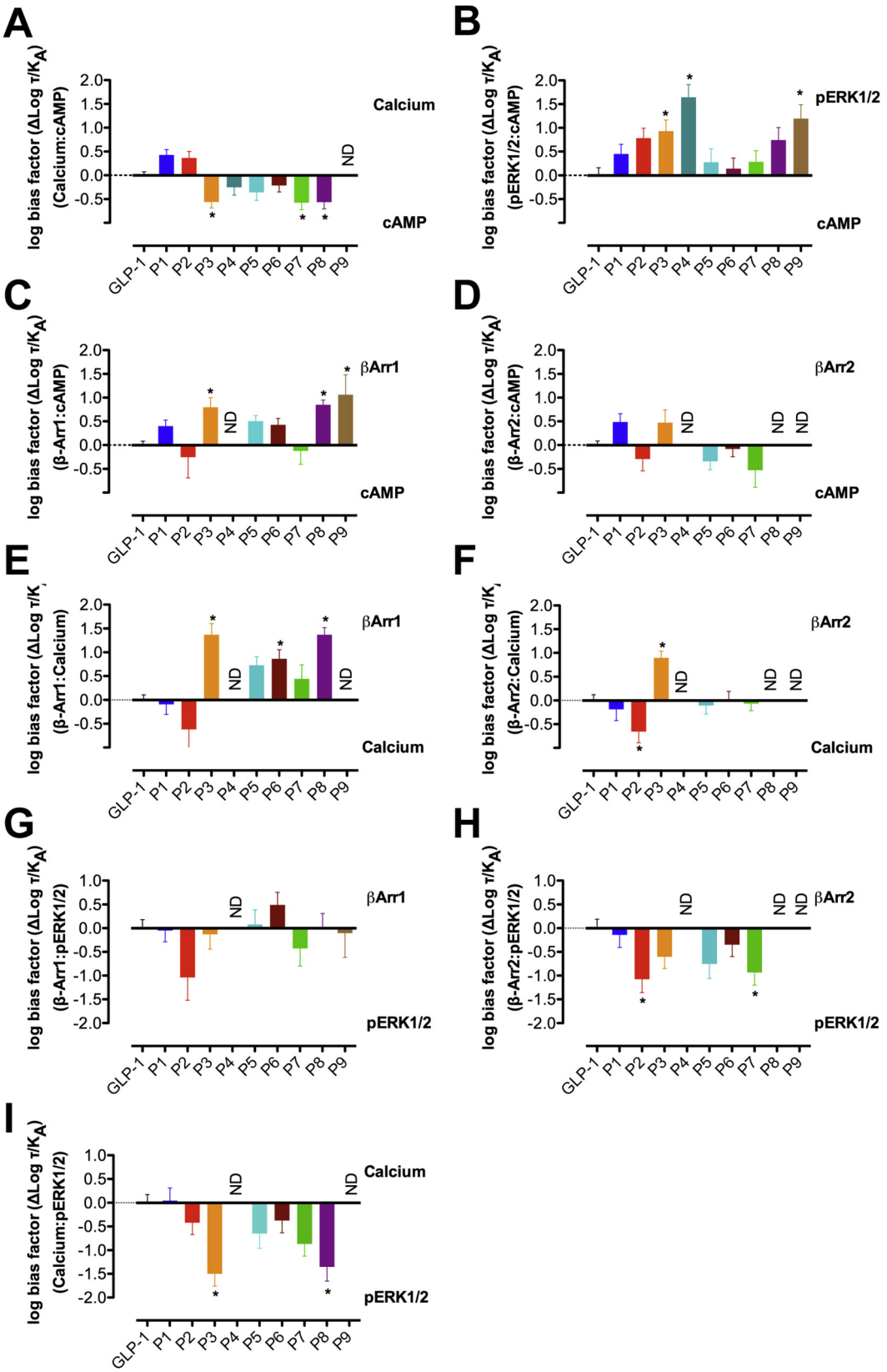

Fig. 3. Bias factors for α- and α/β-peptides **P1–P9** relative to GLP-1 in Ca^{2+} mobilization relative to cAMP accumulation (A), ERK1/2 phosphorylation relative to cAMP accumulation (B), β-Arrestin-1 recruitment relative to cAMP accumulation (C), β-Arrestin-2 recruitment relative to cAMP accumulation (D), β-Arrestin-1 recruitment relative to Ca^{2+} mobilization (E), β-Arrestin-2 recruitment relative to Ca^{2+} mobilization (F), β-Arrestin-1 recruitment relative to ERK1/2 phosphorylation (G), β-Arrestin-2 recruitment relative to ERK1/2 phosphorylation (H), and Ca^{2+} mobilization relative to ERK1/2 phosphorylation (I). Changes in log (τ/K_A) were calculated to provide a measure of the degree of stimulus bias exhibited between different signaling pathways relative to that of the reference agonist GLP-1. Values are the mean ± SEM of three to four individual experiments, conducted in duplicate. * statistically significantly different from GLP-1 using a one-way analysis of variance followed by Dunnett's test.

Please cite this article in press as: M.V. Hager et al., Characterization of signal bias at the GLP-1 receptor induced by backbone modification of GLP-1, Biochem. Pharmacol. (2017), http://dx.doi.org/10.1016/j.bcp.2017.03.018

Table 2
Stimulus bias exhibited by α- and α/β-peptides **P1**–**P9** relative to the reference agonist GLP-1.

	Δlog(τ/K_A)								
	Ca^{2+} vs cAMP	pERK1/2 vs cAMP	βArr1 vs cAMP	βArr2 vs cAMP	βArr1 vs Ca^{2+}	βArr2 vs Ca^{2+}	βArr1 vs pERK1/2	βArr2 vs pERK1/2	Ca^{2+} vs pERK1/2
GLP-1	0.0 ± 0.1	0.0 ± 0.2	0.0 ± 0.1	0.0 ± 0.1	0.0 ± 0.1	0.0 ± 0.1	0.0 ± 0.2	0.0 ± 0.2	0.0 ± 0.2
P1	0.4 ± 0.1	0.5 ± 0.2	0.4 ± 0.1	0.5 ± 0.2	−0.1 ± 0.2	−0.2 ± 0.2	0.0 ± 0.2	−0.1 ± 0.3	0.0 ± 0.2
P2	0.4 ± 0.1	0.8 ± 0.2	−0.3 ± 0.4	−0.3 ± 0.3	−0.7 ± 0.5	−0.7* ± 0.2	−1.0 ± 0.5	−1.0* ± 0.3	−0.4 ± 0.2
P3	−0.6* ± 0.1	0.9* ± 0.2	0.8* ± 0.2	0.5 ± 0.3	1.4* ± 0.2	0.9* ± 0.1	−0.1 ± 0.3	−0.6 ± 0.2	1.5* ± 0.3
P4	−0.2 ± 0.2	1.6* ± 0.3	N.D.	N.D.	N.D.	N.D.	N.D.	N.D.	N.D.
P5	−0.4 ± 0.2	0.3 ± 0.3	0.5 ± 0.1	−0.3 ± 0.2	0.7 ± 0.2	−0.1 ± 0.2	0.1 ± 0.3	−0.8 ± 0.3	−0.6 ± 0.3
P6	−0.1 ± 0.2	0.1 ± 0.2	0.4 ± 0.1	−0.1 ± 0.2	0.9* ± 0.2	0.0 ± 0.2	0.5 ± 0.3	−0.3 ± 0.2	−0.4 ± 0.3
P7	−0.6* ± 0.1	0.3 ± 0.2	−0.1 ± 0.3	−0.5 ± 0.4	0.4 ± 0.3	−0.1 ± 0.1	−0.4 ± 0.4	−0.9* ± 0.3	−0.9 ± 0.3
P8	−0.6* ± 0.1	0.7 ± 0.3	0.8* ± 0.1	N.D.	1.4* ± 0.1	N.D.	0.0 ± 0.3	N.D.	−1.3* ± 0.3
P9	N.D.	1.2* ± 0.3	1.1* ± 0.4	N.D.	N.D.	N.D.	−0.1 ± 0.5	N.D.	N.D.

Stimulus bias exhibited by **P1**–**P9** relative to GLP-1in Ca^{2+} mobilization relative to cAMP accumulation, ERK1/2 phosphorylation relative to cAMP accumulation, β-Arrestin-1 recruitment relative to cAMP accumulation, β-Arrestin-2 recruitment relative to cAMP accumulation, β-Arrestin-1 recruitment relative to Ca^{2+} mobilization, β-Arrestin-2 recruitment relative to Ca^{2+} mobilization, β-Arrestin-1 recruitment relative to ERK1/2 phosphorylation, β-Arrestin-2 recruitment relative to ERK1/2 phosphorylation, and Ca^{2+} mobilization relative to ERK1/2 phosphorylation. Changes in log (τ/K_A) were calculated to provide a measure of the degree of stimulus bias exhibited between different signaling pathways relative to that of the reference agonist GLP-1. Values are the mean ± SEM of three to four individual experiments, conducted in duplicate. *Statistically significantly different from GLP-1 using a one-way analysis of variance followed by Dunnett's test.

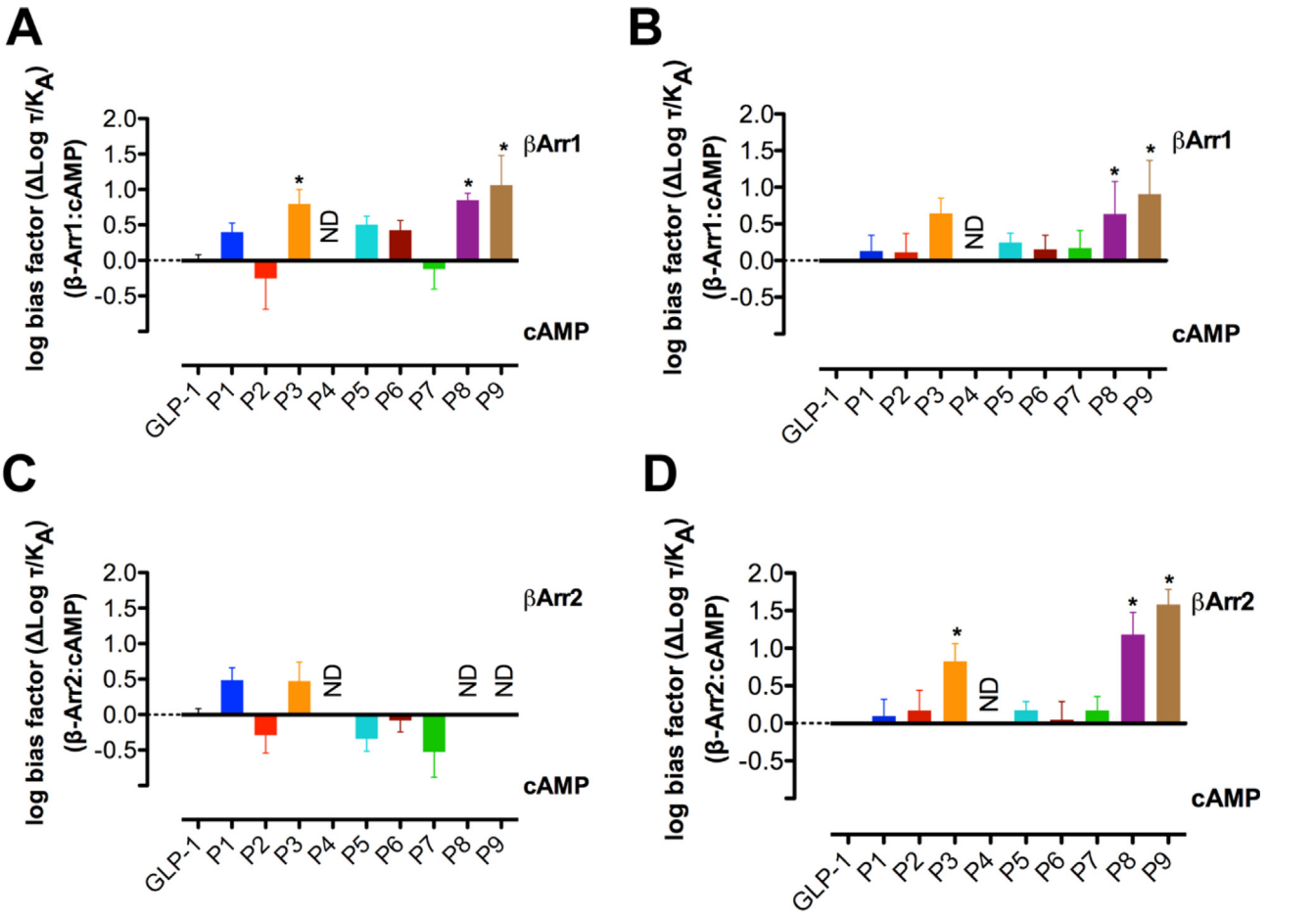

Fig. 4. Comparison of the bias factors for α- and α/β-peptides **P1**–**P9** relative to GLP-1 for β-Arrestin-1 recruitment versus cAMP accumulation between FlpInCHO cells (A) and HEK293 cells [24] (B) and for β-Arrestin-2 recruitment versus cAMP accumulation between FlpInCHO cells (C) and HEK293 cells [24] (D). Changes in log (τ/K_A) were calculated to provide a measure of the degree of stimulus bias exhibited between different signaling pathways relative to that of the reference agonist GLP-1. * statistically significantly different from GLP-1 using a one way analysis of variance followed by Dunnett's test ($P < 0.05$).

Moreover, **P7** favors ERK1/2 phosphorylation over β-arrestin-2 recruitment, while not favoring ERK1/2 phosphorylation over β-arrestin-1 recruitment or vice versa. Cases in which GLP-1 analogues selectively favor or disfavor either β-arrestin-1 or β-arrestin-2 recruitment suggest the intriguing possibility that these analogues could serve as starting points for more strongly biased GLP-1 agonists that could be used to parse the roles of β-arrestin-1 and β-arrestin-2 activity at the GLP-1R. However, this

Please cite this article in press as: M.V. Hager et al., Characterization of signal bias at the GLP-1 receptor induced by backbone modification of GLP-1, Biochem. Pharmacol. (2017), http://dx.doi.org/10.1016/j.bcp.2017.03.018

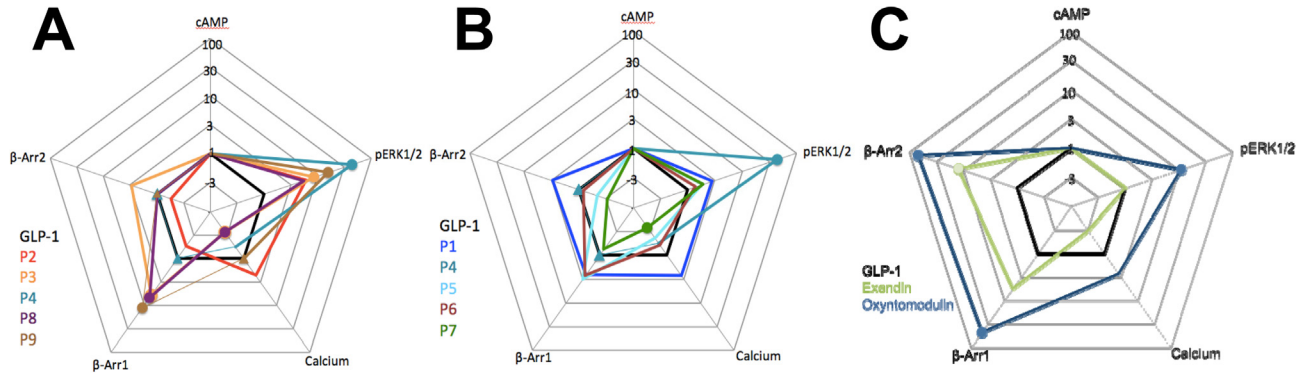

Fig. 5. Webs of bias for α- and α/β-peptides **P1**–**P9** (A, B) and known biased agonists exendin-4 and oxyntomodulin [9] (C) relative to GLP-1 in FlpInCHO cells stably expressing the human GLP-1R. Circles represent data that are significantly biased. Triangles represent data where no value could be defined. The τ/K_A ratio extracted from standard concentration-response data is used to calculate bias factors ($\Delta\Delta(\tau/K_A)$ through normalization of the transduction coefficient (τ/K_A) to a reference ligand (GLP-1) and reference pathway (cAMP accumulation).

possibility would need to be carefully assessed in physiological target cells, because the efficiency of recruitment of each β-arrestin is likely to be influenced by the complement of GRKs that are expressed.

One interesting outlier in the comparison of ERK1/2 phosphorylation and β-arrestin-1 and -2 recruitment for our α/β-peptides is **P2**, which is significantly biased toward ERK1/2 phosphorylation over β-arrestin-2 recruitment (in addition, **P2** trends towards bias of ERK1/2 phosphorylation over β-arrestin-1 recruitment). **P2** is also biased towards calcium mobilization over β-arrestin-2 recruitment (with a trend in this direction for β-arrestin-1), suggesting that the **P2** α/β-peptide may have a novel G protein bias profile.

Several well-studied peptides, including exendin-4 and oxyntomodulin, have been identified as biased agonists of the GLP-1R [9,20,21,25]. Both exendin-4 and oxyntomodulin bias the GLP-1R toward β-arrestin-1 recruitment and β-arrestin-2 recruitment over cAMP accumulation in experiments performed in FlpIn CHO cells [9,20,25]. Oxyntomodulin also biases the GLP-1R toward ERK1/2 phosphorylation over cAMP accumulation, but exendin-4 does not exhibit bias toward ERK1/2 phosphorylation [9,20,25]. The observation that exendin-4 and oxyntomodulin are both biased toward β-arrestin recruitment but only oxyntomodulin is also biased toward ERK1/2 phosphorylation may be explained by different degrees of contribution from β-arrestin-1 and β-arrestin-2 activity in mediating downstream ERK1/2 phosphorylation [9]. The distinct bias profiles for these two peptides indicate different modes of activation of the GLP-1R in response to either oxyntomodulin or exendin-4.

Because the bias factors calculated for **P1**–**P9** in this work are derived from experiments performed in the same FlpIn CHO cells that were used in the experiments to determine bias for exendin-4 and oxyntomodulin, the bias for **P1**–**P9** can be compared to that observed for exendin-4 and oxyntomodulin without concerns that either differences in cellular background or in assay format are the cause of distinct bias profiles between discrete agonists. Fig. 5 provides a graphical summary of bias effects that allows ready comparison of **P1**–**P9** (Fig. 5A, B) or exendin-4 [9] and oxyntomodulin [9] (Fig. 5C) with GLP-1 in terms of all five of the GLP-1R signaling outcomes we monitored. Each "web of bias" is constructed to convey bias relative to the cAMP production pathway. **P4** is illustrated in both Fig. 5A, which highlights ERK1/2 phosphorylation-biased ligands, and 5B as a reference for the α/β peptides.

Comparing the bias profiles for oxyntomodulin and exendin-4 to those for **P3**, **P4**, **P8** and **P9**, which each display significant bias toward either β-arrestin-1 or ERK1/2 phosphorylation or both over cAMP [9,24,25], we can categorize each GLP-1 analogue as being either "oxyntomodulin-like" or "exendin-4-like" in terms of its bias profile. (This categorization is imperfect, because both oxyntomodulin and exendin-4 are also biased toward β-arrestin-2 over cAMP [9,25], while no β-arrestin-2 bias factors could be calculated for any among **P3**, **P4**, **P8** or **P9**.) **P3** and **P9** are both biased toward β-arrestin-1 and ERK1/2 phosphorylation over cAMP, making them "oxyntomodulin-like" biased agonists of the GLP-1R. **P8** is biased toward β-arrestin-1 over cAMP but not toward ERK1/2 phosphorylation over cAMP, and is therefore an "exendin-4-like" biased agonist of the GLP-1R. The differences in bias profiles for **P8** compared to **P3** and **P9** indicate that these sets of analogues differ in how they activate the GLP-1R. **P4** is biased toward ERK1/2 phosphorylation over cAMP production, but no bias factor could be determined for **P4** in terms of β-arrestin-1 over cAMP; thus, the bias profile of **P4** is unique because it differs from the profile of either exendin-4 or oxyntomodulin.

We have previously shown that modifying the backbone of GLP-1 *via* incorporation of β-amino acid residues can generate agonists that engender significant bias toward β-arrestin-1 and/or β-arrestin-2 recruitment over cAMP production relative to GLP-1 itself [24]. Here, we expand the characterization of these biased peptides to include receptor-affinity measurements and additional signaling endpoint measurements. Our new data show that several among the α- and α/β-peptides we characterized are biased toward additional signaling outcomes beyond β-arrestin recruitment, thereby highlighting the importance of monitoring a diverse set of signaling and regulatory endpoints when characterizing novel agonists to identify biased agonists. These new results strengthen the conclusion that α → β residue replacement can alter receptor signaling relative to the parent α-peptide. Thus, α → β residue replacement may prove to be a general method by which receptor selectivity can be engineered into a peptide agonist that activates its cognate receptor to initiate different signaling pathways. The α/β-peptides characterized in this work may have utility as tools to probe the roles of β-arrestin recruitment and ERK1/2 phosphorylation in GLP-1R signaling. Moreover, these α/β-peptides could provide a platform to develop pathway-selective therapeutic agents targeting the GLP-1R.

Conflict of interest statement

The authors declare the following competing financial interest (s): S.H.G. is an inventor on a patent application covering GLP-1 analogues described here; S.H.G. is a cofounder of Longevity Biotech, Inc., which is pursuing biomedical applications of α/β-peptides.

Please cite this article in press as: M.V. Hager et al., Characterization of signal bias at the GLP-1 receptor induced by backbone modification of GLP-1, Biochem. Pharmacol. (2017), http://dx.doi.org/10.1016/j.bcp.2017.03.018

Acknowledgements

This work was supported by the National Institute of General Medical Sciences (NIGMS) (GM056414, to S.H.G.) and the National Health and Medical Research Council of Australia (NHMRC) (project grants [1061044] and [1065410], and NHMRC program grant [1055134] to P.M.S. and D.W.); P.M.S. is a NHMRC Principal Research Fellow. D.W. is a NHMRC Career Development Fellow. M.V.H. was supported in part by a Chemical Biology Interface Training Grant from NIGMS (T32 GM008505). Support for this research was provided by the University of Wisconsin–Madison, Office of the Vice Chancellor for Research and Graduate Education with funding from the Wisconsin Alumni Research Foundation.

References

[1] F. Zaccardi, D.R. Webb, T. Yates, M.J. Davies, Pathophysiology of type 1 and type 2 diabetes mellitus: a 90-year perspective, Postgrad. Med. J. 92 (2016) 63–69.
[2] R.A. DeFronzo, Pathogensis of Type 2 (non-insulin dependent) diabetes mellitus: a balanced overview, Diabetologia 35 (1992) 389–397.
[3] R.S. Hundal, S.E. Inzucchi, Metformin: new understandings, new uses, Drugs 63 (2003) 1879–1894.
[4] S.G. Swinnen, J.B. Hoekstra, J.H. DeVries, Insulin therapy for type 2 diabetes, Diabetes Care 32 (Suppl. 2) (2009) S253–259.
[5] J.J. Holst, F.K. Knop, T. Vilsboll, T. Krarup, S. Madsbad, Loss of incretin effect is a specific, important, and early characteristic of type 2 diabetes, Diabetes Care 34 (Suppl 2) (2011) S251–257.
[6] L.L. Baggio, D.J. Drucker, (2007) Biology of incretins: GLP-1 and GIP, Gastroenterology 132 (2007) 2131–2157.
[7] C. Montrose-Rafizadeh, P. Avdonin, M.J. Garant, B.D. Rodgers, S. Kole, H. Yang, et al., Pancreatic glucagon-like peptide-1 receptor couples to multiple G proteins and activates mitogen-activated protein kinase pathways in chinese hamster ovary cells, Endocrinology 140 (1999) 132–1140.
[8] M. Hallbrink, T. Homqvist, M. Olsson, C.-G. Ostenson, S. Efendic, U. Langel, Different domains in the third intracellular loop of the GLP-1 receptor are responsible for Gas and Gai/Gao activation, Bichim. Biophys. Acta 1546 (2001) 79–86.
[9] D. Wootten, C.A. Reynolds, K.J. Smith, J.C. Mobarec, C. Koole, E.E. Savage, et al., The extracellular surface of the GLP-1 receptor is a molecular trigger for biased agonism, Cell 165 (2016) 1632–1643.
[10] R. Jorgensen, V. Kubale, M. Vrecl, T.W. Schwartz, C.E. Elling, Oxyntomodulin differentially affects glucagon-like peptide-1 receptor beta-arrestin recruitment and signaling through Galpha(s), J. Pharmaocl. Exp. Ther. 322 (2007) 148–154.
[11] N. Sonoda, T. Imamura, T. Yoshizaki, J.L. Babendure, J.C. Lu, J.M. Olefsky, Beta-Arrestin-1 mediates glucagon-like peptide-1 signaling to insulin secretion in cultured pancreatic beta cells, Proc. Natl. Acad. Sci. U.S.A. 105 (2008) 6614–6619.
[12] J. Quoyer, C. Longuet, C. Broca, N. Linck, S. Costes, E. Varin, et al., GLP-1 mediates antiapoptotic effect by phosphorylating Bad through a beta-arrestin 1-mediated ERK1/2 activation in pancreatic beta-cells, J. Biol. Chem. 285 (2010) 1989–2002.
[13] S. Rajagopal, K. Rajagopal, R.J. Lefkowitz, Teaching old receptors new tricks: biasing seven-transmembrane receptors, Nat. Rev. Drug Discov. 9 (2010) 373–386.
[14] E. Reiter, S. Ahn, A.K. Shukla, R.J. Lefkowitz, Molecular mechanism of beta-arrestin-biased agonism at seven-transmembrane receptors, Annu. Rev. Pharmacol. Toxicol. 52 (2002) 179–197.
[15] T. Kenakin, A. Christopoulos, Signalling bias in new drug discovery: detection, quantification and therapeutic impact, Nat. Rev. Drug Discov. 12 (2013) 205–216.
[16] B.K. Kobilka, X. Deupi, Conformational complexity of G-protein-coupled receptors, Trends Pharmacol. Sci. 28 (2007) 397–406.
[17] T. Kenakin, Ligand-selective receptor conformations revisited: the promise and the problem, Trends Pharmacol. Sci. 24 (2003) 346–354.
[18] E.J. Whalen, S. Rajagopal, R.J. Lefkowitz, Therapeutic potential of beta-arrestin- and G protein-biased agonists, Trends Mol. Med. 17 (2011) 126–139.
[19] K.M. Appleton, L.M. Luttrell, Emergent biological properties of arrestin pathway-selective biased agonism, J. Recept. Signal Transduct. Res. 33 (2013) 153–161.
[20] C. Koole, D. Wootten, J. Simms, C. Valant, R. Sridhar, O.L. Woodman, et al., Allosteric ligands of the glucagon-like peptide 1 receptor (GLP-1R) differentially modulate endogenous and exogenous peptide responses in a pathway-selective manner: implications for drug screening, Mol. Pharmacol. 78 (2010) 456–465.
[21] D. Wootten, E.E. Savage, F.S. Willard, A.B. Bueno, K.W. Sloop, A. Christopoulos, et al., Differential activation and modulation of the glucagon-like peptide-1 receptor by small molecule ligands, Mol. Pharmacol. 83 (2013) 822–834.
[22] J. Broichhagen, T. Podewin, H. Meyer-Berg, Y. von Ohlen, N.R. Johnston, B.J. Jones, et al., Optical control of insulin secretion using an incretin switch, Angew. Chem. Int. Ed. Engl. 54 (2015) 15565–15569.
[23] H. Zhang, E. Sturchler, J. Zhu, A. Nieto, P.A. Cistrone, J. Xie, et al., Autocrine selection of a GLP-1R G-protein biased agonist with potent antidiabetic effects, Nat. Commun. 6 (2015) 8918.
[24] M.V. Hager, L.M. Johnson, D. Wootten, P.M. Sexton, S.H. Gellman, Beta-arrestin-biased agonists of the GLP-1 receptor from beta-amino acid residue incorporation into GLP-1 analogues, J. Am. Chem. Soc. 138 (2016) 14970–14979.
[25] D. Wootten, J. Simms, L.J. Miller, A. Christopoulos, P.M. Sexton, Polar transmembrane interactions drive formation of ligand-specific and signal pathway-biased family B G protein-coupled receptor conformations, Proc. Natl. Acad. Sci. U.S.A. 110 (2013) 5211–5216.
[26] L.M. Johnson, S. Barrick, M.V. Hager, A. McFedries, E.A. Homan, M.E. Rabaglia, et al., A potent alpha/beta-peptide analogue of GLP-1 with prolonged action in vivo, J. Am. Chem. Soc. 136 (2014) 12848–12851.
[27] E.V. Denton, C.J. Craig, R.L. Pongratz, J.S. Appelbaum, A.E. Doerner, A. Narayanan, et al., A beta-peptide agonist of the GLP-1 receptor, a class B GPCR, Org. Lett. 15 (2013) 5318–5321.
[28] X. Bai, Y. Niu, J. Zhu, A.Q. Yang, Y.F. Wu, X.S. Ye, A new GLP-1 analogue with prolonged glucose-lowering activity in vivo via backbone-based modification at the N-terminus, Bioorg. Med. Chem. 24 (2016) 1163–1170.
[29] E. Peggion, S. Mammi, E. Schievano, L. Silvestri, L. Schiebler, A. Bisello, et al., Structure-function studies of analogues of parathyroid hormone (PTH)-1-34 containing beta-amino acid residues in positions 11–13, Biochemistry 41 (2002) 8162–8175.
[30] E. Schievano, S. Mammi, E. Carretta, N. Fiori, M. Corich, A. Bisello, et al., Conformational and biological characterization of human parathyroid hormone hPTH(1–34) analogues containing beta-amino acid residues in positions 17–19, Biopolymers 70 (2003) 534–547.
[31] R.W. Cheloha, A. Maeda, T. Dean, T.J. Gardella, S.H. Gellman, Backbone modification of a polypeptide drug alters duration of action in vivo, Nat. Biotechnol. 32 (2014) 653–655.
[32] K.E. Olson, L.M. Kosloski-Bilek, K.M. Anderson, B.J. Diggs, B.E. Clark, J.M. Gledhill Jr, et al., Selective VIP receptor agonists facilitate immune transformation for dopaminergic neuroprotection in MPTP-intoxicated mice, J. Neurosci. 35 (2015) 16463–16478.
[33] R.W. Cheloha, T. Watanabe, T. Dean, S.H. Gellman, T.J. Gardella, Backbone modification of a parathyroid hormone receptor-1 antagonist/inverse agonist, ACS Chem. Biol. 11 (2016) 2752–2762.
[36] W.S. Horne, M.D. Boersma, M.A. Windsor, S.H. Gellman, Sequence-based design of alpha/beta-peptide foldamers that mimic BH3 domains, Angew. Chem. Intl. Ed. Engl. 47 (2008) 2853–2856.
[37] D.S. Steer, R.A. Lew, P. Perlmutter, A.I. Smith, M.-I. Aguilar, Beta-amino acids: versatile peptidomimetics, Curr. Med. Chem. 9 (2002) 811–822.
[41] C. Koole, D. Wootten, J. Simms, L.J. Miller, A. Christopoulos, P.M. Sexton, Second extracellular loop of human glucagon-like peptide-1 receptor (GLP-1R) has a critical role in GLP-1 peptide binding and receptor activation, J. Biol. Chem. 287 (2012) 3642–3658.
[42] C. Koole, D. Wootten, J. Simms, C. Valant, L.J. Miller, A. Christopoulos, et al., Polymorphism and ligand dependent changes in human glucagon-like peptide-1 receptor (GLP-1R) function: allosteric rescue of loss of function mutation, Mol. Pharmacol. 80 (2011) 486–497.
[43] L.T. May, V.A. Avlani, C.J. Langmead, H.J. Herdon, M.D. Wood, P.M. Sexton, et al., Structure-function studies of allosteric agonism at M2 muscarinic acetylcholine receptors, Mol. Pharmacol. 72 (2007) 463–476.
[44] E.E. Savage, D. Wootten, A. Christopoulos, P.M. Sexton, S.G. Furness, A simple method to generate stable cell lines for the analysis of transient protein-protein interactions, Biotechniques 54 (2013) 217–221.
[45] B.F. Binkowski, B.L. Butler, P.F. Stecha, C.T. Eggers, P. Otto, K. Zimmerman, et al., A luminescent biosensor with increased dynamic range for intracellular cAMP, ACS Chem. Biol. 6 (2011) 1193–1197.
[46] R. Jorgensen, L. Martini, T.W. Schwartz, C.E. Elling, Characterization of glucagon-like peptide-1 receptor beta-arrestin 2 interaction: a high-affinity receptor phenotype, Mol. Endocrinol. 19 (2005) 812–823.
[47] M.B. Wheeler, M. Lu, J.S. Dillon, X.-H. Leng, C. Chen, A.E. Boyd, Functional expression of the rat glucagon-like peptide-1 receptor, and evidence for coupling to both adenylyl cyclase, and phospholipase-C, Endocrinology 133 (1993) 57–62.
[48] G.G. Holz, Epac: a new cAMP-binding protein in support of glucagon-like peptide-1 receptor-mediated signal transduction in the pancreatic beta-cell, Diabetes 53 (2004) 5–13.
[49] A. Thompson, V. Kanamarlapudi, Agonist-induced internalisation of the glucagon-like peptide-1 receptor is mediated by the Galphaq pathway, Biochem. Pharmacol. 93 (2015) 72–84.
[50] J.W. Black, P. Leff, Operational models of pharmacological agonism, Proc. R. Soc. Lond. B Biol. Sci. 220 (1983) 141–162.
[51] T. Kenakin, C. Watson, V. Muniz-Medina, A. Christopoulos, S. Novick, A simple method for quantifying functional selectivity and agonist bias, ACS Chem. Neurosci. 3 (2012) 193–203.

Please cite this article in press as: M.V. Hager et al., Characterization of signal bias at the GLP-1 receptor induced by backbone modification of GLP-1, Biochem. Pharmacol. (2017), http://dx.doi.org/10.1016/j.bcp.2017.03.018

Appendix II:
Phase-plate cryo-EM structure of a biased agonist bound human GLP-1 receptor-Gs complex

LETTER

doi:10.1038/nature25773

Phase-plate cryo-EM structure of a biased agonist-bound human GLP-1 receptor–Gs complex

Yi-Lynn Liang[1]*, Maryam Khoshouei[2]*, Alisa Glukhova[1]*, Sebastian G. B. Furness[1], Peishen Zhao[1], Lachlan Clydesdale[1], Cassandra Koole[1], Tin T. Truong[1], David M. Thal[1], Saifei Lei[3,4], Mazdak Radjainia[1,5], Radostin Danev[2], Wolfgang Baumeister[2], Ming-Wei Wang[3,4,6], Laurence J. Miller[1,7], Arthur Christopoulos[1], Patrick M. Sexton[1,6] & Denise Wootten[1]

The class B glucagon-like peptide-1 (GLP-1) G protein-coupled receptor is a major target for the treatment of type 2 diabetes and obesity[1]. Endogenous and mimetic GLP-1 peptides exhibit biased agonism—a difference in functional selectivity—that may provide improved therapeutic outcomes[1]. Here we describe the structure of the human GLP-1 receptor in complex with the G protein-biased peptide exendin-P5 and a $G\alpha_s$ heterotrimer, determined at a global resolution of 3.3 Å. At the extracellular surface, the organization of extracellular loop 3 and proximal transmembrane segments differs between our exendin-P5-bound structure and previous GLP-1-bound GLP-1 receptor structure[2]. At the intracellular face, there was a six-degree difference in the angle of the Gαs–α5 helix engagement between structures, which was propagated across the G protein heterotrimer. In addition, the structures differed in the rate and extent of conformational reorganization of the $G\alpha_s$ protein. Our structure provides insights into the molecular basis of biased agonism.

The GLP-1R, a class B G protein-coupled receptor (GPCR), is a key incretin hormone receptor and an important target for the development of therapies for the treatment of type 2 diabetes and obesity[1]. Biased agonism is commonly observed at the GLP-1R[3–5], and exendin-P5 (ExP5) has been identified as a potent G protein-biased selective agonist of GLP-1R, with diminished coupling to β-arrestins[6] and a unique *in vivo* profile in animal models of diabetes[6]. The prevalence of GLP-1R biased agonism and its therapeutic implications make understanding of the phenomenon at molecular and structural levels crucial for the rational design of novel ligands.

Like all class B GPCRs, the GLP-1R contains a large extracellular N-terminal domain (NTD) and a seven-transmembrane helix bundle, with peptide binding spanning both domains; the NTD interaction positions the peptide N terminus within the receptor core to facilitate receptor activation[7]. Clinically used therapeutic agents, including exendin-4, contain an N-terminal sequence that is relatively conserved with that of the native peptide, GLP-1[8]. Notably, ExP5 shares a common C terminus with exendin-4, but possesses a unique N-terminal domain (Extended Data Fig. 1a) that interacts with the GLP-1R transmembrane core to promote receptor activation.

Cryo-electron microscopy (cryo-EM) has enabled researchers to determine the structures of GPCR complexes without the need to extensively modify the receptor[2,9]. A 4.1 Å full-length active structure of a wild-type rabbit GLP-1R was solved in complex with GLP-1 and heterotrimeric G_s protein[2]. In addition, the full-length active structure of the calcitonin receptor (CTR) was solved to a similar global resolution in complex with a peptide agonist and G_s protein[9] using phase contrast cryo-EM[10–12]. Here, we used Volta phase plate cryo-EM to determine the structure of an active state, human GLP-1R bound to ExP5 in complex with a heterotrimeric G_s protein. The structure provides insights into the binding of ExP5 to the GLP-1R, with implications for receptor activation, G protein coupling and signalling for class B GPCRs.

To form an active, G protein-coupled complex, the GLP-1R was co-expressed with $G\alpha_s$, His-Gβ1, and Gγ2 in *Trichoplusia ni* (Tni) insect cells and stimulated with an excess of ExP5 in the presence of apyrase and the nanobody Nb35, which bridges the G protein α- and βγ-subunits. A dominant-negative $G\alpha_s$ was used to enable the formation of a complex with improved stability. We characterized and purified the complex as described for the CTR[9] (Extended Data Figs 1b, 2a).

Following imaging and initial 2D classification (Extended Data Fig. 2b, c), 3D classification revealed that the majority of the complex had stable features. The exception was the $G\alpha_s$ α-helical domain, the density of which was averaged out at higher resolution because it had substantial flexibility despite occupying a single predominant orientation (Fig. 1a). We used 184,672 particle projections to obtain a cryo-EM density map with nominal global resolution of 3.3 Å (Fig. 1a; Extended Data Fig. 2b).

An atomic resolution structure of the ExP5–GLP-1R–$G\alpha_s$ heterotrimeric G protein complex was built into the map and refined to reveal global features similar to those observed in other class B GPCR structures[2,9,13–15]. Side chains of the majority of amino acid residues are clearly identifiable in the peptide, all of the transmembrane helices and the subunits of the G protein (Extended Data Fig. 3). Although linker region density between the NTD and the transmembrane core was visible in the cryo-EM map, it was less well-resolved than other receptor domains, suggesting substantial flexibility in the ExP5 bound state. Continuous density was observed for helix 8 (H8) and all intracellular and extracellular loops (ICLs and ECLs, respectively), with the exception of ICL3, which was not modelled. In addition, the cryo-EM map was poor for a region of four ECL3 residues (372–375) and therefore only the protein backbone was modelled in this region.

Within the NTD there was discontinuous density in the backbone for some regions. As such, the NTD structure bound to exendin(9–39)[16] was used to perform a rigid body fit into the density. N-terminal residues 24–30 and residues beyond E423 at the receptor C terminus were not resolved. The G protein was well resolved, allowing modelling of all G protein components (with the exception of the Gαs α-helical domain).

The extracellular NTD conformation differs between the three agonist-bound $G\alpha_s$ heterotrimer class B GPCR structures (Extended Data Fig. 4a–c). Whereas multiple NTD conformations were evident for the CTR[9], a single predominant conformation was stabilized in both GLP-1R structures[2]. However, there were subtle differences in the relative positioning of the N terminus relative to the transmembrane

[1]Drug Discovery Biology and Department of Pharmacology, Monash Institute of Pharmaceutical Sciences, Monash University, Parkville 3052, Victoria, Australia. [2]Department of Molecular Structural Biology, Max Planck Institute of Biochemistry, 82152 Martinsried, Germany. [3]University of Chinese Academy of Sciences, 19A Yuquan Road, Beijing 100049, China. [4]The National Center for Drug Screening and CAS Key Laboratory of Receptor Research, Shanghai Institute of Materia Medica, Chinese Academy of Sciences, Shanghai 201203, China. [5]FEI, 5651 GG Eindhoven, The Netherlands. [6]School of Pharmacy, Fudan University, Shanghai 201203, China. [7]Department of Molecular Pharmacology and Experimental Therapeutics, Mayo Clinic, Scottsdale, Arizona 85259, USA.
*These authors contributed equally to this work.

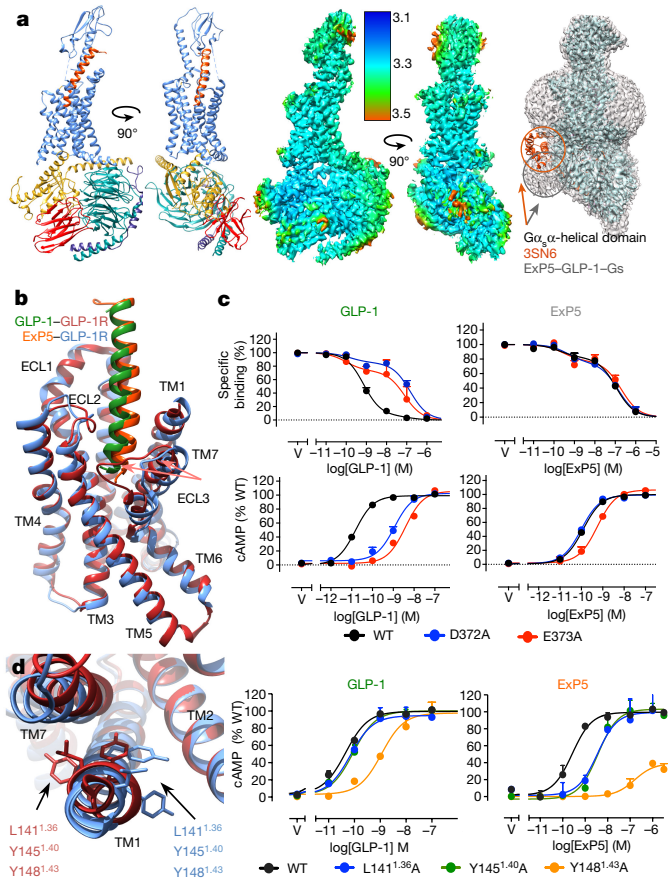

Figure 1 | The ExP5–GLP-1R–Gs cryo-EM structure reveals molecular details linked to GLP-1R biased agonism. a, Left, ExP5–GLP-1R–Gs structure after refinement in the cryo-EM map. Middle, cryo-EM density map coloured by local resolution (Å). Right, low-resolution cryo-EM map highlighting the predominant $G\alpha_s$ α-helical domain location in ExP5–GLP-1R–Gs (grey), compared to β2-AR–Gs (PDB:3SN6, orange). **b**, Transmembrane domain and peptide superimposition reveal backbone differences in ECL3, TM6, TM7 and TM1 when bound by GLP-1 relative to ExP5. ExP5 is located closer to TM1 than GLP-1. **c**, D372 and E373 in ECL3 are important for the pharmacology of GLP-1 and have a limited role in ExP5 affinity and signalling. WT, wild type; V, vehicle. **d**, Left, overlay of the GLP-1–GLP-1R deposited structure[2] (GLP-1R in red) and ExP5–GLP-1R (GLP-1R in blue) reveals a rotation in TM1 side chains. Right, $L141^{1.36}$, $Y145^{1.40}$ and $Y148^{1.43}$ mutations have a larger effect on ExP5-mediated than on GLP-1-mediated cAMP signalling. Whole-cell binding assays and cAMP signalling were assessed in CHOFlpIn cells and data are means + s.e.m. of four (for TM1) and six (for ECL3) independent experiments, performed in duplicate.

bundle that contribute to the positioning of the N termini of GLP-1 and ExP5 (Extended Data Fig. 4b). Notably, the 11-mer agonist-bound GLP-1R structure solved without the $G\alpha_s$ heterotrimer[15] displayed a unique NTD conformation relative to GLP-1 and ExP5 (Extended Data Fig. 4c). Collectively, these structures suggest that the binding of different peptide agonists alters the juxtaposition of the extracellular NTD and transmembrane bundle to regulate the ability of different peptides to activate class B GPCRs.

Compared to inactive class B GPCR transmembrane bundles, the GLP-1R in our structure undergoes similar macroscopic conformational transitions to those previously reported for the GLP-1-bound GLP-1R[2] and calcitonin-bound CTR[9] (Extended Data Fig. 4d–h). These include considerable movements in the extracellular ends of transmembrane (TM) helices 1, 6 and 7, required to open the bundle to accommodate peptide binding, and a large 15–16 Å movement of TM6 away from the central transmembrane domain axis that opens up the cytoplasmic face to accommodate G protein interaction (Extended Data Fig. 4d, f). These large conformational movements are coordinated around the highly conserved class B GPCR $P^{6.47}XXG^{6.50}$ motif in TM6, and $G^{7.50}$ in TM7 (Extended Data Fig. 4d). Nonetheless, there are notable differences in the extracellular face between the activated structures, particularly in the extent of movement of TM6, ECL3 and TM7, which probably reflect the distinct modes with which these ligands activate their respective receptors (Extended Data Fig. 4g, h).

ExP5 is a biased agonist relative to exendin-4[6]. Our pharmacological analysis revealed that ExP5 is also G protein-biased, with limited β-arrestin recruitment relative to GLP-1 (Extended Data Fig. 1d). Comparison of receptor occupancy with ligand potency and efficacy in cellular signalling assays showed that the bias of ExP5 arises primarily from enhanced efficacy in $G\alpha_s$-mediated cAMP signalling, rather than a loss of β-arrestin coupling (Extended Data Fig. 1e). Ligand binding and GTPγS studies performed in insect cells also support enhanced G protein efficacy of ExP5 relative to GLP-1 (Extended Data Fig. 1c). Thus, comparison of the GLP-1 and ExP5-bound GLP-1R–$G\alpha s\beta\gamma$ structures provides insight into conformational differences that may be linked to biased agonism.

The largest distinctions between the GLP-1 and ExP5-bound GLP-1R transmembrane domains occur within TM1, the extracellular portions of TM6 and TM7, and the ECL3 conformation (Fig. 1b, Extended Data Fig. 5a), indicating that these domains may contribute to biased agonism. This is supported by earlier work identifying crucial roles for ECL3, and the extracellular helical boundaries of TM6 and TM7, within the GLP-1R for differential control of GLP-1R-mediated signalling[17]. Alanine scanning mutagenesis confirmed the importance of this domain for the differing pharmacological profiles of GLP-1 and ExP5 (Fig. 1c, Extended Data Table 1). Although some ECL3 residues (G377, R380) had similar roles in both GLP-1 and ExP5 function, the substitutions L379A, D372A and E373A substantially reduced GLP-1 affinity and signalling but had little effect on ExP5 function. Notably, the latter two residues lie within the region of ECL3 where the largest receptor backbone differences are observed between the two structures (Extended Data Fig. 5a), and alanine mutation converts the binding profile of GLP-1 to one that closely resembles the binding profile of ExP5 (Fig. 1c). Mutagenesis of these two residues also had a similar effect on the pharmacology of exendin-4, which has a bias profile similar to that of GLP-1 for these pathways (Extended Data Table 1). Moreover, mutation of $L388^{7.43}$ within the top of TM7 had a greater effect on GLP-1 signalling than on ExP5 signalling (Extended Data Fig. 5b), further supporting the importance of this region in biased agonism of GLP-1R.

There are additional differences between the ExP5-bound structure and the deposited GLP-1-bound GLP-1R structure, in the reported positioning of the TM1 kink and orientation of side chains in the extracellular half of TM1 (Extended Data Fig. 5c, Fig. 1d). The location of the TM1 kink in the 11-mer-bound GLP-1R and the agonist-bound CTR structures is equivalent to that observed in the ExP5-bound structure and an overlay of the ExP5-bound and GLP-1-bound GLP-1R cryo-EM maps reveals that they have similar backbone densities (Extended Data Fig. 5c). Although the limited density in the GLP-1 bound structure precludes confidence, the TM1 backbone can also be modelled in this common conformation, suggesting that the gross positioning of TM1 may be conserved, although comparison of the density maps indicates that the side chain positioning differs between the ExP5- and GLP-1-bound structures, possibly contributing to the biased agonism of ExP5. Indeed, in the deposited GLP-1-bound model, $L141^{1.36}$, $Y145^{1.40}$ and $Y148^{1.43}$ face towards TM7, whereas in the ExP5 structure they reside closer to TM2 (Fig. 1d). Mutation of these residues to alanine had a stronger effect on ExP5-mediated cAMP signalling than on GLP-1 signalling, supporting a role for TM1 in the control of signalling and an interaction between TM1 and TM7–ECL3–TM6 that manifests as altered $G\alpha_s$ efficacy and biased agonism between GLP-1 and ExP5.

Strong density was observed for the entirety of ExP5 extending from the NTD into deep within the transmembrane core (Extended Data Fig. 3).

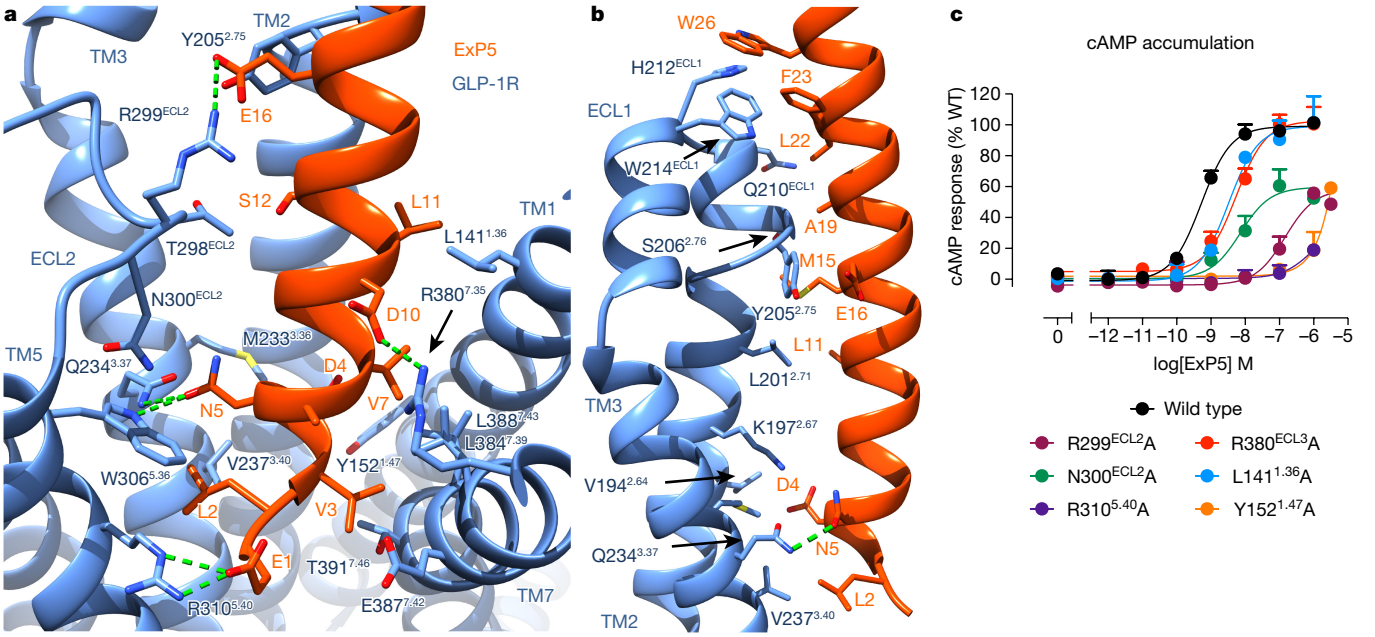

Figure 2 | The ExP5 binding site. a, Key interactions between ExP5 residues and TM1, TM3, TM5, TM7 and ECL2 of the GLP-1R transmembrane bundle (side chains located within 4 Å between the peptide (orange) and the GLP-1R (blue) are shown). ECL3 has been removed for clarity. **b**, Additional interactions formed by ExP5 with TM2, TM3 and ECL1. **c**, The functional effect on Gs-mediated cAMP accumulation following mutagenesis of key ExP5 residues that form interactions (highlighted in **a**) in the refined model supports the role of these residues in ExP5 interactions. cAMP signalling was assessed in CHOFlpIn cells and data are means + s.e.m. of four independent experiments performed in duplicate.

The peptide forms extensive interactions with residues in TMs 1, 2, 3, 5, 7 and all 3 ECLs (Fig. 2, Extended Data Table 2). Alanine mutagenesis confirmed the importance of key residues in the GLP-1R for ExP5 binding (Fig. 2c). Many of these residues lining the ExP5 binding site have previously been implicated as being important for binding of the cognate ligand, GLP-1[7,17–23].

E1 of ExP5 interacts with R310$^{5.40}$ of GLP-1R and is crucial for the ability of ExP5 to promote signalling through Gα_s, with R310$^{5.40}$A almost completely abolishing ExP5-mediated cAMP accumulation (Fig. 2a, c). Very clear density is evident for W306$^{5.36}$, which interacts directly with ExP5 through Van der Waal interactions with the aliphatic region of N5, as well as forming a direct hydrogen bond with N5 in the peptide. N5 also forms a hydrogen bond with Q234$^{3.37}$. N300^{ECL2} points down towards the receptor core within bonding distance of W306$^{5.36}$ and may participate in stabilizing these interactions. A series of contacts occur between residues in TM2 and ExP5, mainly through hydrophobic Van der Waals interactions with either hydrophobic residues or aliphatic regions of polar side chains (Fig. 2b, Extended Data Table 2). Peptide interactions also occur within ECL1, a region that has been implicated in peptide binding of other GLP-1R agonists[17,22] and ECL1 resides close to GLP-1 in the GLP-1-bound cryo-EM structure[2]. Van der Waals interactions are also formed between ExP5 and residues in TM1 and TM7 (Fig. 2a, Extended Data Table 2). In addition, two key electrostatic interactions are formed by R299^{ECL2} in ECL2 and R380$^{7.35}$ at the top of the TM7–ECL3 boundary with E16 and D10 of ExP5, respectively (Fig. 2a). These two residues also formed direct interactions with the 11-mer peptide agonist in the GLP-1R X-ray structure, interacting with a serine at position 8 (R299^{ECL2}) and an aspartic acid at position 9 (R380$^{7.35}$)[15]. D9 in the 11-mer is the equivalent of D10 in ExP5 and D15 in native GLP-1. An interaction between GLP-1 D15 and R380$^{7.35}$ has also been predicted by molecular dynamics simulations[17] and mutagenesis[23], but was not reported in the GLP-1-bound GLP-1R structure[2]. However, side chain densities were poorly resolved in this region of the deposited GLP-1–GLP-1R map; alternative modelling can preserve this interaction and therefore it is likely to be conserved across the three ligands for which structures are now available.

The GLP-1-bound GLP-1R cryo-EM structure also reported that R299^{ECL2} dips into the receptor core to form a direct interaction with H7 of GLP-1[2]. This modelling into the cryo-EM map is also ambiguous and contains an alternate positioning of W306$^{5.36}$ (required for R299^{ECL} to reach into the bundle) to the ExP5-bound and 11-mer-bound GLP-1R structures[15]. Because this positioning of W306$^{5.36}$ is not supported by density, and the described interaction of R299^{ECL2} is highly energetically unfavourable, we hypothesize that W306$^{5.36}$ is more likely to reside in a similar orientation to that observed in the ExP5- and 11-mer-bound structures, supported by good density in these maps. This orientation would promote interactions of R299^{ECL2} with GLP-1 higher up in the peptide.

Owing to the limited density available to define GLP-1 interactions in the GLP-1-bound GLP-1R cryo-EM map, it is difficult to assess direct differences in peptide interactions between the GLP-1- and ExP5-bound structures by relying on the structures alone. Nonetheless, alanine mutation of residues lining the ExP5-binding pocket (highlighted in Fig. 2c, Extended Data Table 1) confirmed a likely overlap of GLP-1R residues involved in interactions with GLP-1 and ExP5, with previous publications highlighting the importance of Y205$^{2.75}$, R299^{ECL2}, N300 ^{ECL2}, R380$^{7.35}$ and R310$^{5.40}$ in GLP-1 affinity and signalling[1,17,20,21], and our results confirming their importance for ExP5 binding (Fig. 2). The nature of these interactions is likely to differ, owing to the variations in peptide sequence and consequent receptor interactions, as highlighted by the TM1, TM7 and ECL3 mutagenesis in this study.

Class B GPCRs contain a number of highly conserved transmembrane polar residues that participate in key hydrogen bond interactions for receptor integrity and maintenance of the apo state. A central polar network formed by residues R$^{2.60}$, N$^{3.43}$, H$^{6.52}$ and Q$^{7.49}$ is located just below the peptide binding site in the ExP5-bound structure[24,25] (Extended Data Fig. 6). Two highly conserved class B GPCR polar networks (TM2–TM3–TM6–TM7: H$^{2.50}$, E$^{3.50}$, T$^{6.42}$, Y$^{7.57}$ and TM2–TM6–TM7–H8: R$^{2.46}$, R/K$^{6.37}$, N$^{7.61}$, E$^{8.41}$) at the cytoplasmic face lock the base of the receptor in an inactive conformation[21,25]. Located between the central hydrogen bond network and the TM2–TM3–TM6–TM7 network is a cluster of conserved residues that form

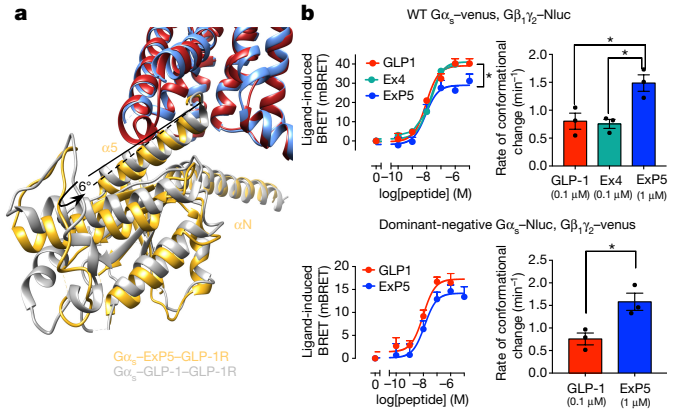

Figure 3 | Comparison of GLP-1R-mediated G protein conformation in GLP-1-bound and ExP5-bound receptors. a, Superimposition of the GLP-1R bundle bound by GLP-1 and by ExP5 reveals distinct angles of $G\alpha_s$ α5 engagement (6° measured using pisco). **b**, Top, BRET measurements show distinct conformational rearrangements between the $G\alpha_s$ α-helical domain and Gγ when the GLP-1R is activated by ExP5, relative to activation by GLP-1 or exendin-4. This is associated with a faster rate of rearrangement at equi-occupant ligand concentrations. Bottom, similar differences are observed with the dominant-negative $G\alpha_s$. Data are means + s.e.m. (left panels) or mean ± s.e.m. (right panels) of three independent experiments performed in triplicate. * $P < 0.05$ by one-way analysis of variance followed by Tukey's multiple comparisons post-test.

hydrophobic packing interactions in the inactive state, stabilizing the TM6 $P^{6.47}XXG^{6.50}$ motif in an inactive conformation (Extended Data Fig. 6). Upon peptide binding, a reorganization of the GLP-1R central hydrogen bond network is associated with destabilization within TM6 around the $P^{6.47}XXG^{6.50}$ motif and a major rearrangement of the central hydrophobic network to form a new packing arrangement that stabilizes the active state (Extended Data Fig. 6, Supplementary Video 1). These major rearrangements break two hydrogen bond networks at the bottom of the receptor, facilitating movement of TM6 away from the transmembrane bundle to create a cavity for G protein binding (Extended Data Figs 6, 7b–d, Supplementary Video 1). $Y^{7.57}$ and $H^{2.50}$ are released from their ground state constraints and reorganize to form part of the hydrophobic network that stabilizes the active state. $E^{3.50}$ maintains a hydrogen bond interaction with $H^{2.50}$, further stabilizing this active conformation.

The GLP-1R active conformation is stabilized by extensive interactions with the $G\alpha_s$ heterotrimeric protein (Extended Data Fig. 7). The receptor–$G\alpha_s$ heterotrimer interface is formed by residues located in TM2, TM3, TM5, TM6, TM7, ICL1, ICL2, ICL3 and H8 of the GLP-1R, and the α5 and αN regions of $G\alpha_s$ and Gβ (Extended Data Table 3).

H8 in all active structures is amphipathic, with bulky aromatic residues on the membrane-proximal face heavily buried in the detergent micelle. Direct interactions of H8 and ICL1 with Gβ are conserved across class B GPCR G protein structures[2,9] (Extended Data Fig. 7e) and these are summarized in Extended Data Table 3. Though the importance of these interactions for the GLP-1R is unclear, truncation of H8 in the CTR reduced receptor expression and peptide-mediated cAMP efficacy, suggesting that receptor–Gβ interactions are important for class B GPCR function[9].

In all structures, the most extensive G protein contacts are formed by the α5 helix of the $G\alpha_s$ Ras-like domain, which inserts into the central GLP-1R transmembrane bundle cytoplasmic cavity formed by the 15 Å outward movement of TM6 (Extended Data Fig. 7). These contacts consist of both polar and hydrophobic Van der Waals interactions and there is, generally, a common interaction pattern between $G\alpha_s$ and the available active class B GPCRs (Extended Data Table 3).

Superimposition of the G proteins of the GLP-1- and ExP5-bound GLP-1R structures reveals only relatively small differences in the receptor-complexed $G\alpha_s$Ras and Gβγ domains (Extended Data Fig. 7f). The largest change was a 4 Å variance in the conformation of the $G\alpha_s\alpha N$ domain at its N terminus, which may reflect a ligand-dependent difference in conformation.

Superimposition of the transmembrane domains of the GLP-1R in the GLP-1- and ExP5- bound structures reveals that, although there are limited differences in the overall $G\alpha_s$Ras and Gβγ conformations, there is a six-degree variance in the angle at which the $G\alpha_s$ α5 helix engages in the GLP-1R cytoplasmic cavity. This results in an overall rotation of the G protein in the ExP5-bound structure relative to the GLP-1-bound structure (Fig. 3a, Extended Data Fig. 7f). Notably, when ExP5 is bound to the GLP-1R, the α4 helix and β3 strand are located further from the receptor core, and no interactions are observed between the α4 helix and the GLP-1R intracellular face, whereas there are potential contacts for the GLP-1-bound structure[2]. In addition, the αN–β3 loop of $G\alpha s$ is located further from ICL2 of the GLP-1R in the ExP5-bound structure; although these side chains are still within bonding distance, their interactions are likely to be weaker than those induced by GLP-1 binding. Notably, there was only very limited density within the backbone for residues in the bottom of TM5–ICL3 (residues 337–343) in the ExP5-bound structure, such that this region is not visible in high-resolution maps, whereas this backbone density was clearly visible for the GLP-1-bound structure (Extended Data Fig. 5d). This suggests that ICL3 of the GLP-1R is less flexible in the GLP-1- and G protein-bound state than in the ExP5- and G protein-bound state.

There are multiple lines of evidence that differences in ligand–receptor conformation propagate to G protein conformation[26,27]. Direct assessment of conformational rearrangement between $G\alpha_s$ and Gγ, using a bioluminescence resonance energy transfer (BRET) assay, revealed that ExP5 promotes a faster conformational change within $G\alpha_s$ than do GLP-1 or exendin-4 at equi-occupant concentrations, accompanied by a lower BRET maximal signal (E_{max}) at saturating concentrations of peptide (Fig. 3b). Together with the structural data, these results are consistent with the distinct flexibilities of the bottom of TM5 and within ICL3 altering the conformational positioning of the $G\alpha_s$ α-helical domain and increasing the rate of G protein activation. Collectively, this may contribute to the enhanced $G\alpha_s$ protein-mediated efficacy of ExP5 that is a key element of its biased agonism.

In conclusion, the structure of the ExP5–GLP-1R–$G\alpha_s$ complex provides insights into the structural reorganization of class B GPCRs upon peptide activation, as well as the distinct engagement of GLP-1R agonists with differential signalling bias. Our results highlight that even when ligands share a common G protein transducer, differences in the mode of G protein binding can have consequences for conformational changes in the G protein that are linked to activation. The findings increase our understanding of biased agonism and may contribute to the rational design of novel therapeutics that target the GLP-1R.

Online Content Methods, along with any additional Extended Data display items and Source Data, are available in the online version of the paper; references unique to these sections appear only in the online paper.

Received 22 September 2017; accepted 17 January 2018.
Published online 21 February 2018.

1. de Graaf, C. *et al.* Glucagon-like peptide-1 and its class B G protein-coupled receptors: a long march to therapeutic successes. *Pharmacol. Rev.* **68,** 954–1013 (2016).
2. Zhang, Y. *et al.* Cryo-EM structure of the activated GLP-1 receptor in complex with a G protein. *Nature* **546,** 248–253 (2017).
3. Hager, M. V., Clydesdale, L., Gellman, S. H., Sexton, P. M. & Wootten, D. Characterization of signal bias at the GLP-1 receptor induced by backbone modification of GLP-1. *Biochem. Pharmacol.* **136,** 99–108 (2017).
4. Koole, C. *et al.* Allosteric ligands of the glucagon-like peptide 1 receptor (GLP-1R) differentially modulate endogenous and exogenous peptide responses in a pathway-selective manner: implications for drug screening. *Mol. Pharmacol.* **78,** 456–465 (2010).
5. Wootten, D. *et al.* Differential activation and modulation of the glucagon-like peptide-1 receptor by small molecule ligands. *Mol. Pharmacol.* **83,** 822–834 (2013).
6. Zhang, H. *et al.* Autocrine selection of a GLP-1R G-protein biased agonist with potent antidiabetic effects. *Nat. Commun.* **6,** 8918 (2015).

7. Mann, R. *et al.* Peptide binding at the GLP-1 receptor. *Biochem. Soc. Trans.* **35,** 713–716 (2007).
8. Manandhar, B. & Ahn, J. M. Glucagon-like peptide-1 (GLP-1) analogs: recent advances, new possibilities, and therapeutic implications. *J. Med. Chem.* **58,** 1020–1037 (2015).
9. Liang, Y. L. *et al.* Phase-plate cryo-EM structure of a class B GPCR–G-protein complex. *Nature* **546,** 118–123 (2017).
10. Danev, R., Buijsse, B., Khoshouei, M., Plitzko, J. M. & Baumeister, W. Volta potential phase plate for in-focus phase contrast transmission electron microscopy. *Proc. Natl Acad. Sci. USA* **111,** 15635–15640 (2014).
11. Khoshouei, M., Radjainia, M., Baumeister, W. & Danev, R. Cryo-EM structure of haemoglobin at 3.2 Å determined with the Volta phase plate. *Nat. Commun.* **8,** 16099 (2017).
12. Khoshouei, M. *et al.* Volta phase plate cryo-EM of the small protein complex Prx3. *Nat. Commun.* **7,** 10534 (2016).
13. Siu, F. Y. *et al.* Structure of the human glucagon class B G-protein-coupled receptor. *Nature* **499,** 444–449 (2013).
14. Hollenstein, K. *et al.* Structure of class B GPCR corticotropin-releasing factor receptor 1. *Nature* **499,** 438–443 (2013).
15. Jazayeri, A. *et al.* Crystal structure of the GLP-1 receptor bound to a peptide agonist. *Nature* **546,** 254–258 (2017).
16. Runge, S., Thøgersen, H., Madsen, K., Lau, J. & Rudolph, R. Crystal structure of the ligand-bound glucagon-like peptide-1 receptor extracellular domain. *J. Biol. Chem.* **283,** 11340–11347 (2008).
17. Wootten, D. *et al.* The extracellular surface of the GLP-1 receptor is a molecular trigger for biased agonism. *Cell* **165,** 1632–1643 (2016).
18. Coopman, K. *et al.* Residues within the transmembrane domain of the glucagon-like peptide-1 receptor involved in ligand binding and receptor activation: modelling the ligand-bound receptor. *Mol. Endocrinol.* **25,** 1804–1818 (2011).
19. Dods, R. L. & Donnelly, D. The peptide agonist-binding site of the glucagon-like peptide-1 (GLP-1) receptor based on site-directed mutagenesis and knowledge-based modelling. *Biosci. Rep.* **36,** e00285 (2015).
20. Koole, C. *et al.* Second extracellular loop of human glucagon-like peptide-1 receptor (GLP-1R) has a critical role in GLP-1 peptide binding and receptor activation. *J. Biol. Chem.* **287,** 3642–3658 (2012).
21. Wootten, D. *et al.* Key interactions by conserved polar amino acids located at the transmembrane helical boundaries in class B GPCRs modulate activation, effector specificity and biased signalling in the glucagon-like peptide-1 receptor. *Biochem. Pharmacol.* **118,** 68–87 (2016).
22. Yang, D. *et al.* Structural determinants of binding the seven-transmembrane domain of the glucagon-like peptide-1 receptor (GLP-1R). *J. Biol. Chem.* **291,** 12991–13004 (2016).
23. Moon, M. J. *et al.* Ligand binding pocket formed by evolutionarily conserved residues in the glucagon-like peptide-1 (GLP-1) receptor core domain. *J. Biol. Chem.* **290,** 5696–5706 (2015).
24. Wootten, D. *et al.* A hydrogen-bonded polar network in the core of the glucagon-like peptide-1 receptor is a fulcrum for biased agonism: lessons from class B crystal structures. *Mol. Pharmacol.* **89,** 335–347 (2016).
25. Wootten, D., Simms, J., Miller, L. J., Christopoulos, A. & Sexton, P. M. Polar transmembrane interactions drive formation of ligand-specific and signal pathway-biased family B G protein-coupled receptor conformations. *Proc. Natl Acad. Sci. USA* **110,** 5211–5216 (2013).
26. Furness, S. G. B. *et al.* Ligand-dependent modulation of G protein conformation alters drug efficacy. *Cell* **167,** 739–749.e11 (2016).
27. Gregorio, G. G. *et al.* Single-molecule analysis of ligand efficacy in β2AR-G-protein activation. *Nature* **547,** 68–73 (2017).

Supplementary Information is available in the online version of the paper.

Acknowledgements The work was supported by the Monash University Ramaciotti Centre for Cryo-Electron Microscopy, the National Health and Medical Research Council of Australia (NHMRC) project grants (1061044, 1065410, 1120919 and 1126857), NHMRC program grant (1055134), Strategic Priority Research Program of the Chinese Academy of Sciences (XDA12020347) and Shanghai Science and Technology Development Fund (15DZ2291600). P.M.S., A.C., D.W. and C.K. are NHMRC Principal Research, Senior Principal Research, Career Development and CJ Martin Fellows, respectively. S.L. received the Postgraduate Overseas Study Fellowship from CAS. We thank J. Plitzko, G. Christopoulos, V. Julita, J. Michaelis, X. Zhang, P. Thompson and M. Liu for assay and technical support and B. Kobilka for technical advice and comments on the manuscript.

Author Contributions Y.-L.L. established the GLP-1R complex expression and purification strategy, expressed and purified the complex, and performed negative stain EM and data acquisition/analysis; Y.-L.L. and M.R. performed preliminary cryo-EM screening; M.K. performed cryo-sample preparation and phase plate imaging to acquire EM data and performed EM map calculations; A.G. built the model and performed refinement; A.G., C.K. and D.M.T. performed pharmacological assays; L.C., T.T.T. and S.L. performed the mutagenesis studies; S.G.B.F. and P.Z. designed and performed the G protein BRET assays; R.D. and W.B. organized and developed the Volta phase plate cryo-EM data acquisition strategy; Y.-L.L., M.K., A.G., S.G.B.F., P.Z., L.C., C.K., D.M.T., T.T.T., S.L., A.C., P.M.S. and D.W. performed data analysis; S.G.B.F., P.Z., C.K., A.C., L.J.M., M.-W.W. and A.C. assisted with data interpretation and preparation of the manuscript; Y.L.L., M.K., A.G., P.M.S. and D.W. interpreted data and wrote the manuscript; P.M.S. and D.W. supervised the project.

Author Information Reprints and permissions information is available at www.nature.com/reprints. The authors declare no competing financial interests. Readers are welcome to comment on the online version of the paper. Publisher's note: Springer Nature remains neutral with regard to jurisdictional claims in published maps and institutional affiliations. Correspondence and requests for materials should be addressed to D.W. (denise.wootten@monash.edu) and P.M.S. (Patrick.sexton@monash.edu).

Reviewer Information *Nature* thanks R. Glaeser, F. Marshall and J. Mayer for their contribution to the peer review of this work.

METHODS

Constructs. The human GLP-1R was unmodified with the exception of replacing the native signal peptide with that of haemagglutinin (HA) to enhance receptor expression and the addition of affinity tags (an N-terminal Flag tag epitope and a C-terminal 8× His tag); both tags are removable by 3C protease cleavage. The construct was generated in both mammalian and insect cell expression vectors. These modifications did not alter receptor pharmacology (Extended Data Fig. 1b). A dominant-negative $G\alpha_s$ ($DNG\alpha_s$) construct was generated by site-directed mutagenesis to incorporate mutations that alter nucleotide handling (S54N[28] and G226A[29]), stabilize the G_0 state (E268A[30]) and substitute residues from $G\alpha_{i2}$ (N271K, K274D, R280K, T284D and I285T[31,32]) that are reported to improve the dominant-negative effect, presumably by stabilizing interactions with the $\beta\gamma$ subunits.

Insect cell expression. Human GLP-1R, human $DNG\alpha_s$, and His_6-tagged human $G\beta_1$ and $G\gamma_2$ were expressed in Tni insect cells (Expression systems) using baculovirus. Cell cultures were grown in ESF 921 serum-free medium (Expression Systems) to a density of 4 million cells per ml and then infected with three separate baculoviruses at a ratio of 2:2:1 for GLP-1R, $DNG\alpha_s$ and $G\beta_1\gamma_2$. The culture was collected by centrifugation 60 h after infection and cell pellets were stored at −80 °C.

Complex purification. Cell pellets were thawed in 20 mM HEPES pH 7.4, 50 mM NaCl, 2 mM $MgCl_2$ supplemented with cOmplete Protease Inhibitor Cocktail tablets (Roche). Complex formation was initiated by addition of 1 μM ExP5 (China Peptides), Nb35–His (10 μg/ml) and apyrase (25 mU/ml, NEB); the suspension was incubated for 1 h at room temperature. Membranes were collected by centrifugation at 30,000*g* for 30 min, and complex was solubilized from membrane using 0.5% (w/v) lauryl maltose neopentyl glycol (LMNG, Anatrace) supplemented with 0.03% (w/v) cholesteryl hemisuccinate (CHS, Anatrace) for 2 h at 4 °C in the presence of 1 μM ExP5 and apyrase (25 mU/ml, NEB). Insoluble material was removed by centrifugation at 30,000*g* for 30 min and the solubilized complex was immobilized by batch binding to M1 anti-Flag affinity resin in the presence of 3 mM $CaCl_2$. The resin was packed into a glass column and washed with 20 column volumes of 20 mM HEPES pH 7.4, 100 mM NaCl, 2 mM $MgCl_2$, 3 mM $CaCl_2$, 1 μM ExP5, 0.01% (w/v) LMNG and 0.006% (w/v) CHS before bound material was eluted in buffer containing 5 mM EGTA and 0.1 mg/ml FLAG peptide. The complex was then concentrated using an Amicon Ultra Centrifugal Filter (MWCO, 100 kDa) and subjected to size-exclusion chromatography on a Superdex 200 Increase 10/300 column (GE Healthcare) that was pre-equilibrated with 20 mM HEPES pH 7.4, 100 mM NaCl, 2 mM $MgCl_2$, 1 μM ExP5, 0.01% (w/v) MNG and 0.006% (w/v) CHS to separate complex from contaminants. Eluted fractions consisting of receptor and G-protein complex were pooled and concentrated. The final yield of purified complex was approximately 0.2 mg per litre of insect cell culture.

SDS–PAGE and western blot analysis. Samples collected from size-exclusion chromatography were analysed by SDS–PAGE and western blot. For SDS–PAGE, precast gradient TGX gels (Bio-Rad) were used. Gels were either stained by Instant Blue (Expedeon) or immediately transferred to PVDF membrane (Bio-Rad) at 100 V for 1 h. The proteins on the PVDF membrane were probed with two primary antibodies, rabbit anti-$G\alpha_s$ C-18 antibody (cat. no. sc-383, Santa Cruz) against the $G\alpha_s$ subunit and mouse penta-His antibody (cat. no. 34660, QIAGEN) against His tags. The membrane was washed and incubated with secondary antibodies (680RD goat anti-mouse and 800CW goat anti-rabbit, LI-COR). Bands were imaged using an infrared imaging system (LI-COR Odyssey Imaging System).

Preparation of vitrified specimen. EM grids (Quantifoil, 200 mesh copper R1.2/1.3) were glow discharged for 30 s in high pressure air using Harrick plasma cleaner. Four microlitres of sample at 1.3 mg/ml was applied to the grid in the Vitrobot chamber (FEI Vitrobot Mark IV). The Vitrobot chamber was set to 100% humidity at 4 °C. The sample was blotted for 5 s with a blot force of 20 and then plunged into propane–ethane mixture (37% ethane and 63% propane).

Data acquisition. Data were collected on a Titan Krios microscope operated at 300 kV (Thermo Fisher Scientific equipped with a Gatan Quantum energy filter, a Gatan K2 summit direct electron detector (Gatan) and a Volta phase plate (Thermo Fisher Scientific)). Videos were recorded in EFTEM nanoprobe mode, with 50-μm C2 aperture, at a calibrated magnification of 47,170 corresponding to a magnified pixel size of 1.06 Å. Each video comprised 50 frames with a total dose of 50 $e^-/Å^2$ and exposure time was 8 s with a dose rate of 7 e^- per pixel per s on the detector. Data acquisition was done using SerialEM software at −500 nm defocus[33].

Data processing. We collected 2,793 movies and subjected them to motion correction using motioncor2[34]. Contrast transfer function (CTF) estimation was done using Gctf software[35] on the non-dose-weighted micrographs. The particles were picked using gautomatch (developed by K. Zhang, MRC Laboratory of Molecular Biology, Cambridge, UK; http://www.mrc-lmb.cam.ac.uk/kzhang/Gautomatch/). An initial model was made using EMAN2[36] based on a few automatically picked micrographs and using the common-line approach. The particles were extracted in RELION 2.03[37] using a box size of 200 pixels. Picked particles (614,883) were subjected to 3D classification with 5 classes. Particles (190,135) from the best-looking class were subjected to 3D auto-refinement in RELION 2.03. The refined particles were subjected to another run of 3D classification with 5 classes and without alignments, after which 184,672 particles were chosen for a final run of 3D auto-refinement in RELION 2.03. The final map was sharpened with a *B*-factor of −50 Å. Local resolution was determined using RELION[37] with half-reconstructions as input maps. The cryo-EM data collection, refinement and validation statistics are reported in Supplementary Table 1.

Modelling. The initial template for GLP-1R transmembrane regions, G protein and Nb35 was derived from rabbit GLP-1R in complex with $G\alpha_s$ (PDB-5VAI)[2] followed by extensive remodelling using COOT[38]. The ECL3 loop residues 372–376 were stubbed owing to insufficient density for unambiguous modelling, and no high-resolution density was present for ICL3 residues N338–T343, which were omitted from the deposited structure. Owing to discontinuous and/or variable density in the GLP-1R ECD region, we used the high-resolution X-ray crystal structure of the GLP-1R ECD–exendin(9–39) (PDB-3C5T)[16] for a rigid body fit with limited manual adjustments. The ExP5 peptide was modelled manually. The final model was subjected to global refinement and minimization in real space using the module 'phenix.real_space_refine' in PHENIX[39]. Validation was performed in MolProbity[40].

Insect cell membrane preparations. Crude membrane preparations were prepared from insect cells produced using the same expression conditions as used for cryo-EM samples. Cells were resuspended in buffer (20 mM HEPES 7.4, 50 mM NaCl, 2 mM $MgCl_2$, with protease inhibitors and benzonase) and dounced 20 times with the tight pestle, followed by centrifugation (10 min, 350*g*, 4 °C). The pellet was resuspended in buffer, dounced and clarified by centrifugation at a low *g*. Membranes were pelleted by centrifugation (1 h, 40,000*g*, 4 °C), resuspended in buffer and sonicated. Protein concentration was determined using Bradford reagent (Bio-Rad).

[^{35}S]GTPγS binding. Measurement of [^{35}S]GTPγS incorporation was performed in 20 mM HEPES pH 7.4; 100 mM NaCl; 10 mM $MgCl_2$; 1 mM EDTA; 0.1% (w/v) BSA; 30 μg/ml saponin. Membranes (50 μg per sample) were pre-incubated with 1 μM GDP and increasing concentrations of ligand for 30 min at 22 °C. Reactions were started by the addition of [^{35}S]GTPγS and ATP (final concentrations: 300 pM and 50 μM, respectively). After 1 h incubation at 30 °C, the reaction was terminated by collecting the membranes on Whatman UniFilter GF/C plates using Filtermate 196 harvester (Packard). Membranes were extensively washed with ice-cold 50 mM Tris pH 7.6, 10 mM $MgCl_2$, 100 mM NaCl, dried, dissolved in 40 μl MicroScint-O scintillation cocktail (Packard) and counted using a MicroBeta LumiJET counter (PerkinElmer). Data from each experiment were normalized to the response of GLP-1R–WT$G\alpha_s$–$G\beta_1\gamma_2$ membranes at 1 μM GLP-1 (100%).

Radioligand competition binding experiments on insect cell membranes. Radioligand binding was performed in 20 mM HEPES, pH 7.4, 100 mM NaCl, 10 mM $MgCl_2$ and 0.1% (w/v) BSA. Competition binding assays with GLP-1 and ExP5 were performed in the presence of 50 pM [^{125}I]-exendin(9–39). Binding reactions were initiated with the addition of 4 μg of GLP-1R-expressing membranes (with or without G protein) followed by 1 h incubation at 30 °C. Membranes were collected on UniFilter GF/C (Whatman) plates using a Filtermate 196 harvester (Packard), extensively washed with ice-cold NaCl, dried, dissolved in 40 μl of MicroScint-O scintillation cocktail (Packard), and counted using a MicroBeta LumiJET counter (PerkinElmer). Data from each experiment were normalized to vehicle control and non-specific binding (1 μM exendin(9–39)). Curves were fit to a one- or two-site competition binding equation in Prism 6.0 (GraphPad).

Generation of mutant receptor constructs in mammalian cell lines. Mutant receptors were generated in a 2× c-Myc epitope-tagged receptor in the pEF5/FRT/V5-DEST vector using QuikChange site-directed mutagenesis (Invitrogen) and sequences confirmed. Mutant receptors were stably expressed in CHOFlpIn cells using the FlpIn Gateway technology system (Invitrogen) and selected using 600 μg/ml hygromyocin B. All cells were tested and found to be free from mycoplasma contamination.

Mammalian whole-cell radioligand binding assays. Cells were seeded at a density of 30,000 cells per well into 96-well culture plates and incubated overnight in DMEM containing 5% FBS at 37 °C in 5% CO_2. Growth medium was replaced with binding buffer (DMEM containing 25 mM HEPES and 0.1% (w/v) BSA) containing 0.1 nM [^{125}I]-exendin(9–39) and increasing concentrations of unlabelled peptide agonists. Cells were incubated overnight at 4 °C, followed by three washes in ice cold 1× PBS to remove unbound radioligand. Cells were then solubilized in 0.1 M NaOH, and radioactivity determined by gamma counting. For all experiments, nonspecific binding was defined by 1 μM exendin(9–39).

Mammalian cAMP assays. Cells were seeded at a density of 30,000 cells per well into 96-well culture plates and incubated overnight in DMEM containing 5% FBS at 37 °C in 5% CO_2. cAMP detection was performed as previously described[3]. All values were converted to cAMP concentration using a cAMP standard curve

performed in parallel and data were subsequently normalized to the response of 100 μM forskolin in each cell line.

β-Arrestin recruitment assay. Cells stably expressing GLP-1R–Rluc8 and β-arrestin1–venus were seeded at a density of 30,000 cells per well into 96-well culture plates and incubated overnight in DMEM containing 5% FBS at 37 °C in 5% CO_2. β-Arrestin recruitment was performed as previously described[41].

Mammalian cell membrane preparations for G protein BRET assays. HEK293AΔS-GLP-1R cells were transfected with $G\alpha_s$–venus (inserted at position 72 of $G\alpha_s$ with a GSSSSG linker) or dominant-negative $G\alpha_s$–nanoluc (inserted at position 72 of $G\alpha_s$ with a GSSSSG linker), $G\beta_1$ and $G\gamma_{2}$–nanoluc or $G\gamma_{2}$–venus (inserted at the N terminus of $G\gamma_2$ with a GSAGT linker) at a 1:1:1 ratio using PEI. Cell membranes were prepared as described previously[26] and stored at −80 °C. Twenty-four hours after transfection, cells were collected with membrane preparation buffer (20 mM BisTris, pH 7.4, 50 mM NaCl, 1 mM $MgCl_2$, 1× P8340 protease inhibitor cocktail (Sigma-Aldrich), 1 mM DTT and 0.1 mM PMSF). Cells were then homogenized, applied to a stepped sucrose gradient (60%, 40%, homogenate) and centrifuged at 22,500 r.p.m. for 2.5 h at 4 °C. The layers between 40% and homogenate were collected, diluted in membrane preparation buffer and centrifuged at 30,000 r.p.m. for 30 min at 4 °C. The final pellet was resuspended in membrane preparation buffer, and stored at −80 °C. Total protein concentration was determined using a NanoDrop.

G protein conformational determination using BRET. HEK293AΔS cells stably expressing the GLP-1R (tested and confirmed to be free from mycoplasma) were transfected with a 1:1:1 ratio of $G\gamma_{2}$:nanoluc–$G\alpha_s$[72]:venus–$G\beta_1$ or $G\gamma_{2}$:venus–dominant-negative $G\alpha_s$[72]:nanoluc–$G\beta_1$ 24 h before collection and preparation of cell plasma membranes (above). Five micrograms per well of cell membrane was incubated with furimazine (1:1,000 dilution from stock) in assay buffer (1× HBSS, 10 mM HEPES, 0.1% (w/v) BSA, 1× P8340 protease inhibitor cocktail, 1 mM DTT and 0.1 mM PMSF, pH 7.4). The GLP-1R-induced BRET signal between $G\alpha_s$ and $G\gamma$ was measured at 30 °C using a PHERAstar (BMG LabTech). Baseline BRET measurements were taken for 2 min before addition of vehicle or ligand. BRET was measured at 15 s intervals for a further 7 min. All assays were performed in a final volume of 100 μl.

Data analysis. Pharmacological data were analysed using Prism 7 (GraphPad). Concentration-dependent response signalling data were analysed as previously described[20] using a three-parameter logistic equation. Signalling bias was quantified by analysis of cAMP accumulation and β-arrestin1 recruitment concentration–response curves using an operational model of agonism modified to directly estimate the ratio of τ/K_A as described previously[5,20,42].

$$Y = \frac{E_{max} \times (\tau_c/K_A)^n \times [A]^n}{[A]^n \times (\tau_c/K_A)^n + (1 + [A]/K_A)^n}$$

in which E_{max} represents the maximal stimulation of the system, K_A is the agonist–receptor dissociation constant in molar concentration, $[A]$ is the molar concentration of ligand and τ is the operational measure of efficacy in the system, which incorporates signalling efficacy and receptor density. All estimated τ/K_A ratios included propagation of error for both τ and K_A. Changes in τ/K_A ratios with respect to GLP-1 for each novel peptide were used to quantify bias between signalling pathways. Accordingly, bias factors included propagation of error from the τ/K_A ratios of each pathway.

Changes in the rate of change in BRET signal were fitted to a one-phase association curve. Normalized AUC for the indicated ligand concentrations was plotted as a concentration–response curve and fitted with a three-parameter logistic curve. Statistical analysis was performed with either one-way analysis of variance and a Tukey's post-test or a paired *t*-test, and significance accepted at $P < 0.05$.

Graphics. Molecular graphics images were produced using the UCSF Chimera package from the Computer Graphics Laboratory, University of California, San Francisco (supported by NIH P41 RR-01081)[43]. Superposition of maps was performed in COOT using "transformation by LSQ model fit"[38]. Measurements of GαRas α5 movements between different structures was performed in Pymol using the psico python module.

Data availability. All relevant data are available from the authors and/or included in the manuscript or Supplementary Information. Atomic coordinates and the cryo-EM density map have been deposited in the Protein Data Bank (PDB) under accession number 6B3J and EMDB entry ID EMD-7039.

28. Cleator, J. H., Mehta, N. D., Kurtz, D. T. & Hildebrandt, J. D. The N54 mutant of Gαs has a conditional dominant negative phenotype which suppresses hormone-stimulated but not basal cAMP levels. *FEBS Lett.* **443,** 205–208 (1999).
29. Lee, E., Taussig, R. & Gilman, A. G. The G226A mutant of Gsα highlights the requirement for dissociation of G protein subunits. *J. Biol. Chem.* **267,** 1212–1218 (1992).
30. Iiri, T., Bell, S. M., Baranski, T. J., Fujita, T. & Bourne, H. R. A Gsα mutant designed to inhibit receptor signaling through Gs. *Proc. Natl Acad. Sci. USA* **96,** 499–504 (1999).
31. Berlot, C. H. A highly effective dominant negative αs construct containing mutations that affect distinct functions inhibits multiple Gs-coupled receptor signaling pathways. *J. Biol. Chem.* **277,** 21080–21085 (2002).
32. Berlot, C. H. & Bourne, H. R. Identification of effector-activating residues of Gsα. *Cell* **68,** 911–922 (1992).
33. Mastronarde, D. N. Automated electron microscope tomography using robust prediction of specimen movements. *J. Struct. Biol.* **152,** 36–51 (2005).
34. Zheng, S. Q. *et al.* MotionCor2: anisotropic correction of beam-induced motion for improved cryo-electron microscopy. *Nat. Methods* **14,** 331–332 (2017).
35. Zhang, K. Gctf: Real-time CTF determination and correction. *J. Struct. Biol.* **193,** 1–12 (2016).
36. Tang, G.*et al.* EMAN2: an extensible image processing suite for electron microscopy. *J. Struct. Biol.* **157,** 38–46 (2007).
37. Kimanius, D., Forsberg, B. O., Scheres, S. H. & Lindahl, E. Accelerated cryo-EM structure determination with parallelisation using GPUs in RELION-2. *eLife* **5,** e18722 (2016).
38. Emsley, P. & Cowtan, K. Coot: model-building tools for molecular graphics. *Acta Crystallogr. D* **60,** 2126–2132 (2004).
39. Adams, P. D. *et al.* PHENIX: a comprehensive Python-based system for macromolecular structure solution. *Acta Crystallogr. D* **66,** 213–221 (2010).
40. Chen, V. B. *et al.* MolProbity: all-atom structure validation for macromolecular crystallography. *Acta Crystallogr. D* **66,** 12–21 (2010).
41. Savage, E. E., Wootten, D., Christopoulos, A., Sexton, P. M. & Furness, S. G. A simple method to generate stable cell lines for the analysis of transient protein–protein interactions. *Biotechniques* **54,** 217–221 (2013).
42. Hager, M. V. J., Johnson, L. M., Wootten, D., Sexton, P. M. & Gellman, S. H. β-Arrestin-biased agonists of the GLP-1 receptor from β-amino acid residue incorporation into GLP-1 analogues. *J. Am. Chem. Soc.* **138,** 14970–14979 (2016).
43. Pettersen, E. F. *et al.* UCSF Chimera—a visualization system for exploratory research and analysis. *J. Comput. Chem.* **25,** 1605–1612 (2004).
44. Ehlert, F. J. The relationship between muscarinic receptor occupancy and adenylate cyclase inhibition in the rabbit myocardium. *Mol. Pharmacol.* **28,** 410–421 (1985).

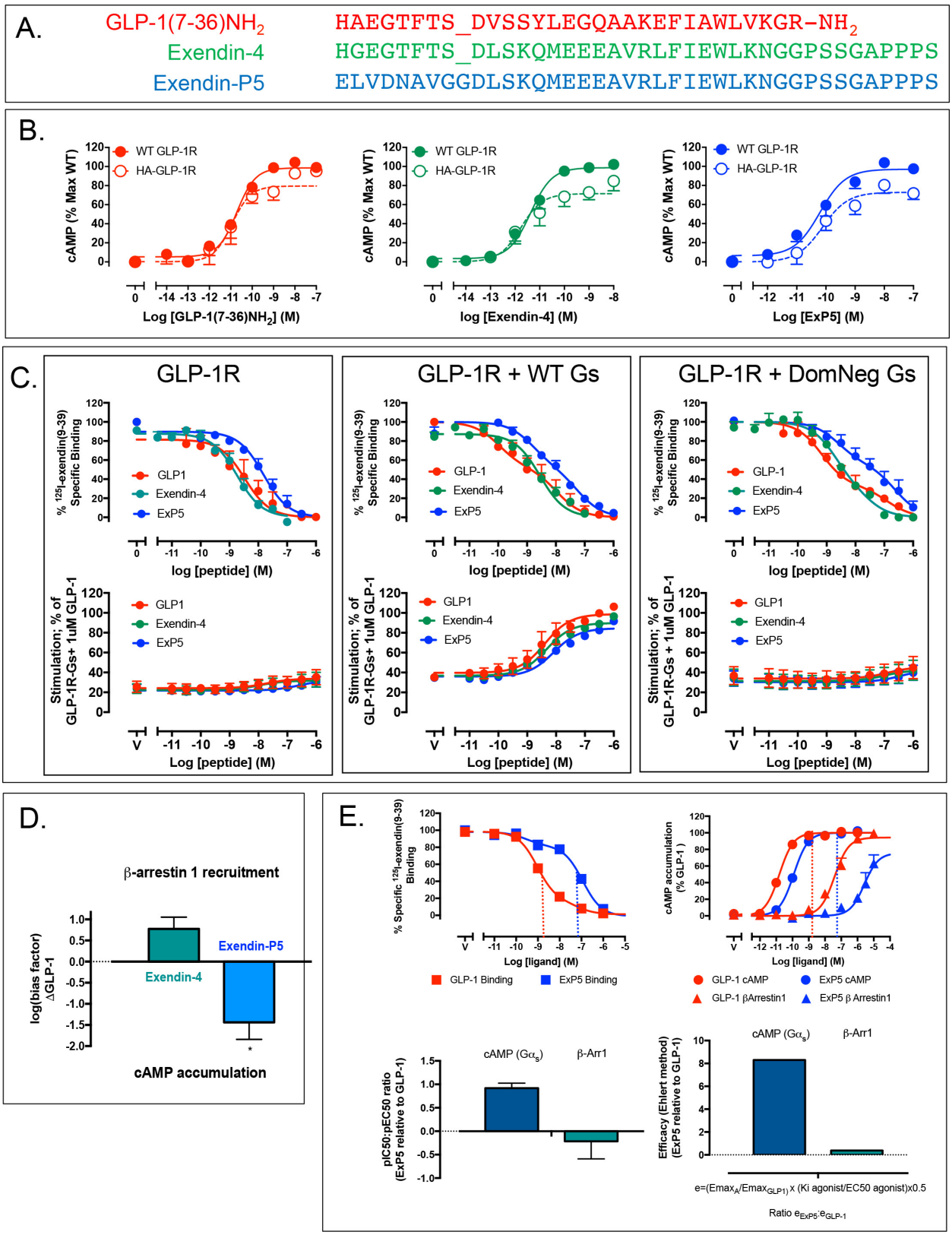

Extended Data Figure 1 | See next page for caption.

Extended Data Figure 1 | GLP-1R pharmacology. a, Peptide sequences. **b**, Pharmacology of untagged GLP-1R (WT GLP-1R) and the purification construct (HA–GLP-1R). **c**, Insect cell pharmacology of HA–GLP-1R. Top, radioligand competition binding. Bottom, GTPγS binding. Left, no Gs protein. ExP5 has lower affinity than GLP-1 and exendin-4 and does not bind GTPγS. Middle, wild-type Gs enhances peptide affinity and promotes GTPγS binding. Right, dominant-negative Gs is similar to wild-type Gs in binding, but does not bind GTPγS. **d**, Bias factors calculated from concentration–response curves using the Black and Leff operational model[5,20,41] (see Methods) confirm that ExP5 is a biased agonist relative to GLP-1. **e**, Top left, pIC_{50} of ExP5 is ~100-fold lower than of GLP-1 (CHOFlpIn whole cell). Top right, GLP-1 and ExP5 have β-arrestin1 coupling with pEC_{50} ~30-fold to the right of their pIC_{50} (dotted lines). ExP5 is more potent than GLP-1 in cAMP signalling (pEC_{50} relative to pIC_{50}). Bottom left, pIC_{50}:pEC_{50} ratios for G protein (cAMP) and β-arrestin1 of ExP5 relative to GLP-1 highlights ExP5 bias arises from enhanced Gs coupling, not reduced β-arrestin1 recruitment. Bottom right, ratio of ExP5 efficacy (calculated using the Ehlert method[44]) relative to GLP-1 in cAMP and β-arrestin1 recruitment confirms that ExP5 bias arises from enhanced $G\alpha_s$ efficacy. Data in **b**, **c** are mean ± s.e.m. of three (insect cells) or four (CHOFlpIn cells) independent experiments, conducted in duplicate or triplicate, respectively. Data in **d**, **e** are from 11 independent experiments performed in duplicate. $^*P < 0.05$ by one-way analysis of variance and Dunnett's post-test.

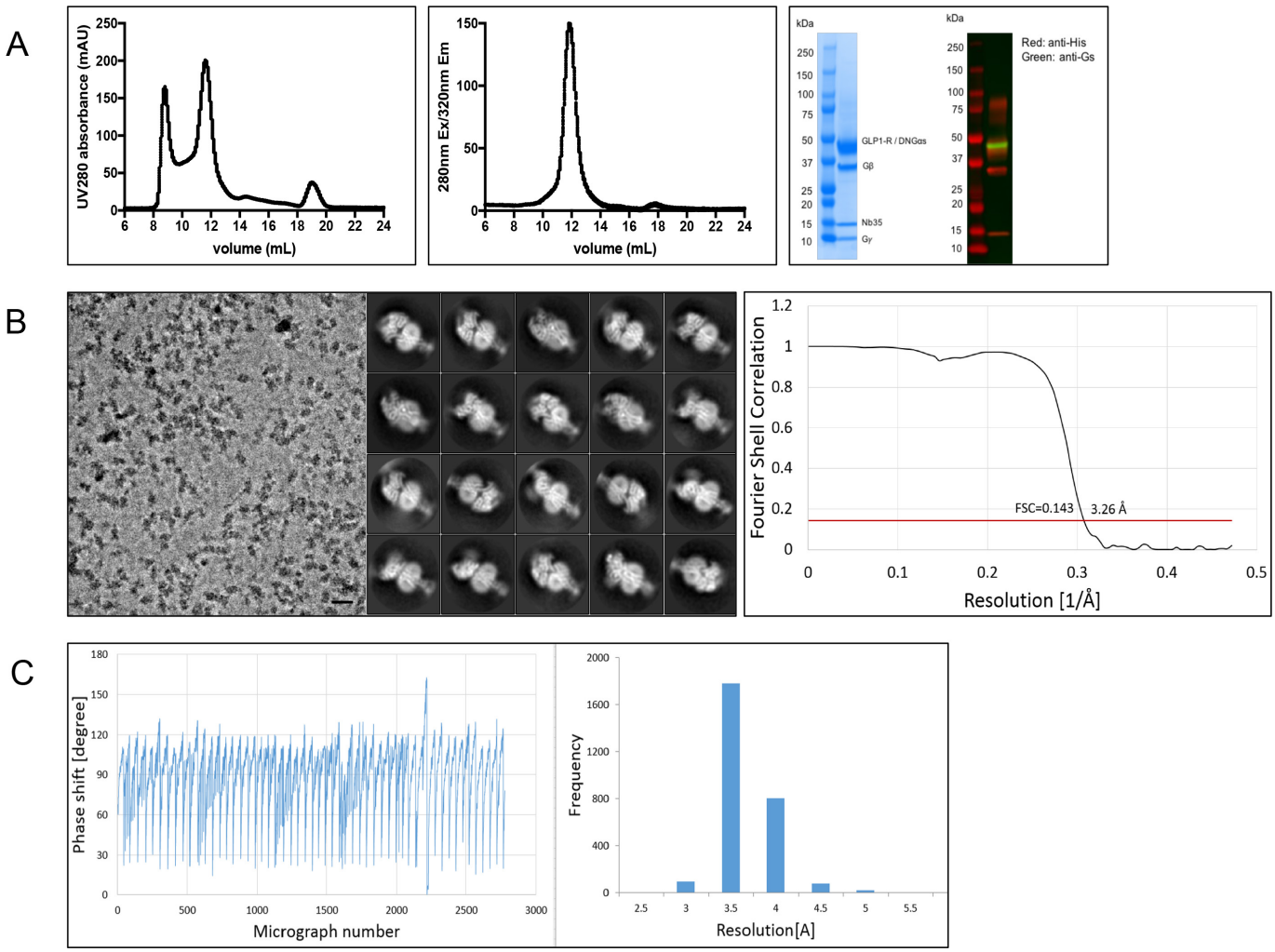

Extended Data Figure 2 | Purification and Volta phase plate imaging of the ExP5–GLP-1R–Gs complex. a, Left, elution profile of the purified complex. Middle, pooled complex fractions, concentrated and analysed by size exclusion chromatography (SEC). Right, SDS–PAGE/Coomassie blue stain and western blot of the complex showing all components. Anti-His antibody detects Flag–GLP-1R–His, Gβ–His and Nb35–His (red) and anti-Gs antibody detects $G\alpha_s$ (green). **b**, Left, Volta phase plate micrograph of the complex (representative of 2,793). Middle, 2D class averages. Right; 'gold standard' Fourier shell correlation (FSC) curves; the overall nominal resolution is 3.26 Å. **c**, Left, Volta phase plate phase shift history throughout the dataset. Right, histogram of the estimated micrograph resolutions from the CTF.

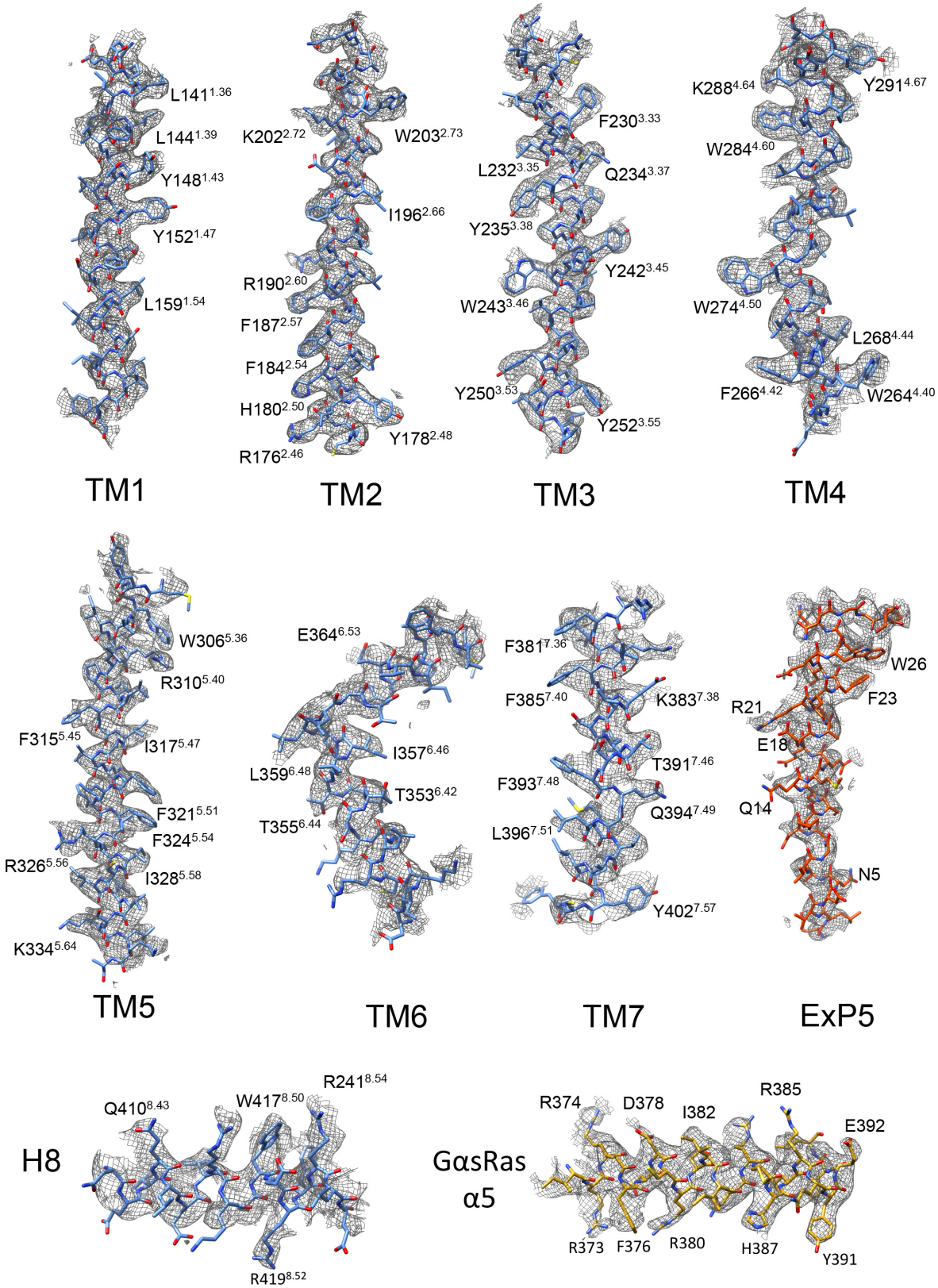

Extended Data Figure 3 | Atomic resolution model of the ExP5–GLP-1R–Gs heterotrimer in the cryo-EM density map. EM density map and model are shown for all seven transmembrane helices and H8 of the receptor, the ExP5 peptide and the α5α helix of the GαSα Ras-like domain. Bulky residues are highlighted. All transmembrane helices exhibit good density, with TM6—which is flexible—being the least well-resolved.

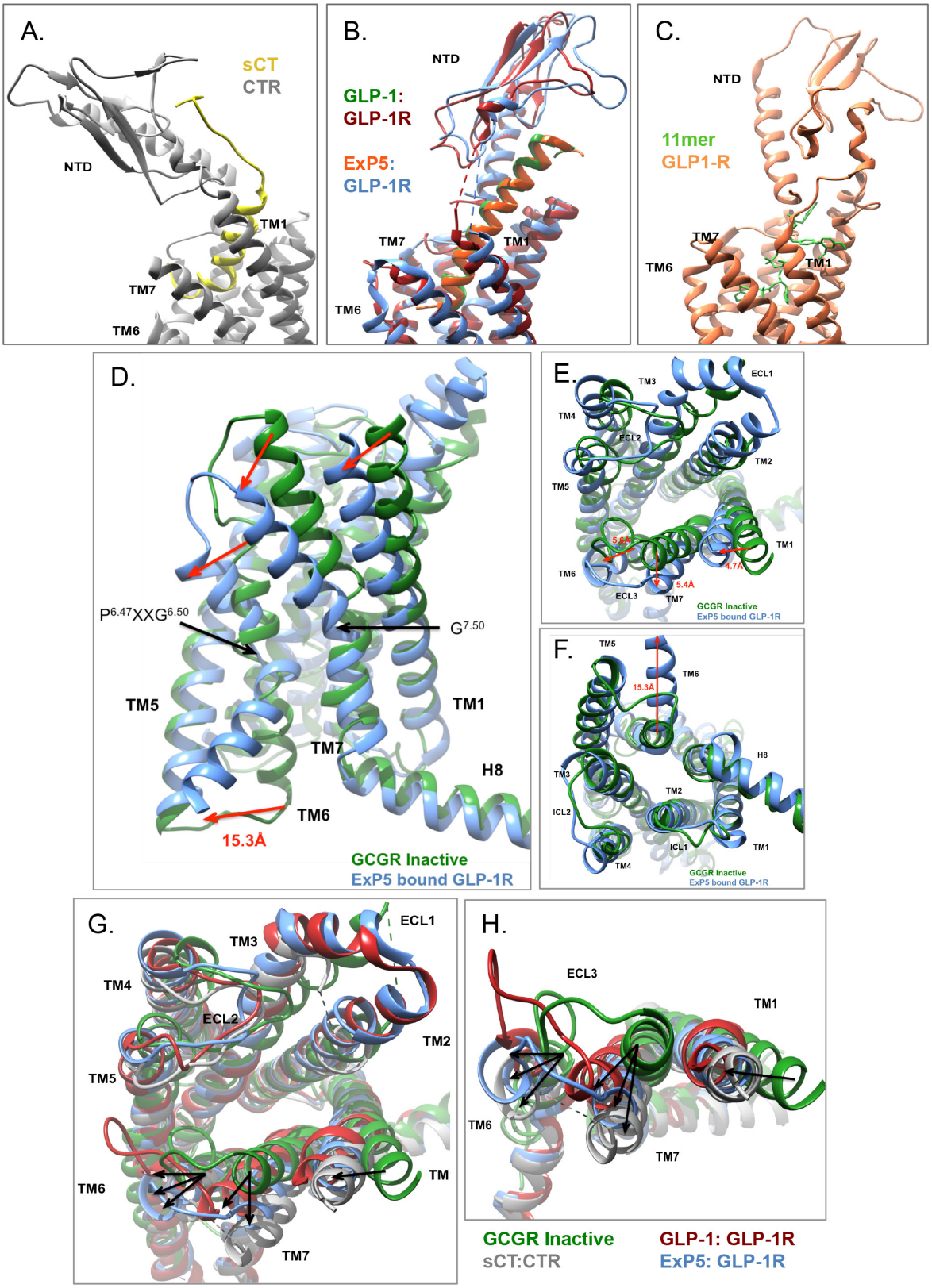

Extended Data Figure 4 | Comparison of class B GPCR structures. **a**–**c**, Agonist-bound full-length structures have distinct NTD orientations. **d**–**f**, Side view (**d**), extracellular view (**e**) and cytoplasmic view (**f**) of the conformational reorganization between inactive (GCGR, PDB 4L6R) and active structures (ExP5-bound GLP-1R). Distances are measured from Cα residues 1.33, 6.58, 7.35 and 6.35. Numbering uses the Wootten class B system. **g**–**h**, Superimposition of transmembrane domains from sCT–CTR–Gs (grey, PDB 5U27), GLP-1–GLP-1R–Gs (red, PDB 5VAI) and ExP5–GLP-1R–Gs with the inactive GCGR (green, PDB 4L6R). The largest differences in active structures relative to the inactive GCGR occur in TM1, TM6, TM7 and ECL3 (**h**), but the nature and extent of conformational change varies.

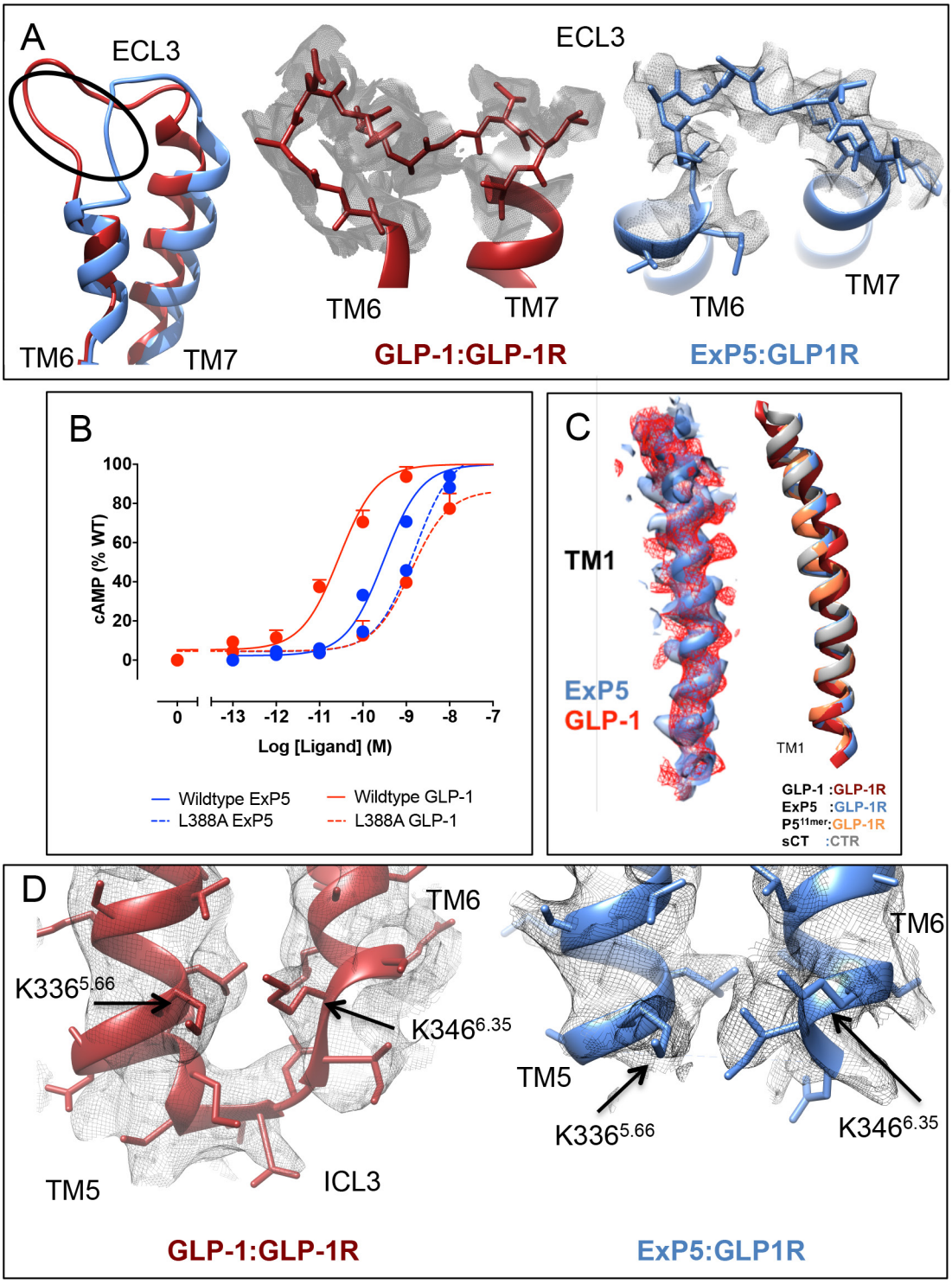

Extended Data Figure 5 | ECL3, TM7, TM1 and ICL3 may be associated with GLP-1R biased agonism. a, Conformational differences in GLP-1R ECL3 between ExP5-bound (blue) and GLP-1-bound (red) GLP-1R structures are supported by density in their respective cryo-EM maps. **b**, L388$^{7.43}$A affected the potency of GLP-1 mediated cAMP more than ExP5 (mean + s.e.m. of four independent experiments). **c**, Right, TM1 overlays from agonist-bound class B GPCR structures reveals a different conformation for GLP-1–GLP-1R. Left, TM1 model overlays of ExP5–GLP-1R and GLP-1–GLP-1R with their associated cryo-EM maps (GLP-1, red ribbon/mesh; ExP5, blue ribbon/surface) reveals limited differences in the TM1 backbone, but potentially distinct side-chain orientations. **d**, Left, ICL3 backbone conformation in GLP-1–GLP-1R (PDB 5VAI) is supported by density (EMD-3653). Limited density is observed for ICL3 (337–343) in ExP5–GLP-1R.

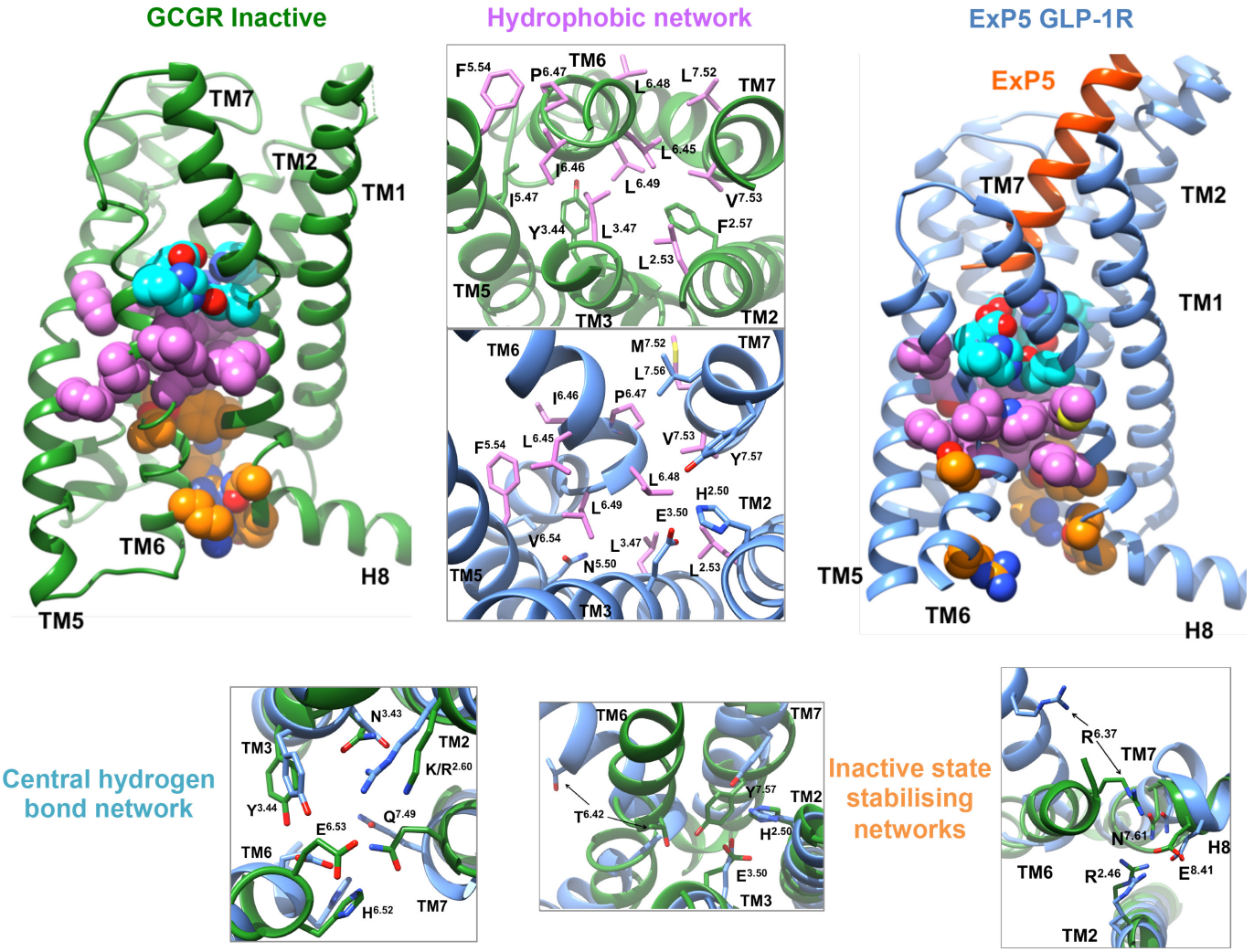

Extended Data Figure 6 | Rearrangement of conserved networks upon GLP-1R binding to ExP5. Comparison of conserved networks in the inactive (green, GCGR) and activated (blue, ExP5–GLP-1R–Gs) states; central polar network (cyan), cytoplasmic polar networks (orange) and hydrophobic residues (pink). Inactive state interactions are incompatible with peptide binding and reorganize on activation. Upper middle, major rearrangements within the hydrophobic network (top, inactive; bottom, activated); side chains involved in ground state stabilization in green, inactive and active state in pink and active state in blue. Lower left and lower right, reorganization of the central hydrogen bond network and cytoplasmic networks, respectively, where green is inactive and blue is active. Subscript, Wootten numbering. These conformational changes are detailed in Supplementary Video 1.

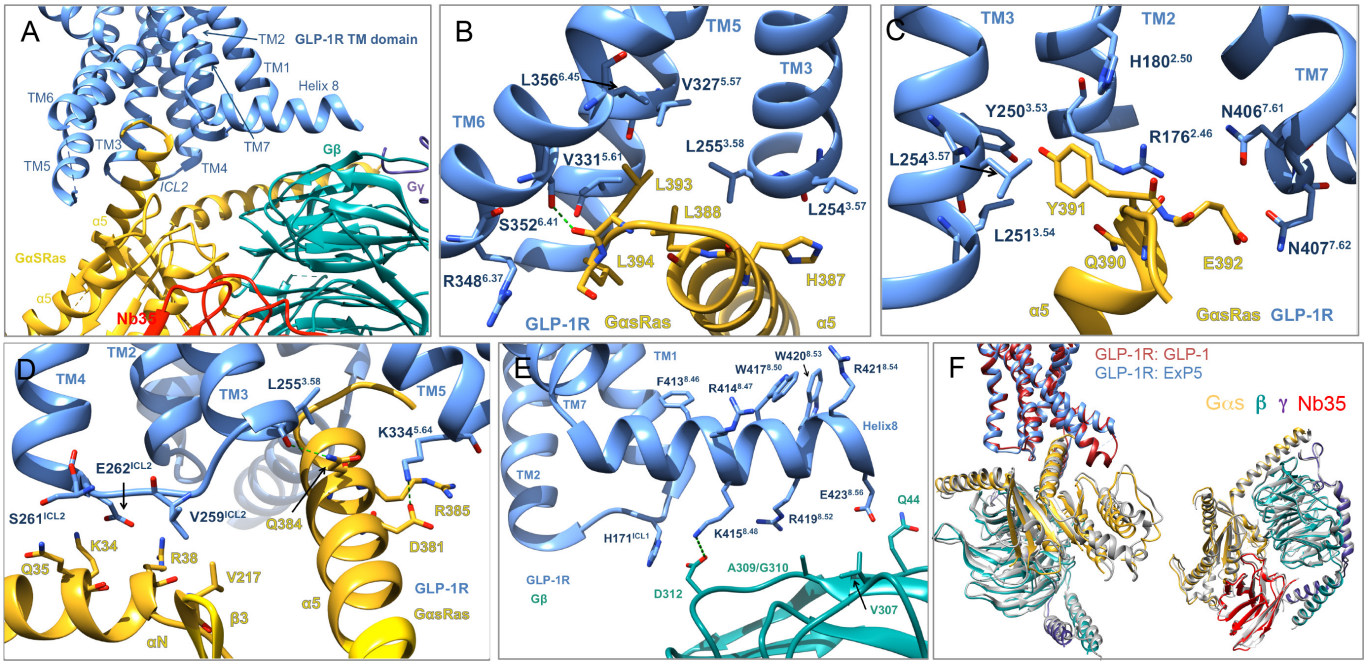

Extended Data Figure 7 | GLP-1R–G protein interactions. a, GLP-1R forms interactions with $G\alpha_s$Ras and Gβ. **b**–**e**, Receptor side chains (blue) within 4.5 Å of $G\alpha_s$ side chains (gold) or Gβ side chains (cyan). **b**–**d**, $G\alpha_s\alpha5$ forms polar and non-polar interactions with the cytoplasmic cavity formed by TM6 opening. Potential interactions also occur between $G\alpha_s\alpha N$ and ICL2 of GLP-1R. **e**, GLP-1R H8 aromatic residues embed within the detergent micelle and polar residues form direct interactions with Gβ. **f**, Left, the distinct engagement angle of $G\alpha_s\alpha5$ with the receptor (Fig. 3) results in an overall rotation of the $G\alpha_s$Ras,β,γ in ExP5–GLP-1R relative to GLP-1–GLP-1R. Right, overlaying $G\alpha_s$ from both structures reveals only minor differences in the G protein upon receptor engagement.

Extended Data Table 1 | Effects of extracellular loop 3 alanine mutants of human GLP-1R on agonist binding and cell surface expression

GLP-1R	Cell surface expression	Whole cell competition radioligand binding pK_i			cAMP Accumulation					
		GLP-1	Exendin-4	Exendin-P5	GLP-1		Exendin-4		Exendin-P5	
					pEC_{50}	E_{max}	pEC_{50}	E_{max}	pEC_{50}	E_{max}
Wild type	100 ± 3	8.81±0.04 -	8.97±0.07 -	9.61±0.45(0.18) 7.05±0.09	10.8±0.04	100±2	11.4±0.04	100±1	9.93±0.04	100±1
D372A	86 ± 4	9.62±0.47 (0.15)	9.29±0.56 (0.14) **7.40±0.21***	9.34±0.41 (0.24) 6.85±0.09	**8.95±0.10***	103±4	**10.1±0.09***	105±3	10.0±0.08	99±2
E373A	94 ± 7	9.80±0.39 (0.26)	9.67±0.42 (0.10) **7.41±0.15***	9.55±0.29 (0.22) 6.71±0.08	**8.45±0.08***	104±4	**9.3±0.09***	99±3	**9.25±0.08***	106±3
H374A	82 ± 8	8.87±0.14 -	8.87±0.09 -	9.94±0.52 (0.10) 7.24±0.13	10.9±0.07	102±2	11.6±0.08	99±2	10.1±0.07	93±2
R376A	92 ± 7	8.53±0.10 -	8.92±0.10 -	9.61±0.48 (0.15) 7.05±0.09	**10.3±0.09***	99±3	11.4±0.12	95±2	9.61±0.14	105±5
G377A	96 ± 3	**8.27±0.06***	9.12±0.25 (0.68) **7.29±0.21***	- 7.03±0.10	**9.9±0.08***	105±3	11.1±0.15	102±4	**9.14±0.15***	106±5
T378A	173 ± 11*	8.87±0.06	8.71±0.11	- 6.75±0.08	10.7±0.10	93±2	11.5±0.17	85±7	10.0±0.10	95±3
L379A	90 ± 6	**8.33±0.07***	**8.15±0.15***	9.61±0.49 (0.15) **6.63±0.11***	**9.74±0.13***	89±3	**10.5±0.20***	92±5	10.2±0.10	96±3
R380A	73 ± 5	**7.35±0.09***	**7.65±0.05***	- **6.65±0.04***	**7.74±0.07***	103±4	**8.81±0.08***	103±3	**8.21±0.11***	97±4
F381A	92 ± 5	8.97±0.06	8.94±0.05	9.22±0.51 (0.19) **6.32±0.15***	10.5±0.06	88±2	11.5±0.08	86±6	10.3±0.06	93±2
I382A	115 ± 6	8.92±0.06	8.91±0.06	9.71±0.51 (0.14) 6.79±0.12	10.9±0.12	99±3	11.3±0.09	95±2	10.2±0.12	102±4

Cell surface expression was determined through antibody detection of the N-terminal c-Myc epitope label and expressed as percentage of wild-type (WT) GLP-1R expression. Whole-cell competition radioligand binding data were analysed using either a one-site (a single pK_i) or a two-site binding curve (two pK_i values are reported with the fraction of receptors in the high affinity site reported in brackets) as determined by an *F*-test in Graphpad Prism. pK_i values represent the negative logarithm of the equilibrium dissociation constant (in molar) of agonist. Data were normalized to specific [^{125}I]-exendin(-9-39) binding. cAMP concentration response data were analysed using a three-parameter logistic curve to determine pEC_{50} and E_{max} values. pEC_{50} values represent the negative logarithm of agonist concentration that produces half maximal response. E_{max} values are maximal response as percentage of WT response. All values are expressed as mean ± s.e.m. of five independent experiments conducted in duplicate. Data were analysed using one-way analysis of variance and Dunnett's post-test. $^*P < 0.05$ (in comparison with WT response).

Extended Data Table 2 | Interactions between the GLP-1R and ExP5

ExP5	Peptide side chain density at Cβ	Peptide side chain density at Cγ	GLP-1R	Interaction
E1	yes	no	R310$^{5.40}$ A368$^{6.57}$	Hydrogen bond
L2	yes	yes	V237$^{3.40}$ I313$^{5.43}$	
V3	yes	N/A	L384$^{7.39}$ E387$^{7.42}$ L388$^{7.43}$ *T391$^{7.46}$*	
D4	no	no	Y152$^{1.47}$ V194$^{2.64}$ M233$^{3.36}$ *K197$^{2.67}$*	Potential H-bond Salt bridge
N5	yes	yes	Q234$^{3.37}$ W306$^{5.36}$	Hydrogen bond Hydrogen bond
A6	yes	N/A		
V7	yes	N/A	L384$^{7.39}$ L388$^{7.43}$	
G8	N/A	N/A		
G9	N/A	N/A		
D10	yes	no	R380$^{7.35}$	Salt bridge
L11	yes	no	L141$^{1.36}$ *Y145$^{1.40}$* *L201$^{2.71}$*	
S12	yes	N/A	T298^{ECL2} L201$^{2.71}$	
K13	yes	yes	R299^{ECL2} backbone	potential H-bond to the backbone
Q14	yes	yes	E138$^{1.33}$ L141$^{1.36}$	no side chain density for E138
M15	yes	yes	L201$^{2.71}$ K202$^{2.71}$ Y205$^{2.75}$ S206$^{2.76}$	
E16	yes	yes	Y205$^{2.75}$ R299^{ECL2} N32	Potential H-bond Salt bridge, Potential H-bond to the backbone
E17	yes	no	*Potentially TM1 stalk*	
E18	yes	yes	*Potentially TM1 stalk*	
A19	yes	N/A	Y205$^{2.75}$	
V20	yes	N/A	*V30^{NTD}* L32^{NTD} P90^{NTD}	
R21	yes	yes	*Potentially TM1 stalk*	
L22	yes	yes	*Q210^{ECL1}*	
F23	yes	yes	W214^{ECL1} *L32^{NTD}* *L35^{NTD}* *V36^{NTD}* W39^{NTD}	
I24	yes	yes	 V20^{NTD} Y69^{NTD} *L89^{NTD}* P90^{NTD} W91^{NTD}	
E25	yes	yes		
W26	yes	yes	H212^{ECL1} W214^{ECL1}	 π-stack
L27-S33			N-terminal interactions	

Residues in black are within 4 Å of the bound peptide. Residues in grey italics are within 4.5 Å of the bound peptide, but out of bonding distance and may form transient interactions. Residues in blue italics are within 4 Å in our model but there is no side-chain density in the cryo-EM map.

Extended Data Table 3 | Interactions formed between class B receptor and Gs heterotrimeric Gs proteins

G protein subunit	G protein Residue no	GLP-1R (ExP5 bound)	GLP-1R (GLP-1 bound) PDB: 5VAI	CTR (sCT bound) PDB:5UZ7
GαRas α5	R380	*F257^{ICL2}*	L256$^{2.59}$bb	K326$^{6.54}$
	D381	K334$^{5.64}$	K334$^{5.64}$	
	I383	*S258^{ICL2}*		V252^{ICL2}
	Q384	L255$^{2.58}$bb K334$^{5.64}$	L255$^{2.58}$bb K334$^{5.64}$	L248$^{2.58}$bb K326$^{5.64}$
	R385	K334$^{5.64}$ bb	K334$^{5.64}$bb	K326$^{5.64}$
	H387	L254$^{3.57}$ L255$^{2.58}$	L254$^{3.57}$	L247$^{3.57}$
	L388	L255$^{2.58}$ V331$^{5.61}$ *K334$^{5.64}$*	V331$^{5.61}$	L323$^{5.61}$
	Q390	R176$^{2.46}$	R176$^{2.46}$ E408$^{8.41}$	R180$^{2.46}$
	Y391	*H180$^{2.50}$* Y250$^{3.53}$ L251$^{3.54}$ ***L254$^{3.57}$***	H180$^{2.50}$ L359$^{6.48}$ L356$^{6.45}$ L251$^{3.54}$	Y253^{ICL2} L244$^{3.54}$
	E392	*N406$^{7.61}$* N407$^{7.62}$	N406$^{7.61}$ V405$^{7.60}$bb L401$^{7.56}$bb	***C394$^{7.60}$bb*** ***N396$^{7.62}$***
	L393	S352$^{6.41}$bb L356$^{6.45}$ ***V327$^{5.57}$*** *V331$^{5.61}$*	*S352$^{6.41}$* L356$^{6.45}$ T353$^{6.42}$	L348$^{6.45}$
	L394	*V331$^{5.61}$* *R348$^{6.37}$ (to L394 backbone)*	*L339$^{5.59}$*	M327$^{5.65}$
GαRas αN	Q35	S261^{ICL2}	S261^{ICL2} E262^{ICL2}	
	R38	E262^{ICL2}		
	Q31	Q263^{ICL2} (not support density)	Q263^{ICL2}	
	K34	*E262^{ICL2}*	Q263^{ICL2}	
GαRas β3	V217	V259^{ICL2}		
GαRas α4	R385	*(N338 not resolved in cryo EM map but likely conserved)*	N338^{ICL3}	
Gβ	D312	H171^{ICL1} K415$^{8.48}$	H171^{ICL1} K415$^{8.48}$	R404$^{8.48}$
	A309/G310 (backbone)	R419$^{8.52}$	R419$^{8.52}$	Q408$^{8.52}$
	Q44	*E423$^{8.56}$*		Q415$^{8.60}$

All receptor residues within 4 Å (4.5 Å in non-bold italics) of G protein that were evident in the cryo-EM maps of the sCT–CTR–Gs, GLP-1–GLP-1R–Gs and ExP5–GLP-1R–Gs complexes are listed. Residues in red are conserved interactions between the three structures, those in blue are conserved between the two GLP-1R structures and those in black are unique in the different structures (bb indicates backbone interactions).

nature research

Corresponding author(s): Patrick M. Sexton, Denise Wootten

☐ Initial submission ☒ Revised version ☐ Final submission

Life Sciences Reporting Summary

Nature Research wishes to improve the reproducibility of the work that we publish. This form is intended for publication with all accepted life science papers and provides structure for consistency and transparency in reporting. Every life science submission will use this form; some list items might not apply to an individual manuscript, but all fields must be completed for clarity.

For further information on the points included in this form, see Reporting Life Sciences Research. For further information on Nature Research policies, including our data availability policy, see Authors & Referees and the Editorial Policy Checklist.

Experimental design

1. Sample size

Describe how sample size was determined. Sample size calculation was not required

2. Data exclusions

Describe any data exclusions. No data were excluded

3. Replication

Describe whether the experimental findings were reliably reproduced. Experimental findings were reliably reproduced

4. Randomization

Describe how samples/organisms/participants were allocated into experimental groups. Randomization was not required

5. Blinding

Describe whether the investigators were blinded to group allocation during data collection and/or analysis. Blinding was not required

Note: all studies involving animals and/or human research participants must disclose whether blinding and randomization were used.

6. Statistical parameters

For all figures and tables that use statistical methods, confirm that the following items are present in relevant figure legends (or in the Methods section if additional space is needed).

n/a	Confirmed
☐	☒ The exact sample size (*n*) for each experimental group/condition, given as a discrete number and unit of measurement (animals, litters, cultures, etc.)
☒	☐ A description of how samples were collected, noting whether measurements were taken from distinct samples or whether the same sample was measured repeatedly
☐	☒ A statement indicating how many times each experiment was replicated
☐	☒ The statistical test(s) used and whether they are one- or two-sided (note: only common tests should be described solely by name; more complex techniques should be described in the Methods section)
☒	☐ A description of any assumptions or corrections, such as an adjustment for multiple comparisons
☐	☒ The test results (e.g. *P* values) given as exact values whenever possible and with confidence intervals noted
☐	☒ A clear description of statistics including central tendency (e.g. median, mean) and variation (e.g. standard deviation, interquartile range)
☐	☒ Clearly defined error bars

See the web collection on statistics for biologists for further resources and guidance.

Software

Policy information about availability of computer code

7. Software

Describe the software used to analyze the data in this GraphPad Prism, ImageJ, Motioncor2, Gctf, Gautomatch, EMAN2, Relion 2.03,

study.	PHENIX, MolProbity, COOT, Pymol, UCSF Chimera

For manuscripts utilizing custom algorithms or software that are central to the paper but not yet described in the published literature, software must be made available to editors and reviewers upon request. We strongly encourage code deposition in a community repository (e.g. GitHub). *Nature Methods* guidance for providing algorithms and software for publication provides further information on this topic.

Materials and reagents

Policy information about availability of materials

8. Materials availability

Indicate whether there are restrictions on availability of unique materials or if these materials are only available for distribution by a for-profit company.	There are no restriction

9. Antibodies

Describe the antibodies used and how they were validated for use in the system under study (i.e. assay and species).	All antibodies were used for Western blot analysis and have been validated. rabbit anti-Gs C-18 antibody (cat no sc-383), Santa Cruz mouse Penta-His antibody (cat no 34660), QIAGEN 680RD goat anti-mouse antibody (LI-COR) 800CW goat anti-rabbit antibody (LICOR)

10. Eukaryotic cell lines

a. State the source of each eukaryotic cell line used.	Cells used in assays were obtained from ATCC
b. Describe the method of cell line authentication used.	No authentication required
c. Report whether the cell lines were tested for mycoplasma contamination.	Cell lines were tested and are free from mycoplasma contamination
d. If any of the cell lines used are listed in the database of commonly misidentified cell lines maintained by ICLAC, provide a scientific rationale for their use.	Cells are not listed in the database

Animals and human research participants

Policy information about studies involving animals; when reporting animal research, follow the ARRIVE guidelines

11. Description of research animals

Provide details on animals and/or animal-derived materials used in the study.	Not applicable

Policy information about studies involving human research participants

12. Description of human research participants

Describe the covariate-relevant population characteristics of the human research participants.	Not applicable

Appendix III:
Two distinct domains of the glucagon-like peptide-1 receptor control peptide-mediated biased agonism

Two distinct domains of the glucagon-like peptide-1 receptor control peptide-mediated biased agonism

Received for publication, April 2, 2018, and in revised form, April 20, 2018 Published, Papers in Press, May 1, 2018, DOI 10.1074/jbc.RA118.003278

Saifei Lei[‡§1], Lachlan Clydesdale[¶], Antao Dai[‡], Xiaoqing Cai[‡], Yang Feng[‡], Dehua Yang[‡], Yi-Lynn Liang[¶], Cassandra Koole[¶2], Peishen Zhao[¶], Thomas Coudrat[¶], Arthur Christopoulos[¶3], Ming-Wei Wang[‡§‖4], Denise Wootten[¶‖5], and Patrick M. Sexton[¶‖6]

From the [‡]National Center for Drug Screening and CAS Key Laboratory of Receptor Research, Shanghai Institute of Materia Medica, Chinese Academy of Sciences, Shanghai 201203, China, the [¶]Drug Discovery Biology, Monash Institute of Pharmaceutical Sciences, Monash University, Parkville, Victoria 3052, Australia, the [§]School of Pharmacy, University of Chinese Academy of Sciences, No. 19A Yuquan Road, Beijing 100049, China, and the [‖]School of Pharmacy, Fudan University, Shanghai 201203, China

Edited by Henrik G. Dohlman

G protein–coupled receptors (GPCRs) can be differentially activated by ligands to generate multiple and distinct downstream signaling profiles, a phenomenon termed biased agonism. The glucagon-like peptide-1 receptor (GLP-1R) is a class B GPCR and a key drug target for managing metabolic disorders; however, its peptide agonists display biased signaling that affects their relative efficacies. In this study, we combined mutagenesis experiments and mapping of surface mutations onto recently described GLP-1R structures, which revealed two major domains in the GLP-1/GLP-1R/G_s protein active structure that are differentially important for both receptor quiescence and ligand-specific initiation and propagation of biased agonism. Changes to the conformation of transmembrane helix (TM) 5 and TM 6 and reordering of extracellular loop 2 were essential for the propagation of signaling linked to cAMP formation and intracellular calcium mobilization, whereas ordering and packing of residues in TMs 1 and 7 were critical for extracellular signal–regulated kinase 1/2 (pERK) activity. On the basis of these findings, we propose a model of distinct peptide–receptor interactions that selectively control how these different signaling pathways are engaged. This work provides important structural insight into class B GPCR activation and biased agonism.

This work was supported in part by National Health and Medical Research Council of Australia Project Grants 1061044, 1065410, and 1126857; National Health and Medical Research Council Program Grant 1055134; Shanghai Science and Technology Development Fund Grant 15DZ2291600; National Natural Science Foundation of China Grant 81573479; and Strategic Priority Research Program of the Chinese Academy of Sciences Grants XDA12020347 and XDA12040308. The authors declare that they have no conflicts of interest with the contents of this article.

[1] Recipient of the Postgraduate Overseas Study Fellowship from the Chinese Academy of Sciences.
[2] National Health and Medical Research Council C. J. Martin Fellow.
[3] National Health and Medical Research Council of Australia Senior Principal Research Fellow.
[4] To whom correspondence may be addressed. E-mail: mwwang@simm.ac.cn.
[5] National Health and Medical Research Council Career Development Fellow. To whom correspondence may be addressed. E-mail: denise.wootten@monash.edu.
[6] National Health and Medical Research Council Principal Research Fellow. To whom correspondence may be addressed. Tel.: 61-3-9903-9069; E-mail: patrick.sexton@monash.edu.

GPCRs[7] are ubiquitous integrators of extracellular signals for the control of cellular responses. As such, they are key drug targets, and ~40% of approved therapeutics act via this receptor class (1). Nonetheless, many potential drugs fail in late-stage clinical trials due to lack of predicted efficacy, indicating gaps in our understanding of drug action and/or the specific contributions of signaling events to the control of diseases.

It has become increasingly evident that GPCRs are highly dynamic proteins that can adopt numerous ligand-specific conformational ensembles with distinct impact on signaling and regulatory profiles, even with ligands acting via a common binding pocket, a phenomenon termed biased agonism (2, 3). This not only provides an unprecedented opportunity to sculpt biological responses for therapeutic benefit, but it also creates increased challenges for drug discovery and developmental programs to identify the spectra of ligand behavior and to elucidate structure–activity relationships linking observed behavior to physiology and disease processes.

Class B peptide hormone GPCRs bind important physiological peptides of about 30–40 amino acids, including calcitonin, amylin, adrenomedullin, calcitonin gene-related peptide, secretin, parathyroid hormones, vasoactive intestinal peptide, gastric inhibitory peptide, glucagon, and the glucagon-like peptides (4, 5). As such, these receptors are crucial targets for treatment of chronic diseases, notably osteoporosis, migraine, obesity, and type 2 diabetes. Class B GPCRs are pleiotropically coupled, and biased agonism is commonly observed when signaling is studied across multiple pathways, creating novel therapeutic opportunities. However, optimally exploiting this property requires detailed mechanistic understanding of the drivers of bias (4).

The glucagon-like peptide-1 (GLP-1) receptor (GLP-1R) is a class B GPCR that is both critical to the natural incretin response of the body and a major target for treatment of metabolic disorders. It is among the best studied for biased agonism, and such bias is readily observed for both naturally occurring

[7] The abbreviations used are: GPCR, G protein–coupled receptor; GLP-1R, glucagon-like peptide-1 receptor; TM, transmembrane; ECL, extracellular loop; pERK, phosphorylation of extracellular signal-regulated kinase 1/2; ECD, extracellular domain; GCGR, glucagon receptor; NAM, negative allosteric modulator; PDB, Protein Data Bank; $[Ca^{2+}]_i$, intracellular calcium; ANOVA, analysis of variance; hGLP-1R, human GLP-1R.

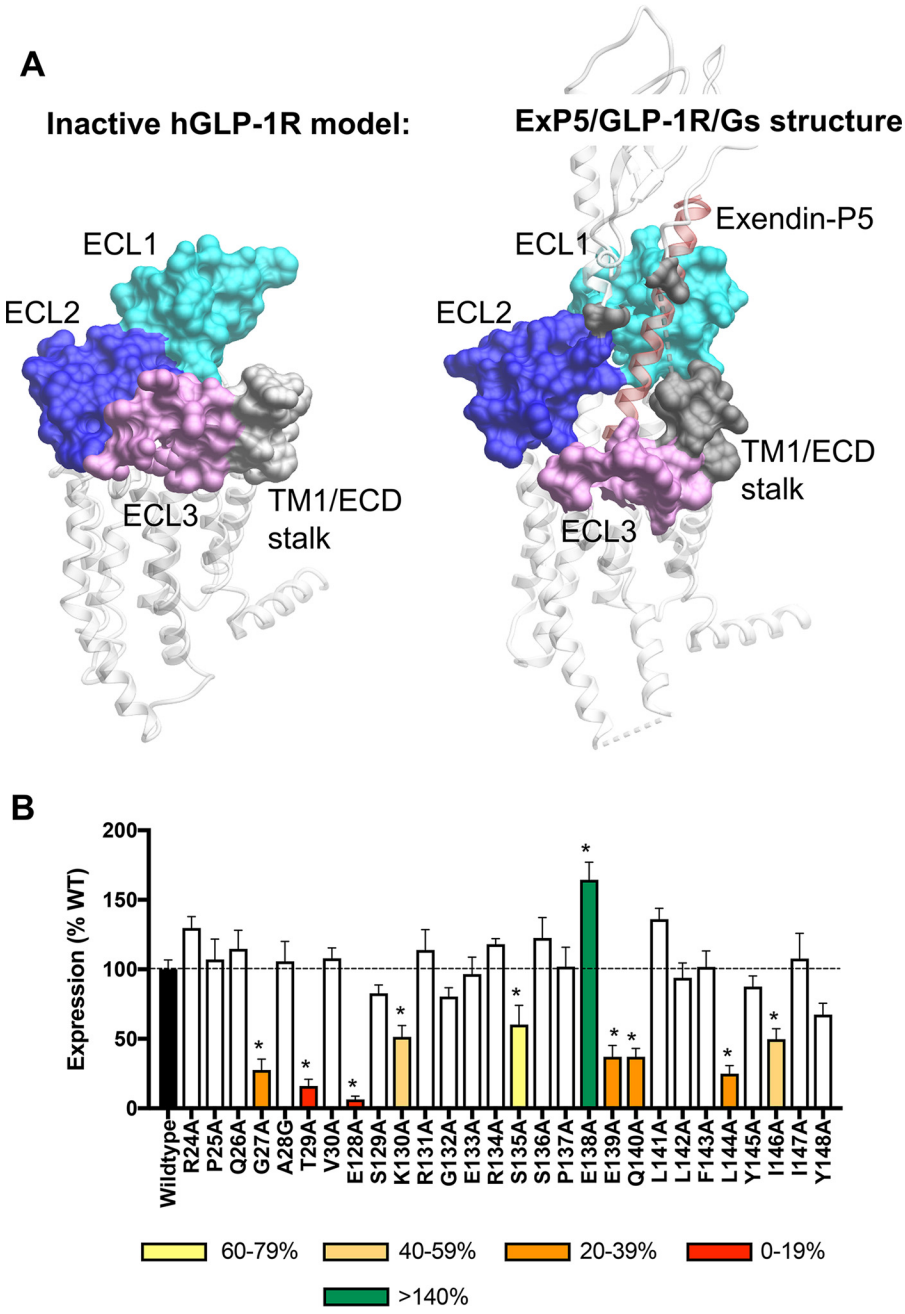

Figure 1. Location of the TM/N-terminal ECD interface in active and inactive models of the human GLP-1R and expression of GLP-1R constructs in stable cell lines. *A,* surface residues of the GLP-1R. *Left-hand panel,* inactive model of the hGLP-1R TM domain (residues 134–422) based on the inactive glucagon receptor (PDB code 4L6R). *Right-hand panel,* active full-length exendin-P5 (*ExP5*)–hGLP-1R–G_s complex (PDB code 6B3J). The far N-terminal ECD (residues 24–30) and the TM1/ECD stalk (residues 128–148) are illustrated in *gray*. ECL residues mutated in previous analyses (11) are colored by ECL. ECL1 (residues 201–223; *cyan*), ECL2 (residues 285–307; *dark blue*), ECL3 (residues 372–387; *light purple*) are shown. The position of exendin-P5 is shown as *red ribbon* representation. *B,* cell-surface expression was determined by ELISA to the N-terminal c-Myc epitope tag on the hGLP-1R and mutant hGLP-1R isogenically expressed in CHO–Flp-In cells. Data were normalized to the WT receptor. All values are mean ± S.E. of four to six independent experiments, conducted in duplicate. One-way ANOVA and Dunnett's post-test were performed to determine statistical differences (*, $p < 0.05$).

and synthetic peptide mimetics (6–11). This biased agonism alters responses in pancreatic β-cells (11) and disease models *in vivo* (10). The prevailing view for class B GPCR peptide binding and receptor activation is a two-domain theory with initial binding of the peptide C terminus to the receptor extracellular domain (ECD) that positions the peptide N terminus relative to the receptor core to facilitate receptor activation (12). The prevalence of GLP-1R biased agonism and the therapeutic implications of this behavior make understanding of the triggers for, and propagation of, bias important for rational drug design and development. We recently revealed that the extracellular loops (ECLs) of the GLP-1R play a crucial role in the biased agonism of exendin-4, oxyntomodulin, and GLP-1(7–36)-NH_2 (GLP-1): the first clinically approved GLP-1 mimetic, a biased endogenous GLP-1R peptide, and the most common circulating form of GLP-1, respectively (11, 13). Nonetheless, interpretation of the data was limited by lack of experimentally determined structure for the GLP-1R core and, indeed, any full-

Table 1

Effects of human GLP-1R TM1/N-terminal mutants on peptide ligand binding and cell-surface expression

Binding data were analyzed using a three-parameter logistic equation and normalized to the maximal binding of the radiolabeled antagonist ^{125}I-exendin-4(9–39) and the nonspecific binding in the presence of 1 μM exendin-4(9–39). pK_i is the negative logarithm of peptide affinity. All the values for binding are mean ± S.E. of three independent experiments, conducted in triplicate. Cell-surface expression was accessed through ELISA detecting the N-terminal c-Myc epitope label on the receptor. Mutant data are compared with the wildtype human GLP-1R expression and shown as percentage. The data for cell-surface expression are mean ± S.E. of four to six independent experiments, conducted in duplicate. One-way ANOVA and Dunnett's post-test were used to determine statistical differences (*, $p < 0.05$). ND, not determined.

	Whole-cell competition radioligand binding (pK_i)				Cell-surface expression (% wildtype)
	GLP-1(7–36)-NH_2	Exendin-4	Oxyntomodulin	Exendin(9–39)	
Wildtype	8.12 ± 0.06	9.31 ± 0.06	7.52 ± 0.08	7.85 ± 0.05	100 ± 7
R24A	8.10 ± 0.08	9.54 ± 0.13	7.69 ± 0.08	7.74 ± 0.06	130 ± 8
P25A	8.17 ± 0.09	9.56 ± 0.12	7.80 ± 0.08	7.71 ± 0.06	107 ± 15
Q26A	7.96 ± 0.09	9.23 ± 0.11	7.56 ± 0.10	7.72 ± 0.07	115 ± 13
G27A	ND	ND	ND	ND	28 ± 8*
A28G	7.67 ± 0.08*	8.89 ± 0.11*	7.07 ± 0.08*	7.61 ± 0.06	106 ± 15
T29A	ND	ND	ND	ND	16 ± 5*
V30A	8.16 ± 0.09	9.31 ± 0.11	7.72 ± 0.08	7.77 ± 0.08	108 ± 8
E128A	ND	ND	ND	ND	6 ± 2*
S129A	8.10 ± 0.11	9.94 ± 0.10	7.71 ± 0.15	7.79 ± 0.10	83 ± 6
K130A	8.12 ± 0.08	9.25 ± 0.07	7.52 ± 0.12	7.64 ± 0.09	51 ± 8*
R131A	8.28 ± 0.12	9.37 ± 0.09	7.72 ± 0.14	7.78 ± 0.09	114 ± 15
G132A	ND	ND	ND	ND	80 ± 6
E133A	8.16 ± 0.07	9.45 ± 0.10	7.70 ± 0.09	7.84 ± 0.10	97 ± 12
R134A	8.12 ± 0.09	9.14 ± 0.08	7.60 ± 0.12	7.65 ± 0.11	118 ± 4
S135A	8.35 ± 0.09	9.40 ± 0.10	7.79 ± 0.09	7.82 ± 0.09	60 ± 14*
S136A	7.84 ± 0.11	9.29 ± 0.07	7.39 ± 0.13	7.59 ± 0.15	123 ± 15
P137A	7.18 ± 0.13*	8.54 ± 0.09*	6.94 ± 0.12*	6.98 ± 0.18*	102 ± 14
E138A	8.22 ± 0.07	9.19 ± 0.10	7.21 ± 0.07	7.87 ± 0.07	164 ± 13*
E139A	ND	ND	ND	ND	37 ± 8*
Q140A	7.84 ± 0.15	8.65 ± 0.13*	7.68 ± 0.21	8.15 ± 0.16	37 ± 6*
L141A	7.50 ± 0.06	8.53 ± 0.06*	6.17 ± 0.28*	7.17 ± 0.06*	136 ± 8
L142A	7.89 ± 0.07	9.23 ± 0.07	6.89 ± 0.10*	7.84 ± 0.07	94 ± 11
F143A	8.19 ± 0.06	9.33 ± 0.09	7.35 ± 0.09	7.65 ± 0.06	102 ± 11
L144A	7.94 ± 0.15	9.41 ± 0.17	7.15 ± 0.19	8.03 ± 0.15	25 ± 6*
Y145A	8.25 ± 0.09	9.51 ± 0.09	7.38 ± 0.10	7.92 ± 0.07	88 ± 8
I146A	8.07 ± 0.09	9.32 ± 0.12	7.57 ± 0.14	7.91 ± 0.09	50 ± 8*
I147A	7.78 ± 0.05	9.00 ± 0.08	7.26 ± 0.08	7.67 ± 0.08	108 ± 18
Y148A	6.79 ± 0.15*	8.06 ± 0.06*	6.26 ± 0.25*	8.09 ± 0.08	67 ± 8

length and active class B GPCR structures. Recently, several near-atomic resolution structures of the GLP-1R have been published that include structures of a stabilized inhibitor-bound human receptor transmembrane (TM) domain (14), a stabilized full-length human receptor bound to a modified 11-mer peptide agonist (15), and GLP-1Rs in complex with heterotrimeric G_s protein and either GLP-1 (16) or a newly identified biased agonist, exendin-P5 (17). In the meantime, the structure of a full-length glucagon receptor (GCGR) in complex with a weak partial agonist (18) and the full-length active calcitonin receptor in complex with peptide agonist and heterotrimeric G_s were also solved (19). Collectively, this work has provided novel insights into gross conformational changes linked to the dynamics of class B GPCR activation, including marked kinking of transmembrane helix (TM) 6, outward movement of helices 6 and 7, and the interlinking ECL3, required for full activation, as well as manifest reorganization of other ECLs (16, 17, 19).

The ECD is structurally linked to the receptor core through extension of TM1, and there is accumulating evidence that the far N terminus of the ECD may have a dynamic role in class B GPCR function, both with respect to maintenance of an inactive state, as has been suggested for the glucagon receptor (GCGR) (20), and in ligand-dependent signaling (21, 22). Notably, the TM1 stalk domain is unstructured in complexes of class B receptors complexed to agonist and G protein, but it maintains an extended α-helix in GCGR bound to a partial agonist but without G protein (18). In this study, we performed alanine-scanning analysis of the GLP-1R surface of the far N-terminal 7 amino acids (residues 24–30, immediately after the receptor signal peptide) and the 21 amino acids that link TM1 and the ECD (residues 128–148), and we assessed cell-surface expression, peptide affinity, and peptide efficacy for activation of pathways linked to cAMP accumulation, intracellular calcium ($[Ca^{2+}]_i$) mobilization and phosphorylation of extracellular signal-regulated kinase 1/2 (pERK). Each of these pathways is of physiological relevance for GLP-1R signaling (4, 23), and both these regions are dynamically involved in GLP-1R peptide affinity and signal transduction. The overlay of the new data and that from our prior mutagenic analysis of the ECLs (11) onto the recently solved GLP-1R structures revealed that changes to the conformation of TMs 5 and 6 and reordering of ECL2 were essential for propagation of cAMP formation and $[Ca^{2+}]_i$ mobilization signaling, whereas ordering and packing of residues in TMs 1 and 7 were critical for pERK that is principally driven by the G_i–G$\beta\gamma$–arrestin interaction in the WT receptor.

Results

The far N-terminal ECD (Arg-24–Val-30) and TM1/ECD linker (Glu-128–Tyr-148) residues of GLP-1R were mutated to alanine by site-directed mutagenesis and stably expressed in CHO–Flp-In cells by isogenic recombination, with the exception of Ala-28 that was mutated to glycine. The location of these amino acids within the GLP-1R extracellular surface is illustrated on inactive (TM1/ECD linker only) and active hGLP-1R models in Fig. 1*A*.

Cell-surface expression levels for WT and mutant GLP-1Rs in the CHO–Flp-In stable cell lines were measured through ELISA of anti–c-Myc antibody binding to the N-terminal

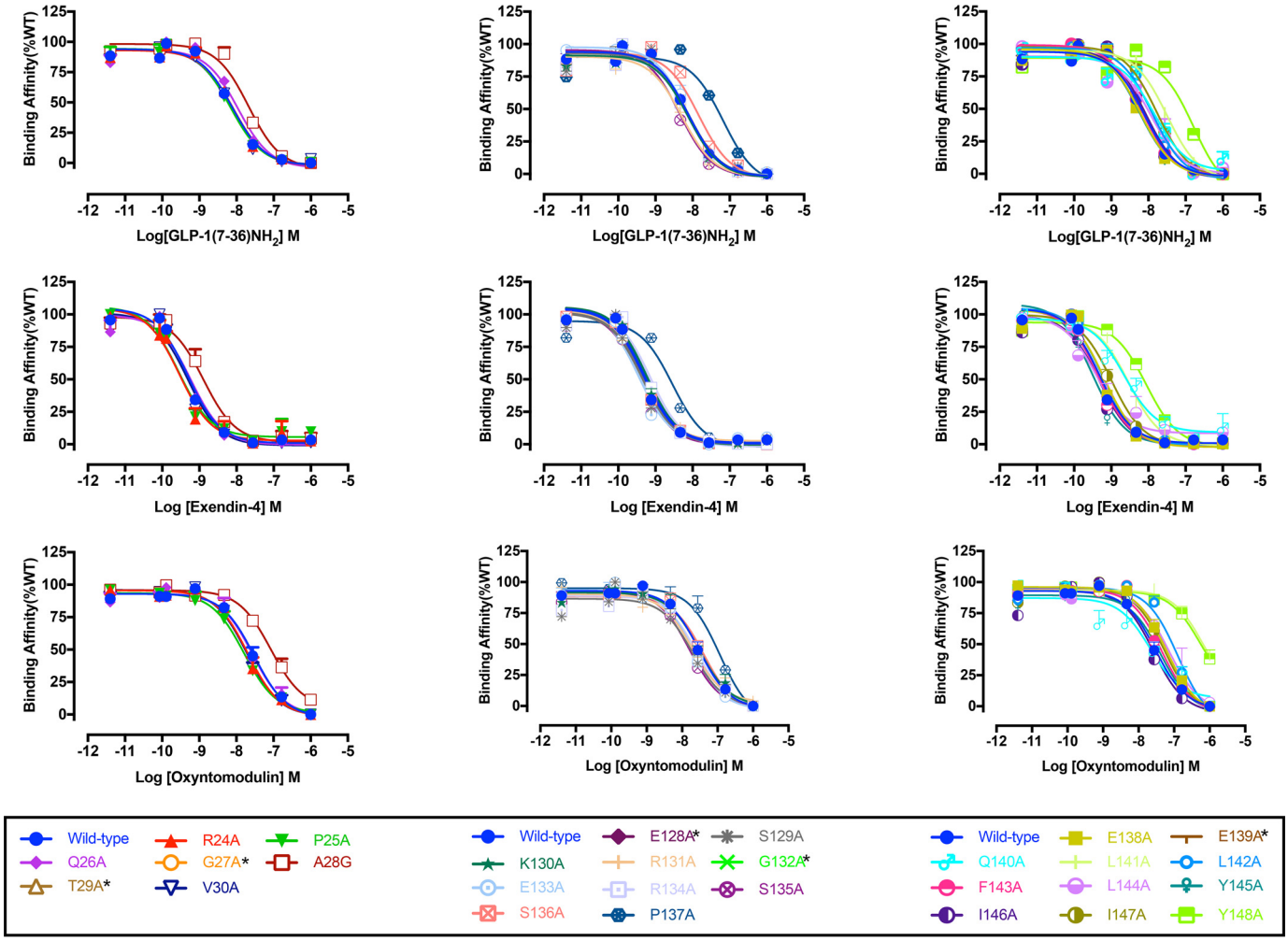

Figure 2. Competitive inhibition of ^{125}I-exendin(9–39) binding by peptide agonists for Ala mutants of the hGLP-1R N-terminal ECD and TM1 and linker region. Binding affinity data are expressed as a percentage of measured bound *versus* bound in the absence of peptide, each corrected for nonspecific binding (measured in the presence of 1 μM unlabeled exendin(9–39)). Inhibition curves of WT and mutant receptors were stimulated by GLP-1(7–36)NH_2 (*upper panels*), exendin-4 (*middle panels*), or oxyntomodulin (*lower panels*) in CHO–Flp-In cells stably expressed WT or mutant receptors. Data were fitted with a three-parameter logistic equation. All values are means ± S.E. of four to six independent experiments, conducted in duplicate.

c-Myc epitope. All receptors were expressed at the cell surface; however, the expression of G27A, T29A, E128A, K130A, S135A, E139A, Q140A, L144A, and I146A mutants was significantly lower and that of E138A was markedly higher than WT GLP-1R. All the other mutant receptors were not significantly different from the WT (Fig. 1*B* and Table 1).

Peptide agonist affinity

Heterologous whole-cell competition binding with ^{125}I–exendin-4(9–39) was performed to determine peptide agonist affinity for the WT and mutant GLP-1Rs. As reported previously (6), at the WT receptor exendin-4 had the highest affinity (pK_i ≈9.31), followed by GLP-1 (pK_i ≈8.12), whereas oxyntomodulin had the lowest affinity (pK_i ≈7.52) (Table 1 and Fig. 2). No specific binding window could be established for the G132A mutant, despite good cell–surface expression by ELISA, or for the low-expressing mutants G27A, T29A, E128A, and E139A; for all others, competitive binding isotherms were established for each of the peptides. Of the far N-terminal ECD residues that exhibited specific binding, only the A28G mutation modified affinity (<5-fold) for GLP-1 and exendin-4, with a similar trend for oxyntomodulin (Figs. 2 and 3*A* and Table 1). Of the TM1/stalk residues, P137A, L141A, and Y148A mutations reduced affinity for each of the agonist peptides, whereas the P137A and L141A mutations also reduced affinity of the antagonist exendin-4(9–39). Ligand-specific reductions in affinity were seen for Q140A (exendin-4) and L142A (oxyntomodulin). All other mutations were without significant effect on peptide affinity (Figs. 2 and 3*A* and Table 1).

Agonist efficacy

Concentration-response curves for each of the peptides were established to determine agonist potency and maximal responses for canonical signaling endpoints, cAMP accumulation, $[Ca^{2+}]_i$ mobilization, and pERK1/2 (Figs. 3, *B–D*, and 4–6 and Tables 2–4). These data were subject to operational modeling (26) to determine affinity-independent measures of efficacy (τ for each pathway). The operational efficacy term "τ" is a measure of the number of receptors that need to be occupied to give a specified response. The τ values were normalized to receptor expression to derive a receptor expression-indepen-

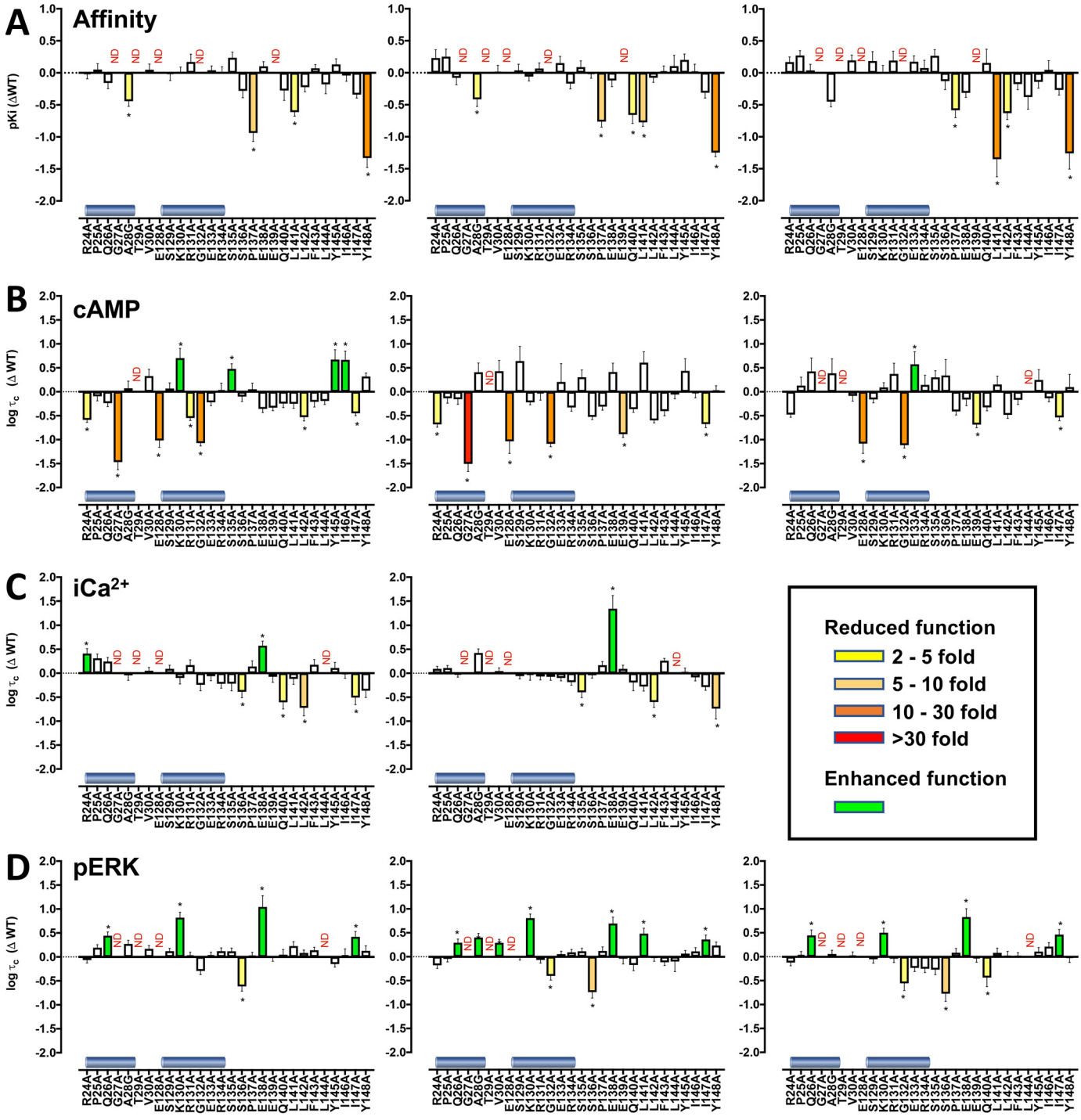

Figure 3. Changes in affinity (*A*) and efficacy (*B–D*) of the agonists GLP-1, exendin-4, and oxyntomodulin at mutant GLP-1Rs. *A*, pK_i values for the agonist peptides were derived from competition of ^{125}I–exendin-4(9–39) binding. Data were plotted as differences in pIC_{50} of the alanine mutants compared with the wildtype (*WT*) hGLP-1R for GLP-1 (*left panel*), exendin-4 (*middle panel*), and oxyntomodulin (*right panel*). All pIC_{50} values were mean ± S.E. of three independent experiments performed in triplicate. *B–D*, $\Delta\log\tau_c$ values are the difference in the coupling efficacy ($\log\tau_c$) for cAMP accumulation (*B*), $[Ca^{2+}]_i$ mobilization (*C*), and ERK phosphorylation (*pERK*) (*D*) of the alanine mutant GLP-1Rs compared with the WT receptor for GLP-1 (*left panels*), exendin-4 (*middle panels*), and oxyntomodulin (*right panels*). All functional values are mean ± S.E. of four to six independent experiments, conducted in duplicate. One-way ANOVA and Dunnett's post-test were performed to determined statistical differences (*, $p < 0.05$), and the *bars* are colored according to the fold-change between WT and mutant receptors (*yellow,* 2–5-fold decrease; *light orange,* 5–10-fold decrease; *dark orange,* 10–30-fold decrease; *red,* >30-fold decrease; *green,* increased affinity (*A*) or efficacy (*B–D*)). *N.D.,* not defined.

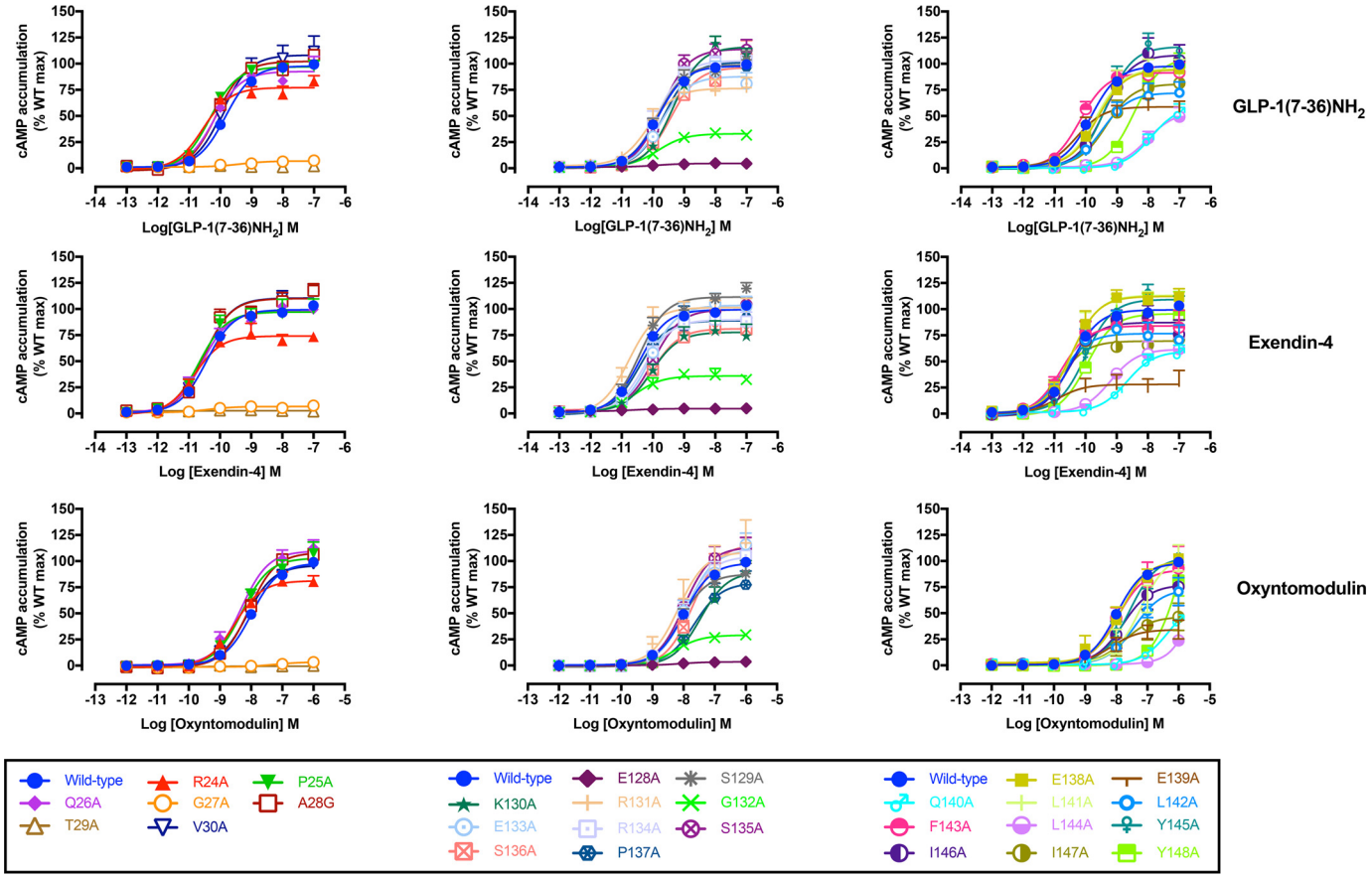

Figure 4. cAMP concentration-response curves for Ala mutants of the hGLP-1R N-terminal ECD and TM1 and linker region. Concentration-response curves for cAMP accumulation of WT and mutant receptors were stimulated by GLP-1(7–36)NH_2 (*upper panels*), exendin-4 (*middle panels*), or oxyntomodulin (*lower panels*) in CHO–Flp-In cells stably expressing WT or mutant receptors. Data were normalized to the response elicited by the WT and analyzed with an operational model of agonism. All values are means ± S.E. of four to six independent experiments, conducted in duplicate.

dent and quantitative measure of pathway activation "τ_c" for individual peptides at each of the mutants (27, 28).

cAMP accumulation

Within the far N terminus of the ECD, mutants G27A and T29A that had poor expression displayed very weak to no measurable cAMP response. Unlike binding affinity, which was unaltered, the R24A mutant had reduced efficacy for GLP-1 and exendin-4 (Figs. 3*B* and 4 and Table 2). Within the TM1/ECD linker there was only limited correlation between effects on binding affinity and cAMP efficacy and on cAMP efficacy between peptides. E128A that was poorly expressed responded very weakly to all peptides. The I147A mutant induced modest loss of efficacy, and the G132A mutant exhibited 10–30-fold decreased efficacy for all peptides. The L142A mutant had a significantly attenuated efficacy for GLP-1, with similar fold decreases for exendin-4 and oxyntomodulin, although these latter effects did not achieve significance. The E139A mutant that had undetectable ^{125}I–exendin-4(9–39) binding had reduced efficacy with exendin-4 and to a lesser extent oxyntomodulin but not GLP-1. There were statistically significant increases in efficacy for oxyntomodulin at E133A, whereas K130A, S135A, Y145A, and I146A caused selective increases in GLP-1 efficacy, and R131A induced a weak and selective decrease in GLP-1 efficacy (Figs. 3*B* and 4 and Table 2).

iCa^{2+} mobilization

Because of relatively weak $[Ca^{2+}]_i$ mobilization by oxyntomodulin, only a single high concentration (~3 μM) was assessed. For GLP-1 and exendin-4, no measurable response was seen at the poorly expressed G27A, T29A, and E128A mutants, whereas the E138A mutant exhibited increased efficacy for both peptides, even after correction for the higher cell-surface expression (Figs. 3*C* and 5 and Table 3). There was decreased efficacy for both peptides with the L142A mutant, whereas L144A abolished $[Ca^{2+}]_i$ mobilization, despite unaltered cAMP efficacy. There was selective loss of exendin-4 efficacy at the S135A and Y148A mutants and of GLP-1 efficacy at the S136A, Q140A, and I147A mutants, although these effects were relatively small (Figs. 3*C* and 5 and Table 3). There was also a weak and selective increase in GLP-1 efficacy at the R24A mutant, whereas the opposite effect was seen for GLP-1–dependent cAMP efficacy (Fig. 3, *C versus B*, and Tables 2 and 3). Of interest, although not quantitative, there was no measurable response for the single high concentration of oxyntomodulin at the P137A and Y148A mutants, despite approximately WT levels of cell-surface receptor expression and limited (for P137A) or no (Y148A) effect of the mutation on oxyntomodulin affinity (Fig. 3*C* and Table 1).

Table 2

Effects of human GLP-1R TM1/N-terminal mutants on agonist-mediated cAMP accumulation

cAMP accumulation data were analyzed using a three-parameter logistic equation to determine pEC_{50} and E_{max} values. pEC_{50} is the negative logarithm of the molar concentration of agonist that induced half the maximal response. E_{max} for mutants is expressed as a percentage of wildtype. $Log\tau_c$ is the operational efficacy value (determined via the Black and Leff operational model (24)), corrected for cell-surface expression of GLP-1R. All values for cAMP accumulation are mean ± S.E. of four to six independent experiments, conducted in duplicate. One-way ANOVA and Dunnett's post-test were used to determine statistical differences (*, $p < 0.05$). ND, not determined.

	Agonist-mediated cAMP accumulation								
	GLP-1(7–36)-NH_2			Exendin-4			Oxyntomodulin		
	pEC_{50}	E_{max}	$Log\tau_c$	pEC_{50}	E_{max}	$Log\tau_c$	pEC_{50}	E_{max}	$Log\tau_c$
Wildtype	9.84 ± 0.04	97.77 ± 1.13	0.77 ± 0.07	10.43 ± 0.03	99.32 ± 0.90	0.81 ± 0.09	7.99 ± 0.03	98.16 ± 1.13	0.73 ± 0.06
R24A	10.55 ± 0.14*	77.09 ± 2.92*	0.18 ± 0.05*	10.83 ± 0.16	74.16 ± 3.10*	0.13 ± 0.06*	8.52 ± 0.11	81.17 ± 2.99	0.25 ± 0.06
P25A	10.33 ± 0.08	97.02 ± 2.21	0.67 ± 0.10	10.67 ± 0.18	97.12 ± 4.65	0.67 ± 0.10	8.29 ± 0.11	102.90 ± 4.26	0.86 ± 0.18
Q26A	10.20 ± 0.09	92.56 ± 2.61	0.53 ± 0.07	10.56 ± 0.08	97.69 ± 2.24	0.66 ± 0.11	8.31 ± 0.10	109.70 ± 3.98	1.15 ± 0.28
G27A	9.36 ± 0.49	6.91 ± 0.99*	−0.70 ± 0.16*	10.39 ± 0.57	6.62 ± 0.94*	−0.70 ± 0.16*	ND	ND	ND
A28G	10.14 ± 0.10	102.20 ± 3.14	0.84 ± 0.15	10.51 ± 0.12	110.00 ± 3.61	1.22 ± 0.19	8.10 ± 0.07	108.20 ± 3.07	1.13 ± 0.30
T29A	ND	ND	ND	ND	ND	ND	ND	ND	ND
V30A	9.93 ± 0.16	108.20 ± 5.48	1.09 ± 0.14	10.50 ± 0.10	110.50 ± 3.01	1.24 ± 0.22	8.14 ± 0.14	95.92 ± 5.19	0.64 ± 0.11
E128A	9.87 ± 0.39	4.59 ± 0.42*	−0.25 ± 0.14*	10.62 ± 0.72	4.63 ± 0.48*	−0.22 ± 0.25	8.08 ± 0.53	4.15 ± 0.83*	−0.35 ± 0.20*
S129A	9.85 ± 0.10	98.92 ± 3.30	0.83 ± 0.12	10.44 ± 0.09	111.50 ± 2.93	1.45 ± 0.31*	8.10 ± 0.11	87.57 ± 3.84	0.57 ± 0.07
K130A	9.35 ± 0.09	116.20 ± 3.83*	1.47 ± 0.20*	10.05 ± 0.18	77.74 ± 4.44*	0.59 ± 0.05	7.46 ± 0.17	89.78 ± 7.01	0.82 ± 0.10
R131A	10.15 ± 0.21	76.34 ± 4.84*	0.22 ± 0.05*	10.78 ± 0.15	101.40 ± 4.12	0.78 ± 0.14	8.16 ± 0.26	108.70 ± 10.93	1.10 ± 0.22
G132A	9.83 ± 0.16	33.04 ± 1.67*	−0.31 ± 0.06*	10.58 ± 0.25	35.90 ± 2.36*	−0.28 ± 0.06*	8.29 ± 0.12	29.04 ± 1.30*	−0.39 ± 0.06*
E133A	9.74 ± 0.17	87.76 ± 4.92	0.55 ± 0.07	10.09 ± 0.16	103.40 ± 5.28	1.01 ± 0.38	7.90 ± 0.11	110.50 ± 5.20	1.30 ± 0.26*
R134A	9.86 ± 0.12	102.80 ± 4.06	0.80 ± 0.15	10.28 ± 0.17	89.67 ± 4.44	0.48 ± 0.08	7.97 ± 0.10	104.30 ± 4.41	0.87 ± 0.20
S135A	9.72 ± 0.15	114.00 ± 5.30*	1.24 ± 0.11*	9.99 ± 0.09	99.42 ± 2.79	1.11 ± 0.15	7.99 ± 0.11	113.40 ± 5.13	1.03 ± 0.14
S136A	9.42 ± 0.23	96.37 ± 7.34	0.67 ± 0.10	10.00 ± 0.10	81.16 ± 2.54*	0.29 ± 0.05	7.70 ± 0.10	116.20 ± 5.12	1.07 ± 0.33
P137A	9.64 ± 0.12	101.30 ± 3.90	0.82 ± 0.13	10.45 ± 0.29	88.74 ± 7.37	0.50 ± 0.07	7.65 ± 0.20	79.11 ± 6.64	0.32 ± 0.07
E138A	9.63 ± 0.15	94.25 ± 4.49	0.41 ± 0.08	10.46 ± 0.14	112.30 ± 4.24*	1.22 ± 0.18	7.86 ± 0.16	100.40 ± 6.56	0.57 ± 0.13
E139A	10.29 ± 0.19	58.81 ± 3.12*	0.43 ± 0.06	10.90 ± 0.51	28.03 ± 3.75*	−0.08 ± 0.07*	8.16 ± 0.31	34.23 ± 3.94*	0.04 ± 0.06*
Q140A	7.91 ± 0.15*	59.59 ± 5.48*	0.52 ± 0.08	8.68 ± 0.14*	59.75 ± 3.60*	0.45 ± 0.07	6.32 ± 0.18*	63.82 ± 9.80	0.40 ± 0.07
L141A	9.68 ± 0.18	95.20 ± 5.60	0.51 ± 0.09	10.43 ± 0.12	113.20 ± 3.68*	1.42 ± 0.23	7.22 ± 0.18*	106.90 ± 10.38	0.88 ± 0.18
L142A	9.48 ± 0.19	72.12 ± 4.84*	0.24 ± 0.08*	10.79 ± 0.27	76.65 ± 5.75*	0.21 ± 0.05	7.41 ± 0.18	72.94 ± 5.98	0.25 ± 0.08
F143A	10.18 ± 0.13	91.47 ± 3.55	0.56 ± 0.11	10.78 ± 0.21	84.00 ± 4.91*	0.41 ± 0.10	7.96 ± 0.24	91.72 ± 9.10	0.56 ± 0.10
L144A	8.03 ± 0.18*	53.89 ± 5.51*	0.57 ± 0.07	8.90 ± 0.14*	68.52 ± 3.71*	0.75 ± 0.09	ND	ND	ND
Y145A	9.36 ± 0.13	116.40 ± 5.51*	1.44 ± 0.21*	10.00 ± 0.09	109.30 ± 3.28	1.25 ± 0.25	7.57 ± 0.11	103.90 ± 4.88	0.98 ± 0.22
I146A	9.41 ± 0.16	108.30 ± 6.35	1.43 ± 0.18*	10.55 ± 0.21	87.23 ± 5.09	0.78 ± 0.10	7.79 ± 0.27	77.14 ± 8.62	0.59 ± 0.07
I147A	9.34 ± 0.20	80.68 ± 5.54*	0.32 ± 0.05*	10.83 ± 0.39	69.46 ± 7.47*	0.14 ± 0.07*	7.74 ± 0.36	46.61 ± 6.97	0.19 ± 0.07*
Y148A	8.45 ± 0.12*	106.20 ± 6.02	1.08 ± 0.07	9.96 ± 0.29	95.57 ± 9.29	0.84 ± 0.10	5.95 ± 0.50*	173.10 ± 106.70*	0.83 ± 0.27

ERK1/2 phosphorylation

As seen with the other pathways, the poorly expressed mutants G27A, T29A, and E128A had no measurable pERK response to any of the peptides. For the far N-terminal ECD mutations, there was a slightly increased efficacy for all peptides with the Q26A mutant and a selective weak increase in efficacy for exendin-4 at the A28G and V30A mutants (Figs. 3*D* and 6 and Table 4). For the TM1/ECD linker, there was increased efficacy for all three peptides at the K130A, E138A and I147A mutants and decreased efficacy at the S136A mutant. A weak loss of efficacy for exendin-4 and oxyntomodulin, but not GLP-1, occurred with the G132A mutant, whereas the L144A mutant abolished pERK response to GLP-1 and oxyntomodulin but did not alter efficacy for exendin-4. Of the remaining mutants, only L141A (increased exendin-4 efficacy) and Q140A (weak loss of oxyntomodulin efficacy) had any significant effect (Figs. 3*D* and 6 and Table 4).

Discussion

Structural insights into GLP-1R biased agonism

Our results indicate that the far N terminus and the linker region between TM1 and the ECD play discrete roles in receptor stability and expression and in peptide-specific signaling. Recent advances in structural determination for class B GPCRs and particularly the GLP-1R provide an unprecedented opportunity to map key surface residues in three-dimensional space relevant to both inactive and active structures. For the GLP-1R, four new structures have recently been solved, which include a modified human GLP-1R TM domain structure bound to negative allosteric modulators (NAMs) (14), a thermostabilized full-length human GLP-1R bound to a modified 11-mer agonist peptide (15), a fully active rabbit GLP-1R in complex with GLP-1 and the heterotrimeric G_s protein (16), and human GLP-1R in complex with the biased agonist, exendin-P5, and the G_s protein (17). Details of structures, including differences from WT human GLP-1R, are described in Table 5. This work complements the previously published inactive structures of the related GCGR (29, 30). The NAM-bound GLP-1R contains structural alterations, including an introduced cysteine bridge between TM helices 5 and 6, that disrupt key networks of the native inactive receptor. As such, we have used the inactive GCGR (PDB code 4L6R) (29) as a template to model the inactive GLP-1R (Fig. 1*A*) (28). The active rabbit GLP-1R complex has a global resolution of 4.1 Å, with limited side-chain resolution and ambiguity in potential modeling of ECLs, whereas the exendin-P5–GLP-1R complex has a global resolution of 3.3 Å with good side-chain resolution for most of the receptor; we have used this structure as the principal template for comparative mapping of the effects of mutations between active and inactive states (Fig. 1*A*). All full-length structures lack density for residues 24–28 of the far N terminus, indicating that this segment is flexible upon ligand binding. However, the position of Val-30 that is resolved in the structures suggests that the far N-terminal residues likely make transient interactions with

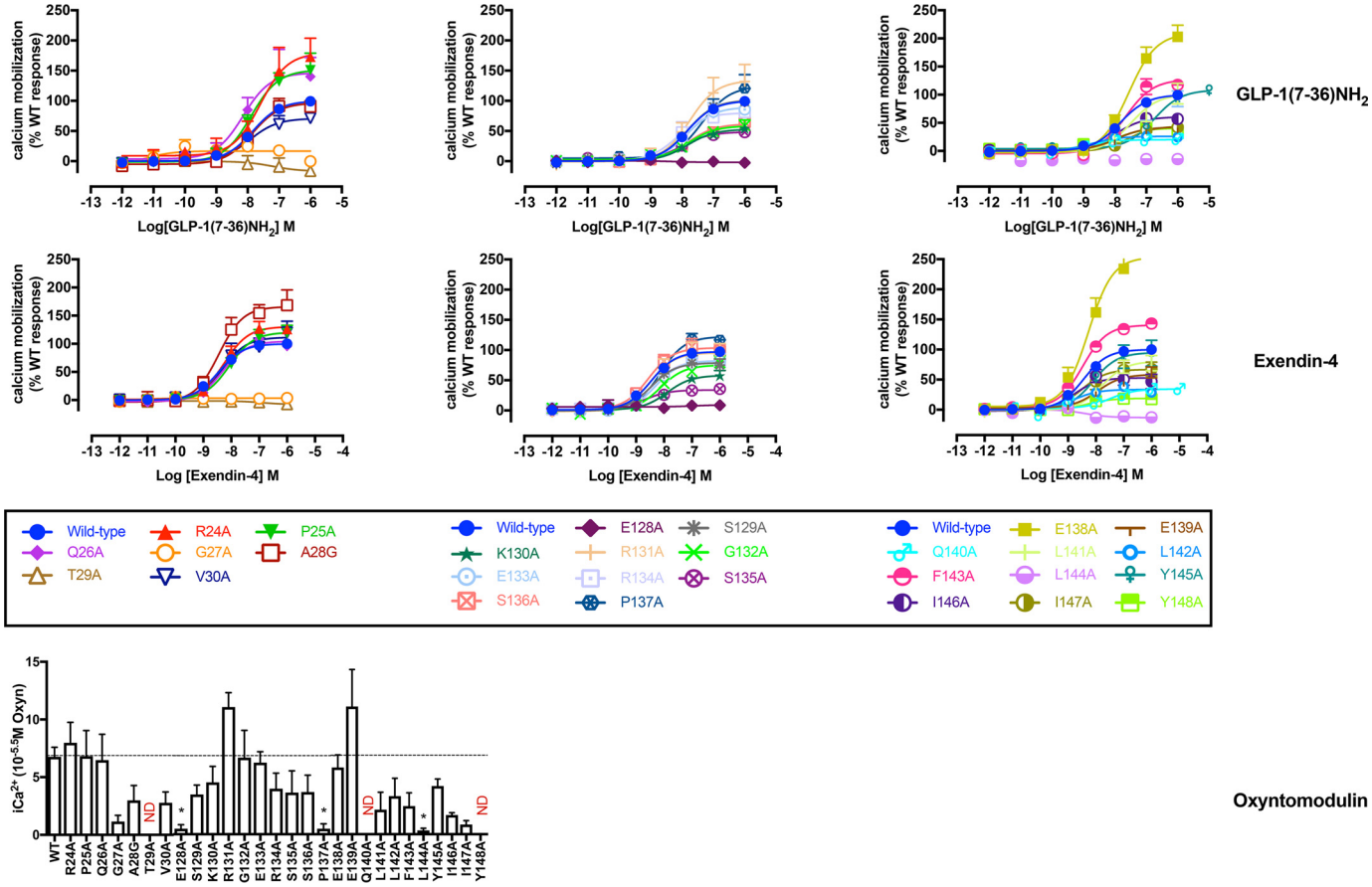

Figure 5. $[Ca^{2+}]_i$ mobilization concentration-response curves for Ala mutants of the hGLP-1R N-terminal ECD and TM1 and linker region. Concentration-response curves of $[Ca^{2+}]_i$ mobilization of WT and mutant receptors were stimulated by GLP-1(7–36)NH_2 (*upper panels*), exendin-4 (*middle panels*), or oxyntomodulin (*lower panels*) in CHO–Flp-In cells stably expressing WT or mutant receptors. Data were normalized to the response elicited by the WT and analyzed with an operational model of agonism. All values are means ± S.E. of four to six independent experiments, conducted in duplicate.

ECLs 2 and 3 and/or the peptide agonist (Fig. 7). The new data are considered holistically consistent with previously published ECL alanine-scanning mutagenesis studies (11, 13) to yield a comprehensive structure-function analysis of signal propagation networks in the GLP-1R. Nonetheless, as with all such structure–function analyses, our observations are influenced by the recombinant cellular environment, including the relative expression of transducer and regulatory proteins that will differ from endogenous sites of receptor expression.

Structural reorganization upon receptor activation

ECD–receptor core interactions—There is accumulating evidence that interactions between the ECD and TM core of class B GPCRs contribute to receptor quiescence and peptide-mediated receptor activation (20, 21, 31). For the related GCGR, interactions of the far N terminus and the residues in ECL3 contribute to maintenance of a quiescent state (20), although ground state interactions at the intracellular face also play a key role (22, 32, 33). As noted above, the far N terminus is dynamic in peptide-bound states (15, 16), making interpretation of mutations in the context of available structures difficult. The dramatic loss of cell-surface expression for G27A and T29A is indicative of the important roles of these amino acids in receptor stability, potentially via loss of stabilizing interaction between Thr-29 and the receptor core that would be consistent with a role of the far N terminus in maintaining receptor quiescence. Nevertheless, the GLP-1R is expressed at the cell surface when the full ECD is truncated (31), suggesting that loss of receptor expression is due to destabilizing interactions of the modified ECD. Glycines provide structural flexibility, and Gly-27 may be required for favorable positioning of Thr-29. In the active GLP-1- and exendin-P5–bound receptors, Thr-29 is proximal to the peptide ligand, although not within hydrogen-bonding distance. In the structure of the modified 11-mer bound receptor, the position of the ECD is not constrained by peptide binding, where Thr-29 interacts with the linker between TM1 and the ECD (Fig. 7*B*).

Class B GPCRs, including the GLP-1R, exhibit an extracellular-oriented V-shape cavity within the TM bundle that provides domain separation of the external facing segments of TMs 1, 7, and 6, and TMs 2–5 (Fig. 8*A*). Nonetheless, in the inactive model, there are key hydrogen-bonded interactions between Asp-198 of TM2 and Tyr-145, Tyr-148, and Thr-149 of TM1 that coordinate Tyr-145 and Tyr-148 away from TM7 (Fig. 9*A*), and this facilitates tight packing of TMs 1 and 7. Consistent with this, D198A mutation leads to marked loss of receptor expression and/or GLP-1-stimulated cAMP signaling (34–36). In the active, exendin-P5–bound structure, this hydrogen bond network is weakened, with loss of interactions between Asp-

Table 3

Effects of human GLP-1R TM1/N-terminal mutants on agonist-mediated $[Ca^{2+}]_i$ mobilization

$[Ca^{2+}]_i$ mobilization data were analyzed using a three-parameter logistic equation to determine pEC_{50} and E_{max} values. pEC_{50} is the negative logarithm of the molar concentration of agonist that induced half the maximal response. E_{max} for mutants is expressed as a percentage of wildtype. $Log\tau_c$ is the operational efficacy value (determined via the Black and Leff operational model (24)), corrected for cell-surface expression of GLP-1R. All values for cAMP accumulation are mean ± S.E. of four to six independent experiments, conducted in duplicate. One-way ANOVA and Dunnett's post-test were used to determine statistical differences (*, $p < 0.05$). ND, not determined.

	Agonist-mediated intracellular calcium mobilization					
	GLP-1(7–36)-NH_2			Exendin-4		
	pEC_{50}	E_{max}	$Log\tau_c$	pEC_{50}	E_{max}	$Log\tau_c$
Wildtype	7.83 ± 0.04	100.00 ± 1.11	−0.22 ± 0.03	8.45 ± 0.04	100.00 ± 1.35	−0.22 ± 0.02
R24A	7.60 ± 0.27	179.60 ± 20.27*	0.19 ± 0.10*	8.25 ± 0.12	130.40 ± 5.76*	−0.12 ± 0.05
P25A	7.89 ± 0.17	151.30 ± 11.07*	0.09 ± 0.09	8.07 ± 0.14	120.50 ± 6.80*	−0.11 ± 0.05
Q26A	8.14 ± 0.29	146.40 ± 16.50*	0.02 ± 0.09	8.31 ± 0.12	104.50 ± 4.87	−0.24 ± 0.05
G27A	ND	16.77 ± 4.36*	ND	ND	ND	ND
A28G	7.86 ± 0.14	96.66 ± 5.98	−0.27 ± 0.10	8.45 ± 0.19	165.90 ± 11.23*	0.21 ± 0.09
T29A	ND	ND	ND	ND	ND	ND
V30A	7.93 ± 0.24	70.75 ± 7.07*	0.17 ± 0.07	8.31 ± 0.24	111.50 ± 9.64	−0.17 ± 0.06
E128A	ND	ND	ND	ND	ND	ND
S129A	7.83 ± 0.12	101.30 ± 5.03	−0.13 ± 0.07	8.47 ± 0.19	80.73 ± 5.52	−0.27 ± 0.06
K130A	7.83 ± 0.18	52.81 ± 4.09*	−0.32 ± 0.13	7.89 ± 0.17	59.33 ± 4.30*	−0.25 ± 0.11
R131A	7.76 ± 0.25	133.80 ± 14.52*	−0.05 ± 0.11	8.50 ± 0.24	98.00 ± 8.13	−0.28 ± 0.07
G132A	7.79 ± 0.20	58.45 ± 4.75*	−0.47 ± 0.13	8.14 ± 0.23	76.96 ± 7.21*	−0.29 ± 0.07
E133A	7.84 ± 0.18	89.51 ± 6.77	−0.28 ± 0.10	8.30 ± 0.21	84.37 ± 6.62	−0.31 ± 0.06
R134A	8.15 ± 0.32	79.99 ± 9.90	−0.44 ± 0.09	8.36 ± 0.19	84.59 ± 5.60	−0.40 ± 0.06
S135A	7.99 ± 0.20	48.35 ± 3.85*	−0.44 ± 0.15	8.71 ± 0.22	34.19 ± 2.48*	−0.61 ± 0.11*
S136A	7.81 ± 0.18	61.68 ± 4.72*	−0.61 ± 0.12*	8.56 ± 0.16	106.70 ± 5.75	−0.26 ± 0.06
P137A	7.35 ± 0.25	124.00 ± 14.18	0.08 ± 0.12	8.13 ± 0.10	126.00 ± 5.21	−0.04 ± 0.08
E138A	7.56 ± 0.13	209.20 ± 11.92*	0.35 ± 0.10*	8.27 ± 0.20	253.40 ± 18.09*	1.13 ± 0.27*
E139A	7.94 ± 0.20	42.50 ± 3.51*	−0.30 ± 0.11	7.94 ± 0.21*	58.47 ± 4.87*	−0.12 ± 0.08
Q140A	8.89 ± 0.30*	20.06 ± 2.38*	−0.83 ± 0.14*	7.49 ± 0.42*	34.38 ± 4.54*	−0.41 ± 0.17
L141A	7.49 ± 0.25	101.00 ± 11.56	−0.34 ± 0.11	7.79 ± 0.18	80.46 ± 6.34	−0.49 ± 0.09
L142A	8.74 ± 0.32*	25.97 ± 2.71*	−0.95 ± 0.17*	8.77 ± 0.23	33.56 ± 2.55*	−0.82 ± 0.11*
F143A	7.65 ± 0.12	127.20 ± 7.06	−0.05 ± 0.11	8.48 ± 0.08	140.70 ± 3.98*	0.05 ± 0.05
L144A	ND	ND	ND	ND	ND	ND
Y145A	6.76 ± 0.20*	108.50 ± 10.35	−0.12 ± 0.12	8.10 ± 0.25	94.96 ± 9.30	−0.19 ± 0.09
I146A	7.97 ± 0.19	60.52 ± 4.60*	−0.23 ± 0.10	8.80 ± 0.28	52.91 ± 5.09*	−0.30 ± 0.07
I147A	7.60 ± 0.22	44.28 ± 4.42*	−0.73 ± 0.15*	8.50 ± 0.28	66.87 ± 6.33*	−0.51 ± 0.07
Y148A	7.99 ± 0.25	40.42 ± 3.79*	−0.59 ± 0.14	8.30 ± 0.21	18.91 ± 1.50*	−0.95 ± 0.22*

198 and both Tyr-148 and Thr-149, facilitating the movement of TM1 toward TM7, whereas the kink in TM1 is stabilized by hydrogen bonding of the side chain of Thr-149 with the backbone oxygen of Tyr-145 (Fig. 9*B*). A similar pattern of interaction is observed in the 11-mer bound structure (Fig. 9*E*). Although the position of the kink in TM1 of the GLP-1/GLP-1R structure is likely conserved (17) (although modeled differently in 5VAI), there is further loss of the interaction between Tyr-145 and Asp-198, and this leads to an anti-clockwise rotation of the upper end of TM1, with a parallel rotation of TM7 that is not seen in the exendin-P5 structure (Fig. 9, *B* and *C*). This likely contributes to the distinct conformation of ECL3 between the GLP-1– and exendin-P5–bound structures that has been linked to efficacy differences of the two peptides (17).

Both Tyr-148 and Thr-149 (37, 38) play important roles in peptide agonist affinity but do not make direct interactions with GLP-1 in the active structure, and the same is true for P137A and L141A in the TM1 stalk. Thus, these residues contribute to the reorganization of TM1 and packing with TM7. These changes are also likely to impact the position of Glu-139. Mutation of this amino acid causes loss of exendin-4(9–39) binding. In the GLP-1–bound active structure, the side chain of Glu-139 is directed toward the GLP-1 peptide, suggesting a direct interaction that may be more prevalent for the truncated exendin peptide (and indeed, this is observed in the exendin-P5/GLP-1R/G_s structure (17)). This would be consistent with the lack of effect of the E139A mutant on GLP-1 signaling, and only limited attenuation of oxyntomodulin and exendin-4–mediated cAMP production (Fig. 3). Of the TM1 stalk residues, only mutations to Thr-149 also translate into a major impact on signaling (37, 38), implying that its role in structural reorganization is also critical for activation transition and effector binding. This loss can be recovered by allosteric modulator binding at the intracellular face of the receptor that is predicted to destabilize ground state interactions at the base of the receptor (14, 37, 38).

In the active and G_s protein-complexed receptor structures, the linker region between the ECD and the core is poorly resolved, suggesting a high degree of flexibility even when the peptide is bound. In the inactive GCGR (PDB 4L6R) (29), the TM1 stalk is present as an extended α-helix, and although this may be partially due to crystal-packing artifacts, an extended α-helix is also present in the structure of the full-length GCGR bound to a partial agonist peptide, NNC1702 (Fig. 7) (18). This suggests that order to disorder transition of the TM1 stalk may be required for full receptor activation. Indeed, this would be required to accommodate the movement of TM1 toward TM7, seen in the active and active-like structures. An important role for the TM1 stalk is supported by our current mutagenesis data (Fig. 3). Polar residues in this region, particularly Ser-136, Lys-130, and Glu-138, had effects on peptide signaling in a pathway- and peptide-specific manner, indicating that formation and disruption of interactions formed by these amino acids contribute to conformational transition for activation. Similar behavior was seen for the G132A mutant, suggesting that backbone flexibility plays a role in these effects. Somewhat surprisingly, E128A had a profound effect on receptor expression, presum-

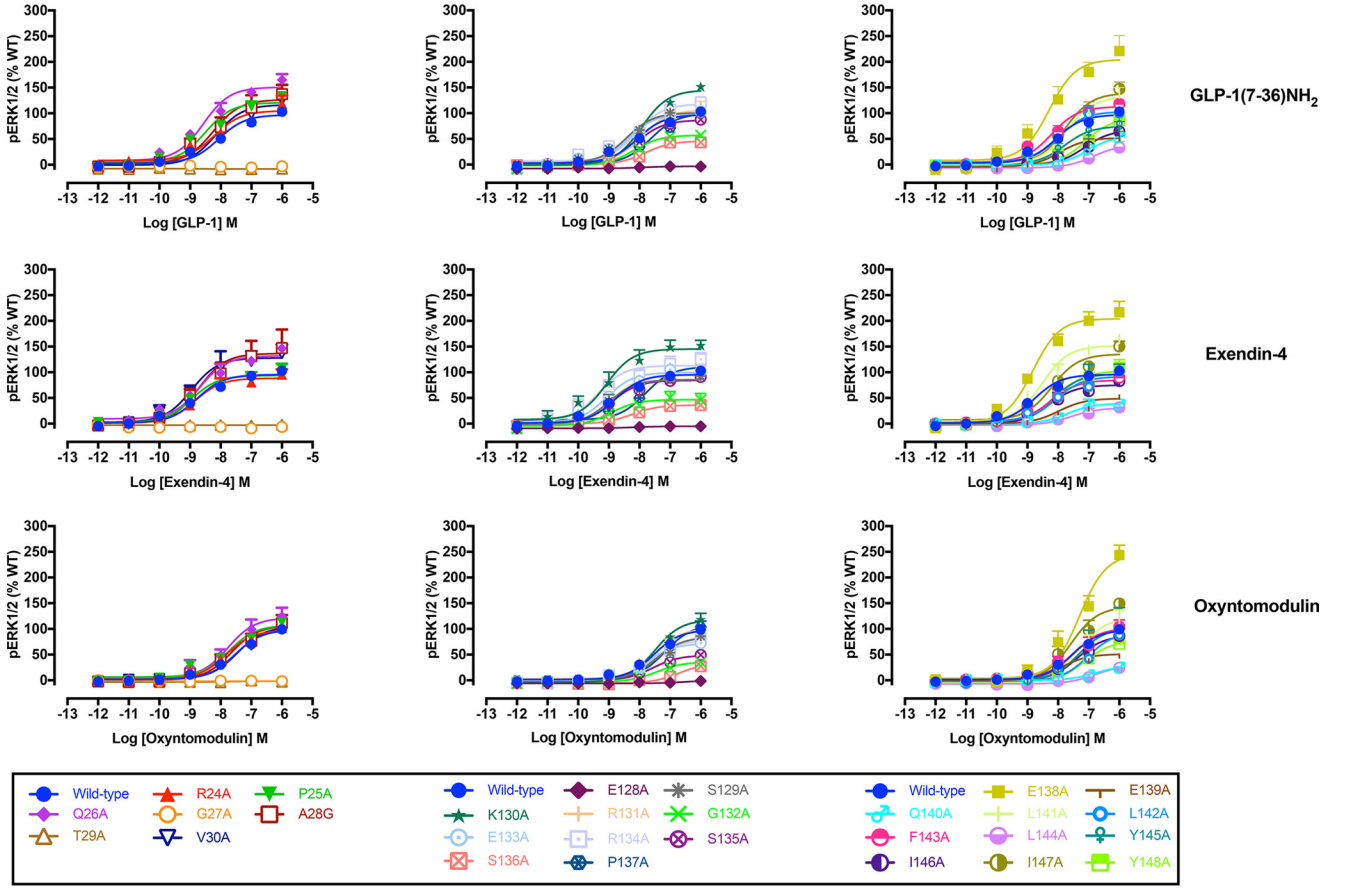

Figure 6. pERK1/2 concentration-response curves for Ala mutants of the hGLP-1R N-terminal ECD and TM1 and linker region. Concentration-response curves of pERK of WT and mutant receptors were stimulated by GLP-1(7–36)-NH_2 (*upper panels*), exendin-4 (*middle panels*), or oxyntomodulin (*lower panels*) in CHO–Flp-In cells stably expressing WT or mutant receptors. Data were normalized to the response elicited by the WT and analyzed with an operational model of agonism. All values are means ± S.E. of four to six independent experiments, conducted in duplicate.

ably via destabilization of the receptor protein, in a similar manner to that observed for the T29A mutant. Although speculative, it is possible that these amino acids are in close proximity in the inactive receptor and form part of an important network that stabilizes this state. In studies where E128A is further overexpressed by transient expression, there is a <3-fold loss of GLP-1 potency and an ~5-fold loss of exendin-4 potency for cAMP production (39), consistent with a limited role of this residue for peptide binding.

In the inactive homology model, the deeper binding cavity occupied by agonist peptides is capped by a series of large aromatic residues, particularly Trp-297 and Tyr-305 (Fig. 8, *B* and *C versus D* and *E*), whose position is predicted to be stabilized by H-bonding. In the active structure, these amino acids undergo large-scale movements associated with reorganization of ECL2 that reorients Trp-297 away from the binding pocket, where it forms interactions with other ECL2 residues, accompanied by small outward movements of Arg-299 and Asn-300 that directly contact the peptide in the active structure. Release of ground state interactions in the inactive ECL2 loop structure enables unwinding of the top of TM6 with an ~180° rotation of Tyr-305 accompanied by an ~9-Å displacement of the Cα carbon. Previous molecular dynamics simulations on the inactive GLP-1R model suggested that this aromatic cap provided a significant energy barrier to deeper entry of the GLP-1 N terminus, with entry facilitated by Glu-9 of the peptide that forms a salt bridge with Arg-190 of the receptor (11). Intriguingly, mutation of Trp-297 and the adjacent Cys-296 (that is covalently linked to Cys-226 in TM3) markedly attenuated GLP-1 and exendin-4 affinity, but it did not impact oxyntomodulin affinity. Oxyntomodulin contains an uncharged Gln, positionally equivalent to GLP-1 Glu-9, and does not interact with Arg-190 in the receptor core (11). It is therefore possible that oxyntomodulin binds in a shallower orientation. A significant and selective decrease in oxyntomodulin affinity for F381A, L142A, and K202A mutants and lack of an effect for the R380A mutant are consistent with this hypothesis (Fig. 10).

Peptide-mediated signaling and bias—Comparison of the position of mutated residues that affect GLP-1–mediated cAMP formation between fully active and inactive models reveals two major networks involved in GLP-1R function (Figs. 10 and 11). The first includes residues of ECL2 and the membrane-proximal TM regions and the proximal segment of ECL3. K288A impacted ligand binding and was critical for propagation of cAMP signaling (13, 24, 40). It stabilizes the center of the ECL2 network and may coordinate interactions between the ECL2 residues. Both exendin-4 and oxyntomodulin were similarly affected by mutations to ECL2 indicating a general role in propagation of cAMP signaling (Figs. 10 and 11). Despite the lack of effect of W297A on oxyntomodulin binding,

Table 4

Effects of human GLP-1R TM1/N-terminal mutants on agonist-mediated pERK1/2

pERK1/2 phosphorylation data were analyzed using a three-parameter logistic equation to determine pEC_{50} and E_{max} values. pEC_{50} is the negative logarithm of the molar concentration of agonist that induced half the maximal response. E_{max} for mutants is expressed as a percentage of wildtype. $Log\tau_c$ is the operational efficacy value (determined via the Black and Leff operational model (24)), corrected for cell-surface expression of GLP-1R. All values for cAMP accumulation are mean ± S.E. of four to six independent experiments, conducted in duplicate. One-way ANOVA and Dunnett's post-test were used to determine statistical differences (*, $p < 0.05$). ND, not determined.

	Agonist-mediated ERK1/2 phosphorylation								
	GLP-1(7–36)-NH_2			Exendin-4			Oxyntomodulin		
	pEC_{50}	E_{max}	$Log\tau_c$	pEC_{50}	E_{max}	$Log\tau_c$	pEC_{50}	E_{max}	$Log\tau_c$
Wildtype	8.07 ± 0.05	100.00 ± 1.87	0.03 ± 0.02	8.77 ± 0.05	98.37 ± 1.56	0.02 ± 0.02	7.53 ± 0.04	101.40 ± 1.64	0.05 ± 0.03
R24A	8.21 ± 0.19	108.50 ± 7.64	−0.03 ± 0.06	8.83 ± 0.18	90.87 ± 5.55	−0.16 ± 0.07	7.82 ± 0.11	100.40 ± 4.85	−0.07 ± 0.07
P25A	8.51 ± 0.13	125.30 ± 5.34	0.22 ± 0.06	8.95 ± 0.18	96.53 ± 5.67	−0.03 ± 0.06	7.73 ± 0.14	110.80 ± 6.22	0.09 ± 0.07
Q26A	8.57 ± 0.16	157.30 ± 7.93*	0.47 ± 0.08*	8.68 ± 0.16	137.30 ± 7.13*	0.31 ± 0.08*	7.76 ± 0.22	126.10 ± 12.12	0.49 ± 0.12*
G27A	ND	ND	ND	ND	ND	ND	ND	ND	ND
A28G	8.25 ± 0.24	131.40 ± 11.84*	0.30 ± 0.08	8.71 ± 0.29	142.10 ± 13.91*	0.42 ± 0.09*	7.66 ± 0.20	110.20 ± 9.56	0.11 ± 0.08
T29A	ND	ND	ND	ND	ND	ND	ND	ND	ND
V30A	8.16 ± 0.12	120.80 ± 5.95	0.20 ± 0.07	8.96 ± 0.23	132.90 ± 10.41*	0.31 ± 0.07*	7.45 ± 0.11	107.80 ± 5.45	0.07 ± 0.08
E128A	ND	ND	ND	ND	ND	ND	ND	ND	ND
S129A	8.42 ± 0.12	104.10 ± 4.55	0.15 ± 0.06	9.00 ± 0.17	87.98 ± 5.16	0.01 ± 0.06	7.45 ± 0.15	86.48 ± 5.89	−0.004 ± 0.08
K130A	7.93 ± 0.08	151.20 ± 5.17*	0.85 ± 0.11*	9.08 ± 0.21	151.40 ± 9.84*	0.83 ± 0.09*	7.51 ± 0.12	122.50 ± 6.66	0.55 ± 0.09*
R131A	7.93 ± 0.16	109.70 ± 7.47	0.06 ± 0.07	8.88 ± 0.13	96.88 ± 4.49	−0.05 ± 0.06	7.50 ± 0.16	104.10 ± 7.36	0.005 ± 0.08
G132A	8.19 ± 0.17	57.61 ± 4.22*	−0.26 ± 0.08	8.93 ± 0.29	46.60 ± 5.30*	−0.38 ± 0.09*	7.45 ± 0.24	35.06 ± 4.55*	−0.51 ± 0.15*
E133A	8.37 ± 0.13	101.80 ± 5.00	0.07 ± 0.06	9.08 ± 0.15	102.90 ± 5.02	0.07 ± 0.06	7.76 ± 0.17	72.90 ± 5.38	−0.19 ± 0.08
R134A	8.09 ± 0.13	122.30 ± 6.33	0.15 ± 0.07	9.36 ± 0.21	116.90 ± 7.21	0.11 ± 0.06	7.63 ± 0.16	79.86 ± 5.78	−0.20 ± 0.08
S135A	8.06 ± 0.18	88.91 ± 6.40	0.15 ± 0.07	8.90 ± 0.19	86.39 ± 5.43	0.13 ± 0.06	7.57 ± 0.14	48.80 ± 3.35*	−0.22 ± 0.10
S136A	7.81 ± 0.16	45.74 ± 3.36*	−0.58 ± 0.10*	8.26 ± 0.16	35.37 ± 2.32*	−0.72 ± 0.13*	6.73 ± 0.25*	32.54 ± 6.85*	−0.73 ± 0.16*
P137A	7.64 ± 0.15	102.70 ± 6.67	0.05 ± 0.07	7.80 ± 0.25*	114.50 ± 11.67	0.14 ± 0.08	7.17 ± 0.16	112.30 ± 9.51	0.13 ± 0.09
E138A	8.29 ± 0.21	214.30 ± 16.04*	1.07 ± 0.24*	8.82 ± 0.13	214.00 ± 9.04*	0.71 ± 0.13*	7.30 ± 0.16	258.30 ± 20.51*	0.88 ± 0.18*
E139A	7.95 ± 0.20	52.17 ± 4.96*	0.02 ± 0.08	7.98 ± 0.24*	48.99 ± 5.12*	−0.02 ± 0.11	7.90 ± 0.18	51.16 ± 4.23*	0.01 ± 0.08
Q140A	7.02 ± 0.21*	57.35 ± 7.44*	0.08 ± 0.11	7.70 ± 0.31*	38.88 ± 5.68*	−0.15 ± 0.12	6.78 ± 0.26*	27.40 ± 5.10*	−0.39 ± 0.19*
L141A	7.71 ± 0.11	137.10 ± 6.84*	0.26 ± 0.09	8.52 ± 0.13	158.10 ± 6.82*	0.50 ± 0.11*	7.30 ± 0.18	126.10 ± 11.22	0.13 ± 0.10
L142A	8.00 ± 0.16	106.40 ± 6.71	0.12 ± 0.06	8.05 ± 0.17*	94.20 ± 6.46	0.00 ± 0.08	7.03 ± 0.19	97.49 ± 11.29	0.06 ± 0.10
F143A	8.22 ± 0.16	116.70 ± 6.85	0.17 ± 0.06	8.24 ± 0.28	86.81 ± 9.12	−0.10 ± 0.07	7.50 ± 0.22	104.80 ± 10.36	0.06 ± 0.08
L144A	ND	ND	ND	7.57 ± 0.36*	29.28 ± 5.54*	−0.08 ± 0.21	ND	ND	ND
Y145A	7.78 ± 0.41	76.36 ± 13.92	−0.12 ± 0.06	8.13 ± 0.28*	99.84 ± 11.07	0.08 ± 0.06	7.32 ± 0.46	106.00 ± 24.78	0.15 ± 0.09
I146A	7.14 ± 0.34*	68.81 ± 13.41*	0.07 ± 0.13	8.30 ± 0.22	76.61 ± 6.48	0.13 ± 0.08	7.38 ± 0.18	89.57 ± 8.13	0.26 ± 0.08
I147A	7.77 ± 0.16	144.90 ± 9.75*	0.45 ± 0.11*	8.21 ± 0.12	140.80 ± 6.46*	0.38 ± 0.09*	7.58 ± 0.17	149.10 ± 11.18*	0.51 ± 0.11*
Y148A	7.11 ± 0.21*	93.43 ± 11.28	0.16 ± 0.11	8.01 ± 0.20*	105.60 ± 8.68	0.25 ± 0.07	7.12 ± 0.17	78.45 ± 7.84	0.03 ± 0.10

Table 5

Sequence variations in published structures

PDB code	Description	Structure fragment	Mutations/differences from hGLP-1R	Missing residues in the structure
5VEW (Song *et al.* 14)	Crystal structure of human GLP-1R transmembrane domain in complex with negative allosteric modulator PF-06372222	Residues 128–431. Residues 258–260 at intracellular loop 2 were replaced with T4 lysozyme. Residues 205–214 from ECL1 were replaced by a GSG linker	S193C, I196F, Y205G, ΔThr-207, ΔAla-208, ΔAla-209, ΔGln-210, ΔGln-211, ΔHis-212, ΔGln-213, W214G, S225A, M233X, S271A, I317C, G318I, K346A, C347F, G361C	Glu-128, Ser-129, Lys-130, Arg-131, Gly-132, Glu-133, Arg-134, Ser-135, Met-204, Asp-215, Glu-373, His-374, Ala-375, Arg-376, Gly-377, Thr-378, Leu-379, Glu-423, His-424, Leu-425, His-426, Ile-427, Gln-428, Arg-429, Asp-430, Ser-431
5NX2 (Jazayeri *et al.* 15)	Crystal structure of human GLP-1 receptor bound to the 11-mer agonist peptide 5	Residues 24–432	T207E, Q211A, D215R, L232F, L260F, G295A, T298A, C329A, P358A, G361A, H363V, V405A	Arg-24, Pro-25, Gln-26, Gly-27, Ala-28, Glu-418, Arg-419, Trp-420, Arg-421, Leu-422, Glu-423, His-424, Leu-425, His-426, Ile-427, Gln-428, Arg-429, Asp-430, Ser-431, Ser-432
5VAI (Zhang *et al.* 16)	Cryo-EM structure of active rabbit GLP-1 receptor in complex with GLP-1 and G_s protein	Residues 24–422	T106A, H112P, Q140R	Arg-24, Pro-25, Gln-26, Gly-27, Ala-28, Ser-129, Arg-130, Arg-131, Gly-132, Glu-133, Ser-134, Leu-422
6B3J (Liang *et al.* 17)	Cryo-EM structure of active human GLP-1 receptor in complex with exendin-P5 and G_s protein	Residues 23–466	None	Ala–23–Thr–29, Ser–129–Ser–136, Asn–338–Thr–342, His–424–Gly–466

it was crucial for signaling of all three peptides. In the active agonist-bound calcitonin receptor, there is a high degree of overlap in the structural organization of ECL2 despite considerable sequence variation; Arg-281 that is positionally equivalent to Lys-288 of the GLP-1R appears to play a similar coordinating role in maintenance of this structure (19, 25). The organization of the ECL2 network is also required for calcium signaling, although it does not appear as important for peptide-mediated pERK (Figs. 10 and 11).

The second network involves residues in TM1 and the TM7 proximal residues of ECL3 (Figs. 10 and 11). This network exhibits a higher degree of peptide-specific effects that are likely related to both differences in the peptide sequences and orientation of the peptides in the active structures. As noted

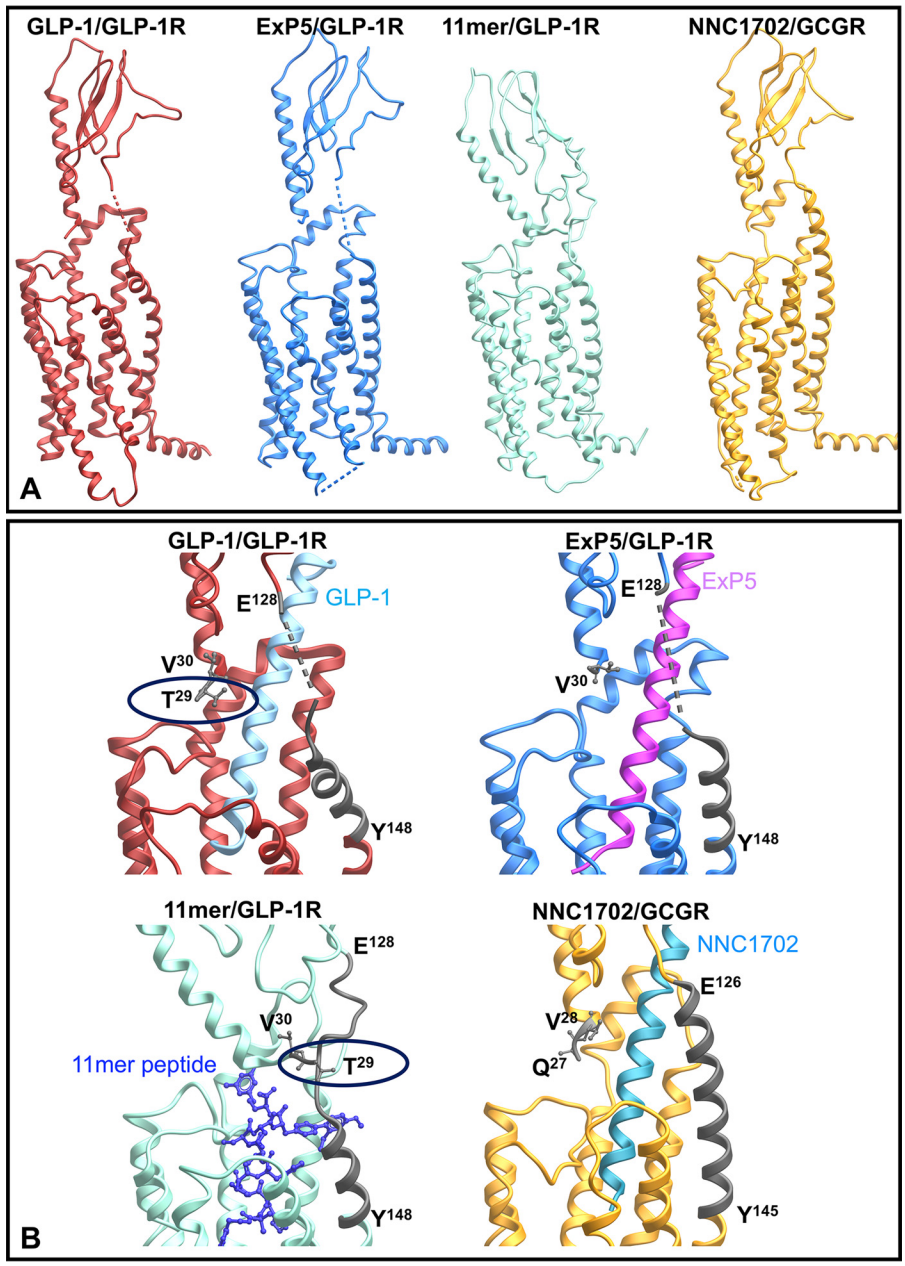

Figure 7. Peptide-bound full-length structures of GLP-1R and GCGR. *A,* full-length structures illustrating the relative position of the N-terminal ECD to the receptor core. *B,* zoom-in of the resolved far N-terminal residue(s) and TM1/ECD stalk (highlighted in *dark gray*). The backbones of the peptide agonists are illustrated in ribbon (GLP-1, exendin-P5 (*ExP5*), and NNC1702) or X-stick (11-mer).

above, this region of the receptor is involved in coordination of TM1 in the inactive structure and the reorganization and packing of TM1 with TM7 in the active structures (Fig. 9). Unlike GLP-1 and exendin-4, oxyntomodulin-mediated cAMP production is also weakly attenuated by mutation to amino acids in ECL1 that sit within the short α-helix formed in the active structure that extends to the ECL2 network. This is likely due to the predicted distinct positioning of oxyntomodulin when bound to the receptor (Fig. 10). The boundary of ECL1 at the top of TM3 is covalently linked to ECL2 by disulfide linkage of Cys-226 (TM3) and Cys-296 (ECL2), whereas Arg-227 in inactive/partially active structures may also stabilize ECL2. R227A mutation decreases affinity of all three peptides, but with minimal impact on signaling efficacy (32). As such, the extent to which the oxyntomodulin-specific effects are due to unique direct interactions with ECL1 *versus* potential differences in Cys-296 and Trp-297 is not clear.

Overall, the pattern of effect of mutation was similar for calcium and cAMP signaling across GLP-1 and exendin-4 where efficacy effects could be quantified, although there was generally a greater magnitude of effect on calcium signaling (Figs. 10 and 11). Previous pharmacological inhibitor studies revealed that both these pathways were regulated by G protein interaction at the WT receptor in the CHO–Flp-In cell background, although G_i and G_q interactions had more prominent roles in calcium mobilization (11); this is indicative of broad similarities in changes required to enable G protein coupling. Exendin-4–mediated signaling is also gen-

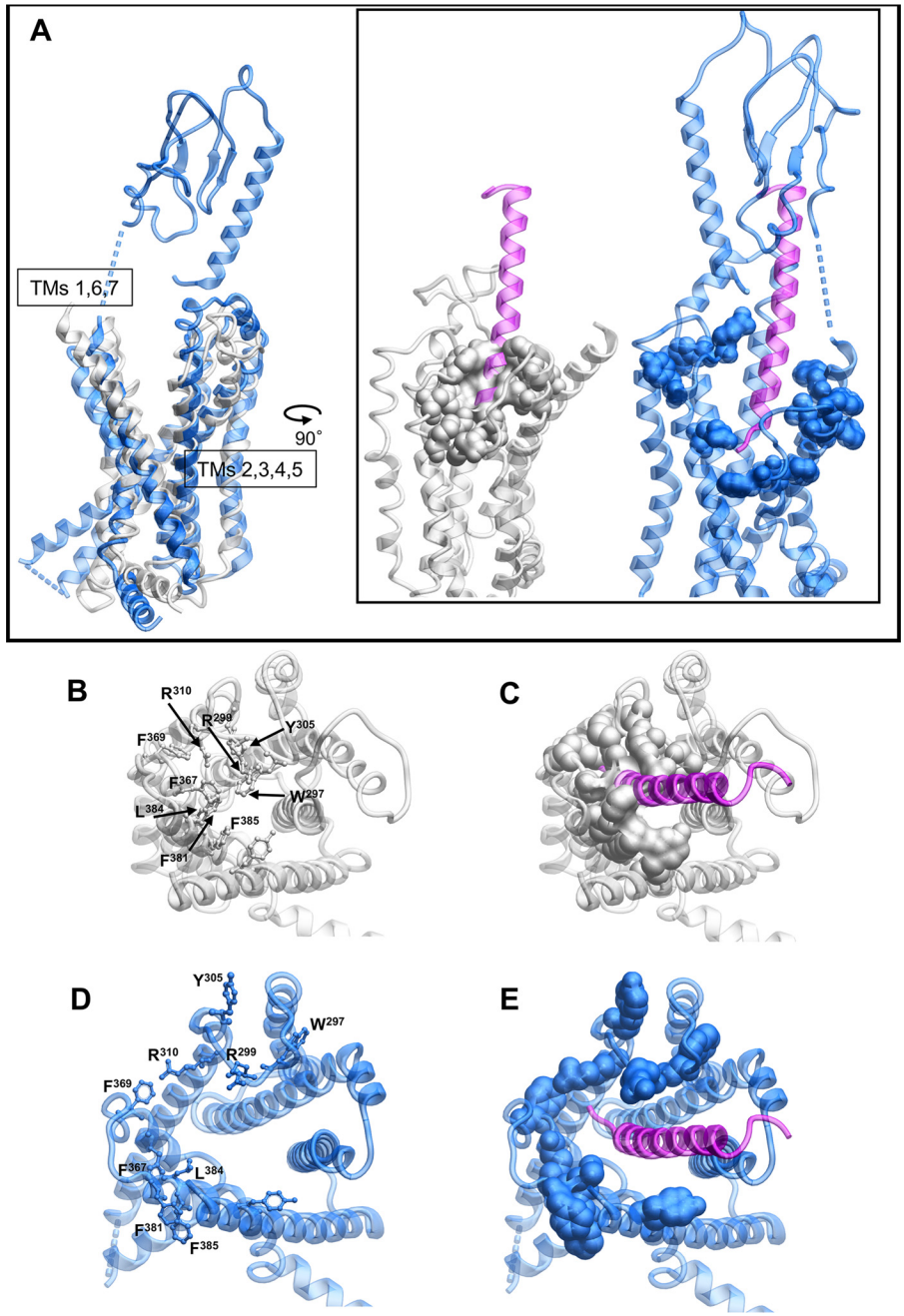

Figure 8. Peptide binding to the GLP-1R requires reorganization of aromatic/hydrophobic residues in the receptor core. *A,* side view of the inactive GLP-1R model (*gray*) or exendin-P5-bound GLP-1R structure (*blue*) with the exendin-P5 peptide illustrated in *purple*. Residues that occupy the core of the receptor in the inactive model are shown as space fill. *B–E,* top view of the structures where the ECD has been omitted for clarity. *B* and *C,* inactive GLP-1R model. *D* and *E,* exendin-P5-bound GLP-1R structure.

erally more sensitive to mutation than that mediated by GLP-1, and the required ECL2 network extends to the top of TM4 for this peptide (Fig. 10).

Peptide-mediated pERK was least sensitive to GLP-1R surface mutations, being principally confined to mutations of the distal ECL3/TM7 boundary, and residues of TM1 and the linker extension that provides physical connection to the ECD, which were revealed in this study (Figs. 10 and 11). This was particularly evident for exendin-4, which was least affected by mutation (Fig. 11). Intriguingly, there was effectively no involvement of the ECL2 residues that were absolutely required for cAMP and calcium signaling. Inhibitor studies at the WT receptor indicated that G_s and G_q have limited contribution to exendin-4–mediated pERK, with signaling principally driven by G_i, $G\beta\gamma$, and arrestin interactions, although those are likely to be at least partly interdependent (11). For GLP-1, and more prominently oxyntomodulin, selective mutations in ECL2 also impacted pERK, and this could relate to greater contribution of G_q (GLP-1) and G_s (oxyntomodulin) in pERK at the WT receptor. Also of interest, for TM1 and ECL3/TM7, the effects of individual mutation were highly peptide-specific (Fig. 10). The data are consistent with a model whereby selective and peptide-specific interactions alter the TM1/TM7 interface linked to G_i/$G\beta\gamma$/arrestin coupling to pERK. Moreover, our mutational

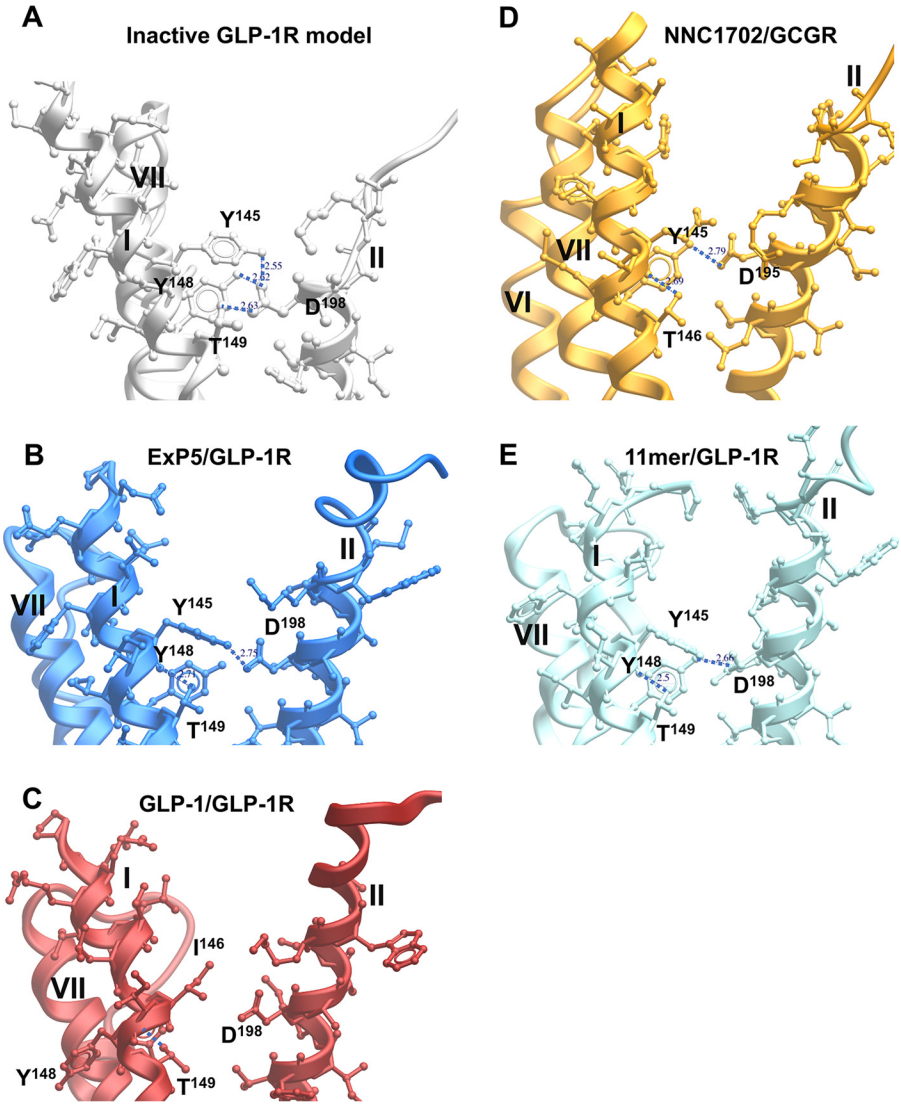

Figure 9. Polar residues in the GLP-1R TM1 are coordinated by Asp-198 (TM2) in the inactive model, orienting key side chains away from TM7 and facilitating tight packing of TM1/TM7. View facing the TM1/TM2 boundary is shown. Key TM1 side chains interacting with Asp-198 are depicted in X-stick representation and labeled. *A*, inactive GLP-1R model. *B*, exendin-P5 (*ExP5*)/GLP-1R structure. *C*, GLP-1/GLP-1R structure. *D*, NNC1702/GCGR structure. *E*, 11-mer agonist/GLP-1R structure. TM helices are labeled in *roman numerals*.

data suggest these changes can occur relatively independent of the reorganization of TMs 5 and 6 that are critical for cAMP formation and $[Ca^{2+}]_i$ mobilization, events that are G_s/G_q-dependent at the WT receptor. Exendin-P5 is a G protein-biased peptide agonist that exhibits bias toward cAMP relative to arrestin interaction, compared with the related exendin-4 peptide and GLP-1 (10, 17). It has distinct actions *in vivo* compared with exendin-4 (10). As noted above, comparison of the exendin-P5– and GLP-1–bound active GLP-1R structures reveals major differences in ECL3 and the upper TM boundaries of TMs 6 and 7 that are linked to distinct rotational differences in the upper region of TM1. Mutation in these domains has confirmed peptide-specific differences in the engagement of GLP-1 *versus* exendin-P5 with amino acids in TM1, as well as the TM6 proximal region of ECL3 (17), thereby providing additional structural evidence for distinctions in the role of these domains in propagation of signaling. An important caveat for extrapolation of our observations to more proximal measures of signaling is that they are based on inferences from WT receptor signaling. Direct measurement of proximal transducer engagement for mutant receptors will be required to validate hypotheses.

The novel structures for the GLP-1R are enabling us to begin to unravel the complexities associated with receptor activation and biased agonism. Combining new data from this study with our previous work on GLP-1R ECLs in the context of inactive and active structures has advanced our understanding of receptor domains that control signaling. Importantly, the work provides evidence for two, at least partially independent, structural domains linked to signaling. The first involves the interface between TMs 5 and 6 and is linked to reorganization of ECL2 into a structured network that is required for propagation of signaling linked to G_s and G_q-dependent pathways at the WT receptor. The second is the interface between TMs 1 and 7 that, although important for at least G_s-dependent cAMP signaling, may be independently linked to $G_i/G\beta\gamma$/arrestin-mediated signaling that is the key driver of pERK at the WT receptor. Our data support a model where dis-

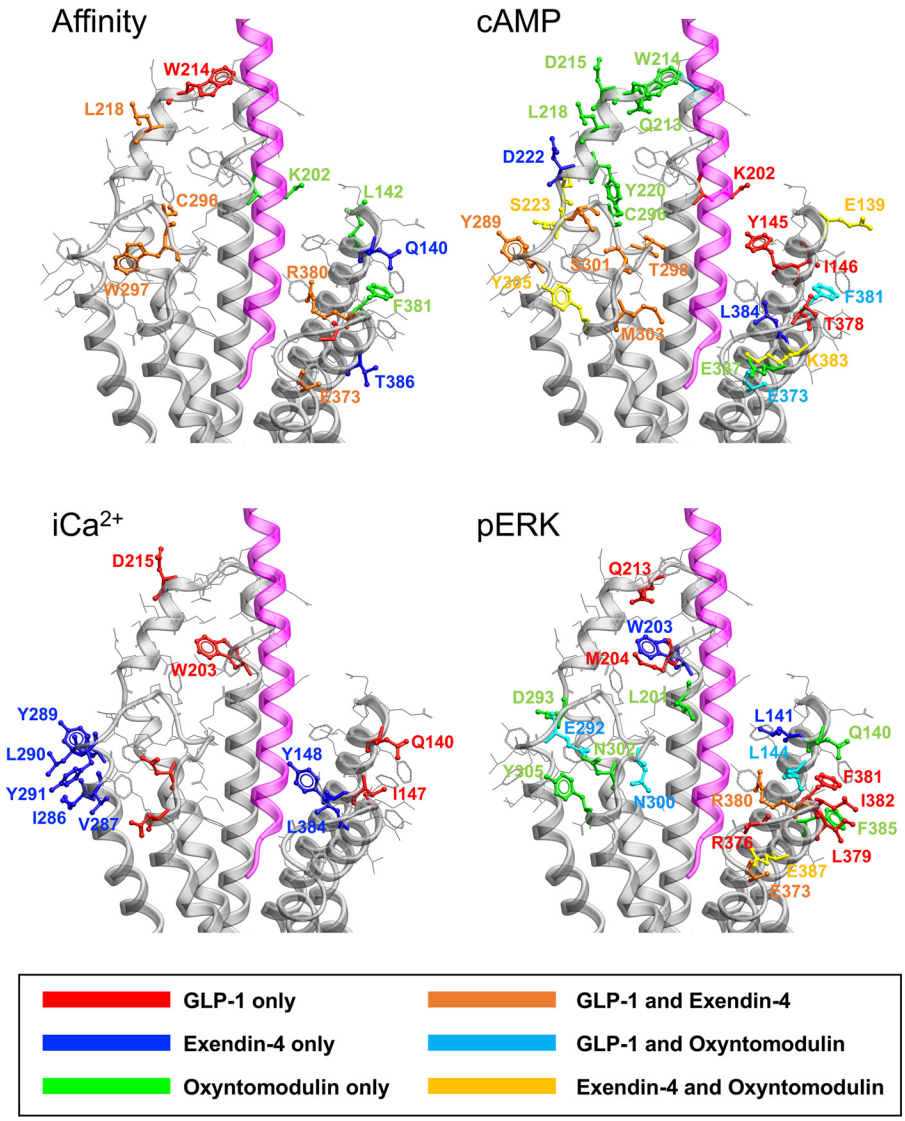

Figure 10. Peptide-selective effects on agonist affinity, cAMP accumulation, $[Ca^{2+}]_i$ mobilization, and pERK. Mutated amino acids with similar effects across peptides are not highlighted. Maps for affinity, cAMP, and pERK include all three peptides. The map for $[Ca^{2+}]_i$ includes only GLP-1 and exendin-4. The exendin-P5 peptide is displayed in *magenta*.

tinct peptide–receptor interactions can provide selective control of how these different networks are engaged.

Experimental procedures

Mutagenesis

Desired mutations were introduced to the N-terminal double c-Myc–labeled human *GLP-1R* gene in pDONR201 (Invitrogen) via the Muta-direct™ kit (Beijing SBS Genetech Co., Ltd., China), and then LR recombination reactions were conducted to transfer the N-terminal double c-Myc–labeled human *GLP-1R* gene into the pEF5/FRT/V5-DEST destination vector using Gateway Technology (Invitrogen). The oligonucleotides for mutagenesis were purchased from GeneWorks (Thebarton, SA, Australia), and mutants were confirmed by automated DNA sequencing.

Stable cell line generation and cell culture

The mutant or wildtype (WT) receptor genes were integrated into the Flp-In-Chinese hamster ovary (Flp-In-CHO) cells, passage 4 (Invitrogen), using the Flp-In™ system. Stable Flp-In expression cell lines were generated through polyclonal selection, screened, and maintained in Dulbecco's modified Eagle's medium supplemented with 10% (v/v) FBS, 600 μg/ml hygromycin B at 37 °C in 5% CO_2. The WT receptor is expressed at ~170,000 receptors/cell. Cell lines were routinely tested for mycoplasma and were mycoplasma free. Stable cells were frozen at passage 14, and all assays were performed with cells between passage 14 and 25.

Heterologous whole-cell competitive binding assay

Competition of ^{125}I–exendin-4(9–39) binding to hGLP-1R was performed as described previously (13) on whole cells in 96-well plates using the radiolabeled antagonist ^{125}I–exendin-4(9–39) (~0.1 nM) and increasing concentrations of unlabeled peptide. Nonspecific binding was defined by co-incubation with 1 μM unlabeled exendin-4(9–39). Following overnight incubation, nonbound ligand was removed, and radioactivity was determined using a gamma counter.

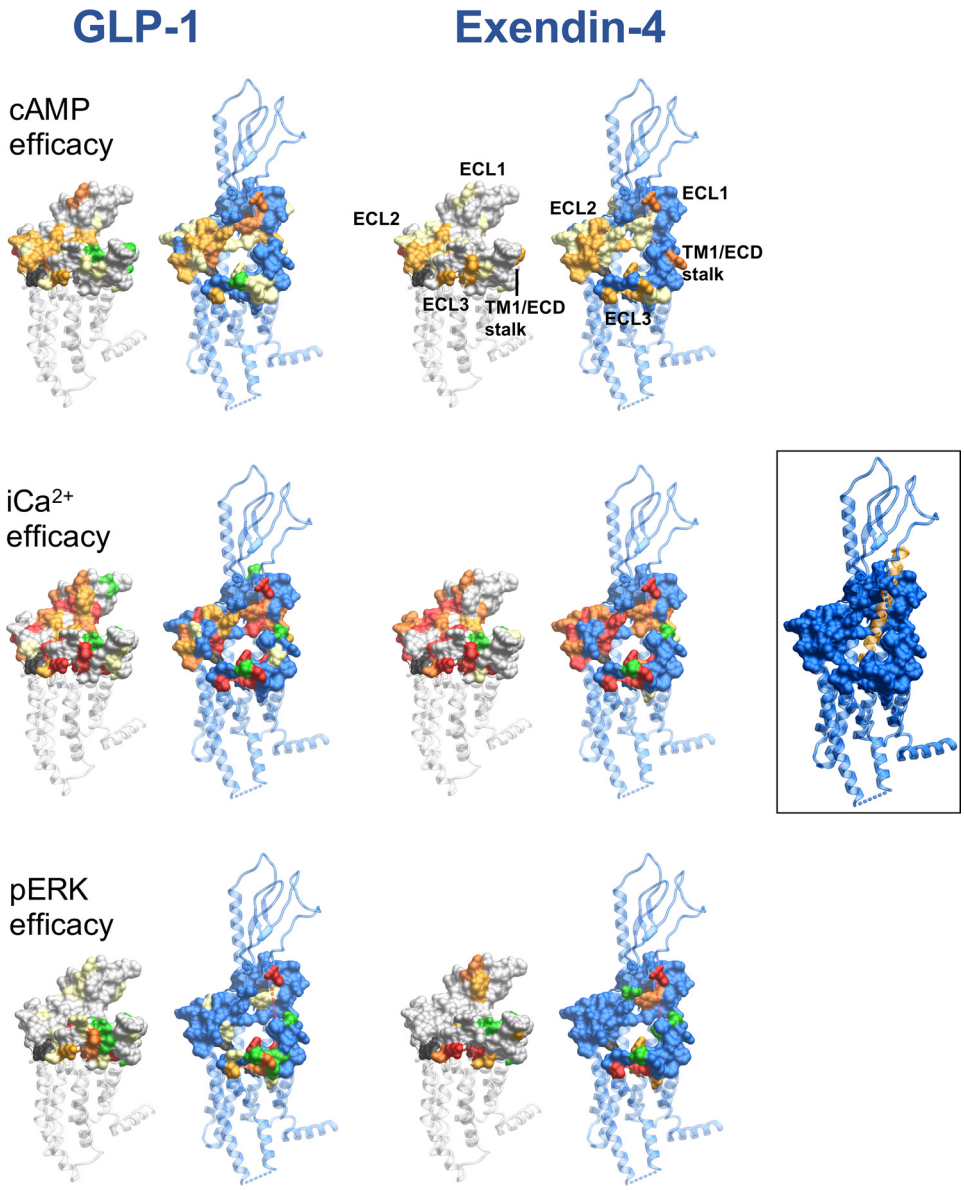

Figure 11. Reorganization of the extracellular surface of the GLP-1R is critical to propagation of signaling. Amino acids involved in efficacy across cAMP (*upper panels*), $[Ca^{2+}]_i$ (*middle panels*), and pERK (*lower panels*) for GLP-1 (*left-hand panels*) and exendin-4 (*right-hand panels*) were mapped onto the inactive GLP-1R model and the fully active exendin-P5 (*ExP5*)-bound GLP-1R structure. Displayed in surface representation are mutated amino acids that affect efficacy: *yellow* (2–5-fold reduction in affinity); *light orange* (5–10-fold reduction in affinity); *red* (>30-fold reduction in affinity); or *green* (increased affinity). Mutated residues not affected are displayed as *gray* (inactive receptor) or *blue* (active receptor).

Cell-surface expression by enzyme-linked immunosorbent assay

1.5×10^5 cells/well were seeded into 24-well culture plates and incubated overnight. Expression was determined through detection of N-terminal double c-Myc of GLP-1R by ELISA as described previously (13). Data were normalized to WT GLP-1R and Flp-In CHO parental cell lines.

Calcium mobilization

3×10^4 cells/well were seeded into 96-well culture plates and incubated overnight. Cells were incubated with Fluo4-AM for 45 min and stimulated with different concentrations of peptides, and fluorescence was determined in a FlexStation® plate reader every 1.36 s for 120 s after ligand addition as described previously (13). Data were normalized to the maximal response elicited by 100 μM ATP.

cAMP accumulation

3×10^4 cells/well were seeded into 96-well culture plates and incubated overnight. Cells were stimulated with increasing concentrations of ligands for 30 min in the presence of isobutylmethylxanthine. The liquid was discarded, changed to absolute ethanol, and volatilized to dry in room temperature. cAMP was detected using a Lance kit (PerkinElmer Life Sciences), as described previously (11). Data were normalized to the response of 100 μM forskolin.

ERK1/2 phosphorylation

3×10^4 cells/well were seeded into 96-well culture plates and incubated overnight. Initially, pERK1/2 time-course experi-

ments were performed over 1 h to identify the time point when the pERK1/2 response is maximal. Subsequently, dose responses for different agonists were determined at this peak time point with stimulation performed after serum starvation overnight. pERK1/2 was detected using an AlphaScreen assay as described previously (13). Data were normalized to the maximal response elicited by 10% FBS determined at 6 min.

Data analysis

IC_{50} values were estimated from competitive inhibition of ^{125}I-exendin(9–39) binding using a three-parameter logistic equation (log(inhibitor *versus* response)) in Prism (version 7, Graphpad). In all cases, the concentration of the radioligand was ≤1% of the K_d values. Under these conditions, the IC_{50} approximates K_i, and such data are reported as pK_i. E_{max} and EC_{50} were estimated from concentration-response curves using with a three-parameter logistic equation in Prism (version 7). These values are a composite of affinity, efficacy, and stimulus response coupling. The Black and Leff operational model of agonism (26) was applied to separate effects on pathway-specific signaling from those that modify ligand affinity. Derived values (τ) were normalized to experimentally determined levels of cell-surface expression to provide a measure of efficacy (τ_c) that is independent of affinity and altered cell-surface receptor expression (11). Log τ_c values for mutant receptors were statistically compared with those of the WT receptor using a one-way analysis of variance (ANOVA) and Dunnett's post-test. Significance was accepted at $p < 0.05$.

Molecular modeling and mapping of mutational effects

A homology model of the inactive GLP-1R TM domain was built using the minimally modified GCGR (PDB code 4L6R) (29), as described previously (28); the first amino acid in this model is Arg-134. The thermostabilized and full-length human GLP-1R bound to modified 11-mer peptide agonist (PDB code 5NX2) (15); the full-length and GLP-1 bound to rabbit GLP-1R in complex with G_s (PDB code 5VAI) (16), and the full-length and exendin-P5 bound to human GLP-1R in complex with G_s (PDB code 6B3J) (16) were used as deposited; the first amino acids in these structures are Thr-29, Thr-29, and Val-30, respectively.

Author contributions—S. L., D. Y., M.-W. W., D. W., and P. M. S. conceptualization; S. L., L. C., D. Y., Y.-L. L., C. K., A. C., and D. W. formal analysis; S. L., L. C., A. D., X. C., Y. F., C. K., P. Z., and T. C. investigation; S. L. methodology; S. L., M.-W. W., D. W., and P. M. S. writing-original draft; S. L., C. K., P. Z., A. C., M.-W. W., D. W., and P. M. S. writing-review and editing; D. Y., M.-W. W., D. W., and P. M. S. supervision; C. K., A. C., M.-W. W., D. W., and P. M. S. funding acquisition; P. M. S. project administration.

References

1. Santos, R., Ursu, O., Gaulton, A., Bento, A. P., Donadi, R. S., Bologa, C. G., Karlsson, A., Al-Lazikani, B., Hersey, A., Oprea, T. I., and Overington, J. P. (2017) A comprehensive map of molecular drug targets. *Nat. Rev. Drug. Discov.* **16,** 19–34 CrossRef Medline
2. Luttrell, L. M., Maudsley, S., and Bohn, L. M. (2015) Fulfilling the promise of "Biased" G protein-coupled receptor agonism. *Mol. Pharmacol.* **88,** 579–588 CrossRef Medline
3. Costa-Neto, C. M., Parreiras-E-Silva, L. T., and Bouvier, M. (2016) A pluridimensional view of biased agonism. *Mol. Pharmacol.* **90,** 587–595 CrossRef Medline
4. Wootten, D., Miller, L. J., Koole, C., Christopoulos, A., and Sexton, P. M. (2017) Allostery and biased agonism at class B G protein-coupled receptors. *Chem. Rev.* **117,** 111–138 CrossRef Medline
5. Hollenstein, K., de Graaf, C., Bortolato, A., Wang, M. W., Marshall, F. H., and Stevens, R. C. (2014) Insights into the structure of class B GPCRs. *Trends Pharmacol. Sci.* **35,** 12–22 CrossRef Medline
6. Koole, C., Wootten, D., Simms, J., Valant, C., Sridhar, R., Woodman, O. L., Miller, L. J., Summers, R. J., Christopoulos, A., and Sexton, P. M. (2010) Allosteric ligands of the glucagon-like peptide 1 receptor (GLP-1R) differentially modulate endogenous and exogenous peptide responses in a pathway-selective manner: implications for drug screening. *Mol. Pharmacol.* **78,** 456–465 CrossRef Medline
7. Hager, M. V., Johnson, L. M., Wootten, D., Sexton, P. M., and Gellman, S. H. (2016) β-Arrestin-biased agonists of the GLP-1 receptor from β-amino acid residue incorporation into GLP-1 analogues. *J. Am. Chem. Soc.* **138,** 14970–14979 CrossRef Medline
8. Hager, M. V., Clydesdale, L., Gellman, S. H., Sexton, P. M., and Wootten, D. (2017) Characterization of signal bias at the GLP-1 receptor induced by backbone modification of GLP-1. *Biochem. Pharmacol.* **136,** 99–108 CrossRef Medline
9. Weston, C., Poyner, D., Patel, V., Dowell, S., and Ladds, G. (2014) Investigating G protein signalling bias at the glucagon-like peptide-1 receptor in yeast. *Br. J. Pharmacol.* **171,** 3651–3665 CrossRef Medline
10. Zhang, H., Sturchler, E., Zhu, J., Nieto, A., Cistrone, P. A., Xie, J., He, L., Yea, K., Jones, T., Turn, R., Di Stefano, P. S., Griffin, P. R., Dawson, P. E., McDonald, P. H., and Lerner, R. A. (2015) Autocrine selection of a GLP-1R G-protein biased agonist with potent antidiabetic effects. *Nat. Commun.* **6,** 8918 CrossRef Medline
11. Wootten, D., Reynolds, C. A., Smith, K. J., Mobarec, J. C., Koole, C., Savage, E. E., Pabreja, K., Simms, J., Sridhar, R., Furness, S. G. B., Liu, M., Thompson, P. E., Miller, L. J., Christopoulos, A., and Sexton, P. M. (2016) The extracellular surface of the GLP-1 receptor is a molecular trigger for biased agonism. *Cell* **165,** 1632–1643 CrossRef Medline
12. Hoare, S. R. (2005) Mechanisms of peptide and nonpeptide ligand binding to class B G-protein coupled receptors. *Drug Discov. Today* **10,** 417–427 CrossRef Medline
13. Koole, C., Wootten, D., Simms, J., Miller, L. J., Christopoulos, A., and Sexton, P. M. (2012) Second extracellular loop of human glucagon-like peptide-1 receptor (GLP-1R) has a critical role in GLP-1 peptide binding and receptor activation. *J. Biol. Chem.* **287,** 3642–3658 CrossRef Medline
14. Song, G., Yang, D., Wang, Y., de Graaf, C., Zhou, Q., Jiang, S., Liu, K., Cai, X., Dai, A., Lin, G., Liu, D., Wu, F., Wu, Y., Zhao, S., Ye, L., *et al.* (2017) Human GLP-1 receptor transmembrane domain structure in complex with allosteric modulators. *Nature* **546,** 312–315 CrossRef Medline
15. Jazayeri, A., Rappas, M., Brown, A. J. H., Kean, J., Errey, J. C., Robertson, N. J., Fiez-Vandal, C., Andrews, S. P., Congreve, M., Bortolato, A., Mason, J. S., Baig, A. H., Teobald, I., Doré, A. S., Weir, M., *et al.* (2017) Crystal structure of the GLP-1 receptor bound to a peptide agonist. *Nature* **546,** 254–258 CrossRef Medline
16. Zhang, Y., Sun, B., Feng, D., Hu, H., Chu, M., Qu, Q., Tarrasch, J. T., Li, S., Sun Kobilka, T., Kobilka, B. K., and Skiniotis, G. (2017) Cryo-EM structure of the activated GLP-1 receptor in complex with a G protein. *Nature* **546,** 248–253 CrossRef Medline
17. Liang, Y. L., Khoshouei, M., Glukhova, A., Furness, S. G. B., Zhao, P., Clydesdale, L., Koole, C., Truong, T. T., Thal, D. M., Lei, S., Radjainia, M., Danev, R., Baumeister, W., Wang, M. W., Miller, L. J., *et al.* (2018) Phase-plate cryo-EM structure of a biased agonist-bound human GLP-1 receptor-Gs complex. *Nature* **555,** 121–125 CrossRef Medline
18. Zhang, H., Qiao, A., Yang, L., Van Eps, N., Frederiksen, K. S., Yang, D., Dai, A., Cai, X., Zhang, H., Yi, C., Cao, C., He, L., Yang, H., Lau, J., Ernst, O. P., *et al.* (2018) Structure of the glucagon receptor in complex with a glucagon analogue. *Nature* **553,** 106–110 CrossRef Medline
19. Liang, Y. L., Khoshouei, M., Radjainia, M., Zhang, Y., Glukhova, A., Tarrasch, J., Thal, D. M., Furness, S. G. B., Christopoulos, G., Coudrat, T., Danev, R., Baumeister, W., Miller, L. J., Christopoulos, A., Kobilka, B. K., *et*

al. (2017) Phase-plate cryo-EM structure of a class B GPCR-G-protein complex. *Nature* **546,** 118–123 CrossRef Medline

20. Mukund, S., Shang, Y., Clarke, H. J., Madjidi, A., Corn, J. E., Kates, L., Kolumam, G., Chiang, V., Luis, E., Murray, J., Zhang, Y., Hötzel, I., Koth, C. M., and Allan, B. B. (2013) Inhibitory mechanism of an allosteric antibody targeting the glucagon receptor. *J. Biol. Chem.* **288,** 36168–36178 CrossRef Medline
21. Zhao, L. H., Yin, Y., Yang, D., Liu, B., Hou, L., Wang, X., Pal, K., Jiang, Y., Feng, Y., Cai, X., Dai, A., Liu, M., Wang, M. W., Melcher, K., and Xu, H. E. (2016) Differential requirement of the extracellular domain in activation of class B G protein-coupled receptors. *J. Biol. Chem.* **291,** 15119–15130 CrossRef Medline
22. Yin, Y., de Waal, P. W., He, Y., Zhao, L. H., Yang, D., Cai, X., Jiang, Y., Melcher, K., Wang, M. W., and Xu, H. E. (2017) Rearrangement of a polar core provides a conserved mechanism for constitutive activation of class B G protein-coupled receptors. *J. Biol. Chem.* **292,** 9865–9881 CrossRef Medline
23. Graaf, Cd., Donnelly, D., Wootten, D., Lau, J., Sexton, P. M., Miller, L. J., Ahn, J. M., Liao, J., Fletcher, M. M., Yang, D., Brown, A. J., Zhou, C., Deng, J., and Wang, M. W. (2016) Glucagon-like peptide-1 and its class B G protein-coupled receptors: a long march to therapeutic successes. *Pharmacol. Rev.* **68,** 954–1013 CrossRef Medline
24. Dods, R. L., and Donnelly, D. (2015) The peptide agonist-binding site of the glucagon-like peptide-1 (GLP-1) receptor based on site-directed mutagenesis and knowledge-based modelling. *Biosci. Rep.* **36,** e00285 Medline
25. Dal Maso, E., Zhu, Y., Pham, V., Reynolds, C. A., Deganutti, G., Hick, C. A., Yang, D., Christopoulos, A., Hay, D. L., Wang, M. W., Sexton, P. M., Furness, S. G. B., and Wootten, D. (2018) Extracellular loops 2 and 3 of the calcitonin receptor selectively modify agonist binding and efficacy. *Biochem. Pharmacol.* **150,** 214–244 CrossRef Medline
26. Black, J. W., and Leff, P. (1983) Operational models of pharmacological agonism. *Proc. R. Soc. Lond. B Biol. Sci.* **220,** 141–162 CrossRef Medline
27. Kenakin, T., and Christopoulos, A. (2013) Signalling bias in new drug discovery: detection, quantification and therapeutic impact. *Nat. Rev. Drug Discov.* **12,** 205–216 Medline
28. Wootten, D., Reynolds, C. A., Koole, C., Smith, K. J., Mobarec, J. C., Simms, J., Quon, T., Coudrat, T., Furness, S. G., Miller, L. J., Christopoulos, A., and Sexton, P. M. (2016) A hydrogen-bonded polar network in the core of the glucagon-like peptide-1 receptor is a fulcrum for biased agonism: lessons from class B crystal structures. *Mol. Pharmacol.* **89,** 335–347 CrossRef Medline
29. Siu, F. Y., He, M., de Graaf, C., Han, G. W., Yang, D., Zhang, Z., Zhou, C., Xu, Q., Wacker, D., Joseph, J. S., Liu, W., Lau, J., Cherezov, V., Katritch, V., Wang, M. W., and Stevens, R. C. (2013) Structure of the human glucagon class B G-protein-coupled receptor. *Nature* **499,** 444–449 CrossRef Medline
30. Jazayeri, A., Doré, A. S., Lamb, D., Krishnamurthy, H., Southall, S. M., Baig, A. H., Bortolato, A., Koglin, M., Robertson, N. J., Errey, J. C., Andrews, S. P., Teobald, I., Brown, A. J., Cooke, R. M., Weir, M., and Marshall, F. H. (2016) Extra-helical binding site of a glucagon receptor antagonist. *Nature* **533,** 274–277 CrossRef Medline
31. Yin, Y., Zhou, X. E., Hou, L., Zhao, L. H., Liu, B., Wang, G., Jiang, Y., Melcher, K., and Xu, H. E. (2016) An intrinsic agonist mechanism for activation of glucagon-like peptide-1 receptor by its extracellular domain. *Cell Discov.* **2,** 16042 CrossRef Medline
32. Wootten, D., Reynolds, C. A., Smith, K. J., Mobarec, J. C., Furness, S. G., Miller, L. J., Christopoulos, A., and Sexton, P. M. (2016) Key interactions by conserved polar amino acids located at the transmembrane helical boundaries in class B GPCRs modulate activation, effector specificity and biased signalling in the glucagon-like peptide-1 receptor. *Biochem. Pharmacol.* **118,** 68–87 CrossRef Medline
33. Wootten, D., Simms, J., Miller, L. J., Christopoulos, A., and Sexton, P. M. (2013) Polar transmembrane interactions drive formation of ligand-specific and signal pathway-biased family B G protein-coupled receptor conformations. *Proc. Natl. Acad. Sci. U.S.A.* **110,** 5211–5216 CrossRef Medline
34. Xiao, Q., Jeng, W., and Wheeler, M. B. (2000) Characterization of glucagon-like peptide-1 receptor-binding determinants. *J. Mol. Endocrinol.* **25,** 321–335 CrossRef Medline
35. López de Maturana, R., and Donnelly, D. (2002) The glucagon-like peptide-1 receptor binding site for the N terminus of GLP-1 requires polarity at Asp198 rather than negative charge. *FEBS Lett.* **530,** 244–248 CrossRef Medline
36. Coopman, K., Wallis, R., Robb, G., Brown, A. J., Wilkinson, G. F., Timms, D., and Willars, G. B. (2011) Residues within the transmembrane domain of the glucagon-like peptide-1 receptor involved in ligand binding and receptor activation: modelling the ligand-bound receptor. *Mol. Endocrinol.* **25,** 1804–1818 CrossRef Medline
37. Koole, C., Wootten, D., Simms, J., Valant, C., Miller, L. J., Christopoulos, A., and Sexton, P. M. (2011) Polymorphism and ligand dependent changes in human glucagon-like peptide-1 receptor (GLP-1R) function: allosteric rescue of loss of function mutation. *Mol. Pharmacol.* **80,** 486–497 CrossRef Medline
38. Koole, C., Wootten, D., Simms, J., Miller, L. J., Christopoulos, A., and Sexton, P. M. (2015) Differential impact of amino acid substitutions on critical residues of the human glucagon-like peptide-1 receptor involved in peptide activity and small-molecule allostery. *J. Pharmacol. Exp. Ther.* **353,** 52–63 CrossRef Medline
39. Underwood, C. R., Garibay, P., Knudsen, L. B., Hastrup, S., Peters, G. H., Rudolph, R., and Reedtz-Runge, S. (2010) Crystal structure of glucagon-like peptide-1 in complex with the extracellular domain of the glucagon-like peptide-1 receptor. *J. Biol. Chem.* **285,** 723–730 CrossRef Medline
40. Al-Sabah, S., and Donnelly, D. (2003) The positive charge at Lys-288 of the glucagon-like peptide-1 (GLP-1) receptor is important for binding the N-terminus of peptide agonists. *FEBS Lett.* **553,** 342–346 CrossRef Medline

Two distinct domains of the glucagon-like peptide-1 receptor control peptide-mediated biased agonism

Saifei Lei, Lachlan Clydesdale, Antao Dai, Xiaoqing Cai, Yang Feng, Dehua Yang, Yi-Lynn Liang, Cassandra Koole, Peishen Zhao, Thomas Coudrat, Arthur Christopoulos, Ming-Wei Wang, Denise Wootten and Patrick M. Sexton

J. Biol. Chem. 2018, 293:9370-9387.
doi: 10.1074/jbc.RA118.003278 originally published online May 1, 2018

Appendix IV:
Glucagon-like peptide-1 receptor internalisation controls spatiotemporal signalling mediated by biased agonists

Biochemical Pharmacology 156 (2018) 406–419

Contents lists available at ScienceDirect

Biochemical Pharmacology

journal homepage: www.elsevier.com/locate/biochempharm

Glucagon-like peptide-1 receptor internalisation controls spatiotemporal signalling mediated by biased agonists

Madeleine M. Fletcher[a], Michelle L. Halls[a], Peishen Zhao[a], Lachlan Clydesdale[a], Arthur Christopoulos[a], Patrick M. Sexton[a,b,*], Denise Wootten[a,b,*]

[a] Drug Discovery Biology, Monash Institute of Pharmaceutical Sciences, Faculty of Pharmacy and Pharmaceutical Sciences, Monash University, Parkville, Melbourne, Victoria 3052, Australia
[b] School of Pharmacy, Fudan University, Shanghai 201203, China

ARTICLE INFO

Keywords:
Glucagon-like peptide 1 receptor
Biased agonism
Receptor trafficking
Internalisation
Spatiotemporal signalling

ABSTRACT

The glucagon-like peptide-1 receptor (GLP-1R) is a major therapeutic target in the treatment of type 2 diabetes due to its roles in regulating blood glucose and in promoting weight loss. Like many GPCRs, it is pleiotropically coupled, can be activated by multiple ligands and is subject to biased agonism. The GLP-1R undergoes agonist mediated receptor internalisation that may be associated with spatiotemporal control of signalling and biased agonism, although to date, this has not been extensively explored. Here, we investigate GLP-1R trafficking and its importance with regard to signalling, including the localisation of key signalling molecules, mediated by biased peptide agonists that are either endogenous GLP-1R ligands or are used clinically. Each of the agonists promoted receptor internalisation through a dynamin and caveolae dependent mechanism and traffic the receptor to both degradative and recycling pathways. This internalisation is important for signalling, with cAMP and ERK1/2 phoshorylation (pERK1/2) generated by both plasma membrane localised and internalised receptors. Further assessment of pERK1/2 revealed that all peptides induced nuclear ERK activity, but ligands, liraglutide and oxyntomodulin that are biased towards pERK1/2 relative to cAMP (when compared to GLP-1 and exendin-4), also stimulated pERK1/2 activity in the cytosol. This compartmentalisation of ERK1/2 signalling was reliant on receptor internalisation, with restriction of receptor localisation to the plasma membrane limiting ERK1/2 signalling to the cytosol. Thus, this study implicates a role of receptor internalisation in spatiotemporal control of ERK1/2 signalling that may contribute to GLP-1R biased agonism.

1. Introduction

The glucagon-like peptide-1 receptor (GLP-1R) has been extensively studied due to its physiological importance in mediating the effects of the incretin hormone GLP-1 in regulation of blood glucose levels. It is a major, validated, therapeutic target for the treatment of type 2 diabetes [1]. The GLP-1R is expressed in pancreatic β-cells where it mediates direct glucoregulatory effects by increasing insulin, and decreasing glucagon, secretion [2]. In addition, GLP-1 increases the mass of pancreatic β-cells by increasing β-cell neogenesis and proliferation, while decreasing apoptosis [3]. Independent of insulin, GLP-1R activation also reduces plasma glucose concentrations through the inhibition of gastric emptying and reduces appetite and body weight, which can assist with controlling obesity, a condition that is often associated with diabetes [4].

The GLP-1R is a class B G protein-coupled receptor (GPCR) that has multiple endogenous agonists, including GLP-1 and oxyntomodulin. It is targeted clinically to treat type 2 diabetes and obesity, with exendin-4 and liraglutide being the two most commonly prescribed of the 6 FDA approved GLP-1R drugs. Upon activation, the receptor predominantly activates Gαs proteins to promote the production of cAMP. However, it is pleiotropically coupled and signals via other G protein-dependent and independent mechanisms, activating downstream pathways including intracellular calcium (iCa^{2+}) mobilisation and phosphorylation of mitogen activated kinases, such as extracellular regulated kinases 1 and 2 (ERK1/2) [5–7]. Due to this pleiotropic coupling, the GLP-1R is subject to biased agonism, where different GLP-1R agonists can induce distinct patterns of receptor signalling and regulation. Relative to GLP-1, oxyntomodulin exhibits bias towards ERK1/2 phosphorylation over cAMP production and iCa^{2+} mobilisation, and both oxyntomodulin and exendin-4 are biased towards β-arrestin recruitment [7,8].

A growing body of evidence suggests that the location (spatial) and

* Corresponding authors at: 381 Royal Parade, Parkville, VIC 3052, Australia.
E-mail addresses: patrick.sexton@monash.edu (P.M. Sexton), denise.wootten@monash.edu (D. Wootten).

https://doi.org/10.1016/j.bcp.2018.09.003
Received 10 July 2018; Accepted 5 September 2018
Available online 07 September 2018

duration (temporal) of signalling within a cell play an important role in the diverse cellular outputs that are mediated by GPCRs and in the generation of differential ligand responses at the same GPCR [9–11] Spatiotemporal compartmentalisation of signalling can arise through multiple mechanisms that include (but are not restricted to) regulatory mechanisms that control the location and duration of receptor activation, such as desensitisation and internalisation [12]. Upon activation, the GLP-1R internalises rapidly and enters pathways that either recycle the receptor back to the plasma membrane or that sort the receptor to lysosomal and recycling pathways [13–15]. GLP-1 and exendin-4 are reported to be 10-fold more potent at inducing internalisation than liraglutide, but GLP-1 causes the receptor to recycle two–three times faster than when stimulated with exendin-4 or liraglutide [13]. The mechanism underlying this internalisation is unclear, with both clathrin- and caveolae-dependent mechanisms being identified that vary with cell type [16–19]. Sustained signalling by internalised GLP-1Rs and colocalisation of intracellular GLP-1R with GLP-1, adenylate cyclase and Gαs has also been reported, with inhibition of receptor internalisation decreasing GLP-1 mediated cAMP formation, ERK1/2 phosphorylation, Ca^{2+} mobilisation and insulin secretion [14,20,21].

To date, the influence of compartmentalised signalling on GLP-1R biased agonism and the role of GLP-1R internalisation in this process has not been extensively explored. In this study, we test the hypothesis that GLP-1R internalisation is important for the spatiotemporal control of signalling and that this in turn may be linked to biased agonism. Here, we characterise signalling, regulatory protein interactions, internalisation and trafficking of the GLP-1R and identify distinct profiles of compartmentalised signalling that are influenced by receptor internalisation for different biased agonists.

2. Materials and methods

2.1. Peptides

GLP-1, exendin-4 and oxyntomodulin were purchased from Mimotopes (Melbourne, VIC, Australia). Liraglutide was purchased from Bachem (Bubendorf, Switzerland). Dulbecco's modified Eagle's medium (DMEM) was purchased from Invitrogen (Carlsbad, CA, USA). AlphaScreen™ reagents, Bolton-Hunter reagent [^{125}I] and 384-well ProxiPlates were purchased from PerkinElmer Life and Analytical Sciences (Waltham, MA, USA). Fetal bovine serum (FBS) was purchased from Thermo Fisher Scientific (Melbourne, VIC, Australia). SureFire™ ERK1/2 reagents were generously supplied by TGR Biosciences (Adelaide, SA, Australia). Unless specifically listed below, all other reagents were purchased from Sigma-Aldrich (St. Louis, MO, USA) or BDH Merck (Melbourne, VIC, Australia) and were of an analytical grade.

2.2. Plasmids and constructs

Human c-myc-GLP1R was generated in the laboratory as previously described [7]. The c-myc-GLP-1R-Rluc8 was generated by removal of the GLP-1R stop-codon and sub-cloning it into a gateway cassette (Invitrogen, Carlsbad, CA) containing a Rluc8 insert. The c-myc and Rluc8 tags have no effect on GLP-1R pharmacology [22]. Caveolin-1 (cav-1) and cav-1 P132L were generated via site-directed mutagenesis to introduce a stop codon in the Cav-1 P132L-mEGFP plasmid (prior to the mEGFP) from Addgene (Cambridge, MA, USA) with the QuikChange mutagenesis kit (Agilent Technologies, Santa-Clara, USA). The BRET sensors Rab5a, Rab7a, Rab11 and KRas-Venus were provided by Nevin Lambert (Augusta University, Georgia) and have been described previously [23,24]. The cAMP FRET sensors were provided by Martin Lohse (cytoEpac2 [25]) and Dermot Cooper (pmEpac2 [26]), the ERK FRET sensors were obtained from Addgene (nucEKAR plasmid 18,681 and cytoEKAR plasmid 18,679 [27]). HA-dynamin I K44E (dyn-K44E) and HA-dynamin I (dyn) constructs were provided by Nigel Bunnett (Columbia University) and have been previously described [28].

2.3. Cell culture and transfection

FlpIn-Chinese hamster ovary (FlpIn-CHO) cells (Invitrogen) were used due to their lack of endogenous GLP-1R expression. GLP-1R signalling has been well-characterised in this cell background [22]. Cells were cultured in Dulbecco's Modified Eagle's Medium (DMEM) (Invitrogen) supplemented with 5% v/v heat-inactivated fetal bovine serum (FBS) (Thermo Electron Corporation, Melbourne, VIC, Australia) at 37°C and 95% O_2 /5% CO_2 in a humidified incubator. FlpIn-CHO cells were either stably transfected with either human c-myc-GLP-1R, or c-myc-GLP-1R-Rluc8 with either β-arrestin1- or β-arrestin2-Venus using gateway technology. These cell lines were characterised and described previously [22,29]. Parental FlpIn-CHO cells were also transiently transfected, using polyethylenimine (PEI) (Polysciences, Warrington, PA), and plated simultaneously. DNA and PEI diluted in 150 mM NaCl were combined in a 1:6 ratio and incubated for 15 min, before the mixture was added to the cell suspension and the cells plated.

2.4. cAMP accumulation

FlpIn-CHO cells stably transfected with human c-myc-GLP-1R cells were seeded at a density of 30,000 cells/well into clear 96-well culture plates and incubated overnight at 37 °C in 5% CO_2. For cAMP accumulation assays in conditions where GLP-1R internalisation was inhibited, parental FlpIn-CHO cells were transiently transfected with 42 ng/well of human c-myc-GLP-1R and 107 ng/well of dyn-K44E or pcDNA3.1 and 15,000 cells/well were seeded into clear 96-well plates and incubated at 37 °C in 5% CO_2 for 48 h.

On the day of assay, growth media was replaced with stimulation buffer [phenol-free DMEM containing 0.1% (w/v) BSA, 1 M HEPES and 0.5 mM 3-isobutyl-1-methylxanthine, pH 7.4] and incubated for 30 min at 37 °C in 5% CO_2 before cells were stimulated with the indicated concentrations of peptide. After 30 min the reaction was terminated by aspiration of the buffer and addition of 50 µl of ice-cold 100% (v/v) ethanol. Upon evaporation of ethanol, 75 µl of lysis buffer [5 mM HEPES, 0.1% (w/v) BSA, 0.3% (w/v) Tween20, pH 7.4)] was added. Five µl of lysate was transferred to a 384-well OptiPlate (PerkinElmer). The cAMP detection was performed using a LANCE TR FRET kit (Perkin Elmer). 5 µl of anti-cAMP antibody (0.5% v/v diluted in the detection buffer) was added in reduced lighting conditions and the plate incubated for 30 min at room temperature. 10 µl of detection mix was added [0.02% v/v Eu-W8044 labelled streptavidin, 0.07% v/v biotin-cAMP diluted in the detection buffer] in reduced-lighting. The plate was incubated for 60 min at RT before measurement on the EnVision multilabel plate reader (PerkinElmer) using the LANCE protocol settings. All values were converted to an absolute concentration of cAMP using a cAMP standard curve performed in parallel. Data were analysed and curve fitting performed using a three-parameter logistic equation using GraphPad Prism version 6.0 (Graphpad Software Inc.).

2.5. ERK1/2 phosphorylation

FlpIn-CHO cells stably transfected with human c-myc-GLP-1R cells were seeded at a density of 30,000 cells/well into clear 96-well culture plates and incubated overnight for 30 min at 37 °C in 5% CO_2, and serum-starved in FBS-free DMEM for 6 h prior to being assayed. For pERK1/2 assyas in conditions where GLP-1R internalisation was inhibited, parental FlpIn-CHO cells were transiently transfected with 75 ng/well of human c-myc-GLP-1R and 75 ng/well of dyn-K44E or pcDNA3.1 and seeded into clear 96-well plates at 30,000 cells/well and assayed 48 h later. Cells were serum-starved overnight before the assay.

On the day of assay, cells were stimulated with ligand for the indicated time periods at 37 °C before stimulation was terminated by removal of media, then the addition of 40 µl of SureFire lysis buffer

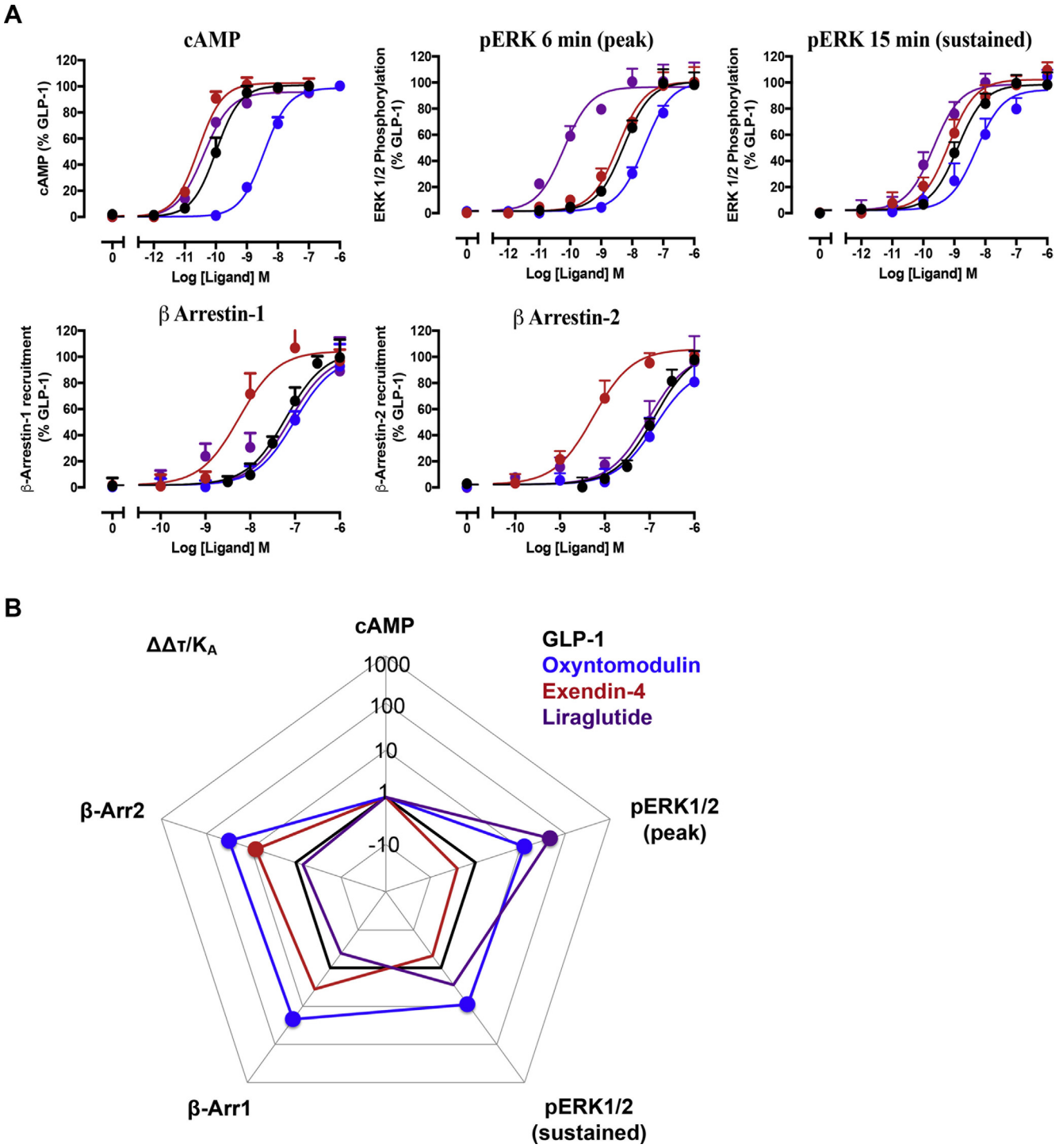

Fig. 1. Signalling bias exhibited by GLP-1R ligands in FlpIn-CHO cells stably expressing the GLP-1R. (A) Concentration-response data for GLP-1 (black), exendin-4 (red), oxyntomodulin (blue) and liraglutide (purple) for cAMP signalling, pERK1/2 signalling at two time points and β-Arrestin (β-Arr) 1 and 2 recruitment. (B) Web of bias illustrating peptide bias relative to GLP-1 and cAMP signalling. Concentration-response data were analysed using the operational model to determine bias factors (τ/K_A). These were normalized to GLP-1 and cAMP accumulation ($\Delta\Delta\tau/K_A$) and plotted on a logarithmic scale on the web. Circles represent data significantly different from GLP-1 as assessed using a one-way ANOVA followed by Dunnett's post test ($P < 0.05$). Data are mean + SEM from four to five experiments performed in duplicate. (For interpretation of the references to colour in this figure legend, the reader is referred to the web version of this article.)

(TGR Biosciences) and the plate agitated for two min. 5 µl of lysate was added to a 384-well ProxiPlate (PerkinElmer), and 8.5 µl of detection buffer [10 parts Activation buffer, 60 parts Reaction buffer, 0.3 parts AlphaScreen acceptor beads, 0.3 parts AlphaScreen donor beads] was added in reduced lighting conditions. The plate was incubated at 37 °C for 1 h, the plate cooled to RT for 30 min, before reading on the EnVision multilabel plate reader (PerkinElmer) (excitation wavelength = 680 nm; emission wavelength = 520–620 nm). All data were expressed as a percentage of the ERK1/2 phosphorylation mediated after 6 or 15 min of exposure to 10% v/v FBS (as stated). Data were analysed and curve fitting performed using a three-parameter logistic equation using GraphPad Prism version 6.0.

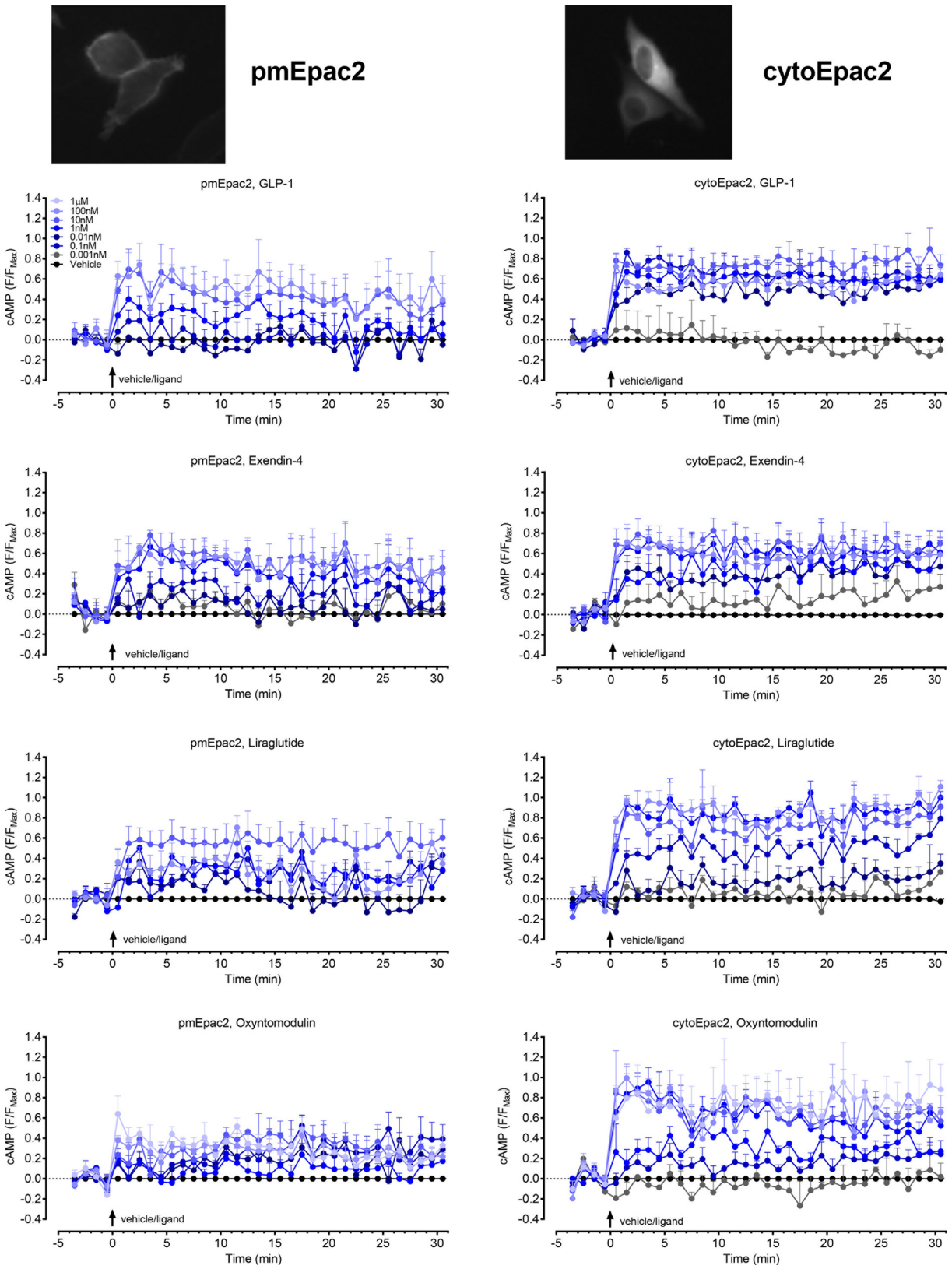

Fig. 2. Compartmentalised cAMP signalling. Time course of cAMP signalling upon stimulation of GLP-1R, by GLP-1, exendin-4, liraglutide and oxyntomodulin as measured by the FRET sensors pmEpac2 and cytoEpac2 in FlpIn-CHO cells following transient transfection of the GLP-1R and the relevant FRET sensor. Cell images for each sensor are shown, confirming the localization of the two sensors to the plasma membrane (pmEpac2) or the cytosol (cytoEpac2). Data are plotted as change in CFP/YFP ratio relative to the maximum response (F_{max}) for each cell and baseline corrected to the vehicle response. Data points are mean + SEM, of 3–6 individual experiments (n), with 48–211 individual cells per condition in each individual n.

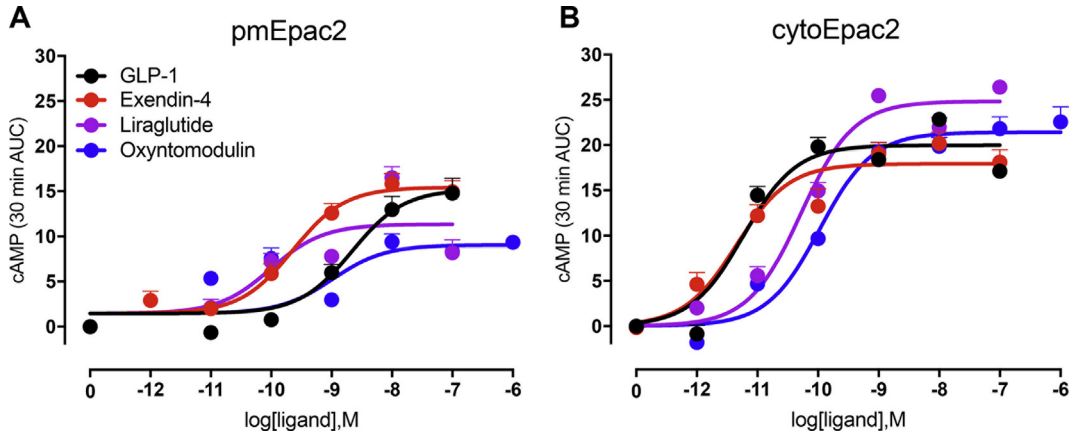

Fig. 3. Concentration-response curves of cAMP signalling upon stimulation of GLP-1R, by GLP-1, exendin-4, liraglutide and oxyntomodulin measured using FRET sensors pmEpac2 and cytoEpac2 in FlpIn-CHO cells following transient transfection of the GLP-1R and the relevant FRET sensor Data are the AUC of F/F_{max} over 30 min as in Fig. 2. Data points are mean + SEM, of 3–6 individual experiments (n), with 48–211 individual cells per condition in each individual n.

Table 1
Summary of the pEC_{50} and E_{max} values of AUC concentration–response curves of cAMP detected by the pmEpac2 and cytoEpac2 sensors upon stimulation of GLP-1R with peptide ligands. pEC_{50} is the negative logarithm of the concentration that produces 50% of the maximal response. E_{max} is the maximal response, as indicated by the maximum of the concentration–response curve. Values are mean ± SEM calculated from a three-parameter curve fit. Statistical tests are one-way ANOVA, followed by Tukey's post-test, # compared to GLP-1 for each sensor, #p < 0.01.

	pEC_{50} (M)			
	GLP-1	Exendin-4	Liraglutide	Oxyntomodulin
pmEpac2	8.66 ± 0.40 (3)	9.64 ± 0.36 (3)	10.01 ± 0.47 (3)	8.98 ± 0.61 (3)
cytoEpac2	11.23 ± 0.20 (3)	11.35 ± 0.23 (5)	10.28 ± 0.17 (3)	9.97 ± 0.18 (3)#
E_{max} (relative units AUC)				
	GLP-1	Exendin-4	Liraglutide	Oxyntomodulin
pmEpac2	15.23 ± 0.28 (3)	15.44 ± 0.77 (3)	11.31 ± 2.44 (3)	9.06 ± 2.24 (3)
cytoEpac2	19.99 ± 1.16 (3)	17.93 ± 1.14 (5)	24.84 ± 1.35 (3)	21.42 ± 1.19 (3)

2.6. Bioluminescence resonance energy transfer (BRET) assays to assess β-arrestin recruitment

FlpIn-CHO cells stably expressing the human c-myc-GLP-1R-Rluc8 and either β-arrestin1- or β-arrestin2-Venus were seeded in 96-well white-walled CulturPlates (PerkinElmer) at a density of 30,000 cells/well and cultured for 24 h. Cells were washed once with HBSS with 0.1% w/v BSA, to remove traces of phenol red and incubated in this solution for a further 15 min. Cells were challenged with drug or vehicle at indicated time points, and the Rluc substrate coelenterazine-h (Nanolight) added to reach a final concentration of 5 μM 10 min before BRET reads. BRET readings were collected using a LumiSTAR Omega (BMG LabTech) that allows sequential integration of signals detected in the 465–505 nm and 515–555 nm windows using filters with the appropriate band pass. The BRET ratio for each sample (515–555 nm emission over 465–505 nm emission) was vehicle subtracted to express results as ligand-induced BRET. This eliminates the requirement for measuring a donor only control sample. Initial time course experiments were performed over 20 min to determine the time at which β-arrestin1 and β-arrestin2 recruitment was maximal for each ligand. Subsequent concentration response data were collected at this peak time. Data were normalized to the maximal response elicited by GLP-1. Data were analysed and curve fitting performed using a three-parameter logistic equation using GraphPad Prism version 6.0.

2.7. BRET assays to assess receptor trafficking

FlpIn-CHO were transiently transfected with 20 ng/well human c-myc-GLP-1R-Rluc8, 80 ng/well BRET biosensor (either Rab5a-, Rab7a-, Rab11- or KRas- Venus) and 50 ng/well of either dyn-K44E, dyn, cav-1, cav-1 P132L or pcDNA3.1. The cells were plated at 15,000 cells/well, into 96-well white-walled CulturPlates (PerkinElmer) and assays performed 48 h later. Cells were washed once with HBSS containing 0.1% w/v BSA and 10 μg/μl cycloheximide (Sigma Aldrich), then incubated in this solution for another 30 min. Cycloheximide was added to prevent *de novo* protein synthesis.

In Pitstop2 studies, 30 μM of Pitstop2 was added to the buffer for the 30 min incubation. Cells were challenged with the drug or vehicle at indicated time-points and washed 30 min after addition. Ten min before reading the plate, coelentrazine h was added to give a final concentration of 5 μM. The plate was read on a LUMIstar Omega using 465–505/515–555 nm filters. The BRET ratio for each sample (515–555 nm emission over 465–505 nm emission) was vehicle subtracted to express results as ligand-induced BRET, and corrected to baseline values at time 0.

2.8. Forster resonance energy transfer assays to assess signalling

FlpIn-CHO cells were transiently transfected with 55 ng/well human c-myc-GLP-1R and 45 ng/well of FRET sensor (cytoEpac2, pmEpac, nucEKAR or cytoEKAR) or for studies assessing the impact of internalisation, 42 ng/well receptor, 45 ng/well biosensor (cytoEpac2, pmEpac, nucEKAR or cytoEKAR) and 63 ng/well of dyn-K44E or pcDNA3.1. Cells were seeded at 15,000 cells/well into 96-well clear-bottomed, black-walled ViewPlates (PerkinElmer). Assays were performed 48 h after transfection and cells were serum-starved overnight before assay. The assay method is adapted from that previously described [30]. On the day of assay cells were equilibrated in HBSS at 37°C for 30 min. Fluorescence was measured on the GE Healthcare high-content INCell 2000 Analyzer, with CFP and YFP filters and a

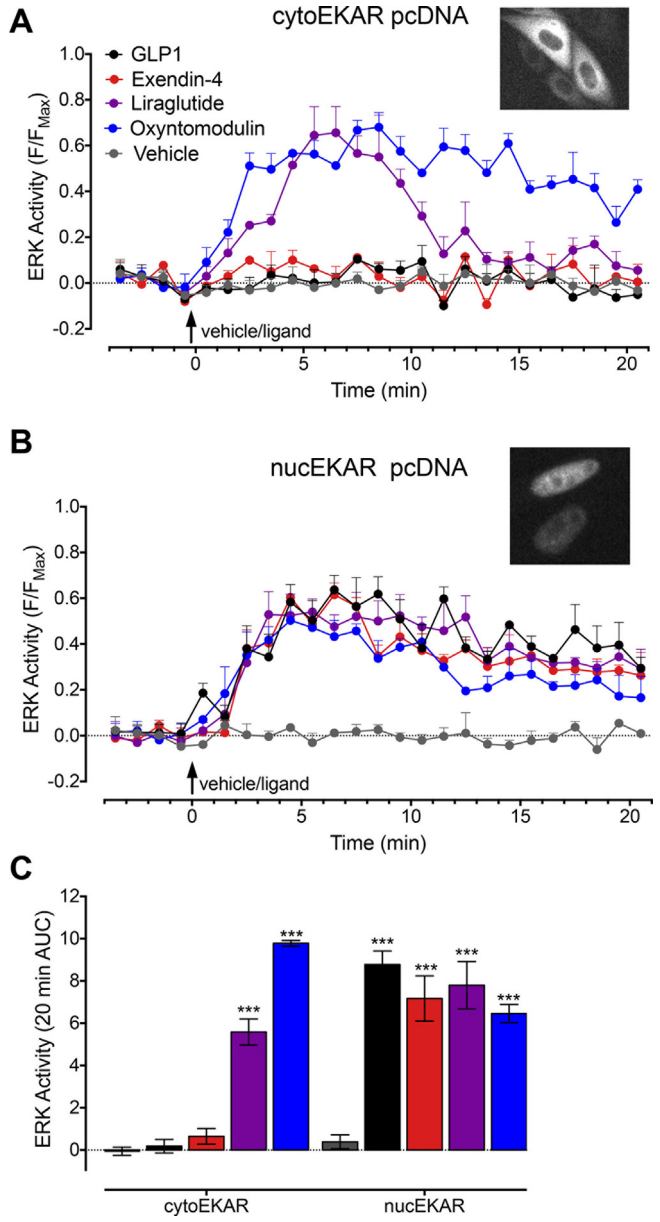

Fig. 4. Time course of ERK activity upon stimulation of GLP-1R, by GLP-1, exendin-4, liraglutide (100 nM) and oxyntomodulin (1 μM) as measured by cytoEKAR (A) and nucEKAR (B) in FlpIn-CHO cells following transient transfection of the human GLP-1R and the relevant FRET sensor. Cell images are shown in A and B to confirm the localization of the sensors to the cytosol (cytoEKAR) or the nucleus (nucEKAR). Data are plotted as change in cerulean/venus ratio relative to the maximum response to FBS (F_{max}) for each cell. Data points are mean + SEM, of three individual experiments (n), with 68–176 total cells per condition. Statistical tests are two-way ANOVA, followed by Dunnett's test compared to vehicle, $^{***}p < 0.001$.

polychroic optimised for the CFP/YFP filter pair (Quad3). Images of up to 14 wells were collected at one min intervals. Baseline emission ratio images were captured for four min. Cells were the challenged with the drug or vehicle and the images captured for 30 min, before the cells were stimulated with the positive control [10 μM forksolin and 100 μM 3-isobutyl-1-methylxanthine (IBMX) for cAMP or 200 nM phorbol-12,13-dibutyrate for ERK] for 10 min to generate maximal FRET, and positive images collected for four min. Data were analysed with three macros that run in the FIJI distribution of Image J, as previously described [30]. Briefly, the baseline, stimulated and positive image stacks were collated and aligned with the StackCreator script. The cells and background were selected, the fluorescence intensity measured across the stack, and the background fluorescence subtracted. The FRET response was graphed as the FRET ratio relative to the positive control (F/F_{max}) for each cell at each time-point. Only cells with > 5% increase in the background corrected FRET ratio (F/F_0) to the positive control were selected for analysis. To generate the concentration–response curves, the area under the curve was plotted against the log concentration of peptide, and the curves were fit in GraphPrism version 6 using a three-parameter logistic equation.

2.9. Bias calculations

To quantify biased agonism, which may be manifested as selective functional affinity (K_A) and/or efficacy (τ) of an agonist for a given pathway, concentration response data were analysed with an operational model of agonism directly modified to estimate the ratio of τ/K_A for each pathway as described previously [7]. All estimated parameters are expressed as logarithms (mean ± S.E.M.).

2.10. Statistics

Comparisons of multiple different groups were assessed using a one-way or two-way analysis of variance (ANOVA) followed by either Sidak's, Dunnett's or Tukey's post-test. Paired or unpaired t-tests were performed to compare the effects of dyn-K44E and pcDNA and differences between the pmEpac2 and cytoEpac2 sensors with regard to potency and maximal responses calculated from concentration response curves. Significance was accepted at $p < 0.05$.

3. Results

3.1. Exendin-4, liraglutide and oxyntomodulin are biased peptides relative to GLP-1

Agonist concentration–response data were generated to assess biased agonism in multiple pathways; cAMP accumulation, ERK1/2 phosphorylation and β-arrestin recruitment (Fig. 1A). cAMP assays were performed as an accumulation assay over 30 min. For β-arrestin recruitment, concentration–response data were generated at the time-point of the peak response (3 min). For ERK1/2 phosphorylation, concentration–response curves were generated at two time points, chosen to reflect peak response (6 min) and the sustained response (15 min), as determined from kinetic time course experiments. Calculation of transduction ratios (tau/Ka) determined from operational fitting to concentration–response data [31], revealed both oxyntomodulin and liraglutide are biased agonists relative to GLP-1, generating greater ERK1/2 phosphorylation relative to the same amount of cAMP (Fig. 1B). This bias was greater for liraglutide than oxyntomodulin at the peak (6 min) response, but oxyntomodulin was greater when measuring the sustained response (15 min time point). When assessing β-arrestin 1 or 2 recruitment, liraglutide displayed no bias relative to cAMP when compared with GLP-1. This was in contrast to oxyntomodulin and exendin-4 that were both biased towards recruitment of β-arrestin 2, similar to previous observations (Fig. 1B), [32]. Oxyntomodulin was also significantly biased towards β-arrestin 1.

3.2. Ligand-dependent spatiotemporal signalling of the GLP-1R

To gain temporal and spatial resolution of GLP-1R signalling, we utilised a cytosolically located (cytoEpac2) and a plasma membrane targeted (pmEpac2) cAMP Epac2 biosensor. cAMP was detected with both sensors, immediately upon stimulation with all peptides (Fig. 2). cAMP signals at lower concentrations of ligand were more transient at the plasma membrane, decreasing back towards baseline over the 30 min after stimulation. Cytosolically localised responses were sustained over this time scale. Taking the area under the curve (AUC) of

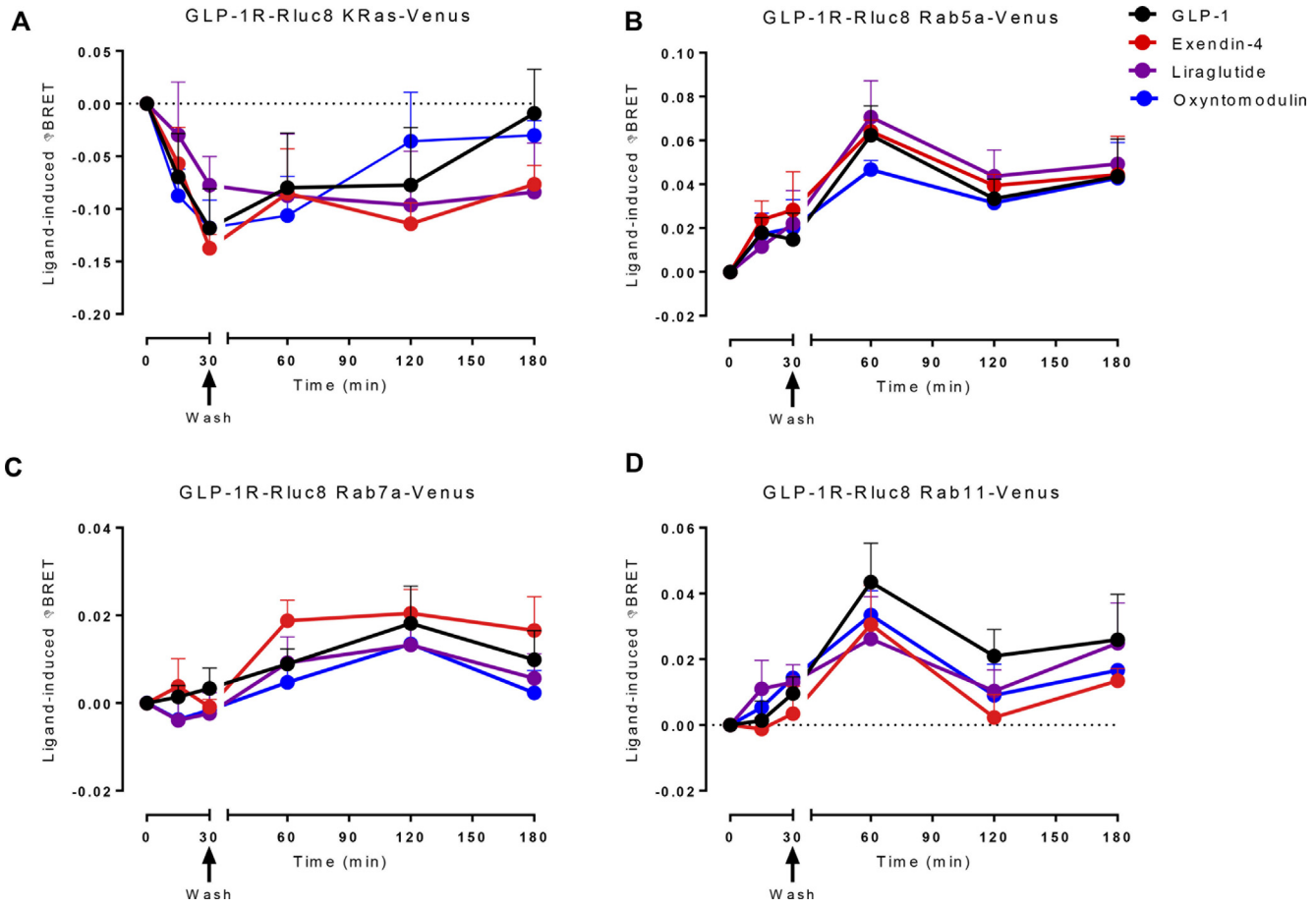

Fig. 5. The trafficking of GLP-1R-Rluc8 in FlpIn-CHO cells upon stimulation with GLP-1 (100 nM), exendin-4 (100 nM), liraglutide (100 nM) and oxyntomodulin (1 μM). Cells were transiently transfected with human GLP-1R-Rluc8 and the relevant BRET sensor targeted to the various subcellular compartments. Cells were challenged with ligand for 30 min before they were washed and BRET measured between GLP-1R-Rluc8 and subcellular markers (A) KRas (plasma membrane), (B) Rab5a (early endosome), (C) Rab7a (late endosome) and (D) Rab11 (recycling endosome). Data are mean + SEM from four to five experiments performed in triplicate.

each of these graphs, concentration–response curves were plotted (Fig. 3, Table 1). Consistent with population-based global assays of cellular cAMP, oxyntomodulin had the weakest response in both cellular compartments with statistically lower potency relative to GLP-1 at the cytoplasmic localised sensor and a lower maximal response than GLP-1 in generating plasma membrane-localised cAMP (Table 1). Interestingly, equipotent responses were measured for liraglutide in both compartments, whereas GLP-1, exendin-4 and oxyntomodulin were 372-, 51- and 10- fold more potent, respectively, in detecting cAMP using the cytosolically localised sensor relative to the plasma membrane localised sensor. Consequently, GLP-1 and exendin-4 were significantly more potent in the generation of cytosolic cAMP than liraglutide. In contrast, GLP-1 was 10-fold less potent than exendin-4 and liraglutide, which were equipotent, in the generation of cAMP at the plasma membrane (albeit these differences did not reach statistical significance for this sensor). These data suggest that individual peptides differentially generate localised pools of cAMP.

Compartmentalised ERK activation was detected in time-course assays using a single saturating concentration of ligand, by ERK activity sensors localised to the cell cytosol (cytoEKAR; Fig. 4A) or nucleus (nucEKAR; Fig. 4B). Nuclear ERK activity was detected upon stimulation with all four peptides, although the oxyntomodulin response was more transient than the other three ligands (Fig. 4B, 4C). In contrast, within the cytosol, a different profile of ERK activity was observed where the biased agonists liraglutide and oxyntomodulin generated cytosolic ERK activity but GLP-1 and exendin-4 did not elicit a response (Fig. 4A and C). Interestingly, the response to oxyntomodulin was sustained over the 20 min time-course, whereas the response to liraglutide was transient, decreasing back to baseline by 15 min.

3.3. GLP-1R internalises into early, recycling and late endosomes upon activation by all peptide ligands

To assess the role of receptor internalisation in GLP-1R signalling, we first assessed the internalisation and trafficking of the GLP-1R using bioluminescence resonance energy transfer (BRET) to measure the co-localisation of a Rluc8 tagged receptor (GLP-1R-Rluc8) with Venus-tagged markers that are targeted to defined subcellular locations (KRas-Venus, Rab5a-Venus, Rab7a-Venus, Rab11-Venus). Upon stimulation with all four peptide ligands, the GLP-1R rapidly internalised as detected by a decrease in co-localisation of the GLP-1R and the plasma membrane marker KRas (decrease in BRET signal) that reached a maximum at 30 min post ligand stimulation (Fig. 5A). Accordingly, this was correlated with increased co-localisation between the GLP-1R and the early endosomal marker Rab5a (increased BRET signal), which peaked at 60 min (Fig. 5B). These data exemplify the GLP-1R leaving the plasma membrane, via internalisation, and entering early endosomes. An increase in BRET was also observed with GLP-1R and the markers Rab11 and Rab7a, peaking at 60 and 120 min, respectively (Fig. 5C and D). This indicates that receptor trafficking diverges into both recycling and late endosomes, from which the receptor is likely trafficked either back to the plasma membrane or to lysosomes. No

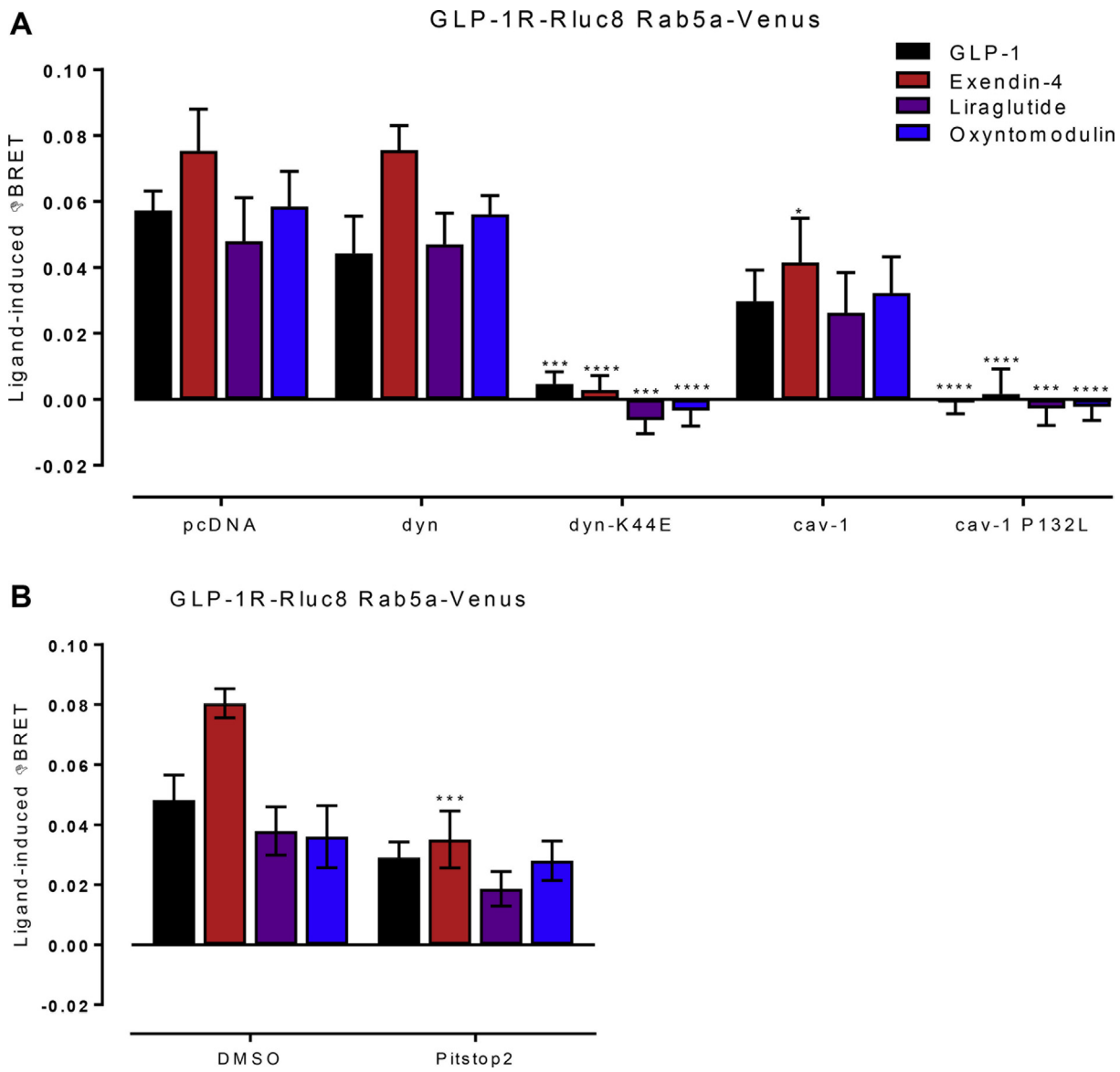

Fig. 6. The co-localisation of GLP-1R-Rluc8 with the early endosome was assessed in FlpIn-CHO cells transiently transfected with GLP-1R-Rluc8, Rab5a-Venus and either dyn, cav-1 or their dominant-negative forms, dyn-K44E and cav-1-P132L (A) or treated with clathrin inhibitor Pitstop2 (B). Cells were treated with peptide agonists GLP-1 (100 nM), exendin-4 (100 nM), liraglutide (100 nM) and oxyntomodulin (1 μM), the ligand was washed out at 30 min and the BRET between GLP-1R-Rluc8 and Rab5a-Venus (early endosome) measured at 60 min. Data points are vehicle-corrected and are mean + SEM from five experiments, performed in triplicate. Statistical tests are two-way ANOVA, (with variables pcDNA3 and each inhibitor) followed by Dunnett's post-test, compared to pcDNA control for each ligand) (A) or two-way ANOVA, (variables DMSO control and Pitstop2), followed by Sidak's post-test, compared to DMSO control for each ligand ($^{*}p < 0.05$, $^{***}p < 0.001$, $^{****}p < 0.0001$) (B).

statistical difference was observed in the kinetics or magnitude of ligand-induced trafficking between the different peptide agonists at any time point assessed.

3.4. GLP-1R internalises via caveolin-1, clathrin and dynamin-dependent mechanisms in FlpIn-CHO cells

Previous literature has provided evidence for clathrin and/or caveolae-mediated GLP-1R internalisation across a range of cellular backgrounds. A partial role of clathrin-coated pits has been implicated in CHO and CHL cells [16,17], whereas a caveolin-1 dependent mechanism has been observed in HEK293 cells, with GLP-1R and caveolin-1 co-localising inside the cell [18,19]. Both clathrin and caveolae-mediated mechanisms are dynamin-dependent. To determine the mechanism by which GLP-1R internalises in the FlpIn-CHO cells used in the current study, we measured BRET between the early endosomal marker, Rab5a-Venus, and the GLP-1R-Rluc8 60 min after ligand stimulation, in the presence or absence of various inhibitors of GPCR internalisation. Consistent with previous reports, overexpression of dyn-K44E, a dominant negative form of dynamin with no GTPase activity [33], abolished all ligand-mediated GLP-1R internalisation when compared to the wild type dynamin and the pcDNA3.1 transfection control (Fig. 6A). Also consistent with published literature, the clathrin-dependent inhibitor, Pitstop2, partially inhibited internalisation for exendin-4 (Fig. B). Caveolin-1 (cav-1) is a key protein in the formation of caveolae, and cav1-P132L, is dominant negative mutant of the protein that is intracellularly retained [34]. Transfection of cav1-P132L also abolished internalisation of GLP-1R compared to wildtype and pcDNA3.1 for all peptides (Fig. 6A).

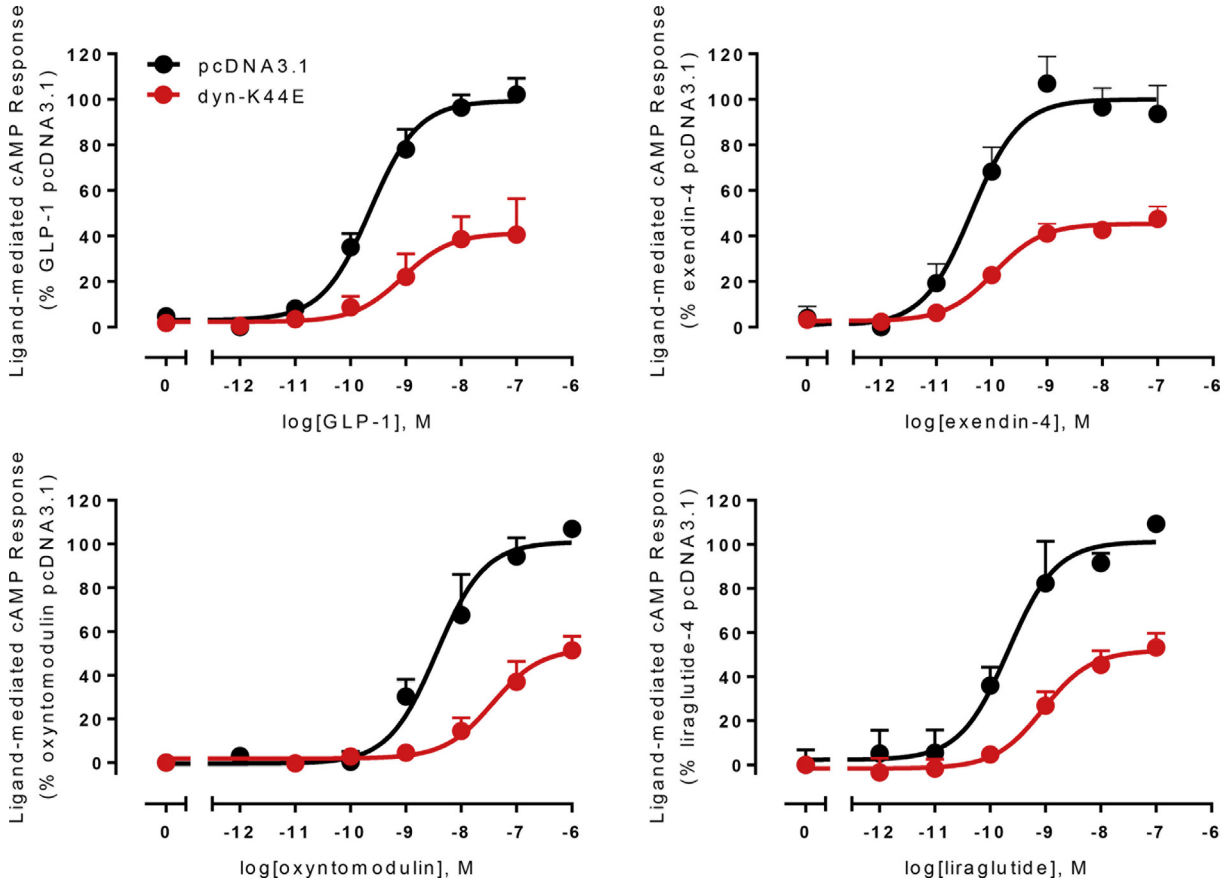

Fig. 7. Concentration-response curves for 30 min cAMP accumulation upon stimulation of the GLP-1R with GLP-1, liraglutide, oxyntomodulin, exendin-4, in FlpIn-CHO cells transiently transfected with GLP1R and either dyn-K44E or pcDNA. Data points are vehicle corrected and represent the mean + SEM from four to five individual experiments performed in triplicate.

Table 2
pEC_{50} and E_{max} values calculated from concentration-response data performed in FlpIn CHO cells transfected with either dyn-K44E or pcDNA3.1. E_{max} is the maximal response expressed as a percentage of the pcDNA3.1 control. Values represent the mean ± SEM from 3 to 5 individual experiments performed in triplicate. Individual number of experiments are shown in brackets. Statistical tests are unpaired students t-tests comparing dyn-K44E to the pcDNA3.1 control for each ligand
$^{*}p < 0.05$.

		GLP-1		Exendin-4		Liraglutide		Oxyntomodulin	
		pEC_{50}	E_{max}	pEC_{50}	E_{max}	pEC_{50}	E_{max}	pEC_{50}	E_{max}
cAMP	pcDNA3.1	9.65 ± 0.12 (5)	100 ± 4	10.4 ± 0.19 (5)	100 ± 5	9.76 ± 0.22 (5)	100 ± 7	8.45 ± 0.17 (4)	100 ± 6
	dyn-K44E	8.97 ± 0.29 (4)	47 ± 6*	9.95 ± 0.15 (5)	45 ± 2*	8.98 ± 0.19 (5)	51 ± 4*	7.43 ± 0.23 (4)*	51 ± 5*
pERK1/2	pcDNA3.1	8.93 ± 0.11 (3)	100 ± 4	9.18 ± 0.17 (5)	100 ± 6	9.63 ± 0.15 (5)	100 ± 5	8.23 ± 0.19 (4)	100 ± 7
	dyn-K44E	7.98 ± 0.43 (3)	65 ± 12*	8.88 ± 0.41 (5)	60 ± 7*	8.72 ± 0.22 (5)*	73 ± 7*	7.03 ± 0.35* (4)	64 ± 12*

3.5. Inhibition of GLP-1R internalisation decreases global cAMP formation and ERK1/2 phosphorylation

To determine the influence of GLP-1R internalisation on cAMP mediated signalling, cAMP production was assessed in a population-based accumulation assay in the presence of dyn-K44E to completely abolish ligand-mediated receptor internalisation (Fig. 7). Over-expression of dyn-K44E reduced the maximal cAMP response for all peptides by approximately 50% (Fig. 7, Table 2). In contrast, there was only limited attenuation of GLP-1, exendin-4 or liraglutide potency for cAMP signalling, while a significant reduction of potency was observed for oxyntomodulin (Fig. 7, Table 2).

To assess the influence of receptor internalisation on ERK1/2 phosphorylation, an initial kinetic assay was performed in a population-based cell assay with GLP-1 in the absence or presence of dyn-K44E (Fig. 8A). A decrease in pERK1/2 response in the presence of dyn-K44E was evident across the entire time-course with the greatest reduction occurring at 15 min. As such, concentration response curves for ERK1/2 phosphorylation were performed at 15 min. Treatment of cells with dyn-K44E attenuated responses of all four ligands (Fig. 8B). For liraglutide and oxyntomodulin, both potency and maximal responses, relative to the control, were statistically reduced upon inhibition of internalisation (Fig. 8B, Table 2). For GLP-1 and exendin-4, there was little effect on potency, however a similar reduction in maximal response (Fig. 8B, Table 2).

3.6. GLP-1R internalisation plays a role in the control of spatiotemporal signalling

To observe if the reduced cAMP production and pERK1/2 observed

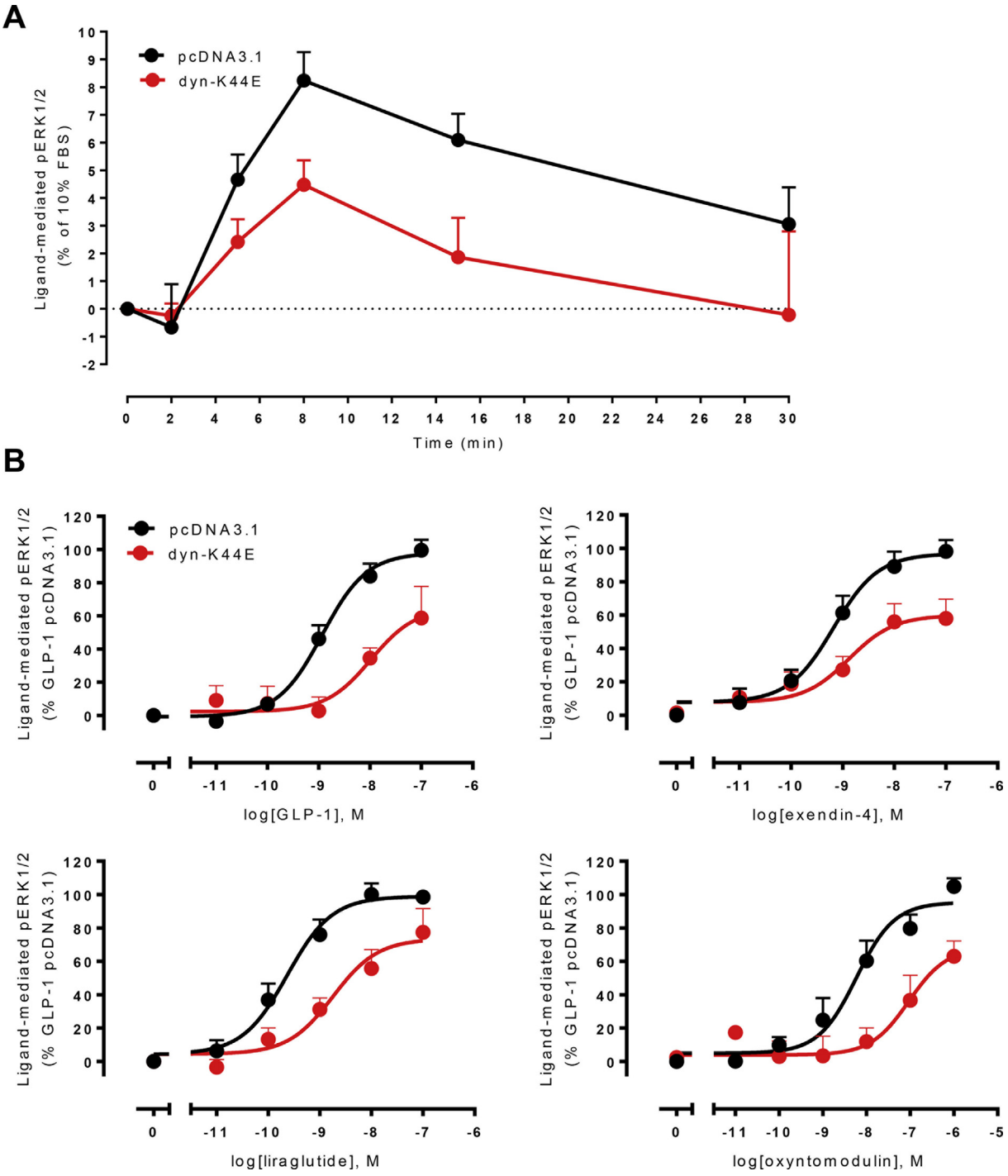

Fig. 8. pERK1/2 in FlpIn-CHO cells transiently transfected with the GLP-1R and either pcDNA or dyn-K44E. **A)** Time course of ERK1/2 phosphorylation over 30 min after stimulation with GLP-1 (100 nM) normalised to FBS response at 6 min. dyn-K44E reduced pERK1/2 relative the control (pcDNA3). B) Concentration-response curves for pERK1/2 after 15 min stimulation with GLP-1, liraglutide, exendin-4 and oxyntomodulin. Data are vehicle-corrected and mean + SEM from three (A) or three-five (B) experiments performed in triplicate.

upon inhibition of GLP-1R internalisation in global assays is correlated to alterations in spatiotemoral profiles of cAMP production or ERK1/2 activity, a single saturating concentration of peptide was used to assess the role of receptor internalisation in the generation of compartmentalised cAMP and pERK1/2 activity. Inhibition of GLP-1R internalisation using dyn-K44E attenuated cAMP signaling in both compartments, although the magnitude of the effect was both peptide- and compartment-dependent. Using the plasma membrane-localised sensor, there was a reduction in AUC response for exendin-4 and liraglutide in the presence of dyn-K44E, but no effect on oxyntomodulin (Fig. 9A and C). In contrast, cAMP production measured with the cytosolically-localised sensor was attenuated for GLP-1, exendin-4 and oxyntomodulin, but not liraglutide, following inhibition of GLP-1R internalisation (Fig. 9B and C).

Intriguingly, inhibition of GLP-1R internalisation using dyn-K44E eliminated all nuclear ERK activity. In contrast, inhibition of GLP-1R internalisation revealed cytoEKAR responses to GLP-1 and exendin-4 that did not produce cytosolic signalling under control conditions

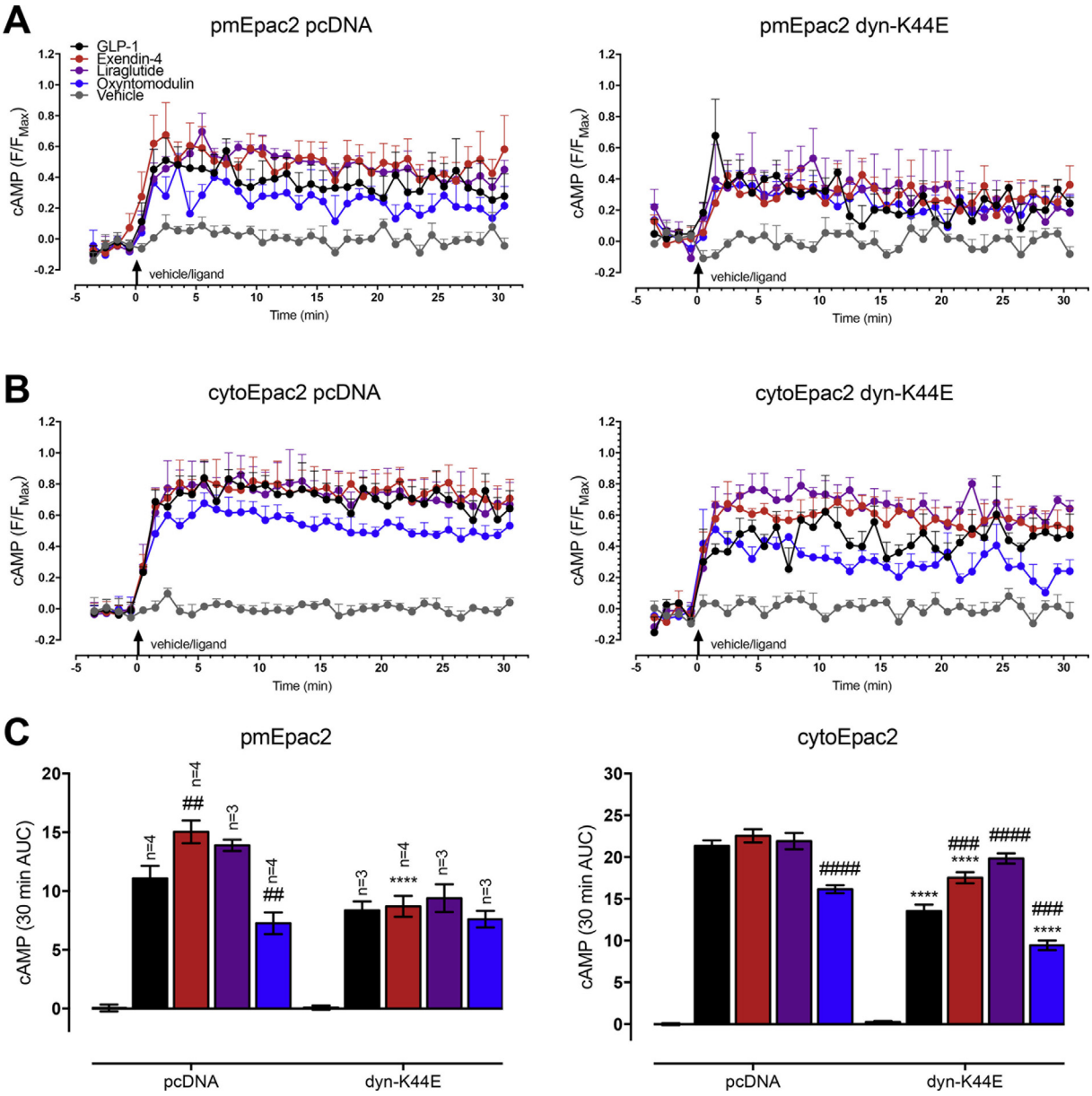

Fig. 9. Time course of cAMP signalling upon stimulation of GLP-1R, in FlpIn-CHO cells transiently transfected with the GLP-1R, the relevant FRET sensor and either pcDNA or dyn-K44E, by equi-occupant concentrations of GLP-1, exendin-4, liraglutide (1 nM) and oxyntomodulin (10 nM) as measured by FRET sensors pmEpac2 and cytoEpac2. Data are plotted as change in CFP/YFP ratio relative to the maximum response to forskolin and IBMX (F_{max}) for each cell. Data points are mean ± SEM, of three-four individual experiments for pmEpac2 and three individual experiments for cytoEpac2, with 141–324 total cells per condition. Statistical tests are two-way ANOVA, (variables pcDNA and dyn-K44E), followed by Sidak's post test to compare each ligand in the different treatments, ($^{****}p < 0.0001$) or Dunnett's post test, to compare each ligand to GLP-1 within each treatment ($^{\#\#}p < 0.01$, $^{\#\#\#}p < 0.001$, $^{\#\#\#\#}p < 0.0001$).

(Fig. 10A–C). In addition, the temporal profile of liraglutide ERK activity within the cytosol switches from a transient response to a sustained profile, consistent with retention of the receptor at the plasma membrane. Consequently, a similar degree of sustained cytosolic ERK activity was observed for all four peptides following inhibition of internalisation (Fig. 10A and C).

4. Discussion

Biased agonism is well established at the GLP-1R and multiple recent studies have implicated a role for receptor internalisation in the control of GLP-1R signalling that may have clinical implications for development of novel therapeutics. Here, we reveal important and unappreciated roles of internalisation and trafficking in the control of differential GLP-1R activation that leads to distinct spatiotemporal signalling profiles by GLP-1R biased agonists.

Consistent with previous publications [32], this study confirmed oxyntomodulin as a biased GLP-1R agonist favouring pERK1/2 and β-arrestin recruitment relative to cAMP when compared with GLP-1. The clinically used ligands exendin-4 and liraglutide are also biased agonists; for liraglutide this manifests as bias towards pERK1/2 in the absence of β-arrestin bias relative to cAMP, whereas exendin-4 displayed a modest degree of bias towards β-arrestin recruitment with no change in pERK1/2 relative to cAMP. pERK1/2 is predicted to be downstream of β-arrestin recruitment, however the lack of direct correlation between pERK1/2 and β-arrestin bias relative to cAMP for some ligands suggest multiple signalling and regulatory pathways link GLP-1R activation and signalling to downstream mediators, such as pERK1/2. This is consistent with our earlier work that demonstrates both β-arrestin and G protein mediated pathways play a role in

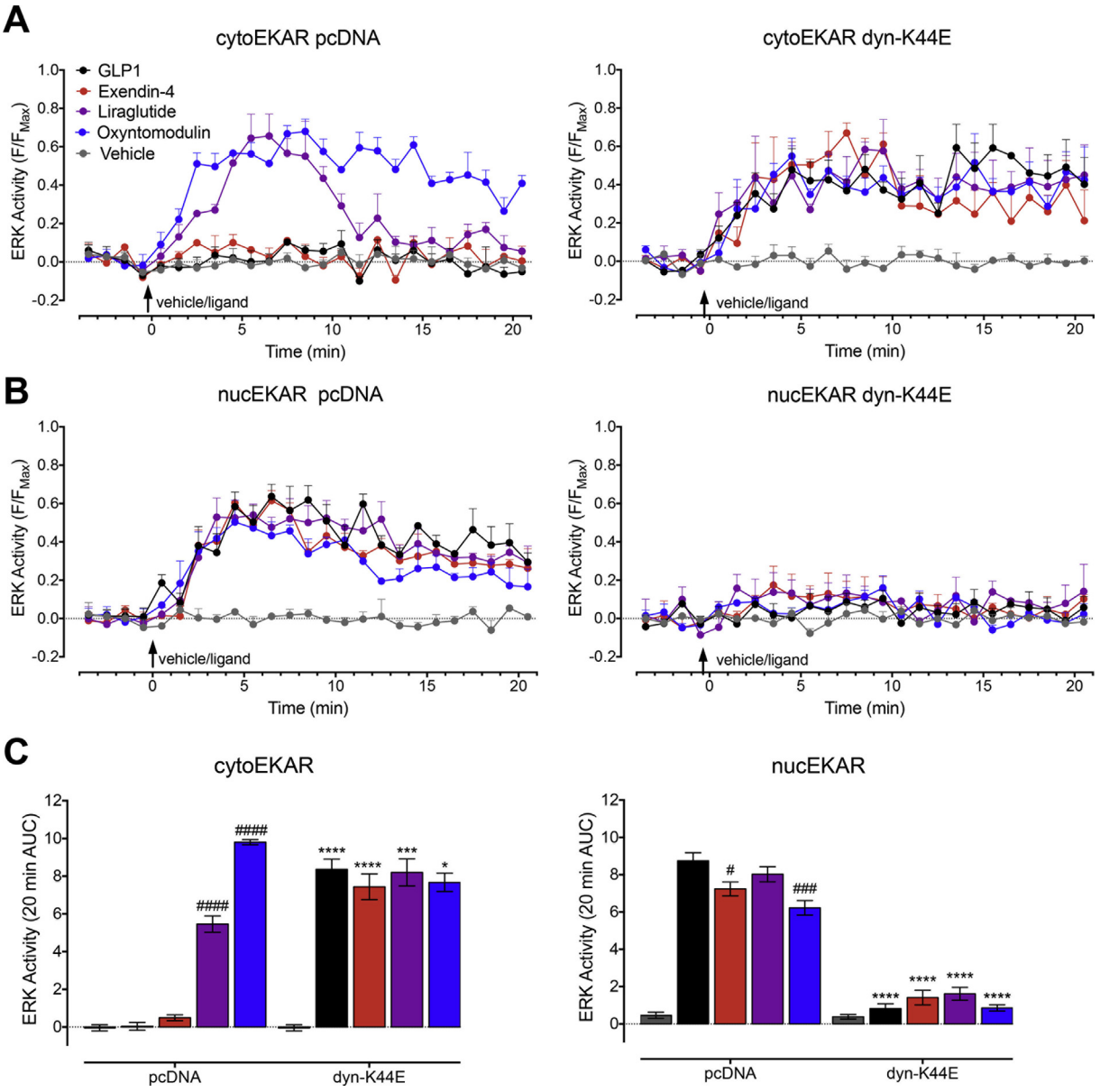

Fig. 10. Time course of ERK activity upon stimulation of GLP-1R in FlpIn-CHO cells transiently transfected with the GLP-1R, the relevant FRET sensor and either pcDNA or dyn-K44E, by GLP-1 (100 nM), exendin-4 (100 nM), liraglutide (100 nM) and oxyntomodulin (1 μM) as measured by cytoEKAR (A) and nucEKAR (B). Data are plotted as change in cerulean/venus ratio relative to the maximum response to FBS (F_{max}) for each cell. Data points are mean ± SEM, of 3 individual experiments, with 75–253 cells per condition. Statistical tests are two-way ANOVA (variables pcDNA and dyn-K44E), followed by Sidak's post test to compare each ligand in the different treatments, ($^{*}p < 0.05$, $^{***}p < 0.001$, $^{****}p < 0.0001$) or followed by Dunnett's post test, to compare each ligand to GLP-1 within each treatment ($^{\#}p < 0.05$, $^{\#\#\#}p < 0.001$, $^{\#\#\#\#}p < 0.0001$).

activating this pathway [32].

Using biophysical approaches to assess GLP-1R signalling in real time revealed differential activation of the GLP-1R leads to distinct spatiotemporal profiles of signalling, particularly for ERK1/2 activity that may, in part, account for some of the observed GLP-1R biased agonism. Strikingly, while GLP-1, exendin-4, liraglutide and oxyntomodulin all promoted nuclear localised ERK1/2 activity (albeit with slightly different temporal properties), only the pERK1/2 biased agonists liraglutide and oxyntomodulin were able to generate cytosolic pERK1/2. Interestingly, oxyntomodulin produced a more sustained response than liraglutide, a kinetic profile consistent with the observed bias relative to cAMP observed from global ERK assays, whereby oxyntomodulin was biased when assessed at two distinct time points (6 and 15 mins), but liraglutide was only biased at the 6 min time point. This highlights the importance that spatiotemporal profiles of signalling can play in engendering biased agonist profiles, as has been noted for other receptor systems [35]. Interestingly, these two ligands each have a different profile for β-arrestin recruitment, with oxyntomodulin being a biased agonist favouring recruitment, while liraglutide displayed similar recruitment relative to GLP-1. β-arrestins are scaffolding proteins that can regulate GPCR signalling. Speculatively, this β-arrestin bias may in part lead to the differences in the cytosolic ERK1/2 kinetic profile. Indeed, β-arrestin 1-dependent GLP-1R ERK1/2 activation is reported to be sustained and cytosolically restricted, at least in β-cells [36].

Differences in temporal cAMP signalling were less striking than those for ERK activity, nonetheless some important observations were revealed in our study. Whereas all ligands displayed sustained signalling that was detected within the cytosol, responses detected by the plasma membrane localised sensor for GLP-1 and exendin-4 had greater

E_{max} values immediately following ligand stimulation, but they were also more transient in nature than those generated by liraglutide and oxyntomodulin. Of particular interest was the relative rank order of potencies where GLP-1 and exendin-4 were more potent at production of cAMP within the cytosol than liraglutide, but GLP-1 had weaker potency than exendin-4 and liraglutide detectable by the plasma membrane localised sensor. This reveals that different ligands may display distinct spatiotemporal profiles of signalling that may differentially influence physiological functions.

Assessment of GLP-IR internalisation in our system revealed that the receptor internalises rapidly when activated by GLP-1, exendin-4, liraglutide and oxyntomodulin, where it traffics into early endosomes, before moving through either recycling or degradative pathways, illustrated by co-localisation with both Rab7a and Rab11 biosensor reporters. This is consistent with previous observations in HEK293 cells and the insulinoma cell line, BRIN-BD11 [13,14]. In our study no significant differences between the ligands could be established, in the route or in kinetics of trafficking, however these studies were performed with saturating concentrations of ligand and it is possible that distinction in recycling versus degradative trafficking may occur with lower ligand concentrations. Unfortunately, limitations in the sensitivity of this assay for Rab7a and Rab11 markers precluded establishment of concentration responses. Nonetheless, it has been reported that liraglutide induces greater receptor internalisation than GLP-1 and exendin-4 [15] and that exendin-4 and liraglutide stimulated receptors recycle slower than those activated with GLP-1 [13]. These data suggest that the differences in spatiotemporal profiles of signalling that we observed using our localised FRET sensors may be linked to the internalisation and localisation of the receptor following ligand stimulation.

Dynamin, clathrin and caveolin are important for GLP-1R internalisation in the cells assessed within this study with inhibition of dynamin and caveolin completely ablating receptor internalisation and clathrin inhibition resulting in a partial reduction. Consistent with previous studies [14,21], inhibition of GLP-1R internalisation markedly decreased global cAMP accumulation and pERK1/2 mediated by GLP-1 and exendin-4. This was also true for the pERK1/2 biased ligands oxyntomodulin and liraglutide suggesting that, for all four ligands, internalised receptors contribute to the overall signalling response. Intriguingly, inhibition of internalisation had differential effects on the integrated cAMP signaling from equi-occupant concentrations of individual peptides when localised signaling was examined (Fig. 9). This may be related to the subtle differences in ligand-dependent receptor trafficking noted above [13,15]. Perhaps not surprisingly, cAMP responses were still measurable with the cytosolic Epac2 sensor despite inhibition of internalisation, indicating that plasma membrane generated cAMP is likely to rapidly diffuse into the cytosol (and maybe vice versa), contributing to the measured response. Thus, while our data illustrates that compartmentalisation of cAMP signaling is a likely component of observed biased agonism, more discriminative tools will be required to fully understand these behaviours. In contrast to the limitations with the cAMP biosensors, there was clear separation of signaling with the cytosolic and nuclear localized ERK sensors that revealed important, localisation-dependent, distinctions in peptide-mediated ERK activity. Maintaining the GLP-1R at the plasma membrane eliminated all nuclear ERK signaling, while either preserving (liraglutide, oxyntomodulin) or engendering (GLP-1, exendin-4) cytosolic ERK activity. This indicates that GLP-1R-mediated nuclear ERK activity is generated from internalised receptors while cytosolic ERK is generated by plasma membrane localised receptors. These different localised signals are likely to produce distinct cellular outcomes. Indeed, cytosolic and nuclear ERK activity have been implicated in different physiological roles with nuclear translocation involved in transcriptional control [36] and cytosolically restricted ERK mediating anti-apoptotic effects in β cells [36].

Mechanistic insight into GLP-1R biased agonism at the cellular level is of importance due to the broad therapeutic relevance of the receptor to diseases ranging from diabetes and obesity through to neurodegenerative diseases including Parkinson's and Alzheimer's. Our study further highlights the role of receptor internalisation in control of spatiotemporal GLP-1R signalling that contributes to biased agonism. Promising recent studies in rodent models of diabetes suggest that biased GLP-1R agonists with a reduced ability to internalise may offer a therapeutic advantage as they produce greater long-term insulin release, faster agonist dissociation rates and elicit glycemic benefits without signs of nausea in animal models, which is a common side effect of GLP-1R therapies [15]. Our work, combined with this recent study, thus emphasises the need to fully understand the interplay between GLP-1R internalisation, spatiotemporally organised signalling and biased agonism and how these ligand behaviours can be utilised to develop novel, optimised disease-specific therapeutics.

5. Conflict of interest statement

The authors declare no competing interests.

Acknowledgements

This work was supported by the National Health and Medical Research Council of Australia (NHMRC) (project grants [1061044], [1065410] and [1126857], and NHMRC program grant [1055134]); P.M.S. is a NHMRC Principal Research Fellow and A.C. is a NHMRC Senior Principal Research Fellow. M.L.H and D.W. are NHMRC RD Wright Career Development Fellows (1061687 (M.L.H), 1089966 (D.W).

References

[1] C. Orskov, A. Wettergren, J.J. Holst, Biological effects and metabolic rates of glucagonlike peptide-1 7–36 amide and glucagonlike peptide-1 7–37 in healthy subjects are indistinguishable, Diabetes 42 (5) (1993) 658–661.
[2] D.J. Drucker, J. Philippe, S. Mojsov, W.L. Chick, J.F. Habener, Glucagon-like peptide I stimulates insulin gene expression and increases cyclic AMP levels in a rat islet cell line, Proc. Natl. Acad. Sci. U.S.A. 84 (10) (1987) 3434–3438.
[3] L. Farilla, A. Bulotta, B. Hirshberg, S. Li Calzi, N. Khoury, H. Noushmehr, et al., Glucagon-like peptide 1 inhibits cell apoptosis and improves glucose responsiveness of freshly isolated human islets, Endocrinology 144 (12) (2003) 5149–5158.
[4] J.D. Roth, M.R. Erickson, S. Chen, D.G. Parkes, GLP-1R and amylin agonism in metabolic disease: complementary mechanisms and future opportunities, Br. J. Pharmacol. 166 (1) (2012) 121–136.
[5] C. Montrose-Rafizadeh, P. Avdonin, M.J. Garant, B.D. Rodgers, S. Kole, H. Yang, et al., Pancreatic glucagon-like peptide-1 receptor couples to multiple G proteins and activates mitogen-activated protein kinase pathways in Chinese hamster ovary cells, Endocrinology 140 (3) (1999) 1132–1140.
[6] N. Sonoda, T. Imamura, T. Yoshizaki, J.L. Babendure, J.C. Lu, J.M. Olefsky, Beta-Arrestin-1 mediates glucagon-like peptide-1 signaling to insulin secretion in cultured pancreatic beta cells, Proc. Natl. Acad. Sci. U.S.A. 105 (18) (2008) 6614–6619.
[7] C. Koole, D. Wootten, J. Simms, C. Valant, R. Sridhar, O.L. Woodman, et al., Allosteric ligands of the glucagon-like peptide 1 receptor (GLP-1R) differentially modulate endogenous and exogenous peptide responses in a pathway-selective manner: implications for drug screening, Mol. Pharmacol. 78 (3) (2010) 456–465.
[8] R. Jorgensen, V. Kubale, M. Vrecl, T.W. Schwartz, C.E. Elling, Oxyntomodulin differentially affects glucagon-like peptide-1 receptor beta-arrestin recruitment and signaling through Galpha(s), J. Pharmacol. Exp. Ther. 322 (1) (2007) 148–154.
[9] S. Ferrandon, T.N. Feinstein, M. Castro, B. Wang, R. Bouley, J.T. Potts, et al., Sustained cyclic AMP production by parathyroid hormone receptor endocytosis, Nat. Chem. Biol. 5 (10) (2009) 734–742.
[10] D. Calebiro, V.O. Nikolaev, M.C. Gagliani, T. de Filippis, C. Dees, C. Tacchetti, et al., Persistent cAMP-signals triggered by internalized G-protein-coupled receptors, PLoS Biol. 7 (8) (2009) e1000172.
[11] R. Irannejad, V. Pessino, D. Mika, B. Huang, P.B. Wedegaertner, M. Conti, et al., Functional selectivity of GPCR-directed drug action through location bias, Nat Chem Biol 13 (7) (2017) 799–806.
[12] K. Eichel, D. Jullie, M. von Zastrow, beta-Arrestin drives MAP kinase signalling from clathrin-coated structures after GPCR dissociation, Nat Cell Biol 18 (3) (2016) 303–310.
[13] S.N. Roed, P. Wismann, C.R. Underwood, N. Kulahin, H. Iversen, K.A. Cappelen, et al., Real-time trafficking and signaling of the glucagon-like peptide-1 receptor, Mol Cell Endocrinol 382 (2) (2014) 938–949.
[14] R.S. Kuna, S.B. Girada, S. Asalla, J. Vallentyne, S. Maddika, J.T. Patterson, et al., Glucagon-like peptide-1 receptor-mediated endosomal cAMP generation promotes glucose-stimulated insulin secretion in pancreatic beta-cells, Am J Physiol

Endocrinol Metab 305 (2) (2013) E161–70.
[15] B. Jones, T. Buenaventura, N. Kanda, P. Chabosseau, B.M. Owen, R. Scott, et al., Targeting GLP-1 receptor trafficking to improve agonist efficacy, Nat Commun 9 (1) (2018) pp. 1602–018-03941-2.
[16] C. Widmann, W. Dolci, B. Thorens, Agonist-induced internalization and recycling of the glucagon-like peptide-1 receptor in transfected fibroblasts and in insulinomas, Biochem. J. 310 (Pt 1) (1995) 203–214.
[17] P. Vazquez, I. Roncero, E. Blazquez, E. Alvarez, The cytoplasmic domain close to the transmembrane region of the glucagon-like peptide-1 receptor contains sequence elements that regulate agonist-dependent internalisation, J. Endocrinol. 186 (1) (2005) 221–231.
[18] C.A. Syme, L. Zhang, A. Bisello, Caveolin-1 regulates cellular trafficking and function of the glucagon-like peptide 1 receptor, Mol. Endocrinol. 20 (12) (2006) 3400–3411.
[19] A. Thompson, V. Kanamarlapudi, Agonist-induced internalisation of the glucagon-like peptide-1 receptor is mediated by the Galphaq pathway, Biochem Pharmacol 93 (1) (2015) 72–84.
[20] S.B. Girada, R.S. Kuna, S. Bele, Z. Zhu, N.R. Chakravarthi, R.D. DiMarchi, et al., Galphas regulates Glucagon-Like Peptide 1 Receptor-mediated cyclic AMP generation at Rab5 endosomal compartment, Mol Metab 6 (10) (2017) 1173–1185.
[21] S.N. Roed, A.C. Nøhr, P. Wismann, H. Iversen, H. Bräuner-Osborne, S.M. Knudsen, et al., Functional consequences of glucagon-like peptide-1 receptor cross-talk and trafficking, J. Biol. Chem. 290 (2) (2015) 1233–1243.
[22] D. Wootten, E.E. Savage, F.S. Willard, A.B. Bueno, K.W. Sloop, A. Christopoulos, et al., Differential activation and modulation of the glucagon-like peptide-1 receptor by small molecule ligands, Mol. Pharmacol. 83 (4) (2013) 822–834.
[23] T.H. Lan, Q. Liu, C. Li, G. Wu, N.A. Lambert, Sensitive and high resolution localization and tracking of membrane proteins in live cells with BRET, Traffic 13 (11) (2012) 1450–1456.
[24] H.R. Yeatman, J.R. Lane, K.H.C. Choy, N.A. Lambert, P.M. Sexton, A. Christopoulos, et al., Allosteric modulation of M1 muscarinic acetylcholine receptor internalization and subcellular trafficking, J. Biol. Chem. 289 (22) (2014 May 30) 15856–15866.
[25] V.O. Nikolaev, M. Bunemann, L. Hein, A. Hannawacker, M.J. Lohse, Novel single chain cAMP sensors for receptor-induced signal propagation, J. Biol. Chem. 279 (36) (2004) 37215–37218.
[26] S. Wachten, N. Masada, L.J. Ayling, A. Ciruela, V.O. Nikolaev, M.J. Lohse, et al., Distinct pools of cAMP centre on different isoforms of adenylyl cyclase in pituitary-derived GH3B6 cells, J. Cell Sci. 123 (Pt 1) (2010) 95–106.
[27] C.D. Harvey, A.G. Ehrhardt, C. Cellurale, H. Zhong, R. Yasuda, R.J. Davis, et al., A genetically encoded fluorescent sensor of ERK activity, Proc. Natl. Acad. Sci. U.S.A. 105 (49) (2008) 19264–19269.
[28] F. Schmidlin, O. Dery, K.O. DeFea, L. Slice, S. Patierno, C. Sternini, et al., Dynamin and Rab5a-dependent trafficking and signaling of the neurokinin 1 receptor, J Biol Chem 276 (27) (2001) 25427–25437.
[29] E.E. Savage, D. Wootten, A. Christopoulos, P.M. Sexton, S.G. Furness, A simple method to generate stable cell lines for the analysis of transient protein-protein interactions, BioTechniques 54 (4) (2013) 217–221.
[30] M.L. Halls, D.P. Poole, A.M. Ellisdon, C.J. Nowell, M. Canals, Detection and quantification of intracellular signaling Using FRET-based biosensors and high content imaging, Methods Mol. Biol. 1335 (2015) 131–161.
[31] T. Kenakin, C. Watson, V. Muniz-Medina, A. Christopoulos, S. Novick, A simple method for quantifying functional selectivity and agonist bias, ACS Chem. Neurosci. 3 (3) (2011) 193–203.
[32] D. Wootten C.A. Reynolds K.J. Smith J.C. Mobarec C. Koole E.E. Savage et al. The extracellular surface of the GLP-1 receptor Is a molecular trigger for biased agonism Cell 2016 165 7 1632 1643.
[33] J.S. Herskovits, C.C. Burgess, R.A. Obar, R.B. Vallee, Effects of mutant rat dynamin on endocytosis, J. Cell Biol. 122 (3) (1993 Aug) 565–578.
[34] H. Lee, D.S. Park, B. Razani, R.G. Russell, R.G. Pestell, M.P. Lisanti, Caveolin-1 mutations (P132L and null) and the pathogenesis of breast cancer: caveolin-1 (P132L) behaves in a dominant-negative manner and caveolin-1 (-/-) null mice show mammary epithelial cell hyperplasia, Am. J. Pathol. 161 (4) (2002 Oct) 1357–1369.
[35] C. Klein Herenbrink, D.A. Sykes, P. Donthamsetti, M. Canals, T. Coudrat, J. Shonberg, et al., The role of kinetic context in apparent biased agonism at GPCRs, Nat. Commun. 24 (7) (2016 Feb) 10842.
[36] J. Quoyer, C. Longuet, C. Broca, N. Linck, S. Costes, E. Varin, et al., GLP-1 mediates antiapoptotic effect by phosphorylating Bad through a beta-arrestin 1-mediated ERK1/2 activation in pancreatic beta-cells, J. Biol. Chem. 285 (3) (2010) 1989–2002.

Appendix V:
Activation of the GLP-1 receptor by a non-peptidic agonist

Article

Activation of the GLP-1 receptor by a non-peptidic agonist

https://doi.org/10.1038/s41586-019-1902-z

Received: 10 May 2019

Accepted: 8 November 2019

Published online: 8 January 2020

Peishen Zhao[1,9], Yi-Lynn Liang[1,9], Matthew J. Belousoff[1,9], Giuseppe Deganutti[2,9], Madeleine M. Fletcher[1], Francis S. Willard[3], Michael G. Bell[3], Michael E. Christe[3], Kyle W. Sloop[3], Asuka Inoue[4], Tin T. Truong[1], Lachlan Clydesdale[1], Sebastian G. B. Furness[1], Arthur Christopoulos[1], Ming-Wei Wang[5,6], Laurence J. Miller[7], Christopher A. Reynolds[2], Radostin Danev[8]*, Patrick M. Sexton[1,6]* & Denise Wootten[1,6]*

Class B G-protein-coupled receptors are major targets for the treatment of chronic diseases, including diabetes and obesity[1]. Structures of active receptors reveal peptide agonists engage deep within the receptor core, leading to an outward movement of extracellular loop 3 and the tops of transmembrane helices 6 and 7, an inward movement of transmembrane helix 1, reorganization of extracellular loop 2 and outward movement of the intracellular side of transmembrane helix 6, resulting in G-protein interaction and activation[2–6]. Here we solved the structure of a non-peptide agonist, TT-OAD2, bound to the glucagon-like peptide-1 (GLP-1) receptor. Our structure identified an unpredicted non-peptide agonist-binding pocket in which reorganization of extracellular loop 3 and transmembrane helices 6 and 7 manifests independently of direct ligand interaction within the deep transmembrane domain pocket. TT-OAD2 exhibits biased agonism, and kinetics of G-protein activation and signalling that are distinct from peptide agonists. Within the structure, TT-OAD2 protrudes beyond the receptor core to interact with the lipid or detergent, providing an explanation for the distinct activation kinetics that may contribute to the clinical efficacy of this compound series. This work alters our understanding of the events that drive the activation of class B receptors.

Class B peptide G-protein-coupled receptors (GPCRs) regulate the control of glucose and energy homeostasis, bone turnover, and cardiovascular development and tone[1]. Several peptide agonists are clinically approved for disorders of energy and bone metabolism[1]; however, attempts to develop non-peptide, orally available analogues have yielded only limited success. Understanding the structural basis of class B GPCR activation is crucial to the rational development of peptidic and non-peptidic drugs. Recent structural determination of full-length, active class B receptors bound to peptide agonists[2–6] confirmed that the N terminus of the peptide ligands, required for receptor activation, binds deep within the seven-transmembrane helical bundle. This is associated with an outward movement of the tops of transmembrane helices (TM) 6 and 7 (and interconnecting extracellular loop (ECL) 3) and a large kink in the centre of TM6 that opens up the intracellular face of the receptor to allow G-protein coupling[2–4,7–10]. In parallel, a conformational reorganization of ECL2 and an inward movement of TM1 facilitates peptide interaction and receptor activation.

The GLP-1 receptor (GLP-1R) is an established therapeutic target for type 2 diabetes and obesity[11]. Despite their clinical success, GLP-1R peptide drugs are suboptimal owing to their route of administration and side-effect profiles, most notably nausea and vomiting that reduce patient compliance[11]. For many years, oral GLP-1R agonists have been pursued, with recent studies reporting promising clinical trial data for oral semaglutide—a new formulation of the approved peptide semaglutide[12,13]. However, it induced slightly greater severity of nausea and gastrointestinal side effects than those observed with injectable GLP-1 mimetics[13]. Future development of non-peptide drugs could offer more traditional small molecule absorption characteristics that may assure better long-term patient compliance with the potential for reduced gastrointestinal liability, especially for patients who are co-administering with other medications.

Several non-peptidic GLP-1R agonists have been identified[14]. One class form covalent interactions with C347$^{6.36}$ (in which the superscript denotes the Wootten class B GPCR numbering) and are predicted to allosterically disrupt polar networks at the base of the receptor, promoting activation[15], whereas other small molecule compounds bind to unknown sites at the receptor extracellular face[14,16,17]. However, it is assumed that these molecules may need to mimic key interactions of the peptide N terminus deep within the transmembrane core to initiate receptor activation, as is seen for short stabilized 11-mer peptides, that occupy an overlapping site to full-length peptides[18].

[1]Drug Discovery Biology, Monash Institute of Pharmaceutical Sciences, Monash University, Parkville, Victoria, Australia. [2]School of Biological Sciences, University of Essex, Colchester, UK. [3]Lilly Research Laboratories, Eli Lilly and Company, Indianapolis, IN, USA. [4]Graduate School of Pharmaceutical Sciences, Tohoku University, Sendai, Miyagi, Japan. [5]The National Center for Drug Screening and CAS Key Laboratory of Receptor Research, Shanghai Institute of Materia Medica, Chinese Academy of Sciences, Shanghai, China. [6]School of Pharmacy, Fudan University, Shanghai, China. [7]Mayo Clinic, Scottsdale, AZ, USA. [8]Graduate School of Medicine, University of Tokyo, Hongo, Bunkyo-ku, Tokyo, Japan. [9]These authors contributed equally: Peishen Zhao, Yi-Lynn Liang, Matthew J. Belousoff, Giuseppe Deganutti. *e-mail: rado@m.u-tokyo.ac.jp; patrick.sexton@monash.edu; denise.wootten@monash.edu

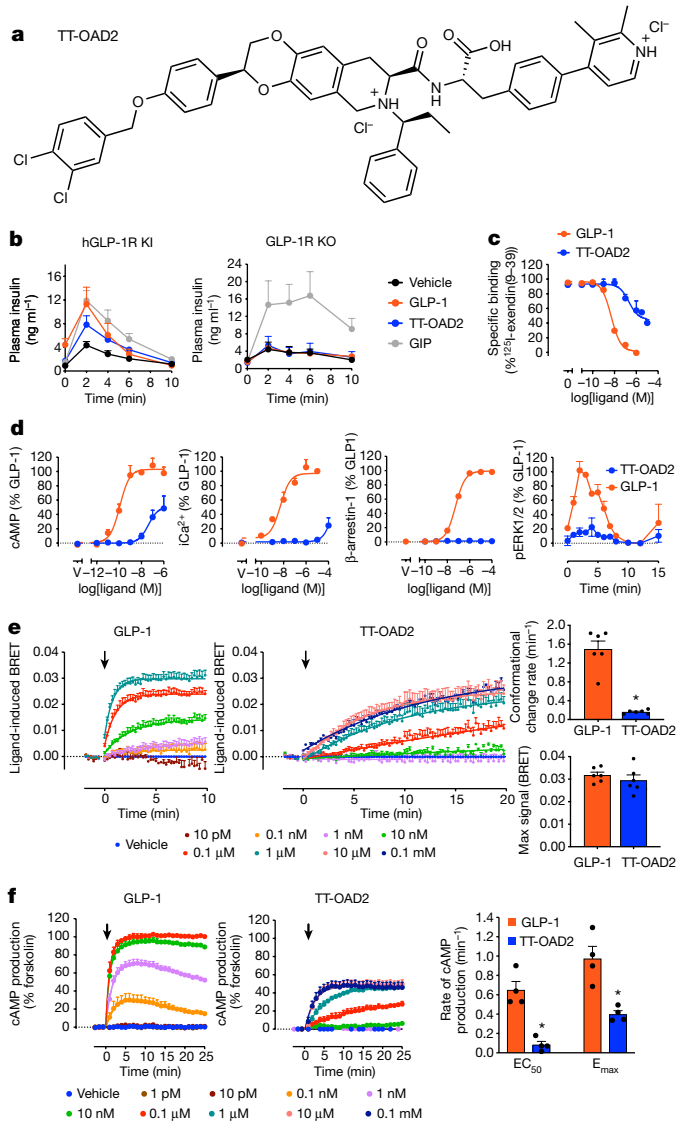

Fig. 1 | Pharmacology exhibited by TT-OAD2 relative to GLP-1. a, Chemical structure of TT-OAD2. **b**, Plasma insulin induced by GLP-1 (10 μg kg^{-1}), TT-OAD2 (3 mg kg^{-1}) or gastric inhibitory polypeptide (GIP; 25 μg kg^{-1}) in an acute IVGTT on humanized GLP-1R knock-in (KI) and GLP-1R knockout (KO) mice. **c**, Whole-cell binding assays showing the ability of GLP-1 and TT-OAD2 to displace ^{125}I-exendin(9-39). **d**, cAMP accumulation, intracellular calcium mobilization, β-arrestin-1 recruitment and ERK1/2 phosphorylation (pERK1/2). **e**, Agonist-induced changes in trimeric G_s conformation in cell plasma membrane preparations for GLP-1 (left) and TT-OAD2 (middle). Rates (top right) and plateau (bottom right) at saturating concentrations (1 μM GLP-1, 10 μM TT-OAD2) were quantified by applying a one-phase association curve. **f**, Kinetics of cAMP production measured by an EPAC biosensor for GLP-1 (left) and TT-OAD2 (middle). Rates were quantified using approximate EC_{50} and E_{max} concentrations (1 nM and 0.1 μM for GLP-1, 0.1 μM and 10 μM for TT-OAD2) by applying a one-phase association curve. In **e** and **f**, arrows refer to the time at which ligand or vehicle was added. Parameters derived from kinetic data are represented as scatter plots with each individual experiment shown by black circles. All experiments were performed in GLP-1R expressing HEK293A cells. Data in **b** are mean + s.e.m. from 4–5 mice per treatment, representative of 3 independent experiments. Data in **c**–**f** are mean + s.e.m. of 4–5 independent experiments (in duplicate or triplicate). *P < 0.05, Student's paired t-test.

Here we investigate TT-OAD2 (Fig. 1a), a non-peptidic compound reported in the patent literature and part of the chemical series that contains the vTv Therapeutics investigational drug candidate, TTP273. TTP273, an orally administered GLP-1R agonist, successfully completed phase IIa efficacy trials for type 2 diabetes (ClinicalTrials.gov Identifier: NCT02653599), in which it met its primary endpoint, reducing levels of glycated haemoglobin in patients with type 2 diabetes, with no reported cases of nausea[19], suggesting a potential clinical advantage for compounds of this series. Little has been disclosed about the molecular properties of this compound series; however, recent progression of TTP273 has been hampered by unexpected complexity in identifying optimal dosing that may be linked to a lack of understanding of its mechanism of action. Assessment of acute in vivo activity in humanized GLP-1R mice revealed that TT-OAD2 is insulinotropic and that this effect is dependent on the GLP-1R (Fig. 1b).

TT-OAD2 is a biased agonist with slow kinetics

In HEK293 cells that overexpress GLP-1R, TT-OAD2 only partially displaced the orthosteric probes ^{125}I-exendin(9–39) and ROX-exendin-4 (Fig. 1c, Extended Data Fig. 1a), consistent with an allosteric mode of interaction[16]. Although GLP-1R signals to several cellular pathways, TT-OAD2 activated only a subset of these responses; it was a low-potency partial agonist for cAMP accumulation, with only weak responses detected for mobilization of intracellular Ca^{2+} and phosphorylation of ERK1/2 at very high concentrations (100 μM) (Fig. 1d) and no detectable recruitment of β-arrestin-1. These data are indicative of bias towards cAMP and away from these other pathways relative to endogenous GLP-1. There is considerable interest in exploiting biased agonism at GPCRs to maximize the beneficial effects of receptor activation, while minimizing on-target side-effect profiles.

CRISPR-engineered HEK293 cells in which $G_{s/olf}$ or $G_{i/o/z}$ proteins were deleted revealed that G_s was essential for the production of cAMP; however, this response, for both ligands, was also dependent on the presence of $G_{i/o/z}$ proteins. (Extended Data Fig. 1b). Assessment of proximal activation of G_s and G_i transducers using split luciferase NanoBit G-protein sensors (Extended Data Fig. 1c) determined GLP-1-decreased luminescence in a bi-phasic, concentration-dependent, manner for both G proteins with similar potencies in each phase. For TT-OAD2, the G_i sensor gave a similar decrease in luminescence to GLP-1; however, enhanced luminescence was observed for the G_s sensor, which suggests a different mechanism of G_s activation. To probe these differences further, we used membrane-based assays of bioluminescence resonance energy transfer (BRET) G-protein sensors to assess the rate and nature of the G_s conformational change. In contrast to the rates of change in the conformation of G_i, which were similar for both ligands (Extended Data Fig. 1), there was a marked distinction in kinetics for G_s coupling. GLP-1 promoted a rapid conformational change in G_s protein, whereas for TT-OAD2 this was very slow (Fig. 1e). However, both agonists induced a similar plateau of the measured response (Fig. 1e) that was reversed by excess GTP (Extended Data Fig. 1d), indicative of a similar overall conformational rearrangement. Together, this suggests that slower G_s conformational transitions, required for the exchange of GDP for GTP and G_s activation, would result in lower turnover of G protein and rate of cAMP production by TT-OAD2. Direct kinetic measurements of cAMP production validated this hypothesis (Fig. 1f, Extended Data Fig. 1e). Overall, these data revealed TT-OAD2 as a biased agonist that can only activate a subset of pathways with limited efficacy and with distinct activation kinetics relative to peptide agonists.

TT-OAD2 has an unexpected binding mode

To understand how TT-OAD2 binds and activates the GLP-1R, we determined the GLP-1R structure bound to TT-OAD2 and the transducer heterotrimeric G_s protein (Fig. 2). Complex formation was initiated in *Tni* insect cells by stimulation with 50 μM TT-OAD2, and complexes were then solubilized and purified (Extended Data Fig. 2a). Vitrified complexes were imaged by single-particle cryo-electron microscopy (cryo-EM) on a Titan Krios. Following 2D and 3D classification, the most

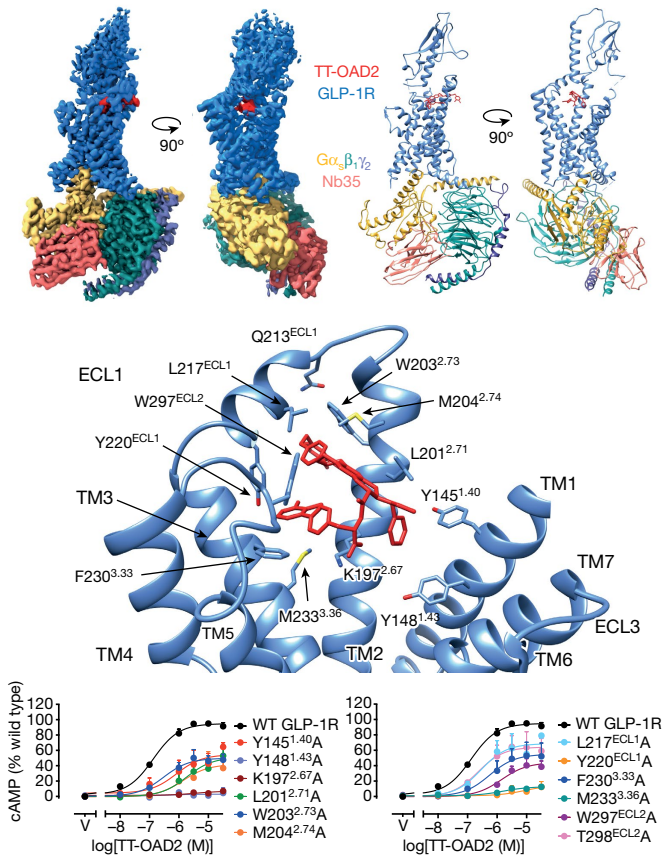

Fig. 2 | TT-OAD2–GLP-1R–G_s cryo-EM structure reveals non-peptide binding site. Top, orthogonal views of the TT-OAD2–GLP-1R–G_s complex cryo-EM map (left) and the structure after refinement in the cryo-EM map (right), colour-coded to protein chains; GLP-1R (blue), TT-OAD2 (red), heterotrimeric G_s (α: gold, β: dark cyan, γ: purple, Nb35: salmon). Middle, TT-OAD2 interacts with the top of the GLP-1R bundle. Interacting residues of GLP-1R (blue) with TT-OAD2 (red). Bottom, TT-OAD2-mediated cAMP production by receptors containing alanine mutants of key residues assessed in ChoFlpIn cells. Data are mean + s.e.m. of four independent experiments performed in duplicate. WT, wild type.

abundant class was resolved to 3.0 Å (Extended Data Fig. 2c–f, Supplementary Table 1). The cryo-EM density map allowed unambiguous assignment of the TT-OAD2-binding site and pose, and clear rotamer placement for most amino acids within the receptor core and G protein (Fig. 2, Extended Data Figs. 3, 4a, b). The GLP-1R extracellular domain (ECD) and the $G\alpha_s$ α-helical domain were not resolved at high resolution, consistent with their greater mobility. Rigid body fitting of an available X-ray structure of the GLP-1R ECD domain (PDB code 3C5T)[20] was performed into the density to generate a full-length model.

TT-OAD2 bound high up in the helical bundle interacting with residues within TM1, TM2, TM3, ECL1 and ECL2 (Fig. 2, Extended Data Fig. 4a). Most interactions are hydrophobic in nature (Fig. 2), including numerous π–π stacking interactions between receptor aromatic residues and phenolic regions within the ligand. Unexpectedly, TT-OAD2 adopts a 'boomerang-like' orientation within the binding site with the 3,4-dichloro-benzyl ring of TT-OAD2 protruding beyond the receptor core through transmembrane helices 2 and 3, interacting with $W203^{2.73}$, and embedding in the detergent micelle, consistent with probable interactions with the lipid bilayer in a native system. $F230^{3.33}$ and $W297^{ECL2}$ interact with the 2,3-dimethyl-pyridin-4-yl-phenol region, $Y220^{ECL1}$ forms a hydrogen bond with the 2,3-dimethyl-pyridine ring and $K197^{2.67}$ forms a polar interaction with the propionic acid part of the ligand. Additional hydrophobic contacts are formed with TT-OAD2 by $Y145^{1.40}$, $L201^{2.71}$, $I196^{2.69}$, $A200^{2.70}$, $L217^{ECL1}$, $V229^{3.32}$ and $M204^{3.36}$ (Fig. 2, Extended Data Fig. 4a). Molecular dynamics simulations of the TT-OAD2–GLP-1R–G_s complex predicted further transient interactions with TM1, TM2, TM3, ECL1, ECL2 and the ECD of GLP-1R (Extended Data Table 1). Assessment of TT-OAD2-induced cAMP production at alanine mutants of key receptor residues within the binding site revealed reduced potency (negative logarithm of the half-maximal effective concentration, pEC_{50}), reduced maximal responses (E_{max}) or both relative to the wild-type receptor (Fig. 2, Supplementary Table 2). Application of the operational model of agonism revealed these mutations directly alter TT-OAD2 functional affinity (K_A) and/or efficacy (τ) (Supplementary Table 2), which highlights the importance of these residues in TT-OAD2 function.

Peptide versus non-peptide binding sites

The TT-OAD2-binding pose has very limited overlap with full-length peptides, GLP-1 and exendin-P5 (ExP5)[3,6] (Fig. 3, Extended Data Fig. 5). Structural comparisons, combined with associated molecular dynamics simulations performed on models generated from the cryo-EM data, identified only 10 out of 29 residues that interact with both TT-OAD2 and GLP-1. Moreover, the persistence and nature of ligand interactions formed by common residues differed (Fig. 3c, Extended Data Table 1). In contrast to TT-OAD2, peptide ligands engage transmembrane helices 5–7 in addition to extensive interactions deep within the bundle in transmembrane helices 1–3 (Fig. 3, Extended Data Fig. 5, Extended Data Table 1).

The relatively limited overlap between the peptide- and TT-OAD2-binding sites suggests that this compound series may modulate peptide function in a physiological setting. To address this, we assessed the effect of TT-OAD2 on the signalling of two physiological ligands (Extended Data Fig. 6). TT-OAD2 inhibited GLP-1- and oxyntomodulin-mediated cAMP, calcium, pERK1/2 and β-arrestin responses in a concentration-dependent manner (Extended Data Fig. 6). This suggests that the profile of signalling observed from the GLP-1R when using TT-OAD2-like compounds as drugs may depend on the dose administered; at high concentrations, their presence would probably inhibit all endogenous peptide effects, biasing receptor responses primarily to cAMP formation mediated by the compound itself. However, at lower concentrations, some endogenous peptide signalling may still occur. Notably, TTP273 was reported to exhibit greater clinical efficacy at lower concentrations, indicating that maintenance of some aspects of physiological signalling may be important for clinical efficacy[19].

GLP-1R conformational changes and activation

At a gross level, the TT-OAD2-complexed GLP-1R helical bundle displays the key hallmarks of activated, peptide-occupied, class B GPCRs[2–6]. At the extracellular face, this includes the large outward movement of TM6, ECL3 and TM7, inward movements of TM1, helical extensions within TM2 and TM3, a reordering of ECL1, and conformational transitions within ECL2 that increases upward towards the extracellular side (Extended Data Fig. 5). At the intracellular side, there is an equivalent large outward movement of TM6 away from the centre of the helical bundle, and the smaller outward movement of TM5. It is important to note that the fully active state is driven in part by allosteric conformational changes, including those in the extracellular face, linked to G protein binding[21]. Nonetheless, all the GLP-1R structures are solved with the same G protein yet reveal conformational differences at their extracellular face, including within the extent of movement of TM6, ECL3, ECL7 and the conformation of the ECD, TM2–ECL1 and ECL2 that are linked to the bound agonists (Fig. 3a, b, Extended Data Fig. 5b, c). This suggests that distinct receptor activation triggers converge to common changes at the intracellular face that allow coupling to transducers.

Although the low resolution of the receptor ECD for the TT-OAD2 complex indicates extensive mobility, it occupied a distinct orientation

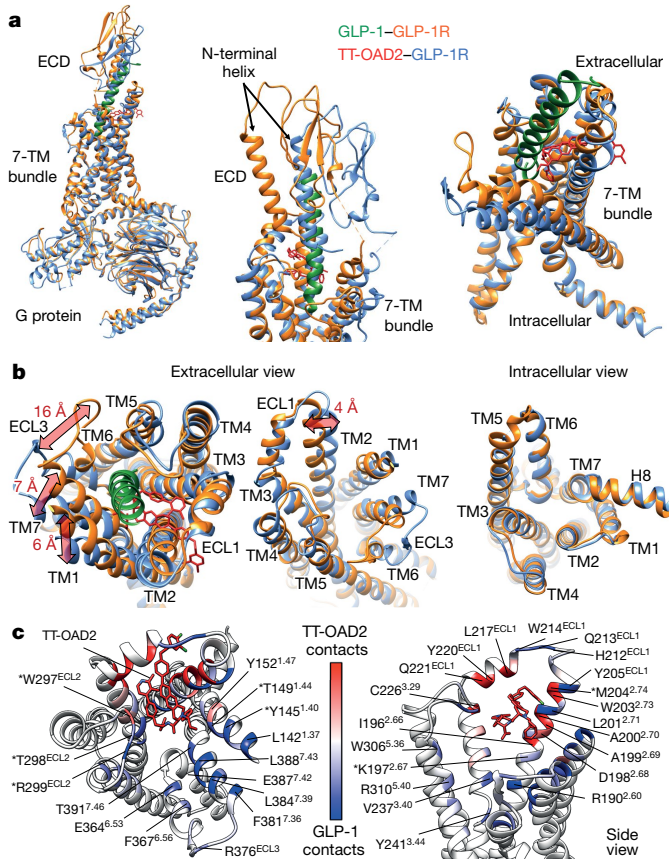

Fig. 3 | Comparisons of GLP-1R conformations induced by GLP-1 and TT-OAD2. a, **b**, Superimposition of the GLP-1R from PDB 5VAI (GLP-1R or G protein: orange, GLP-1: green) and the TT-OAD2 structure (GLP-1R or G protein: blue, TT-OAD2: red) reveals partial overlap of peptide- and TT-OAD2-binding sites and conformational differences in the receptor. **a**, Left, full complex; middle, close up of ECD and the top of the seven-transmembrane (7-TM) bundle; right, close up of the transmembrane bundle. **b**, Left, 16 Å, 7 Å and 6 Å differences occur in the location of TM6/ECL3, TM7 and TM1, respectively. Middle, a 4 Å shift in the location of the top of TM2 result in distinct conformations of ECL1. Right, the intracellular region of the GLP-1R helical bundles have similar overall backbone conformations. **c**, Comparison of the GLP-1R–TT-OAD2 and GLP-1R–GLP-1 contacts during molecular dynamics simulations performed on the GLP-1R–TT-OAD2–G_s and GLP-1R–GLP-1–G_s complexes. Top (left) and side (right) views of the GLP-1R transmembrane domain (ribbon representation, TT-OAD2 in red sticks, GLP-1 not shown). TT-OAD2 made contacts (red coloured ribbon) with ECL1 and residues located at the top of TM2 and TM3. GLP-1 was able to engage TM5, TM6 and TM7 of the receptor and side chains located deep in the bundle (blue coloured ribbon). Residues that are involved both in the GLP-1R–TT-OAD2–G_s and GLP-1R–GLP-1–G_s complexes are indicated by asterisks, and coloured according to the algebraic difference in occupancy (contact differences in percentage frames) between GLP-1R–TT-OAD2–G_s and GLP-1R–GLP-1–G_s. Red indicates regions more engaged by TT-OAD2 and blue more engaged by GLP-1. The ECD is not shown. Plotted data are summarized in Extended Data Table 1.

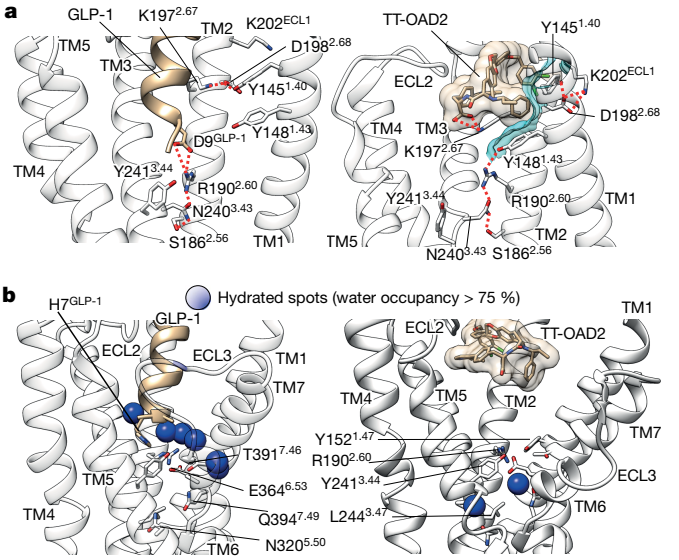

Fig. 4 | TT-OAD2 interactions lead to reorganization and stabilization of the central polar network via a distinct mechanism to GLP-1. Summaries of interactions observed in molecular dynamics simulations (Supplementary Video 2) on TT-OAD2- and GLP-1-bound GLP-1R that predict interactions stabilizing the active conformation of the central polar network. **a**, Left, GLP-1 (brown ribbon) residue D^9 (brown stick) forms an ionic interaction (red dotted lines) with $R190^{2.60}$, which is involved in key hydrogen bonds with $N240^{3.43}$ (in turn interacting with $S186^{2.56}$). At the top of TM2, $K197^{2.67}$, $D198^{2.68}$ and $Y145^{1.40}$ are stabilized in polar interactions (red dotted lines). Right, TT-OAD2 (brown stick and transparent surface) forms ionic interaction (red dotted lines) with $K197^{2.67}$ and hydrophobic contacts with $Y145^{1.40}$ and $Y148^{1.43}$ (cyan transparent surfaces) modifying the interaction network at the top of TM1. $Y148^{1.43}$ transiently interacts with $R190^{2.60}$ and partially reorients $N240^{3.43}$ and $S186^{2.56}$. TM6 and TM7 were removed for clarity. **b**, GLP-1R transmembrane helix sites are occupied by structural water molecules; blue spheres indicate receptor volumes occupied by low-mobility water molecules (occupancy more than 75% frames). Left, the GLP-1R–GLP-1–G_s complex stabilizes the central transmembrane polar residues by waters interacting with $Y152^{1.47}$, $T391^{7.46}$, $R190^{2.60}$ and $E364^{5.53}$ (Supplementary Video 1). Right, the GLP-1R–TT-OAD2–G_s complex is characterized by structural water molecules interacting with $N320^{5.50}$ and $E364^{6.53}$ (Supplementary Video 1).

relative to the transmembrane core in comparison to peptide-bound complexes, whereas both GLP-1- and ExP5-bound receptors stabilized a similar conformation[3,6] (Extended Data Fig. 5a). Similarly, the short 11-mer peptide HepP5 forms few interactions with the ECD[18] and occupies a distinct orientation relative to GLP-1 and ExP5, but this conformation also differs from that stabilized by TT-OAD2 (Extended Data Fig. 5c). The cryo-EM map of the TT-OAD2-bound receptor complex supports extended interactions of the ECD with ECL1 and ECL2 (Extended Data Fig. 4c) and this is supported by molecular dynamics simulations that predicts interactions of $R40^{ECD}$ with $D215^{ECL1}$ and $E34^{ECD}$ with $R299^{ECL2}$ (Extended Data Table 2). This later interaction is particularly important as $R299^{ECL2}$ directly, and stably interacts with peptide ligands, but in the TT-OAD2-bound receptor, stabilizes the N terminus of the ECD in a position that may have an analogous role to the peptide in stabilizing ECL2. Indeed, in our models, the position of the far N-terminal ECD helix overlapped with the location of the C-terminal region of GLP-1 and ExP5 when comparing the TT-OAD2- and peptide-bound structures (Fig. 3a). Thus, the ECD is likely to be important for both stabilizing the TT-OAD2-binding site and facilitating receptor activation, as previously proposed for different classes of peptide ligands[22,23].

Distinctions from peptide-bound receptors observed within TM2/ECL1 and ECL2 (Fig. 3b) are probably driven by direct ligand interactions by TT-OAD2 (Fig. 2), whereas those within TM6 and TM7 by direct interactions formed by peptide agonists. Molecular dynamics simulations also support a role of membrane lipid interactions in directly stabilizing both these regions within the TT-OAD2-bound structure (Extended Data Fig. 7). Notably, the helical bundle of the TT-OAD2-complexed receptor is in a more open conformation than the peptide-occupied receptors, largely owing to the top of TM6/ECL3, TM7 and TM1 residing 16 Å, 6 Å and 7 Å further outwards relative to the GLP-1-bound structure (measured from the Cα atoms of $D372^{6.62/ECL3}$, $F381^{7.37}$ and $P137^{1.32}$, respectively (Fig. 3b). The orientation of TM6, ECL3 and TM7 also differs between ExP5- and GLP-1-bound structures, with ExP5 adopting a more open conformation[3]; however, the outward positioning of ECL3 induced by TT-OAD2 is much larger (Extended Data Fig. 5b). Peptide-bound

structures of all solved class B GPCRs revealed direct interactions of the engaged peptide with residues within TM5, TM6, TM7 and ECL3 with the peptide volume (minimally) presumed to actively contribute to the outward conformational change in this region[2–4,8,9,24]. In the apo-state of the glucagon receptor, interactions occur between ECL3 and the ECD that contribute to maintenance of receptor quiescence[7,8,25,26]. Molecular dynamics simulations on the GLP-1R structures, performed after the removal of either TT-OAD2 or GLP-1, predict that the GLP-1R ECD also adopts both open and closed conformations in the apo-state, in which it can form transient interactions with both ECL2 and ECL3[25] (Extended Data Fig. 8). Combining this information with the GLP-1R active structures suggests that interactions, with either peptide or non-peptide agonists, can release ECL3-ECD constraints, lowering the energy barrier for receptor activation. However, the degree of ligand interaction with TM6–ECL3–TM7 determines the extent to which the transmembrane bundle opens, and this in turn directly contributes to G-protein efficacy and biased agonism, as these regions (TM6–ECL3–TM7 and TM1) have been identified as key drivers for these phenomena, particularly for the GLP-1R[3,27–29].

Despite the different binding modes, commonalities observed in interactions with TT-OAD2 and peptide with transmembrane helices 1–3 and stabilization of ECL2 are sufficient to initiate conformational transitions that propagate to a similar reorganization of the class B GPCR conserved central polar network that is linked to activation, albeit the mechanism for this differs for peptide agonists versus TT-OAD2 (Fig. 4a, Supplementary Video 1, Extended Data Fig. 9). Molecular dynamics simulations of the GLP-1-bound GLP-1R predicted persistent interactions between Y152$^{1.47}$, R190$^{2.60}$, Y241$^{3.44}$ and E364$^{6.53}$ and the N terminus of GLP-1 that directly engage the central polar network (Fig. 4a, Extended Data Tables 1, 2, Supplementary Video 1). By contrast, TT-OAD influences the central polar network allosterically via interactions with K197$^{2.67}$, Y145$^{1.40}$ and Y148$^{1.43}$. TT-OAD2 also promotes unique hydrogen bond networks with crucial residues in TM2 (Fig. 4a, Extended Data Table 2) that result in different interaction patterns at the top of TM1 and TM2 relative to peptide-occupied receptors. These effects propagate to the polar network through transient contacts between TT-OAD2 with Y148$^{1.43}$ and Y152$^{1.47}$ that in turn interact with R190$^{2.60}$ of the central polar network (Supplementary Video 2). When bound by GLP-1, the polar network is stabilized by ligand and a network of water molecules, whereas for TT-OAD2, this occurs via a distinct network of structural waters rather than by the ligand (Fig. 4b, Supplementary Video 1). These differences in the mechanism of conformational transitions and stabilization of conserved polar networks (summarized in Extended Data Fig. 9) may contribute to the different kinetic profiles of G-protein activation, as well as the full versus partial agonism for cAMP production.

Collectively, our work provides key advances in understanding the activation of class B GPCRs and G_s protein efficacy, identifying a non-peptide binding site within the GLP-1R that can promote distinct efficacy and biased signalling relative to peptide ligands, and this may extend to other class B GPCRs. The demonstration that non-peptide agonists of the GLP-1R are not required to mimic the extensive receptor contacts formed by peptides within the transmembrane cavity to promote receptor activation will advance the pursuit of non-peptide agonists for therapeutically important class B receptors.

Online content

Any methods, additional references, Nature Research reporting summaries, source data, extended data, supplementary information, acknowledgements, peer review information; details of author contributions and competing interests; and statements of data and code availability are available at https://doi.org/10.1038/s41586-019-1902-z.

1. Bortolato, A. et al. Structure of class B GPCRs: new horizons for drug discovery. *Br. J. Pharmacol.* **171**, 3132–3145 (2014).
2. Liang, Y. L. et al. Cryo-EM structure of the active, G_s-protein complexed, human CGRP receptor. *Nature* **561**, 492–497 (2018).
3. Liang, Y. L. et al. Phase-plate cryo-EM structure of a biased agonist-bound human GLP-1 receptor-Gs complex. *Nature* **555**, 121–125 (2018).
4. Liang, Y. L. et al. Phase-plate cryo-EM structure of a class B GPCR-G-protein complex. *Nature* **546**, 118–123 (2017).
5. Zhao, L. H. et al. Structure and dynamics of the active human parathyroid hormone receptor-1. *Science* **364**, 148–153 (2019).
6. Zhang, Y. et al. Cryo-EM structure of the activated GLP-1 receptor in complex with a G protein. *Nature* **546**, 248–253 (2017).
7. Siu, F. Y. et al. Structure of the human glucagon class B G-protein-coupled receptor. *Nature* **499**, 444–449 (2013).
8. Zhang, H. et al. Structure of the full-length glucagon class B G-protein-coupled receptor. *Nature* **546**, 259–264 (2017).
9. Zhang, H. et al. Structure of the glucagon receptor in complex with a glucagon analogue. *Nature* **553**, 106–110 (2018).
10. Song, G. et al. Human GLP-1 receptor transmembrane domain structure in complex with allosteric modulators. *Nature* **546**, 312–315 (2017).
11. Htike, Z. Z. et al. Efficacy and safety of glucagon-like peptide-1 receptor agonists in type 2 diabetes: A systematic review and mixed-treatment comparison analysis. *Diabetes Obes. Metab.* **19**, 524–536 (2017).
12. Aroda, V. R. et al. PIONEER 1: Randomized clinical trial comparing the efficacy and safety of oral semaglutide monotherapy with placebo in patients with type 2 diabetes. *Diabetes Care* **42**, dc190749 (2019).
13. Pratley, R. *et al*. Oral semaglutide versus subcutaneous liraglutide and placebo in type 2 diabetes (PIONEER 4): a randomised, double-blind, phase 3a trial. *Lancet* **394**, 39–50 (2019).
14. Wootten, D. et al. Differential activation and modulation of the glucagon-like peptide-1 receptor by small molecule ligands. *Mol. Pharmacol.* **83**, 822–834 (2013).
15. Nolte, W. M. et al. A potentiator of orthosteric ligand activity at GLP-1R acts via covalent modification. *Nat. Chem. Biol.* **10**, 629–631 (2014).
16. Freeman, J. W. S. et al. TTP273: Oral, G protein pathway selective clinical-stage GLP-1 receptor (GLP-1R) agonist. *Keystone Symposium, Keystone, CO February 22* http://vtvtherapeutics.com/wp-content/uploads/pdf/GLP1_poster_animation_Keystone_CO_FINAL.pdf (2016).
17. Chen, D. et al. A nonpeptidic agonist of glucagon-like peptide 1 receptors with efficacy in diabetic *db/db* mice. *Proc. Natl Acad. Sci. USA* **104**, 943–948 (2007).
18. Jazayeri, A. et al. Crystal structure of the GLP-1 receptor bound to a peptide agonist. *Nature* **546**, 254–258 (2017).
19. Freeman, J. D. C., Dunn, I. & Valcarce, C. TTP273, Oral (nonpeptide) GLP-1R agonist: improved glycemic control without nausea and vomiting in phase 2. *American Diabetes Association 77th Scientific Sessions, San Diego, CA, June 9–13, 2017* http://vtvtherapeutics.com/wp-content/uploads/pdf/ADA_Logra_study_results_poster_1220-P%20Final.pdf (2017).
20. Runge, S., Thøgersen, H., Madsen, K., Lau, J. & Rudolph, R. Crystal structure of the ligand-bound glucagon-like peptide-1 receptor extracellular domain. *J. Biol. Chem.* **283**, 11340–11347 (2008).
21. DeVree, B. T. et al. Allosteric coupling from G protein to the agonist-binding pocket in GPCRs. *Nature* **535**, 182–186 (2016).
22. Yin, Y. et al. An intrinsic agonist mechanism for activation of glucagon-like peptide-1 receptor by its extracellular domain. *Cell Discov.* **2**, 16042 (2016).
23. Zhao, L. H. et al. Differential requirement of the extracellular domain in activation of class B G protein-coupled receptors. *J. Biol. Chem.* **291**, 15119–15130 (2016).
24. Ehrenmann, J. et al. High-resolution crystal structure of parathyroid hormone 1 receptor in complex with a peptide agonist. *Nat. Struct. Mol. Biol.* **25**, 1086–1092 (2018).
25. Yang, L. et al. Conformational states of the full-length glucagon receptor. *Nat. Commun.* **6**, 7859 (2015).
26. Wootten, D., Simms, J., Miller, L. J., Christopoulos, A. & Sexton, P. M. Polar transmembrane interactions drive formation of ligand-specific and signal pathway-biased family B G protein-coupled receptor conformations. *Proc. Natl Acad. Sci. USA* **110**, 5211–5216 (2013).
27. dal Maso, E. et al. The molecular control of calcitonin receptor signaling. *ACS Pharmacol. Transl. Sci.* **2**, 31–51 (2019).
28. Wootten, D. et al. The extracellular surface of the GLP-1 receptor is a molecular trigger for biased agonism. *Cell* **165**, 1632–1643 (2016).
29. Lei, S. et al. Two distinct domains of the glucagon-like peptide-1 receptor control peptide-mediated biased agonism. *J. Biol. Chem.* **293**, 9370–9387 (2018).

Methods

Data reporting

No statistical methods were used to predetermine sample size. The experiments were not randomized and investigators were not blinded to allocation.

TT-OAD2 synthesis

Several azoanthracene-based derivatives are reported as potent agonists of the GLP-1R (WO10114824), and a compound from this series known as OAD2 was selected for our studies (WO14113357). OAD2, (*S*)-2-{[(3S,8S)-3-[4-(3,4-dichloro-benzyloxy)-phenyl]-7-((*S*)-1-phenyl-propyl)-2,3,6,7,8,9-hexahydro-[1,4]dioxino[2,3-g]isoquinoline-8-carbonyl]-amino}-3-[4-(2,3-dimethyl-pyridin-4-yl)-phenyl]-propionic acid, was synthesized using procedures previously described (see example 179 in WO10114824), and a dihydrochloride salt form (OAD2.2HCl) was prepared by standard methods from the free base. Therefore, TT-OAD2 is the dihydrochloride salt of OAD2 in patent WO14113357. The purity of TT-OAD2 was determined by liquid chromatography–mass spectrometry (LC–MS) to be 98.62%.

Constructs

GLP-1R was modified to contain either a 2xcMyc-N-terminal epitope tag (for signalling and radioligand-binding assays) or a Nanoluc tag (with a 12xGly linker; for NanoBRET binding studies) after the native signal peptide. For β-arrestin recruitment assays, a C-terminal Rluc8 was fused to the C terminus of the receptor. For G-protein conformational assays, a Nanoluc flanked by SGGGGS linkers was inserted into $G\alpha_s$ and $G\alpha_{i2}$ after G(h1ha10) in $G\alpha_s$ or E(HA.03) in $G\alpha_{i2}$ as previously described[30,31]. These were used in conjunction with an N-terminally Nluc-labelled $G\gamma_2$. For G-protein steady-state assays, G-protein NanoBit-split luciferase constructs were generated by fusing the LgBIT after G(h1ha10) in $G\alpha_s$ or E(HA.29) in $G\alpha_{i2}$ and the SmBIT to $G\gamma_2$. For structural studies, human GLP-1R in the pFastBac vector was modified to include an N-terminal Flag tag epitope and a C-terminal 8×histidine tag; both tags are removable by 3C protease cleavage. These modifications did not alter the pharmacology of the receptor[3]. A dominant-negative $G\alpha_s$ construct was generated previously by site directed mutagenesis to incorporate mutations that alter nucleotide handling, stabilize the G_0 state and interactions with the βγ subunits[30].

Insect cell expression

GLP-1R, human dominant-negative $G\alpha_s$, His6-tagged human $G\beta_1$ and $G\gamma_2$ were expressed in *Tni* insect cells (Expression systems) using baculovirus. Cell cultures were grown in ESF 921 serum-free media (Expression Systems) to a density of 4 million cells per ml and then infected with three separate baculoviruses at a ratio of 2:2:1 for GLP-1R, dominant-negative $G\alpha_s$ and $G\beta_1\gamma_2$. Cells were obtained by centrifugation 60 h after infection and the cell pellet was stored at −80 °C.

Purification of the TT-OAD2–GLP-1R–G_s complex

Cell pellet was thawed in 20 mM HEPES, pH 7.4, 50 mM NaCl, 2 mM $MgCl_2$ supplemented with cOmplete Protease Inhibitor Cocktail tablets (Roche). Complex formation was initiated by addition of 50 μM TT-OAD2, Nb35–His (10 μg ml^{-1}) and apyrase (25 mU ml^{-1}, NEB) to catalyse hydrolysis of unbound GDP and allow for stabilization of the G_0 state; the suspension was incubated for 1 h at room temperature. Membrane was solubilized by 0.5% (w/v) lauryl maltose neopentyl glycol (LMNG, Anatrace) supplemented with 0.3% (w/v) cholesteryl hemisuccinate (CHS, Anatrace) for 2 h at 4 °C. Insoluble material was removed by centrifugation at 30,000*g* for 30 min and the solubilized complex was immobilized by batch binding to M1 anti-Flag affinity resin in the presence of 3 mM $CaCl_2$. The resin was packed into a glass column and washed with 20 column volumes of 20 mM HEPES pH 7.4, 100 mM NaCl, 2 mM $MgCl_2$, 3 mM $CaCl_2$, 1 μM OAD, 0.01% (w/v) MNG and 0.006% (w/v) CHS before bound material was eluted in buffer containing 5 mM EGTA and 0.1 mg ml^{-1} Flag peptide. The complex was then concentrated using an Amicon Ultra Centrifugal Filter (molecular mass cut off 100 kDa) and subjected to size-exclusion chromatography on a Superdex 200 Increase 10/300 column (GE Healthcare) that was pre-equilibrated with 20 mM HEPES pH 7.4, 100 mM NaCl, 2 mM $MgCl_2$, 1 μM OAD, 0.01% (w/v) MNG and 0.006% (w/v) CHS to separate complex from contaminants. Eluted fractions consisting of receptor and G-protein complex were pooled and concentrated. Final yield of purified complex was approximately 0.15 mg per litre of insect cell culture.

Electron microscopy

Samples (3 μl) were applied to a glow-discharged Quantifoil R1.2/1.3 CuRh 200 mesh holey carbon grid (Quantifoil GmbH) and were flash frozen in liquid ethane using the Vitrobot mark IV (Thermo Fisher Scientific) set at 100% humidity and 4 °C for the prep chamber. Data were collected on a Titan Krios microscope (Thermo Fisher Scientific) operated at an accelerating voltage of 300 kV with a 50 μm C2 aperture at an indicated magnification of 105 K in nanoprobe EFTEM mode. Gatan K3 direct electron detector positioned post a Gatan Quantum energy filter, operated in a zero-energy-loss mode with a slit width of 25 eV was used to acquire dose fractionated images of the GLP-1R TT-OAD2-bound sample without an objective aperture. Movies were recorded in hardware-binned mode (previously called counted mode on the K2 camera) yielding a physical pixel size of 0.826 Å pixel^{-1} with an exposure time of 3.715 s amounting to a total dose of 65.6 e^- Å^{-2} at a dose rate of 12.2 e^- pixel^{-1} s^{-1}, which was fractionated into 62 subframes. A second dataset of 1,568 micrographs was also recorded using the same microscope but in 'super-resolution' mode on the K3 detector, the physical pixel size was 0.413 Å with an exposure time of 4.015 s amounting to a total dose of 63.5 e^- Å^{-2}, which was fractionated into 67 subframes. Defocus range was set between −0.7 and −1.5 μm. A total of 3,158 plus 1,568 movies were collected in two data collection sessions.

Electron microscopy data processing

Movies were motion-corrected with UCSF MotionCor2[32] (movies collected in super-resolution mode were Fourier scaled by a factor of ×2 to match the pixel size of the larger data set). This was followed by CTF estimation sing the GCTF software packag[33]. Particles were picked from the micrographs using the automated reference-free procedure in RELION[34,35]. Reference free 2D and 3D classification (by generating multiple ab initio models with no structural identity enforced) was carried out in CryoSPARC (v.2.5.0)[36]. A homogeneous subset of particles was then subjected to movie refinement and Bayesian particle polishing as implemented in RELION (v.3.0). This homogeneous subset of polished particles was used in a 3D refinement in RELION and then further classified into 3D classes with alignment of Euler angles not taken into account. Particles belonging to the 3D class that yielded the best resolved map were then subjected to signal subtraction to subtract density due to the detergent micelle and the alpha domain of the G protein. Final 3D refinement was performed in RELION (3.0) yielded a map of resolutions 3.01 Å. Local resolution estimations were performed using the ResMAP software packag[37].

Atomic model refinement

Fitting the model to the cryoEM electron density map was achieved using the MDFF routine in namd[38]. The fitted model was further refined by rounds of manual model building in coot[39] and real space refinement as implemented in the Phenix software package[40], the model restraints for the TT ligand were prepared by using the coordinates generated from Chem3D and the ELBOW software package[41]. The ligands were fitted after the first round of real-space refinements, manually first in coot[39], then refined using Phenix real-space refinement[42]. Ramachandran, rotamer and secondary structure restraints were applied for the first round of real-space refinement, and after manual inspection and

adjustment of the model in coot further real-space refinements were carried out with only Ramachandran and rotamer restraints applied and the model/data weight was allowed to freely refine. The density around the extracellular domain was poorly resolved (local resolution estimated at >8 Å) and was not modelled.

Modelling methods for preparation of molecular dynamic simulations

The two missing receptor loops, namely the stalk region and ICL3, were generated using PLOP[43]; ICL3 was also minimized in the presence of Gα to eliminate steric clashes. On the basis of the electron density of our structures, TM1 for the GLP-1-bound 5VAI structure[6] was replaced by TM1 from the P5-bound structure (PDB code 6B3J)[3] by the method of molecular superposition. The missing residues in the stalk region were reconstructed using Modeller[44] subject to the constraint that the high variability positions[45] in the GLP-1R multiple sequence alignment (E133–R134) faced outwards. The missing loops in the G protein were generated by molecular superposition, using VMD[46], of the corresponding loops in the β_2-adrenergic receptor–G protein complex[47], PDB code 3SN6 to the flank either side of the gap, since this particular X-ray structure (with 99% identity to the G protein used in this study) generally gave a lower root mean squared deviation value on molecular superposition than plausible alternative G-protein structures (for example, PDB 5VAI). The joining point was taken as the closest atom pairs (usually separated by approximately 0.2 Å) that maintained an appropriate Cα–Cα distance (3.7–3.9 Å) across the join; selected residues spanning the join were minimized using PLOP where additional refinement was deemed necessary. The exception to this was the loop between A249–N264, which was completed using the shorter loop from the adenosine A_{2A} receptor–G-protein complex, PDB code 5G53[48]. The helical domain, between residues G47 and G207, which is not visible in the cryo-EM structure, was omitted as in earlier work.

Molecular dynamics methods

Four GLP-1R complexes (GLP-1R–TT-OAD2–G_s; GLP-1R–TT-OAD2; GLP-1R–GLP-1–G_s; and GLP-1R–GLP-1; Supplementary Table 3) and two apo GLP-1R structures (obtained by removing both the G_s protein and the ligands; Supplementary Table 3) were prepared for simulation with the CHARMM36 force field[49], through use of in-house python htmd[50] and TCL (Tool Command Language) scripts. The pdb2pqr[51] and propka[52] software were used to add hydrogen atoms appropriate for a pH of 7.0; the protonation of titratable side chains was checked by visual inspection. The coordinates were superimposed on the corresponding GLP-1R coordinates from the OPM database[53] so as to orient the receptor before insertion[54] in a rectangular pre-built 125 Å × 116 Å 1-palmitoyl-2-oleyl-*sn*-glycerol-3-phosphocholine (POPC) bilayer; lipid molecules overlapping the receptor were removed. TIP3P water molecules were added to the 125 Å × 116 Å × 195 Å simulation box using the VMD Solvate plugin 1.5 (Solvate Plugin, v.1.5; http://www.ks.uiuc.edu/Research/vmd/plugins/solvate/). Overall charge neutrality was maintained by adding Na^+ and Cl^- counter ions to a final ionic concentration of 150 mM using the VMD Autoionize plugin 1.3 (Autoionize Plugin, v.1.3; http://www.ks.uiuc.edu/Research/vmd/plugins/autoionize/). CGenFF force field parameters[55–57] and topology files for TT-OAD2 were retrieved from the Paramch[56] webserver. No further optimization was performed because the obtained parameters were associated to low penalty scores.

Systems equilibration and molecular dynamics simulation settings

ACEMD[58] was used for both equilibration and molecular dynamics productive simulations. Isothermal-isobaric conditions (Langevin thermostat[59] with a target temperature of 300 K and damping of 1 ps^{-1} and Berendsen barostat[60] with a target pressure 1 atm) were used to equilibrates the systems through a multi-stage procedure (integration time step of 2 fs). Initial steric clashes between lipid atoms were reduced through 3,000 conjugate-gradient minimization steps, then a 2 ns molecular dynamics simulation was run with a positional constraint of 1 kcal mol^{-1} $Å^{-2}$ on protein atoms and lipid phosphorus atoms. Subsequently, 20 ns of molecular dynamics simulations were performed constraining only the protein atoms. In the final equilibration stage, protein backbone alpha carbons constraints were applied for a further 60 ns.

Productive trajectories in the canonical ensemble (NVT) at 300 K (four 500-ns-long replicas for each GLP-1R complex; Supplementary Table 3) were computed using a thermostat damping of 0.1 ps^{-1} with an integration time step of 4 fs and the M-SHAKE algorithm[61] to constrain the bond lengths involving hydrogen atoms. The cut-off distance for electrostatic interactions was set at 9 Å, with a switching function applied beyond 7.5 Å. Long-range Coulomb interactions were handled using the particle mesh Ewald summation method (PME)[62] by setting the mesh spacing to 1.0 Å. Trajectory frames were written every 100 ps of simulations.

Molecular dynamics analysis

The first half (500 ns) of the molecular dynamics replicas involving GLP-1R–TT-OAD2, GLP-1R–GLP-1 complexes as well as the apo-GLP-1R (TT-OAD2), and apo-GLP-1R (GLP-1) systems (Supplementary Table 3) were considered as part of the equilibration stage and therefore not considered for analysis. Atomic contacts (atom distance less than 3.5 Å) were computed using VMD[46]. Hydrogen bonds were identified using the GetContacts analysis tool (https://getcontacts.github.io/), with the donor-acceptor distance set to 3.3 Å and the angle set to 150°. Videos were generated using VMD[46] and avconv (https://libav.org/avconv.html). Root mean square fluctuation (RMSF) values were computed using VM[46] after superposition of the molecular dynamic trajectories frames on the alpha carbon of the transmembrane domain (residues $E138^{1.33}$–$V404^{7.60}$). The orientation of the N-terminal helix of the ECD of GLP-1R was drawn in VMD considering a representative frame every 10 ns. To detect volumes within the transmembrane domain of GLP-1R occupied by water molecules with low mobility (structural water molecules), the AquaMMapS[63] analysis was performed on 10-ns-long molecular dynamics simulations of the GLP-1R–TT-OAD2–G_s and GLP-1R–GLP-1–G_s complexes (coordinates were written every 10 ps of simulation); all the alpha carbons were restrained in analogy with the approach proposed previously[64].

Whole-cell radioligand binding assays

HEK293 cells (confirmed mycoplasma negative) were seeded at 30,000 cells per well in 96-well culture plates and incubated overnight in DMEM containing 5% FBS at 37 °C, 5% CO_2. Media was replaced with HBSS containing 25 mM HEPES and 0.1% (w/v) BSA with 0.1 nM ^{125}I-exendin(9–39) and increasing concentrations of unlabelled agonist. Cells were incubated overnight at 4 °C, washed three times in ice-cold buffer and then solubilized in 0.1 M NaOH. Radioactivity was determined by gamma counting. Non-specific activity was defined using 1 μM exendin(9–39).

cAMP accumulation assays

HEK293 cells (confirmed mycoplasma negative) were seeded at a density of 30,000 cells per well into 96-well culture plates and incubated overnight in DMEM containing 5% FBS at 37 °C in 5% CO_2. cAMP detection was performed as previously described in the presence of the phosphodiesterase inhibitor 3-isobutyl-1-methylxanthin[65]. All values were converted to cAMP concentration using a cAMP standard curve performed in parallel and data were subsequently normalized to the response of 100 μM forskolin in each cell line. In one series of experiments, vehicle or increasing concentrations of TT-OAD2 was added 30 min before assay of peptide response.

cAMP kinetics studies

HEK293A cells (confirmed mycoplasma negative) were transfected with an Epac-cAMP sensor (CAMYEL) and human GLP-1R at an optimized

ratio. Ligand-mediated cAMP production was measured 48 h after transfection. In brief, culture media was replaced with assay buffer (1× HBSS, 10 mM HEPES, 0.1% BSA, pH 7.4). BRET signals were measured at 1 min intervals using a PHERAstar plate reader (BMG LabTech) in the absent or present of increasing concentration of ligands. Forskolin (100 μM) was used as a positive control, and data were normalized to the forskolin response.

β-arrestin recruitment assays

HEK293 cells (confirmed mycoplasma negative) were transiently transfected with GLP-1R-Rluc8 and β-arrestin1-Venus at a 1:4 ratio and seeded at a density of 30,000 cells per well into 96-well culture plates and incubated for 48 h in DMEM containing 5% FBS at 37 °C in 5% CO_2. β-arrestin recruitment was performed as previously described[66]. In one series of experiments, vehicle or increasing concentrations of TT-OAD2 was added 30 min before assay of peptide response.

ERK1/2 phosphorylation assays

HEK293 cells (confirmed mycoplasma negative) expressing stably expressing the GLP-1R were seeded at a density of 30,000 cells per well into 96-well culture plates and incubated overnight at 37 °C in 5% CO_2. Receptor-mediated pERK1/2 was determined using the AlphaScreen ERK1/2 SureFire protocol as previously described[14]. Data were normalized to the maximal response elicited by 10% FBS determined at 6 min. In one series of experiments, vehicle or increasing concentrations of TT-OAD2 was added 30 min before assay of peptide response.

Ca^{2+} mobilization assays

HEK293 cells (confirmed mycoplasma negative) stably expressing the GLP-1R were seeded at a density of 30,000 cells per well into 96-well culture plates and incubated overnight at 37 °C in 5% CO_2, and receptor- mediated intracellular calcium mobilisation determined as previously described[65]. Fluorescence was determined immediately after ligand addition, with an excitation wavelength set to 485 nm and an emission wavelength set to 520 nm, and readings taken every 1.36 s for 120 s. The peak value was used to create concentration-response curves. Data were normalized to the maximal response elicited by 100 μM ATP. In one series of experiments, vehicle or increasing concentrations of TT-OAD2 was added 30 min before assay of peptide response.

Generation of stable cell lines containing wild-type and mutant GLP-1R

Mutant receptors were generated in a 2xc-Myc epitope-tagged receptor using QuikChange site-directed mutagenesis (Invitrogen) and sequences confirmed. Wild-type and mutant receptors were stably expressed in CHOFlpIn cells (confirmed mycoplasma negative) using the FlpIn Gateway technology system and selected using 600 μg ml^{-1} hygromyocin B.

NanoBRET ligand binding

HEK293A cells were transiently transfected with Nluc-hGLP-1R. Forty-eight hours after transfection, cells were collected and plasma membrane was extracted as described previously[31]. Cell membrane (1 μg per well) was incubated with furimazine (1:1,000 dilution from stock) in assay buffer (1× HBSS, 10 mM HEPES, 0.1% (w/v) BSA, 1× P8340 protease inhibitor cocktail, 1 mM DTT and 0.1 mM PMSF, pH 7.4). RhodamineX-Ex4 (Rox-Ex4) was used as fluorescent ligand in the NanoBRET binding assay. BRET signal between Nluc-hGLP-1R and Rox-Ex4 was measured using PHERAstar (BMG LabTech) at 10 s interval (25 °C), a 2 min baseline was taken before addition of Rox-Ex4 (K_d concentration 3.16nM, determined previously), the measurement continued for 15 min followed by adding increasing concentration of TT-OAD2, or unlabelled Ex4 as a control. Data were corrected for baseline and vehicle treated samples.

G-protein conformation assays

HEK293AΔS/Q/12/13 cells stably expressing GLP-1R (tested and confirmed to be free from mycoplasma) were transfected with a 1:1:1 ratio of Nanoluc-$G\alpha_s$ (Nanoluc inserted at position 72): $G\beta_1$:Venus-$G\gamma_2$ 24 h before collection and preparation of cell plasma membranes. Cell membrane (5 μg per well) was incubated with furimazine (1:1,000 dilution from stock) in assay buffer (1× HBSS, 10 mM HEPES, 0.1% (w/v) BSA, 1× P8340 protease inhibitor cocktail, 1 mM DTT and 0.1 mM PMSF, pH 7.4). The GLP-1R-induced BRET signal between $G\alpha_s$ and Gγ was measured at 30 °C using a PHERAstar (BMG LabTech). Baseline BRET measurements were taken for 2 min before addition of vehicle or ligand. BRET was measured at 15-s intervals for a further 7 min. All assays were performed in a final volume of 100 μl.

G-protein NanoBIT assays

HEK293A wild-type cells stably express human GLP-1R were transiently transfected with Gα-LgBIT, $G\beta_1$, $G\gamma_2$-SmBIT (1:5:5) 48 h before the assays. Cells were then incubated with coelenterazine H (5 μM) for 1 h at room temperature. Luminescence signals were measured using a Clariostar plate reader (BMG LabTech) at 30 s intervals before and after ligand addition (25 °C). Data were corrected to baseline and vehicle treated samples.

In vivo IVGTT assays

Intravenous glucose tolerance tests were performed in male human GLP-1R knock-in and knockout mice (all on C57/BL6 background[67]). Catheters were placed in the right carotid artery and left jugular vein of mice 6–11 months of age. Approximately one week later, mice (n = 4–5 per group) were fasted overnight and the catheters were exteriorized as mice acclimated to test cages. Vehicle (5% DMSO, 20% Captisol in $NaHPO_4$, pH 2, 1 ml kg^{-1}), GLP-1(7-36)NH_2 at 10 μg kg^{-1}, GIP(1-42) at 25 μg kg^{-1}, or OAD2 at 3 mg kg^{-1} was administered intravenously one minute before glucose load (0.5 g kg^{-1}). Blood samples were collected at −10, 0, 2, 4, 6, 10, 20 and 30 min to determine blood glucose concentrations via glucometer (Roche, Aviva) and plasma insulin measurement (Alpco, 80-INSMSU-E10). All mouse experiments were performed in accordance with the Institutional Animal Care and Use Committee of Eli Lilly and Company and the NIH Guide for the Use and Care of Laboratory Animals.

Data analysis

Pharmacological data were analysed using Prism 7 (GraphPad). Concentration response signalling data were analysed using a three-parameter logistic equation, or via operational analysis. Changes in the rate of change in BRET kinetic data were fitted to one-phase association curve. Statistical analysis was performed with either one-way analysis of variance and a Dunnetts post-test or a paired t-test, and significance accepted at $P < 0.05$.

Graphics

Molecular graphics images were produced using the UCSF Chimera package from the Computer Graphics Laboratory, University of California, San Francisco (supported by NIH P41 RR-01081).

Reporting summary

Further information on research design is available in the Nature Research Reporting Summary linked to this paper.

Data availability

All relevant data are available from the authors and/or included in the manuscript or Supplementary Information. Atomic coordinates and the cryo-EM density map have been deposited in the Protein Data Bank

(PDB) under accession number 6ORV and Electron Microscopy Data Bank (EMDB) accession EMD-20179.

30. Liang, Y.-L. et al. Dominant negative G proteins enhance formation and purification of agonist-GPCR-G protein complexes for structure determination. *ACS Pharmacol. Transl. Sci.* **1**, 9 (2018).
31. Furness, S. G. B. et al. Ligand-dependent modulation of G protein conformation alters drug efficacy. *Cell* **167**, 739–749.e711 (2016).
32. Zheng, S. Q. et al. MotionCor2: anisotropic correction of beam-induced motion for improved cryo-electron microscopy. *Nat. Methods* **14**, 331–332 (2017).
33. Zhang, K. Gctf: Real-time CTF determination and correction. *J. Struct. Biol.* **193**, 1–12 (2016).
34. Nakane, T., Kimanius, D., Lindahl, E. & Scheres, S. H. Characterisation of molecular motions in cryo-EM single-particle data by multi-body refinement in RELION. *eLife* **7**, e36861 (2018).
35. Zivanov, J. et al. New tools for automated high-resolution cryo-EM structure determination in RELION-3. *eLife* **7**, e42166 (2018).
36. Punjani, A., Rubinstein, J. L., Fleet, D. J. & Brubaker, M. A. cryoSPARC: algorithms for rapid unsupervised cryo-EM structure determination. *Nat. Methods* **14**, 290–296 (2017).
37. Kucukelbir, A., Sigworth, F. J. & Tagare, H. D. Quantifying the local resolution of cryo-EM density maps. *Nat. Methods* **11**, 63–65 (2014).
38. Chan, K. Y., Trabuco, L. G., Schreiner, E. & Schulten, K. Cryo-electron microscopy modeling by the molecular dynamics flexible fitting method. *Biopolymers* **97**, 678–686 (2012).
39. Emsley, P., Lohkamp, B., Scott, W. G. & Cowtan, K. Features and development of Coot. *Acta Crystallogr. D* **66**, 486–501 (2010).
40. Adams, P. D. et al. PHENIX: a comprehensive Python-based system for macromolecular structure solution. *Acta Crystallogr. D* **66**, 213–221 (2010).
41. Moriarty, N. W., Grosse-Kunstleve, R. W. & Adams, P. D. electronic Ligand Builder and Optimization Workbench (eLBOW): a tool for ligand coordinate and restraint generation. *Acta Crystallogr. D* **65**, 1074–1080 (2009).
42. Afonine, P. V. et al. Real-space refinement in PHENIX for cryo-EM and crystallography. *Acta Crystallogr. D* **74**, 531–544 (2018).
43. Jacobson, M. P. et al. A hierarchical approach to all-atom protein loop prediction. *Proteins* **55**, 351–367 (2004).
44. Eswar, N. et al. Comparative protein structure modeling using Modeller. *Curr Protoc Bioinformatics* **Chapter 5**, Unit 5.6 (2006).
45. Vohra, S. et al. Similarity between class A and class B G-protein-coupled receptors exemplified through calcitonin gene-related peptide receptor modelling and mutagenesis studies. *J. R. Soc. Interface* **10**, 20120846 (2012).
46. Humphrey, W., Dalke, A. & Schulten, K. VMD: visual molecular dynamics. *J. Mol. Graph* **14**, 33–38 (1996).
47. Rasmussen, S. G. et al. Crystal structure of the β_2 adrenergic receptor–G_s protein complex. *Nature* **477**, 549–555 (2011).
48. Carpenter, B., Nehmé, R., Warne, T., Leslie, A. G. & Tate, C. G. Structure of the adenosine A_{2A} receptor bound to an engineered G protein. *Nature* **536**, 104–107 (2016).
49. Huang, J. & MacKerell, A. D. Jr. CHARMM36 all-atom additive protein force field: validation based on comparison to NMR data. *J. Comput. Chem.* **34**, 2135–2145 (2013).
50. Doerr, S., Harvey, M. J., Noé, F. & De Fabritiis, G. HTMD: high-throughput molecular dynamics for molecular discovery. *J. Chem. Theory Comput.* **12**, 1845–1852 (2016).
51. Dolinsky, T. J., Nielsen, J. E., McCammon, J. A. & Baker, N. A. PDB2PQR: an automated pipeline for the setup of Poisson–Boltzmann electrostatics calculations. *Nucleic Acids Res.* **32**, W665–W667 (2004).
52. Olsson, M. H., Søndergaard, C. R., Rostkowski, M. & Jensen, J. H. PROPKA3: consistent treatment of internal and surface residues in empirical pka predictions. *J. Chem. Theory Comput.* **7**, 525–537 (2011).
53. Lomize, M. A., Lomize, A. L., Pogozheva, I. D. & Mosberg, H. I. OPM: orientations of proteins in membranes database. *Bioinformatics* **22**, 623–625 (2006).
54. Sommer, B. Membrane packing problems: a short review on computational membrane modeling methods and tools. *Comput. Struct. Biotechnol. J.* **5**, e201302014 (2013).
55. Vanommeslaeghe, K. et al. CHARMM general force field: a force field for drug-like molecules compatible with the CHARMM all-atom additive biological force fields. *J. Comput. Chem.* **31**, 671–690 (2010).
56. Vanommeslaeghe, K. & MacKerell, A. D. Jr. Automation of the CHARMM General Force Field (CGenFF) I: bond perception and atom typing. *J. Chem. Inf. Model.* **52**, 3144–3154 (2012).
57. Vanommeslaeghe, K., Raman, E. P. & MacKerell, A. D. Jr. Automation of the CHARMM General Force Field (CGenFF) II: assignment of bonded parameters and partial atomic charges. *J. Chem. Inf. Model.* **52**, 3155–3168 (2012).
58. Harvey, M. J., Giupponi, G. & Fabritiis, G. D. ACEMD: Accelerating Biomolecular Dynamics in the Microsecond Time Scale. *J. Chem. Theory Comput.* **5**, 1632–1639 (2009).
59. Loncharich, R. J., Brooks, B. R. & Pastor, R. W. Langevin dynamics of peptides: the frictional dependence of isomerization rates of *N*-acetylalanyl-*N*'-methylamide. *Biopolymers* **32**, 523–535 (1992).
60. Berendsen, H. J. C., Postma, J. P. M., van Gunsteren, W. F., DiNola, A. & Haak, J. R. Molecular dynamics with coupling to an external bath. *J. Chem. Phys.* **81**, 3684 (1984).
61. Kräutler, V. G., van Gunsteren, W. F. & Hünenberger, P. H. A fast SHAKE algorithm to solve distance constraint equations for small molecules in molecular dynamics simulations. *J. Comput. Chem.* **22**, 501–508 (2001).
62. Essmann, U. P. & Berkowitz, L. M.L. A smooth particle mesh Ewald method. *J. Chem. Phys.* **103**, 8577 (1995).
63. Cuzzolin, A., Deganutti, G., Salmaso, V., Sturlese, M. & Moro, S. AquaMMapS: an alternative tool to monitor the role of water molecules during protein-ligand association. *ChemMedChem* **13**, 522–531 (2018).
64. Wall, M. E., Calabró, G., Bayly, C. I., Mobley, D. L. & Warren, G. L. Biomolecular solvation structure revealed by molecular dynamics simulations. *J. Am. Chem. Soc.* **141**, 4711–4720 (2019).
65. Koole, C. et al. Allosteric ligands of the glucagon-like peptide 1 receptor (GLP-1R) differentially modulate endogenous and exogenous peptide responses in a pathway-selective manner: implications for drug screening. *Mol. Pharmacol.* **78**, 456–465 (2010).
66. Savage, E. E., Wootten, D., Christopoulos, A., Sexton, P. M. & Furness, S. G. A simple method to generate stable cell lines for the analysis of transient protein-protein interactions. *Biotechniques* **54**, 217–221 (2013).
67. Jun, L. S. et al. A novel humanized GLP-1 receptor model enables both affinity purification and Cre-LoxP deletion of the receptor. *PLoS One* **9**, e93746 (2014).

Acknowledgements The work was supported by the Monash University Ramaciotti Centre for Cryo-Electron Microscopy, the Monash MASSIVE high-performance computing facility, the National Health and Medical Research Council of Australia (NHMRC) project grants (1061044, 1065410, 1120919 and 1126857) and NHMRC program grants (1055134 and 1150083), the Japan Society for the Promotion of Science (JSPS) KAKENHI no. 18H06043 and Japan Science and Technology Agency (JST) PRESTO no. 18069571 (to R.D.). P.M.S. and A.C. are NHMRC Senior Principal Research Fellows and D.W. is an NHMRC Senior Research Fellow. S.G.B.F. is an ARC Future Fellow. A.I. was funded by the PRIME JP17gm5910013 and the LEAP JP17gm0010004 from the Japan Agency for Medical Research and Development, and JSPS KAKENHI 17K08264. We are grateful to G. Christopoulos, V. Julita, T. Fields, C. Lafuente, J. M. Minguez, G. C. Sanz and F. Qu for assay and technical support.

Author contributions P.Z. designed and performed most of the pharmacological studies with assistance from T.T.T.; Y.-L.L. expressed and purified the complex; R.D. performed cryo-sample preparation and imaging to acquire electron microscopy data; M.J.B. and R.D. processed the electron microscopy data and performed electron microscopy map calculations; M.J.B. built the model and performed refinement; M.M.F. performed the mutagenesis studies, L.C. performed studies in the HEK293 CRISPR-knockout cells; G.D. and C.A.R. designed, performed and analysed the molecular dynamics simulations; F.S.W. and M.G.B. provided TT-OAD2. M.E.C., M.G.B. and K.W.S. designed and oversaw the in vivo studies; P.Z., Y.-L.L., M.J.B., G.D., C.A.R., F.S.W., K.W.S., R.D., P.M.S. and D.W. performed data analysis; P.Z., Y.-L.L., M.J.B., G.D., C.A.R., F.S.W., K.W.S., A.C., L.J.M., M.-W.W. and R.D. assisted with data interpretation, figure and manuscript preparation; P.M.S. and D.W. designed and supervised the project, interpreted the data and wrote the manuscript.

Competing interests F.W.S., M.E.C. and K.W.S. are employees of Eli Lilly and Company.

Additional information

Supplementary information is available for this paper at https://doi.org/10.1038/s41586-019-1902-z.

Correspondence and requests for materials should be addressed to R.D., P.M.S. or D.W.

Peer review information *Nature* thanks Doryen Bubeck, Dave D'Alessio, Nita R. Shah and the other, anonymous, reviewer(s) for their contribution to the peer review of this work.

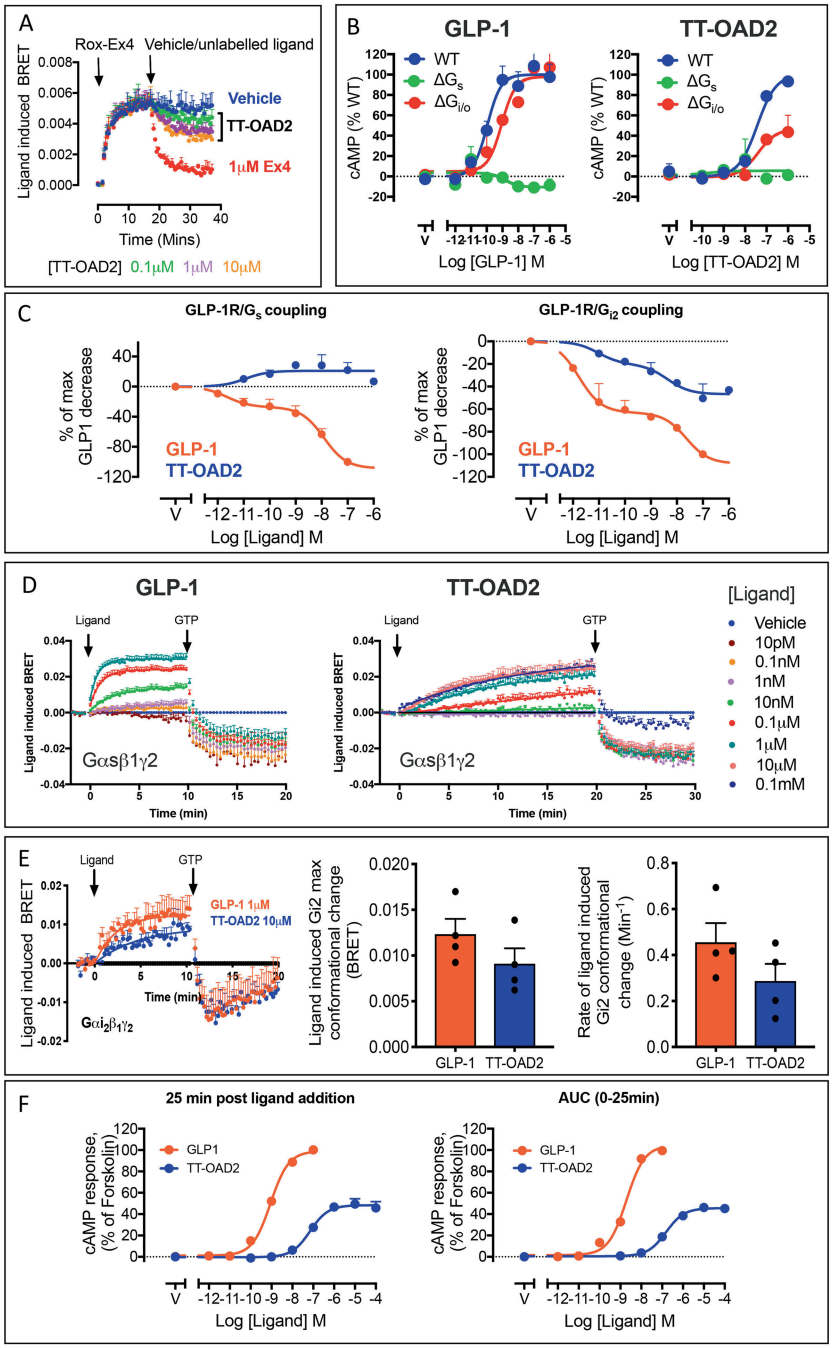

Extended Data Fig. 1 | Binding, transducer coupling and signalling mediated by TT-OAD2. a, Kinetic ligand-binding assay using ROX-exendin-4 as the fluorescent probe. TT-OAD2 is only able to partially displace the probe and with slower kinetics relative to exendin-4 that shows complete displacement of the probe with rapid kinetics. **b**, cAMP accumulation studies using GLP-1 and TT-OAD2 as the agonist in wild-type HEK293 cells and HEK293 cells in which $G_{s/olf}$ (ΔG_s) or all $G_{i/o/z}$ ($\Delta G_{i/o/z}$) have been depleted using CRISPR–Cas9. **c**, HEK293A cells transiently transfected with the GLP-1R and the NanoBit constructs for $G\alpha_s$ and $G\alpha_{i2}$ (Gα-LgBIT, $G\gamma_2$-SmBIT). Luminescence signal was assessed over time (0–20 min) in the presence of increasing concentrations of GLP-1 and TT-OAD2. Concentration response curves are expressed as AUC (0–20 min) for each concentration and normalized to the negative response observed by GLP-1 at 1 μM. **d**, Agonist-induced changes in trimeric G_s protein conformation. Ligand-induced changes in BRET were measured in plasma membrane preparations performed in kinetic mode until kinetic equilibrium was reached for vehicle or increasing concentrations of GLP-1 (left) and TT-OAD2 (right). The addition of GTP dissociated the trimeric G protein complex stabilized by GLP-1-occupied and TT-OAD2-occupied GLP-1R. **e**, Agonist-induced changes in trimeric G_{i2} protein conformation. Left, ligand-induced changes in BRET were measured in plasma membrane preparations performed in kinetic mode until kinetic equilibrium with a saturating concentration of GLP-1 and TT-OAD2. The BRET signal decreased in the presence of GTP, which suggests that GTP dissociated the G_{i2} protein complex stabilized by GLP-1-occupied and TT-OAD2-occupied GLP-1R. Quantification of the plateau (middle) and the rate of ligand-induced conformational change (right) for each agonist (1 μM GLP-1 and 10 μM TT-OAD2) was calculated by applying a one-phase association curve to the kinetic data with values from each individual experiment show in black circles. **f**, Concentration–response curves of production in live HEK293 cells expressing the GLP-1R and an EPAC BRET biosensor in the presence of different concentrations of GLP-1 and TT-OAD2. Left, cAMP response taken 25 min after ligand addition. Right, area under the curve (AUC) analysis of the response calculated as AUC across the full kinetic trace for each ligand concentration (from data in Fig. 2d). Data are mean + s.e.m. of 4–6 independent experiments performed in duplicate or triplicate.

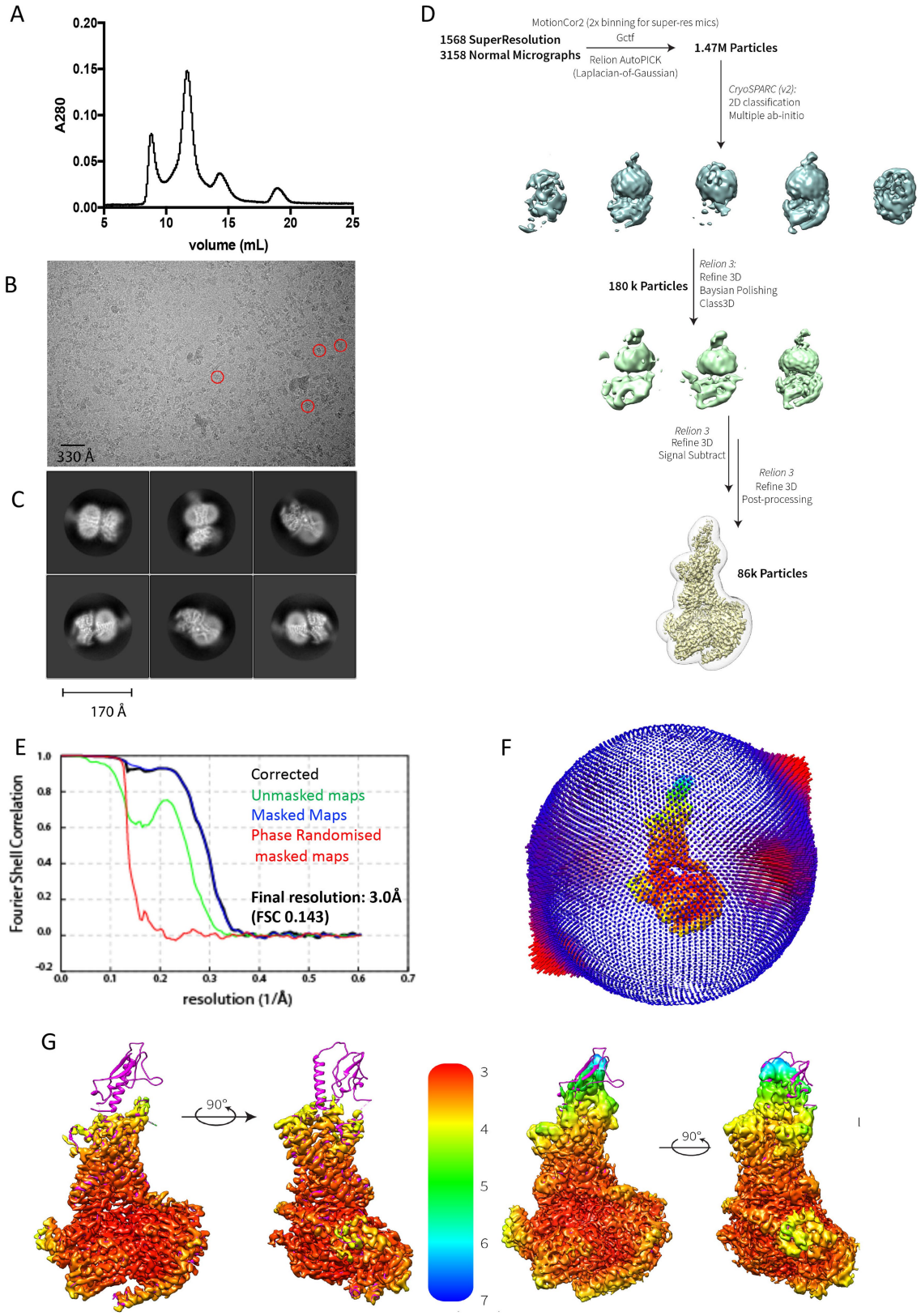

Extended Data Fig. 2 | Purification, cryo-EM data imaging and processing of the TT-OAD2–GLP-1R–G_s complex. a, Representative elution profile of Flag-purified complex on Superdex 200 Increase 10/30 SEC. **b**, Representative micrograph of the TT-OAD2–GLP-1R–G_s complex. Red circles highlight examples of individual particles. **c**, Two-dimensional class averages of the complex in maltose-neopentyl glycol (MNG) micelle. **d**, Cryo-EM data processing workflow. **e**, Gold-standard Fourier shell correlation (FSC) curves, showing the overall nominal resolution at 3.0 Å. **f**, 3D histogram representation of the Euler angle distribution of all the particles used for the in the reconstruction overlaid on the density map drawn on the same coordinate axis (map is coloured according to local resolution as in **g**). **g**, Cryo-EM density map coloured according to resolution. Left, map with the GLP-1R ECD masked; right, map including the ECD of GLP-1R.

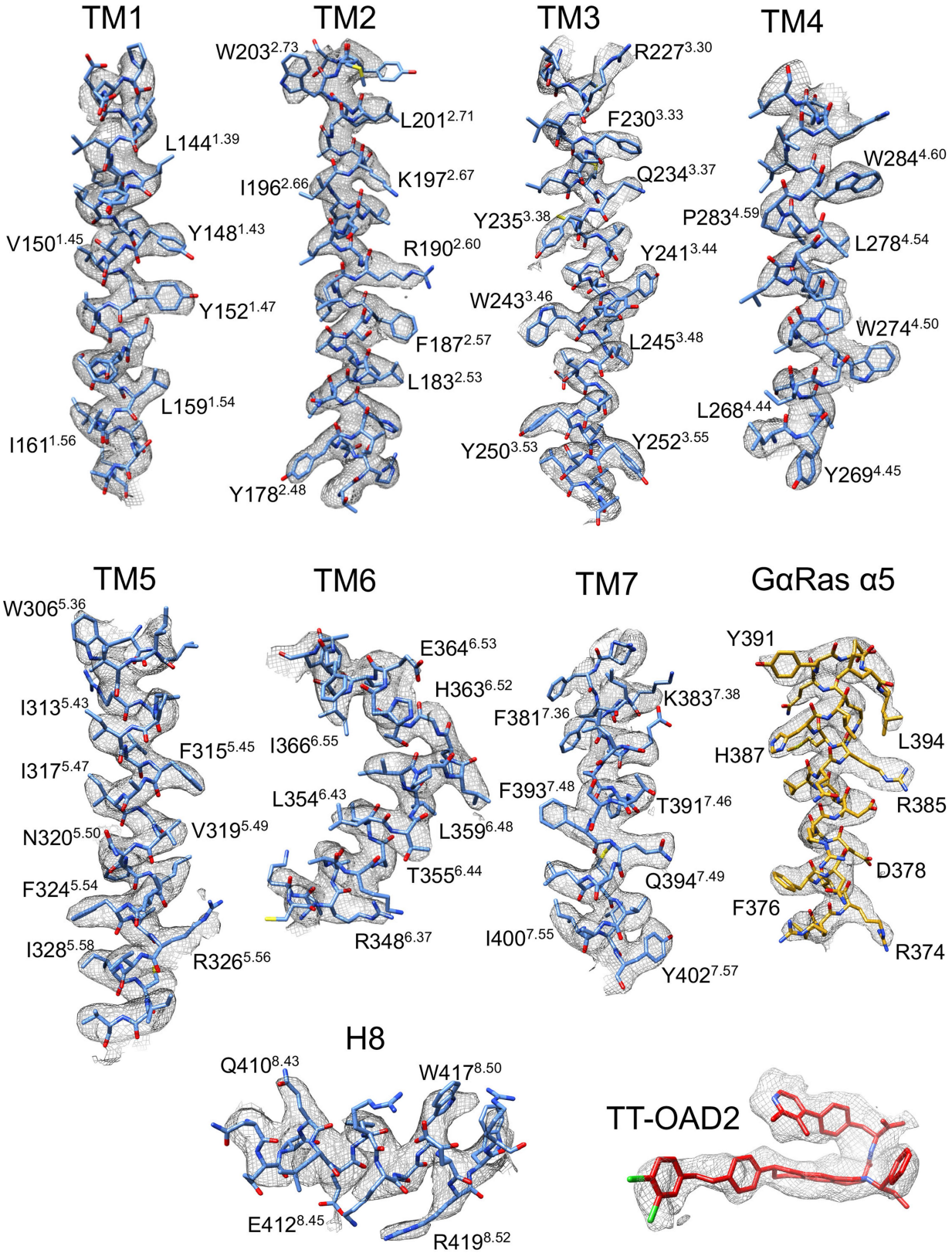

Extended Data Fig. 3 | The atomic resolution model of the TT-OAD2–GLP-1R–Gα_s heterotrimer in the cryo-EM density map. Electron microscopy density map and the model are shown for all seven transmembrane helices and helix 8 (H8) of the receptor, the α5 helix of the Gα_s Ras-like domain and TT-OAD2. All transmembrane helices exhibit good density, with TM6 that displays flexibility being the least well resolved region.

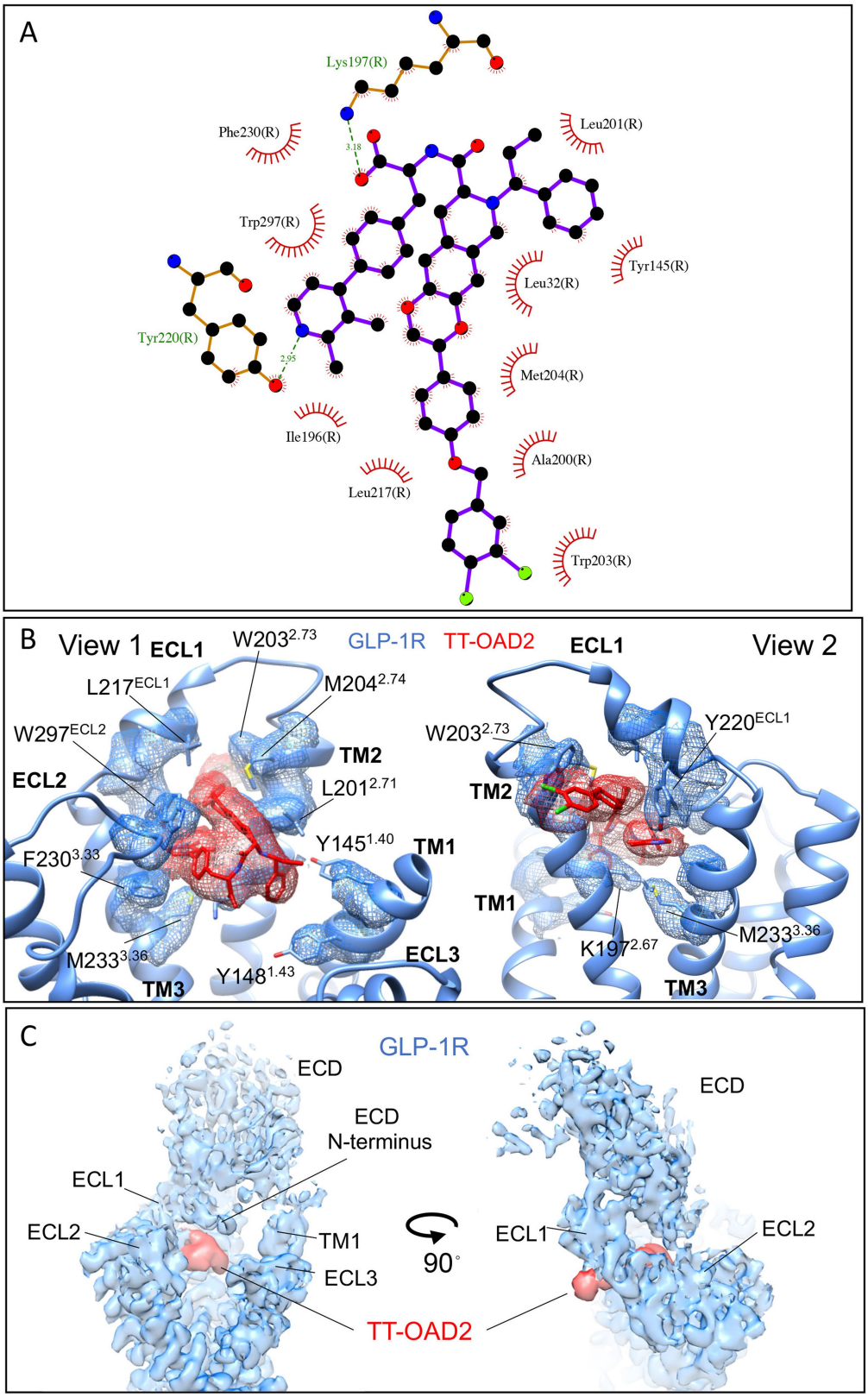

Extended Data Fig. 4 | Cryo-EM density supports ligand interactions in the TT-OAD2-binding site. a, Interacting residues predicted by LigPlot using the full-length model with ECD. **b**, The pose of TT-OAD2 and interactions with residues within TM1, TM2, TM3, ECL1 and ECL2 are supported by well-resolved density in the cryo-EM map. **c**, Density for the ECD was visible in the cryo-EM and supports extended interactions of the ECD with ECL1 and ECL2, as well as with the ligand TT-OAD2.

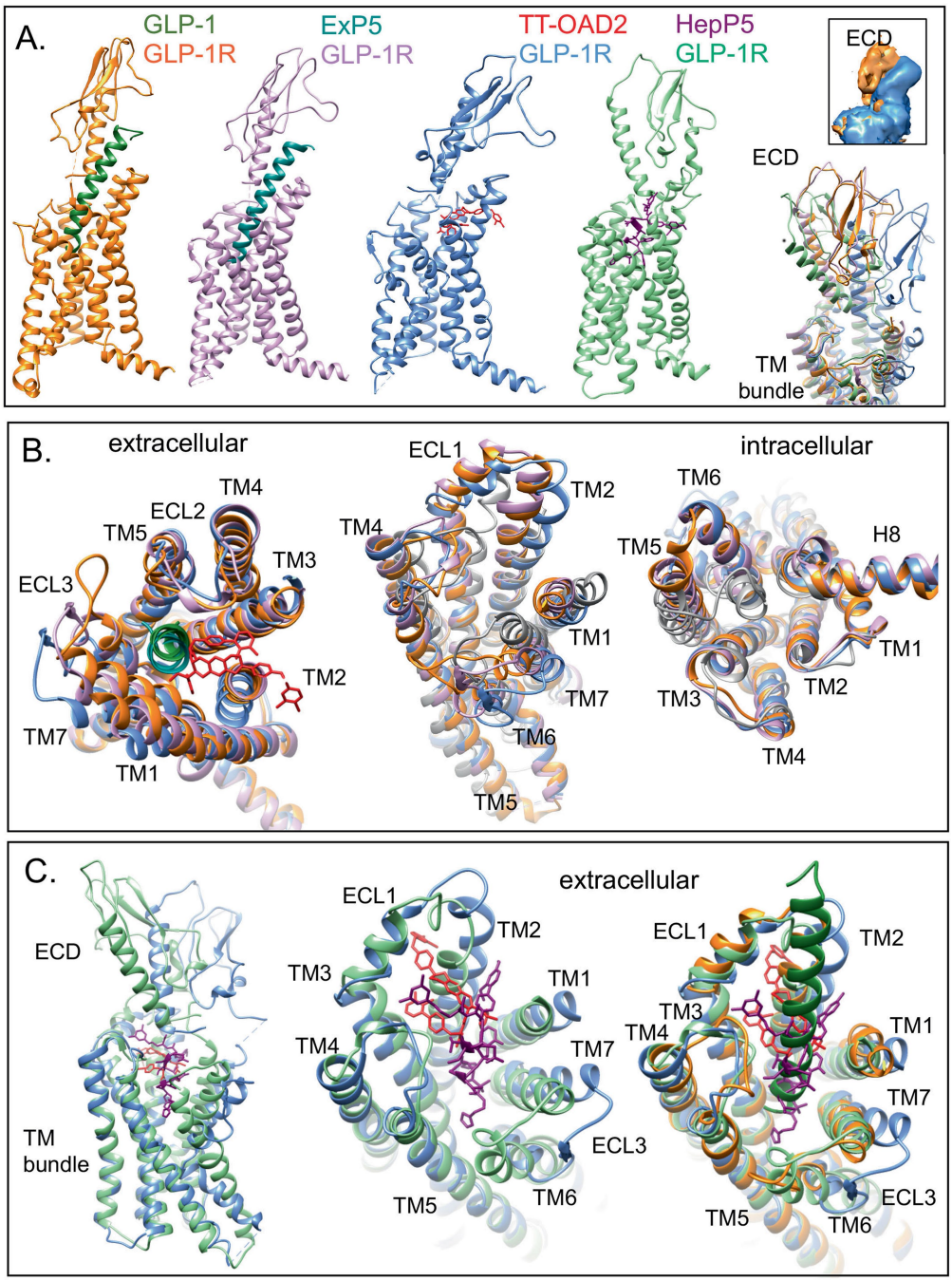

Extended Data Fig. 5 | Comparison of the TT-OAD2–GLP-1R–G_s complex with peptide agonist-bound GLP-1R structures and the inactive class B GPCR glucagon receptor transmembrane helices. a, Structures of agonist-bound GLP-1R; from left to right: GLP-1R (orange) bound to GLP-1 peptide (green) in an active conformation, GLP-1R (pink) bound to ExP5 peptide (cyan) in an active conformation, GLP-1R (blue) bound to non-peptide TT-OAD2 (red) in an active conformation, GLP-1R (pale green) bound to 11-mer peptide HepP5 (purple) in a partially active conformation. Far right, overlay of GLP-1R agonist-bound structures highlighting variations within the ECD position in the different structures. Inset, differences in the location of the ECD are supported by density in the cryo-EM maps; shown are the GLP-1-bound (orange) and TT-OAD2 bound (blue) GLP-1R. **b**, **c**, Various overlays of these structures (using the same colours) to compare conformational differences between the different structures. **b**, Overlay of TT-OAD2-bound GLP-1R G_s structure with the full-length peptide bound G_s structures and the inactive glucagon receptor (GCGR; grey) bundle reveals common conformational transitions occur in all agonist-bound structures relative to the inactive GCGR, but the extent of these movements differ. A more open helical bundle is observed for the TT-OAD2-bound GLP-1R than either GLP-1- or ExP5-bound owing to a distinction in the conformations of TM1, TM6, TM7 and ECL3 at the extracellular side of the receptor induced by the binding of the different ligands (left and middle). Middle, differences in the conformation of TM2 between the inactive and peptide-agonist-bound structures is also evident. Right, at the intracellular face all active structures display a similar large outward movement of TM6 and a smaller movement within TM5. **c**, Comparison of TT-OAD2-bound GLP-1R with the small peptide HepP5-bound GLP-1R structure. Left, TT-OAD2 and Hep-P5 occupy a partially overlapping binding site but promote distinct conformations of the ECD and transmembrane bundle of the GLP-1R. Middle, HepP5 engages deeper in the helical bundle than TT-OAD2 and promotes a more closed helical bundle owing to differences induced in the conformation of TM1, TM6, TM7 and ECL3. Right, overlay of the TT-OAD2-, Hep-P5- and GLP-1-bound GLP-1R transmembrane bundles reveals HepP5 induces a similar conformation of the helical bundle to GLP-1 whereas TT-OAD2 induces a distinct conformation.

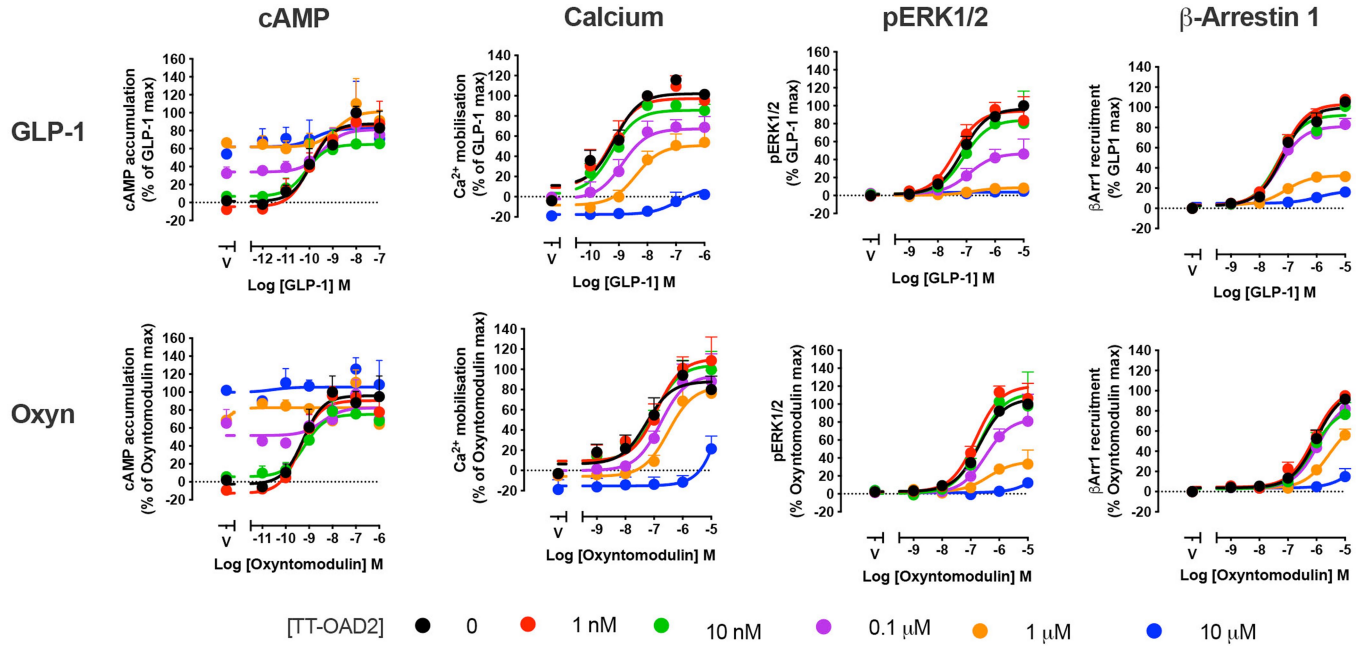

Extended Data Fig. 6 | Pharmacological responses exhibited by endogenous ligands GLP-1 and oxyntomodulin in the presence of TT-OAD2. Signalling profiles of GLP-1 and oxyntomodulin, after 30 min preincubation of vehicle (0) or increasing concentrations of TT-OAD2. Data were performed in HEK293A cells stably expressing the GLP-1R, and are mean + s.e.m. of 3–4 independent experiments performed in duplicate.

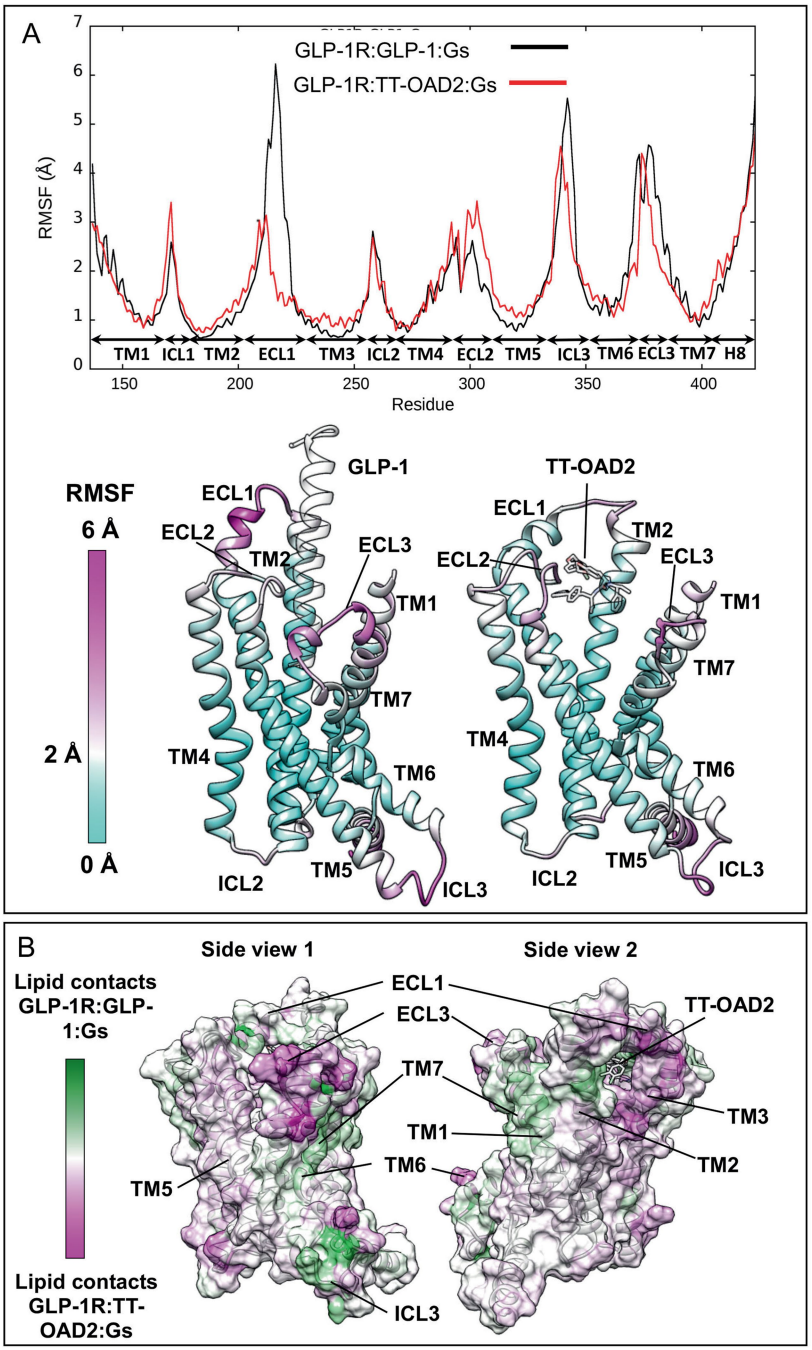

Extended Data Fig. 7 | GLP-1R domains are stabilized by either ligand contacts or lipid interactions. a, Top, RMSF values of alpha carbons computed during MD simulations of the GLP-1R–GLP-1–G_s complex (black line) and the GLP-1R–TT-OAD2–G_s complex (red line); transmembrane helices, intracellular loops (ICLs), and ECLs positions are indicated. Bottom left, RMSF values plotted on the GLP-1R structure bound to GLP-1 (transparent ribbon). Bottom right, RMSF values plotted on the GLP-1R structure bound to TT-OAD2 (transparent stick representation). ECL1 and ECL3 were more dynamic in the GLP-1-bound receptor than the TT-OAD2-bound structure. By contrast, ECL2 and the top end of TM5 were more mobile in the GLP-1R–TT-OAD2–G_s complex. **b**, GLP-1R contacts formed with membrane lipids during molecular dynamic simulations of the GLP-1R–TT-OAD2–G_s and the GLP-1R–GLP-1–G_s systems. Two sides views of the receptor are shown (ribbon and transparent surface). When bound to TT-OAD2, ECL1, TM3, the distal end of TM6, and ECL3 are more in contact with the membrane lipids (magenta). By contrast, TM1 and TM7 are more prone to interact with the membrane when GLP-1 is bound (green). The outward movement of ECL3 in the GLP-1R–TT-OAD2–G_s complex (stabilized by a hydrogen bond network different than GLP-1R–GLP-1–G_s; Extended Data Table 2) produces more interactions with the lipids, possibly further stabilizing the open conformation of TM6, ECL3 and TM7.

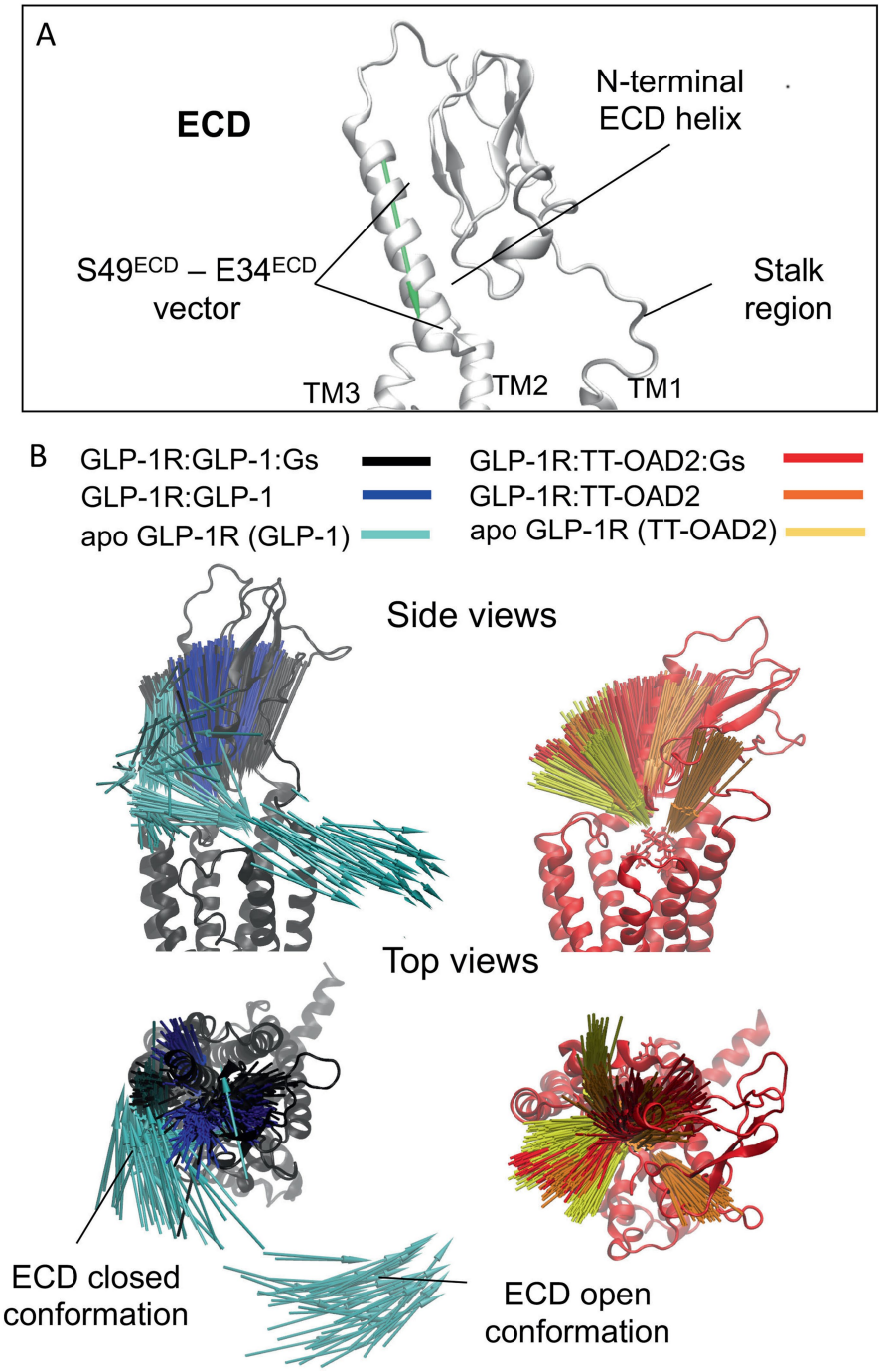

Extended Data Fig. 8 | Dynamics of the ECD of GLP-1R. a, The vector (shown here as a green arrow) connecting $S49^{ECD}$ and $E34^{ECD}$ alpha carbons (ECD N-terminal helix) are shown in the box. **b**, Left, ECD N-terminal helix orientations observed during the molecular dynamics simulation of the GLP-1R–GLP-1–G_s (black arrows), the GLP-1R–GLP-1 complex (obtained by removing G protein; blue arrows), and the apo-GLP-1R (obtained by removing both the G_s protein and GLP-1; cyan arrows) are shown on the left viewed from the top and side of the bundle. The receptor is shown as a dark grey ribbon. During molecular dynamic simulations with GLP-1 bound, the N-terminal helix was oriented vertically (black and blue arrows), whereas in the apo-form the ECD N-terminal helix was more dynamic and experienced both open and closed conformations (this is analogous to the suggested ECD dynamics for the glucagon receptor). Right, ECD N-terminal helix orientations of the GLP-1R–TT-OAD2–G_s (red arrows), the GLP-1R–TT-OAD2 complex (obtained by removing G protein; orange arrows), and the apo-GLP-1R (obtained by removing both the G_s protein and TT-OAD2; yellow arrows) are shown. The receptor is shown as a red ribbon. The distal end ($S49^{ECD}$) of the helix was more mobile than the proximal one ($E34^{ECD}$), which had an overall tendency to remain in the proximity of the TT-OAD2-binding site, driven by transient interactions with the ligand (Extended Data Table 1) and hydrogen bonds with the $R299^{ECL2}$ side chain (Extended Data Table 2). Molecular dynamics simulations therefore suggest a different behaviour for residue $R299^{ECL2}$, which is stably involved in interactions with the peptide in the GLP-1-R–GLP-1–G_s complex (Extended Data Table 1), and instead interacts with $E34^{ECD}$ and other residues located at the ECL2 ($E294^{ECD}$, $D293^{ECD}$ and $N300^{ECD}$) in the GLP-1R–TT-OAD2–G_s complex (Extended Data Table 2).

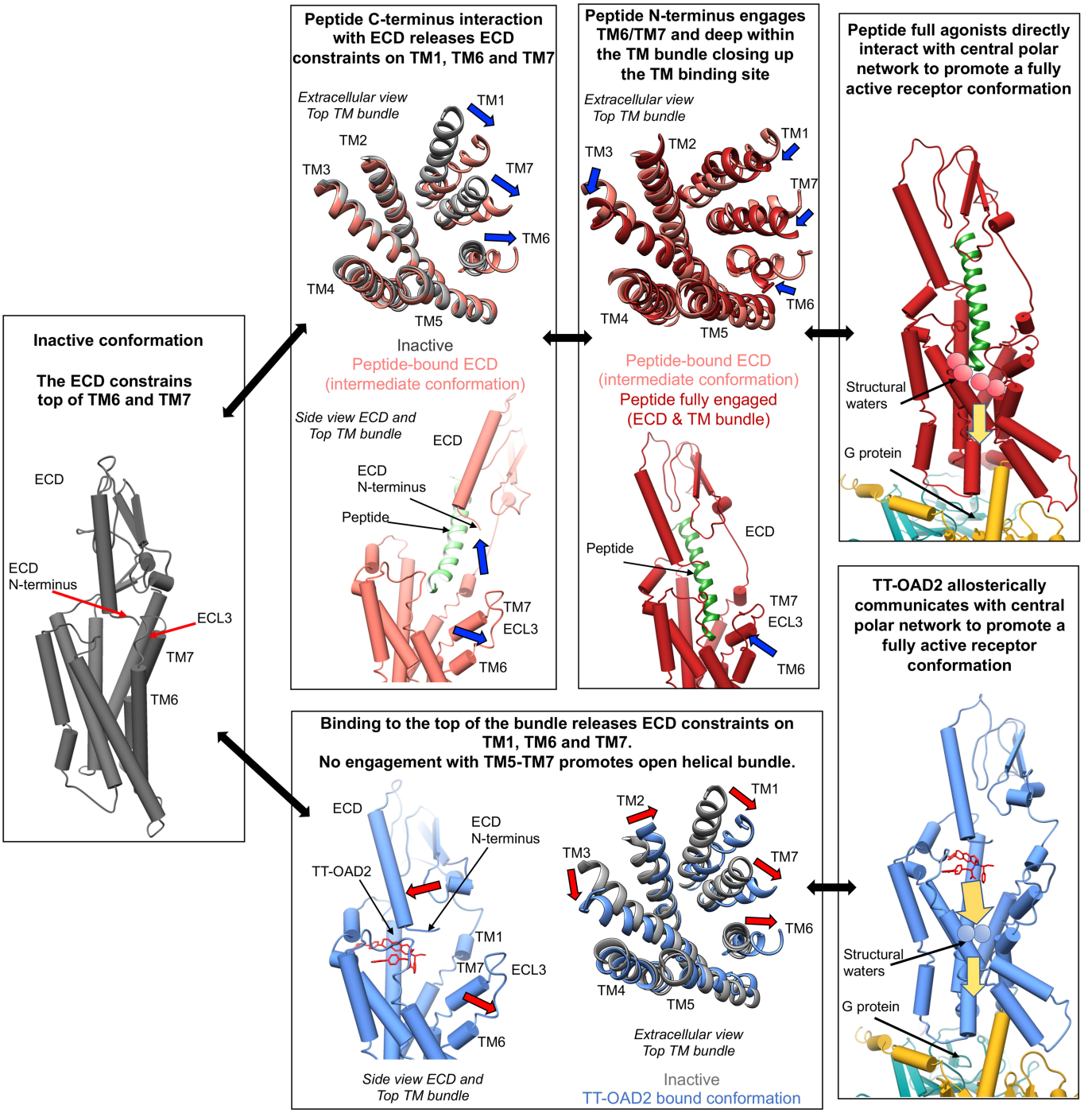

Extended Data Fig. 9 | Proposed activation mechanism of class B GPCRs. Left, in the inactive conformation, the top of the transmembrane domain is stabilized by interactions of the ECD with the TM6–ECL3–TM7 region. Top, activation of class B GPCRs by peptides occurs via a two domain mechanism. Top left, engagement of the peptide with the receptor ECD releases ECD constraints on the transmembrane domain promoting outward movements of TM1, TM6 and TM7 by peptide. Middle, interaction of the peptide N terminus in the bundle within TM1, TM2, TM3, TM5, TM6 and TM7 promotes TM1, TM6 and TM7 to close in around the peptide. Direct engagement of peptides with the central polar network facilitates conformational transitions required for G protein coupling and activation. Top right, the active conformation of the central polar network is stabilized by a series of structural waters. Bottom, interaction of the non-peptide TT-OAD2 at the top of the GLP-1R transmembrane bundle releases ECD constraints on the transmembrane bundle resulting in movements of TM1, TM6 and TM7 outwards. TT-OAD2 does not engage TM5–TM7 and the bundle remains open. TT-OAD allosterically promotes conformational rearrangement of the central polar network to stabilize the fully active receptor conformation that allows coupling to G protein. Bottom right, the central polar network is stabilized by a distinct network of structural waters relative to peptide-mediated activation.

Extended Data Table 1 | GLP-1R–TT-OAD2 and GLP-1R–GLP-1 contacts during molecular dynamics simulations performed on the GLP-1R–TT-OAD2–G_s and GLP-1R–GLP-1–G_s complexes

GLP-1R:TT-OAD2 (TM) Residues	Contacts occupancy (% frames)	GLP-1R:GLP-1 (TM) Residues	Contacts occupancy (% frames)
*K197$^{2.67}$	100.0	*R299^{ECL2}	302.9
A200$^{2.70}$	100.0	L388$^{7.43}$	288.0
Y220^{ECL1}	100.0	L201$^{2.71}$	273.2
*F230$^{3.33}$	99.9	L384$^{7.39}$	266.2
*M204$^{2.74}$	99.8	Y205^{ECL1}	261.3
*W297^{ECL2}	99.8	L142$^{1.37}$	222.5
W203$^{2.73}$	99.7	L141$^{1.36}$	196.2
C226$^{3.29}$	99.7	*Y145$^{1.40}$	193.2
*M233$^{3.36}$	99.5	F381$^{7.36}$	187.4
V229$^{3.32}$	99.2	R190$^{2.60}$	151.1
L201$^{2.71}$	98.9	*K197$^{2.67}$	140.8
L217^{ECL1}	98.1	*M233$^{3.36}$	139.1
I196$^{2.66}$	88.6	E387$^{7.42}$	132.1
*Y145$^{1.40}$	68.9	*Y148$^{1.43}$	131.2
Q221^{ECL1}	67.4	H212^{ECL1}	124.1
A199$^{2.69}$	52.4	Q213^{ECL1}	111.8
Q234$^{3.37}$	48.6	E364$^{6.53}$	103.7
D198$^{2.68}$	44.4	T391$^{7.46}$	101.3
T29^{ECD}	43.9	W214^{ECL1}	93.2
*Y148$^{1.43}$	43.4	V237$^{3.40}$	89.6
*V194$^{2.64}$	42.6	*F230$^{3.33}$	87.3
S31^{ECD}	41.5	*T298^{ECL2}	86.6
C296^{ECL2}	40.3	*V194$^{2.64}$	81.0
W33^{ECD}	38.7	Y241$^{3.44}$	80.3
A28^{ECD}	36.4	W306$^{5.36}$	76.6
L32^{ECD}	25.1	R376^{ECL3}	69.1
T149$^{1.44}$	23.6	*$^{\#}$W297^{ECL2}	67.0
*R299^{ECL2}	22.0	F367$^{6.56}$	62.6
*T298^{ECL2}	20.1	R310$^{5.40}$	59.6
		F385$^{7.40}$	57.0
		I313$^{5.43}$	56.7
		*M204^{ECL1}	52.7

Contacts involving the GLP-1R transmembrane domain are determined as the sum of the occupancy (reported as percentage of frames) of all the contacts involving each residue. Values higher than 100% indicate residues able to interact with more than one peptide side chain. A contact was considered productive if the distance between the residue and the ligand was less than 3.5 Å. Data are summarized in Fig. 4c. TT-OAD2 mainly interacted with TM2, ECL1 and TM3. Interactions with TM1 and ECL2 were present but not persistent (with the exception of W297^{ECL2}). The N-terminal helix of the ECD was engaged in (many) transient interactions. Overall, GLP-1 interacted with a different set of residues and was able to further involve TM5, TM6 and TM7. TT-OAD2 and GLP-1 common contact residues (indicated by an asterisk) were located at TM1, TM2 and ECL2. Ligand contacts formed via interaction with the receptor backbone rather than a side chain interaction are indicated by a hash symbol.

Extended Data Table 2 | Main GLP-1R–GLP-1R intramolecular hydrogen bonds during molecular dynamics simulation

GLP-1R residues involved in intramolecular hydrogen bonds		GLP-1R:TT-OAD2:Gs	GLP-1R:GLP-1:Gs	GLP-1R:GLP-1:Gs / GLP-1R:TT-OAD2:Gs Δ occupancy [a]
R40^{ECD}	D215^{ECL1}	38.2	68.6	30.4
R176$^{2.46}$	E408^{H8}	35.7		-35.7
R176$^{2.46}$	E247$^{3.50}$	46.7	97.9	51.2
N182$^{2.52}$	W274$^{4.50}$	73	81.4	8.4
R190$^{2.60}$	E364$^{6.53}$	4	5	1
R190$^{2.60}$	Y241$^{3.44}$	13.9	14.2	0.3
R190$^{2.60}$	N240$^{3.43}$	78,2	93.1	14.9
D198$^{2.68}$	K202^{ECL1}	60.2	18.8	-41.4
D198$^{2.68}$	Y145$^{1.40}$	74	59.2	-14.8
D198$^{2.68}$	K197$^{2.67}$	0.2	59.6	59.4
R227$^{3.30}$	D222^{ECL1}	4.1		-4.1
R227$^{3.30}$	D293^{ECL2}	63.5	31.9	-31.6
R227$^{3.30}$	S223^{ECL1}		37	37
N240$^{3.43}$	S186$^{2.56}$	54.9	69.1	14.2
E247$^{3.50}$	Y402$^{7.47}$	60.4	77.6	17.2
D293^{ECL2}	K288$^{4.64}$	23.4	4.9	-18.5
D293^{ECL2}	Y220^{ECL1}		13.6	13.6
E294^{ECL2}	S301^{ECL2}	0.8		-0.8
E294^{ECL2}	T298^{ECL2}	11.1		-11
E294^{ECL2}	K288$^{4.64}$	42.5	39	-3.5
R299^{ECL2}	E34^{ECD}	56.5	0.1	-56.4
R299^{ECL2}	E294^{ECL2}	26.5		-26.5
R299^{ECL2}	D293^{ECL2}	17.8		-17.8
R299^{ECL2}	N300^{ECL2}	16.2		-16.2
R299^{ECL2}	E373^{ECL3}		19.6	19.6
N300^{ECL2}	E292$^{4.68}$	13.9		-13.9
R310$^{5.40}$	E364$^{6.53}$	31.4	3.3	-28.1
R310$^{5.40}$	D372^{ECL3}		29,6	29.6
D344$^{6.33}$	K346$^{6.35}$	48.9	11,2	-37.7
H363$^{6.52}$	T391$^{7.46}$	38.5	0,5	-38
E364$^{6.53}$	Y241$^{3.44}$	48.6	59,6	11
D372^{ECL3}	K383$^{7.38}$	23.2	0,6	-22.6
R376^{ECL3}	D372^{ECL3}		21,2	21.2
R376^{ECL3}	E373^{ECL3}	13.4	42,7	29.3
R380$^{7.35}$	D372^{ECL3}	60.7	1	-59.7
R380$^{7.35}$	E387$^{7.42}$	2.4	44,7	42.3
E387$^{7.42}$	K383$^{7.38}$	62.6	2.2	-60.4

Data expressed as the occupancy (percentage of frames) in which the interactions were present in the GLP-1R–TT-OAD2–G_s and GLP-1R–GLP-1–G_s complexes. Differences between GLP-1R–GLP-1–G_s and GLP-1R–TT-OAD2–G_s are reported in the right column; green indicates more contacts in GLP-1 versus TT-OAD2, and red denotes more contacts in TT-OAD2 versus GLP-1. Grey cells indicate that hydrogen bonds were not present.

Corresponding author(s): Radostin Danev, Patrick M. Sexton, Denise Wootten

Reporting Summary

Nature Research wishes to improve the reproducibility of the work that we publish. This form provides structure for consistency and transparency in reporting. For further information on Nature Research policies, see Authors & Referees and the Editorial Policy Checklist.

Statistical parameters

When statistical analyses are reported, confirm that the following items are present in the relevant location (e.g. figure legend, table legend, main text, or Methods section).

n/a	Confirmed	
☐	☒	The exact sample size (*n*) for each experimental group/condition, given as a discrete number and unit of measurement
☐	☒	An indication of whether measurements were taken from distinct samples or whether the same sample was measured repeatedly
☐	☒	The statistical test(s) used AND whether they are one- or two-sided *Only common tests should be described solely by name; describe more complex techniques in the Methods section.*
☐	☒	A description of all covariates tested
☐	☒	A description of any assumptions or corrections, such as tests of normality and adjustment for multiple comparisons
☐	☒	A full description of the statistics including central tendency (e.g. means) or other basic estimates (e.g. regression coefficient) AND variation (e.g. standard deviation) or associated estimates of uncertainty (e.g. confidence intervals)
☐	☒	For null hypothesis testing, the test statistic (e.g. *F*, *t*, *r*) with confidence intervals, effect sizes, degrees of freedom and *P* value noted *Give P values as exact values whenever suitable.*
☐	☒	For Bayesian analysis, information on the choice of priors and Markov chain Monte Carlo settings
☒	☐	For hierarchical and complex designs, identification of the appropriate level for tests and full reporting of outcomes
☒	☐	Estimates of effect sizes (e.g. Cohen's *d*, Pearson's *r*), indicating how they were calculated
☒	☐	Clearly defined error bars *State explicitly what error bars represent (e.g. SD, SE, CI)*

Our web collection on statistics for biologists may be useful.

Software and code

Policy information about availability of computer code

Data collection	SerialEM
Data analysis	GraphPad Prism, UCSF Chimera, VMD, GetContacts analysis tool, avconv, AquaMMapS, ACEMD, Modeller, MDFF, Coot, Phenix, Chem3D, Relion 3.0, CryoSPARC 2.5.0, ResMAP, MotionCor2, Gctf, EMAN2

For manuscripts utilizing custom algorithms or software that are central to the research but not yet described in published literature, software must be made available to editors/reviewers upon request. We strongly encourage code deposition in a community repository (e.g. GitHub). See the Nature Research guidelines for submitting code & software for further information.

Data

Policy information about availability of data

All manuscripts must include a data availability statement. This statement should provide the following information, where applicable:

- Accession codes, unique identifiers, or web links for publicly available datasets
- A list of figures that have associated raw data
- A description of any restrictions on data availability

Atomic coordinates and the cryo-EM density map have been deposited in the Protein Data Bank under accession number 6ORV and EMDB entry ID 20179

Field-specific reporting

Please select the best fit for your research. If you are not sure, read the appropriate sections before making your selection.

☒ Life sciences ☐ Behavioural & social sciences ☐ Ecological, evolutionary & environmental sciences

For a reference copy of the document with all sections, see nature.com/authors/policies/ReportingSummary-flat.pdf

Life sciences study design

All studies must disclose on these points even when the disclosure is negative.

Sample size	Sample size calculation was not required
Data exclusions	No data were excluded
Replication	Experimental findings were reliably reproduced
Randomization	Randomization was not required
Blinding	Blinding was not performed

Reporting for specific materials, systems and methods

Materials & experimental systems

n/a	Involved in the study
☐	☐ Unique biological materials
☐	☒ Antibodies
☐	☒ Eukaryotic cell lines
☐	☐ Palaeontology
☐	☒ Animals and other organisms
☐	☐ Human research participants

Methods

n/a	Involved in the study
☐	☐ ChIP-seq
☐	☐ Flow cytometry
☐	☐ MRI-based neuroimaging

Unique biological materials

Policy information about availability of materials

Obtaining unique materials	*Describe any restrictions on the availability of unique materials OR confirm that all unique materials used are readily available from the authors or from standard commercial sources (and specify these sources).*

Antibodies

Antibodies used	rabbit anti-Gs C-18 antibody (cat no sc-383), Santa Cruz mouse Penta-His antibody (cat no 34660), QIAGEN 680RD goat anti-mouse antibody (LI-COR) 800CW goat anti-rabbit antibody (LICOR)
Validation	All antibodies were used for Western blot analysis and have been validated.

Eukaryotic cell lines

Policy information about cell lines

Cell line source(s)	Cells used in assays were obtained from ATCC
Authentication	No authentication required
Mycoplasma contamination	Cell lines were tested and are free from mycoplasma contamination

Commonly misidentified lines (See ICLAC register)	Cells are not listed in the database

Palaeontology

Specimen provenance	Not applicable
Specimen deposition	Not applicable
Dating methods	Not applicable

☐ Tick this box to confirm that the raw and calibrated dates are available in the paper or in Supplementary Information.

Animals and other organisms

Policy information about studies involving animals; ARRIVE guidelines recommended for reporting animal research

Laboratory animals	C57/Bl6
Wild animals	Not applicable
Field-collected samples	Not applicable

Human research participants

Policy information about studies involving human research participants

Population characteristics	Not applicable
Recruitment	Not applicable

ChIP-seq

Data deposition

☐ Confirm that both raw and final processed data have been deposited in a public database such as GEO.

☐ Confirm that you have deposited or provided access to graph files (e.g. BED files) for the called peaks.

Data access links *May remain private before publication.*	Not applicable
Files in database submission	Not applicable
Genome browser session (e.g. UCSC)	Not applicable

Methodology

Replicates	Not applicable
Sequencing depth	Not applicable
Antibodies	Not applicable
Peak calling parameters	Not applicable
Data quality	Not applicable
Software	Not applicable

Flow Cytometry

Plots

Confirm that:

☐ The axis labels state the marker and fluorochrome used (e.g. CD4-FITC).

☐ The axis scales are clearly visible. Include numbers along axes only for bottom left plot of group (a 'group' is an analysis of identical markers).

☐ All plots are contour plots with outliers or pseudocolor plots.

☐ A numerical value for number of cells or percentage (with statistics) is provided.

Methodology

Sample preparation	Not applicable
Instrument	Not applicable
Software	Not applicable
Cell population abundance	Not applicable
Gating strategy	Not applicable

☐ Tick this box to confirm that a figure exemplifying the gating strategy is provided in the Supplementary Information.

Magnetic resonance imaging

Experimental design

Design type	Not applicable
Design specifications	Not applicable
Behavioral performance measures	Not applicable

Acquisition

Imaging type(s)	Not applicable
Field strength	Not applicable
Sequence & imaging parameters	Not applicable
Area of acquisition	Not applicable

Diffusion MRI ☐ Used ☒ Not used

Preprocessing

Preprocessing software	Not applicable
Normalization	Not applicable
Normalization template	Not applicable
Noise and artifact removal	Not applicable
Volume censoring	Not applicable

Statistical modeling & inference

Model type and settings	Not applicable
Effect(s) tested	Not applicable

Specify type of analysis: ☐ Whole brain ☐ ROI-based ☐ Both

Statistic type for inference (See Eklund et al. 2016)	Not applicable

Correction	Not applicable

Models & analysis

n/a	Involved in the study
☒	☐ Functional and/or effective connectivity
☒	☐ Graph analysis
☒	☐ Multivariate modeling or predictive analysis